UNIVERSITY OF SOUTHAMPTON

A Sensor System to Detect Events in Gait for the Correction of Abnormalities in Neurological Patients

by

Noreha Abdul Malik

A thesis submitted in partial fulfilment for the degree of Doctor of Philosophy

in the

Faculty of Physical and Applied Sciences

School of Electronics and Computer Science

October, 2010

UNIVERSITY OF SOUTHAMPTON

ABSTRACT

FACULTY OF PHYSICAL AND APPLIED SCIENCES
SCHOOL OF ELECTRONICS AND COMPUTER SCIENCE

Doctor of Philosophy

by Noreha Abdul Malik

Contraction of the hamstrings or gluteals muscles, using electrical stimulation, could improve the abnormal gait in neurological patients. The stimulation timing which follows the normal muscle activity is impractical to achieve using the traditional sensor (the footswitch). This study focuses on the development of a new sensor system for the detection of events in the gait cycle to trigger stimulation of hamstrings or gluteals muscles for preventing knee hyperextension into early stance or reducing the excessive hip flexion/adduction at heel strike. A sensor unit, consisting of four accelerometers, has been designed to determine the angles and linear accelerations of a segment without the need for integration. Tests have been carried out to verify the error of the sensor unit angle measurement by comparing it with the output from a potentiometer of a simple inverted pendulum. In five healthy subjects during walking, assessments have been carried out to compare the segment angle of the thigh, shank and foot calculated from the sensor unit, with the same angles measured using a motion capture system (Vicon^{TM}). The results show that the shank segment angles have a similar pattern. A sensor system to detect gait events has been developed. It consists of the sensor unit, a correlation coefficient calculation and a set of rules with thresholds. The system has detected reliably all heel strikes and a place in the gait cycle representing the tibia vertical position of five healthy subjects. Two sample windows selected from one set of the subject data have been used to detect all of the events. Using the same system, all tibial vertical events have been detected reliably compared to the footswitch in six neurological patients. In five patients, the same sample window, selected from the healthy subject, was used in the detection. For one patient, a sample window selected from the same patient data was used. Further work will be needed to implement the system in real time and evaluate it's use with electrical stimulation as well as to establish the effect of stimulation in patients using the sensor unit as the trigger.

Contents

List of Figures

List of Tables

Declaration of Authorship

I, Noreha Abdul Malik declare that the thesis entitled ‘A Sensor System to Detect Events in Gait for the Correction of Abnormalities in Neurological Patients’and the work presented in the thesis are both my own, and have been generated by me as the result of my own original research. I confirm that:

1. This work was done wholly or mainly while in candidature for a research degree at this University;
2. Where any part of this thesis has previously been submitted for a degree or any other qualification at this University or any other institution, this has been clearly stated;
3. Where I have consulted the published work of others, this is always clearly attributed;
4. Where I have quoted from the work of others, the source is always given. With the exception of such quotations, this thesis is entirely my own work;
5. I have acknowledged all main sources of help;
6. Where the thesis is based on work done by myself jointly with others, I have made clear exactly what was done by others and what I have contributed myself.
7. Parts of this work have been published as listed in section 1.5 of this thesis.

Signed:…….....

Date:…….

Acknowledgements

Thanks to God for his blessing and bestowal which had enables me to complete this PhD thesis.

I would like to express my utmost appreciation and gratitude towards Dr. Paul H. Chappell for being my supervisor and for his great assistance and guidance throughout the development of the project.

I would also like to express my wonderful thanks to my second supervisors, Dr. Duncan E. Wood and Dr. Paul N. Taylor for sharing their valuable knowledge and time for the project enhancement.

My special thanks go to my beloved husband, Khairil with all the love and support he gave me, who motivate and advice me, my parents, Abdul Malik and Rahimah; my parents-in-law Shaari and Arbaie, still don't forget my dearest family members Faridah, Zulkafli, Nazri, Rozita and Iznan for their support.

Thank you to my colleague in IIUM, Dr Faiz Ahmed, all the staff of ECS especially Barry, Richard and Jeff for their technical support, and to all the staff at the Department of Clinical Science and Engineering, Salisbury District Hospital especially Mohamed. Thank you to my dearest friends Ivo, Norsaremah, Dzun, Fadzlin, Amy, Yang, Darren, Ingrid, Joanna, Rod, Somphop, Kiwi, Ghaithaa, Anom, Aizam, Munzilah, Zuhaila and Zurina. I would also like to thank my employer IIUM and my sponsor the Ministry of Higher Education Malaysia. Not to forget, special thanks to all the participants who volunteered in the study. Lastly, thank you to all Malaysian students in Southampton who gave me a strength and support throughout my PhD life in UK.

Glossary

Abduction	A movement of a limb from the midline, in the frontal plane.
Adduction	A movement of a limb towards the midline, in the frontal plane.
Antagonist	Muscles with opposing actions.
Bilateral	Involving right and left limbs (sides of the body).
Cerebral palsy	Neurological disorder with spasticity and incoordination, usually caused by brain damaged before birth.
Cerebrovascular accident	Brain damage due to blood clot or hemorrhage; also known as stroke.
Clonus	A form of movement marked by contractions and relaxations of muscle, occurring in rapid succession, after forcible extension or flexion of a part.
Contralateral	Taking place or originating in a corresponding part on an opposite side, as pain or paralysis in a part opposite the site of a lesion.
Coronal plane	*see frontal plane*
Dorsiflexion	A movement of the foot towards the knee.
Dysphasia	Impairment of speech and verbal comprehension, especially when associated with brain injury.
Evert, eversion	An internal rotation about the long axis of the foot.
Extension	A sagittal plane movement at a joint, the distal segment usually moving posteriorly (anteriorly at the knee).
External rotation	Rotation of a limb about its long axis, the anterior surface moving laterally.
Equinus	A toe-down position of the foot, in which the forefoot is lower than the heel.
Feet adjacent	An event in the swing phase of the gait cycle when the foot of the swinging leg passes the supporting foot.
Flexion	A sagittal plane movement at a joint, the distal segment usually moving anteriorly (posteriorly at the knee).
Foot flat	A point in the stance phase of the gait cycle at which the forefoot contacts the ground, when initial contact has been made by the

	heel.
Foot slap	An abrupt and audible lowering of the foot following initial contact.
Forefoot	The five metatarsal bones and the toes.
Frontal plane	Divides a body part into front and back portions.
Heel rise	An event in the stance phase of the gait cycle at which the heel lifts away from the supporting surface.
Heel strike	A distinct impact the heel and the ground at initial contact.
Hemianaesthesia	Loss of sensation on one side of the body.
Hemiparesis	A partial paralysis affecting one side of the body.
Hemiplegia	A complete paralysis affecting one side of the body.
Hemorrhage	An abnormal bleeding. Hemorrhage into the brain is a common cause of brain damage.
Intial contact	An event in the gait cycle when first contact is made between the foot and the ground; made by the heel in normal gait. Marks the transition from swing phase to stance phase.
Internal rotation	A rotation of a limb about its long axis, the anterior surface moving medially.
Invert, inversion	An external rotation about the long axis of the foot.
Ipsilateral	On the same side of the body.
Lateral	Away from the midline of the body.
Loading response	A period in the stance phase of the gait cycle between initial contact and opposite toe off.
Medial	Towards the midline of the body.
Mid-stance	A period in the stance phase of the gait cycle between opposite toe off and heel rise.
Mid-swing	A period in the stance phase of the gait cycle between feet adjacent and tibia vertical.
Myelin	A white fatty material, composed chiefly of lipids and lipoproteins, that encloses certain axons and nerve fibers.
Opposite initial contact	An event in the stance phase of the gait cycle when other foot makes initial contact with the ground; occurs at around 50% of the cycle in normal gait.

Opposite toe off	An event in the stance phase of the gait cycle when the other foot is leaving the ground. Generally close in the foot flat.
Paralysis	A loss of the ability to voluntarily contract the muscle.
Paraplegia	A complete paralysis of the legs, usually due to disease or injury of the spinal cord.
Plantarflexion	A movement of the foot away from the knee.
Posterior	To the back of the body (in the anatomical position).
Pre-swing	A period in the stance phase of the gait cycle between opposite initial contact and toe off.
Push off	*see pre-swing*
Sagittal plane	Divides part of the body into right and left portions.
Spasticity	Involuntary resistance of muscles to being stretched.
Sphincter	A ring-shaped muscle that encircles an opening or passage in the body.
Stance phase	The part of the gait cycle for one side in which the foot is on the ground.
Swing phase	The part of the gait cycle for one side in which the foot is off the ground, moving through the air.
Terminal stance	A period in the stance phase of the gait cycle between heel rise and opposite initial contact.
Terminal swing	A period in the stance phase of the gait cycle between tibia vertical and the next initial contact.
Thrombosis	Formation of a clot in the blood that either blocks, or partially blocks a blood vessel.
Tibia vertical	An event in the swing phase of gait in which the tibia passes through the vertical in moving from behind the body to in front of it.
Toe-off	An event in the gait cycle when the foot (generally the toe) leaves the ground. Marks the transmission from the stance phase to the swing phase.
Upper motor neuron	A nerve fiber producing muscular contraction, running from the brain to the spinal cord, where it connects with lower motor neurons.

Nomenclature

ALN	Adaptive Logic Network
CNS	Central nervous system
CP	Cerebral Palsy
CVA	Cerebrovascular accident
EC	End contact
FA	Feet adjacent
FES	Functional electrical stimulation
FSR	Force sensing resistor
GC	Gait cycle
HR	Heel rise
HS	Heel strike
IC	Initial contact
IMU	Inertial Measurement Unit
MEMS	Micro-Electro-Mechanical Systems
MS	Multiple sclerosis
PNS	Peripheral nervous system
PVC	Polyvinyl chloride
RMSD	Root mean squared deviation
RMSE	Root mean squared error
RS	Rough Sets
SCI	Spinal cord injury
SD	Standard deviation
TE	Time of tibial vertical event
TO	Toe Off
TV	Tibia Vertical
WHO	World Health Organization

Chapter 1

Overview

1.1 Introduction

According to the World Health Organization (WHO) report in 2007, up to one billion people globally are affected by neurological disorders (World Health Organization (2010)). In the UK alone, each year about 600,000 people are newly diagnosed with a neurological condition (Neurological Alliance (2003)). However, this is only an estimate and there are no accurate figures for the incidence of neurological disorders in the UK (Smith (2006)). Furthermore, the data included a wide range of neurological disorders for example headache, stroke, epilepsy, multiple sclerosis, dementia and head injury. Cerebrovascular accident (CVA) or stroke, multiple sclerosis (MS) and spinal cord injury as a result of trauma are the neurological disorders that would result in gait abnormalities and patients with these disorders are recruited for this study. It is estimated that about 120,000 (National Institute for Health Research (2011)) and 80,000 (Sawcer (1997)) people suffer from stroke and MS each year in UK, respectively. Spinal cord injury affects 17 people per 100,000 of the population per year in the UK (Neurological Alliance (2003)).

Neurological disorders are caused by a disturbance of the central and peripheral nervous system which includes the brain, spinal cord, cranial nerves, peripheral nerves, nerve roots, autonomic nervous system, neuromuscular junction and muscle. The disturbance is due to a developmental abnormality, disease, injury or toxin. Some of the disorders such as stroke and multiple sclerosis would result in a severe disability

including loss of motor control, altered sensation, poor coordination, cognitive and language impairment. The loss of motor control affects a patients' mobility and leads to abnormal gait. Patients having abnormal gait experienced walking difficulties, an increased risk of falling, more effort to walk and a reduction in walking speed.

Dropped foot is the most common abnormal gait accounted in neurological patients. It is a condition whereby the patients are not able to lift their foot off during the swing phase of walking as a result of muscle paralysis. The muscle function can be restored by stimulating the common peroneal nerve using functional electrical stimulation (FES) and this was first introduced in the nineteen sixties (Liberson et al. (1961)). The use of FES has shown improvements in the gait of various neurological patients including stroke (Kottink et al. (2004), Robbins et al. (2006)), multiple sclerosis (Carnstam et al. (1977), Swain et al. (2000) and Swain et al. (2003)) and children with cerebral palsy (Durham et al. (2004)). Improvement includes increased walking speed, less effort needed to walk and placement of initial foot contact. There are several examples of commercially available stimulators (single and two channel), for example Odstock stimulator, Salisbury and MikroFes, Ljubljana, Slovenia.

As well as dropped foot, there are other gait abnormalities observed in neurological patients such as knee hyperextension in early and terminal stance, insufficient knee flexion during swing and excessive hip flexion/adduction at heel strike. In these circumstances, a second channel is used to stimulate different muscles such as gluteals or hamstrings depending on the problems. Stimulation of gluteals or hamstrings muscles can further improve the gait of neurological patients (Wright et al. (1999) and Wilkinson and Taylor (2004)), but the timing of stimulating these muscle groups, such as following the normal muscle activity times, is critical.

The current sensor used to trigger a stimulator, either single or two channel, is the footswitch. It is a reliable sensor placed under the heel of shoe insole used to trigger the stimulator for correction of dropped foot. It detects events such as heel contact and uncontact with the ground, also known as heel strike and heel rise. The main issue with the footswitch is when it is used to trigger the stimulator for correction of other abnormal gaits. The clinician has to set a fixed time delay based on the heel rise and heel strike events, that is not easy to predict and therefore to set. Also, the time setting

does not adapt well to changes in walking speed. Therefore, there is a need for an alternative sensor that can detect specific gait events which coincide with the time needed to trigger the stimulator.

The gait problems that would be addressed in the study are the retracted hip/hip adduction at heel strike and knee hyperextension into early stance. According to the literature, the muscles groups such as gluteals (medius or maximus) start to contract at about 5-6% of gait cycle before initial contact while the hamstrings muscles start to contract at about 12-18% of gait cycle before initial contact in normal walking (Perry (1992)). Therefore in this study, the closest event that occurs before the initial contact that is the tibial vertical event will be detected in the neurological patients. In normal walking, the tibial vertical event occurs 13% of gait cycle before the initial contact (normally the heel strike) (Perry (1992)) and could be used to trigger the stimulator for hamstrings or gluteals muscles groups.

1.2 Clinical Problem

The Odstock Two Channel Stimulator (O2CHS II) is used to assist the neurological patients' walking by restoring the paralysed muscle function. The first channel of the stimulator is normally used to correct dropped foot by stimulating the common peroneal nerve or tibialis anterior muscle. A second channel is used to stimulate other muscles such as hamstrings, gluteals, quadriceps or calf muscle for correction of other abnormal gaits. Figure 1-1 shows the examples of electrodes positions (active and indifferent electrodes) for gluteals, hamstrings and calf muscles stimulation. The positions are for gluteals (the active is placed just below the dimples at the top of sacrum and the indifferent is placed approximately one hands breadth below the active electrode, roughly level with coccyx), hamstrings (the indifferent is placed at the bottom of the hamstrings, just above the back of the knee and the active is placed over the centre of the muscle, about two hand widths above the indifferent) and calf muscles (the indifferent is placed towards the bottom of the calf muscles and the active is placed just above the widest part of the calf muscles) (Taylor (2004a)).

Two common abnormal gaits that will be addressed in the study are the knee hyperextension into early stance and the excessive hip flexion/adduction at heel strike.

The knee hyperextension into early stance is prevented by stimulating the hamstrings muscles and the stimulation profile is shown in Figure 1-2. The excessive hip flexion/adduction is corrected by stimulating the gluteals muscles which reduced hip flexion/adduction at heel strike as shown in the stimulation profile (Figure 1-3).

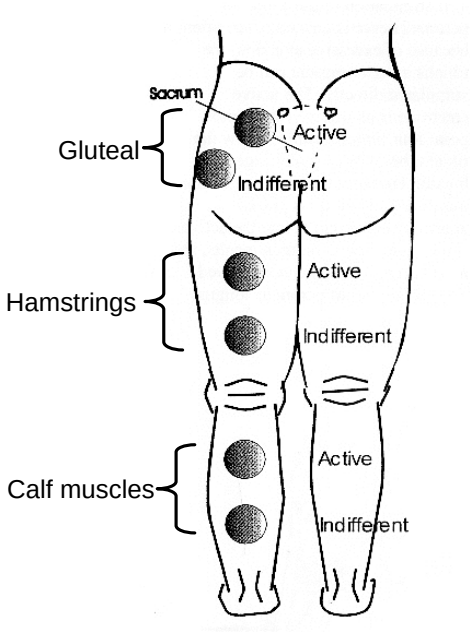

Figure 1-1 The electrodes positions (active and indifferent) for gluteals, hamstrings or calf muscles stimulation (Taylor (2004a)).

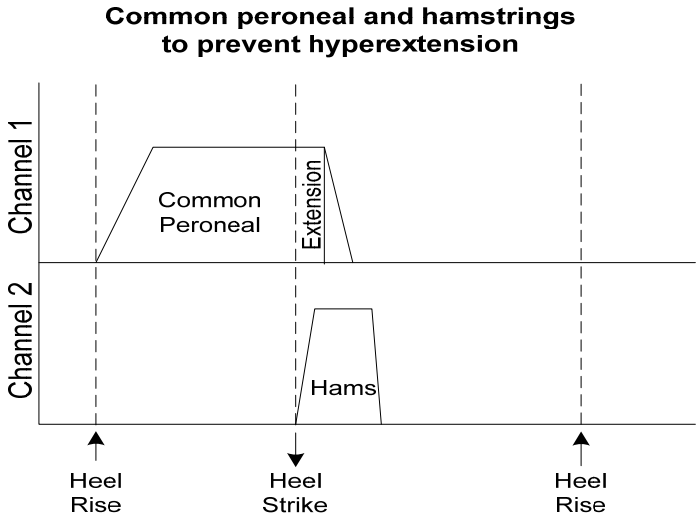

Figure 1-2 A stimulation profile to correct dropped foot and to prevent knee hyperextension into early stance by stimulating the common peroneal and the hamstrings muscles (Taylor (2004a)).

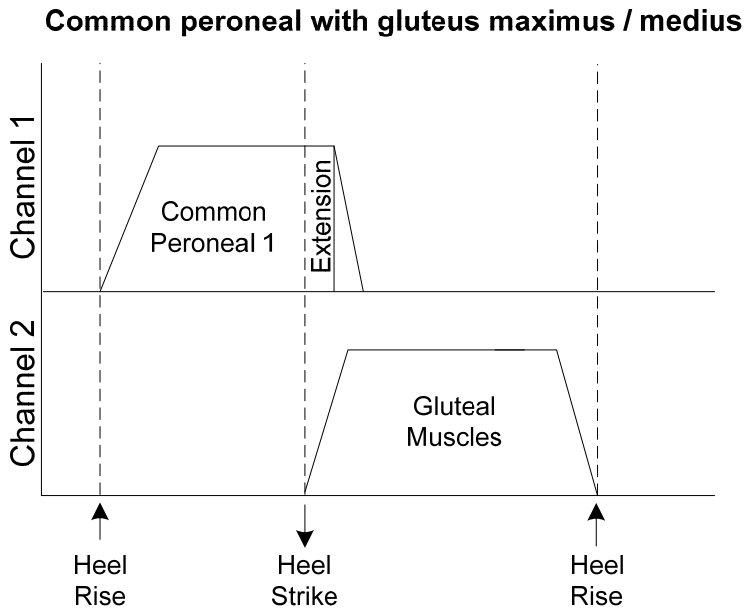

Figure 1-3 A stimulation profile to correct dropped foot and to reduce hip flexion/adduction at heel strike by stimulating the common peroneal and the gluteals muscles (Taylor (2004a)).

The hamstrings and gluteals muscles stimulation start at initial heel contact as can be seen in Figure 1-2 and Figure 1-3 respectively. However, this is quite late in initiating the muscles contraction to correct for specified abnormal gaits. The current sensor used to trigger the O2CHS II is the footswitch, which only detects heel rise, heel strike, toe rise and toe strike, and these events do not coincide with the timing needed to trigger the stimulator for correction of the specified abnormal gaits. According to the timing of the normal muscle activity, these muscles begin their contraction before initial heel contact. The muscles groups such as gluteals (medius or maximus) start to contract at about 5-6% of gait cycle before initial contact while the hamstrings muscles start to contract at about 12-18% of gait cycle before initial contact in normal walking (Perry (1992)). The timing of the normal muscle activity as a percentage of gait cycle before initial heel contact for hamstrings and gluteals muscles are summarised in Table 1-1. These timings are the means data of normal subjects walking with normal cadence. In this study, tibial vertical event will be inferred in the neurological patients as it is the closest event that occurs before the initial heel contact. In normal walking, the tibial vertical event occurs at 13% of gait cycle before the initial contact (normally the heel strike) (Perry (1992)) and could be used to trigger the stimulator for or gluteals muscles groups. In the study, although it is anticipated that the occurrence of tibial vertical event is variable in the healthy subjects and patients, the event detected is compared to

the 13% of gait cycle before initial contact and the earliest stimulation trigger should be about 5% (18% minus13%) before the detected event. The relationship between the timing of the normal muscle activity and the gait cycle is described in section 3.2.1 (Chapter 3, p30).

Table 1-1 The timings of gluteals and hamstrings muscles activity as a percentage of gait cycle before initial heel contact (the means data of normal subjects walking with normal cadence). The hamstrings consist of the biceps femoris long head, semimembranosis and semitendinosis muscles (Perry, 1992).

Muscles	% of gait cycle before initial heel contact
gluteus maximus	5
gluteus medius	4
biceps femoris long head	18
semimembranosis	17
semitendinosis	12

The hamstrings (bicep femoris long head, semimembranosis and semitendinosis) are knee flexor muscles that start their activity at late midswing and the peak intensity occurs at early terminal swing. These muscles contract eccentrically or isometrically to decelerate the shank and the leg at terminal swing. The gluteals muscles are hip extensor and abductor that start their contraction at late terminal swing to decelerate the hip from further flexion and advancement. Once the hamstrings activity has reduced and the thigh has stopped the advancement at late swing, the quadriceps become active and completes the knee extension for preparation of weight acceptance. However, over and unopposed activity of the quadriceps muscles as a result of hamstrings paralysis will lead to hyperextension of the knee into early stance. Stimulation of hamstrings is needed to flex the knee for preventing the knee hyperextension. The balance is still right although the hamstrings extend the hip as the quadriceps activity is in excess. In another instance, hip flexion contracture or spasticity may result in excessive hip flexion which limits hip extension in stance. Stimulation of gluteals muscles is needed to reduce the excessive hip flexion/adduction. In another instance, hip flexion

contracture or spasticity may result in excessive hip flexion which limits hip extension in stance.

1.3 The Project

The main objective of the project is to design a sensor system that could detect tibial vertical event in neurological patients with the future aim to trigger a stimulator for hamstrings or gluteals muscles stimulation to prevent knee hyperextension into early stance or to reduce hip flexion/adduction at heel strike. In the following list are the specific aims in order to achieve the main objective of the project.

- To search for a potential sensor to be used in the study by reviewing various sensors used for kinematic measurements and gait events detection during walking.
- To develop a sensor unit algorithm that could measure the angle and linear accelerations of a segment by using four accelerometers arranged in a specific configuration.
- To identify the sensor unit algorithm output in static and dynamic conditions as well as to verify the signs of terms in the equations describing the system.
- To verify the angle measurement from the sensor unit algorithm. The angle measured from the sensor unit is compared with the angle calculated from potentiometer of a test apparatus (inverted pendulum).
- To demonstrate the kinematic measurement during walking and leg swing in a healthy subject using the sensor unit algorithm.
- To assess the thigh, shank and foot segments angles measured using the sensor unit in five healthy subjects during walking compared to the angle measured from Vicon^{TM}. The two measurements have different cut-off frequencies, sampling rates and mathematical models for the angle measurement. It is anticipated that the results will have a large deviation due to the differences in the two measurements.
- To develop a sensor system that integrates the sensor unit algorithm and detection algorithm. The detection algorithm uses a correlation coefficient calculation, thresholds and a set of rules. The correlation coefficient is

calculated between the angle measurement from the sensor unit and a sample window selected from one data set.

- To evaluate heel strike and tibial vertical events detected in five healthy subjects using the sensor system as compared to footswitch output. The system is reliable if all the events are detected as compared to the footswitch. The tibial vertical event is detected based on 13% of gait cycle before initial contact detected by the footswitch. The tibial vertical event is anticipated to be detected close to 13% or 15% of gait cycle before initial heel contact and would have a small variability.
- To detect tibial vertical events in six neurological patients using the sensor system as compared to footswitch output. The variability of the events detected in patients is anticipated to be more variable than the healthy subjects due to slightly prolonged swing phase in the patients. Also, it is anticipated that the time of the events detected would be different from the healthy subjects.

1.4 Ethics

The study involved five normal subjects and seven impaired subjects. All five normal subjects were recruited from the staff of the Department of Clinical Science and Engineering, Salisbury District Hospital while all seven impaired subjects were the patients using the two channel FES undergoing treatment at Salisbury. All trials were carried out in the gait laboratory. The study was granted ethical approval by the Wiltshire Research Ethics Committee (REF reference number: 08/H0104/77) and the participants gave informed consent.

1.5 Published Papers

Chappell, P. H., Abdul Malik, N., Lane, R. P. and Wood, D. E. 2007. *Determination of angles between segments using accelerometers in a gravitational field.* United Kingdom patent application 0721839.9. 7 November 2007.

Abdul Malik, N., Chappell, P. H., Wood, D. E. and Taylor, P. N. (2008) Measurement of the relative joint angle and acceleration of the lower limb during walking IN:13th Annual Conference of International FES Society Freiburg, Germany.

Chappell, P. H., Abdul Malik, N., Lane, R. P. and Wood, D. E. 2010. *Accelerometer assembly and the use thereof.* United Kingdom patent application PCT/GB2010/000990. 19 May 2010.

Abdul Malik, N., Chappell, P. H., Wood, D. E. and Taylor, P. N. (2010) Event detection for gluteal or hamstring stimulation during walking in neurological patients IN:10th Vienna International Workshop on Functional Electrical Stimulation and 15th IFES Annual Conference, Vienna, Austria.

1.6 Thesis Outline

The overall structure of the study takes the form of eleven chapters, including this introductory chapter. The next chapter, Chapter 2 briefly describes spasticity and paralysis that causes the abnormal gaits, followed by examples of neurological disorders such as stroke, multiple sclerosis and spinal cord injury. A brief introduction of functional electrical stimulation system is also presented.

Chapter 3 describes the events of a gait cycle and the timing of muscle activity with relations to the gait cycle followed by a review of sensors and methods used to detect gait events/phases for FES. The next part of the chapter describes the sensors used for kinematic measurement.

Chapter 4 explains the theory of the algorithm used in the study to develop the sensor unit for angle and acceleration calculation. The derivation of the equations for the sensor unit algorithm is also presented.

Chapter 5 provides the experimental methods and results to verify the sensor unit algorithm for both static and the dynamic conditions. The verification of the angle measurement error is also presented. This chapter also includes some experiments to demonstrate the kinematic measurement of a normal subject during walking and a leg swings while seated.

Chapter 6 provides the experimental procedures and results of the assessment of the lower limb segments angles during walking in five healthy subjects using the sensor unit and compared with measurement from the Vicon™.

Chapter 7 describes the events detection algorithm. The processes involved in the algorithm are detailed in the chapter. This includes the selection of the sample window, the correlation coefficient calculation and the sets of rules used in the algorithm.

Chapter 8 provides the experimental procedures and results of the evaluation of the heel strike event detection in five healthy subjects with a footswitch as the reference measurement.

Chapter 9 provides the experimental procedures and results of the evaluation of the tibial vertical event detection in five healthy subjects with a footswitch as the reference measurement.

Chapter 10 provides the experimental procedures and results of the detection of tibial vertical event in neurological patients with footswitches as the reference measurement.

Finally in Chapter 11, the final conclusions of the research carried out and the future work are presented.

Chapter 2
Neurological Disorders

2.1 Introduction

This chapter briefly described the neurological disorders affecting patients in this study that include cerebrovascular accident (CVA), spinal cord injury (SCI) and multiple sclerosis (MS). These disorder causes muscle paralysis as reflected by the abnormal gait and dropped foot is the most common abnormal gait accounted in these patients. As a result, the patients were not able to lift their foot during the swing phase of their walking. In order to restore this muscle function, the tibialis anterior or peroneal nerve is stimulated using the functional electrical stimulation. The functional electrical stimulation is one of the options of functional therapy. It helps to restore muscle function in these patients to enable them to walk with less effort and energy. As described in literature by Kottink et al. (2004), Robbins et al. (2006), Carnstam et al. (1977), Swain et al. (2000) and Swain et al. (2003), Durham et al. (2004), neurological patients using FES showed improvement in their gait. Stimulation of other muscles groups such as gluteals or hamstrings can further improve the gait of neurological patients (Wright et al. (1999) and Wilkinson and Taylor (2004)).

2.2 Motor System

The human nervous system is divided into two parts: the central and the peripheral nervous systems as shown in Figure 2-1. The central nervous system (CNS) consists of the brain and the spinal cord. It plays an important role in coordinating all parts of the

body activities including the control of voluntary movement. The branching nerves that supply the arms, legs and other part of the body is the peripheral nervous system (PNS).

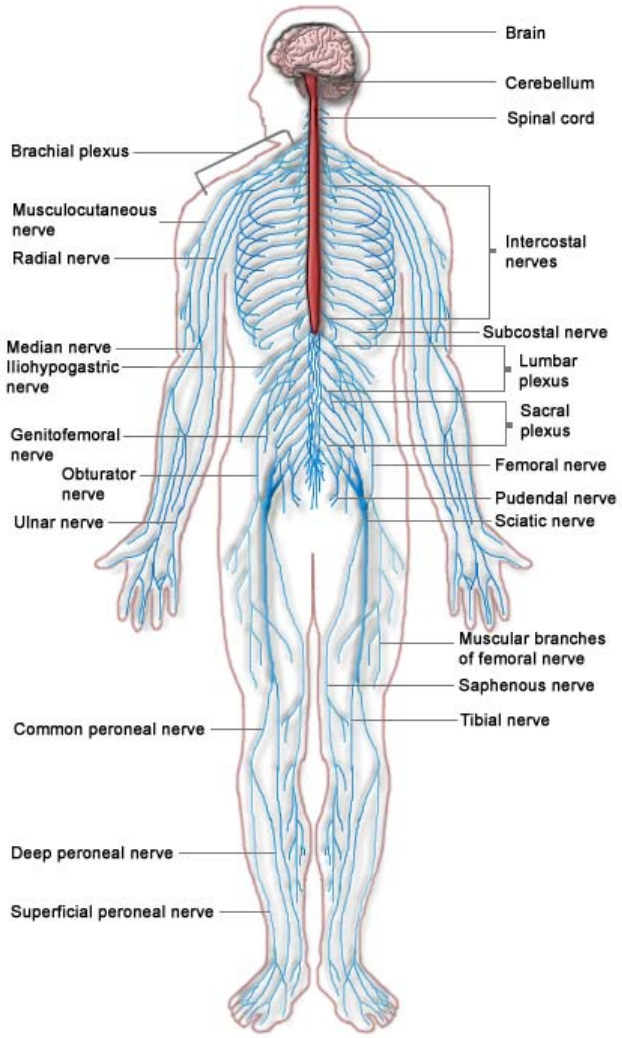

Figure 2-1 Central and peripheral nervous system, red=central nervous system and blue=peripheral nervous system (Persian Poet Gal (2006)).

The motor system is part of central nervous system that is involved with movement. The motor pathway (pyramidal tract or corticospinal tract) starts in the motor center of the cerebral cortex (Figure 2-2). Fibres from the cerebral cortex come close together in the internal capsule which passes close to the thalamus and basal ganglia and then descend the brain stem. These are the upper motor neurones of the corticospinal tract.

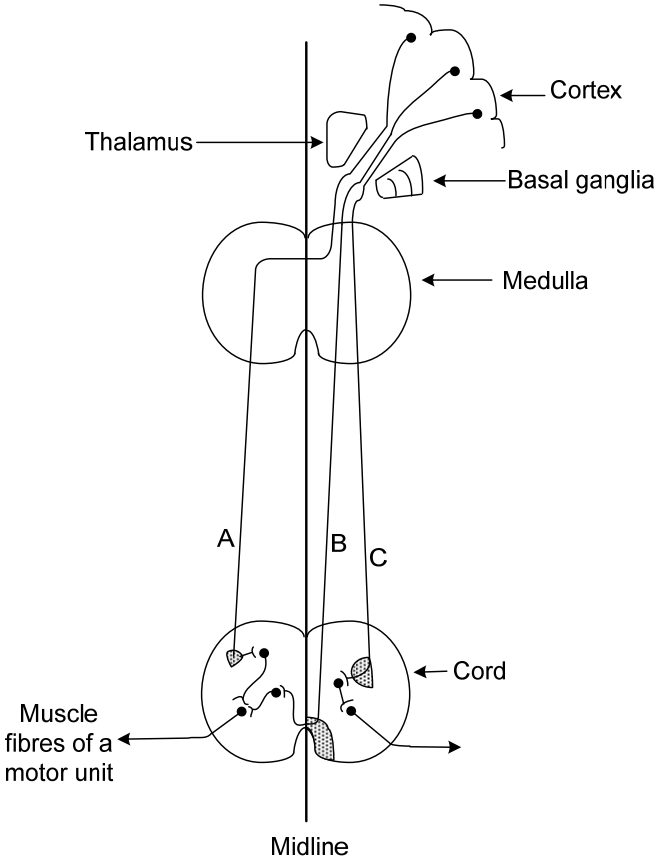

Figure 2-2 Motor system adapted from (Burton (1997)).

In Figure 2-2,

(A) In the lower medulla, the majority of fibres decussate (pass to the opposite side) and descend in the lateral corticospinal (crossed pyramidal) tracts.

(B) Some fibres do not decussate, but descend in the anterior corticospinal tract to supply muscles in the neck.

(C) A few fibres descend directly in the lateral corticospinal tract with the crossed fibres from the contralateral cortex.

Most muscle fibres relay information to the neurones in the anterior horn cells of the grey matter of spinal cord and their fibres to form a final common pathway that is also called a motor unit. (Figure 2-3). This is where the lower motor neurones are located.

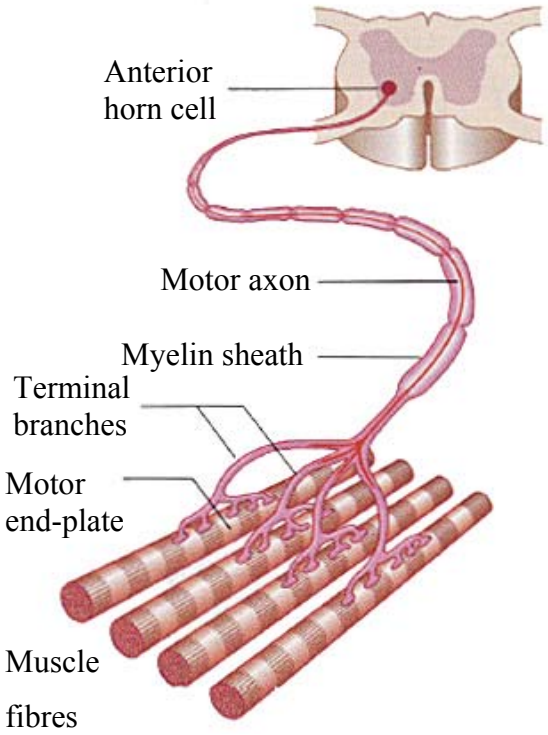

Figure 2-3 Motor unit (Davidson et al. (1995)).

The motor impulses are transmitted from the anterior horn to the voluntary muscles by the somatic motor neurones which resulted in the stimulation of the muscle fibres it supplied. These processes will initiate contraction. Movements are then achieved by contraction and relaxation of these skeletal muscles.

2.3 Paralysis and Spasticity

Injury to the pyramidal tract will result in upper motor neurone syndrome while injury to the motor unit will cause lower motor neurone syndrome. Examples of diseases or injury that result in upper motor neurone syndrome are stroke, multiple sclerosis and spinal cord injury. This syndrome is characterised by 'spastic paralysis' as contrast to lower motor neurone syndrome that shows signs of 'flaccid paralysis'.

Paralysis is loss of strength in affected limb or muscle group that results from dysfunction at any point in the motor system and it can be partial or complete (Newsom-Davis (2010)). The level at which the dysfunction occurs will determine the pattern of paralysis. Damage to the pyramidal tract above the decussate level causes

paralysis on the contralateral side of the body whereas damage to the pyramidal tract below the medulla causes ipsilateral weakness. If the lesion is in the cortex, weakness may be limited to one limb or part of it. Damage at the site where the fibres are closely compacted (internal capsule) may result in weakness of the whole of one side of the body (hemiparesis).

Spasticity is characterized by loss of voluntary movements, increased muscle tone (spasticity or clasped knife rigidity), increased tendon reflexes and clonus and exhibit extensor plantar response. The extensors are weaker than the flexors in the arm, but the reverse is true in the legs, thus resulting in the 'spastic' posture. There will be little or no muscular wasting (Davidson et al. (1995)).

Paralysis and spasticity leads to abnormal gait in the neurological patients. "Walking abnormalities are unusual and uncontrollable walk patterns, usually caused by disease or injuries to the legs, feet, brain, spine or inner ear" (Dugdale et al. (2009)). Some examples of walking abnormalities are propulsive, scissors, spastic, steppage and waddling gait. Table 2-1 presents some examples of walking abnormalities and the characteristics of the walking.

Table 2-1 The abnormal gaits and the characteristics (Dugdale et al. (2009)).

Abnormal gait	**Characteristics**
Propulsive gait	A stooped, rigid posture with the head and neck bent forward
Scissors gait	Legs flexed slightly at the hips and knees, giving the appearance of crouching, with the knees and thighs hitting or crossing in a scissors like movement
Spastic gait	A stiff, foot dragging walk caused by one-sided, long-term, muscle contraction
Steppage gait	Foot drop where the foot hangs with the toes pointing down, causing the toes to scrape the ground while walking
Waddling gait	A distinctive duck-like walk that may appear in childhood or later in life

The scissors, spastic and steppage gait are the abnormal gaits that associated with damage to the nervous system or muscles or combination of these. Dropped foot is the most common abnormal gait in neurological patients and it is characterised by the steppage gait. The other abnormal gaits associated with the spasticity and paralysis are the abnormal hip rotation, excessive knee extension or flexion and abnormal foot contact or rotation.

2.4 FES as a Functional Therapy for Walking

FES is a therapy to restore muscle function of the paralysed limb in neurological patients. In hemiplegic patients, the stimulation of the common peroneal nerve has successfully increased the speed of walking and reduced the effort of walking (Burridge (1997)). Similar improvements are also reported for stroke or multiple sclerosis patients especially when they walk on an uneven surface (Burridge et al. (2007)).

FES is the process of electrically stimulating nerves or muscles to react as though they are receiving impulses from the brain and as the result the muscles are contracted and the function is restored. The electrical stimulation system consists of a stimulator that generates electrical current pulses to the nerves of the paralysed muscle via surface or implanted electrodes as in Figure 2-4.

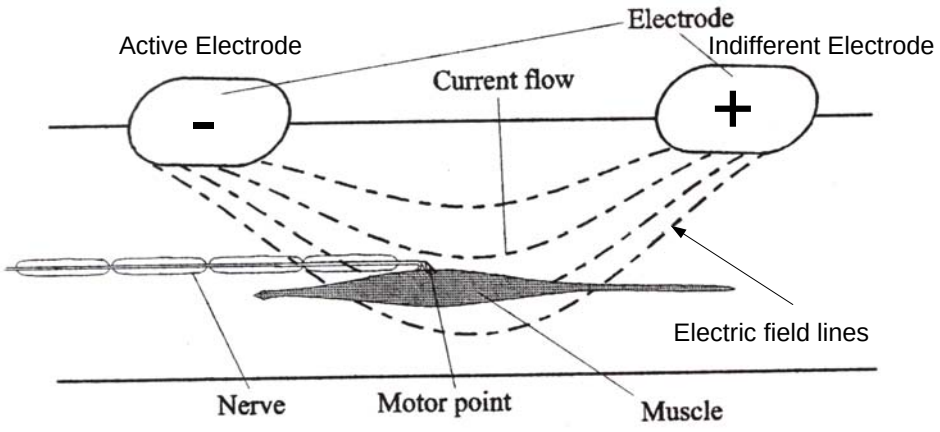

Figure 2-4 Electrical current pulses to the nerves of paralysed muscle (Kennaugh (2007)).

2.4.1 FES System

A typical FES system consists of three main components: sensor, stimulator with controller and electrodes. The basic operation of the FES system is shown in Figure 2-5. The sensor is used to detect events/phases (for example heel rise and heel strike) during the gait and triggers the stimulator. In a closed loop system, as well as to trigger the stimulator, the sensor is used to measure quantities of motion such as joint angle and foot contact pressure. These measurements are then used as a feedback to the stimulator controller to enable it to modify the stimulation parameters in the next cycle of the gait. The foot switch is the sensor of choice in a FES system and is used in most of the stimulators either single or two channel, detecting gait events like heel strike and heel rise during locomotion. However, there are some limitations/disadvantages of the footswitch reported such as no potential for implant (Willemsen et al. (1990a) and Mansfield and Lyons (2003)), lack of reliability with tendency to detect small forces exerted during swing (Mansfield and Lyons (2003)), unable to use for barefoot walk and may have a different function with different terrain or types of shoes (Dai et al. (1996)). Due to these limitations/disadvantages, several studies (Willemsen et al. (1990a), Catalfamo et al. (2010) and Dai et al. (1996)) have proposed sensors such as accelerometer(s), gyroscope(s) and tilt to replace the footswitch.

The stimulator generates voltage pulses and hence current flows in the load to depolarise nerves that results in muscle contraction. For drop foot correction, the peroneal nerve stimulation is on during swing phase and off during stance phase.

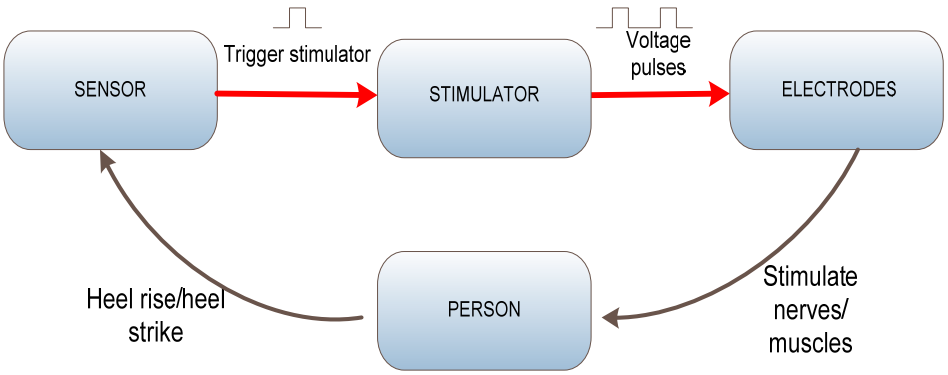

Figure 2-5 Functional block diagram of FES system.

Currently, there are two types of electrodes used, namely surface electrodes and implanted electrodes. Surface electrodes are usually attached to the skin daily and can be used with a conductive gel to reduce the electrical resistance. The electrodes contain a flexible material, such as rubber and conductive materials. The other type, the implanted electrodes are made of platinum or stainless steel foil used with the implanted drop foot stimulator (Stimustep, Odstock Medical Limited and Actigait®, Neurodan A/S). This type of electrode is permanently fixed to the nerves therefore no daily placement is needed. It also helps to reduce the sensation of the stimulation since it requires a lower stimulation current. The problem with this type of electrode is that the person needs to undergo surgery to place the electrode or replace them when necessary. Also, it is more expensive to produce, compared to a surface electrode system. However, the similar functional benefits in walking can be obtained with either system.

Figure 2-6 shows the Odstock Dropped Foot Stimulator (ODFS III) manufactured by Odstock Medical Limited at Salisbury District Hospital in the UK. Table 2-2 shows the stimulation parameters for the ODFSIII (Taylor (2004b)). The ODFSIII has been replaced with a digital stimulator, the ODFS® Pace. Table 2-3 shows several commercially available stimulators for gait correction and the sensors used to trigger the stimulators.

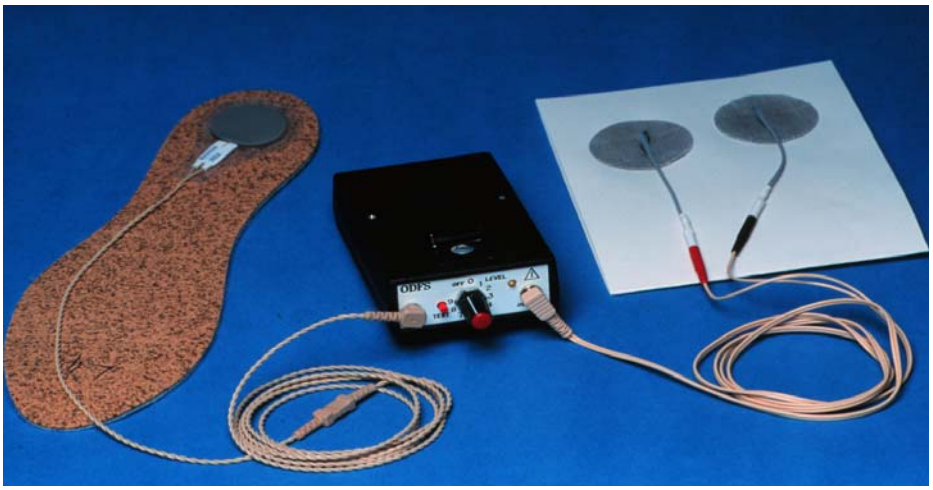

Figure 2-6 From left: foot switch, ODFS III stimulator and surface electrodes.

Table 2-2 Specification for ODFSIII.

Pulse width	3-350μs
Output current	20-100mA
Output voltage	100V into 1kΩ
Rising ramp	0-2s
Stimulation frequency	40Hz
Stimulation time	0.5-6s
Extension	0-1.5s
Descending ramp	0-2s

Table 2-3 The commercially available stimulators for gait correction.

Stimulator	Number of Channel(s)	Sensor Used	Company or Manufacturer
ODFSIII/ O2CHS (Odstock Medical Limited (2008))	Single/Two Channel(s)	Footswitch(es)	Odstock Medical Limited, UK
WalkAide (Innovative Neurotronics (2006))	Single Channel	Tilt Sensor	Innovative Neurotronics, Canada
Parastep (Sigmedics (2000))	Four/Six Channels	Hand-controlled switch	Sigmedic Inc., USA
Mikrofes (Ru"zi"c (1996))	Single Channel	Footswitch	Gorenja, Slovenia
ActiGait (Neurodan A/S (2008))	Four Channels	Wireless Heelswitch	Neurodan A/S, Denmark
NESS L300 (Bioness Inc. (2010))	Single Channel	Wireless Heelswitch (Intelli Sense Gait Sensor™)	Bioness Inc., USA
STIMuSTEP (Finetech Medical (2008))	Implanted Single Channel	Footswitch	Finetech Medical Ltd., UK

2.4.2 FES Profiles

A stimulation profile is the pattern of electrical current pulses that has been generated from the stimulator during the stimulation process. Typically the stimulation frequency is constant. Either the pulse width or the pulse amplitude may be varied to increase or decrease the stimulation. A typical approach is to hold the amplitude constant and vary the pulse width. The first electrical stimulation profile has a rectangular shape proposed by Liberson et al. (1961) (Figure 2-7 solid line). The stimulation profile indicates that the stimulation is on during swing and off during stance for dropped foot correction during gait.

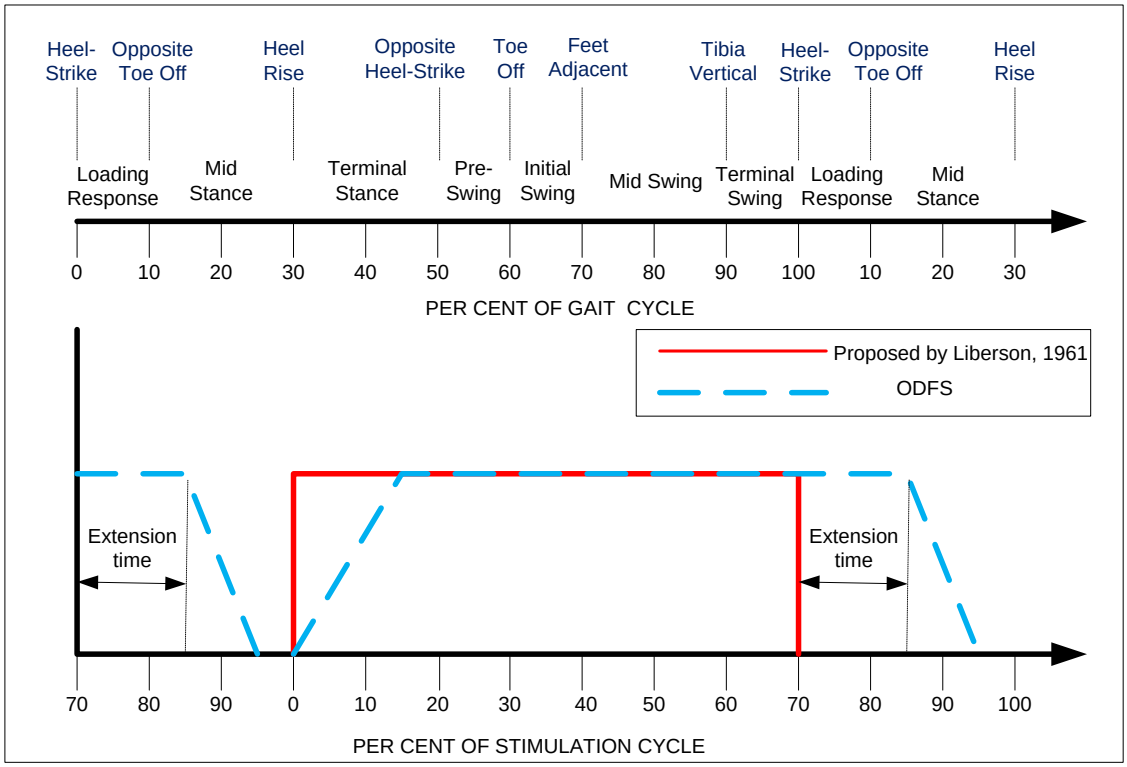

Figure 2-7 Liberson's original rectangular stimulation profile and contemporary trapezoidal stimulation profile.

After a few decades, the stimulation profile pattern has been changed into a trapezoidal shape (Figure 2-7 dashed line), that improved the loading response and helps to avoid the incident of foot-slap during gait (Taylor (2004b)). The stimulation profile is used in the commercial stimulator, the ODFS. This stimulation intensity ramps up at heel rise and maintained constant throughout the swing phase. Next, it continues with the

extension time of stimulation after heel strike before ramps down. The rising edge ramp helps to reduce the stretch reflex in the calf muscle.

O'Halloran et al. (2004) have investigated a different pattern of stimulation profile to improve the gait of a dropped foot patient. One of the tested stimulation profiles is as shown in Figure 2-8. The stimulation profile has a second ramp up prior to heel strike which is about 10 percent of the gait cycle and the intensity level is maintained after heel strike before ramp down. In the investigation, it has been proved that by increasing stimulation intensity prior to heel strike and maintaining the intensity level during the loading response results in a better effect on heel rocker and the trajectory of ankle angle becomes closer to normal gait. This extra activity allowed the tibialis anterior muscle to lower the foot to the ground after heel strike.

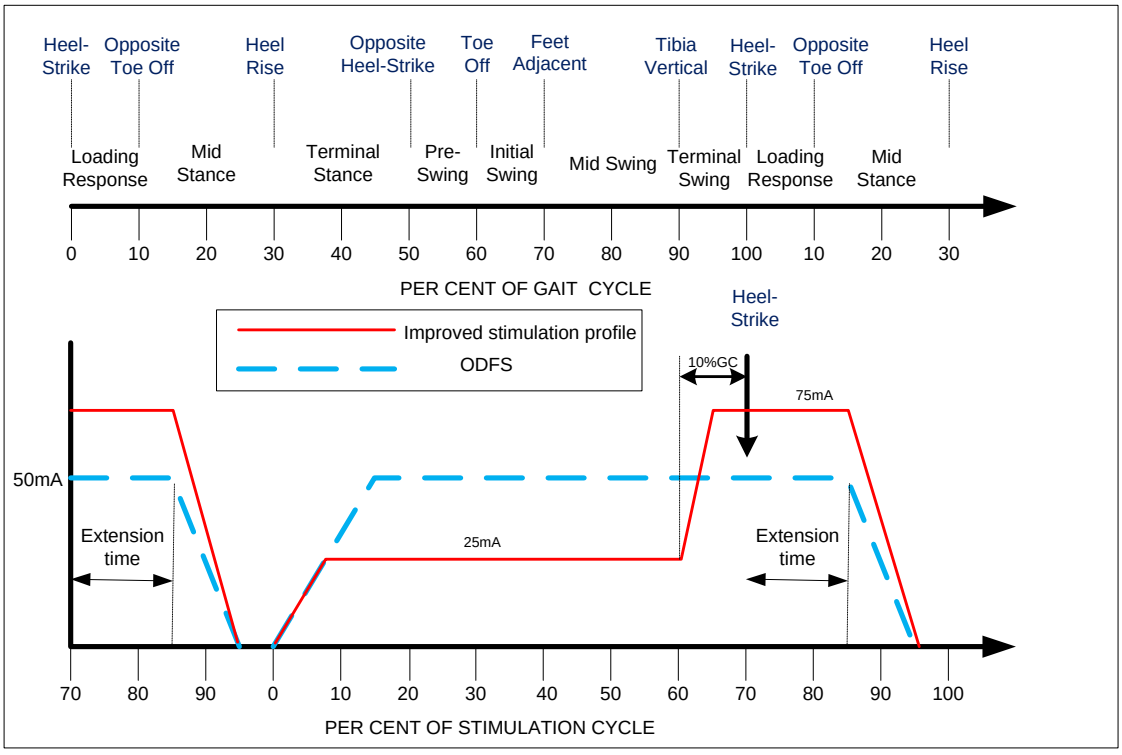

Figure 2-8 Stimulation profile with increased stimulation intensity prior to heel strike proposed by O'Halloran et al. (2004).

Normally for dropped foot correction, the frequency of stimulation of the tibialis anterior muscle is constant. However, in order to improve the gait of the dropped foot patient with a greater torque at the ankle, different stimulation profiles could be applied

(Hart et al. (2006)). For example, doublets of pulses may provide an increased torque that follows the natural activity of the muscle. The simple and rectangular profile of Liberson et al. (1961) has been added to and improved with functional shaping possible in the future. However such profiles will require good detection of gait cycle events using sensors.

2.5 Potential Users of the Odstock Dropped Foot Stimulator (ODFS) (Taylor (2011))

2.5.1 Stroke

It is estimated that about 120,000 people suffer from stroke each year in UK (National Institute for Health Research (2011)). One third of these patients succumb to this disease, another one third recovered and the rest were left with disability. Of those with disability, half may possibly be ODFS users (20,000) and this makes up about 47.4% of all ODFS users in Salisbury. However, not many patients over 75 years use an ODFS, even though strokes occurring in this group of patients constitute about 62.4% and 68.0% of the total for men and women, respectively. Stroke occurrence per year according to age for men and women in UK are presented in Table 2-4 and Table 2-5 respectively. Estimation of ODFS users in Salisbury was also included in the tables.

Table 2-4 Stroke occurrences per year and total population for UK men.

Age	% of all strokes*	Total number Per year	ODFS users	Average Life (years)	Total number in population
15 - 24	0.2%	120	20	55	1,100
25 - 44	0.3%	180	30	45	1,350
45 - 64	7.8%	4,680	780	20	15,600
65 - 74	29.3%	17,580	2930	5	14,650
75 +	62.4%	37,440	†6240	-	-
Totals		60,000	3,760	-	32,700

*Bases on data from (McCormick (2011)), † not calculated in total

Table 2-5 Stroke occurrences per year and total population for UK women.

Age	% of all strokes*	Total number Per year	ODFS users	Average Life (years)	Total number in population
15 - 24	0.3%	180	30	55	1,650
25 - 44	0.5%	300	50	45	2,250
45 - 64	6.3%	3,780	630	20	12,600
65 - 74	24.0%	14,440	2406	5	12,000
75 +	68.8%	41,300	†6883	-	-
Totals	-	60,000	3,116	-	28,500

*Based on data from (McCormick (2011)), † not calculated in total

Stroke results from the interruption of blood flow to part of the brain due to either infarction or haemorrhage (Davidson et al. (1995)). Infarction happens when thrombosis (blood clots) block the artery supplying the brain therefore causing impaired oxygen supply to the brain. Haemorrhage, or bleeding occurs when blood vessels break either from trauma or excess internal pressure. Lack of oxygen supply to brain cells as well as pressure from fluid accumulation leads to cell death and results in cerebral dysfunction. The majority of patients will present with hemiparesis, dysphasia (if the dominant hemisphere is involved), and hemianaesthesia. Contralateral muscle weakness is common but reduced strength on the ipsilateral side of the lesion has also been documented (Sunnerhagen et al. (1999)). The exact combination of these signs depends on the area of cerebral cortex involved.

2.5.2 Multiple Sclerosis

Multiple sclerosis affects approximately 80,000 people in UK each year (Sawcer (1997)). It is one of the commonest neurological causes of long-term disability. The cause of the disease remains unknown (Davidson et al. (1995)). In these patients, the nerves of the central nervous system (brain and spinal cord) degenerate. Inflammation that occurs leads to demyelination or causes myelin to disappear. Myelin is a nerve sheath that improves the conduction of impulses along the nerves and also important in

maintaining the health of the nerves. The electrical impulses that travel along the nerves decelerate as a consequence of demyelination process. In addition, the nerves themselves are damage. As more and more nerves are damage, there will be progressive interference of nervous system function including the motor system.

Common presentation in multiple sclerosis includes weakness or loss of control of one or more limbs, visual symptoms and sensory symptoms. Patient may present with spastic paralysis which may be only slowly progressive. The physical signs will depend on the localisation of areas of demyelination.

In Salisbury, multiple sclerosis makes up 20.7% of FES users. The number of patients who have dropped foot or who could benefit from using the ODFS is not known. However, 31.0% of MS patients have (Expanded Disability Status Scale) EDSS scores of between 4 and 7 and it is this group who have effected walking but are still mobile (Jacobs et al. (1999)). Dropped foot will be the most significant gait deficit and approximately half of these patients may be suitable for FES that is about 12,400 patients.

2.5.3 Incomplete Spinal Cord injury

SCI affects 17 people per 100,000 of the population per year in the UK (Neurological Alliance (2003)). Approximately 10% of SCI patients could be ODFS users and this would be about 100 patients per year in the UK. It predominantly occurs in male and young age group in which more than half of these injuries are due to mechanical trauma (Winter and Pattani (2008)). Injury to the spinal cord could be either due to trauma or space occupying lesion that compresses on spinal cord or interfering with the blood supply (Davidson et al. (1995)). Patients with cord compression that is due to space occupying lesions for example tumours may present with progressive weakness and sensory loss. Sphincter disturbances occur at a late stage. Patients will normally demonstrate lower motor neurone signs at level of compression and spasticity below the level.

2.5.4 Other Groups

Cerebral palsy makes up about 3.4% of FES users in Salisbury. However, this area of use is underdeveloped and it is not yet known of how many people may benefit from using this ODFS. This unknown benefit also applies to cases such as head injury and Parkinson syndrome.

About 11% of FES users in Salisbury are grouped as others in the database which includes cases of upper motor neurone lesions due to various or uncertain diagnoses and hereditary spastic paraparesis. Hereditary spastic paraparesis shows an increasing trend. About 10% of people do not have a diagnosis recorded.

2.6 Conclusions

Functional electrical stimulation (FES) helps to restore muscle function to improve gait in neurological patients. As a result, less effort is needed to walk and the speed of walking is increased. The Odstock Dropped Foot Stimulator (ODFS) in Salisbury is one of the commercially available single channel electrical stimulation devices. From the database (Taylor, 2011)), the total ODFS users is about (42,194) and the percentages of ODFS users in Salisbury are 47.4% of stroke, 20.7% of MS, 7% of SCI, 3.4% of CP, 11% of various or uncertain diagnoses and about 10% of no diagnosis. The potential Odstock Two Channel Stimulator (O2CHS II) users are assumed to be one fifth of the ODFS users (about 8,439 people) (Taylor, 2011)). These are the users that would benefit from the study, where a sensor system will be developed to detect the tibial vertical event. The sensor system would ensure the hamstrings or gluteals muscles are stimulated about the right time for correction of other abnormal gaits such as knee hyperextension into early stance or excessive hip flexion/adduction at heel strike.

Chapter 3

Sensors for Gait Events Detection

3.1 Introduction

In the study, two major gait events will be investigated that are the heel strike and when the tibial is vertical. The main focus is to detect the tibial vertical event, replace the footswitch and trigger a stimulator for patients having specific gait abnormalities such as knee hyperextension into early stance or excessive hip flexion/adduction at heel strike to further improve their gait. The right timing is needed to stimulate muscles such as the hamstrings or gluteals which follow the normal muscle activity as described in section 1.2 (Chapter 1, p3). A controller will need to synchronise to an event in the gait cycle so as to trigger the stimulator. From normal data this event occurs when the tibia is vertical. In the study, the calculation of the tibial vertical event is based on 13% of the gait cycle before initial contact/heel strike detected by a footswitch. Therefore, the heel strike event is another event to be detected and evaluated. The footswitch used in the study has an accuracy of -7 ms ± 19 ms when compared to force plate measurements in the detection of heel contact (Findlow et al. 2004).

In the literature, the tibial vertical event has been detected using images from cameras in healthy subjects by Sousa et al. (2007a, 2007b) while using a tilt sensor attached to the shank in healthy subjects and patients by Park et al. (2007). However, none of the studies have reported on the accuracy of the tibial vertical event detection. This chapter reviews the sensors proposed by other researchers to detect events/phases during gait with the aim of finding an appropriate sensor to detect the specific event to control the

timing of FES. At the end of the chapter, the sensors reviewed are compared to make an informed choice for the sensor to be used in the study.

3.2 Events/Phases of a Gait Cycle

"A gait cycle is defined as the time interval between two successive occurrences of one of the repetitive events of walking" (Whittle (2007)). It is divided into two phases known as stance and swing. These phases are subdivided into seven periods of the gait cycle with four in the stance phase (for weight acceptance and single limb support) and three in the swing phase (for limb advancement) (Perry (1992)). A study of gait maturation by Kaufman and Sutherland (2006) have showed that the temporal/distance parameters reached a plateau by the age of 20 years and remained unchanged throughout most of adult life. These parameters include the velocity, cadence, stride length and percentage of gait cycle for opposite toe-off, duration of stance and swing. For the stance phase, the duration is between 60-61% and for swing phase, the duration is between 39-41% (Kaufman and Sutherland (2006)). The percentage of gait cycle for opposite toe off is between 9%-11% (Kaufman and Sutherland (2006)) and for toe off is between 58%-63% (Winter and Yack (1987)). In the study, patients and healthy subjects are more than 20 years old so their gait parameters have stabilized. Moreover, the trials were conducted at normal speed for both healthy subjects and patients. Therefore a comparison with the normal data is considered to be acceptable. The subdivided periods with percent of gait cycle in the stance phase and swing phase are presented in Table 3-1.

There are seven major events that occur during the gait cycle and they are described in Figure 3-1. The two phases: stance and swing; and the seven subdivided phases are shown in the same figure. In the figure, the right foot (yellow colour) is used to define the gait cycle in which the cycle begins with initial contact of the right foot until it touches the ground again.

Table 3-1 The subdivided periods with percent of gait cycle in the stance phase and swing phase in normal gait (the mean data of normal subjects walking with natural cadence).

Period	% Gait Cycle (Perry (1992))	% Gait Cycle (Kaufman and Sutherland (2006))
Loading response	0-10	0-12
Mid-stance	10-30	12-50
Terminal stance	30-50	
Pre-swing	50-60	50-62
Initial swing	60-73	62-75
Mid swing	73-87	75-85
Terminal swing	87-100	85-100

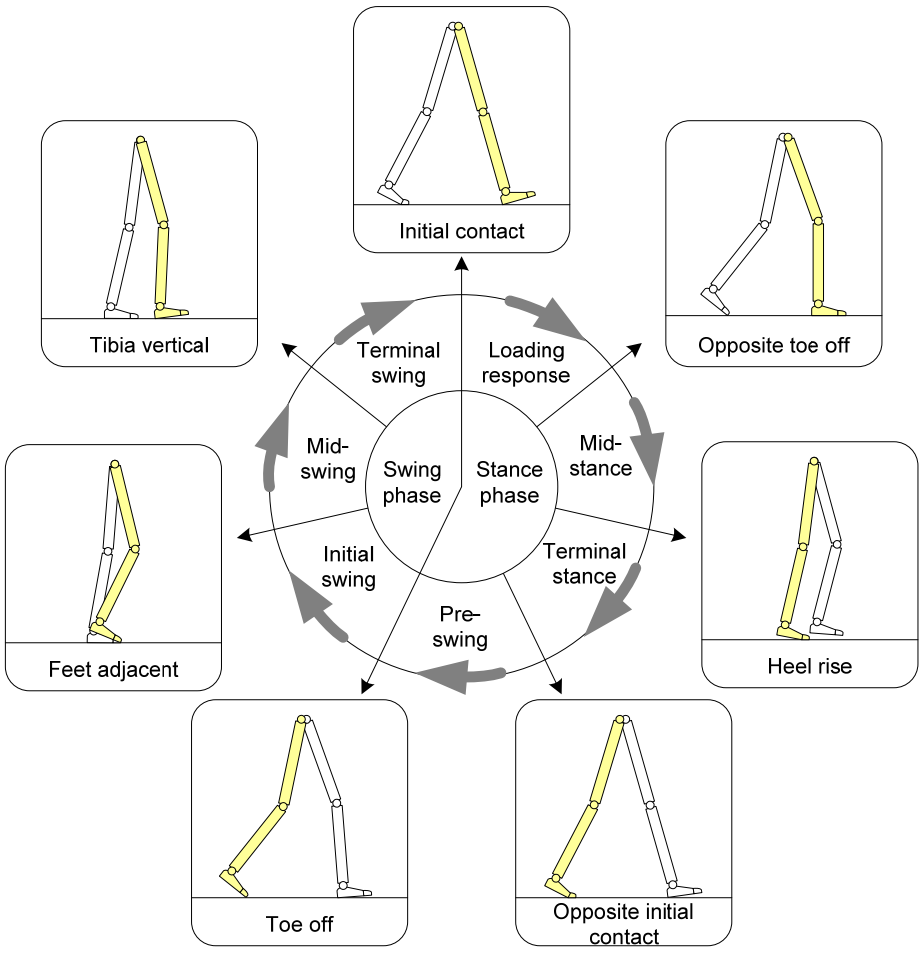

Figure 3-1 Major events during single gait cycle (Right foot defines the gait cycle, begins with initial contact) adapted from (Whittle (2007)).

The diagram that has been used in Figure 3-1 is the standard way of describing the phases in a single gait cycle. Sometimes, different researchers use a different way of describing the gait cycle in their research study. For example, Skelly and Chizeck (2001) subdivided the stance phase into weight acceptance, mid stance and terminal stance; and the swing phase into early swing and late swing. The subdivided phases are divided into five events: foot flat, heel off, toe off, max knee flexion and heel strike. Williamson and Andrews (2000) divide the gait cycle into five phases, namely the loading response, mid-stance, terminal stance, pre swing and swing to be used in their gait events detector.

3.2.1 Timing of Muscle Activity during Gait Cycle (Perry (1992), Boakes and Rab (2006))

In order to produce normal walking, muscles must contract and relax in timely and organized pattern. These muscles have their own role in producing normal walking activity as defined by phasic contraction. Out of phasic muscle contraction will lead to abnormal movement.

Figure 3-2 shows the extensor muscles sequence for stance in normal subjects. Extensor muscle of the limb plays a crucial role during stance phases of gait by producing weight bearing stability, shock absorption and progression over the supporting foot.

Initial contact involves the ankle to be in neutral dorsiflexion, the knee extended and the hip flexed in approximately 30^0. This action will decelerate the body. Action of the hip flexion is made to happen by contraction of the extensor muscles group that is, the hamstrings and single joint muscles (gluteus maximus and adductor magnus). Quadriceps action at the knee is minimal at the time of initial contact. Concurrent activity of the hamstring will prevent hyperextension of the knee. At the same time, tibialis anterior muscle contraction will ensure neutral dorsiflexion of the ankle and prevent it from slapping down on the floor.

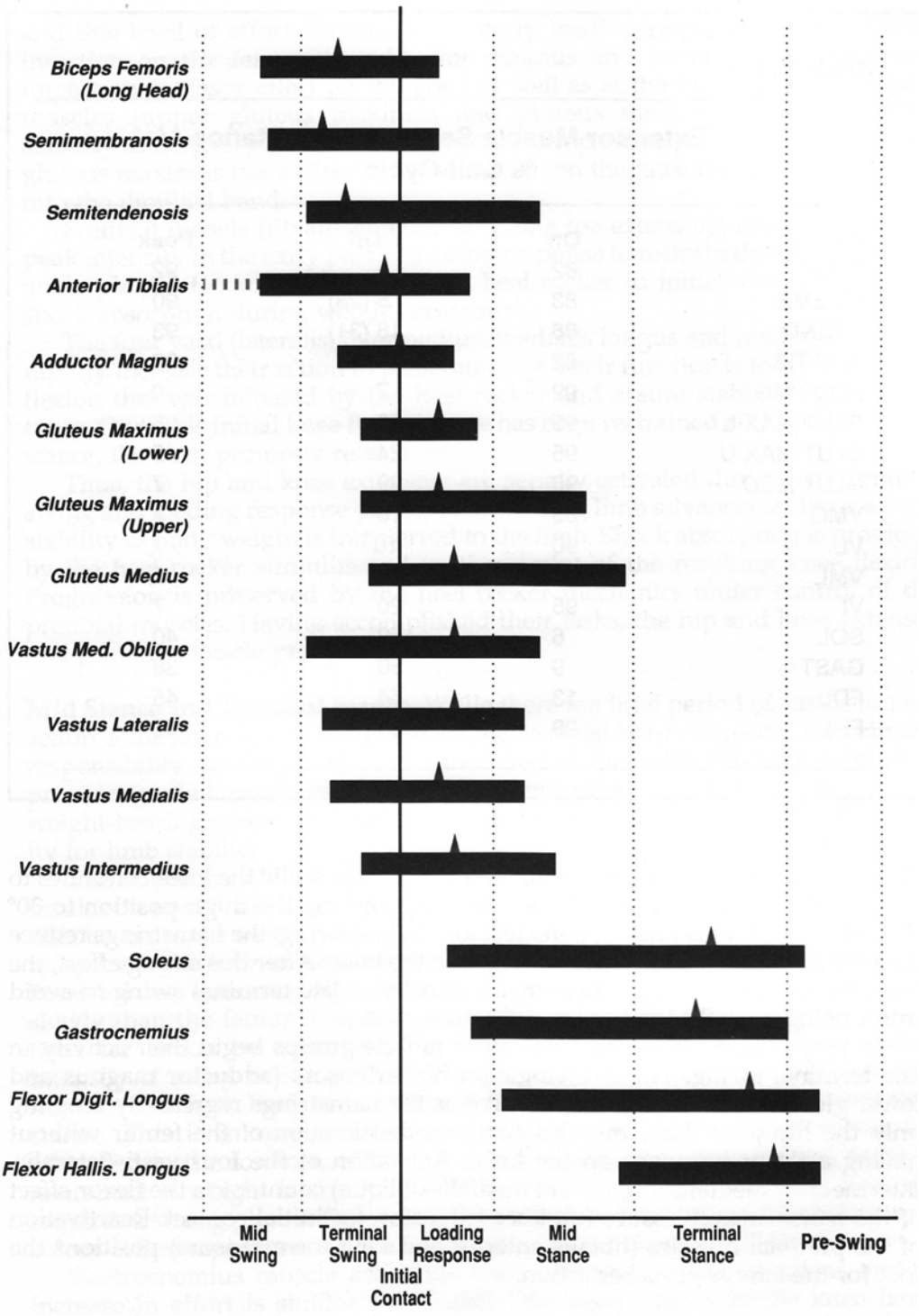

Figure 3-2 Normal extensor muscles activity sequence for stance and the relationship with gait events (the mean data of normal subjects walking with natural cadence) (Perry (1992)).

Early **loading response** happens when the limb accepts the weight of the body by rapidly increasing the contraction of the knee extensors (vasti). The four vasti that are involved are the lateralis, intermedius, medialis longus and medialis oblique muscles.

This process is aided by the action of ankle plantar flexors (eccentric contraction) which result in plantar flexion of the ankle. Simultaneously, the actions of single joint hip extensors rapidly increase. The gluteus medius and upper gluteus maximus (hip abductor) will then contract isometrically and stabilizes the pelvis in response to contralateral drop of the pelvis.

During **midstance**, the mechanical goals are to produce knee stabilization and momentum preservation. The muscles involved are the gastrocnemius and soleus muscles. Soleus muscle contraction happens first and results in ankle plantar flexion to ensure limb stability during weight-bearing period. This action rapidly increases and peaks near the end of **terminal stance** to serve the purpose of acceleration of the body forward. Passive knee extension continues and also assists in hip extension with no action of both knee and hip extensors. Gastrocnemius muscle contraction happens after soleus and its activity is similar to soleus muscle. Lastly, the toe flexors (flexor digitorum longus and flexor hallucis) also help in the support of the forefoot.

The important muscle group that is involved in **preswing** is the hip flexors. There will be no activity of the ankle plantar flexors and the hip flexors (iliopsoas and rectus femoris) will start to lift the limb and swing it forward. This action starts as the opposite limb is in contact with the floor and about to start the loading response.

Figure 3-3 shows the flexor muscles sequence for swing in normal subjects. During the **initial swing** phase, the activity of iliopsoas and rectus femoris muscles started to cease. The activity of sartorius, iliacus and gracilis muscles take place and help to swing the lower limb. The foot is now prepared to clear off ground with the action of ankle dorsiflexors (anterior tibialis, extensor hallucis, extensor digitorum longus) and adequate knee flexion for toe clearance by biceps femoris activity.

The activity of ankle dorsiflexion by anterior tibialis muscle continues in **midswing** phase and reaches a peak. The activity of gracilis muscle also continues.

The mechanical goals of **terminal swing** are to decelerate shank and body, foot positioning and to prepare for contact. Deceleration is achieved by contraction of the hamstrings (semimembranosus, semitendinosus, biceps femoris long head)

eccentrically or isometrically. As a result, both hip flexion and knee extension activities decrease progressively. The hip extensors (adductor magnus and lower gluteus maximus) become active as the activity of hamstrings decreased. In addition, the anterior tibialis muscle contraction is activated to prepare for foot contact. The cycle then repeats as the initial contact event is initiated.

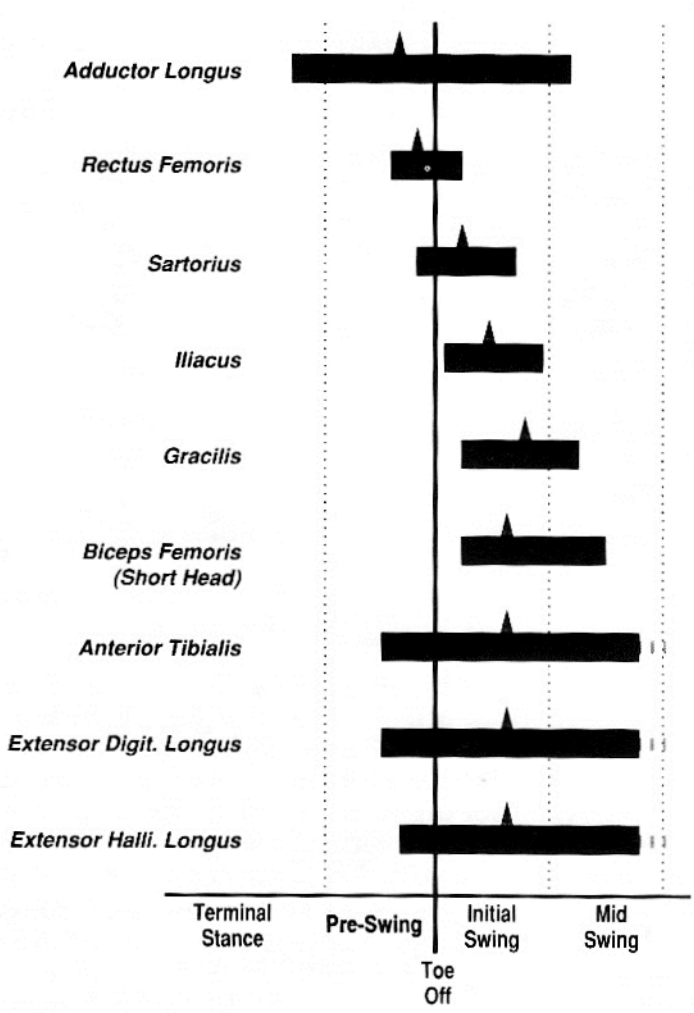

Figure 3-3 Normal flexor muscles activity sequence for swing and the relationship with gait events (the mean data of normal subjects walking with natural cadence) (Perry (1992)).

Winter and Yack (1987) have reported on the analysed variability of EMG magnitude of sixteen muscles during gait cycle of normal subjects. The result showed that the EMG patterns of the proximal muscles are more variable than the distal muscles although the distal muscles are more active. However the variability of the muscles activity timing with relations to gait cycle was not reported. Mickelborough et al. (2004) have described the patterns of phasic muscle during gait initiation in normal elderly people which include those ages more than 65 years old. The muscle activities

tend to be more variable in the preparatory phase than the stepping phase. It was found that the event timing of muscle onset for gluteus medius at initial contact was 81.6% (18.4% of gait cycle before initial contact) with standard deviation (2.4%). Although there was a difference, the data could not be directly compared to subjects in this study as subjects below 65 years of age were also included.

3.3 Sensors Proposed for FES

A sensor used for triggering a FES system should be able to detect important events/phases during gait to control the stimulation timing. A traditional method to detect heel rise and heel strike for peroneal nerve or tibialis anterior muscle stimulation is by using a footswitch placed on an insole under the heel of the affected leg. This method has been used in most of the commercially available stimulators Odstock (Odstock Medical Limited (2008)), ActiGait® (Neurodan A/S (2008)) and MikroFes (Ru”zi”c(1996)). In some cases, when a patient has a problem with a heel or foot contact with the ground, the footswitch is then placed under the heel of the unaffected leg (contralateral leg). In this circumstance, the stimulation will start when the sensor detects heel strike and stop when it detects heel rise. Or sometimes, a footswitch is placed under the first metatarsal head to detect toe rise and toe strike to trigger the start and stop of the peroneal stimulation.

Several sensors have been proposed to detect events/phases of gait for FES using force sensing resistors (FSRs) (Smith et al (2002)), accelerometer(s) (Mansfield and Lyons (2003), Williamson and Andrews (2000a), Williamson and Andrews (2000b), Matsunaga et al. (2007), Shimada et al. (2005) and Willemsen et al. (1990a)), gyroscope (Ghoussayni et al. (2004), Monaghan et al. (2009) and Catalfamo et al. (2010)) and tilt sensors (Dai et al. (1996), Ando et al. (1999), Shimada et al. (2000) and Park et al. (2007)). Also combinations of sensors have been used such as accelerometer(s) with gyroscope(s) (Kotiadis et al. (2004), Kotiadis et al. (2010) and Simcox et al. (2005)) and FSRs with a gyroscope (Pappas et al. (2001) and Pappas et al. (2004)). Other than these artificial sensors, there are also natural sensors proposed. The natural sensors are the ENG (electroneurogram) recorded from Sural nerve (Hansen et al. (2002) and Hansen et al. (2004)) and the EMG (electromyographic) signal recorded from two different quadriceps muscles (vastus lateralis and rectus femoris) (Lauer et al.

(2005)). As well as cosmetically acceptable, easy to don and doff, small in size, low power consumption and inexpensive, the sensor used with FES system should demonstrate an acceptable accuracy in the detection of the events needed to trigger the stimulator.

Willemsen et al. (1990a) have distinguished between the stance and swing phase by measuring the acceleration of the lower limb using an accelerometer. The authors have attached four one-dimensional accelerometers to a PVC bracket and placed on the lower limb using Velcro straps to measure the radial, tangential and equivalent acceleration during the gait. A syntactic detection approach has been used to subdivide the acceleration signal into smaller units (stance, push-off, swing and foot-down). After the signal has been divided into these four small units, the phases were then detected by their own individual algorithm. The heel strike detection in a healthy subject was -30 ± 60 ms. The method proposed used only accelerometers for joint angle measurement without the need for integration, however a bracket is required to place the sensors on the lower limb segment that make them cumbersome and impractical for clinical and everyday use.

Williamson and Andrews (2000a) have detected five phases of gait using a cluster of three accelerometers which produce three dimensional accelerations and a machine learning technique (Rough Sets) to control a FES system for walking. The cluster was attached to the shank of three able bodied subjects at the anterior of the tibial crest. The overall results showed that the detection accuracy of the five phases of gait was greater than 80% when compared to the forces recorded beneath the foot. In a latter study, Williamson and Andrews (2000b) have used a single cluster of accelerometers placed on the shank of three able bodied subjects with two induction rule algorithms, the Rough Sets (RS) and the Adaptive Logic Networks (ALNs) to detect five phases of gait. The accuracy of the two algorithms was compared with the handcrafted rule based algorithm. The results showed that the accuracy of stance/swing detection sampled at 100Hz using RS, ALN and handcrafted was 94-97%, 87-94% and 87-95% respectively. For detection of five phases of gait, the overall accuracy was 82-89% (RS) and 86-91% (ALN). According to the authors, although the average duration of error reported was

smaller in ALN compared to RS, the RS computation was faster and it uses less memory which makes it suitable for real time operation.

Mansfield and Lyons (2003) placed an accelerometer on the trunk (lumbar spine) of four able bodied subjects to detect heel contact events of both legs. The accelerometer was used to measure the anterior-posterior horizontal acceleration in three different walking modes in the healthy subjects (steady, changing or hemiplegic walking). As noted by the authors, the heel contact detection in four healthy subjects using an accelerometer was slightly better than the footswitch (reference sensor) with the percentage ranged between 98.2% and 99.8%, and between 92.4% and 98.7% respectively. The trials however, have not been tested on patients and with different types of footswitch to confirm the reliability.

Shimada et al. (2005) have used an acceleration sensor and a neural network technique as a detector to detect swing phase during gait. The sensor was placed on the thigh and measured the acceleration of the affected leg in the sagittal and gravitational directions. The trials were carried out on five healthy and three stroke subjects. The detector was able to detect the swing phase during the gait in both subjects similar to the heel switch signal. The maximum time difference between the output signal from the detector compared to that from the heel switch was less than 60 ms in healthy subjects and was less than 80 ms in stroke subjects.

Dai et al. (1996) have investigated various types of tilt sensors to replace the foot switch. A tilt sensor was mounted on the shank that measures the tilt of the lower leg during walking. Two thresholds were set on the tilt signal to determine the on and off timing of the peroneal stimulation. This method has improved the cosmesis of the FES user by integrating the sensor with the stimulator without any external wiring as compared to when using a footswitch. However, the errors in the step detection have been observed in subjects who have limited movement of the leg during swing.

Ando et al. (1999) and Shimada et al. (2000) have used a tilt sensor to replace the footswitch and the sensor was mounted on the anterior of the thigh. Ten healthy subjects and one stroke patient have been recruited in the trials to detect toe off during walking using the tilt sensor. The point detected as the toe off using the tilt sensor

signal in the healthy subjects and a patient were 66.6 ± 6.9% and 94.7 ± 0.4% of gait cycle. While using the automatic coordination system the results were 65.0 ± 5.8% and 79.8 ± 1.8% of gait cycle. The actual toe off occurs at about 60% of gait cycle, therefore the difference between the actual toe off and the tilt sensor is about 35% and automatic coordinate system is about 20% of gait cycle for the patient results. The authors however assumed that the tilt sensor can be used to time the stimulation of peroneal nerve during swing in the stroke patient since the result was reproducible and the deviation was very small at about 0.4%.

Catalfamo et al. (2010) used a single gyroscope placed on a shank to detect initial contact and foot off events for level and incline surface. The gyroscope's raw data and filtered signals at nine different frequencies ranged between 5-40Hz obtained from one unimpaired and one cerebral palsy subjects were analysed to investigate the effects on the gait events detection. The results showed that the initial contact detection was more affected by the filtering compared to foot off detection. The cut off frequencies of less than 20Hz have given a higher delay in the detection of initial contact. The authors have used cut off frequency at 35 Hz for the other analysis to evaluate the sensor for the events detection. The other analysis was carried out to detect the initial contact and foot off events during level ground, incline up and incline down walking using rule-based algorithm and the detection was compared with FScan Mobile System. The reliability of the detection reported was above 98% for both events (initial contact and foot off) for all terrains. The accuracy of the detection was between -8ms and -21ms for initial contact while for foot off was between 43ms and 73ms for all terrains. The main problem with the measurement from the gyroscope when it is used for extended period of time is the effect of the temperature drift (fluctuation of stationary output due to changes in ambient temperature). The measurement could be imprecise due to the drift problem. However, the authors suggested that a high pass filter should be used to overcome the drift if it is going to be used for an extended period of time. However, if it is going to be implemented in the real time system with FES, a high pass filter is needed. Adding the filter will introduce a delay to the system and the stimulation will be incorrectly timed.

Smith et al. (2002) evaluated the use of force sensing resistors (FSRs) placed on the insole of both legs to detect the transition between five main phases (loading response,

mid stance, terminal stance, pre swing and initial swing) during gait in cerebral palsy children. The reliability of the sensor for all the events was 94.5% and this has been tested in seven subjects with 35 steps missing out of 642 steps. The accuracy was evaluated using the Vicon 3D marker-based kinematic system as reference and the mean differences were ranged from +35ms (FSR detects the event earlier than it actually happened) to -55ms (FSR detects the event after it actually happened). The mean and standard deviation of the loading response, mid stance, terminal stance, pre swing and initial swing detection were -30 ± 125ms, -27 ± 149ms, -55 ± 151ms, -7 ± 107ms and 35 ± 80ms respectively. The wide distributions in the differences were due to the intrasubject (step-to-step) and the intersubject variability. However, the stimulation timing can be affected with the wide variability in the differences.

Skelly and Chizeck (2001) have used FSRs in the insole of both legs as a gait detector. The authors employed fuzzy logic and a supervised rule method in the detector system to estimate the phases of gait (late swing, early swing, terminal stance, mid-stance and weight acceptance) and determine the events (heel strike, foot flat, heel off, toe off and knee max) in real time. Three complete spinal cord injury subjects have been recruited in the trials. The results showed that two important events, heel strike and toe off were detected within 12% of the gait cycle and within 50% the detection information has become available to the stimulator controller. Therefore, the authors assumed that the system could be used to modify the stimulation intensity and timing in the next cycle of the gait.

Pappas et al. (2004) detected in real time the transition between phases/events (stance, heel off, swing and heel strike) during gait using three FSRs and a gyroscope to control a FES trigger. The gyroscope was used to measure the angular velocity of the foot and the FSRs were used to measure the exerted forces by the foot. All the sensors and a microcontroller were embedded in a shoe insole. The system works robustly in different walking environments such as flat, rough or inclined terrain without any false trigger. The authors set the rules based on the gyroscope and FSRs signal to time the electrical stimulation sequences in the preliminary work (Pappas et al. (2001)). The system was tested on ten able bodied and six impaired gait subjects to walk on different terrains and to ascend and descend stairs. The successful detection rate obtained for walking in different terrains was above 99% in both subjects, whereas for ascending

and descending stairs the rate was above 99% in the able bodied subjects and above 96% in the impaired gait subjects.

Kotiadis et al. (2010) have detected heel off and heel down events in a post stroke (CVA) patient using inertial measurement unit consists of three accelerometers and three gyroscopes. Four algorithms have been developed; the first algorithm used a single accelerometer to measure the radial acceleration of the shank. The second algorithm used two accelerometers to measure radial and tangential acceleration of the shank. The third algorithm used a single gyroscope to measure the angular velocity of the shank and the fourth algorithm is the combination of all the algorithms. The third and fourth algorithms have showed the best results with 100% detection for walking on flat surface and rough terrain, and walking stairs up. However, poor detection has been reported for walking stairs down. The delay for heel off detection reported was less than 150ms when using the third and fourth algorithms while for the first and second algorithm the delay was greater than 150ms.

None of the studies has focussed on using these sensor configurations to detect important events during gait to trigger a stimulator for hamstrings or gluteals muscles stimulation for correction of other gait abnormalities in neurological patients. Most of the studies were more focused on the control of a FES for dropped foot correction by choosing an appropriate sensor:

- To replace the footswitch with a more reliable sensor (Mansfield and Lyons (2003))
- To improve the accuracy of gait events detection (Williamson and Andrews (2000a))
- To propose a design which is cosmetically acceptable (Dai et al. (1996))
- To have the potential for an implantable system (Willemsen et al. (1990a))
- To don and doff easily (Shimada et al. (2000, 2005), Ando et al. (1999))
- To be suitable for different environments (Pappas et al. (2004), Kotiadis et al. (2010) and Catalfamo et al. (2010))

Sousa et al. (2007a, 2007b) have proposed to detect events such as initial contact, opposite toe off, heel rise, opposite initial contact, toe off, feet adjacent and tibia

vertical using image from cameras in seven healthy subjects. Twenty one retro reflective markers have been attached to the subject body segments following the model Simi Motion (Simi Reality Motion Systems, Unterschleissheim, Germany). The image captured from the cameras was analysed to detect the events using a visual method and then compared with the data from the force platform. The visual method was tested with two different camera speeds: normal (50Hz) and high-speed (100Hz). The result for two of the events (initial heel contact and toe off) for both speeds was reported. For the normal speed of operation, the differences are -83 ms ± 51 ms (initial contact) and -1.9 ms ± 25 ms (toe off). For high-speed cameras, the differences are 7.3 ms ± 6.4 ms (initial contact) and 15 ms ± 25 ms (toe off). However, the result for the other events was not reported.

Park et al. (2007) have proposed to detect initial contact, heel off, toe off and tibia vertical in twelve healthy subjects and five hemiplegic patients using output from a tilt sensor attached to the shank. The measurement was taken during normal walking. The events were defined using the positive peak, negative peak and offset of the voltage output from the tilt sensor. The detection was compared with a three dimensional movement analysis device and four force plates. The initial contact and tibia vertical were detected 100% in healthy subjects. The heel off and toe off were detected about 85% and 79% respectively. The detection of other events was not reported. Also not reported is the accuracy of the events detected.

This study will focus on choosing an appropriate sensor that can be used to detect when the tibia is vertical to trigger the stimulation of muscles such as the hamstrings or gluteals for preventing knee hyperextension into early stance or reducing the excessive hip flexion/adduction at heel strike in neurological patients. Although, Park et al. (2007) have detected the tibial vertical event in hemiplegic subjects using a tilt sensor attached to the shank, the reliability and accuracy of the detection were not reported. Sousa et al. (2007a, 2007b) have detected the tibial vertical event using image from cameras in healthy subjects for gait analysis. However, the accuracy of the detection method for detection of tibial vertical event was not reported. Moreover, the method was not suitable for use with FES system and outside the laboratory as it needs a proper set up for the cameras and the cameras are expensive. Since no accuracy has been reported for the detection of tibial vertical event in the studies (Park et al. (2007) and

Sousa et al. (2007a, 2007b)), it is not possible to predict the impact on patients when stimulation is applied using the proposed method. To the best knowledge of the author, no other studies have reported on the accuracy and reliability of tibial vertical event detection in various neurological patients. Therefore, a study is needed to report on the accuracy and reliability of tibial vertical event detection in various neurological patients as well as to discuss the possible impact based on the accuracy of the detection on stimulation of hamstrings and gluteals muscles.

Different sensor positions and kinematic measurements have been used to detect gait events/phases such as at the thigh, shank, foot and trunk while the kinematic measurement used are the joint/segment angle, angular velocity and acceleration. Several methods have been proposed to use with the sensors to detect the gait events/phases such as Adaptive Logic Network (ALN)(Williamson and Andrews (2000b)), neural network (Shimada et al. (2005)), fuzzy logic (Skelly and Chizeck (2001)) and threshold (Dai et al. (1996), Lau and Tong (2008)). In the study, three sensor positions (at the thigh, shank and foot) and the kinematic measurement (segment angle and linear accelerations) will be explored and considered for use in the detection of the specific event. Also, the trials will be carried out in various neurological patients such as stroke, multiple sclerosis and spinal cord injury and not limited to one type of patient.

3.4 Kinematic Measurement

A traditional method of measuring joint angles is to use goniometers. Mulder et al. (1990) and Veltink et al. (1993) have used goniometers in an experimental test to measure knee angle and angular velocity. From this information, the transition from knee lock to unlock positions can be distinguished and the stimulation level of quadriceps muscle can be controlled appropriately in assisted standing. Goniometers, however are not very popular in everyday use with FES systems due to limitations. Practical considerations are that attachment usually requires double-sided tape and these devices also tend to be bulky around the joint. It has been reported that a goniometer can easily slide from the original position attached to the joint; therefore it needs to be re-calibrated every time a measurement is taken (Patrick et al. (1986) and Williamson and Andrews (2001)).

The gyroscope is another sensor that has a good potential in performing kinematic measurement. This micro-machine sensor is tiny, quite expensive and lightweight. The output signal from the sensor is proportional to angular velocity that on integration can produce the angle information. Recently, a gyroscope has been used as a gait detector to control stimulation timing (Ghoussayni et al. (2004), Monaghan et al. (2004), Monaghan et al. (2009) and Pappas et al. (2004)). Unlike the footswitch, this sensor not only detects heel strike and heel rise but it is also capable of determining the position of leg/foot during the gait cycle. However a gyroscope has one common problem which is drift caused by integration (Veltink et al. (1996)). For extended period of time the effect of the temperature drift (fluctuation of stationary output due to changes in ambient temperature) in a gyroscope can caused inaccuracy in the angular velocity measurement and the drift can be eliminated by adding a high pass filter to the output of the sensor (Catalfamo et al. (2010)). For a short time measurement, drift can be a significant problem even if there is little variation in the DC offset/zero frequency component (Monaghan et al. (2004)). The authors however managed to prevent this problem by resetting the detection system process each time before the new integration takes place. Tong and Granat (1999) investigated the single uni-axial gyroscope to be used in the portable motion analysis system. A significant drift problem occurs when there is a change in direction or turning during the gait. By either resetting the system for every step of the gait or using high pass filter, the drift problem can be overcome successfully. However, the foot switch is still needed to detect foot contact for automatically resetting the system.

Another micro-machined sensor, the accelerometer is also small, inexpensive, light weight and has low power. The output signal is proportional to linear acceleration. An accelerometer has many applications; typically it is used to measure tilt/roll, vehicle skid, impact and detect vibration. In a gait system particularly, accelerometers have been used to measure lower limb joints angles in real-time (Willemsen et al. (1990b)), evaluate everyday physical movement (Bouten et al. (1997)) and detect gait events during walking (Mansfield and Lyons (2003), Willemsen et al. (1990a), Williamson and Andrews (2001)). Integration is needed to calculate an angle from angular acceleration or angular velocity when using an accelerometer which produces incorrect results due to drift. Willemsen et al. (1990b) have presented promising results for the calculated lower limb joints angles during walking, sitting and standing without the

need to use integration. The system however was not very comfortable for everyday use because the accelerometers need to be mounted on the brackets placed on the thigh and shank for angle measurement. Also for the angle measurement, the sensors have to be at the same distance from the joint.

Williamson and Andrews (2001) used a combination of two sensors, accelerometers and gyroscopes to estimate knee angle and angular velocity. The offset and drift from the gyroscopes have been cancelled out by using auto-resetting and auto-nulling algorithms. The measurement of angle and angular velocity of individual sensors during standing up trials have shown a higher RMS error when FES was used. However, this error has been reduced by using a 10Hz low pass filter and also was reduced using a gyroscope, from 0.102° to 0.038° for angles and from 19.53°s^{-1} to 6.47°s^{-1} for angular velocities. Using an accelerometer there was a reduction from 7.105° to 1.777° for angle and 904.58°s^{-1} to 233.03°s^{-1} for angular velocity. The results showed that the angle and angular measured using a gyroscope are better than the low pass filtered accelerometer measurement. For sit-stand-sit trial in normal subjects, the combination sensors with auto reset and auto null method were able to estimate the knee angle better than the accelerometer measurement alone. However, the system has not been tested for walking trials. In a different study, Veltink et al. (1996) have compared two methods, the first using the integration signal of a gyroscope and the second using tangential and radial acceleration from an accelerometer together with a differentiated signal of the gyroscope to estimate knee angle. In the study, it shows that the second method gives more accurate results while the first method has drift problems due to the signal integration. All of these methods combine information from different sources resulting in additional hardware and processing that add complexity, cost, weight and increased power consumption for body worn systems.

Jasiewicz et al. (2006) have used a sensor pack consists of a gyroscope and two biaxial accelerometers to detect toe off and heel strike events in nineteen normal and thirteen spinal cord injury subjects (ASIA D). The sensor was attached to the shank and foot of both lower limbs. The events were detected using maximum and minimum peaks based on foot acceleration, foot or shank angular velocities. The events detected were compared with footswitches (heel and toe switch). Figure 3-4 (a) and (b) show the results of the delays found from their results. It is apparent that the delays are small

compared to the time that a stride takes and are of the order of a few percent. These results demonstrate that MEMS sensors could be used to good effect with FES systems and introduce only small timing delays in the heel strike and toe off that are negligible.

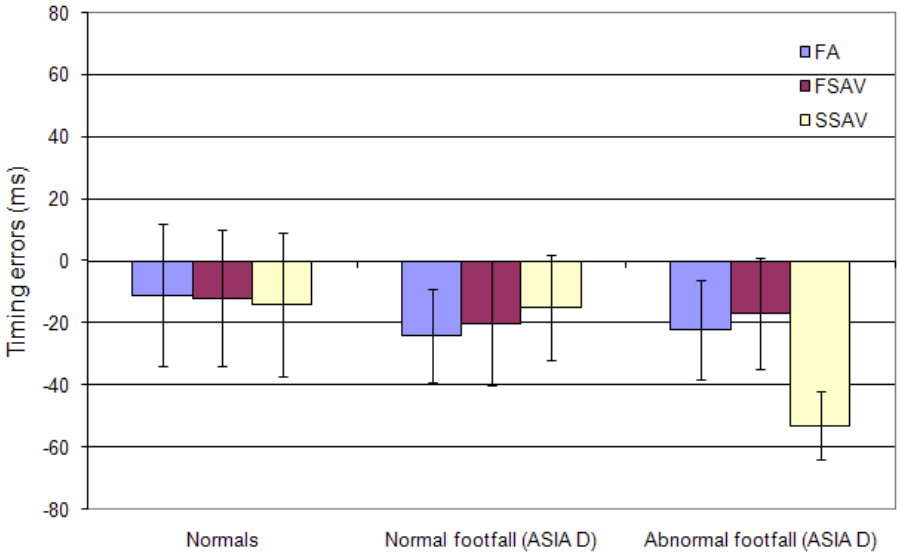

(a)

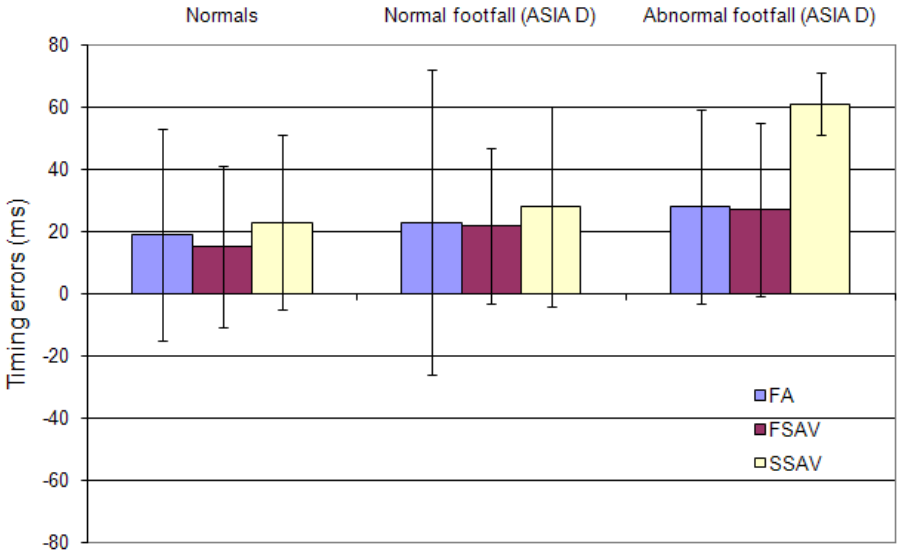

(b)

Figure 3-4 Results of timing errors for (a) initial contact and (b) end contact detection in normal and ASIA D subjects compared to footswitch. (FA=foot acceleration, FSAV=foot sagittal angular velocity and SSAV=shank sagittal angular velocity).

Lau and Tong (2008) have attached a sensor unit consisting of one dual axis accelerometer and one single axis gyroscope at the thigh, shank and foot of the affected

limb of ten hemiparetic patients with dropped foot and the dominant limb of three normal subjects. Each sensor unit was used to measure anterior-posterior (AP) acceleration, superior-inferior (SI) acceleration and AP angular velocity of each locations. The performance index (PI) and timing variation were calculated to evaluate threshold detection method in classification of gait events. The lowest timing variation in dropped foot subject during stance was 1.29% (shank AP angular velocity TP_{max}) and during swing was 4.10% (foot AP angular velocity TP_{min}) while in normal subjects during stance was 0.76% (thigh AP angular velocity TP_{max}) and during swing 1.21% (foot SI acceleration TP_{max}). The highest performance index in dropped foot subject during stance was 0.987 (shank AP angular velocity TP_{min}) and during swing was 0.954 (foot SI acceleration TP_{max}) while in normal subjects during stance was 0.992 (thigh AP angular velocity TP_{max}) and during swing 0.988 (foot SI acceleration TP_{max}). The limitation of the turning point detection method is when there are more peaks and troughs of higher amplitude in the measured signal, especially in abnormal gait. This limitation will reduce the reliability of the detection method.

Favre et al. (2008) have used two inertial measurement units (IMUs), each consisting of a tri-axial gyroscope and an accelerometer attached to the thigh and shank of the subjects to calculate for 3D knee joint angle. A comparison has been made with measurements from the Liberty® magnetic tracking device (Polhemus, USA). Ten healthy young subjects were recruited to perform four movements such as abduction/adduction of both hips and level ground walking of 30m. The method estimates the orientation of the thigh and shank that is then aligned to the reference frame of the two orientation measurements. The system has estimated the 3D knee joint angle during walking with a small offset error for flexion/extension and abduction/adduction (less than 3°) but high offset error for internal/external rotation (up to 9°). However, the sensor system is not suitable for everyday use with FES as the reference frame needs to be defined based on the initial orientation of the IMUs for every new attachment of the sensor to calculate for the joint angle.

Simcox et al. (2005) have measured sagittal plane angle of the thigh, shank and trunk of a normal subject using a sensor pack consisting of a gyroscope and two accelerometers during walking and sit-stand trial. The measurements were compared with a 3D motion analysis (Eva HiRes, Motion Analysis Corporation, California). The root mean squared

error (RMSE) for walking trial was less than 5° and sit-stand trial was less than 6°. The correlation coefficient for walking was between 0.9 and 0.99 and for sit-stand trial was between 0.97 and 0.99.

The inertial measurement unit (IMU) is a sensor that measures three dimensional translation and rotation but these are more bulky and the power consumption is high. Unfortunately these two factors are important for a battery powered neuromuscular stimulator if it is to be durable and reliable, yet also unobtrusive and aesthetic to the person. A two axis rate gyro for example dissipates 20.4 mW (LPY430AL, 6.8mA at 3V) while a three axis accelerometer dissipates 2.1 mW (LIS331AL, 0.65mA and 3V). The cost of the rate gyro is USD 7.36 while for the accelerometer is USD 5.38.

In different study, sensors such as an accelerometer and gyroscope have been used in gait analysis and movement kinematic measurement. Brandes et al. (2006) have assessed gait parameters such as the number of steps, walking distance and walking time in healthy children using three orthogonally mounted accelerometers (MIniMod) attached to the lower back of the trunk. Auvinet et al. (2002) have used a system known as Locometrix^{TM} consisting of two accelerometers, recording device and software to process the acceleration signal in 282 healthy adults and elderly people aged between 20-98 years (144 women and 138 men). The system was attached to the waist of the subject using a belt to obtain stride frequency, step symmetry, stride regularity, cranial-caudal activity, harmonic analysis and kinetic variables during walking by measuring the cranial-caudial and median-lateral acceleration at the point close to the centre of gravity of the body. Miyaoka et al. (2005) have used two dual axis accelerometers to estimate the functional coupling between the head movement and trunk drift. Each of the accelerometers was attached to the centre of the eye glasses and to the centre point between the scapulae. Henriksen et al. (2004) have used a triaxial accelerometer attached to the trunk (lumbar spine) using an elastic belt to evaluate the sensor reliability in estimating mean acceleration, cadence, step and stride length at standardised walking speed in twenty healthy subjects. Moe-Nilssen and Helbostad (2004) have used a triaxial accelerometer placed at the lower trunk of two normal subjects to estimate cadence, step length and measures of gait regularity and symmetry over a range of self administered speeds using the signal analysed by autocorrelation function. Boonstra et al. (2006) have used two boxes of sensors, each consisting of two

accelerometers and a gyroscope placed on the waist with a neoprene belt. The boxes were also attached to the sternum and frontal side of upper leg to assess the accuracy of the sensors for measuring angle and angular velocity of the upper body (thorax and pelvis) and upper leg during rising from a chair in five healthy subjects. The accelerometers signals were low pass filtered and the measurement was improved by high pass filtering of the gyroscope signal and the measurement was compared with an optical motion analysis system (Optotrak®, Northern Digital Inc., Waterloo, Ontario, Canada). The mean squared error was improved from 2.9°, 3.5° and 2.6° to 0.8°, 1.1° and 1.7° for angle measurement and from 9.4°s^{-1}, 18.4°s^{-1} and 11.5°s^{-1} to 2.6°s^{-1}, 4.0°s^{-1} and 4.9°s^{-1} for angular velocity measurement of the thorax, pelvis and upper leg respectively. The optimal cut-off frequencies for the low pass filter were 1.05Hz, 1.30Hz and 1.05Hz and for combined signal were 0.18Hz, 0.20Hz and 0.38Hz (thorax, pelvis and upper leg). The loss of information from the low pass filtering of signals would make these systems unsuitable for the accurate timing of stimulation pulses in FES. Mayagoitia et al. (2002) have used a sensor system consisting of four accelerometers and a gyroscope mounted on an aluminium strip attached to the thigh and the shank of the subject. The trials were carried out with ten healthy subjects and the measurement was compared with Vicon® System. The root mean squared error for the shank angle, shank angular velocity and shank angular acceleration was less than 7% and the coefficient of multiple correlation was above 0.98. For the knee linear acceleration the root mean squared error was between 11% and 15% while the coefficient of multiple correlation was 0.93. Luinge and Veltink (2005) have used an inertial measurement unit (IMU) consisting of three single axis accelerometers and three single axis gyroscopes placed on the pelvis, trunk and forearm to measure the orientation and compared with the Vicon system. A Kalman filter was used to estimate the gyroscope offset that fluctuated as the effect of drift in the measurement. Two subjects were recruited; the first subject lifted a stack of six empty crates and the second subject performed feeding routines and morning routine tasks. The method proposed has estimated the inclination within 3° (root mean squared) and the offset error after two minutes of measurement was about 5% of the initial offset error. The following table (Table 3-2) presents the examples of various kinematic sensors used in various studies.

Table 3-2 The kinematic sensors used in various studies.

Researchers	**Sensor used**	**Kinematic measurement**	**Studies**
Brandes et al. (2006)	Accelerometers	Accelerations measured at lower trunk	Gait assessment in children
Jasiewicz et al. (2006)	Gyroscope and accelerometers	Foot linear accelerations, foot sagittal angular velocity and shank sagittal angular velocity	Determine the timing of initial contact (IC) and end contact (EC) events in normal and spinal cord injured subjects.
Henriksen et al. (2004)	Accelerometer	Anterior-posterior, mediolateral and vertical accelerations at lumbar spine	Clinical gait analysis in healthy subjects
Auvinet et al. (2002)	Accelerometer	Vertical acceleration at the lower trunk (waist)	Gait analysis in adult
Moe-Nilssen and Helbostad (2004)	Accelerometer	Trunk acceleration	Gait cycle characteristics measurement
Miyaoka et al. (2005)	Accelerometer	Head tilt	Analysis of head movement
Simcox et al. (2005)	Gyroscope and accelerometers	Trunk and lower limb angle	FES system (sit-stand-sit and walking)
Williamson and Andrews (2001)	Gyroscopes and accelerometers	Knee angle and angular velocity	FES system (sit-stand-sit)
Luinge and Veltink (2005)	Gyroscopes and accelerometers	Orientation of the pelvis, trunk and forearm	Evaluate the performance of the orientation estimation algorithm in different daily life task.

Mayagoitia et al. (2002)	Gyroscope and accelerometers	Linear acceleration, angle and angular velocity of the thigh and shank	Motion analysis.
Favre et al. (2008)	Gyroscope and accelerometer	Knee joint angle	Assessment of 3D knee joint angle measurement during walking.
Boonstra et al. (2006)	Gyroscopes and accelerometers	Angle and angular velocity of the upper body and upper leg	Kinematic measurement of rising from a chair.
Lau and Tong (2008)	Gyroscopes and accelerometers	Accelerations and angular velocity of the thigh, shank and foot	Identification of gait events in dropped foot patients.

Based on the review, accelerometer and gyroscope has become an alternative sensor proposed to detect gait events for use with FES. The sensors have been used to measure the angles, accelerations and the angular velocities in various part of the human body such as trunk and lower limb. These sensors are more practical and easy to set up compared to the standard system such as motion capture system (Vicon^{TM}) and force plate.

Kotiadis et al. (2010) have defined the acceptable timing limits for heel rise detection as 100 ms before or 100 ms after the heel rise. Heel strike detection is less of a problem and their recommendation is 150 ms before or 150 ms after the heel strike of a heel switch for control of dropped foot stimulation. Shimada et al. (2005) and Willemsen et al. (1990a) have demonstrated an acceptable accuracy of their sensors as compared to footswitch in the detection of events such as heel strike and/or heel rise. A sensor should be as near to 100% reliable as possible in the detection of heel rise or toe rise to ensure that there is no missing trigger of the tibialis anterior muscles during stimulation that lifts the foot and provides the foot clearance of the ground. If a missing event occurred, this may caused patients to fall over. Heel strike event detection is less critical and therefore if a system is less than 100% reliable it is acceptable but it should

be at least as reliable as the existing sensor, the footswitch. The reliability of a sensor could be different when used in different conditions such as walking on slopes, stairs and level ground. Also, the speed of walking could also affect the reliability of a sensor in gait event detection. The best reference would be the 'gold standard system' (Findlow et al. 2004) such as force plate to detect heel contact and heel off. However, this is not possible for walking in different terrain such as slopes, stairs and outside the laboratory.

As well as for use with FES, most researchers (Table 3-2) have used these sensors in the gait analysis. Between these sensors, the accelerometer has become the sensor of choice for the author of this thesis. It consumes low power, is light weight, small and inexpensive which makes it suitable for an application in everyday use. For example an accelerometer ADXL203CE (£6.04, 0.7mA x 5V = 3.5mW, 5mm x 5mm x 2mm = 50mm^3) (Analog Devices Inc. (1995c)) is cheaper, consumes less power and is smaller in size than a gyroscope ENC-03R (£7.69, 3mA x 5.5V = 16.5mW, 8mm x 4mm x 2mm = 64mm^3) (Murata (2011)). Both sensors are lightweight and less than 1 gram. However, the algorithm that will be developed in the study should not use integration in the measurement to avoid any drift problems.

3.5 Conclusions

In the study, the tibial vertical event will be detected in neurological patients. This event occurs during the swing phase of the gait cycle. The traditional sensor used with FES, the footswitch is not a sensor of choice for this study as it can only detect foot contact and lift off from the ground and therefore no information during the swing can be obtained. Kinematic measurements such as angle, linear acceleration and angular velocity have been made for gait event detection using sensors such as tilt devices, gyroscopes and accelerometers (Willemsen et al. (1990b), Mansfield and Lyons (2003), Catalfamo et al. (2010)). These sensors measure the leg or foot position throughout the gait cycle including the swing phase.

Accelerometers and gyroscopes are the potential sensors that could be considered in the study. However, the main problem with the gyroscope is its drifting output signal due to fluctuations in the ambient temperature when used for extended periods of time

(Catalfamo et al. (2010)) or integration of the angular velocity signal to calculate angles (Veltink et al. (1996)). A high pass filter is needed to eliminate the drift (Tong and Granat (1999) and Catalfamo et al. (2010)). Williamson and Andrews (2001) have used auto-resetting and auto-nulling algorithms with accelerometers to eliminate the drift. These additional requirements will only add delays or consume more power as well as extra cost to the system. On the other hand, an accelerometer can measure an angle without integration and therefore the drift is totally avoided (Willemsen et al. (1990b)). Moreover, an accelerometer has some advantages over a gyroscope. For example an accelerometer ADXL203CE (£6.04, 0.7mA x 5V = 3.5mW, 5mm x 5mm x 2mm = 50mm^3) (Analog Devices Inc. (1995c)) is cheaper, consumes less power and is smaller in size than a gyroscope ENC-03R (£7.69, 3mA x 5.5V = 16.5mW, 8mm x 4mm x 2mm = 64mm^3) (Murata (2011)). Both sensors are lightweight and less than 1 gram.

To the best knowledge of the author, no studies have reported on the accuracy and reliability of the tibial vertical event detection in patients and therefore it is not possible to do a direct comparison between the systems. An accelerometer has become a sensor of choice to be developed in the study. Although the method used by Willemsen et al. (1990b) has shown promising results, the accelerometers need to be mounted on brackets placed on the thigh and shank for angle measurement and have to be at the same distance from the joint. This arrangement is cumbersome to the users and not suitable for use with FES. Therefore, a new algorithm will be developed that should calculate the angle without the use of integration to avoid drift in the measurement. The algorithm should be independent of the distance of the sensor from a joint. The algorithm developed using this sensor will be described in the next chapter.

Chapter 4

The Sensor Unit Algorithm

4.1 Introduction

This chapter presents an algorithm to calculate a segment angle and accelerations using outputs from a sensor unit. The sensor unit consists of two dual axis accelerometers arranged in a specific configuration. The angle and linear accelerations are determined analytically without using integration. The sensor unit when attached to the lower limb segment, measures the angle and accelerations with a future aim of triggering a stimulator for the contraction of the hamstrings or gluteals muscles. The minimum range that the sensor unit should be able to measure is 0° to 70° as this is the largest range of angle motion of the lower limb during walking which occurs in the knee (Perry (1992)). Accelerometers with a range of ±2g (Zijlstra and Hof (2003), Jasiewicz et al. (2006), Simcox et al. (2005), Williamson and Andrews (2001), Lau and Tong (2008)) and ±5g (Mayagoitia et al. (2002) and Favre et al. (2008)) have been used to measure angle, angular velocity and acceleration of the lower limb. In the study presented in this thesis, the minimum ±2g and maximum ±6g ranges will be considered.

The advantages of using an accelerometer are that it has a low power consumption, is small in size, lightweight, and inexpensive, making it suitable for everyday use with FES systems. Also, it can provide the kinematic measurements such as angle and acceleration throughout the gait cycle and be used for event detection. It is not possible to measure angles with the sensor unit when all the sensing axes are orthogonal to the

Earth's gravitational field. However the lower limb segments move in the same plane as the gravitational field so the angles can be measured.

4.2 The Basic Principle of an Accelerometer (Johnson (1997))

Most accelerometers operate by applying a spring-mass principle. The principle is based on Newton's and Hooke's laws. Consider a simple spring-mass system (Figure 4-1(a)) which permits the mass, m, to slide freely on the base. If the spring is in the equilibrium position and the mass is not moving, there is zero net force exerted on the spring and the mass. If a mass, *m*, is undergoing an acceleration, *a*, then there must be a force, *F*, acting on the mass and given by $F=ma$ as stated by the Newton's law. If a spring with spring constant *k* is extended from its equilibrium position for a distance Δx, then there must be a force acting on the spring given by $F=k\Delta x$ as stated by Hooke's law.

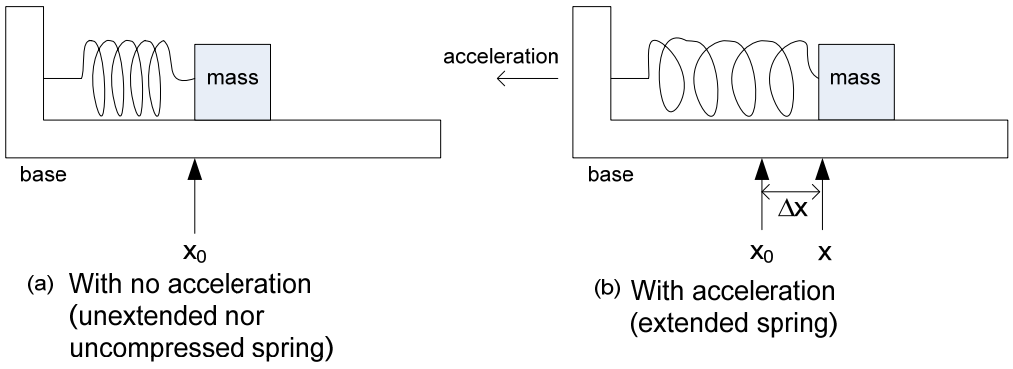

Figure 4-1 The basic spring-mass system which describes the principle of an accelerometer adapted from (Johnson (1997)).

When the spring-mass system is accelerated to the left (Figure 4-1(b)), the spring extends in order to provide the force necessary to accelerate the mass with Δx displacement. This can be described by equating Newton's and Hooke's laws with equality of forces exist:

$$ma = k\Delta x \qquad (4\text{-}1)$$

where,

k = spring constant in N/m

Δx = spring extension in m

m = mass in kg

a = acceleration in m/s^2

Hence, the measurement of acceleration, a is reduced to a measurement of the spring extension, Δx which is a linear displacement measurement because

$$a = \frac{k}{m}\Delta x \tag{4-2}$$

If the acceleration is reversed, the same principle would apply, except that the spring is compressed instead of extended. The Equation 4-2 describes the relationship between the spring displacement (extended or compressed) and the acceleration (output of the accelerometer).

4.3 The Static and Dynamic Forces

The spring displacement is the output from force(s) exerted on the spring and the mass of the accelerometer. Let s be the acceleration output of a single axis accelerometer that is proportional to the spring displacement, when the sensing axis is orthogonal to the gravitational field direction, there will be no force acting on the mass and the spring, therefore there is no spring displacement and s is equal to 0g (Figure 4-2(a) and 4-2(c)). In a different orientation, if the sensing axis is parallel to the gravitational field (Figure 4-2(d)), s is equal to +1g (positive displacement indicates the spring is extended). If the sensing axis is parallel but in the opposite direction to the gravitational field (Figure 4-2(b)), s is equal to -1g (negative displacement indicates the spring is compressed). The magnitude of the acceleration in this case is 1, which is the gravitational acceleration, 1g or typically 9.80665ms^{-2} depending on latitude.

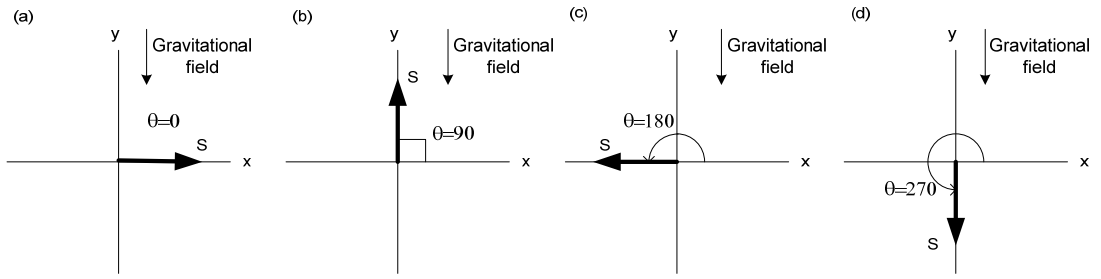

Figure 4-2 The static force.

For general conditions, when a dynamic force (external force) is present as well as a static force, there are two forces acting on the spring and the mass. The output signal, *s*, will be equal to the total acceleration (spring displacement) due to the two forces. Let $\ddot{x}$ be the horizontal acceleration (right or left direction) and $\ddot{y}$ be the vertical acceleration (up or down direction). When the sensing axis is at 0° and the accelerometer is accelerated horizontally (Figure 4-3(a) and 4-3(b)), there will be an external force acting on the mass causing the spring to be displaced (extended or compressed) but when the accelerometer is accelerated vertically (Figure 4-3(c) and 4-3(d)), there will be no force acting on the spring and the mass therefore there will be no spring displacement.

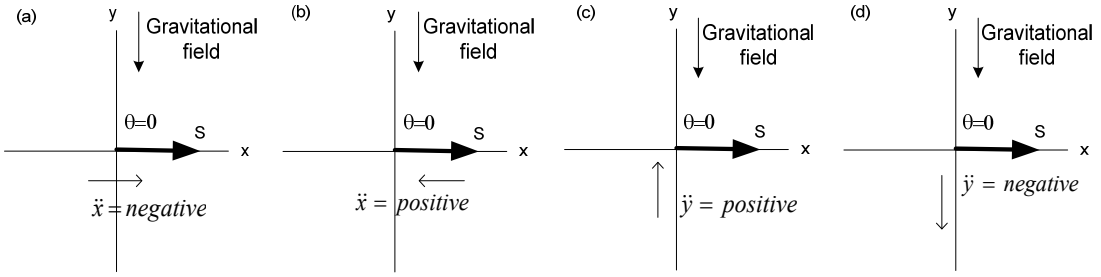

Figure 4-3 The static and dynamic forces (sensing axis at 0°) with dynamic accelerations shown by the arrows.

For the sensing axis inclined at 90°, when the accelerometer is accelerated horizontally (Figure 4-4(a) and 4-4(b)), there will be a spring displacement only due to the gravitational field and when the accelerometer is accelerated vertically (Figure 4-4(c) and 4-4(d)), there will be a spring displacement due to both forces (gravitational and external force) acting on the spring and the mass. It can be concluded that when the

sensing axis is parallel to any force(s), this force(s) will act on the spring and the mass, therefore there will be a spring displacement. However, when the sensing axis is orthogonal to any force(s), this force(s) will not act on the spring and the mass, therefore there will be no spring displacement.

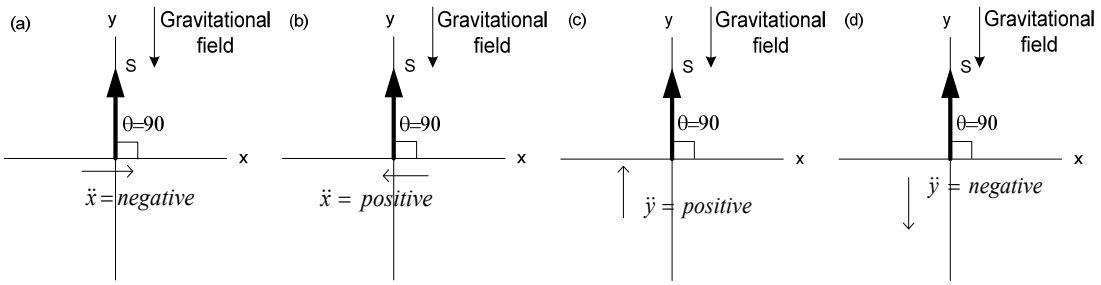

Figure 4-4 The static and dynamic forces (sensing axis at 90°) with dynamic accelerations shown by the arrows.

4.4 The Sensor Unit Algorithm

Based on the basic operation of the accelerometer which has been discussed earlier in this chapter, an algorithm for calculating angle and acceleration has been developed. In the algorithm, both accelerations due to gravitational field and external force have been considered in the derivation of the sensor unit output. The accelerations ($\ddot{y}$, vertically and $\ddot{x}$, horizontally) and the angle of a single segment, θ can be calculated based on the following configuration: the first axis of a dual axis accelerometer, s_1 is aligned to the segment of interest and the second axis of the accelerometer, s_2 is $\pi/2$ degrees from the first axis as shown in Figure 4-5. The angle, θ is the angle between the segment of interest and the x-axis (earth horizontal see Appendix A). Normally, θ is measured as positive in anti-clockwise direction and negative in clockwise direction.

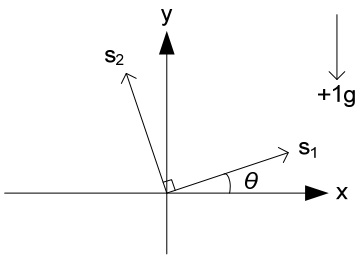

Figure 4-5 The configuration of the first accelerometer for the sensor unit algorithm.

The output of the first accelerometer, s_1 and s_2 can be written as,

$$s_1 = \ddot{x}\cos\theta - \ddot{y}\sin\theta - g\sin\theta \tag{4-3}$$

and

$$s_2 = -\ddot{x}\sin\theta - \ddot{y}\cos\theta - g\cos\theta \tag{4-4}$$

where

$\ddot{x}$ = horizontal acceleration in g

$\ddot{y}$ = vertical acceleration in g

g = gravity acceleration (1g)

Each output consists of two acceleration components, static and dynamic. $\ddot{x}$ and $\ddot{y}$ represent the dynamic acceleration, whereas g represents the static acceleration. As there are three unknowns: $\ddot{x}$, $\ddot{y}$ and θ, at least three equations are needed to solve for all the unknowns. In the algorithm, four equations are needed to solve the unknowns analytically. Therefore, the second dual axis accelerometer is placed between the first accelerometer with π/4 degrees from the s_1 as shown in Figure 4-6.

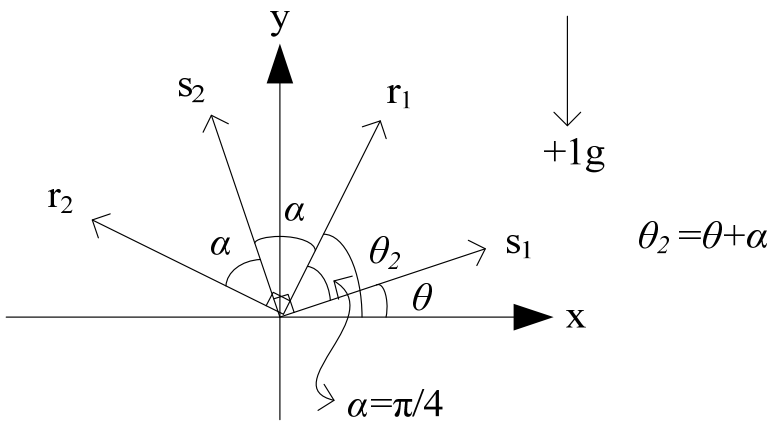

Figure 4-6 The configuration of the first and second accelerometers for the sensor unit algorithm.

The output of the second accelerometer, r_1 and r_2 can be written as,

$$r_1 = \ddot{x}\cos\theta_2 - \ddot{y}\sin\theta_2 - g\sin\theta_2 \tag{4-5}$$

and

$$r_2 = -\ddot{x}\sin\theta_2 - \ddot{y}\cos\theta_2 - g\cos\theta_2 \tag{4-6}$$

By multiplying Equation (4-3) with $\cos\theta$ and Equation (4-4) with $\sin\theta$, s_1 and s_2 can be written as,

$$s_1\cos\theta = \ddot{x}\cos^2\theta - \ddot{y}\sin\theta\cos\theta - g\sin\theta\cos\theta \tag{4-7}$$

and

$$s_2\sin\theta = -\ddot{x}\sin^2\theta - \ddot{y}\sin\theta\cos\theta - g\sin\theta\cos\theta \tag{4-8}$$

By subtracting Equation (4-8) from Equation (4-7), the $\ddot{x}$ is given by,

$$\ddot{x} = s_1\cos\theta - s_2\sin\theta \tag{4-9}$$

By multiplying Equation (4-3) with $\sin\theta$ and Equation (4-4) with $\cos\theta$, s_1 and s_2 can be written as,

$$s_1\sin\theta = \ddot{x}\sin\theta\cos\theta - \ddot{y}\sin^2\theta - g\sin^2\theta \tag{4-10}$$

and

$$s_2\cos\theta = -\ddot{x}\sin\theta\cos\theta - \ddot{y}\cos^2\theta - g\cos^2\theta \tag{4-11}$$

By adding Equation (4-10) and Equation (4-11), $\ddot{y}$ is given by,

$$\ddot{y} = -s_1 \sin\theta - s_2 \cos\theta - g \tag{4-12}$$

Now by multiplying Equation (4-5) with $\cos\theta_2$ and Equation (4-6) with $\sin\theta_2$, then multiplying Equation (4-5) with $\sin\theta_2$ and Equation (4-6) with $\cos\theta_2$, r_1 and r_2 can be written as,

$$r_1 \cos\theta_2 = \ddot{x}\cos^2\theta_2 - \ddot{y}\sin\theta_2\cos\theta_2 - g\sin\theta_2\cos\theta_2 \tag{4-13}$$

and

$$r_2 \sin\theta_2 = -\ddot{x}\sin^2\theta_2 - \ddot{y}\sin\theta_2\cos\theta_2 - g\sin\theta_2\cos\theta_2 \tag{4-14}$$

also,

$$r_1 \sin\theta_2 = \ddot{x}\sin\theta_2\cos\theta_2 - \ddot{y}\sin^2\theta_2 - g\sin^2\theta_2 \tag{4-15}$$

and

$$r_2 \cos\theta_2 = -\ddot{x}\sin\theta_2\cos\theta_2 - \ddot{y}\cos^2\theta_2 - g\cos^2\theta_2 \tag{4-16}$$

By subtracting Equation (4-14) from Equation (4-13), $\ddot{x}$ is given by,

$$\ddot{x} = r_1\cos\theta_2 - r_2\sin\theta_2 \tag{4-17}$$

By adding Equation (4-15) and Equation (4-16), $\ddot{y}$ is given by,

$$\ddot{y} = -r_1\sin\theta_2 - r_2\cos\theta_2 - g \tag{4-18}$$

To solve for θ Equation (4-9) is equated to the negative of Equation (4-17),

$$\theta = \tan^{-1}\left(\frac{-s_1 - r_1\cos\alpha + r_2\sin\alpha}{-s_2 - r_1\sin\alpha - r_2\cos\alpha}\right) \quad (4\text{-}19)$$

4.5 Inverse Tangent Function and Quadrants

The calculation of the angle of a sensor unit, θ, requires the use of the inverse tangent function. For this function, positive values mean that an angle is either in the first quadrant (Q1) or third quadrant (Q3) and negative values are associated with either the second quadrant (Q2) or fourth quadrant (Q4) (Figure 4-7). Therefore, it is very important to know the sign of the numerator and the denominator of Equation 4-19 to determine the exact angle. When the arctan is positive value, the angle is either in the Q1 or Q3, and if the arctan is negative value, the angle is either in Q2 or Q4 as shown in Figure 4-8.

By knowing the sign of the denominator and the numerator, the angle can be determined as follows:

If in Q1, θ = arctan(n/d) + 0°,

If in Q2, θ= arctan(n/d) + 180°,

If in Q3, θ= arctan(n/d) + 180°,

If in Q4, θ = arctan(n/d) + 360°.

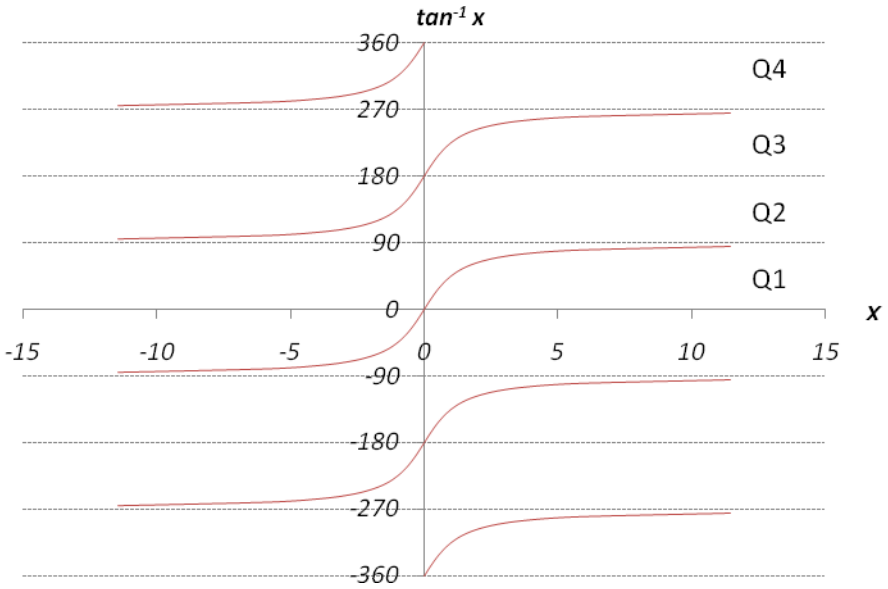

Figure 4-7 The quadrants of tangent inverse function to determine the exact angle.

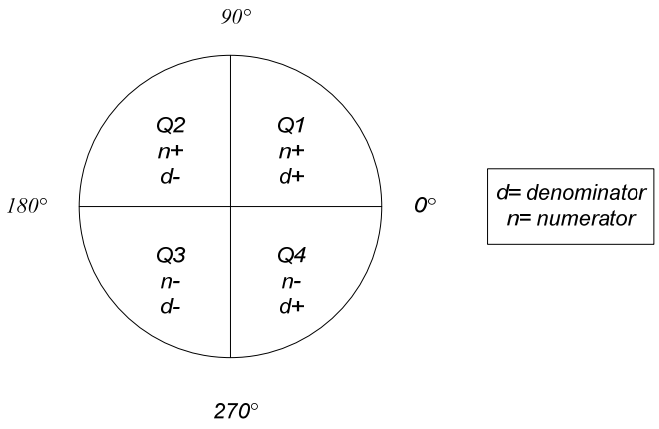

Figure 4-8 Four quadrants with different signs of the denominator and numerator to determine the angle.

4.6 The Sensor Unit

The sensor unit has been designed to measure a segment angle with respect to the horizontal plane of the earth and linear accelerations during walking using the algorithm discussed earlier. Researchers have used accelerometers with an acceleration range of ±2g (Zijlstra and Hof (2003), Jasiewicz et al. (2006), Simcox et al. (2005), Williamson and Andrews (2001), Lau and Tong (2008)) and ±5g (Mayagoitia et al. (2002) and Favre et al. (2008)) for the measurement of angle, angular velocity and accelerations of the lower limb. At the beginning of the study, two dual-axis accelerometers (ADXL311, Analog Devices (1995a)) with a sensitivity of ±2g were used in the sensor unit to calculate angles and linear accelerations. However, data taken in the earlier experiments contained parts that were saturated due to an insufficient acceleration range. The same problem has been reported in the literature (Gaffney et al. (2009)). Therefore, the ADXL311 was substituted with the LIS2L02AS4 from STMicroelectronics (STMicroelectronics (2007)) for a higher range of acceleration (±6g). The LIS2L02AS4 was selected as it was available in the laboratory at the time the experiment was carried out and could be easily soldered to a circuit board. The examples of other accelerometer that can be used are MMA6270QT from Freescale™ Semiconductor (Freescale Semiconductor (2006)) and ADXL302 from Analog Devices (Analog Devices (1995b)) which have a ±5g acceleration range. Various sampling rates have been used by other researchers, for example 40Hz (Simcox et al. (2005)), 100Hz (Williamson and Andrews (2001), Mayagoitia et al. (2002) and Zijlstra and Hof

(2003)), 240Hz (Favre et al. (2008) and Lau and Tong (2008)). In the study, the accelerometers cut-off frequency was set to its maximum of 500Hz and 1kHz sampling rate was used.

The accelerometers were soldered on to two self built printed circuit boards (Figure 4-9(a)) and placed in a small sensor box with dimensions of 64x25x43mm (Figure 4-9(b)). One of the circuit boards is placed on top of the other using four spacers at the corners of the board. The first accelerometer is parallel to the board and the second accelerometer is inclined at an angle of $\pi/4$ as shown on the left hand side in the Figure 4-9(a). Power consumption of each sensor unit is (3.3 x 1.8mA=5.94mW).

In the sensor unit development, the second axis of a two-axis accelerometer is assumed to be 90° with respect to the first axis. When measured, it was found that the difference between s_1 and s_2 is 0.67° (89.33^0 for the first accelerometer) and between r_1 and r_2 is 1.50° (88.5^0 for the second accelerometer). There is no tolerance specified by the manufacturer on the setting of the 90^0 angle between the two accelerometers. Another error can exist when there is a misalignment between the first and second accelerometers. As in the algorithm, the second accelerometer should be placed 45° from the first accelerometer. The error found for the misalignment is 2.11° corresponding to 42.89^0. However, this error could be minimised by making sure that the accelerometers are soldered neatly and aligned with the PCB footprint.
The effects of a lack of the two axes not being set at 90^0 during manufacture can be minimised by measuring the sensitivity of one accelerometer (Vg^{-1}) and moving the MEMS circuit package through $\pm 90^0$ to determine the sensitivity of the second accelerometer. The sensitivity of the first accelerometer is measured by observing the static voltage output at a minimum value (corresponding to –g) then it is rotated (through 180^0) until the maximum value is found (corresponding to +g). The second axis could also be set up this way but then the output signal would contain a dc offset corresponding to the misalignment of the two accelerometers. In a similar way the sensitivity of the other two accelerometers are set by moving the whole unit through increments of 45^0. Therefore, calibration of the sensor can reduce (minimise) any systematic errors (offset) gains.

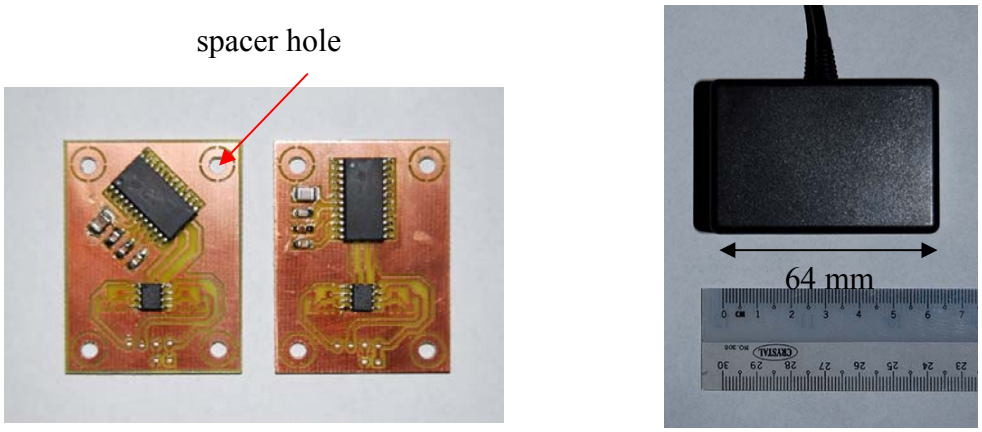

(a) (b)

Figure 4-9 (a) the circuit boards with soldered accelerometers, second accelerometer (left) and first accelerometer (right) (b) the sensor unit.

In order to apply the algorithm, the output of the individual axis of the sensor unit needs to be calculated using the earth gravitational field. Each of the axes produces a single output in voltage. This output can be calculated in unit of g using the following equation:

$$s_{out} = \frac{V_{out} - V_{zero-offset}}{V_{sensitivity}} \qquad (4\text{-}20)$$

where,

s_{out} = output of the accelerometer axis in g

V_{out} = output of the accelerometer axis in Volts

$V_{zero\text{-}offset}$ = accelerometer axis zero-offset in Volts

$V_{sensitivity}$ = accelerometer axis sensitivity in Vg^{-1}

($V_{zero\text{-}offset}$ and $V_{sensitivity}$ will be discussed in the calibration process)

4.6.1 The Axes and the Angles

To describe the angle of the individual axis of the sensor unit with respect to the earth horizontal plane, three angles the φ, β and γ are introduced. As has been explained earlier in this chapter, the angle between the adjacent axes is the α or 45° and the angle

measured using the algorithm is the angle between the s_1 and the horizontal plane, which is the θ. Let θ, φ, β and γ be the angles made between the individual axis (s_1, s_2, r_1 and r_2) of the sensor and the earth horizontal plane, the sensor unit can be represented as in Figure 4-10. The relationship between these angles are ($\varphi=\theta+45°$, $\beta=\theta+90°$, $\gamma=\theta+135°$).

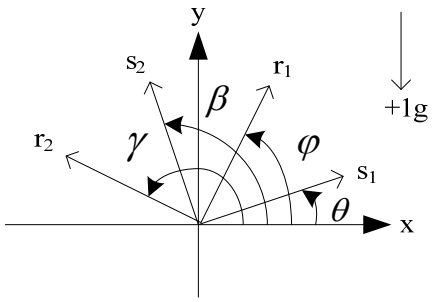

Figure 4-10 The angles of the accelerometers axes in the sensor unit.

4.6.2 The Sensor Unit Circuit

The schematic diagram of the accelerometer circuit board is shown in Figure 4-11. It is divided into two parts, the accelerometer and the operational amplifier. In the accelerometer part, the typical decoupling capacitors used for the power supply are 10uF and 0.1uF. A 3.3nF capacitor was chosen for the filter to set the cut-off frequency at 500Hz and placed at the accelerometer output. The output of the accelerometer can be buffered using an operational amplifier such as the ICL7621. The resistors, R1, R2, R3 and R4 can be set to adjust the overall gain of the signal.

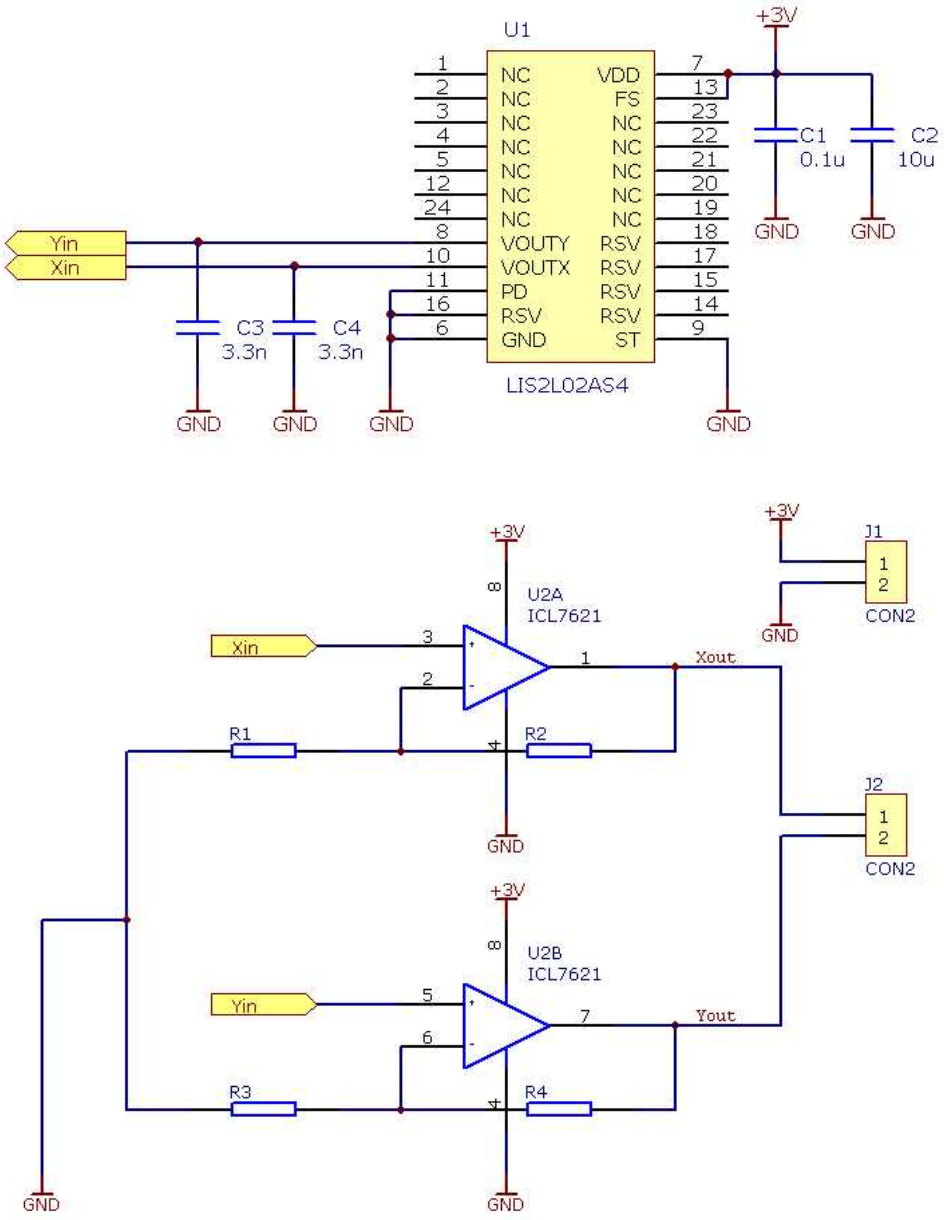

Figure 4-11 The accelerometer circuit board schematic diagram.

4.6.3 The Calibration Process

The accelerometers in the sensor unit need to be calibrated before any experiment is carried out. The sensitivity and the zero offset were determined and used to calculate the accelerometers output in unit of g. The sensitivity is a measure of how much the output of a sensor changes as the input acceleration changes and it is measured in Vg^{-1}. In the experiment, the sensor was rotated such that the sensing axis was orthogonal to

the earth's surface. First, it was aligned vertically ($\theta = \pi/2$) and then it was rotated through an angle of ($\theta=\pi$) corresponding to measurement of +1g and -1g as shown in Figure 4-12. According to the datasheet (STMicroelectronics (2007)), LIS2L02AS4 accelerometer has a typical non-linearity value of ±0.3% for the full scale of 2g. It is assumed that the same value can be applied to the full scale 6g to estimate the effect on the angle calculation using the sensor unit algorithm (Equation 4-19). In the equation, there are three additions/subtractions for the numerator and three for the denominator. This would mean an error of 0.3% + 0.3% + 0.3% for the numerator and the same for the denominator. Hence, there will be 1.8% typically as an error. The most effect will be near to 0 degree, for example ATAN of 0 is 0 degree and the ATAN of 0.018 is 1.03 degrees. Therefore, the typical expected error due to the non-linearity is ±1 degree which has only a small effect on the estimation of the angle. The sensitivity, $V_{sensitivity}$ can be calculated using equation 4-21, where V_{1g} is the measurement at +1g and V_{-1g} is the measurement at -1g.

$$V_{sensitivity} = \frac{1}{2g}\left(V_{1g} - V_{-1g}\right) \tag{4-21}$$

The zero offset, $V_{zero\text{-}offset}$ is to centre the output around zero and set as the midpoint between the +1g and the -1g measurements as described by equation 4-22.

$$V_{zero-offset} = \frac{1}{2}\left(V_{1g} + V_{-1g}\right) \tag{4-22}$$

The calibration is done for all axes s_1, s_2, r_1 and r_2.

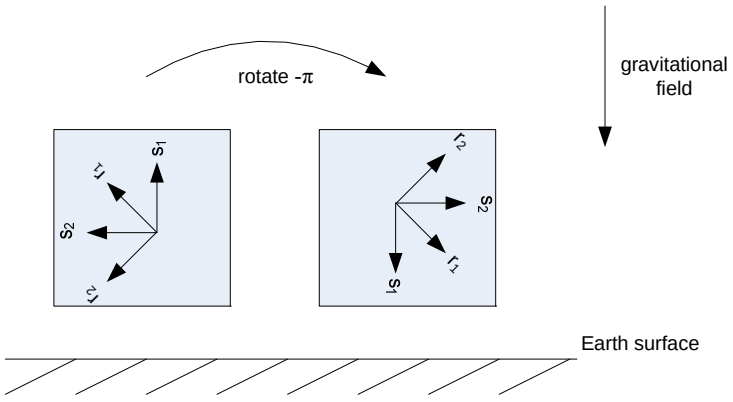

Figure 4-12 Schematic representation of two dual-axis accelerometers in a gravitational field under calibration process, s_1 measurement at -1g (left) and +1g (right). The process is repeated for s_2, r_1 and r_2.

4.7 The Data Acquisition and the Software

The data acquisition system used in the experiment was the DAQPad-6015 from National Instrument Ltd. The acquisition system has sixteen analog inputs if used as single ended or eight analog inputs if used as differential. It has a sampling rate of $200kSs^{-1}$ and if all sixteen channels are used, the rate is $12.5kSs^{-1}$ for each channel. The system has 16-bit resolution ADC. All signals in the experiments were sampled at 1kHz using the continuous analog mode. All measurements were taken using LabVIEW™ 8.0 and the data was stored in the pc memory. The data was then analysed off-line using Microsoft Office Excel© and Matlab® R2006b.

4.8 Discussion

The algorithm has been derived using four sensors output to calculate for segment angle, horizontal acceleration and vertical acceleration. To solve for the three variables analytically, four equations were needed instead of three. This redundancy could makes the measurement become more robust. There are no limits on the bandwidth of angle, horizontal acceleration or vertical acceleration and so the full frequency response of the accelerometers can be exploited (for the devices tested this is 500Hz). Some work has been done to solve the three variables analytically using only three equations (three sensor outputs), however there is no solution (Appendix B). Equation B-15 and B-20 will have a division by zero when Equation B42 and B43 are substituted into the equations. Another arrangement has been considered by placing three single axis accelerometers with $2\pi/3$ (120°) between the axes and the equations derived show that they are linearly dependent and therefore have a unique solution (Appendix C).

Pure accelerations which are not influenced by any gravitational field can be measured by arranging two of the sensor units as in Figure 4-13. The first sensor unit should be orthogonal to the second sensor unit. The first sensor unit will detect whether the second sensor unit is in a horizontal plane or not. If the second sensor unit is in a horizontal plane then the signals coming out from the individual axes of the sensor are the pure accelerations which are not influenced by any gravitational field.

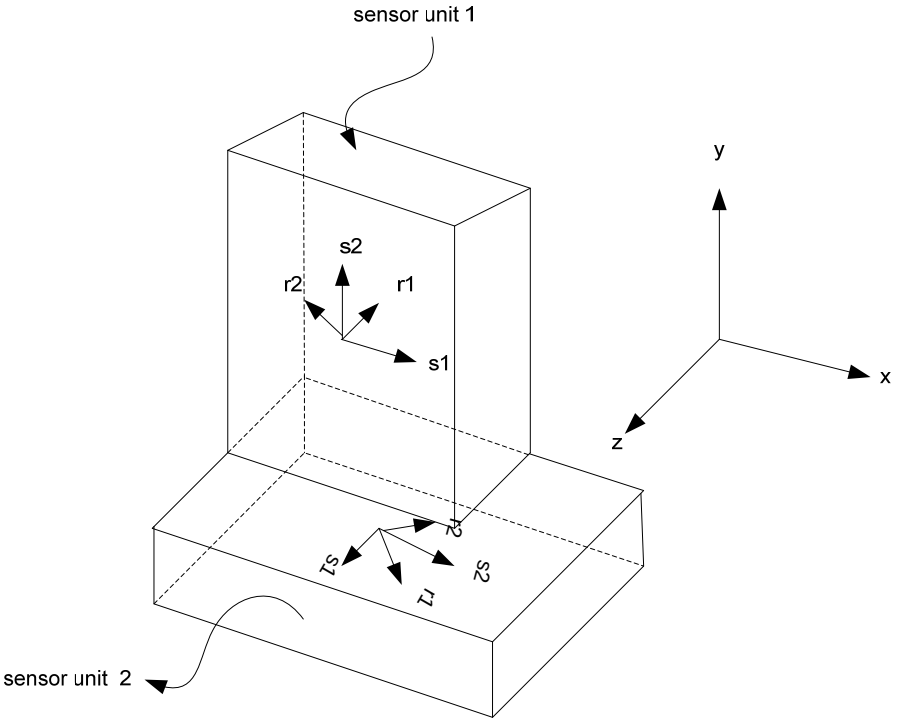

Figure 4-13 Two sensor units arrangement for measuring pure accelerations.

4.9 Conclusions

The sensor unit algorithm has been developed using two dual axis accelerometers arranged with 45 degrees between the sensor axes. The sensor unit algorithm has been designed to measure a segment angle from 0 to 360 degrees with respect to the earth's horizontal plane, however the sign of the numerator and the denominator of the equation in the algorithm must be take into account when calculating the angle. This range is more than sufficient to measure the segment angle of the lower limbs. The typical expected error due to the non-linearity of the accelerometer is ±1 degree which has only a small effect on the estimation of the angle. Each sensor unit consists of two dual axis accelerometers and consumes about 5.94mW of power. The accelerometers have been set to ±6g, with a cut-off frequency of 500Hz and sampled at1kHz to measure the angle and linear accelerations of a segment.

Chapter 5
Verification of the Sensor Unit Algorithm

5.1 Introduction

The sensor unit algorithm has been developed in the previous chapter. This chapter presents the experimental methods and results on some experiments using the sensor unit algorithm. The experiments are to

- identify the output of the individual axes of the sensor unit in static and dynamic conditions. The output is used to verify the signs of the terms in the equation of the sensor unit algorithm. It is important to ensure that the signs used in the equations are correct.
- verify the angle measurement from the sensor unit with a test apparatus, consisting of an aluminium arm with a potentiometer to provide a second measurement for comparison with the unit. The angle measurement to be verified ranges around a full circle (360 degrees). Since the test apparatus can only rotate up to 240 degrees, the test apparatus is also placed upside down and clamped to a table for the remaining range of angle measurement.
- demonstrate the kinematic measurement of a normal subject during walking and leg swing while seated using the sensor unit algorithm. From these measurements, some observations were made such as the maximum linear accelerations (horizontal and vertical) and angle range during walking. This is

to ensure that the acceleration range and cut off frequency used are sufficient for application.

5.2 The Experimental Methods and Materials

5.2.1 The Test Apparatus (Barnes et al. (2006))

The test apparatus used to verify the angle measurement of the sensor unit algorithm is a mechanical arm which is a simple inverted pendulum driven by a dc motor as shown in Figure 5-1. The angle of the arm is measured by a potentiometer that is supplied with a constant voltage. The voltage from the wiper terminal of the potentiometer is proportional to the angle that the arm makes with the Earth's horizontal axis. The full range of the arm is 240° and the directions of the swing can be controlled by changing the voltage polarity of a slider (50Ω potentiometer). The speed of the swing is adjusted by varying the current supply to the dc motor. The dc motor together with the circuit board was powered with ± 7V and 500mA supply for operation. For the tests, a sensor unit (Chapter 4, p62) was attached to the arm of the test apparatus using a double sided tape at two different locations as shown in Figure 5-1: 70mm and 230mm from rotation point.

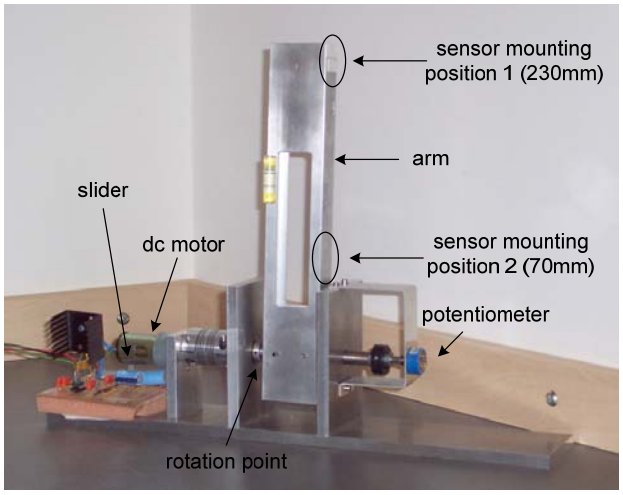

Figure 5-1 Test apparatus used to verify sensor unit algorithm by comparing the angle calculated from the potentiometer and angle calculated from the sensor unit.

The angle, θ (shown on the right in Figure 5-2) is calculated using Equation 5-1 for the range 0° to 200°. Equation 5-2 is used when the platform of the apparatus turned upside down and the range is 180° to 360°.

$$\theta = \frac{V_\theta - V_0}{V_{180} - V_0} \times 180° \tag{5-1}$$

where

V_θ = potentiometer output at angle θ in Volts
V_0 = potentiometer output at 0 degree in Volts
V_{180} = potentiometer output at 180 degrees in Volts

and

$$\theta = \left[\frac{V_\theta - V_{180}}{V_{360} - V_{180}} \times 180° \right] + 180° \tag{5-2}$$

where

V_θ = potentiometer output at angle θ in Volts
V_{180} = potentiometer output at 180 degrees in Volts
V_{360} = potentiometer output at 360 degrees in Volts

It is important to ascertain the accuracy of the test apparatus potentiometer as it will be used as a reference to validate angle measurement of the sensor unit algorithm. To obtain the potentiometer accuracy, the voltage output from the potentiometer was measured at five different orientations at 0°, 45°, 90°, 135° and 180° with respect to the horizontal plane using a protractor and a sprit level. The measurements were taken five times for each of the angles.

Table 5-1 shows the calculated mean and the range of the voltage output from the potentiometer at five different calibrated angles using protractor and spirit level as references. The protractor had graduations every 1^0. As the arm was set at integer

values then the arm could be set at angle with an accuracy of about $\pm 0.5^0$. The angles from the potentiometer measurements presented in section 5.3.3 could therefore have an error of 0.5^0.

Table 5-1 The mean and the range of the voltage output of the potentiometer, N=5.

Angle (°)	**0**	**45**	**90**	**135**	**180**
Mean (volts)	1.094	1.482	1.888	2.281	2.693
Range(volts)	1.093-1.095	1.480-1.485	1.879-1.894	2.280-2.282	2.691-2.695

Table 5-2 shows the mean and the range of the calculated angle using the voltage output from the potentiometer. The angle was calculated using the Equation 5-1. The angle calculation was accurate to 1.3° at 45 degrees, 0.6° at 90 degrees and 1.4° at 135 degrees using the voltage output from the potentiometer. The 0° and 180° were used as the references in the calculation of the angle.

Table 5-2 The mean and the range of the angle calculated from the potentiometer output.

Angle (°)	**0**	**45**	**90**	**135**	**180**
Mean (°)	0.0	43.7	89.4	133.6	180.0
Range (°)	0.0-0.0	43.4-44.2	88.4-90.2	133.5-133.8	180.0-180.0

5.2.2 The Static Acceleration Experimental Method

To verify the sign (plus or minus) of the gravitational acceleration (static acceleration) or g in the sensor unit algorithm (Chapter 4, p57), the sensor unit is attached to the test apparatus's arm (Figure 5-2) and the outputs were measured at angles of 0°, 90°, 180° and 270°. The measurements were recorded for each of the angles orientation when the test apparatus's arm was stationary. For the 270° measurement, the test apparatus was turned upside down and attached to a table using G-clamps. A spirit level and a protractor were used to calibrate the angle of the test apparatus's arm relative to the horizontal plane. All the measurements were taken approximately seven seconds. The voltage outputs of the sensor unit were recorded using the data acquisition system,

DAQPad-6015 and the individual axis of the sensor unit was then calculated in unit of g using Equation 4-20.

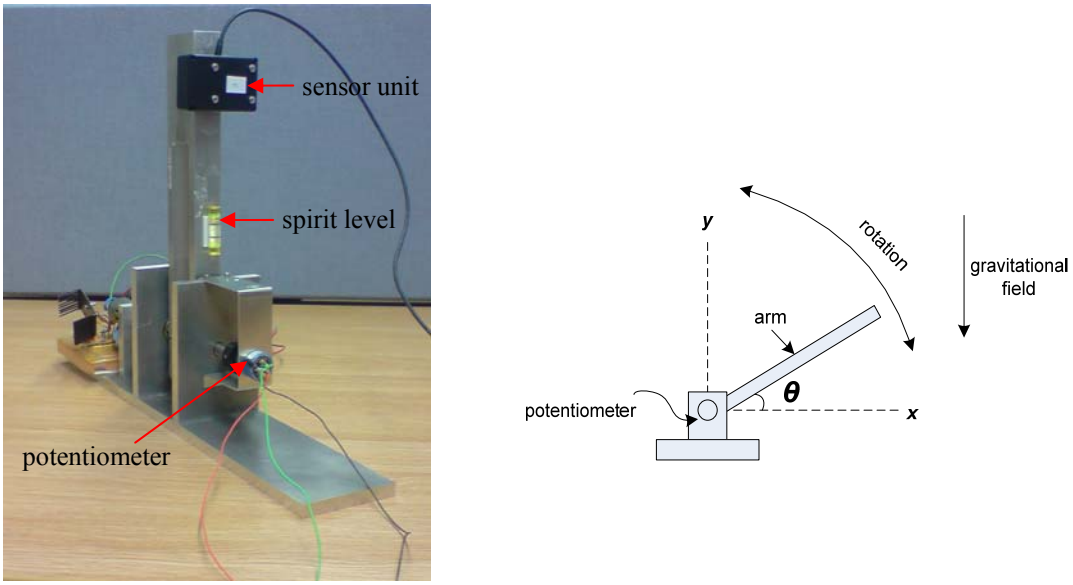

Figure 5-2 The sensor unit attached to the test apparatus arm which swing as inverted pendulum with potentiometer as the point of rotation.

5.2.3 The Dynamic Acceleration Experimental Method

The experiment is designed to identify the outputs of the sensor unit when it is accelerated in various directions at different angles. The outputs are used to verify the signs (plus or minus) of the horizontal acceleration, $\ddot{x}$ and the vertical acceleration, $\ddot{y}$ in the algorithm compared to the theoretical equations. The spirit level and the protractor were used to calibrate the angle between the test apparatus's arm and the horizontal plane. The sensor unit was attached to the test apparatus's arm which was inclined in a specific angle, θ as shown in Figure 5-2. The first measurement was taken with the test apparatus's arm inclined horizontally at θ equals to 0°. The other measurements were taken at angles of 90°, 180° and 270°. Initially, the test apparatus was stationary, and then the apparatus was accelerated by moving it in a specific direction and stopped. For each of angle, the measurements were taken for about two seconds. For each of the angle, the apparatus was moved in four directions to the right (+x), left (-x), up (+y) and down (–y) (Figure 5-3). In the procedure, the arm of the test apparatus was maintained at a constant angle as far as possible since the apparatus was moved manually. Although the accelerometers have been set to 6g acceleration range,

the speed of the movement was controlled for about 2g performed in 0.5s to produce uniform plots. The most important observation in this experiment is the sign of the signal, whether it is going positively or negatively, when a movement is applied to the sensor from a static state. From this, the sign (plus or minus) in the algorithm's equations can be validated. The voltage outputs of the sensor unit were recorded and the individual axis of the sensor unit was then calculated in g using the Equation 4-20.

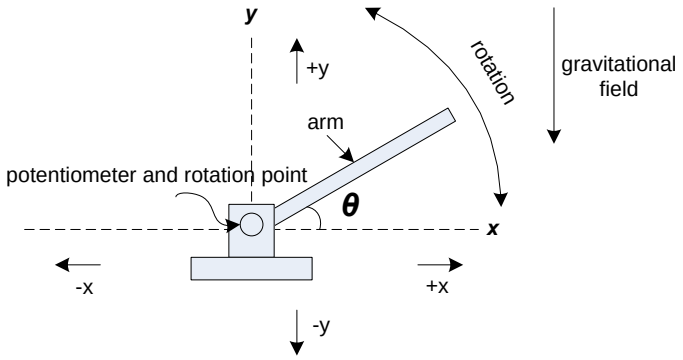

Figure 5-3 The angle and the accelerations directions for dynamic acceleration measurement.

5.2.4 Experimental Method for Angle Measurements during Rotation of the Arm

The purpose of the experiment is to verify the angle measurement of the sensor unit algorithm derived in Chapter 4. The sensor unit was attached to the test apparatus's arm (Figure 5-2) and the measurement of the sensor unit outputs as well as the voltage output from the potentiometer were recorded using the data acquisition DAQPad-6015 during rotation of the arm from 0° to 200° and back to 0° with respect to horizontal plane. The apparatus was then turned upside down, for the measurements of θ from 180° to 360° and back to 180°. These measurements were taken when the sensor unit was placed on the test apparatus's arm at distances of 230mm and 70mm (only measurements from 180° to 360° and back to 180° were performed) away from the rotation point (Figure 5-3). This procedure is carried out to investigate the effect of the different distances of the sensor attachment from the rotation point on the angle measurement of the sensor unit algorithm. The voltage output from the potentiometer was used in Equation 5-1 and 5-2. The sensor unit outputs were calculated in unit of g using Equation 4-20 and then the angle calculated using Equation 4-19. The angle

measurement of the sensor unit was compared with the angle measurement of the potentiometer.

5.2.5 Experimental Method for the Kinematic Measurement of a Normal Subject during Walking and Leg Swing while Seated

The experiment was designed to demonstrate the kinematic patterns such as angles and accelerations of a lower limb segment during walking. In the experiment, a sensor unit was attached on a shank of a normal subject just below the knee as shown in Figure 5-4. A footswitch as a reference sensor was placed in the shoe under the heel of the same leg to detect heel rise and heel strike events during walking. A measurement from both sensors during the subject walking for 4 metres on a carpeted surface with self selected speed has been recorded. The algorithm in (Chapter 4, p57) was used to calculate the angle (angle between the leg segment and the horizontal plane), the vertical acceleration and the horizontal acceleration using the output from the sensor unit. These calculated angle and accelerations were then plotted to demonstrate the kinematic pattern of the lower limb segment during walking. The test was repeated ten times to investigate the consistency of the measurements.

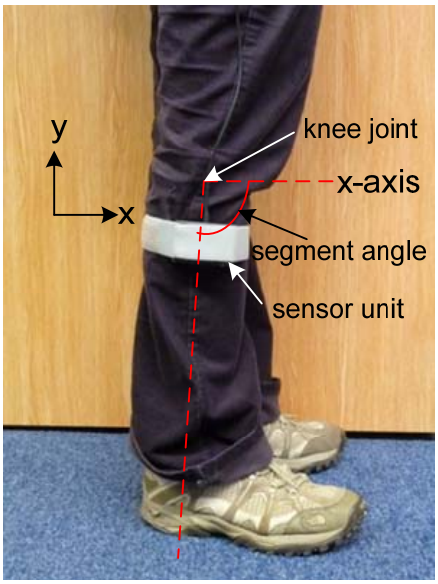

Figure 5-4 The sensor unit attached to the shank showing a single segment angle.

Another test to demonstrate the kinematic of the lower limb segment was carried out with the same sensor attachment (Figure 5-4) but this time while the leg was swinging as a simple pendulum. The subject was seated on a high bench while the leg swings freely. By using the algorithm (Chapter 4, p57), the angle (angle between the leg segment and the horizontal plane), the vertical acceleration and the horizontal acceleration were calculated.

5.3 The Experimental Results

5.3.1 The Static Acceleration

The theoretical and measured (mean and standard deviation) outputs of the stationary sensor unit at different angles of θ equal to 0, 90, 180 and 270 degrees are summarised in Table 5-3 for comparison.

Table 5-3 Theoretical (in grey) and measured values of the sensor unit outputs in unit of g at different angles when the sensor unit is stationary. The mean and standard deviation of the sensor unit output measurement taken over seven seconds (7000 points). ($\varphi=\theta+45°$, $\beta=\theta+90°$, $\gamma=\theta+135°$)

Sensor unit angle, θ (°) mean(SD)	**s_1 at θ mean(SD)**	**s_2 at β mean(SD)**	**r_1 at φ mean(SD)**	**r_2 at γ mean(SD)**
0	0	-1	-0.7071	-0.7071
0.85(0.1833)	-0.0380(0.0044)	-0.9992(0.0031)	-0.7109(0.0027)	-0.7224(0.0029)
90	-1	0	-0.7071	0.7071
90.45(0.1079)	-1.0181(0.0034)	0.0233(0.0024)	-0.7083(0.0026)	0.6975(0.0027)
180	0	1	0.7071	0.7071
180.44(0.1840)	0.0142(0.0037)	0.9962(0.0023)	0.7058(0.0029)	0.7040(0.0030)
270	1	0	0.7071	-0.7071
270.59(0.0838)	0.9951(0.0031)	-0.0166(0.0019)	0.7088(0.0023)	-0.7147(0.0024)

As can be seen in the table, based on the theory, the output of the sensor unit (the individual axis: s_1, s_2, r_1 and r_2) follows the negative sine of the individual angle (θ, φ, β and γ see Figure 4-10, (Chapter 4, p65) and has the value between -1g and 1g. The

measured output is close to the theory. Noted that, θ, φ, β and γ are the angles made between the individual axis (s_1, s_2, r_1 and r_2) and the horizontal plane. The result shows that when an angle (either θ, φ, β or γ) is between 0 and 180 degrees , the output is negative and when the angle is between 180 and 360 degrees the output is positive. The output for the angle at 0, 180 and 360 degrees can be either 0g, slightly positive or slightly negative. In the theory, the output for the angle at 0, 180 and 360 degrees is 0g.

5.3.2 The Dynamic Acceleration

Figure 5-5 to Figure 5-8 show the output waveforms when the sensor unit at a specific angle was initially static, then moved in the +x, -x, +y and –y directions (Figure 5-3) and back to being stationary. The rest of the sensor unit outputs can be found in Appendix D. In these figures, regions A and C show the output when no movement occurred, region B shows the output when a movement occurred. The vertical dotted line between region A and B in the figures indicates the starting point and between B and C the stopping point. Observations of s_1 (section B in the top left plot of Figure 5-5) show that when the unit is accelerated in the +x direction, s_1 is negative. This general effect is shown as the "<0g" entry in the top left of Table 5-4. In the second part of the waveform in section B of Figure 5-5, s_1 is positive where the unit is decelerated as expected. Similarly, the signal s_2 in the top right plot of Figure 5-5 has a value of "-1g" as shown in the first entry of the column labelled s_2 (β=90^0). The range in this signal over the time labelled B in this plot is -0.98g to -0.19g with a mean value of -0.98g (SD = 0.31). All the entries in Table 5-4 have been determined using the waveforms from the figures and show the correct behaviour of the devices from these experimental observations.

In Figure 5-5 to Figure 5-8, all the movements were carried out manually. The means for the signals when they are constant are very close to the expected values for example s_2 equals to -1.00g in Figure 5-6. The variability in this signal is not large (SD = 0.16) and is due to the imprecise movements that have been made manually. Table 5-4 summarise the outputs in region B with specific angles and movement directions (+x, -x, +y and –y). From the first two rows in the tables, it is evident that when the individual axis of a sensor unit is orthogonal to the horizontal plane, movement to +x

and –x the output is constant for example (s_2 at β=90°, s_1 at θ=90°, s_2 at β=270° and s_1 at θ=270°). When the individual axis of the sensor unit is parallel to the horizontal plane, movement to +y and –y the output is constant for example (s_1 at θ=0°, s_2 at β=180°, s_1 at θ=180° and s_2 at β=360°). The other outputs are more negative when the sensor unit is moved in the same direction as the sensing axis and more positive when the sensor unit is moved in opposite direction of the sensing axis for +x and –x directions as can be seen in the first two rows of the tables (Table 5-4) and for +y and –y directions as can be seen in the last two rows of the same table.

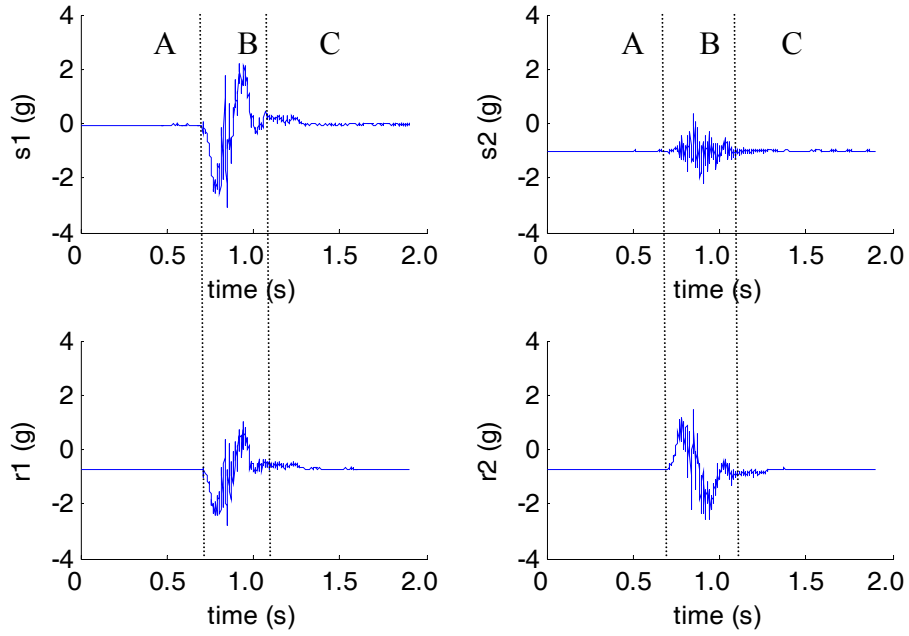

Figure 5-5 The sensor unit outputs (s_1, s_2, r_1 and r_2) in unit of g at θ equals to 0 degree with movement to the right (+x). The means and standard deviations over the time in section B are -0.19g (±1.26), -0.98g (±0.31), -0.80g (±0.85) and -0.62g (±0.91) for s_1, s_2, r_1 and r_2 respectively.

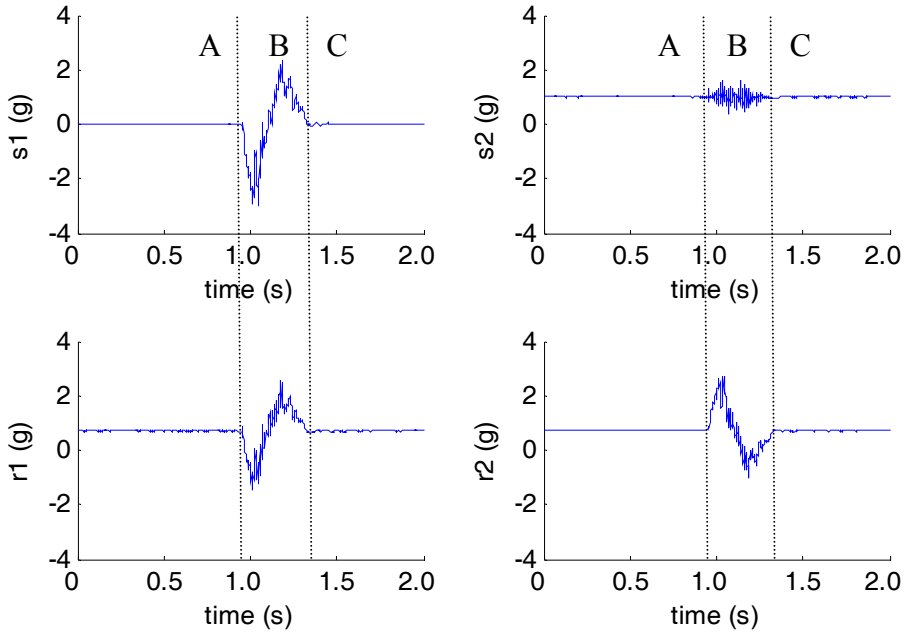

Figure 5-6 The sensor unit output (s_1, s_2, r_1 and r_2) in unit of g at θ equals to 180 degrees with movement to the left (-x). The means and standard deviations over the time in section B are 0.02g (±1.22), -1.00g (±0.16), 0.72g (±0.85) and 0.71g (±0.86) for s_1, s_2, r_1 and r_2 respectively.

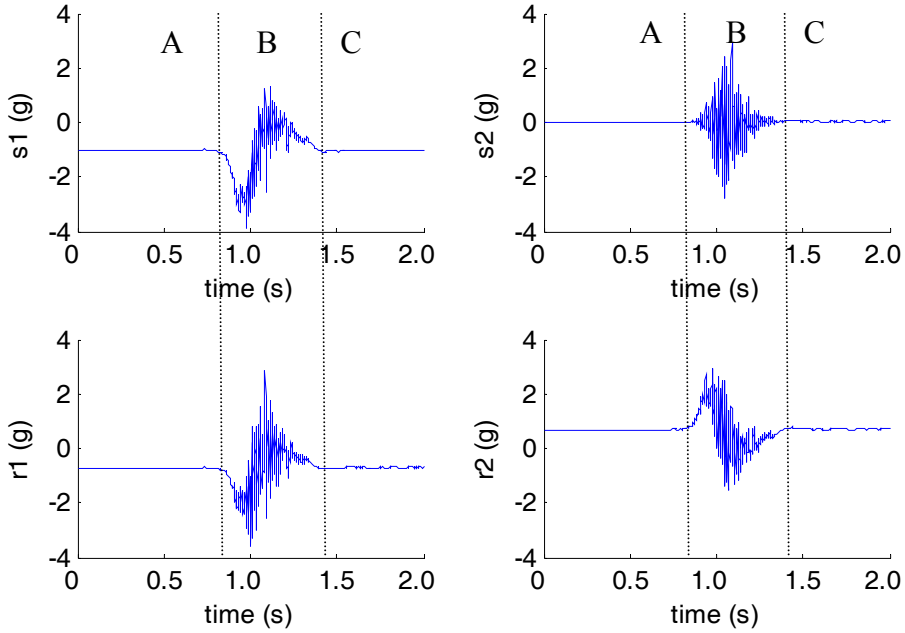

Figure 5-7 The sensor unit output (s_1, s_2, r_1 and r_2) in unit of g at θ equals to 90 degrees with movement to up (+y). The means and standard deviations over the time in section B are -1.02g (±0.97), 0.00g (±0.57), -0.72g (±0.82) and 0.68g (±0.76) for s_1, s_2, r_1 and r_2 respectively.

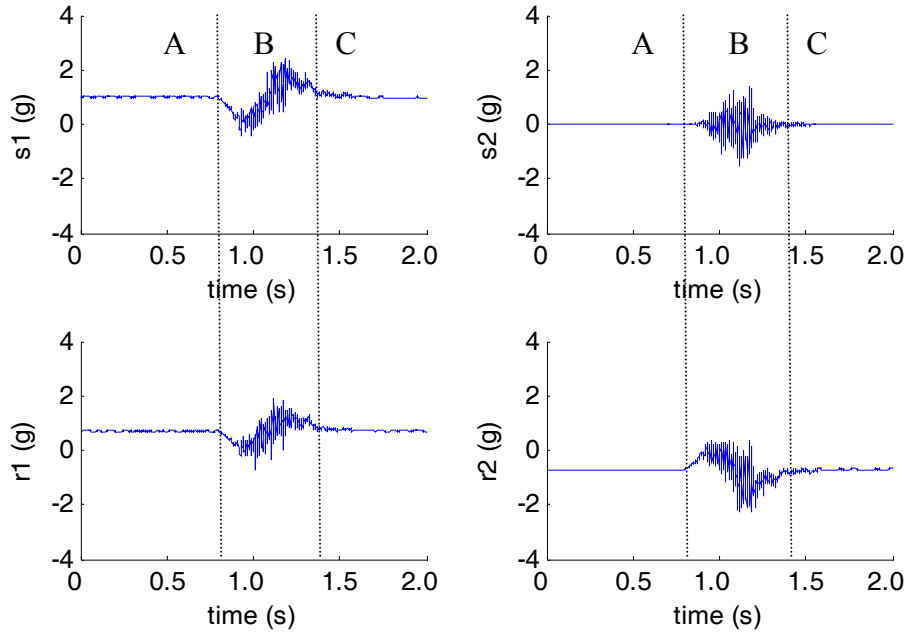

Figure 5-8 The sensor unit output (s_1, s_2, r_1 and r_2) in unit of g at θ equals to 270 degrees with movement to down (-y). The means and standard deviations over the time in section B are 0.98g (±0.53), -0.02g (±0.31), 0.70g (±0.40) and -0.71g (±0.46) for s_1, s_2, r_1 and r_2 respectively.

Table 5-4 The sensor output in unit of g for different movement directions and angles, θ ($\varphi=\theta+45°$, $\beta=\theta+90°$, $\gamma=\theta+135°$).

Movement at $\theta=0°$	**s_1 ($\theta=0°$)**	**s_2 ($\beta=90°$)**	**r_1 ($\varphi=45°$)**	**r_2 ($\gamma=135°$)**
right, +x	< 0g	-1g	< -0.7071g	> -0.7071g
left, -x	> 0g	-1g	> -0.7071g	< -0.7071g
up, +y	0g	< -1g	< -0.7071g	< -0.7071g
down, -y	0g	> -1g	> -0.7071g	> -0.7071g

Movement at $\theta=90°$	**s_1 ($\theta=90°$)**	**s_2 ($\beta=180°$)**	**r_1 ($\varphi=135°$)**	**r_2 ($\gamma=225°$)**
right ,+x	-1g	> 0g	> -0.7071g	> 0.7071g
left, -x	-1g	< 0g	< -0.7071g	< 0.7071g
up, +y	< -1g	0g	< -0.7071g	> 0.7071g
down, -y	> -1g	0g	> -0.7071g	< 0.7071g

Table 5-4 (continued)

Movement at *θ=180°*	**$s_{1\ (\theta=180°)}$**	**$s_{2\ (\beta=270°)}$**	**$r_{1\ (\varphi=225°)}$**	**$r_{2\ (\gamma=315°)}$**
right, +x	> 0g	1g	> 0.7071g	< 0.7071g
left, -x	< 0g	1g	< 0.7071g	> 0.7071g
up, +y	0g	> 1g	> 0.7071g	> 0.7071g
down, -y	0g	< 1g	< 0.7071g	< 0.7071g

Movement at *θ=270°*	**$s_{1\ (\theta=270°)}$**	**$s_{2\ (\beta=360°)}$**	**$r_{1\ (\varphi=315°)}$**	**$r_{2\ (\gamma=45°)}$**
right, +x	1g	< 0g	< 0.7071g	< -0.7071g
left, -x	1g	> 0g	> 0.7071g	> -0.7071g
up, +y	> 1g	0g	> 0.7071g	< 0.7071g
down, -y	< 1g	0g	< 0.7071g	> -0.7071g

5.3.3 The Angle Measurement of the Sensor Unit Algorithm

The angular difference between the sensor unit measurement and the potentiometer measurement has been calculated. After smoothing, a second difference between the sensor unit and the potentiometer was also calculated. The angle measured using the sensor unit was smoothed using a moving average with different windows lengths. A 0.3s window was found to give acceptable smoothing of the data. Shorter lengths did not remove the spiky nature of the raw data enough while longer lengths removed too much of the signal response. Figure 5-9 to Figure 5-12 show the waveforms of the angle measurement of the sensor unit and the potentiometer, the angular difference between the two measurements and the angular difference with a 0.3s of moving average when the sensor unit was at 230mm from the rotation point. Figure 5-13 and Figure 5-14 show the waveforms of the angle measurement of the sensor unit and the potentiometer, the angular difference between the two measurements and the angular difference with 0.3s of moving average when the sensor unit was at 70mm from the rotation point. The pattern of the angle measured using the sensor unit and the angle measured using the potentiometer was similar for example decreasing from 180 degrees

to 0 degree as in Figure 5-9(a) and Figure 5-9(b). The angular difference was more apparent when the arm of the apparatus swung between 250 and 270 degrees (the apparatus facing down) and between 70 and 90 degrees (the apparatus facing up) which may be caused by the jerky rotation of the arm. In Figure 5-9(a) to Figure 5-12(a), there is spike at time 3.8s, 4.2s, 3.8s and 1.8s respectively, caused by a jerky movement of the test apparatus when the angular difference ranged from 20 to 30 degrees in the raw data. These jerky effects are caused by the gearbox backlash of the motor which connects to the potentiometer shaft and the insufficient power of the motor used to rotate the test apparatus arm. As well as the jerky effect, the angular difference is caused by the slipping of the sensor unit attachment from the origin position when the arm swings.

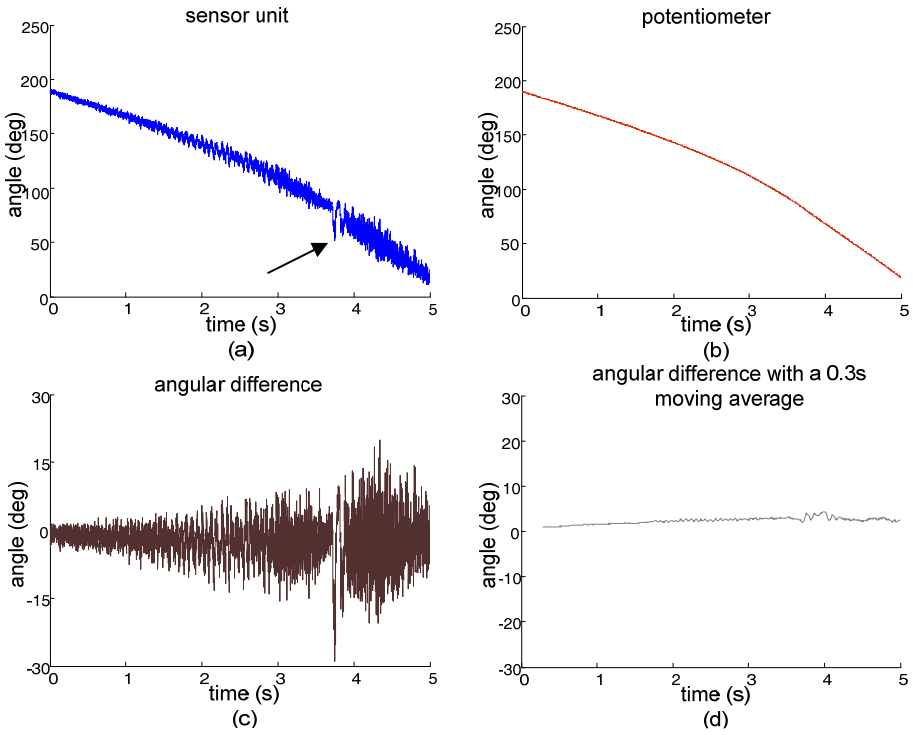

Figure 5-9 The angle measurement (180° to 0°) of (a) sensor unit at 230mm from rotation point and (b) potentiometer. The two angle measurements (c) difference and (d) difference with a 0.3s moving average.

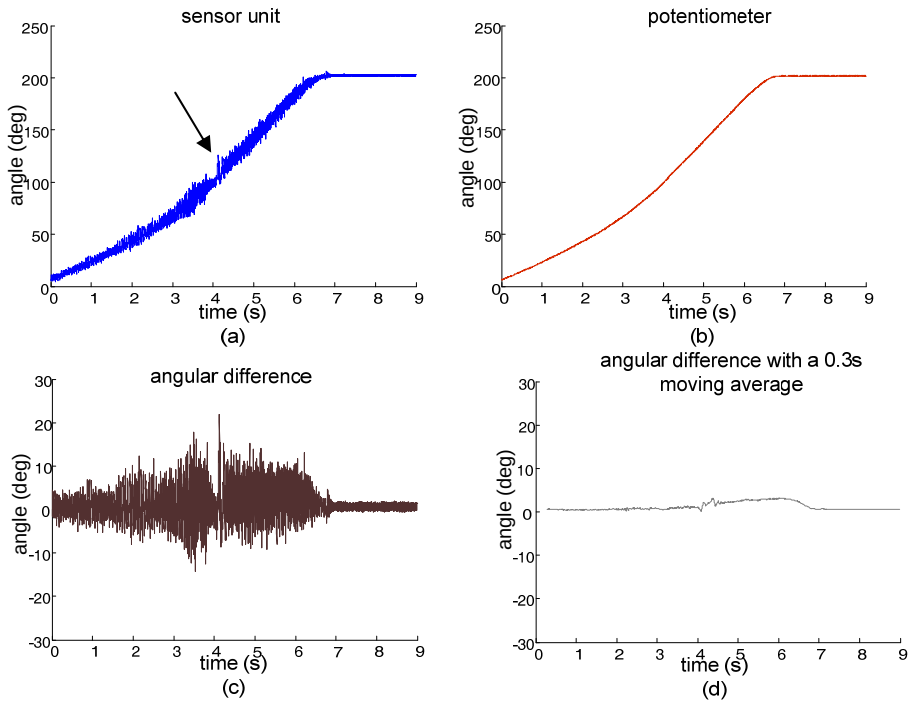

Figure 5-10 The angle measurement (0° to 180°) of (a) sensor unit at 230mm from rotation point and (b) potentiometer. The two angle measurements (c) difference and (d) difference with a 0.3s moving average.

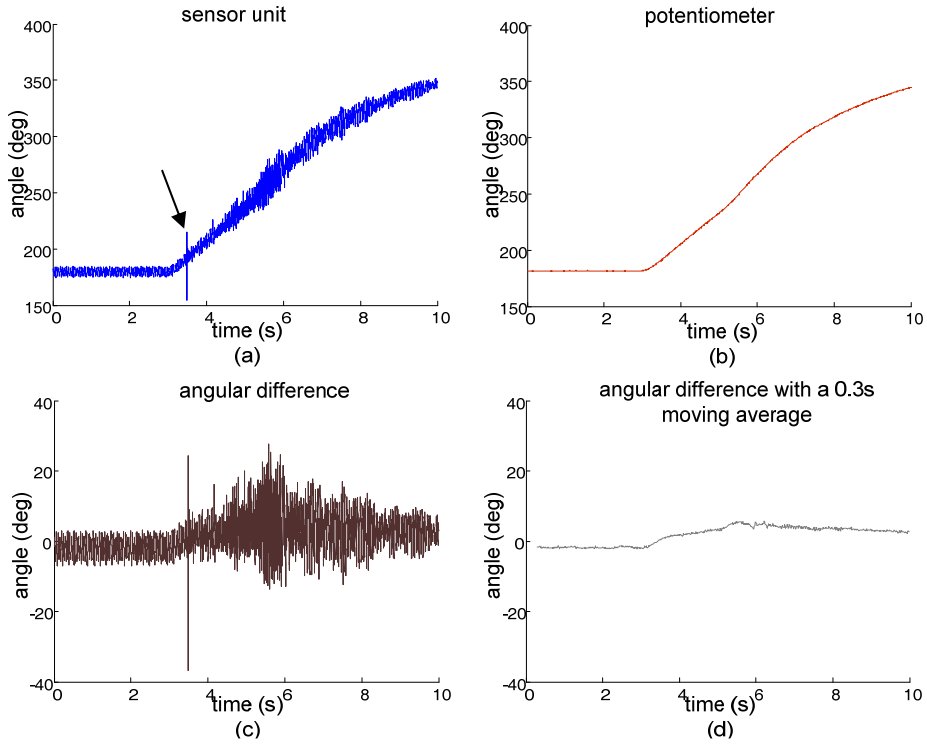

Figure 5-11 The angle measurement (180° to 360°) of (a) sensor unit at 230mm from rotation point and (b) potentiometer. The two angle measurements (c) difference and (d) difference with a 0.3s moving average.

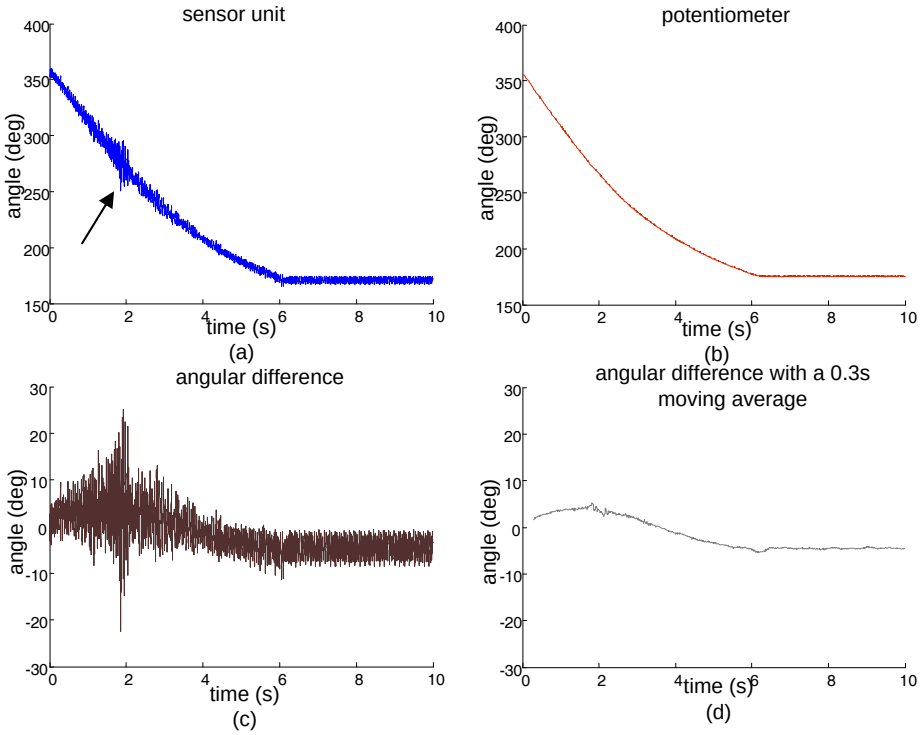

Figure 5-12 The angle measurement (360° to 180°) of (a) sensor unit at 230mm from rotation point and (b) potentiometer. The two angle measurements (c) difference and (d) difference with a 0.3s moving average.

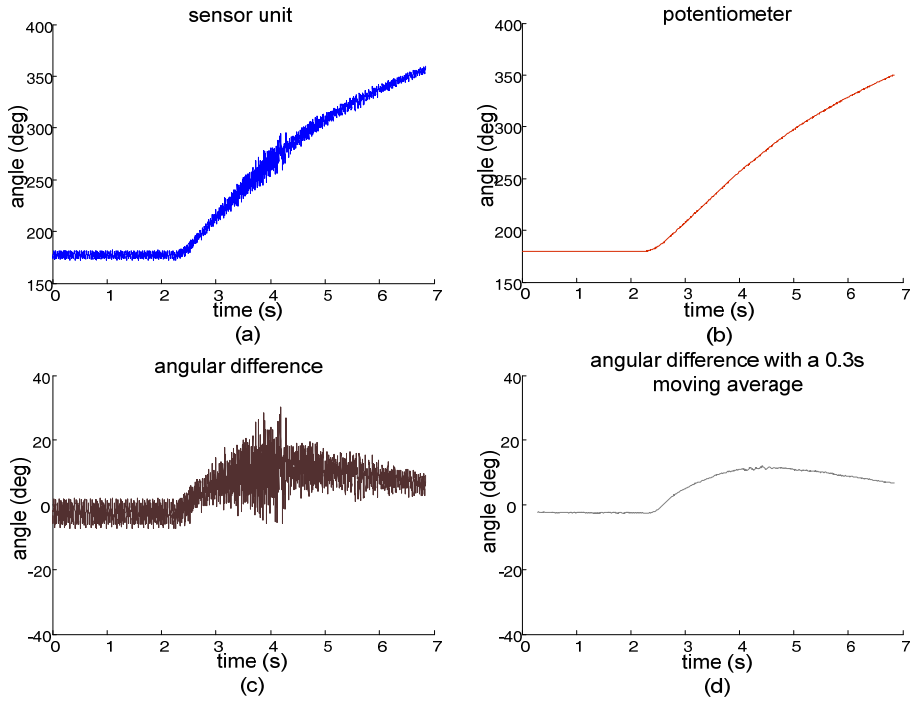

Figure 5-13 The angle measurement (180° to 360°) of (a) sensor unit at 70mm from rotation point and (b) potentiometer. The two angle measurements (c) difference and (d) difference with a 0.3s moving average.

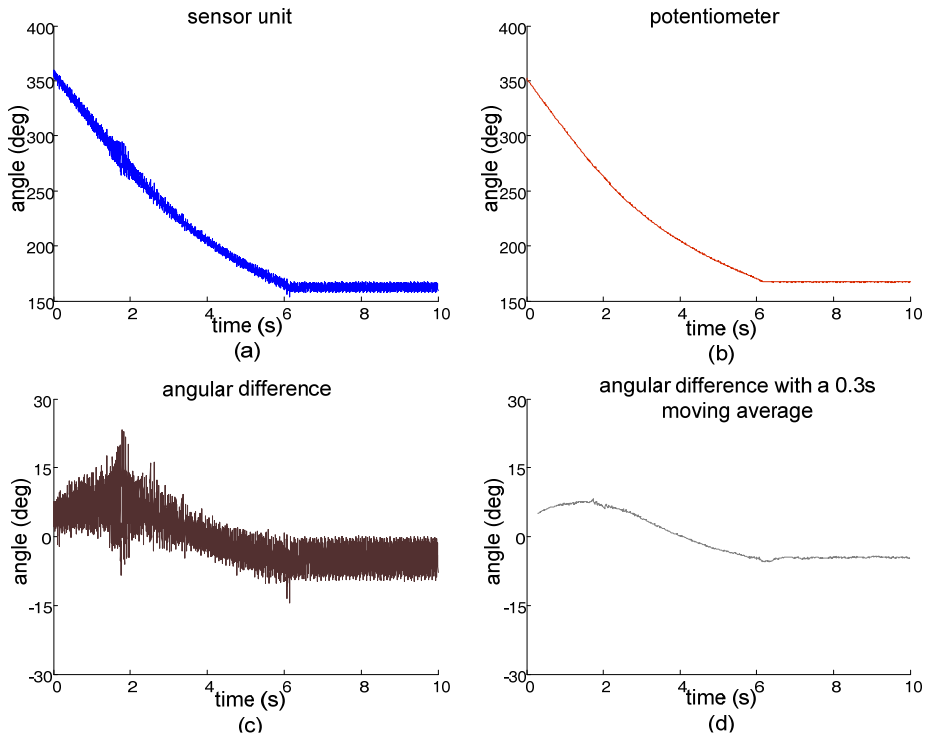

Figure 5-14 The angle measurement (360° to 180°) of (a) sensor unit at 70mm from rotation point and (b) potentiometer. The two angle measurements (c) difference and (d) difference with a 0.3s moving average.

The median, mean difference and standard deviation of the angle measurement between sensor unit and potentiometer are shown in Table 5-5 and 5-6. An analysis of the data shows that there is a possible error of between 0.68° and 4.33°. However, the results demonstrate that the sensor unit responds correctly. The possible sources of these errors have been discussed (Chapter 4, p66) and the error of the potentiometer measurement (section 5.2.1). Further experiments are needed to improve the test apparatus and confirm the known sources of error so that they can be reduced. In typical goniometry experiments, the typical accuracy is $\pm 2^0$ over the range ±90° (Biometrics Ltd (2010)) with a precision of 1^0. The sensor unit therefore has a similar performance for accuracy (mean difference) from the results shown in table 5-5 but the SD is much higher. A future aim would be to improve the precision to about 2^0 or better.

The results showed that the SD is smaller when a moving average is applied to the data. All of the data are very close to being normally distributed and this is shown in the histogram and high linearity of the cumulative plots presented in Appendix E. In Figure 5-16, there was an oscillation at around 4s of the trial shown in Figure 5-10. The mean

and SD of the data without this oscillation have showed a reduce mean from 1.37^0 to 0.63^0 and SD from 3.62^0 to 3.33^0.

Table 5-5 The median, mean difference and standard deviation of the angle measurement between sensor unit (at 230mm from rotation point) and potentiometer.

Angle range	Median (°)	Mean ± SD(°)	Median (°) with a 0.3s moving average	Mean ± SD(°) with a 0.3s moving average
180° to 0°	-1.97	-2.30 ± 4.54	-2.43	-2.34 ± 0.68
0° to 180°	1.11	1.37 ± 3.62	0.89	1.40 ± 0.96
180° to 360°	2.76	3.11 ± 4.15	3.35	3.23 ± 1.27
360° to 180°	-0.32	0.24 ± 4.65	1.11	0.36 ± 3.10

Table 5-6 The median, mean difference and standard deviation of the angle measurement between sensor unit (at 70mm from rotation point) and potentiometer.

Angle range	Median (°)	Mean ± SD (°)	Median (°) with a 0.3s moving average	Mean ± SD(°) with a 0.3s moving average
180° to 360°	8.48	8.51 ± 4.67	9.54	8.89 ± 2.44
360° to 180°	2.02	2.17 ± 5.44	3.10	2.32 ± 4.33

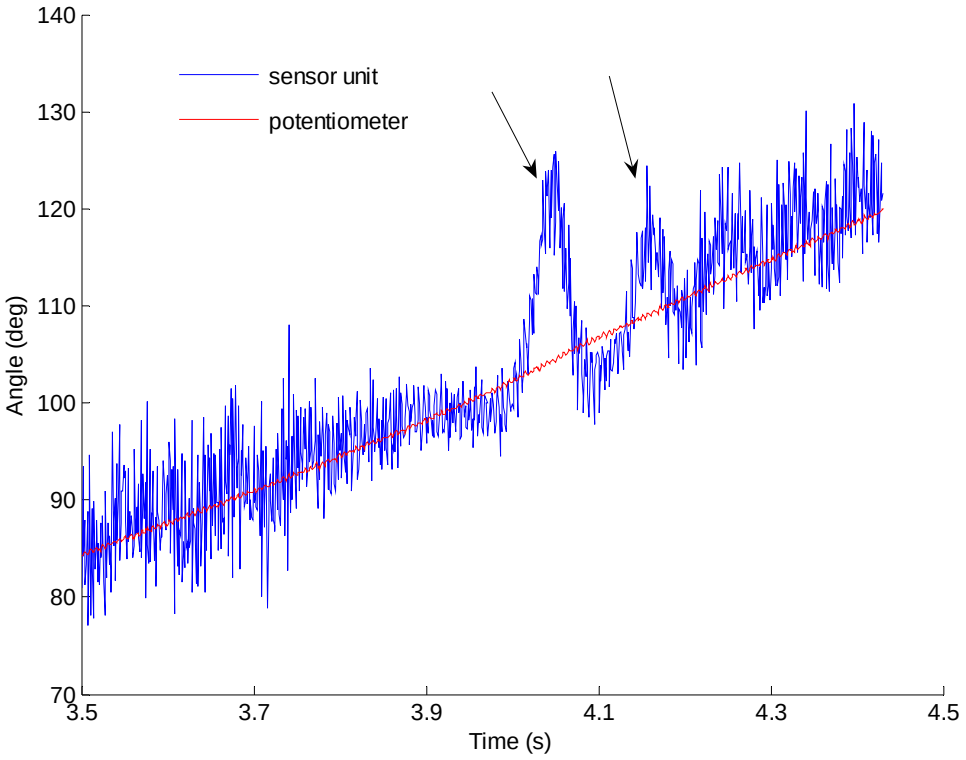

Figure 5-15 The angle signal oscillation occurs at around 4s for angle measurement from 0° to 180° when the sensor unit was at 230mm from rotation point.

5.3.4 The Kinematic Measurement of a Normal Subject during Walking and Leg Swings while Seated

Figure 5-16 and Figure 5-17 show the kinematic measurement of a normal subject walking with a footswitch as a reference. In both figures, the kinematic measurement such as the relative angle, the horizontal *x* acceleration and the vertical *y* acceleration calculated from the algorithm using the sensor output show a consistent repetitive pattern during the stance and swing phase for the five gait cycles. This preliminary result suggests that the algorithm and the sensor could be applied to the neurological patients to obtain a consistent repetitive pattern during walking which then could be used to detect important events to control an electrical stimulator. Shown in Figure 5-16 the maximum extension of the knee angle occurs about 100ms before heel strike in every cycle and this would be very useful to detect the events needed for example prior to heel strike, to stimulate the hamstrings muscle for preventing the knee

hyperextension at heel strike. The maximum shank segment angle with respect to the earth's horizontal plane during walking measured using the sensor unit is about 140 degrees. The maximum horizontal and vertical accelerations observed were 0.5g and 2.5g respectively.

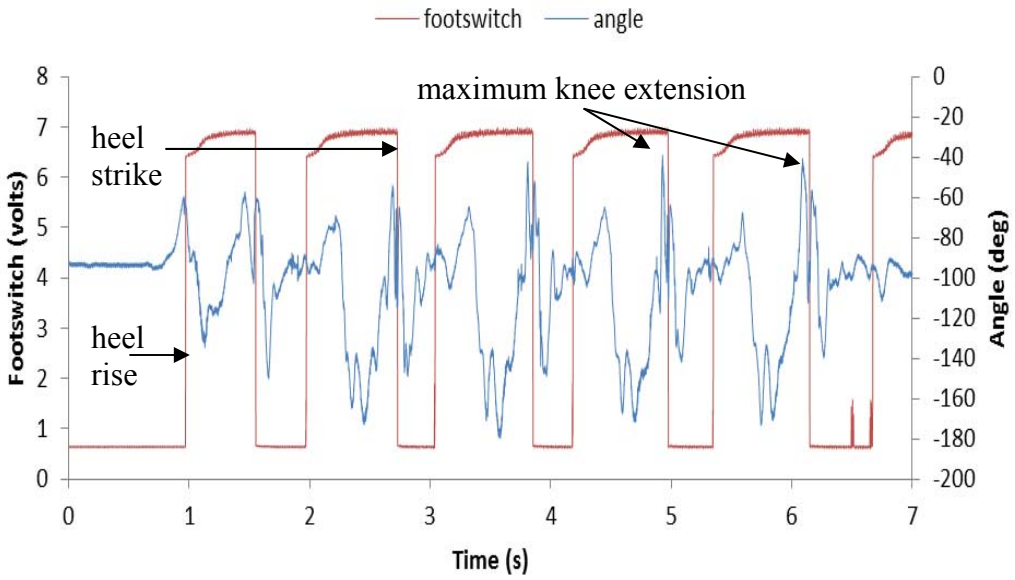

Figure 5-16 Angle determined from the sensor unit and voltage output from the footswitch against time during walking with self selected speed.

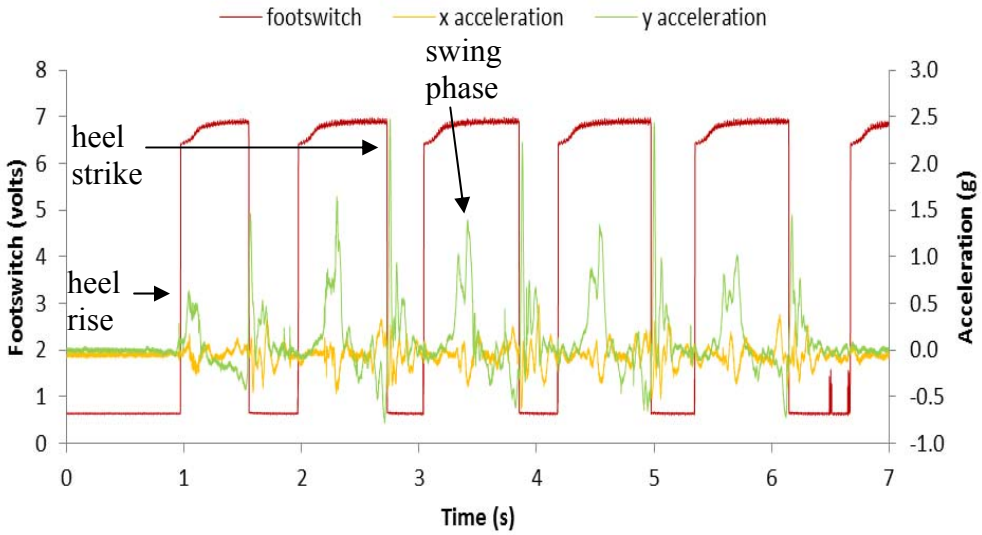

Figure 5-17 Vertical and horizontal accelerations determined from the sensor unit and the voltage output from the footswitch against time during walking with self selected speed.

Figure 5-18 represents the vertical acceleration for a single gait cycle. From the figure, it can be seen that the vertical *y* acceleration has the same timing with the footswitch and there was a high acceleration signal immediately after when the heel strike occurs.

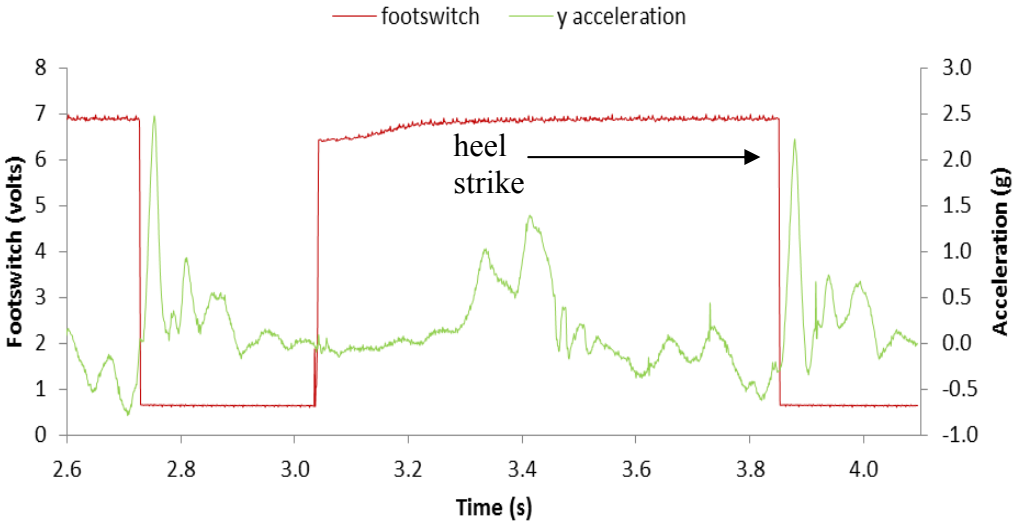

Figure 5-18 The vertical acceleration and voltage output from the footswitch during walking for single gait cycle.

Figure 5-19 and Figure 5-21 show the horizontal acceleration and vertical acceleration with the angle calculated from the algorithm, when a leg swings as pendulum. The leg movement was controlled by the subject making the same range of angle with the sensor mounted on the shank just below the knee. In the figures, it can be seen that the horizontal *x* acceleration is smaller compared to the vertical *y* acceleration. In Figure 5-20, at maximum flexion there is a maximum deceleration of the leg (negative values) while at maximum extension the deceleration of the leg is not as pronounced (positive values). In Figure 5-22, at maximum extension there is a maximum deceleration of the leg (negative values) while at maximum flexion the deceleration of the leg is not as pronounced (positive values).

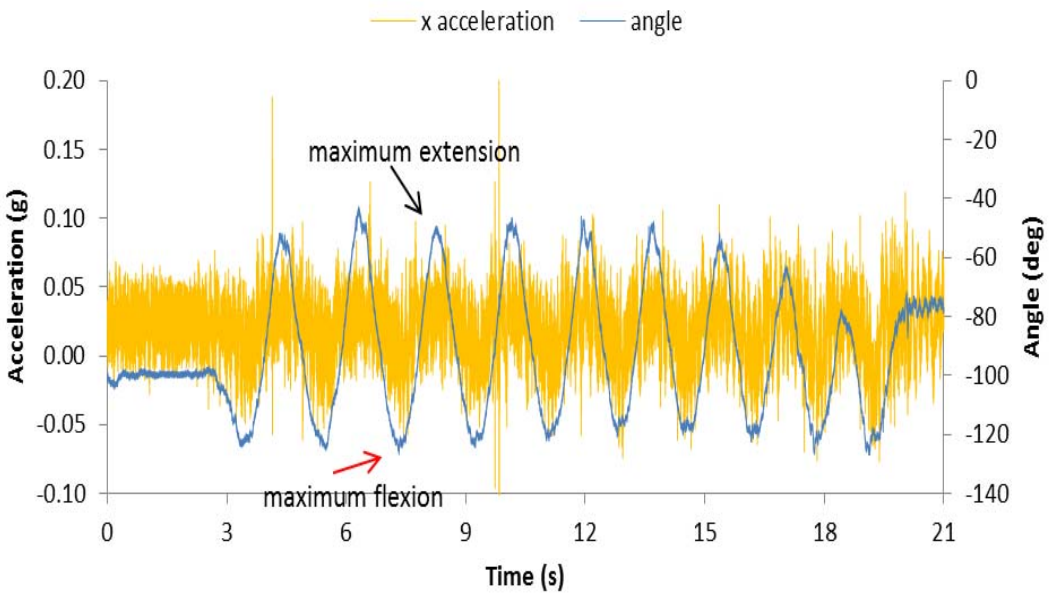

Figure 5-19 Horizontal acceleration and angle against time when a leg swing.

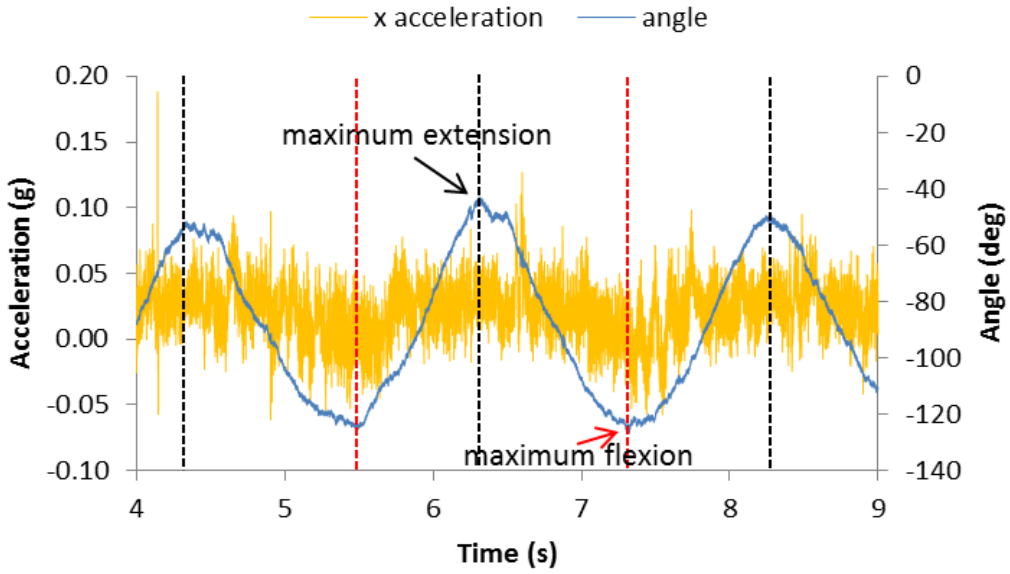

Figure 5-20 Horizontal acceleration and angle against time (expanded of Figure 5-19).

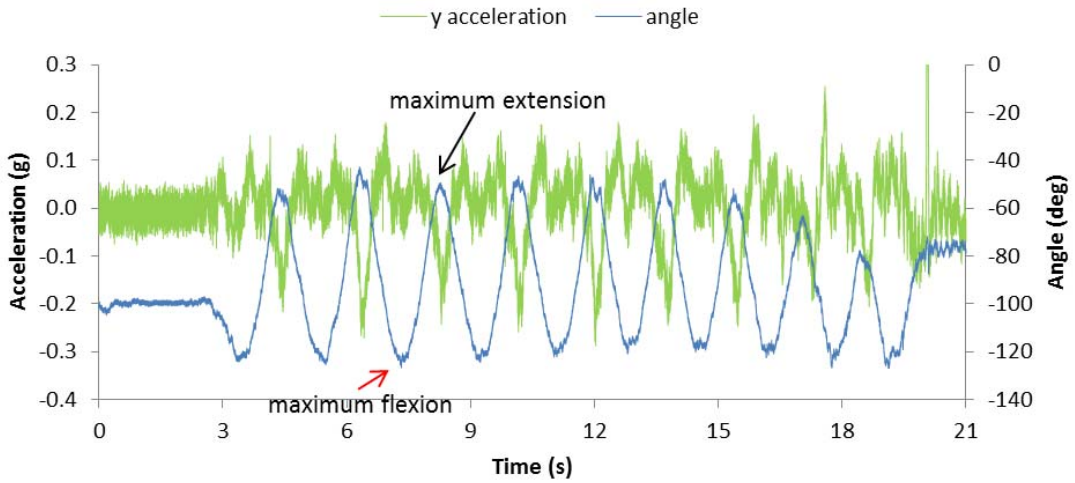

Figure 5-21 Vertical acceleration and angle against time when a leg swing.

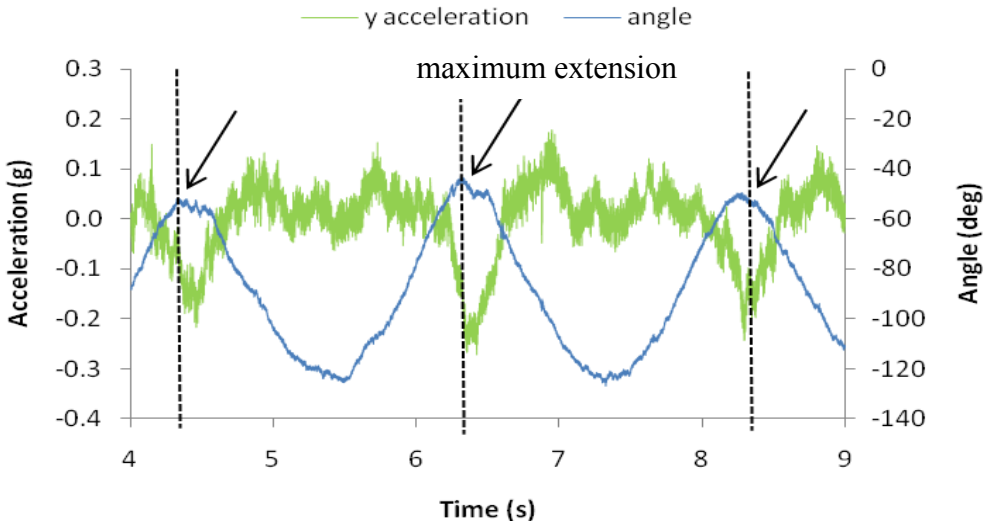

Figure 5-22 Vertical acceleration and angle against time (expanded of Figure 5-21).

5.4 Discussion

In the algorithm, when the sensor unit is stationary, the output (Equation 4-3, 4-4, 4-5 and 4-6) for s_1, s_2, r_1 and r_2 will be reduced to the static acceleration term. The equations become $(-g \sin \theta)$ for the s_1 and $(-g \cos \theta)$ for s_2, while for r_1 and r_2, they will be equal to $(-g \sin \theta_2)$ and $(-g \cos \theta_2)$ respectively. Noted that θ_2 is equal to $(\theta+\alpha)$ and in this case α is equal to $\pi/4$. The result agreed with the theory when negative sign is given to all of the static terms in the equations. The negative sign also applied to the

vertical acceleration, $\ddot{y}$, in the equations although the vertical acceleration has the opposite direction from the gravitational field direction.

The sensor unit algorithm does not work when all of the sensing axes are parallel to the horizontal plane as there will be no output due to the gravitational field. Therefore if all the sensor unit axes are parallel to the horizontal plane, the angle measurement in the transverse plane could not be measured. In this circumstance, a gyroscope could be employed.

The experiments described in this chapter are carried out in the x-y plane (refer Figure 4-13 (Chapter 4, p69) for the plane). A more general test of the system would require the use of for example an industrial robot arm that can be programmed to move the sensor unit over a wider range of operation. All three variables, $\ddot{y}$, $\ddot{x}$ and θ horizontally can then be varied within their ranges. Alternatively, a Vicon™ camera system could be used where the accelerometer unit is attached to the calibration wand. The disadvantage of this method is that a person would carry out the movement of the wand. The robot arm method would be the best one to test the three dimensional use of two sensor units in Figure 4-13 (Chapter 4, p69). The experiment to investigate the effect of placing the sensor unit at different distances from the rotation point could be improved by putting two sensor units at two different distances from the rotation point on the same segment. However, only one sensor unit has been produced at the time the experiment was carried out.

The sensor unit algorithm (Chapter 4, p57) could be used in the two dimensional human walking measurement in gravitational field. The ranged of the angle tested may be more than sufficient if the sensor unit is to be applied for the lower limb segment angle measurement in sagittal or coronal planes. The sensor unit algorithm has the advantage of avoiding the integration for the angle measurement that could cause a drift problem.

5.5 Conclusions

When static, an output of the sensor unit (a signal from the individual axes: s_1, s_2, r_1 and r_2) follows the negative sine of the individual angle (θ, φ, β and γ) with respect to

earth's horizontal plane and has a value between -1g and 1g. The standard deviation of a signal from the stationary sensor unit is between 0.0019g and 0.0044g. The mean angle measured in degrees (SDs) using the sensor unit are 0.85 (0.1833) at 0 degree, 90.45 (0.1078) at 90 degrees, 180.44 (0.1840) at 180 degrees and 270.59 (0.0838) at 270 degrees. In dynamic condition, the standard deviations of the output of the sensor unit are between 0.16g and 0.57g for the axes that are not influenced by the test apparatus movement and between 0.46g and 1.48g for the axes that are influenced by the test apparatus movement. The output from the sensor unit shows more variable in the dynamic condition compared to static condition. The error in the measurement of angle can be lowered from 3.62^0 and 5.44^0 to 0.96^0 and 4.33^0 with a moving average of 0.3s.

An advantage of using the algorithm is that there was no drift in the measurement of angle during a leg swing of 21 seconds. The kinematic measurement of a lower limb segment from the sensor unit has demonstrated a consistent repetitive pattern during stance and swing phase in a normal subject during walking. The maximum shank segment angle with respect to the earth's horizontal plane during walking measured using the sensor unit is about 140 degrees. The maximum horizontal and vertical accelerations are 0.5g and 2.5g respectively. Therefore, ±2g acceleration range is not sufficient for measurement of linear acceleration during walking although it has been used by other researchers (Zijlstra and Hof (2003), Jasiewicz et al. (2006), Simcox et al. (2005), Williamson and Andrews (2001), Lau and Tong (2008)).

Chapter 6

Assessment of the Lower Limb Segment Angle during Walking

6.1 Introduction

This chapter is concerned with an assessment of the lower limb segment angle during walking using the sensor unit algorithm (Chapter 4, p57). The segment angle measured will be compared with the angle measured from the motion analysis system (Vicon ^{TM}). It consists of passive markers placed on a person and infrared cameras to capture the images. The minimum of three markers are needed to define every segment. Lu and O'Connor (1999) have reported that the position of the markers is easily displaced and rotated from the origin with respect to the underlying bone. This is due to a skin movement artefact which contributes to the largest error in calculating the joint angles. Depending on the software model used, the joint angle calculation is also affected by the accuracy of the reconstruction of missing markers (Churchill et al. (2007)).

In the study, the comparison steps are not straight forward as the two systems (sensor unit and Vicon^{TM}) have differences in:

- sampling rates
- physical principles and frequency response
- mathematical model used for the angle measurement and segment reference plane
- data processing (filtering)

Due to the differences between the two systems and errors in calculating the angles from the individual system, it is anticipated that the minimum deviation would be about 5.44° (the largest standard deviation) as reported in the previous chapter (Chapter 5, p88).

The best possible steps have been carried out to minimise the differences between the two systems by:

- down sampling the sensor unit measurement from 1kHz to 100Hz
- using a moving average of the angle calculated from the sensor unit
- changing the reference plane of the sensor unit measurement to match with the Vicon™ reference plane (from horizontal to vertical for thigh and shank segment). However, these verticals are not the same. The Vicon™ verticals are with respect to specific segment plane while the sensor unit verticals are with respect to the Earth horizontal plane.
- using a simple switch to synchronous the start and stop of the data acquisition of both systems.
-

However, the raw data from the Vicon™ was not accessible which made the comparison process more difficult.

6.2 Procedures

6.2.1 Subjects

Five healthy subjects were recruited to participate in the trials. All the subjects were male adult with their weight between 45-80kg. The subjects have no known neurological problem and were medically stable. The study was granted ethical approval by the Wiltshire Research Ethics Committee and the subjects gave informed consent.

6.2.2 Set Up and Protocol

For every subject, data was collected from both of the lower limbs except for Subject 1 (only right limb). The set up (as in Figure 6-1) consisted of:

i. Six sensor units attached laterally to both of the lower limbs segments: thigh and shank using the Velcro strap (black and grey colour) and foot (on the shoe) using double sided tape.

ii. Four footswitches were used; one was placed under the heel and one under the first metatarsal head of the shoe insole for each foot. The footswitch data will be used later in Chapter 8 and 9 for event detection.

iii. Retro-reflective markers were placed on the foot, shank, thigh and waist which follow the modified Helen Hayes model for the lower limb. The Helen Hayes pelvic model as has been adopted for use with Vicon™ systems and is the model developed in the USA (Davis et al. (1991)). A total of sixteen markers were attached to both of the lower limbs using a double sided tape as listed in the table and figure shown in Appendix F.

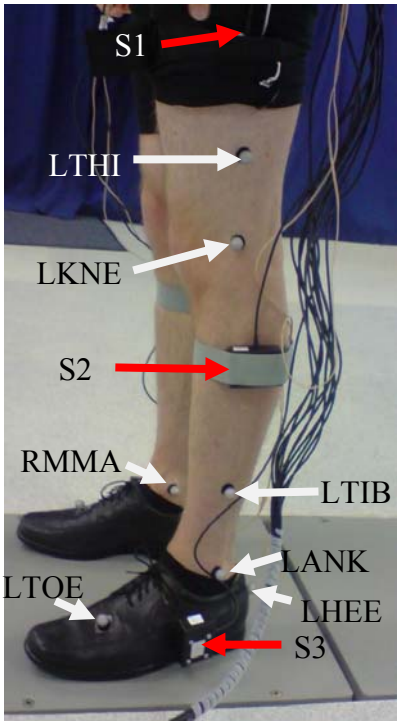

Figure 6-1 Left lateral view of the lower limb with sensor units (red arrows) and retro-reflective markers (white arrows). Five markers were not shown in the figure (LASI/RASI, LPSI/RPSI and LMMA) and the rest of right limb markers except RMMA.

The subjects wore the shoes they normally used in their daily activities. They were asked to walk for about 4 metres for each trial (12 trials) in the Salisbury Gait Laboratory (SGL). A remote switch was used to synchronise the start and stop of the data collection from both systems (Vicon™ and sensor unit). The Vicon™ system was operated by a person who had been trained. The static calibration of the system was carried out for every subject at the beginning of the trials. Six cameras were used by the Vicon™ system to capture the images.

6.2.3 The Data Acquisition and Software

The data acquisition systems used in the experiment were the DAQPad-6015 and DAQ6036E from National Instrument Ltd. For every data acquisition, fourteen analog inputs were used as a single ended input configuration for twelve of the sensor units output and two of the footswitches output. It has a sampling rate of 200 kSs^{-1} for sixteen channels. The system has 16-bit resolution ADC. All signals from the sensor units in the experiments were sampled at 1 kHz using the continuous analog mode. All measurements were taken using LabVIEW™ 8.0 and the data was stored in a PC memory. The data was then analysed off-line using Microsoft Office Excel© and Matlab® R2006b. The sampling rate used for the Vicon™ system is 100Hz and the signal was smoothed using Woltring filter which acts like a low pass filter. This filter is commonly used in Vicon™ data.

6.2.4 Data Analysis

Only the data obtained within the Vicon™ capture volume (restricting the captured walking distance to 3.5 metres) was acquired and analysed. For each subject, the data from two trials were analysed except for Subject 1 and 3, when only one trial was analysed (right limb). The data collected from the sensor unit has been used to calculate the segment angle in the sagittal plane with respect to horizontal plane (anteriorly) as shown in Figure 6-2 using the algorithm in Chapter 4. The data captured from the retro-reflective markers was analysed using the Vicon™ Nexus software by the person in charge of the Vicon™ system. As mentioned earlier in this chapter, the assessment

process is not straight forward as there are many differences between the two systems. The best possible steps were carried out to perform the comparison between the two systems. These processes are:

- The segment angle calculated from the sensor unit with respect to the horizontal plane was recalculated with respect to vertical plane (global) to match with the angle from the Vicon™ system for thigh and shank segment and horizontal plane (global) for foot segment. However, the vertical used by the Vicon™ for the thigh segment angle calculation is orthogonal to the pelvic plane and the vertical for the shank segment angle calculation is parallel to thigh segment. For the foot segment, both systems calculated the angle with respect to the horizontal plane. However, the Vicon™ horizontal plane is orthogonal to the shank segment.
- The sampling rate of the angle measurement from the sensor unit is decreased from 1kHz to 100Hz using the decimation function in Matlab® R2006b.
- The down sampled angle measurement was smoothed using a moving average of 50 to 100 points to match the data with Vicon™ waveforms.
- Both angle measurements, from the sensor unit and the Vicon™ are plotted together and the correlation coefficient and the root mean squared deviation were calculated.

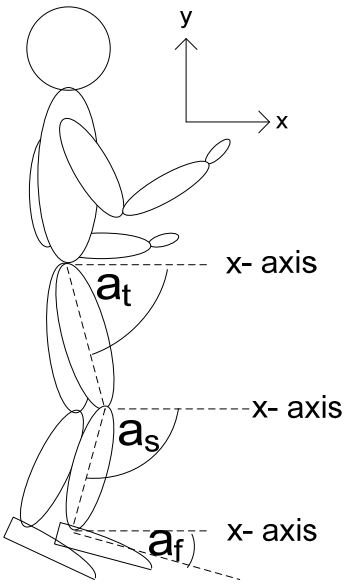

Figure 6-2 Right lateral view of the segment angles: a_t: thigh segment angle, a_s: shank segment angle and a_f: foot segment angle.

The joint angles defined by the Vicon™ system are shown in Figure 6-3. The hip angle (thigh segment angle) is the angle between the thigh segment plane and the vertical plane that is orthogonal to the pelvic plane. The thigh segment was defined by the hip joint centre (HJC) ((Bell et al. (1989), Kadaba et al. (1990), Vicon™ (2010)), thigh wand and lateral knee marker. The knee angle (shank segment angle) is the angle between the shank segment plane and the thigh segment plane. The shank segment was defined by the knee joint centre (KJC) (Kadaba et al. (1990), Vicon™ (2010)), tibial wand and lateral ankle marker. The ankle angle (foot segment angle) is between the foot segment plane and the horizontal plane that is orthogonal to the shank segment plane.

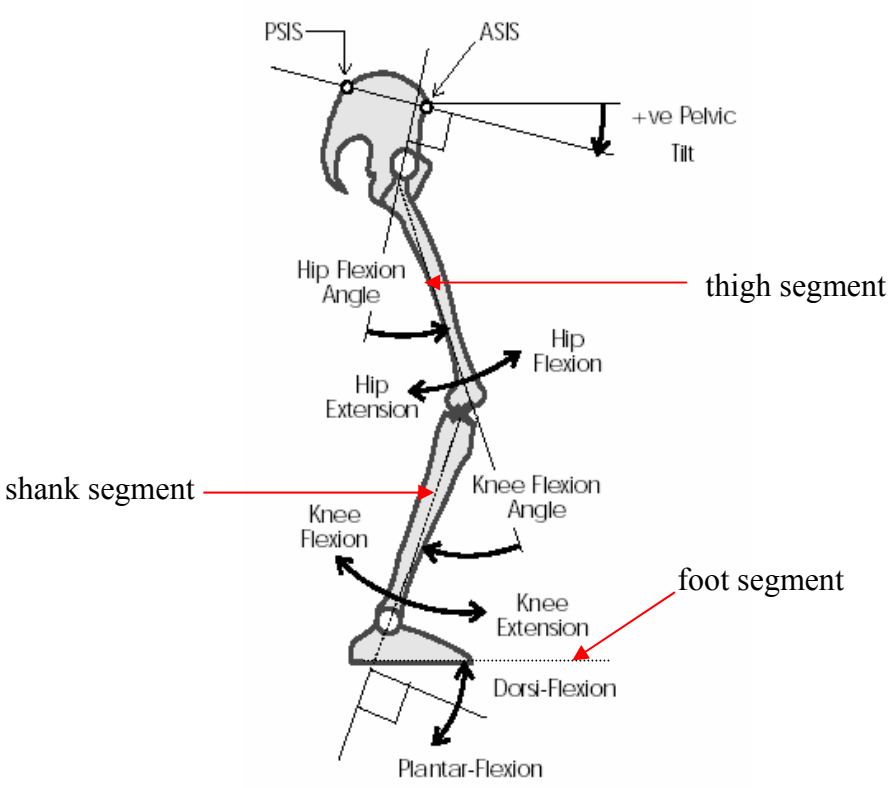

Figure 6-3 Right lateral view of the joint/segment angles defined by the Vicon™ system (Vicon™ (2010)).

6.3 Results and Discussion

Figure 6-4 to Figure 6-45 show the shank, foot and thigh segment angle of a single gait cycle measured from the sensor unit and the Vicon™ system for Subject 1, 2, 3, 4 and 5. For all five subjects, the shank segment angle shows a similar pattern between the

two measurements. A difference can be seen during the stance phase of the gait between 0% and 50% where the angle from the sensor unit shows less smoothing with more detail in the signal. Within this gait cycle, the soleus and gastrocnemius are actively contracting to plantar flex the ankle to ensure limb stability during weight-bearing period. This action rapidly increases and peaks near the end of terminal stance (30%-50% of gait cycle) to serve the purpose of accelerating of the body forward. The more detail information in the segment angle measured using the sensor unit could be from the skin movement artefact due to the muscle action that is actively contracts. The range of the correlation coefficient and standard deviation calculated from the two measurements for shank segment are between (r = 0.834 and r = 0.992) and (2.83°and 13.72°) respectively. The deviation due to the phase shift (delay) as the effect of low filtering can be seen clearly in Figure 6-19 and Figure 6-22 with standard deviation equal to 13.72° and 12.20° respectively.

For all five subjects, the thigh and foot segments angles are not similar throughout a gait cycle between the two measurements (sensor unit and the Vicon^{TM}). The range of the correlation coefficient and standard deviation calculated from the two measurements for thigh and foot segments are between (r = 0.185 and r = 0.643) and (r = 0.363 and r = 0.898) and (10.29°and 19.19°) and (3.48°and 18.27°) respectively. In Vicon^{TM}, the vertical and horizontal planes were defined using the limb segment while in the sensor unit, all the measurements are with respect to global horizontal plane. Moreover, in Vicon^{TM} the pelvic angle is used in the thigh segment angle calculation but not in the sensor unit. The difference reference plane and mathematical model used that caused the angle measurement from the sensor unit deviate from the Vicon^{TM}. The skin movement artefact due to muscle contraction at the thigh and the shank is also another caused of the angle measurement deviation and the muscles at the thigh are all the bulky type such as hamstrings and quadriceps. As the sensor unit only measured the angle in the sagittal plane, the movement such as inversion/eversion has caused the deviation of the angle measurement in the foot segment. Moreover, the reference planes used by the two measurements are not the same. However, the thigh and foot segments angles patterns are similar and consistent between the subjects using the same sensor (either sensor unit or Vicon^{TM}).

The two systems have different sampling frequencies and smoothing techniques. For all the plots, the phase shift (delay) can be seen clearly in the Vicon™ angle as the effect of the low pass filtering. As mentioned earlier in this chapter, the assessment of the angle measurement process is not straight forward. There are many factors that could contribute to the dissimilarities and large deviation between the angle measured from the Vicon™ and the sensor unit such as different sampling frequency, angle calculation method, data processing and underlying physics. It may be possible to minimise the measurement deviation if the data collection had used the same sampling rate, cut-off frequency for filtering and angle calculation model. However, the raw data from the Vicon™ is not accessible and the cut off frequency used for analysis of the Vicon™ data is not known. Other factors which can contribute to the angle measurement error are the effect of the skin movement on the sensor unit alignment and attachment due to muscles contracting. In the data collection method, the sensor units were attached to the laptops with long cables and it is possible that when the subject walks the cables pull and therefore the sensor unit moves from the original position.

As well as the sensor unit, the deviation is also contributed from the Vicon™ measurement. As mentioned earlier in this chapter, the skin movement artefact and the accuracy of the software used to reconstruct the missing marker can contribute to the error. According to Lu and O'Connor (1999), the calculation method used by Kadaba et al. (1990) has the largest error in the angle measurement and the hip joint centre is the most affected. As reported by Churchill et al. (2007), the most accurate reconstruction affecting the segment angle calculation can be up to ±2.3° while the least accurate reconstruction can be up to ±27.48°. Churchill et al. (2007) found that the most accurate reconstruction occurred when the marker chosen for the reconstruction is close to the missing marker. However, in the study, the errors contributed from the Vicon™ system are beyond the control of the experimenter.

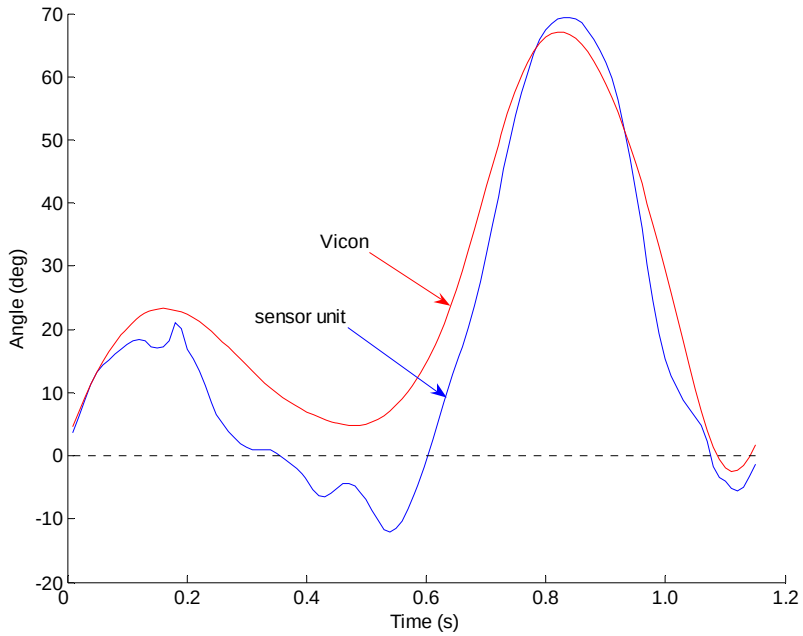

Figure 6-4 Shank segment angle in Subject 1(right limb) of a single gait cycle from heel contact with r = 0.976 and rmsd=9.35°. A positive angle represents knee flexion, a negative angle represents knee extension and 0° represents neutral position.

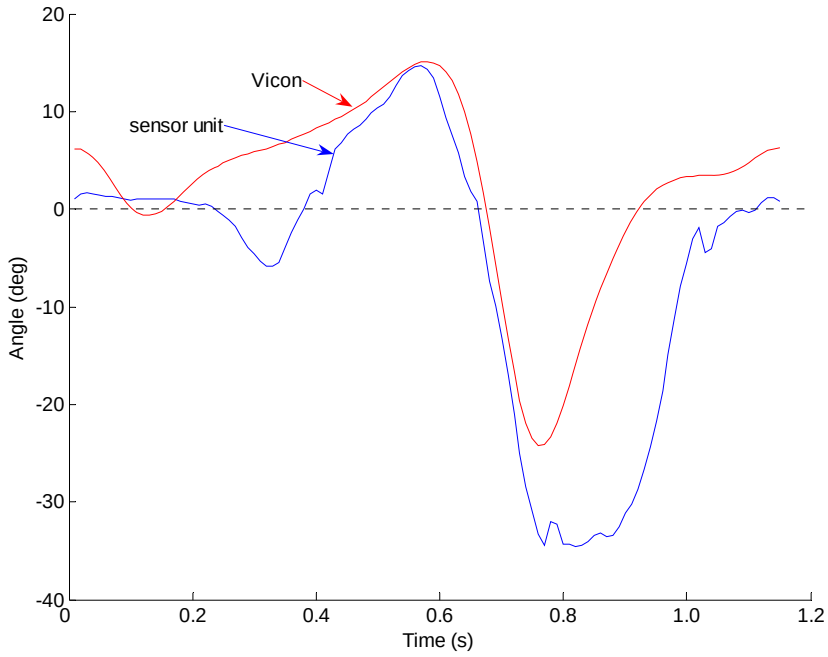

Figure 6-5 Foot segment angle in Subject 1(right limb) of a single gait cycle from heel contact of with r = 0.859 and rmsd=10.98°. A positive angle represents foot dorsiflexion, a negative angle represents foot plantarflexion and 0° represents neutral position.

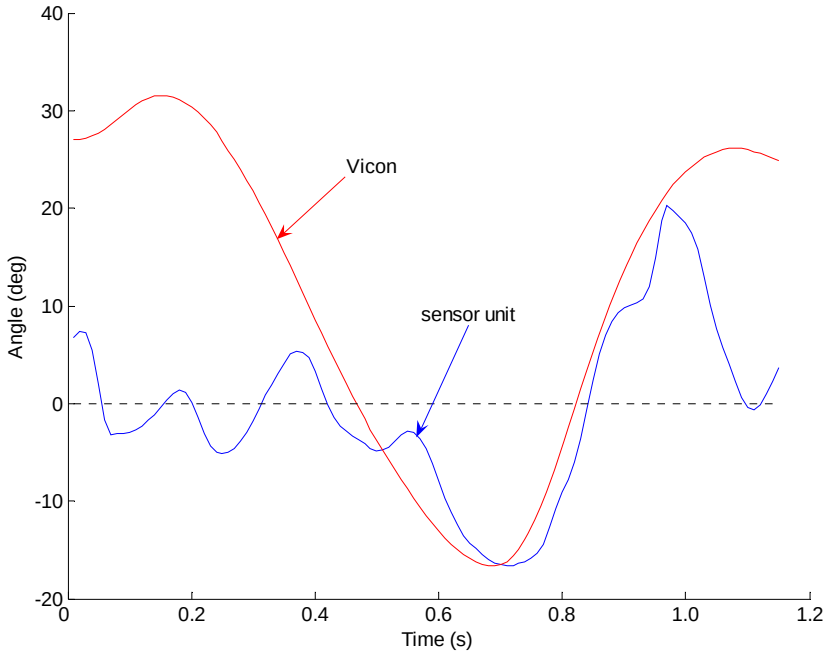

Figure 6-6 Thigh segment angle in Subject 1(right limb) of a single gait cycle from heel contact with r = 0.643 and rmsd=17.60°. A positive angle represents hip flexion, a negative angle represents hip extension and 0° represents neutral position.

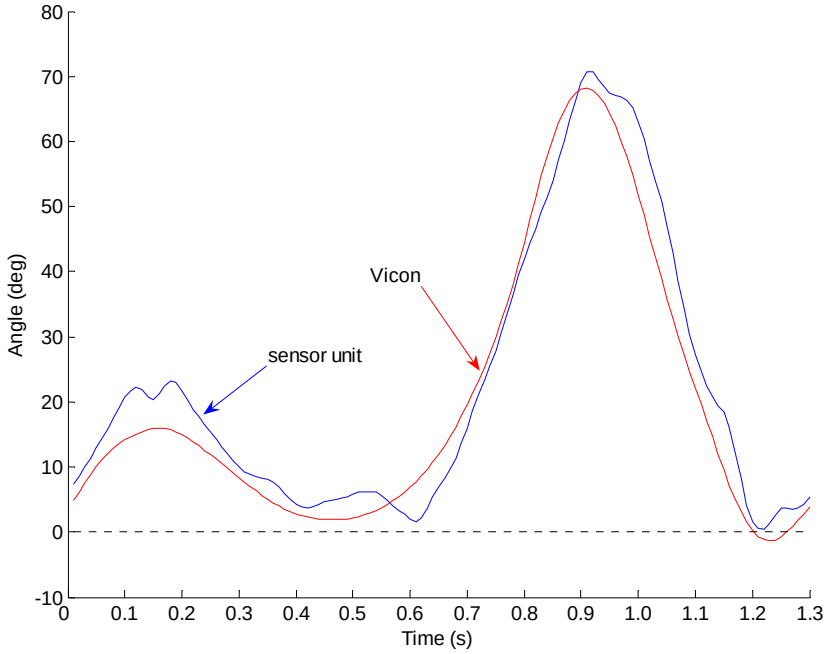

Figure 6-7 Shank segment angle in Subject 2 (right limb) of a single gait cycle from heel contact with r = 0.977 and rmsd=5.03°. A positive angle represents knee flexion, a negative angle represents knee extension and 0° represents neutral position.

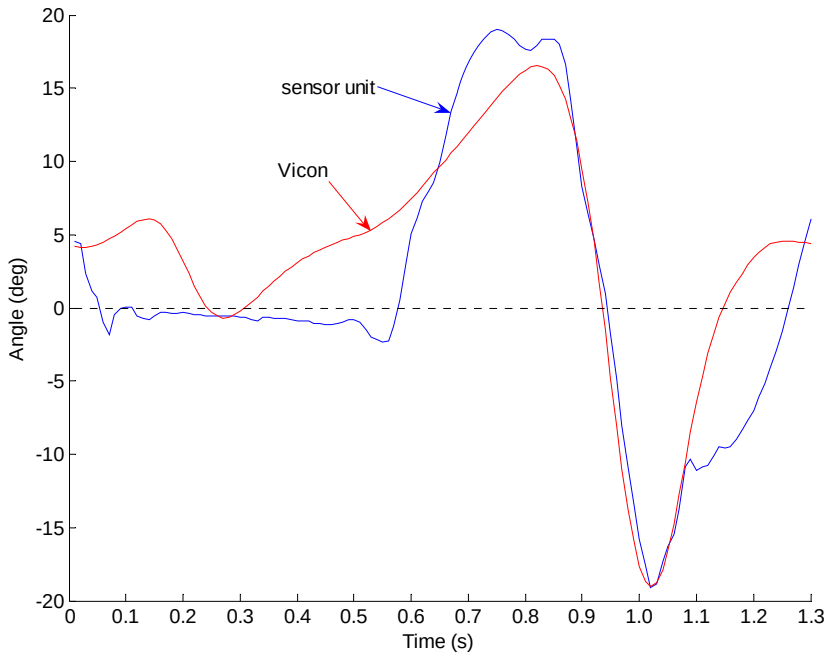

Figure 6-8 Foot segment angle in Subject 2 (right limb) of a single gait cycle from heel contact with r = 0.898 and rmsd=4.76°. A positive angle represents foot dorsiflexion, a negative angle represents foot plantarflexion and 0° represents neutral position.

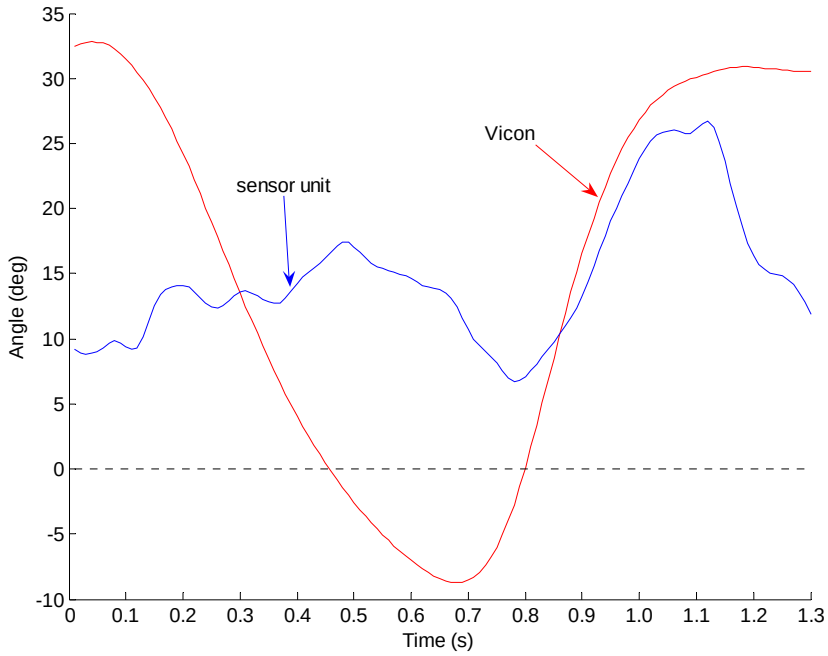

Figure 6-9 Thigh segment angle in Subject 2 (right limb) of a single gait cycle from heel contact with r = 0.344 and rmsd=14.13°. A positive angle represents hip flexion, a negative angle represents hip extension and 0° represents neutral position.

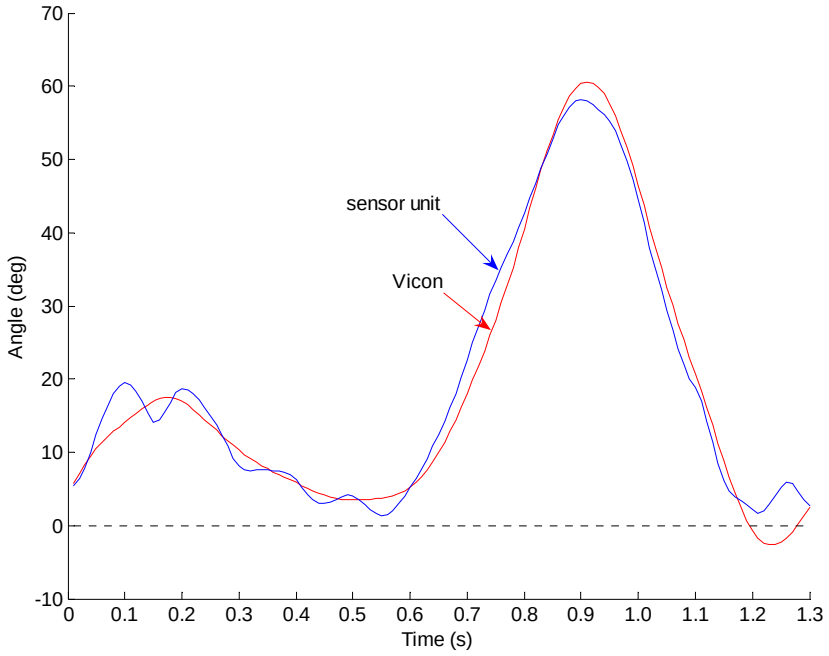

Figure 6-10 Shank segment angle in Subject 2 (left limb) of a single gait cycle from heel contact with r = 0.988 and rmsd=2.83°. A positive angle represents knee flexion, a negative angle represents knee extension and 0° represents neutral position.

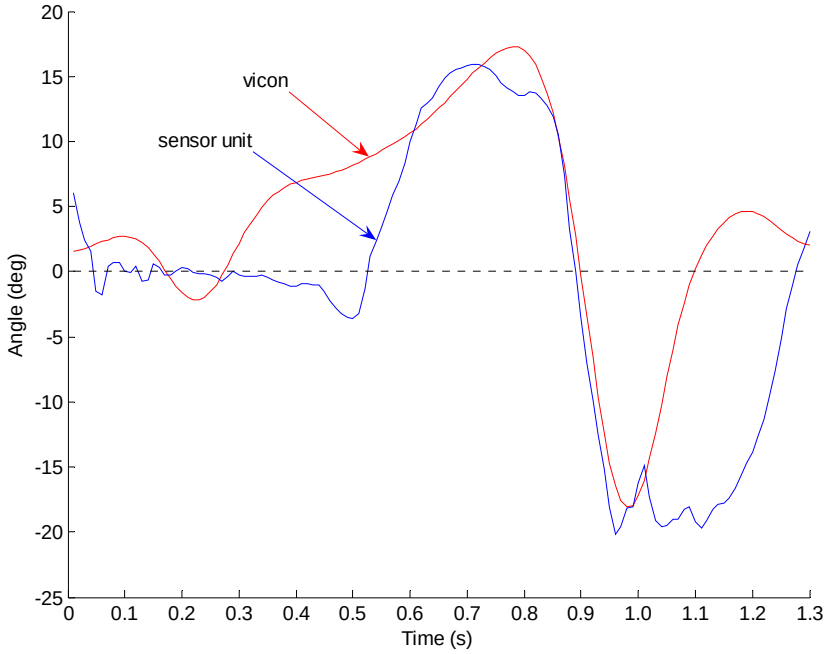

Figure 6-11 Foot segment angle in Subject 2 (left limb) of a single gait cycle from heel contact with r = 0.793 and rmsd=8.28°. A positive angle represents foot dorsiflexion, a negative angle represents foot plantarflexion and 0° represents neutral position.

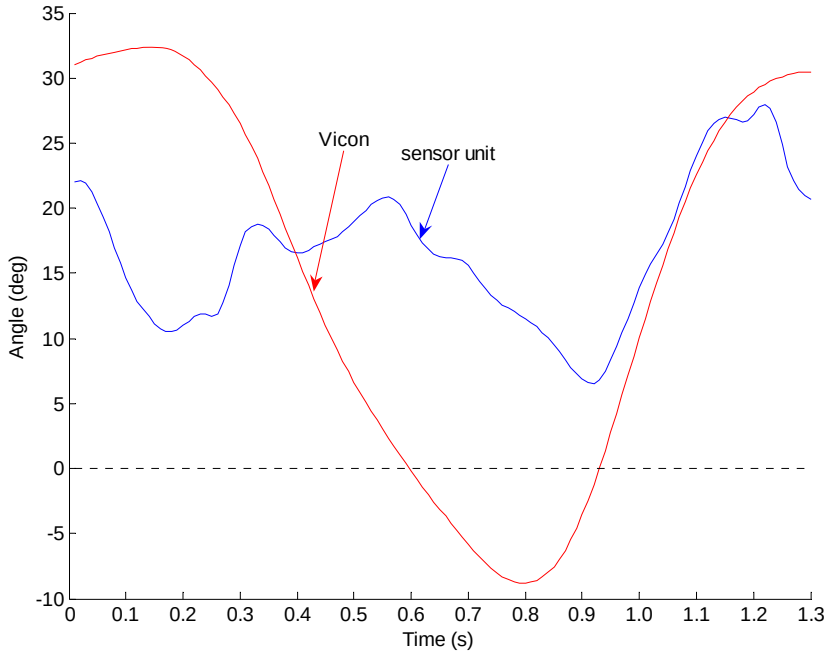

Figure 6-12 Thigh segment angle in Subject 2 (left limb) of a single gait cycle from heel contact with r = 0.428 and rmsd=10.29°. A positive angle represents hip flexion, a negative angle represents hip extension and 0° represents neutral position.

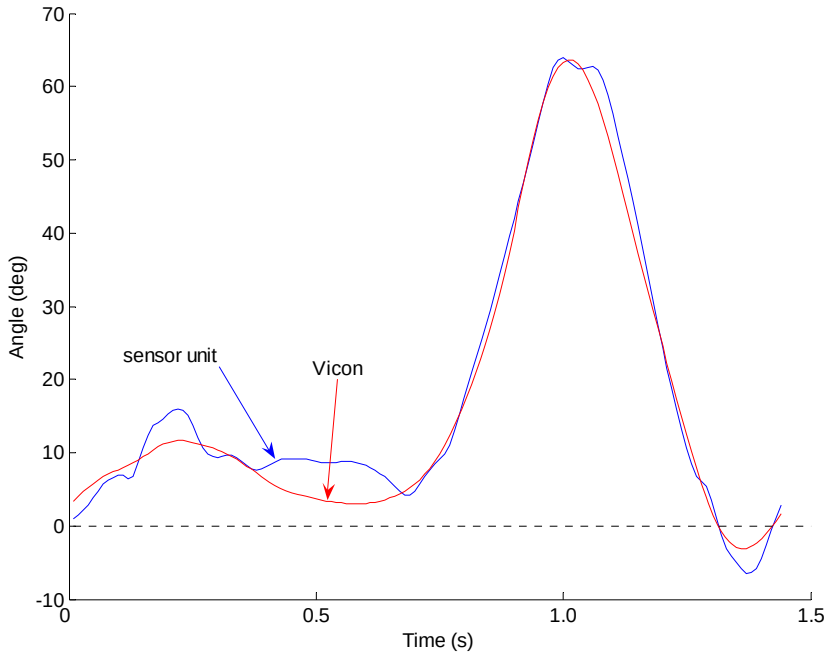

Figure 6-13 Shank segment angle in Subject 2 (right limb) of a single gait cycle from heel contact with r = 0.992 and rmsd=2.83°. A positive angle represents knee flexion, a negative angle represents knee extension and 0° represents neutral position.

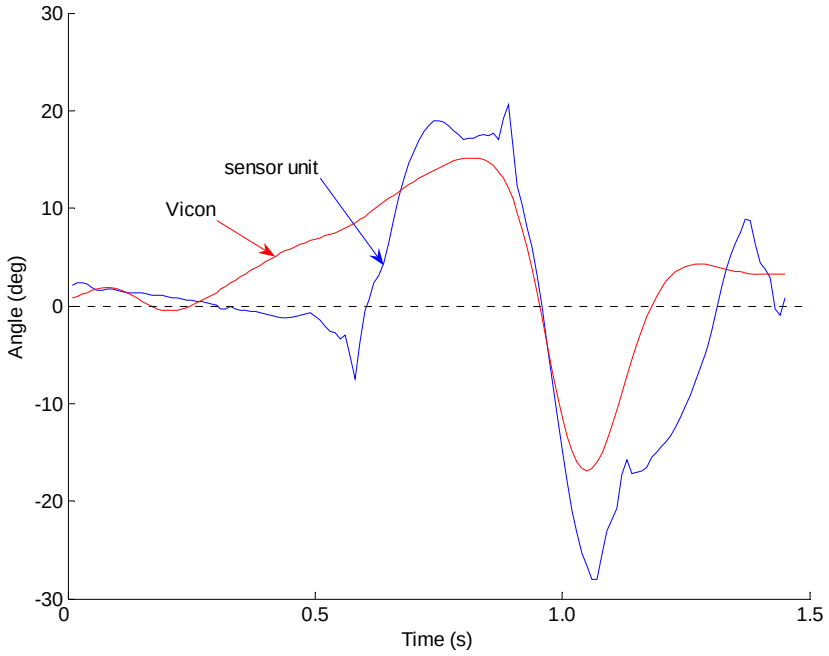

Figure 6-14 Foot segment angle in Subject 2 (right limb) of a single gait cycle from heel contact with r = 0.860 and rmsd=7.02°. A positive angle represents foot dorsiflexion, a negative angle represents foot plantarflexion and 0° represents neutral position.

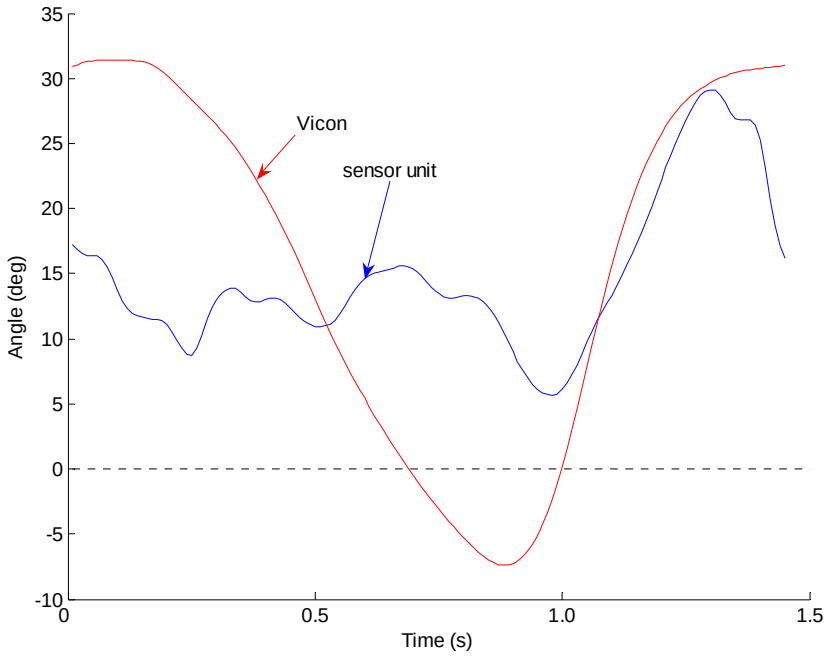

Figure 6-15 Thigh segment angle in Subject 2 (right limb) of a single gait cycle from heel contact with r = 0.511 and rmsd=12.14°. A positive angle represents hip flexion, a negative angle represents hip extension and 0° represents neutral position.

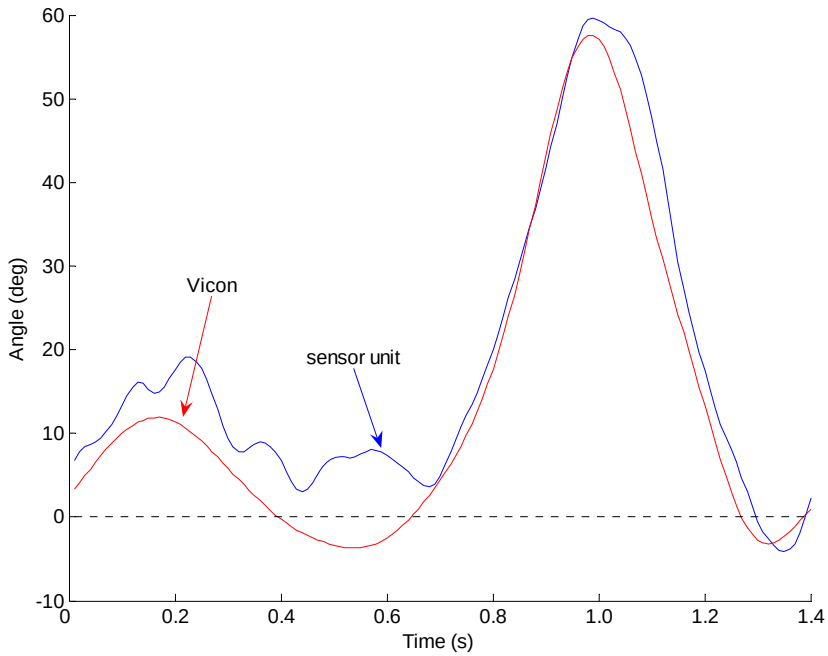

Figure 6-16 Shank segment angle in Subject 2 (left limb) of a single gait cycle from heel contact with r = 0.979 and rmsd=5.86°. A positive angle represents knee flexion, a negative angle represents knee extension and 0° represents neutral position.

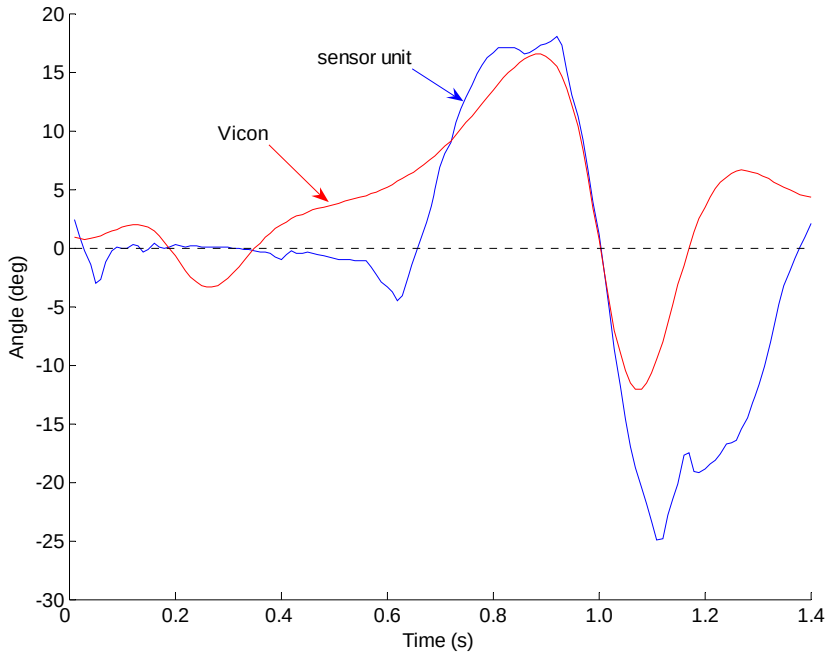

Figure 6-17 Foot segment angle in Subject 2 (left limb) of a single gait cycle from heel contact with r = 0.728 and rmsd=8.81°. A positive angle represents foot dorsiflexion, a negative angle represents foot plantarflexion and 0° represents neutral position.

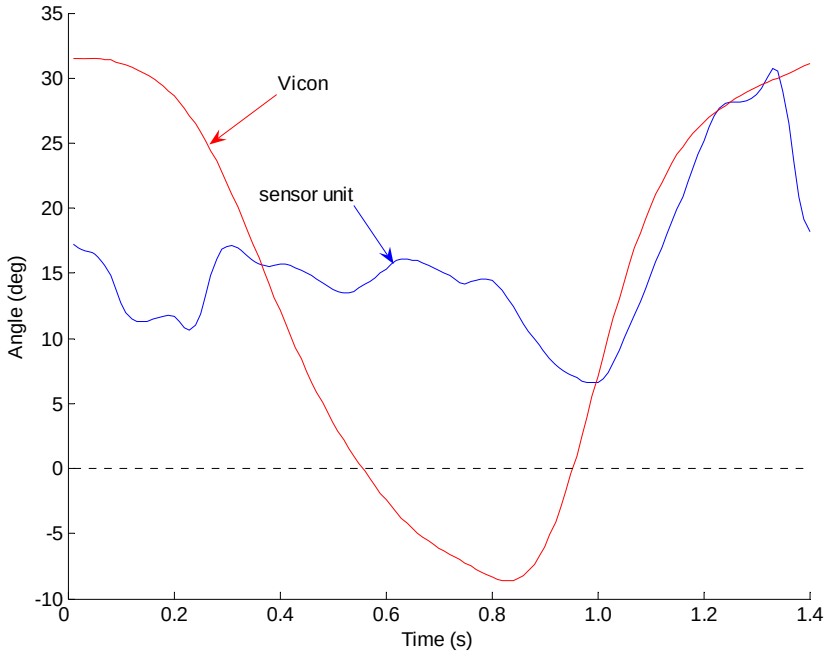

Figure 6-18 Thigh segment angle in Subject 2 (left limb) of a single gait cycle from heel contact with r = 0.467 and rmsd=13.22°. A positive angle represents hip flexion, a negative angle represents hip extension and 0° represents neutral position.

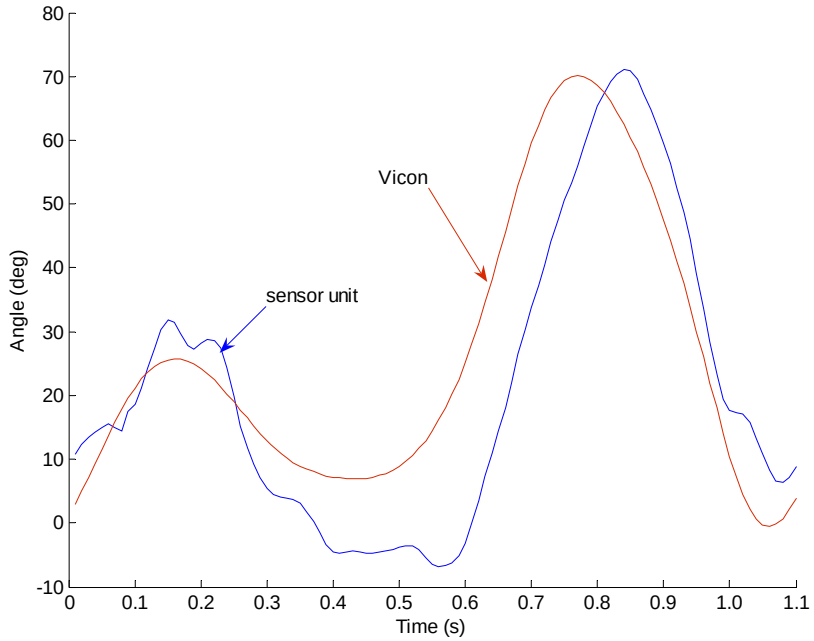

Figure 6-19 Shank segment angle in Subject 3 (right limb) of a single gait cycle from heel contact with r = 0.834 and rmsd=13.72°. A positive angle represents knee flexion, a negative angle represents knee extension and 0° represents neutral position.

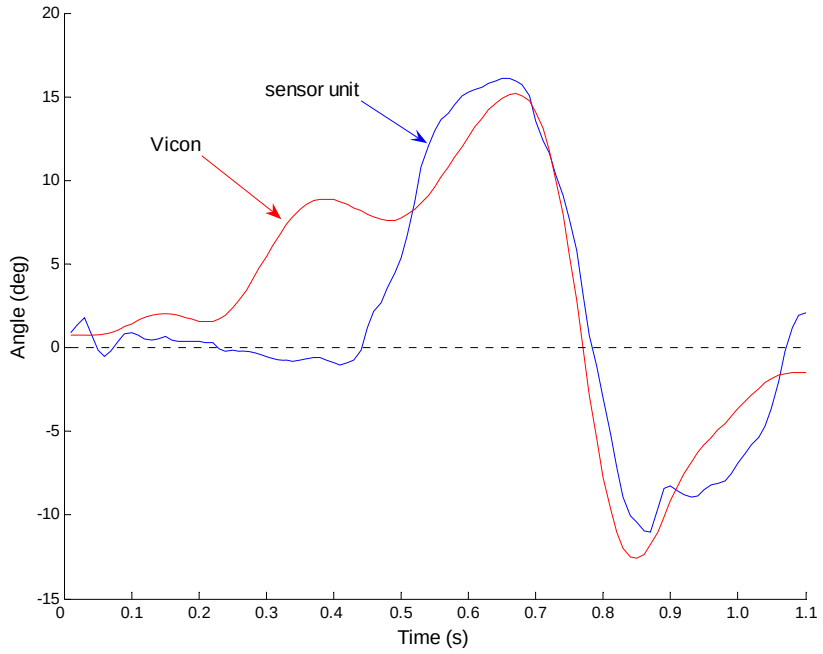

Figure 6-20 Foot segment angle in Subject 3 (right limb) of a single gait cycle from heel contact of with r = 0.871 and rmsd=4.01°. A positive angle represents foot dorsiflexion, a negative angle represents foot plantarflexion and 0° represents neutral position.

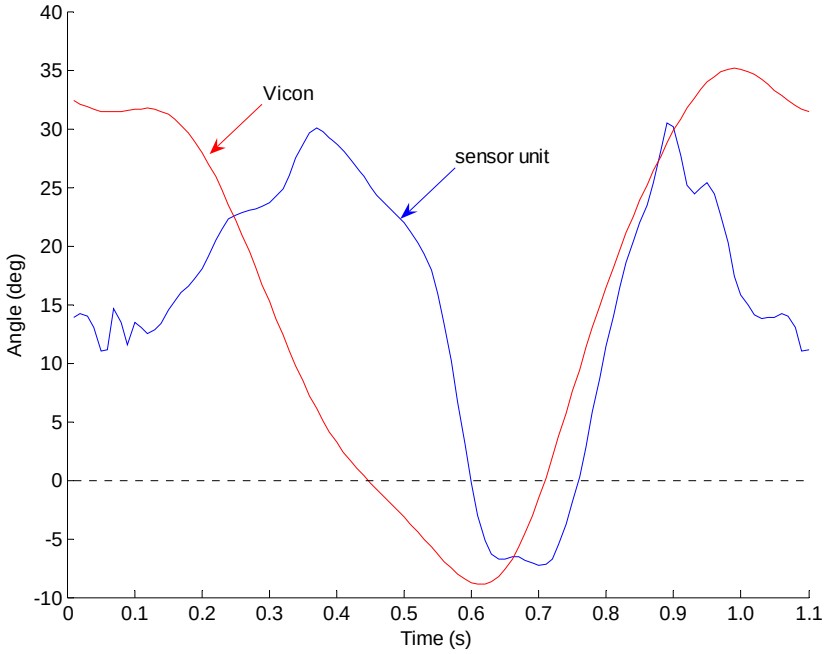

Figure 6-21 Thigh segment angle in Subject 3 (right limb) of a single gait cycle from heel contact with r = 0.330 and rmsd=15.69°. A positive angle represents hip flexion, a negative angle represents hip extension and 0° represents neutral position.

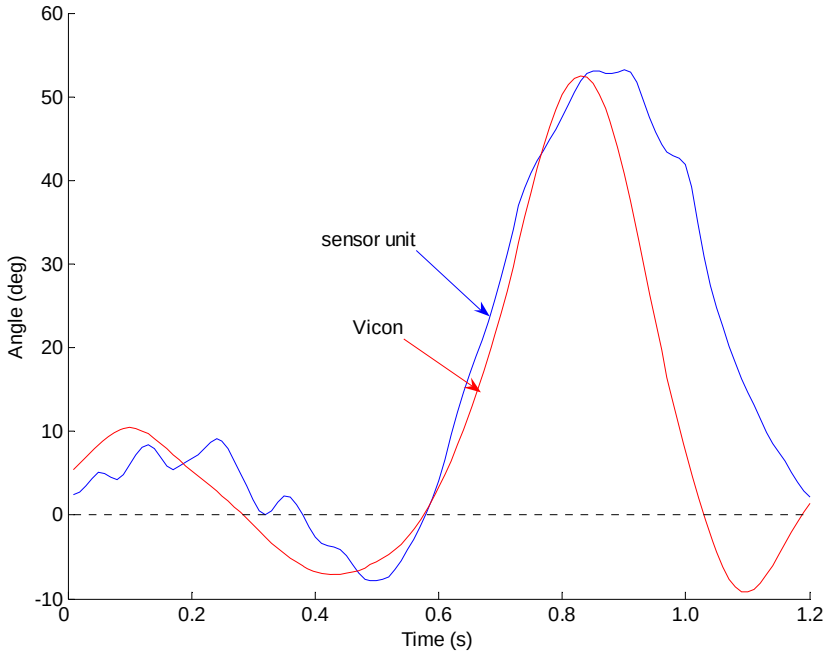

Figure 6-22 Shank segment angle in Subject 4 (right limb) of a single gait cycle from heel contact with r = 0.850 and rmsd=12.20°. A positive angle represents knee flexion, a negative angle represents knee extension and 0° represents neutral position.

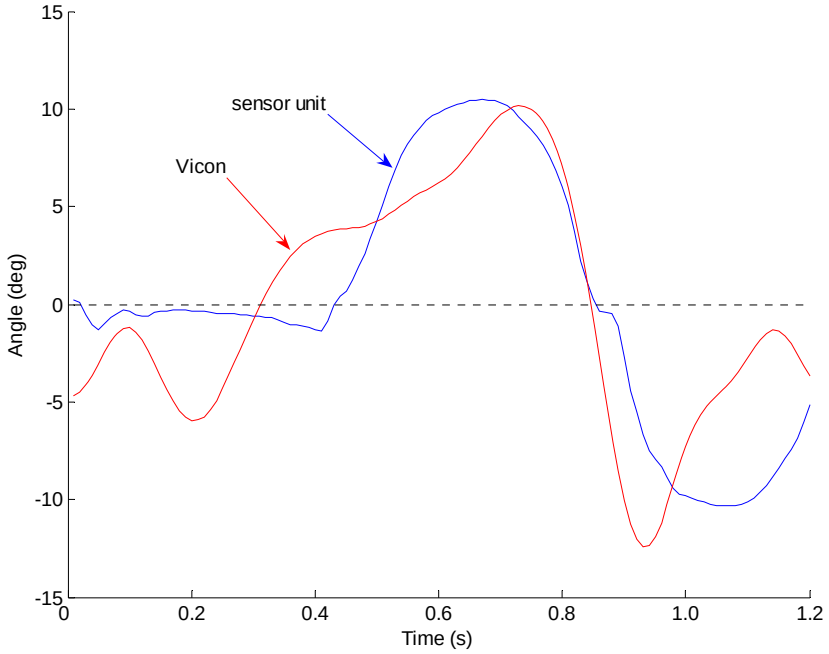

Figure 6-23 Foot segment angle in Subject 4 (right limb) of a single gait cycle from heel contact with r = 0.807 and rmsd=3.86°. A positive angle represents foot dorsiflexion, a negative angle represents foot plantarflexion and 0° represents neutral position.

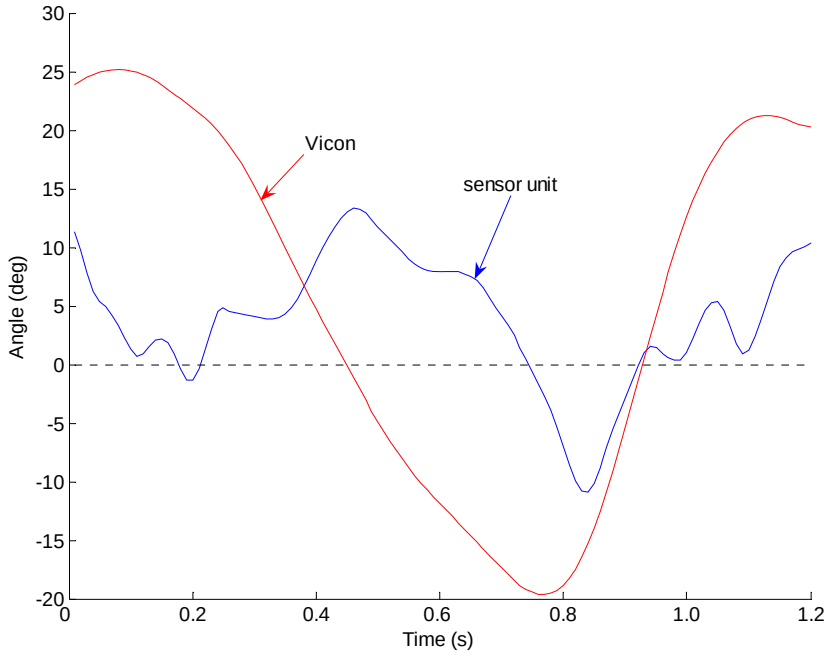

Figure 6-24 Thigh segment angle in Subject 4 (right limb) A single gait cycle from heel contact with r = 0.185 and rmsd=15.73°. A positive angle represents hip flexion, a negative angle represents hip extension and 0° represents neutral position.

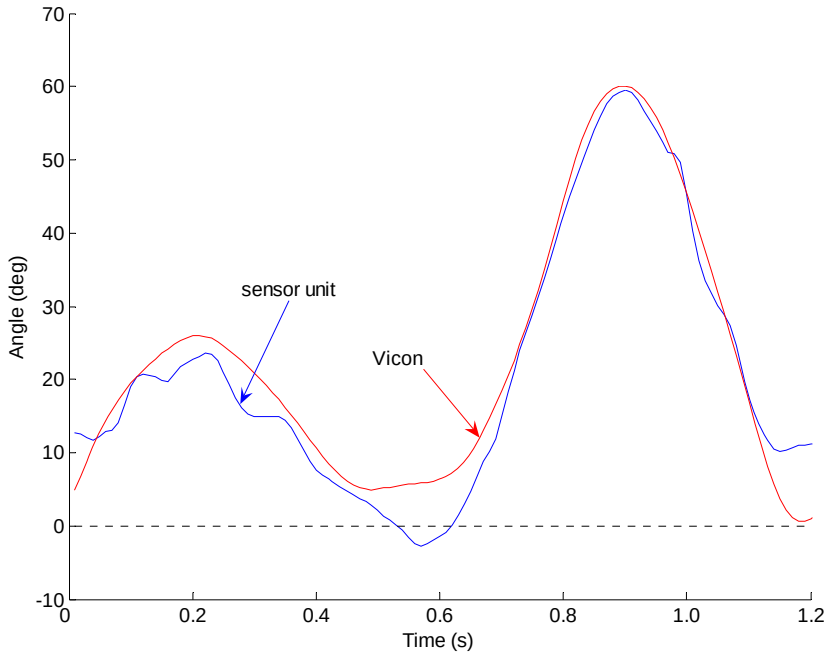

Figure 6-25 Shank segment angle in Subject 4 (left limb) of a single gait cycle from heel contact with r = 0.974 and rmsd=4.29°. A positive angle represents knee flexion, a negative angle represents knee extension and 0° represents neutral position.

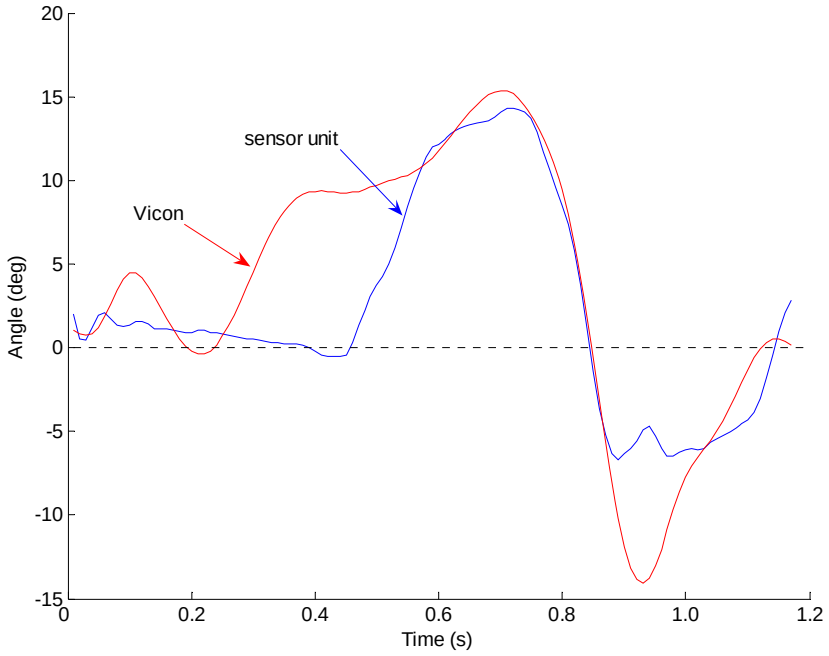

Figure 6-26 Foot segment angle in Subject 4 (left limb) of a single gait cycle from heel contact with r = 0.862 and rmsd=4.24°. A positive angle represents foot dorsiflexion, a negative angle represents foot plantarflexion and 0° represents neutral position.

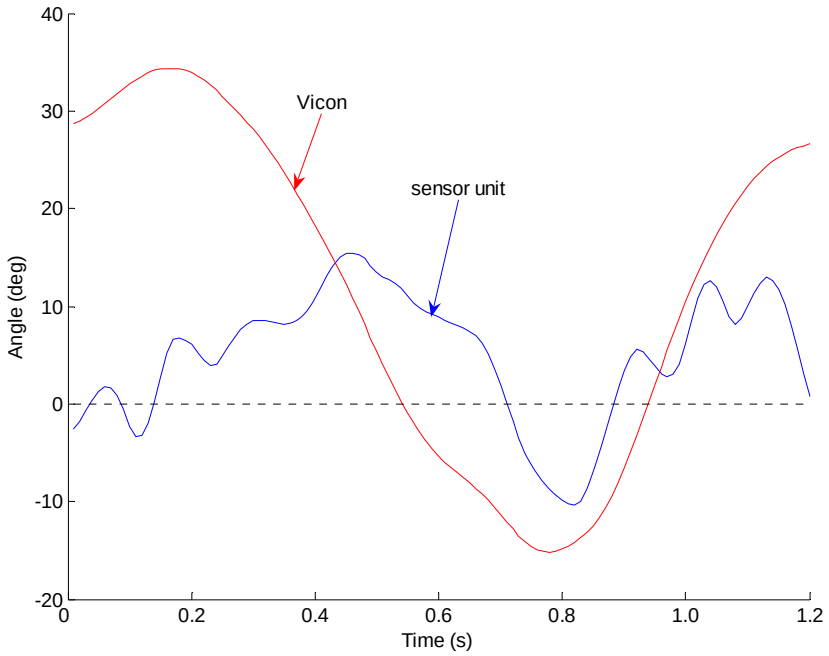

Figure 6-27 Thigh segment angle in Subject 4 (left limb) of a single gait cycle from heel contact with r = 0.289 and rmsd=17.89°. A positive angle represents hip flexion, a negative angle represents hip extension and 0° represents neutral position.

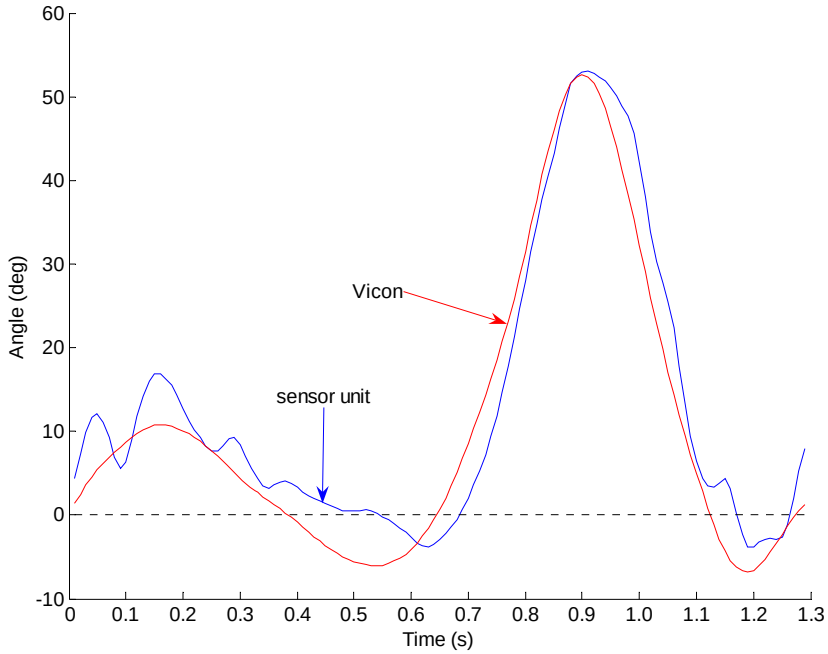

Figure 6-28 Shank segment angle in Subject 4 (right limb) of a single gait cycle from heel contact with r = 0.989 and rmsd=4.77°. A positive angle represents knee flexion, a negative angle represents knee extension and 0° represents neutral position.

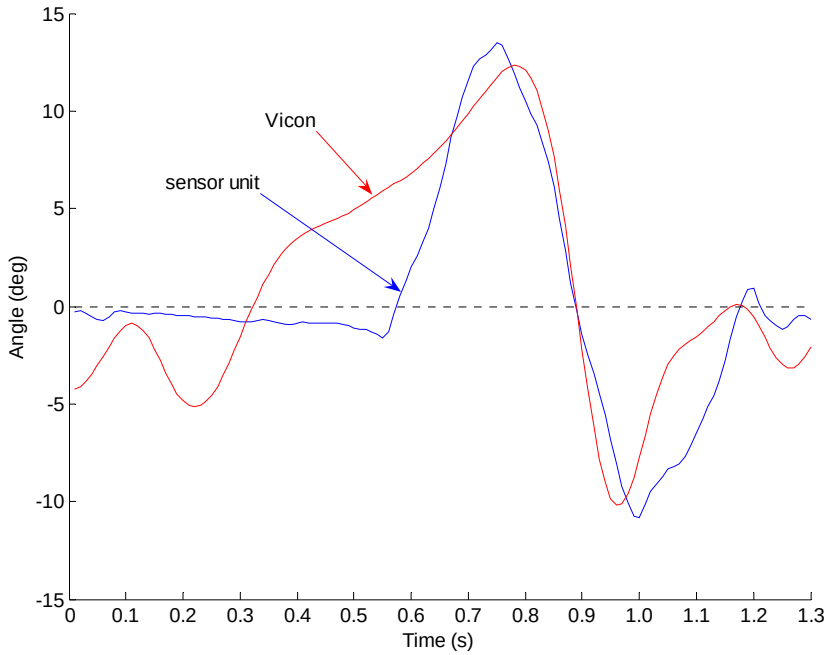

Figure 6-29 Foot segment angle in Subject 4 (right limb) of a single gait cycle from heel contact with r = 0.824 and rmsd=3.48°. A positive angle represents foot dorsiflexion, a negative angle represents foot plantarflexion and 0° represents neutral position.

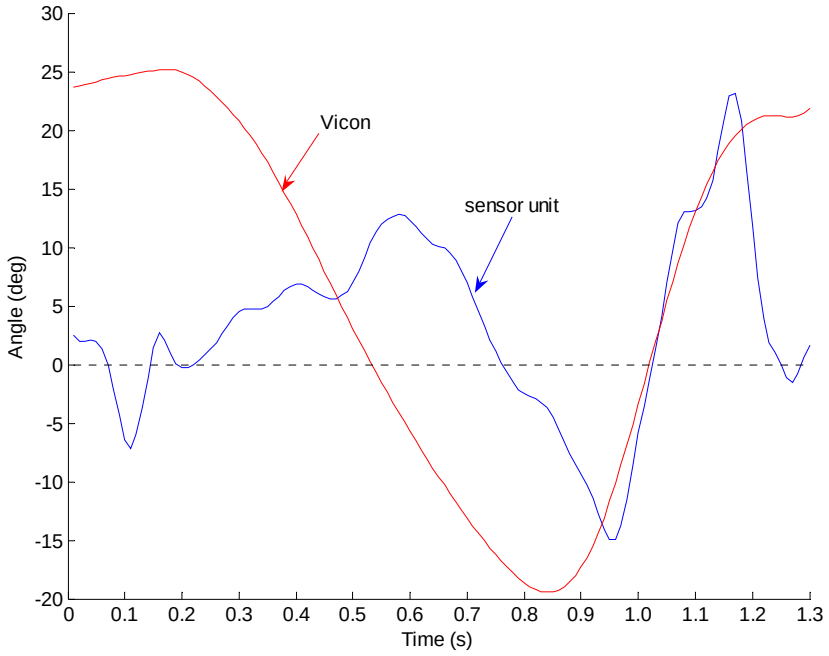

Figure 6-30 Thigh segment angle in Subject 4 (right limb) of a single gait cycle from heel contact with r = 0.243and rmsd=16.18°. A positive angle represents hip flexion, a negative angle represents hip extension and 0° represents neutral position.

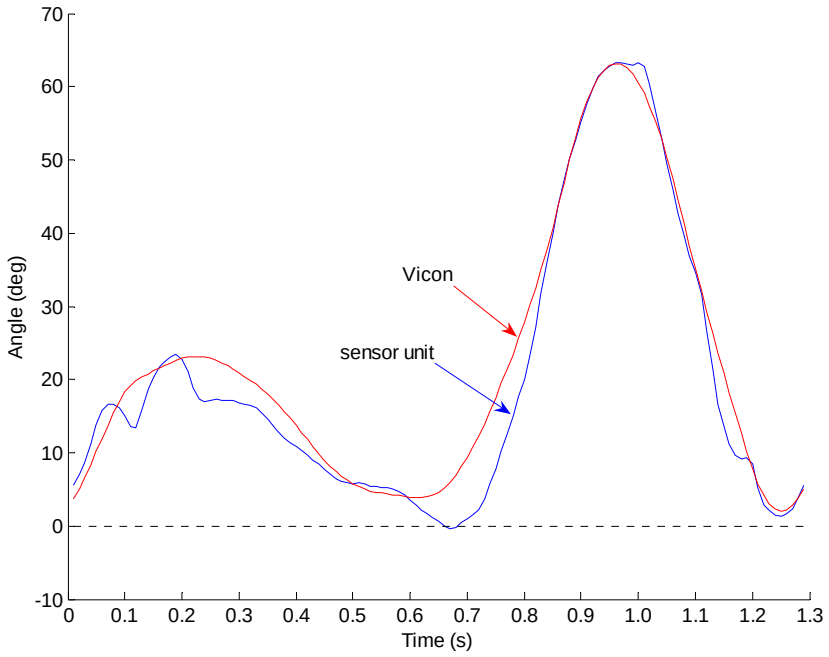

Figure 6-31 Shank segment angle in Subject 4 (left limb) of a single gait cycle from heel contact with r = 0.985 and rmsd=3.99°. A positive angle represents knee flexion, a negative angle represents knee extension and 0° represents neutral position.

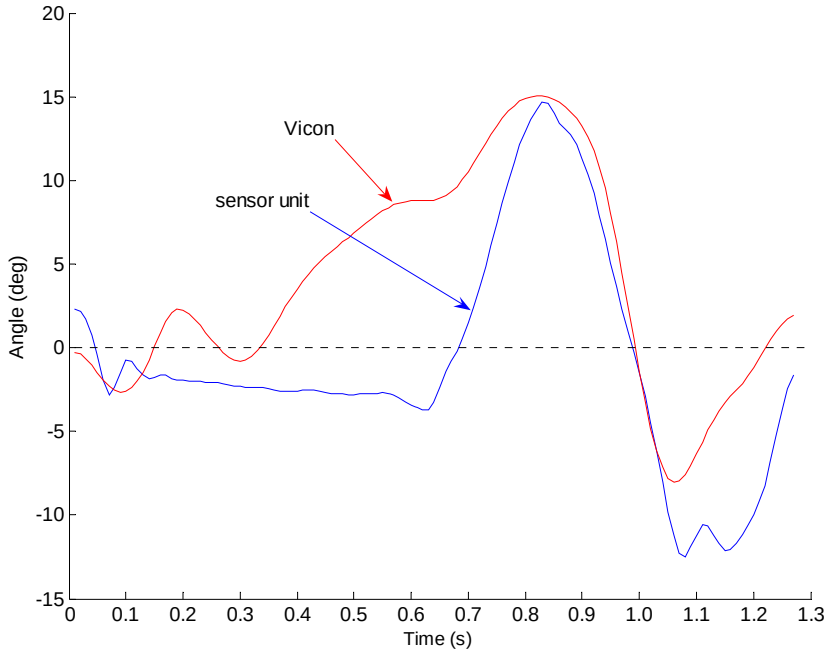

Figure 6-32 Foot segment angle in Subject 4 (left limb) of a single gait cycle from heel contact with r = 0.811 and rmsd=6.22°. A positive angle represents foot dorsiflexion, a negative angle represents foot plantarflexion and 0° represents neutral position.

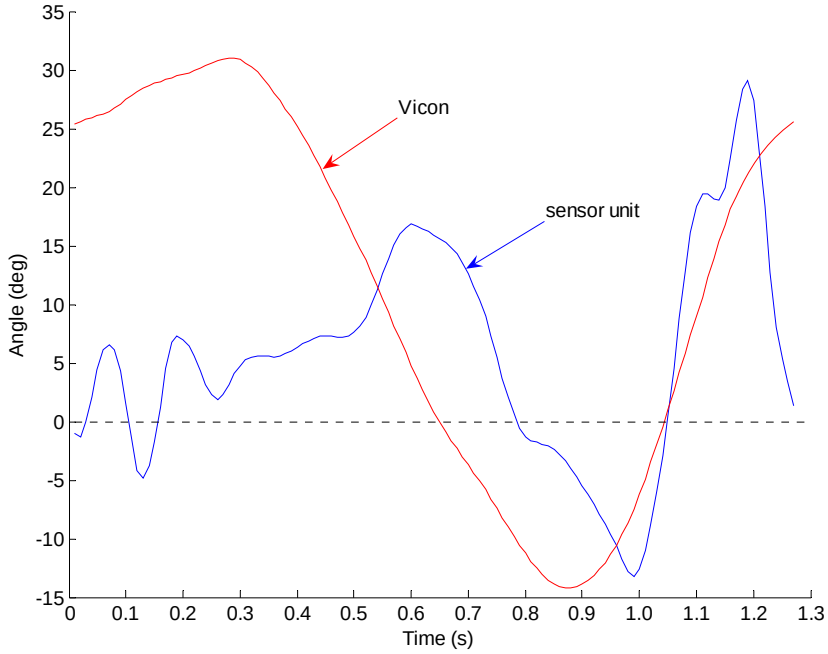

Figure 6-33 Thigh segment angle in Subject 4 (left limb) of a single gait cycle from heel contact with r = 0.288 and rmsd=16.83°. A positive angle represents hip flexion, a negative angle represents hip extension and 0° represents neutral position.

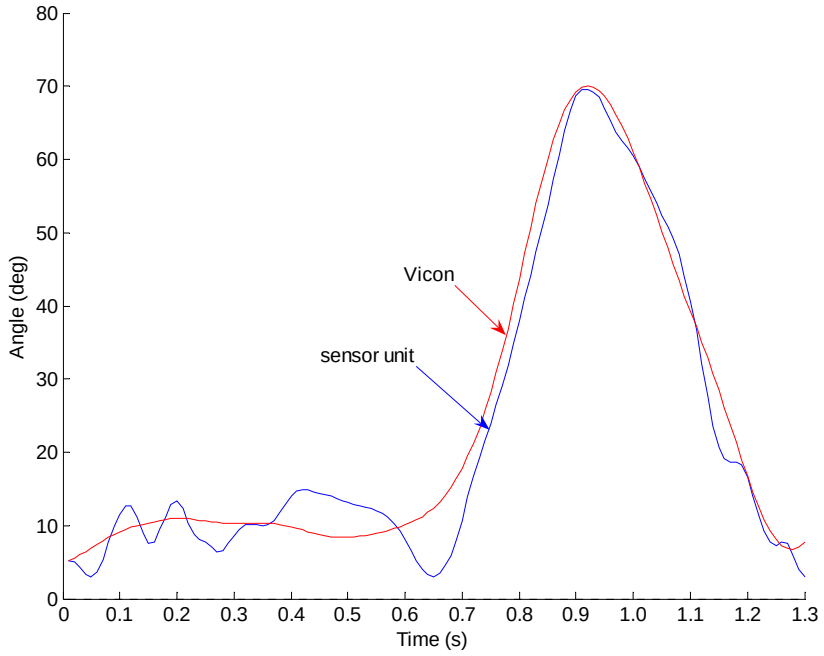

Figure 6-34 Shank segment angle in Subject 5 (right limb) of a single gait cycle from heel contact with r = 0.983 and rmsd=4.00°. A positive angle represents knee flexion, a negative angle represents knee extension and 0° represents neutral position.

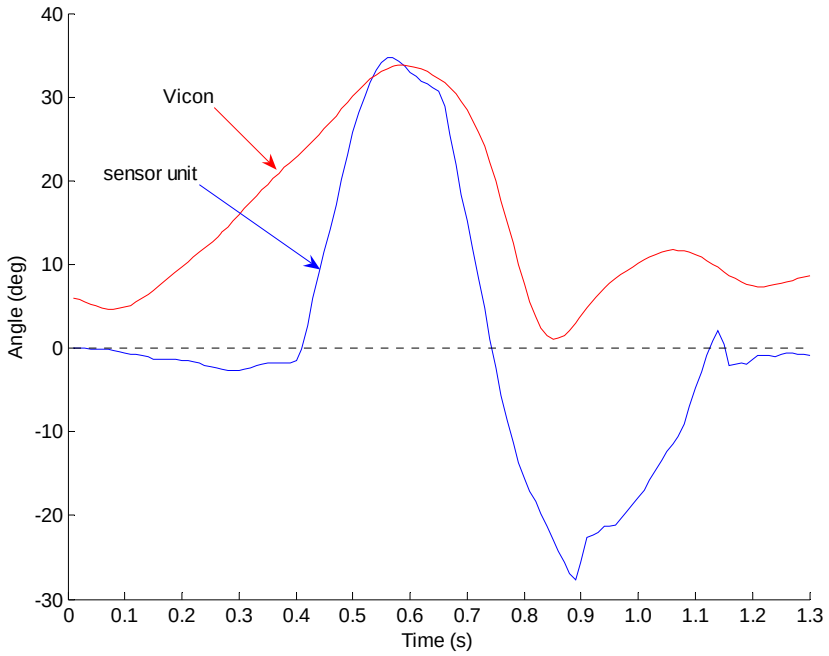

Figure 6-35 Foot segment angle in Subject 5 (right limb) of a single gait cycle from heel contact with r = 0.851 and rmsd=16.95°. A positive angle represents foot dorsiflexion, a negative angle represents foot plantarflexion and 0° represents neutral position.

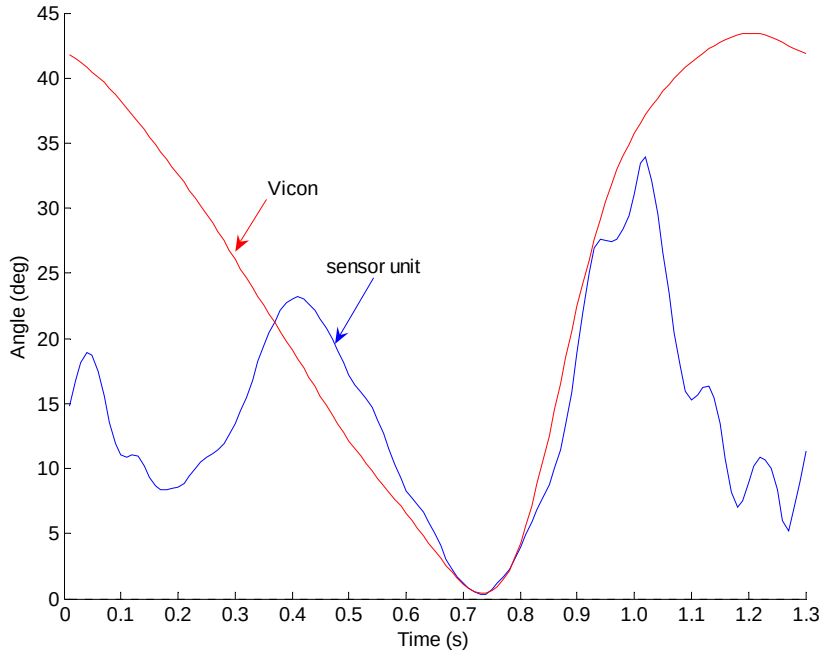

Figure 6-36 Thigh segment angle in Subject 5 (right limb) of a single gait cycle from heel contact with r = 0.380 and rmsd=17.77°. A positive angle represents hip flexion, a negative angle represents hip extension and 0° represents neutral position.

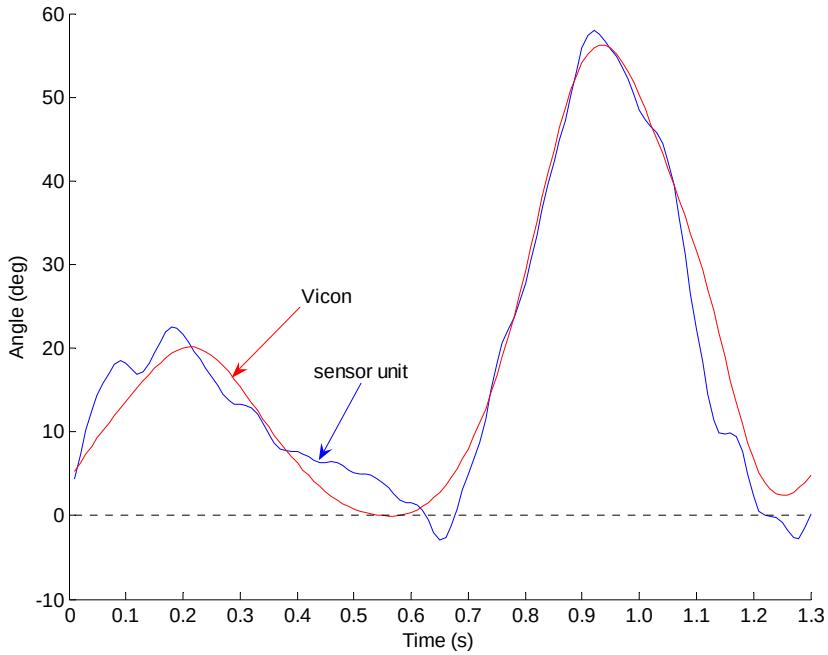

Figure 6-37 Shank segment angle in Subject 5 (left limb) of a single gait cycle from heel contact with r = 0.975 and rmsd=3.89°. A positive angle represents knee flexion, a negative angle represents knee extension and 0° represents neutral position.

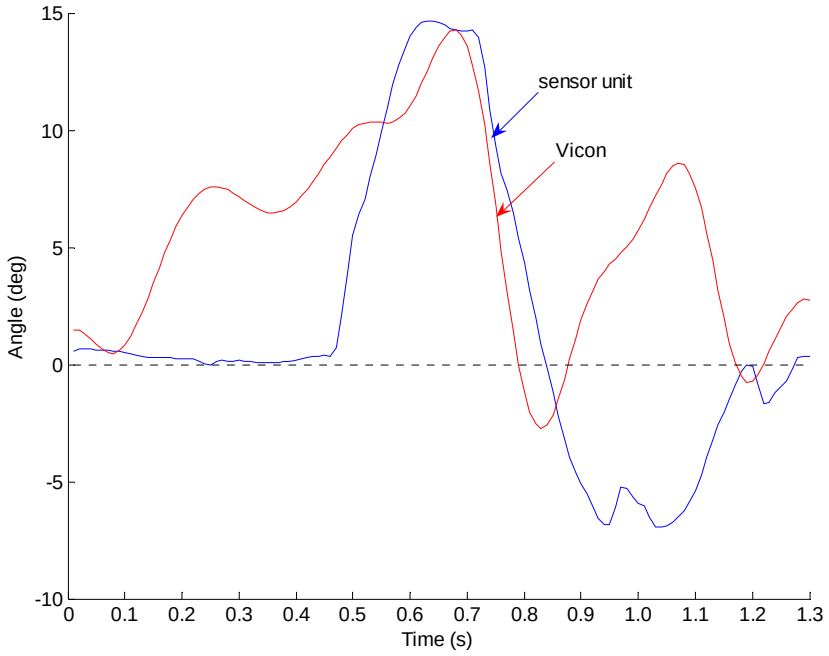

Figure 6-38 Foot segment angle in Subject 5 (left limb) of a single gait cycle from heel contact with r = 0.555 and rmsd=6.50°. A positive angle represents foot dorsiflexion, a negative angle represents foot plantarflexion and 0° represents neutral position.

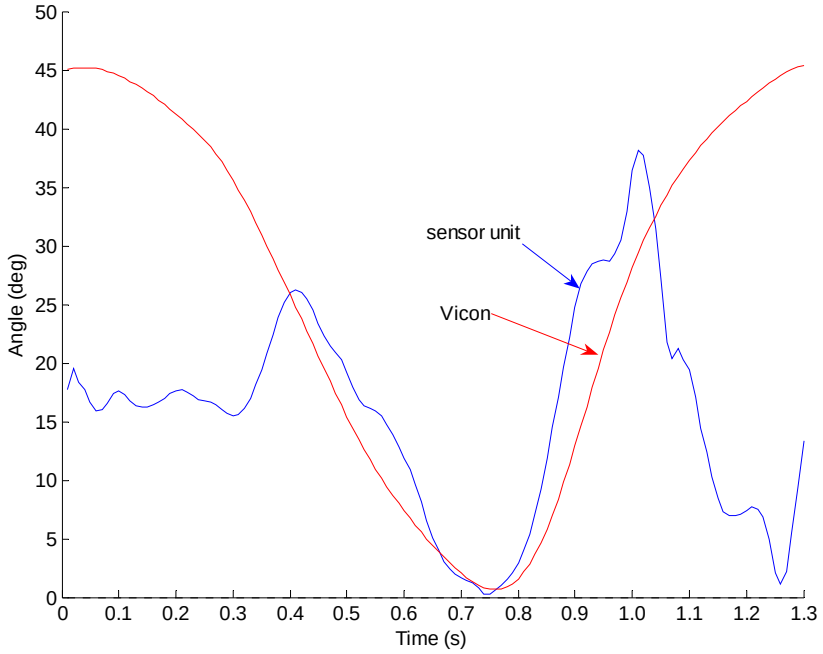

Figure 6-39 Thigh segment angle in Subject 5 (left limb) of a single gait cycle from heel contact with r = 0.253 and rmsd=19.19°. A positive angle represents hip flexion, a negative angle represents hip extension and 0° represents neutral position.

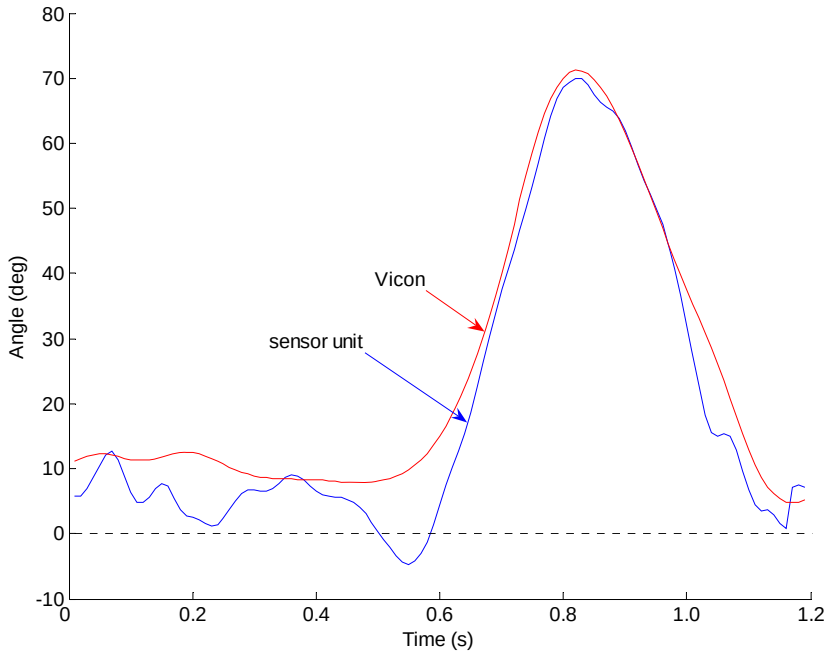

Figure 6-40 Shank segment angle in Subject 5 (right limb) of a single gait cycle from heel contact with r = 0.986 and rmsd=6.17°. A positive angle represents knee flexion, a negative angle represents knee extension and 0° represents neutral position.

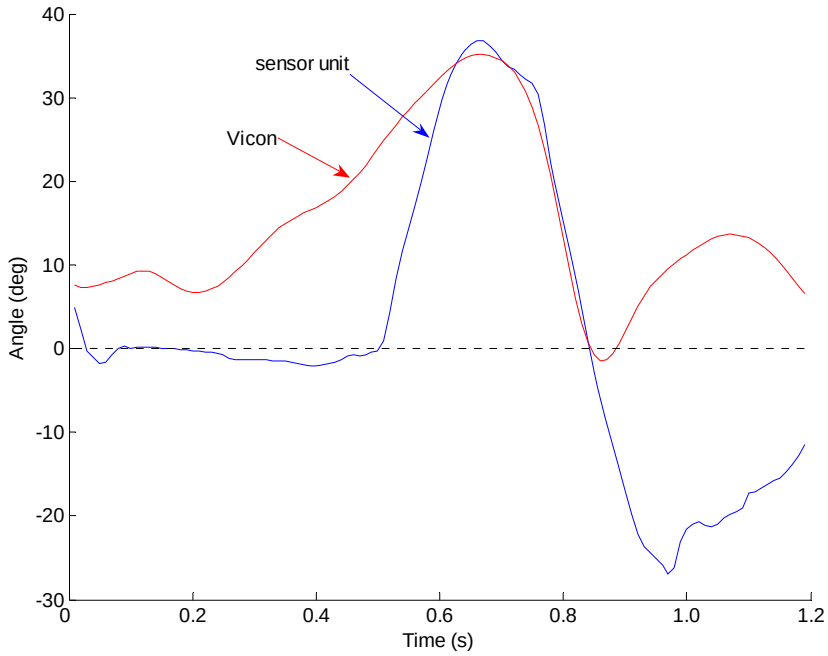

Figure 6-41 Foot segment angle in Subject 5 (right limb) of a single gait cycle from heel contact with r = 0.768 and rmsd=18.27°. A positive angle represents foot dorsiflexion, a negative angle represents foot plantarflexion and 0° represents neutral position.

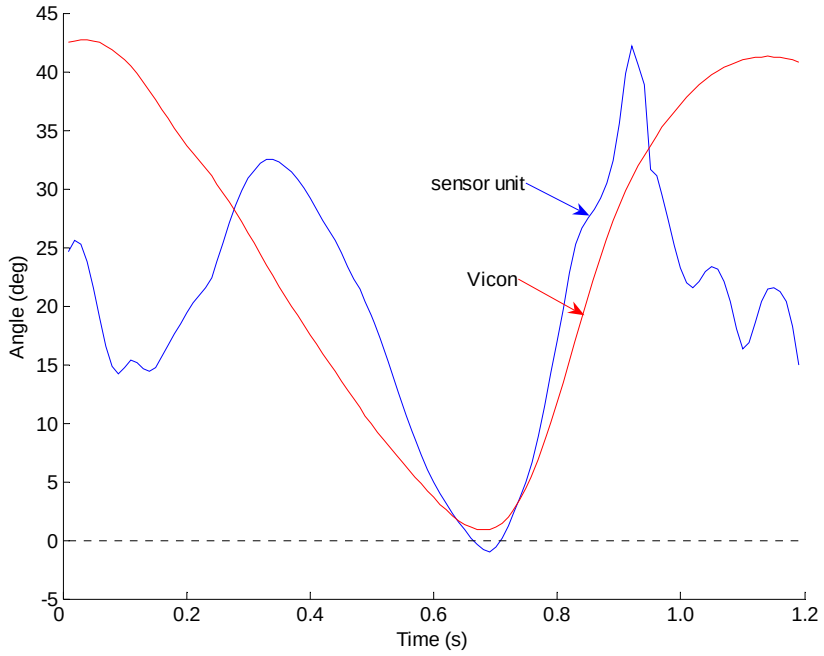

Figure 6-42 Thigh segment angle in Subject 5 (right limb) of a single gait cycle from heel contact with r = 0.509 and rmsd=13.53°. A positive angle represents hip flexion, a negative angle represents hip extension and 0° represents neutral position.

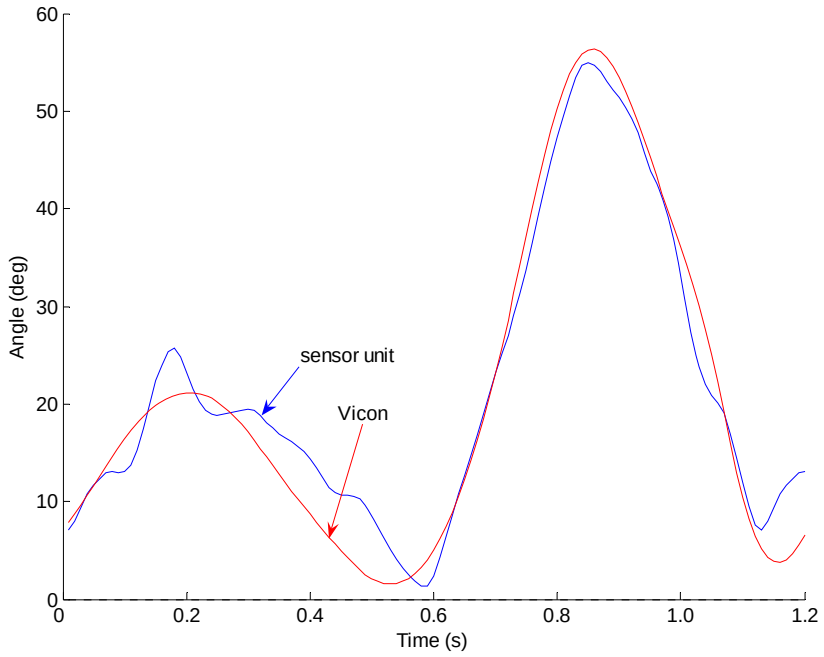

Figure 6-43 Shank segment angle in Subject 5 (left limb) of a single gait cycle from heel contact with r = 0.983 and rmsd=3.46°. A positive angle represents knee flexion, a negative angle represents knee extension and 0° represents neutral position.

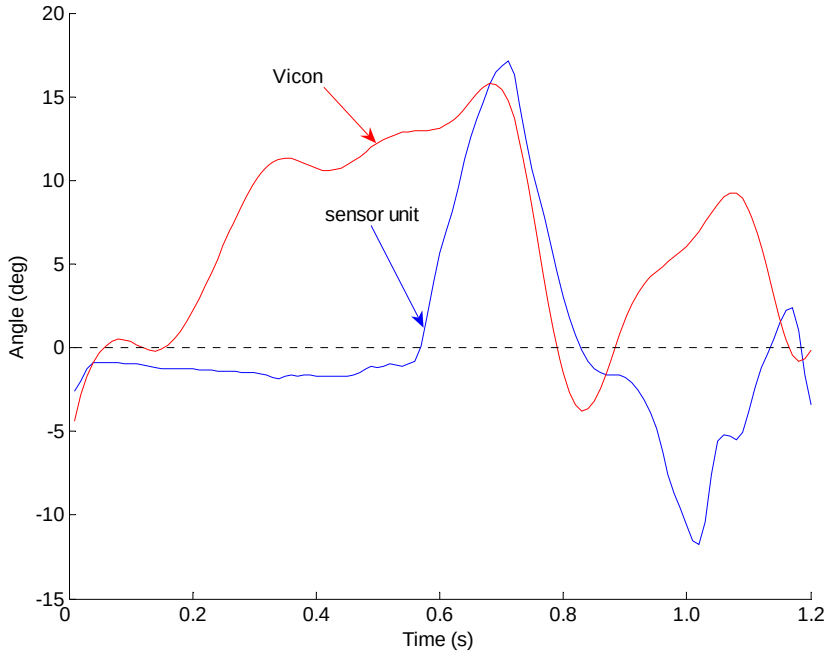

Figure 6-44 Foot segment angle in Subject 5 (left limb) of a single gait cycle from heel contact with r = 0.363 and rmsd=8.98°. A positive angle represents foot dorsiflexion, a negative angle represents foot plantarflexion and 0° represents neutral position.

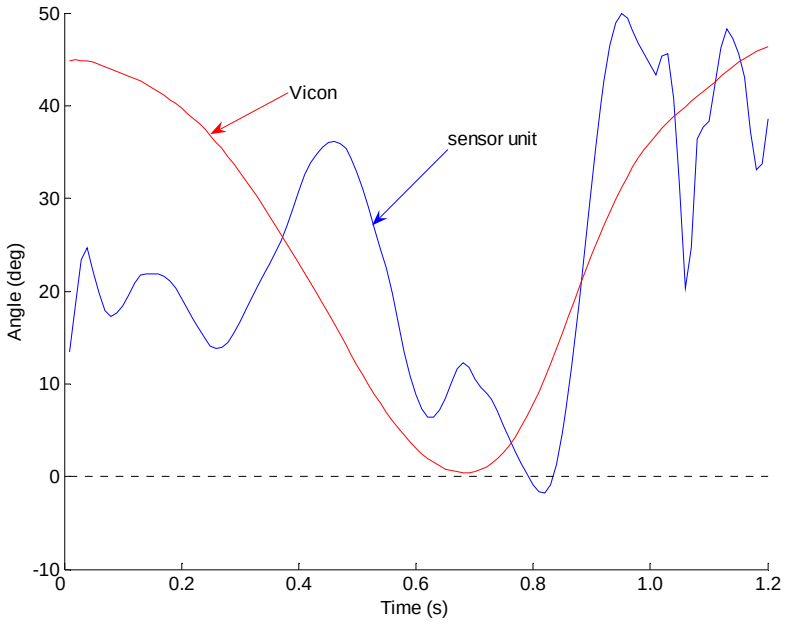

Figure 6-45 Thigh segment angle in Subject 5 (left limb) of a single gait cycle from heel contact with r = 0.514 and rmsd=14.90°. A positive angle represents hip flexion, a negative angle represents hip extension and 0° represents neutral position.

Table 6-1 lists the correlation coefficient (r) and the standard deviation (SD) of segment angle or joints angles measured using various sensors compared to various reference systems as reported by other researchers. The other term such as root mean squared error (RMSE) or root mean squared deviation (RMSD) has also been used by other researchers to report on the SD. In the table, (Tong and Granat (1999), Heyn et al. (1996), Simcox et al. (2005) and Dejnabadi et al. (2005, 2006)) have compared their angle measurement with motion analysis system. The range of the RMSE reported for shank inclination/absolute angle is between 0.026° and 3°. For knee angle the RMSE is 1.3°. The range of RMSE and correlation coefficient/cross correlation of the thigh inclination angle are between (1.6° and 4.99°) and (0.9 and 0.99). Willemsen et al. (1990b) have compared their knee angle measurement in a healthy subject during walking with goniometer and the SD reported has a range between 0.04 rad (5.73°) and 0.09 rad (11.46°). However, it is not appropriate to make a comparison between the result from the study and other studies reported in the table as different subjects (healthy and SCI), protocol (walking with self selected speed and walking with three different speeds), reference sensor/system (Vicon^{TM}, Zebris CMS-HS and goniometer) and calculation methods have been used.

Table 6-1 The correlation coefficient (r) and the standard deviation (SD) of lower limb joint and segment angle as reported by other researchers. Note that RMSE is the same statistic as SD.

Researchers	**Participants**	**Sensor used and positioned**	**Reference sensor/ system used**	**RMSE or SD and r**
Tong and Granat (1999)	One unimpaired and one incomplete spinal cord injury (SCI). Subject walked at their preferred speed along a walk path.	A gyroscope placed on the thigh and shank (anterior) of the affected leg of SCI subject using a strap.	Motion analysis system (Vicon)	For SCI subject Shank inclination angle: RMSE = 4.95° r = 0.92 Knee angle: RMSE = 6.42° r = 0.93 Thigh inclination angle: RMSE = 4.99° r = 0.90
Heyn et al. (1996)	Male volunteers	Four pairs uniaxial accelerometer and a gyroscope placed on an aluminium strip attached to thigh and shank of the	Vicon™	Shank absolute angle : RMSE = 0.026° r = 0.995 (result from one trial, walking at normal speed)

Willemsen et al. (1990b)	A healthy subject.	Eight uniaxial accelerometers on the PVC brackets attached to thigh and shank using VELCRO strap.	goniometer	Knee angle during walking: (without filtering) Std Dev= 0.1 - 0.2 rad (5.73°-11.46°) (with 5Hz filtering) Std Dev = 0.04- 0.09 rad (2.29°- 5.16°)
Simcox et al. (2005)	An able bodied subject. Walked in a straight line at self selected speed.	Sensor pack consists of uniaxial gyroscope and two 2D accelerometers attached to trunk, thigh and shank using straps.	3D Motion analysis system by EVa HiRes, Motion Analysis Corporation, California	Shank angle (left and right) RMSE = 3.0° Cross correlation = 0.97 Thigh angle (left) RMSE = 4.2° Cross correlation = 0.99 Thigh angle (right) RMSE = 2.9° Cross correlation = 0.99
Dejnabadi et al. (2005, 2006)	Eight healthy subjects. Walked on a flat treadmill at three different speeds.	Two accelerometers and one gyroscope (one module). Each module attached to the left shank and thigh using a strap.	Zebris CMS-HS (Zebris, D) ultrasound based motion measurement system	Knee angle: RMSE = 1.30°, r = 0.997 Shank angle: RMSE = 1.0°, r = 0.999 Thigh angle RMSE = 1.6°, r = 0.998

6.4 Conclusions

The thigh, shank and foot segment angle of five healthy subjects during walking have been assessed. For all five healthy subjects walking with normal speed, the range of the correlation coefficient and standard deviation calculated between measurements from the sensor unit and Vicon™ for thigh and foot segments angle for a single stride are between (r = 0.185 and r = 0.643) and (r = 0.363 and r = 0.898) and (10.29°and 19.19°) and (3.48°and 18.27°) respectively. For shank segment angle for a single stride, the correlation coefficient and standard deviation are between (r = 0.834 and r = 0.992) and (2.83°and 13.72°) respectively. The possible deviation in shank and thigh segments angles contributed from the two measurements is believed to be due to the skin movement artefact. For all the three segments thigh, shank and foot, there are differences in the cut-off frequency, sampling rate and mathematical model (mainly the reference plane) used between the two systems. The phase shift (delay) as the effect of the low pass filtering is also a source of the deviation. The comparison process was not developed fully as the raw data from the Vicon™ was not accessible. As well as the sensor unit, there are errors from the Vicon™ measurement. The skin movement artefact and the accuracy of the software used to reconstruct the missing marker can contribute to the error. As reported by Churchill et al. (2007), the most accurate reconstruction affecting the segment angle calculation can be up to ±2.3° while the least accurate reconstruction can be up to ±27.48°.

From all the segments measured using the sensor unit, only the shank segment angle has a similar pattern with the angle measured using the Vicon™ for inter-subject and intra-subject. For thigh and foot angles, the measurements from the two systems have a different pattern. However, the thigh and foot segment angle measured using the sensor unit are similar and consistent between the subjects. Therefore, the angle from any of the segments such as thigh, shank and foot can be considered to be used in the detection of heel strike and tibial vertical event in the healthy subjects which will be presented in the next chapter.

Chapter 7
Event Detection Algorithm

7.1 Introduction

This chapter presents the detection algorithm used for the detection of a heel strike event in the healthy subjects and a tibial vertical event in healthy subjects and patients. The algorithm consists of a set of rules which has been derived from a moving correlation coefficient calculated between kinematic data during walking and a selected sample window. To detect an event, a sample window is needed. Based on the results in the previous chapter, the shank segment angle measured using the sensor unit has shown the most identical pattern to the segment angle measured using the Vicon™. However, to detect a gait event, for example heel strike, a sample window selected from the shank segment angle requires more data points (about 200 more) compared to the sample window selected from the foot segment angle. Therefore, the sample window selected from the foot segment angle has been used to detect the heel strike and tibial vertical event. Less processing time will be required when a small sample window is used, thus this criterion is essential if the algorithm is going to be developed in a real time system.

7.2 The Detection Algorithm

In general, the algorithm consists of four major components (Figure 7-1). There were three sensor units attached to every limb at the thigh, shank and foot for measurement of the segment angle and linear accelerations. The sensing axis of each sensor unit was aligned with the thigh, shank and foot segment. For the thigh, the sensor unit was

attached at lateral side of the femur with the same distance from great trochanter and lateral condyle using a Velcro strap. For the shank, the sensor unit was attached at the lateral side of the shank just below the knee (about 100mm from the knee joint) using a Velcro strap. A sensor unit was attached to the foot at the cuboid (between the calcaneus and metatarsals using a double sided tape.

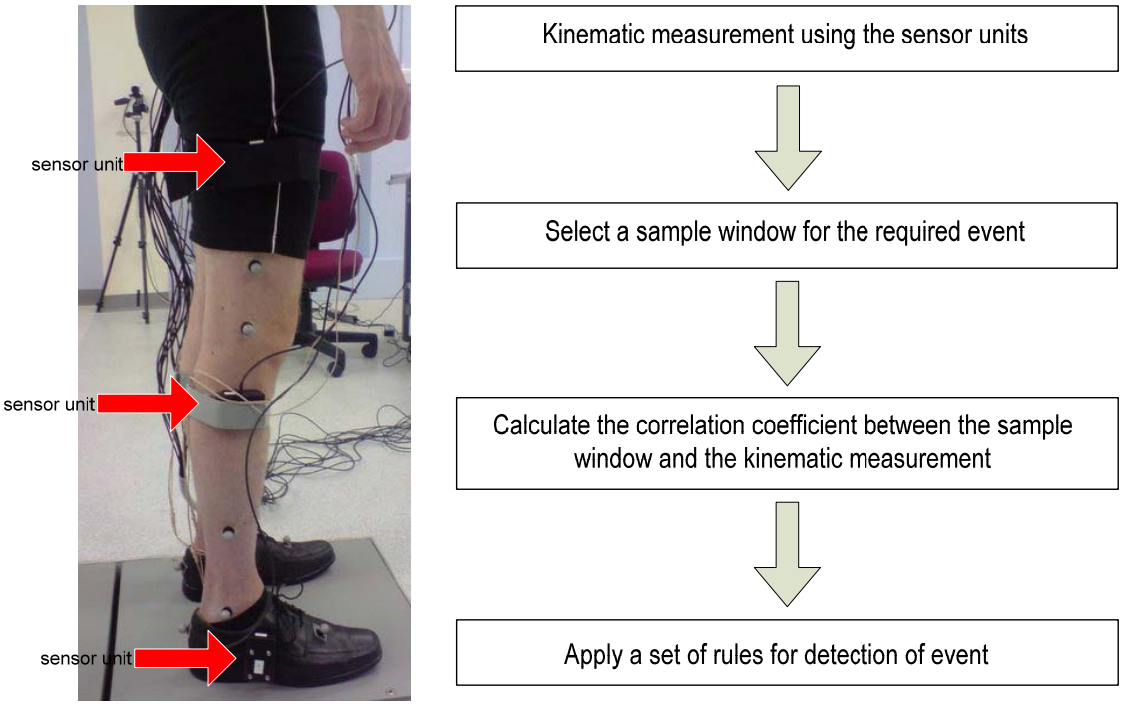

Figure 7-1 Location of the sensor units and the steps involved in the detection of events.

The sensor unit algorithm (Chapter 4, p57) is used to obtain the kinematic measurement such as segment angle and linear accelerations during walking. A sample window which coincides with the desired event is selected from the kinematic signal. After the sample window has been determined, the correlation coefficient between the sample window and the kinematic signal is calculated. A set of rules is then applied to the correlation coefficient signal to detect the desired events.

In the study, the foot segment angle has been used in the algorithm to detect the heel strike events in the healthy subjects and the tibial vertical events in the patients. The sample window selected from the foot segment angle was smaller compared to the sample window selected from the shank segment angle. The set of rules used with healthy subjects to detect heel strike is different from that used to detect that the tibia is

vertical in patients. These rules have been derived from the correlation coefficient signal obtained from the relation of the kinematic signal and the sample window selected to detect the required events.

7.3 Heel Strike and Tibial Vertical Event Detection

As mentioned earlier in this chapter, the heel strike events will be detected in the healthy subjects and the tibial vertical events will be detected in the healthy subjects and the neurological patients. The detection of heel strike event in healthy subjects will evaluate the reliability and accuracy of the detection algorithm. Also, this event will be used as a reference in the detection of tibial vertical event in the patients. This section describes those relevant processes.

7.3.1 Heel Strike Event Detection

The foot segment angle is the kinematic measurement used in the detection algorithm (refer to Figure 6-2). The typical foot segment angle of a healthy subject measured during walking using the sensor unit algorithm (Chapter 4, p57) obtained from Subject 5 is shown in Figure 7-2. In the figure, the main events occur during gait are labelled from heel rise to the next consecutive heel rise which represents a single gait cycle. Three of the events, the heel rise (HR), toe off (TO) and heel strike (HS) were determined by the events detected using the footswitches, while two of the events, the feet adjacent (FA) and tibia vertical (TV) were 27% and 13% of the gait cycle before initial contact based on HS detected by the footswitches. Ideally these events would have been determined from a force plate but this equipment was not available. Alternatively the events should have been determined from the Vicon^{TM} data. However the foot segment angle measured using the sensor unit does not aligned perfectly with the foot segment angle measured using the Vicon^{TM}. The differences are due to the two measurements using different sampling rates, the cut off frequency and the method used for filtering the Vicon^{TM} data was not known. Unfortunately, the raw data from the Vicon was not available. The angle pattern throughout the gait is described below.

- At heel rise, the angle starts to become more negative as the toe is pointing further down and continues until the angle reaches a negative peak before becoming almost parallel with the ground.
- When the next negative peak is reached, the toe starts to lift from the ground and the angle changes to a positive value instantaneously, reaching the positive peak for limb advancement as the foot initiated dorsiflexion. The amplitude of the angle decreases when the foot is in the middle of swing phase.
- When the swinging foot moves adjacent to the other shank (feet adjacent event), the segment angle becomes almost equal to zero (parallel to the horizontal plane).This angle is maintained to avoid foot slap to the ground and then becomes negative as the toe points down just after the tibia is vertical.
- The next part of the gait cycle is where the knee is fully extended with the toe pointing up in preparation for the heel to make contact with the ground. A sharp positive peak occurs in the angle signal and it has a sharp rise and fall with high frequency content due to the impact of the heel with the ground. The foot becomes flat on the ground to provide limb stability and the cycle starts again.

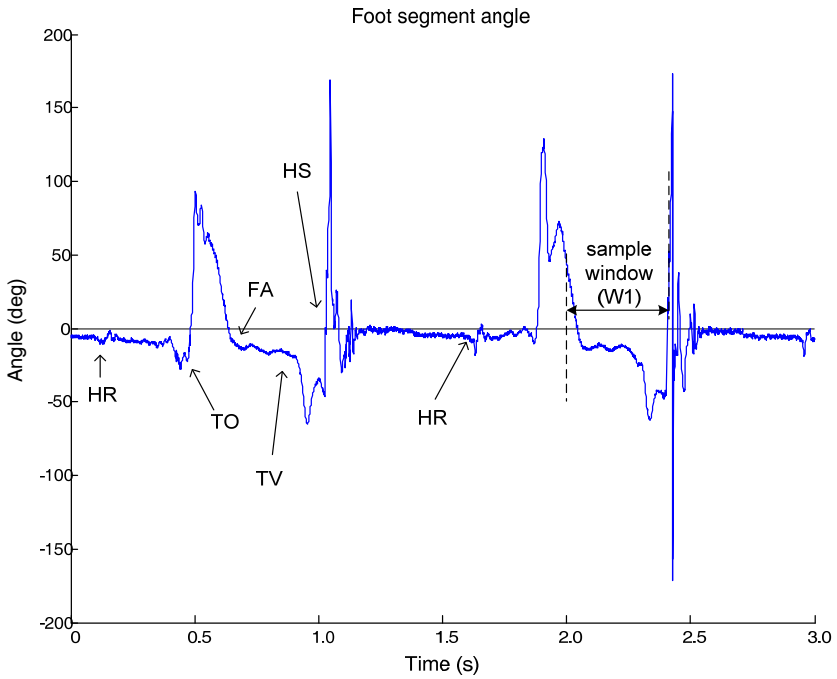

Figure 7-2 A typical foot segment angle of a healthy subject during walking (HR=Heel rise, TO=Toe Off, FA=Feet adjacent, TV=Tibia vertical, HS=Heel strike).

The foot segment angle fragment that coincides with the desired event has been selected as a sample window shown in Figure 7-2. Figure 7-3 shows the sample window (W1) selected from the foot segment angle data from a healthy subject (Subject 5) to detect the heel strike events. The sample window consists of 350 points (0.35ms). The signal begins just before the feet adjacent event ends at heel strike. This sample window is used in the detection of the heel strike events in the healthy subjects in Chapter 8. It was found that the selected template worked very well with other subject data in Chapter 8. While no further templates were investigated from the other four healthy subjects, it is anticipated that very good results would also be obtained. The window size could be reduced to less than 350 points but there will be a size at which the algorithm starts to fail to detect events reliably. The chosen size incorporated data producing a representative pattern for robust event detection.

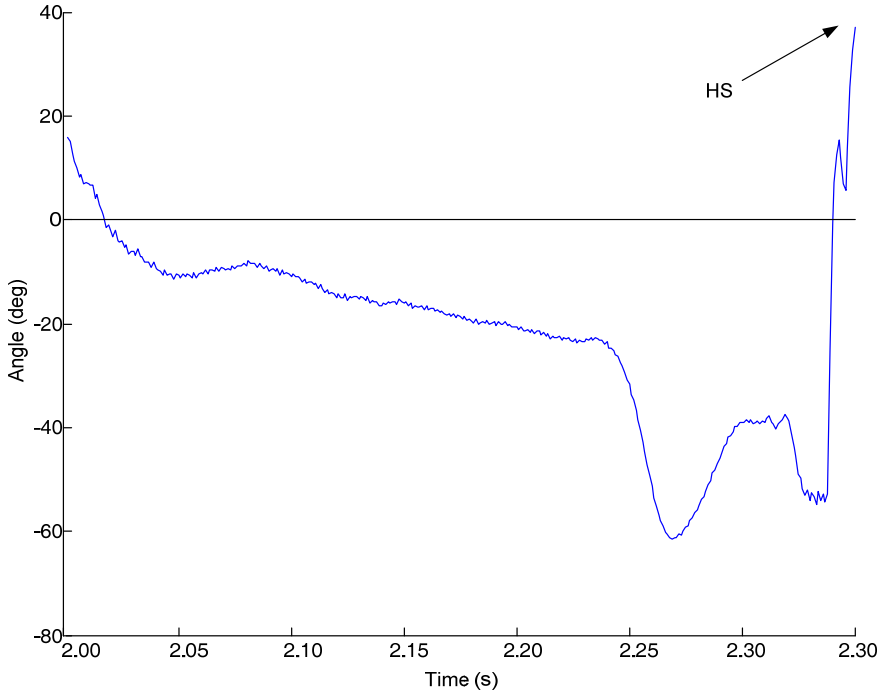

Figure 7-3 A sample window (W1) selected from a foot segment angle of a healthy subject for heel strike event detection in healthy subjects (expansion of the data from Figure 7-2).

The correlation coefficient is a measure of the strength of relationship between two variables. The value can vary from -1 (perfect negative correlation) through 0 (no correlation) to +1 (perfect positive correlation) and can be calculated using Equation 7-1.

$$r_{xy} = \frac{\sum_{i=1}^{n}(x_i - \bar{x})(y_i - \bar{y})}{(n-1)S_x S_y}$$
$$= \frac{n\sum x_i y_i - \sum x_i \sum y_i}{\sqrt{n\sum x_i^{\,2} - (\sum x_i)^2}\sqrt{n\sum y_i^{\,2} - (\sum y_i)^2}} \qquad (7\text{-}1)$$

where $\bar{x}$ and $\bar{y}$ are the mean, S_x and S_y are the standard deviation with i=1,2,3….,n

In the algorithm, the correlation coefficient is calculated between the selected sample window and the segment angle data. The first value of the correlation coefficient is obtained by correlating the whole sample window points with the same number of points of the segment angle for example 350 points as shown in Figure 7-4. The next correlation coefficient value was obtained by correlating the 350 points of the sample window with the next 350 points of the segment angle data (moving correlation coefficient). Figure 7-5 shows example of the correlation coefficient signal calculated from the healthy subject data. In this figure, the desired event that occurs in every cycle has been labelled. The most positive peak is where the event occurred and this peak should be the one after the most negative peak is reached in every cycle.

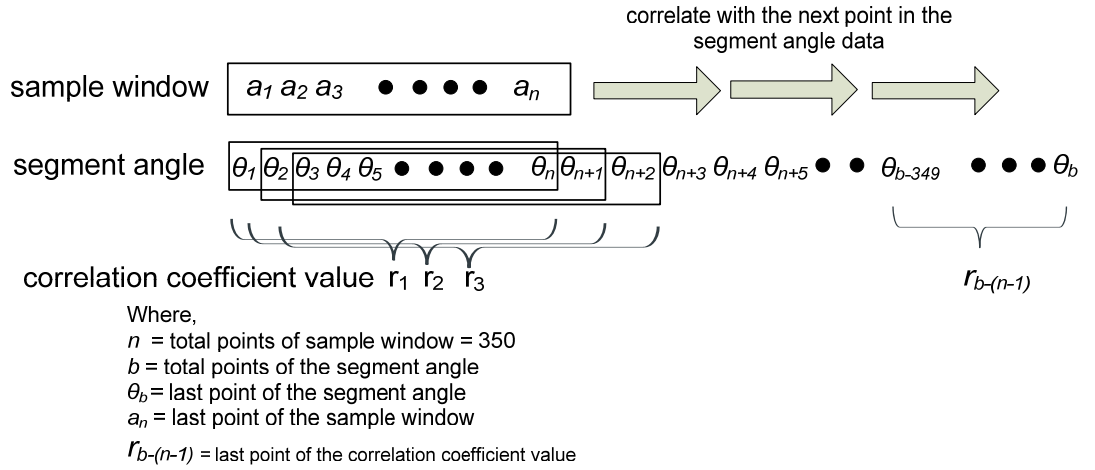

Figure 7-4 Correlation coefficient calculation. The sample window is moved to the next point in the segment angle.

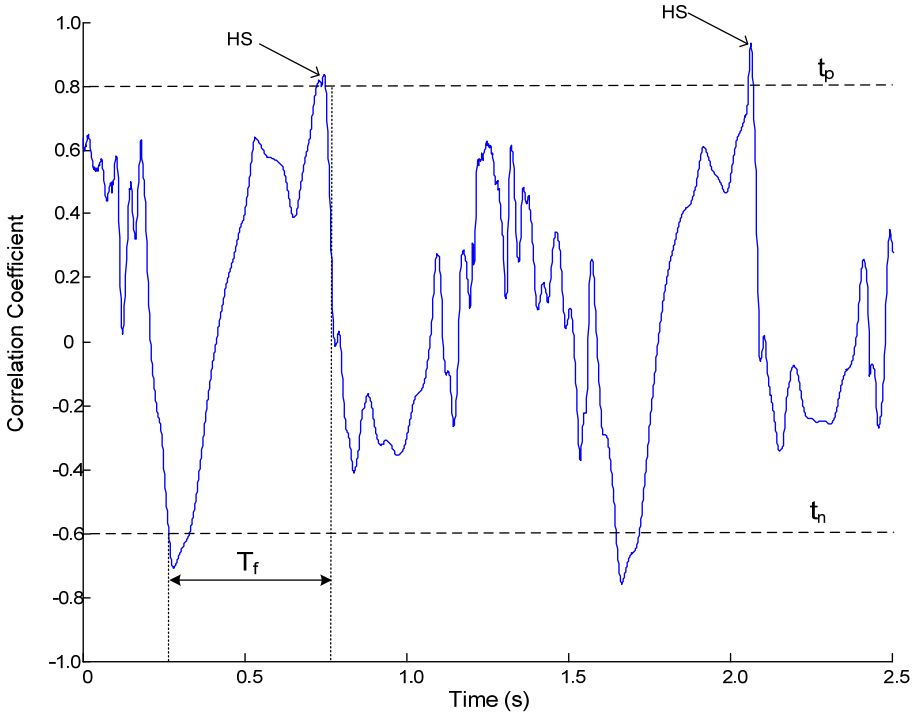

Figure 7-5 Correlation coefficient signal of a healthy subject and the heel strike events (HS), (t_n = negative threshold, t_p = positive threshold and T_f = time frame).

In the algorithm, the set of rules is derived from the correlation coefficient signal to detect the required events. The correlation coefficient signal with the corresponding set of rules (Rules I) to detect the heel strike events in the healthy subjects is shown in Figure 7-5 and the rules are as follows:

i. Begin by searching for the negative threshold (t_n) (refer to Figure 7-5), once the negative threshold (t_n) is reached, start counting for T_f (time frame). Within T_f the positive threshold (t_p) must be reached and the first maximum value (m) after positive threshold (t_p) is reached is where the event detected. The event is detected slightly earlier than the actual event occurred (maximum value). If within the T_f the positive threshold (t_p) is not reached then no event detected and the algorithm will start again by return to (i).

ii. Once an event is detected, the algorithm returns to (i).

7.3.2 Tibial Vertical Event Detection

The typical foot segment angle of a neurological patient during walking with stimulation off and with stimulation on is shown in Figure 7-6 and Figure 7-7 respectively. The main events during the gait have been labelled starting from heel rise to the next consecutive heel rise. The foot segment angle pattern measured in the patient is slightly different from the foot segment angle measured in the healthy subject. The most notable difference is just after toe off where the angle during stimulation goes positive during the swing phase. However, the pattern is almost similar between the patients except for Patient 3 and Patient 4 (Appendix H). As can be seen in Figure 7-6, at toe off there is a sudden change in angle that reaches zero but does not go positive or have a large change when compares to angle for a normal subject (Figure 7-2). However the angle goes positive (Figure 7-7) when the patient walked with stimulation on since the tibialis anterior muscles dorsiflexes the ankle with a greater torque and reduced plantarflexion during swing.

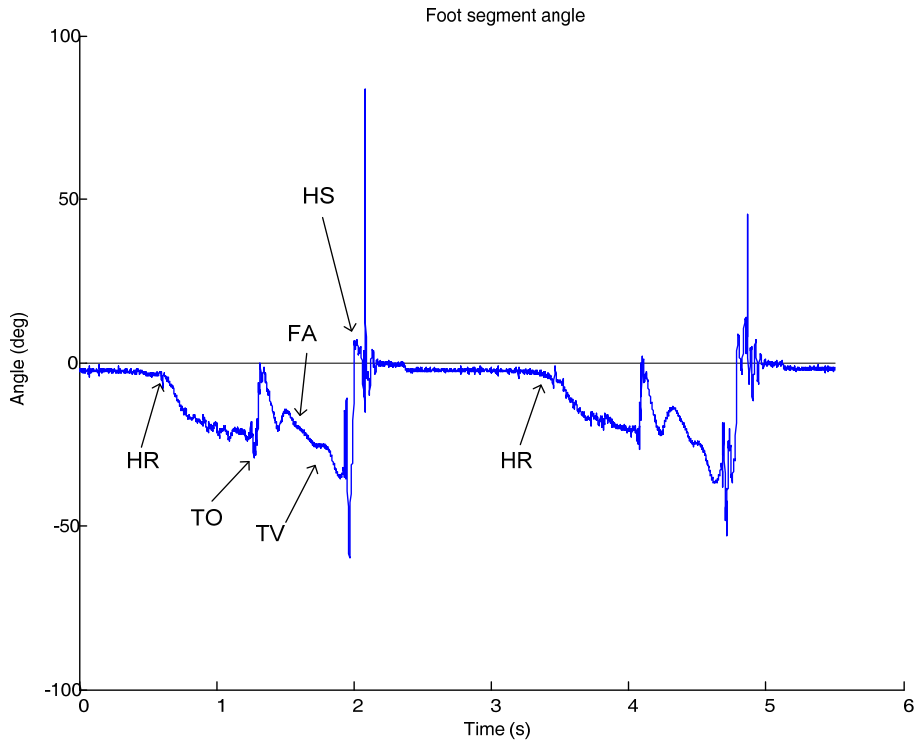

Figure 7-6 A typical foot segment angle of Patient 1 during walking with stimulation off, (HR=Heel rise, TO=Toe Off, FA=Feet adjacent, TV=Tibia vertical, HS=Heel strike).

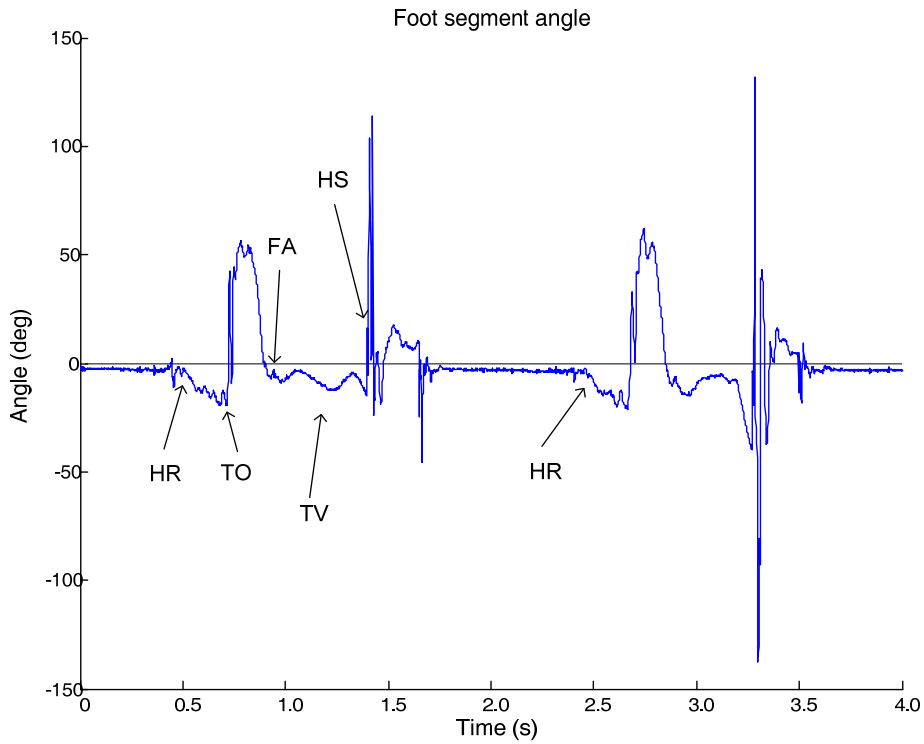

Figure 7-7 A typical foot segment angle of Patient 1 during walking with stimulation on (gluteal and tibialis anterior muscles), (HR=Heel rise, TO=Toe Off, FA=Feet adjacent, TV=Tibia vertical, HS=Heel strike).

The same sample window (W1) is used in the detection of tibial vertical events in five out of seven neurological patients P1, P2, P5, P6 and P7 in Chapter 10. The same sample window used in the detection of tibial vertical event in P1, P2, P5, P6 and P7 has been used in P3. However, the event detected was heel strike event and not tibial vertical event. This could be that the foot segment angle of P3 is similar with the foot segment angle of the healthy subjects. Therefore, a sample window was selected from data of P3 as shown in Figure 7-8 to detect the tibial vertical event. Figure 7-9 shows a sample window (W2) selected from the foot segment angle of a patient (Patient 3) to detect the tibial vertical events for the respective patient. The signal selected start from about the mid of toe off to the tibial vertical event and consists of 350 points (0.35s).

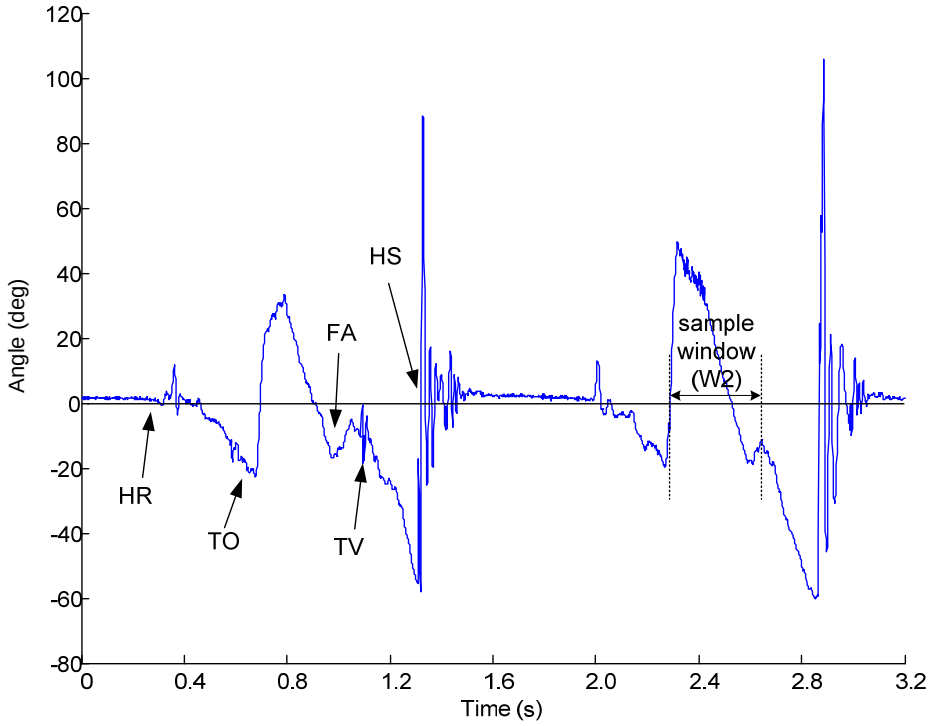

Figure 7-8 The foot segment angle of a patient (Patient 3) during walking with stimulation on.

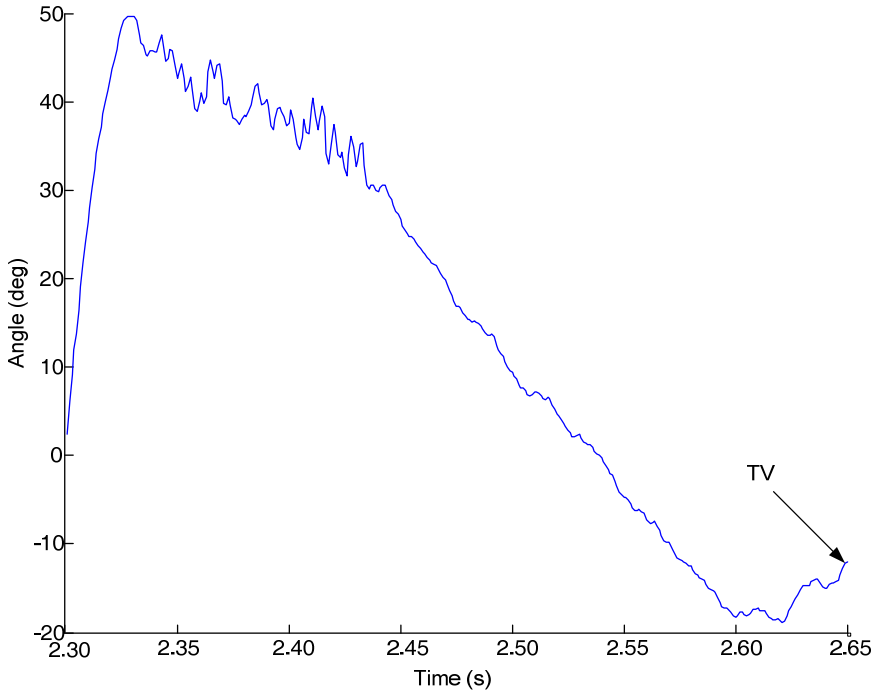

Figure 7-9 A sample window (W2) selected from the foot segment angle of a patient (Patient 3) for tibial vertical events detection in Patient 3, (expansion of the data from Figure 7-8).

The next step will be to correlate the sample windows with the segment angle data to obtain the correlation coefficient signal for the events detection. Figure 7-10 shows example of the correlation coefficient signal calculated from the patient data. In this figure, the desired event that occurs in every cycle has been labelled. The most positive peak is where the event occurred and this peak should be the one after the most negative peak is reached in every cycle.

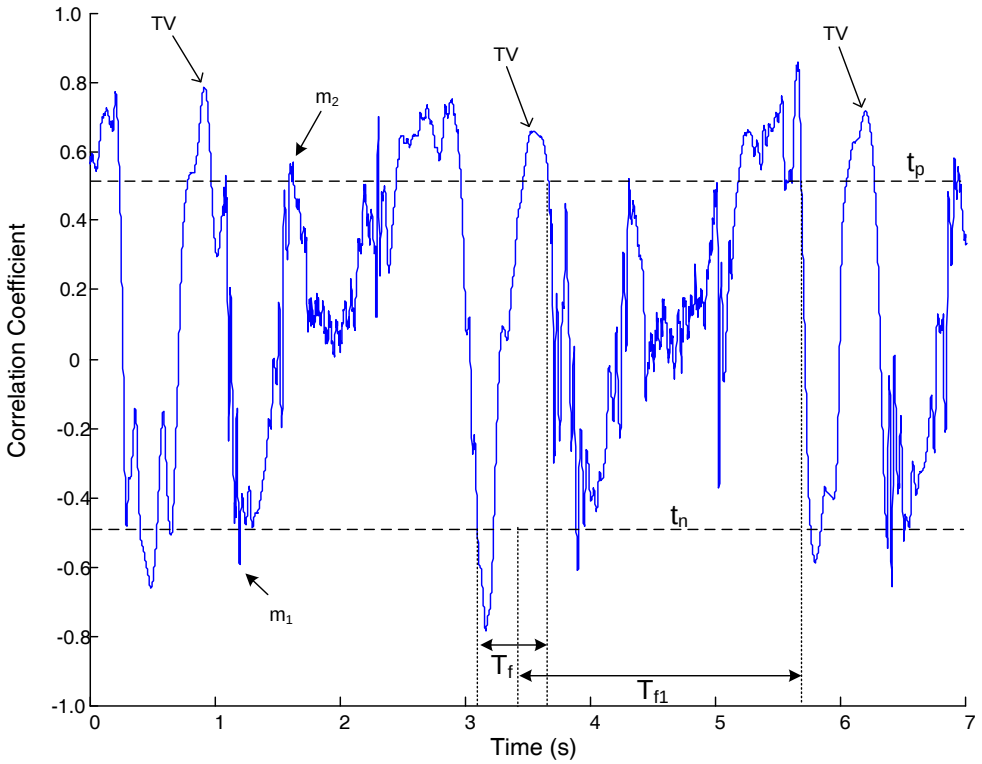

Figure 7-10 Correlation coefficient signal of a patient and the tibial vertical events (TV), (t_n = negative threshold, t_p = positive threshold, T_f = time frame and T_{f1} = time frame 1).

The occurrence of the desired event in the correlation coefficient signal is identified. A dedicated set of rules is derived that is based on the signal to detect the events. A time frame is introduced into the rules to refine the detection algorithm. This extra process is necessary as there is an additional minimum, followed by a maximum value in the correlation coefficient signal (m_1 and m_2 in Figure 7-10).

Figure 7-10 shows the correlation coefficient signal with the corresponding set of rules (Rules II) to detect the tibial vertical events in the neurological patients and the rules are as follows:

i. Begin by searching for the negative threshold (t_n) (refer to Figure 7-10), once the negative threshold (t_n) is reached, start counting for T_f (time frame). Within T_f the positive threshold (t_p) must be reached and the first maximum value (m) after positive threshold (t_p) is reached is where the event detected. If within the T_f the positive threshold (t_p) is not reached then no event occurred and the algorithm will start again. The event is detected slightly earlier than the actual event occurred (maximum value).

ii. Once an event is detected, start counting for T_{fl} (time frame 1). Within the T_{fl} any detection will be cancelled. After T_{fl} has ended, the algorithm returns to (i).

7.4 The Footswitch Circuit (Taylor (2005))

The circuit used with the footswitch is the same circuit used by the ODFSIII V6.22 stimulator. The circuit consists of a voltage divider (R1, R2 and R3), low pass filter (C1 and R4) and tracking comparator (LP324M) as shown in Figure 7-11. The force sensitive resistor (FSR) contained in the footswitch (Figure 7-12) is sensitive to the force applied on it. Whenever there is a force applied upon the FSR the resistance will reduce from about 2MΩ to 2kΩ. The footswitch is connected to the jack socket (JACK1) and part of the voltage divider circuit. When the FSR resistance varies the voltage across the R2 and R3 will also vary. The voltage divider output is low pass filtered using a 33.86kHz cut off frequency filter. This voltage will charge the capacitors C2 through the resistor R5. The capacitor used is a low leakage electrolytic. When the voltage at the non-inverting input is higher than the voltage at the inverting input, the output is high. When the input at the inverting input is higher than the voltage at the non-inverting input, the output is low. The resistor R6 provides a hysteresis to the comparator output and the capacitor C3 is used to prevent the oscillation.

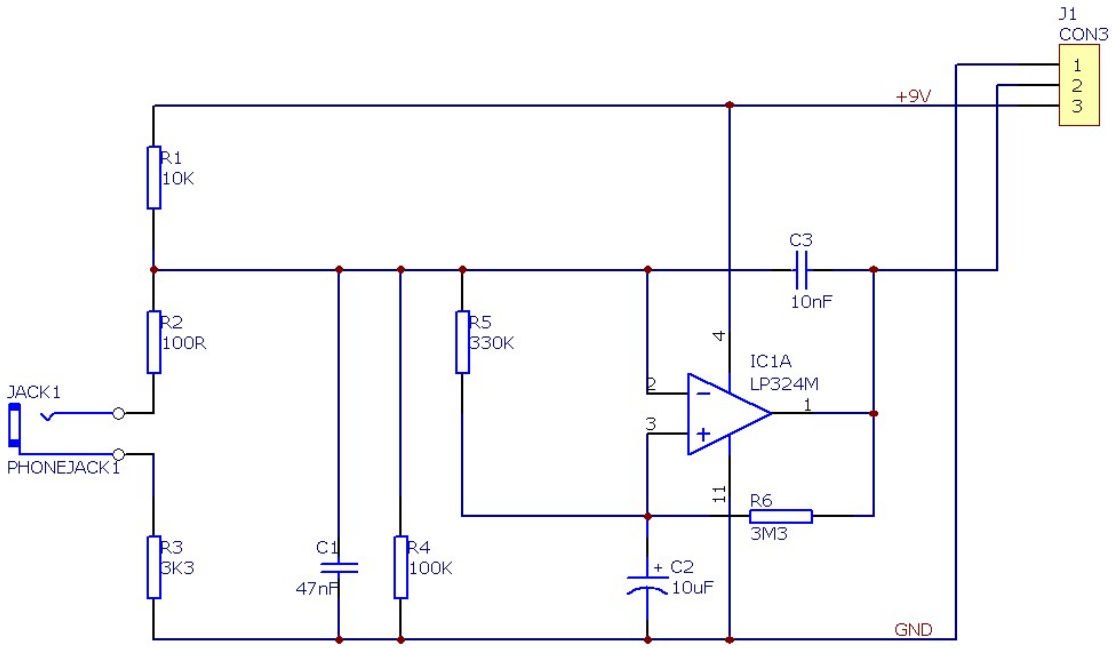

Figure 7-11 The footswitch circuit diagram.

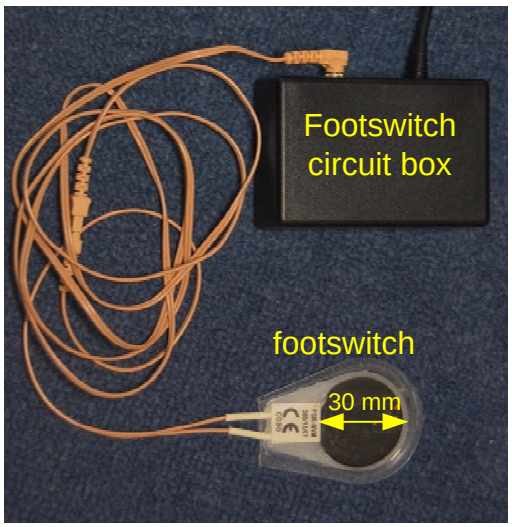

Figure 7-12 The footswitch and circuit box.

Some tests have been carried out to investigate the effect of fast and slow loading and unloading on the footswitch. The tests use force sensor (FSG15N1A by Honeywell) which the output changes correspond to the force applied on it. The results are presented in Appendix I. From the results, the footswitch shows a fast output voltage response. The hysteresis between high and low is small enough to cause uncertainty in the output resulting in a feathered edge.

7.5 Conclusions

An algorithm to detect heel strike events in the healthy subjects and tibial vertical events in the neurological patients is presented. A sample window (W1) to detect these events uses 350 data points selected from the foot segment angle of one healthy subject (Subject 5). The signal begins just before the feet adjacent event ends at heel strike. The sample window is correlated with the foot segment angle to obtain a signal where the event is detected using a set of rules. A single time frame has been used to detect the heel strike event in healthy subjects and two time frames to detect tibial vertical in patients. These time frames are used to avoid any false detection when the thresholds in the set of rules have been achieved. The threshold values and time frame can be set for individual subjects by adjustment. This procedure is based on the correlation coefficient signals from all trials of the individual subjects to optimise the detection time. The algorithm will be evaluated off-line in the next three chapters to detect heel strike (in healthy subjects) and tibial vertical events in healthy subjects and patients.

Chapter 8
Evaluation of Heel Strike Event Detection in Healthy Subjects

8.1 Introduction

This chapter reports on detecting heel strike events in five healthy subjects using the sensor unit algorithm (Chapter 4, p57) and detection algorithm (Chapter 7, p133). A sample window selected from one subject (Subject 5) will be used to detect the heel strike event in all five subjects using the algorithm. It is anticipated that the sample window could be used to detect the event in all five healthy subjects as reliable and as accurate as the footswitch. As the algorithm will be used later to detect important events such as when the tibia is vertical during gait with the future aim to trigger a two channel stimulator for different gait problems, it is important to determine the reliability and the accuracy of the algorithm. In the study, the footswitch is used as a 'gold standard' for detection of heel strike event. The same footswitch used has been evaluated by (Findlow et al. (2004)) in their study and the time difference reported was -7 ± 19ms as compared to the force plate. Ideally, the force plate would have been used as the reference in the study to detect the heel strike event. However, the force plate was not available. Also, there is a drawback of using the force plate as a single force plate can only detect a foot contact from a single step during stance. In the future, if the trials are going to be conducted outside the laboratory for walking on different terrains such as slopes or stairs, it is not possible to use the force plate as well. For these

reasons, a simple yet reliable sensor such as footswitch is the best alternative to detect heel contact events.

Traditionally, the heel strike event has been used as the time to end the stimulation of tibialis anterior muscles or peroneal nerve that dorsiflexed the ankle during swing. The timing for this event is not critical, however Kotiadis et al. (2010) has set 150ms before and after the event as the acceptable timing limits. Therefore, the heel strike event detected in the study should be within the reported timing limits.

8.2 Procedures

8.2.1 Subjects, Set-up and Protocol

The data of five healthy subjects obtained from the experiments described in section 6.2.1, 6.2.2 (i & ii) and 6.2.3 has been used in the analysis for the detection of the heel strike events. The analysis was done off-line using the algorithm described in the previous chapter. Data from a footswitch was used as a reference in the analysis to evaluate the algorithm. Time differences between the outputs from the algorithm and the footswitch were used to determine the accuracy of the algorithm. The number of events detected by the algorithm compared to the footswitch is used to determine the reliability of the algorithm.

8.3 Data Analysis

8.3.1 Heel Strike Events Detection

For every subject, the segment angle shown in Figure 6-2 (Chapter 6, p101) obtained from the sensor units and the data from the footswitches of both lower limbs were analysed off-line. Only the foot segment angle was used to detect the heel strike events using the algorithm described in the previous chapter. All of the subjects had heel strike as initial contact. Only the footswitch placed under the heel was used in the analysis. During the experiments, the heel footswitch sometimes did not register a heel strike. Under these circumstances the footswitch under the toe was used to register that the foot had made contact with the ground (foot flat). A sample window (W1) (Chapter 7,

p135) selected from a foot segment angle data from one of the subject (Subject 5) was used in the correlation coefficient calculation for all the other subjects (five in total) to detect the heel strike events. For two of the subjects (Subject 1 and Subject 3), only the right lower limb data was analysed. All program routines are included in Appendix G. The negative and positive threshold values and time frame which satisfied with all the trials for that respective subject have been determined. Table 8-1 lists the threshold values and time frame used in the algorithm for the detection of the heel strike events for every subject. The threshold values and time frame were set for individual subject based on the correlation coefficient signal obtained. For every subject, two horizontal lines which represent the thresholds were drawn on the correlation coefficient signal beginning with 0.3 for positive threshold and -0.3 for negative threshold (refer to Figure 7-5 (Chapter 7, p137) for a correlation coefficient signal). The line was moved by 0.5 towards 1 for positive threshold and -1 for negative threshold. The last value before the line started to go beyond the positive or negative peak of the correlation coefficient signal in all trials for the respective subject, was set as the threshold. The time frame, T_f was set for individual subject which start at the signal crossing the negative threshold (down slope) before the event and end slightly after the event has been detected and after crossing the positive threshold (down slope).

Table 8-1 The thresholds for the correlation coefficient signal and time frame for heel strike events detection.

Subject	*Positive threshold, t_p*	*Negative threshold, t_n*	*Time frame, T_f in ms*
Subject 1	0.80	-0.45	450
Subject 2	0.70	-0.40	450
Subject 3	0.70	-0.60	450
Subject 4	0.75	-0.60	500
Subject 5	0.80	-0.60	500

8.3.2 Time Difference Calculation

The time difference between the heel strike events detected by the algorithm (Chapter 7, p133) and the footswitch is described in Figure 8-1 and Figure 8-2. The time difference is negative when the algorithm detects the event earlier than the footswitch and positive when the footswitch detects the event earlier than the algorithm. The time difference can be calculated using Equation 8-1.

$$\text{time difference} = t_a - t_s \qquad (8\text{-}1)$$

where t_a is the time of heel strike event detected using algorithm and t_s is the time of heel strike event detected using the footswitch.

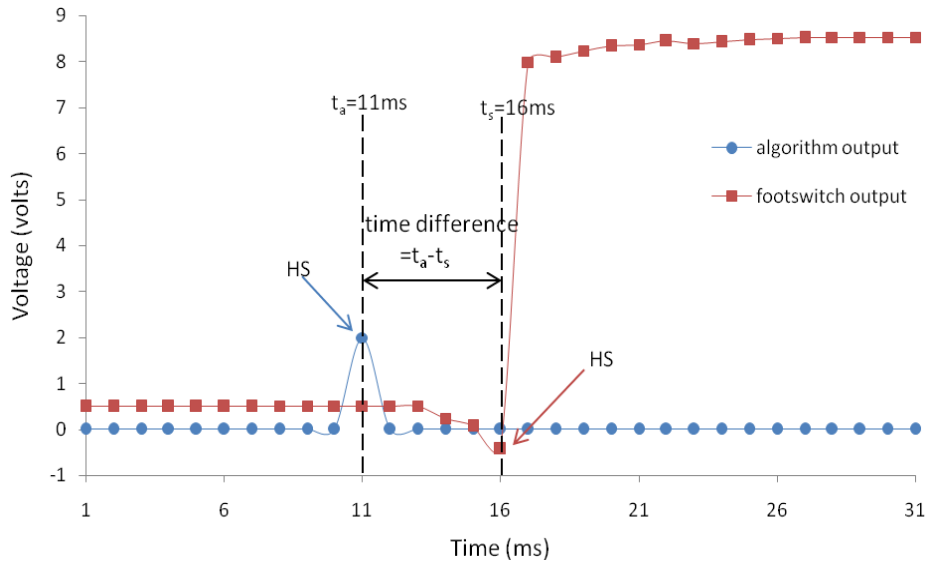

Figure 8-1 An example to illustrate a negative time difference. Shown in the plot is a time difference of -5ms between the heel strike detected by the algorithm (blue arrow) and the footswitch (heel switch, red arrow) from the data of subject 5.

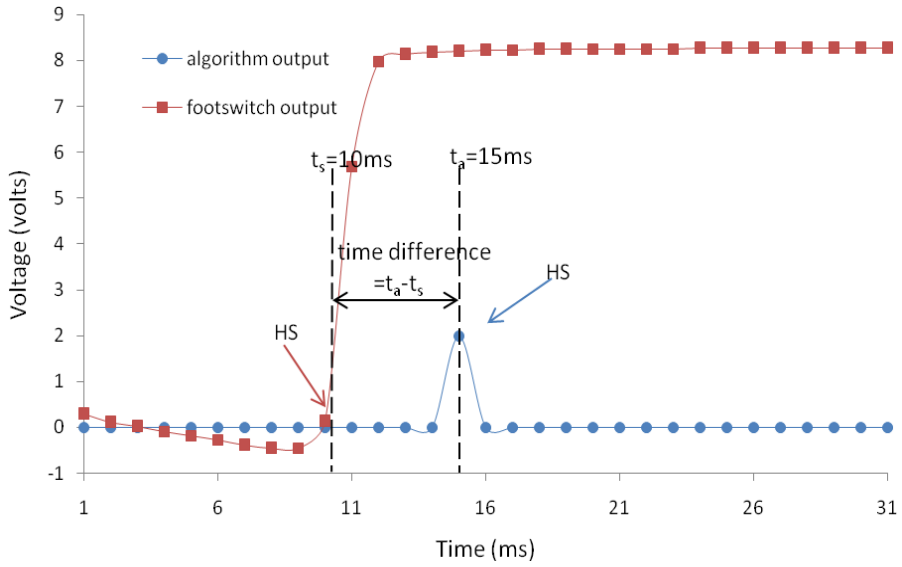

Figure 8-2 An example to illustrate a positive time difference. Shown in the plot is a time difference of 5ms between the heel strike detected by the algorithm (blue arrow) and the footswitch (heel switch, red arrow) from the data of subject 5.

8.4 Results

8.4.1 Heel Strike Events Detection

Figure 8-3 to Figure 8-7 show examples of the heel strike events detection in Subjects 1, 2, 3, 4 and 5 respectively compared to footswitch (heel switch). The rest of the plots are appended in Appendix J. In Figure 8-3 to Figure 8-7, there is a spike in the foot segment angle signal for every heel strike event and this is aligned with the heel strike event detected by the footswitch and the positive peak that crossed the positive threshold after negative peak that crossed the negative threshold of the correlation coefficient signal. Although there was a positive peak that crossed the positive threshold of the correlation coefficient signal at time 2.4s in Figure 8-4(b) and Figure 8-6(b), this peak has not been detected as the heel strike event by the algorithm as before that there was no negative peak that crossed the negative threshold. A total of 161 true heel strike events have been detected using the algorithm (Chapter 7, p133) with no missing events when compared to the footswitch. The footswitch however has detected false trigger events at (1.14s and 2.46s) and (1.24s, 1.33s and 2.46s) as shown in Figure 8-4(d) and Figure 8-6(d) respectively. There are a total of 14 and 8 false detections in Subject 2 (left foot) and Subject 4 (right foot) respectively. No false events were found

in the data from subject 1,3 and 5. In Figure 8-6(d), the toe switch has been used to confirm the false heel strike events detected by the heel switch. The toe switch showed no contact with the ground which indicate that the leg is in the swing phase of the gait.

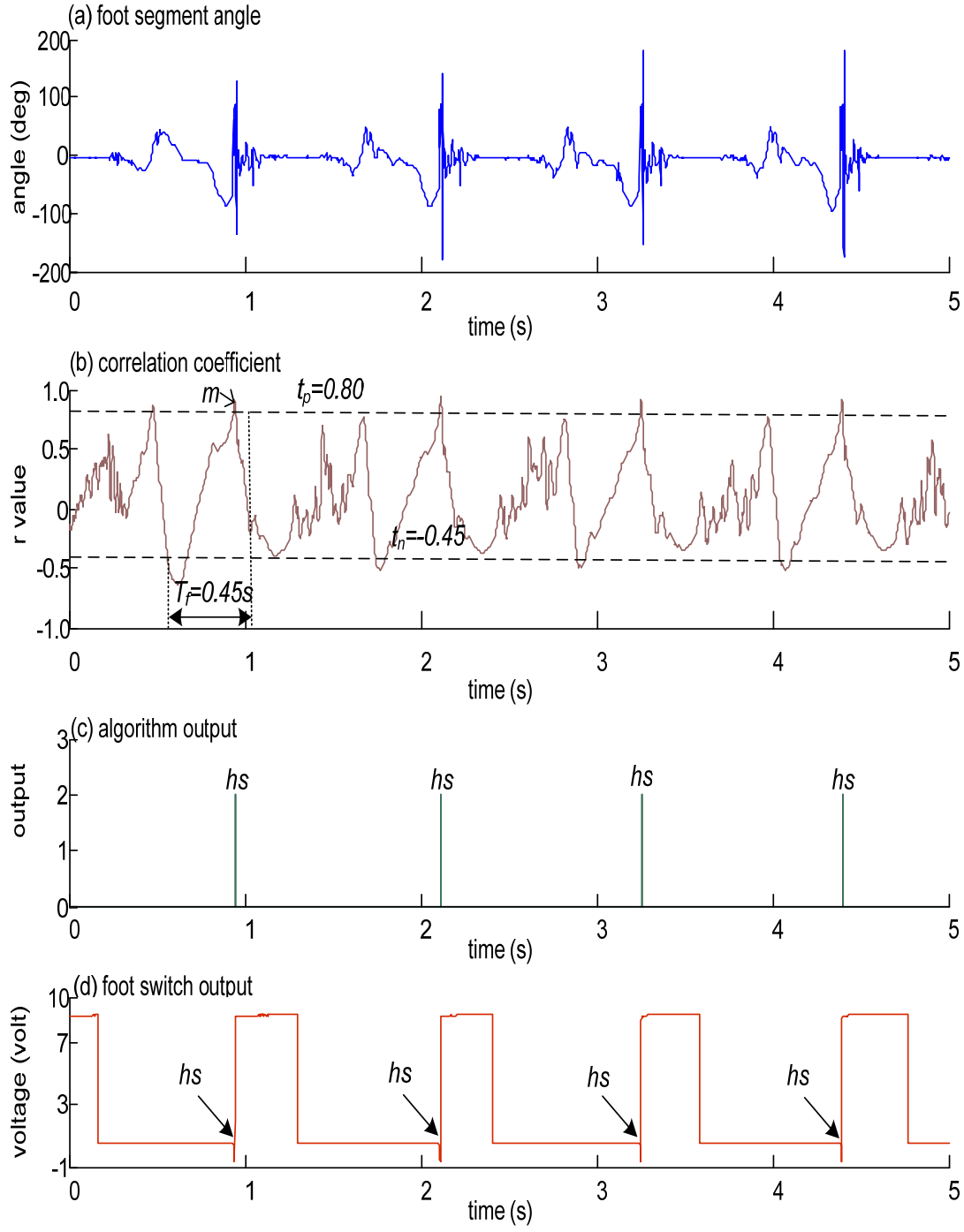

Figure 8-3 Heel strike events in Subject 1 (right foot). (a) foot segment angle (b) correlation coefficient between foot segment angle and a sample window (t_p = positive threshold, t_n = negative threshold, T_f= time frame and m=first maximum point) (c) algorithm output (0=no event, 2=event detected and hs=heel strike) and (d) heel switch output.

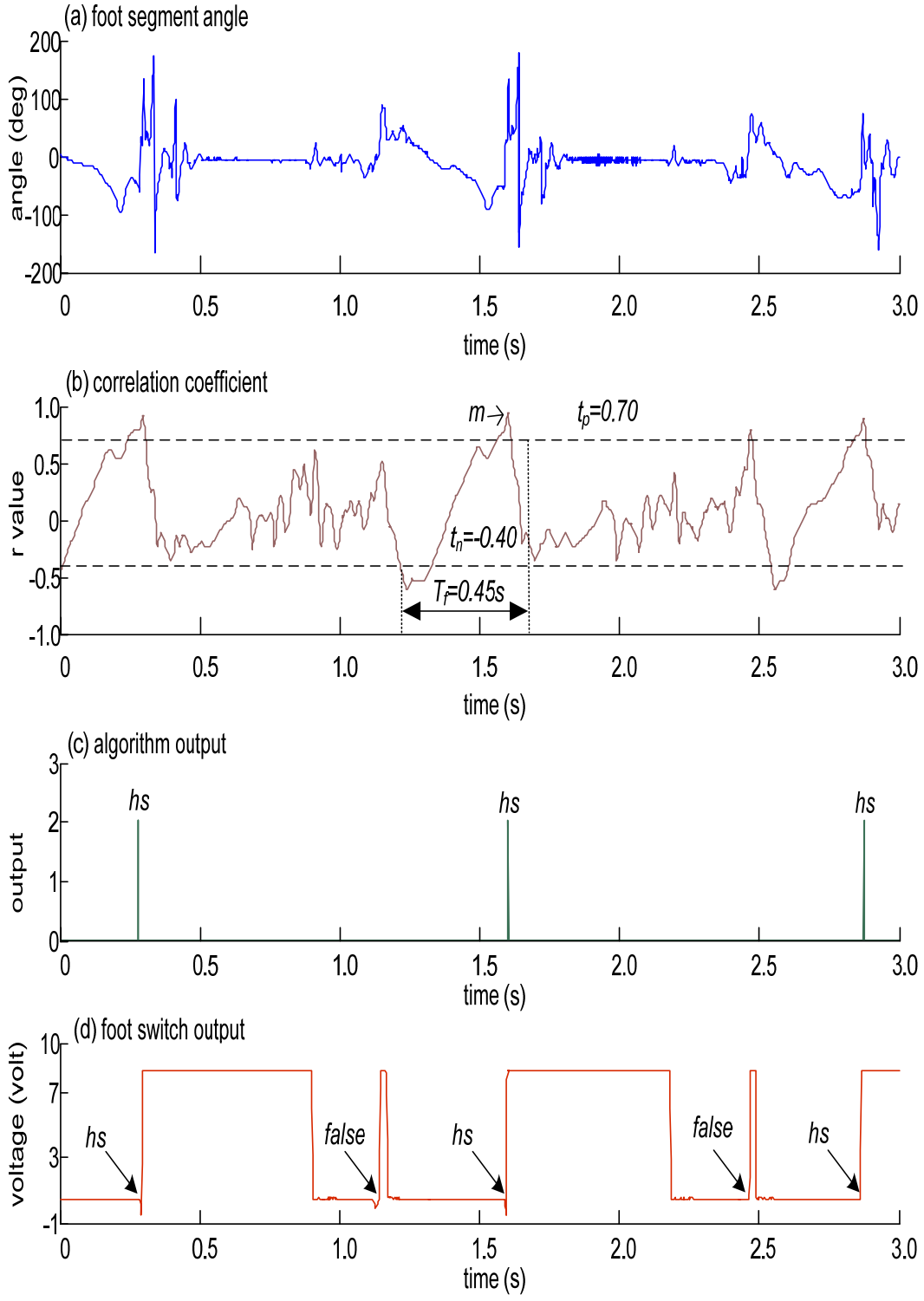

Figure 8-4 Heel strike events in Subject 2 (left foot). (a) foot segment angle (b) correlation coefficient between foot segment angle and a sample window (t_p = positive threshold, t_n = negative threshold, T_f= time frame and m=first maximum point) (c) algorithm output (0=no event, 2=event detected and hs=heel strike) and (d) heel switch output.

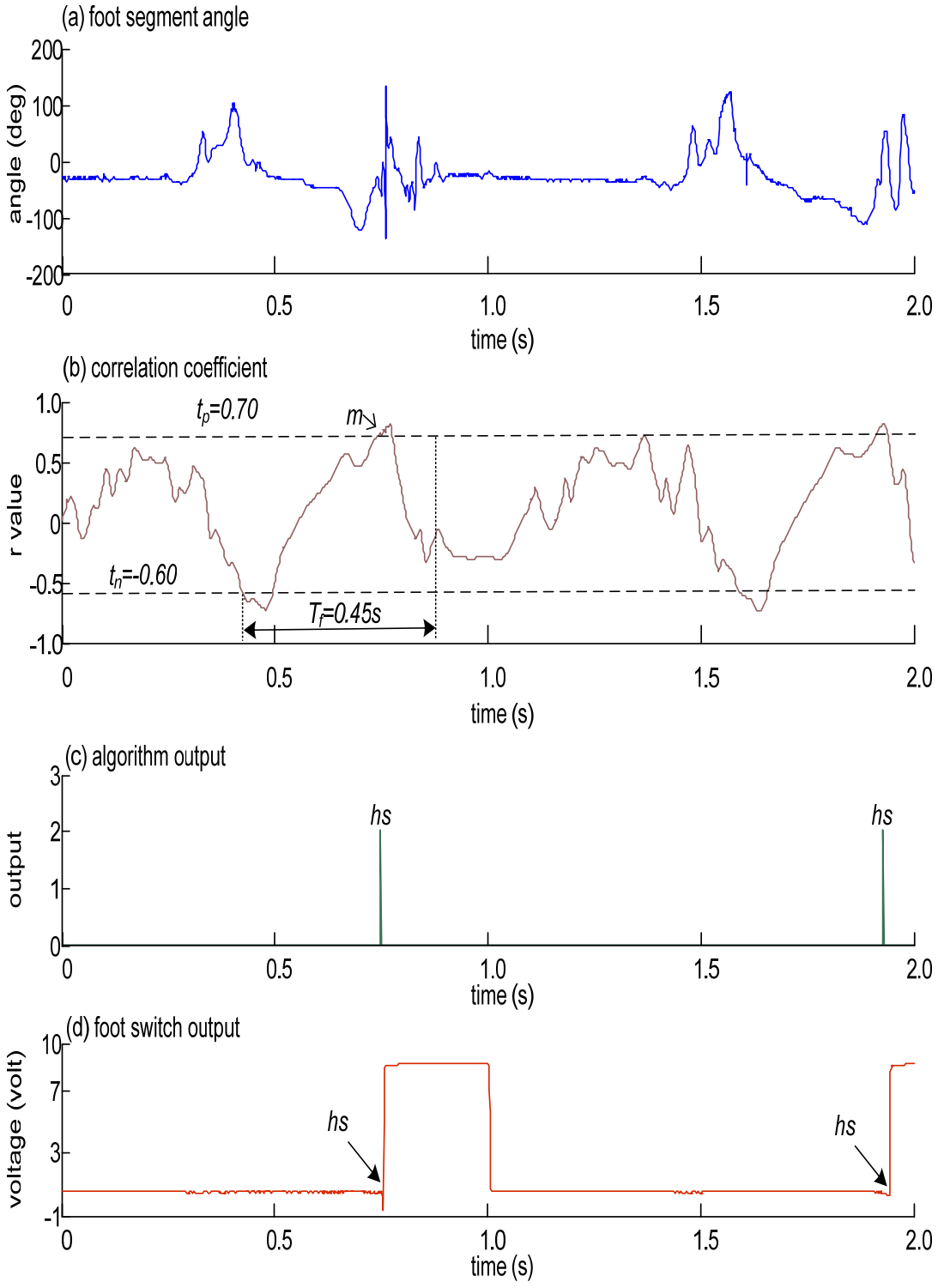

Figure 8-5 Heel strike events in Subject 3 (right foot). (a) foot segment angle (b) correlation coefficient between foot segment angle and a sample window (t_p = positive threshold, t_n = negative threshold, T_f= time frame and m=first maximum point) (c) algorithm output (0=no event, 2=event detected and hs=heel strike) and (d) heel switch output.

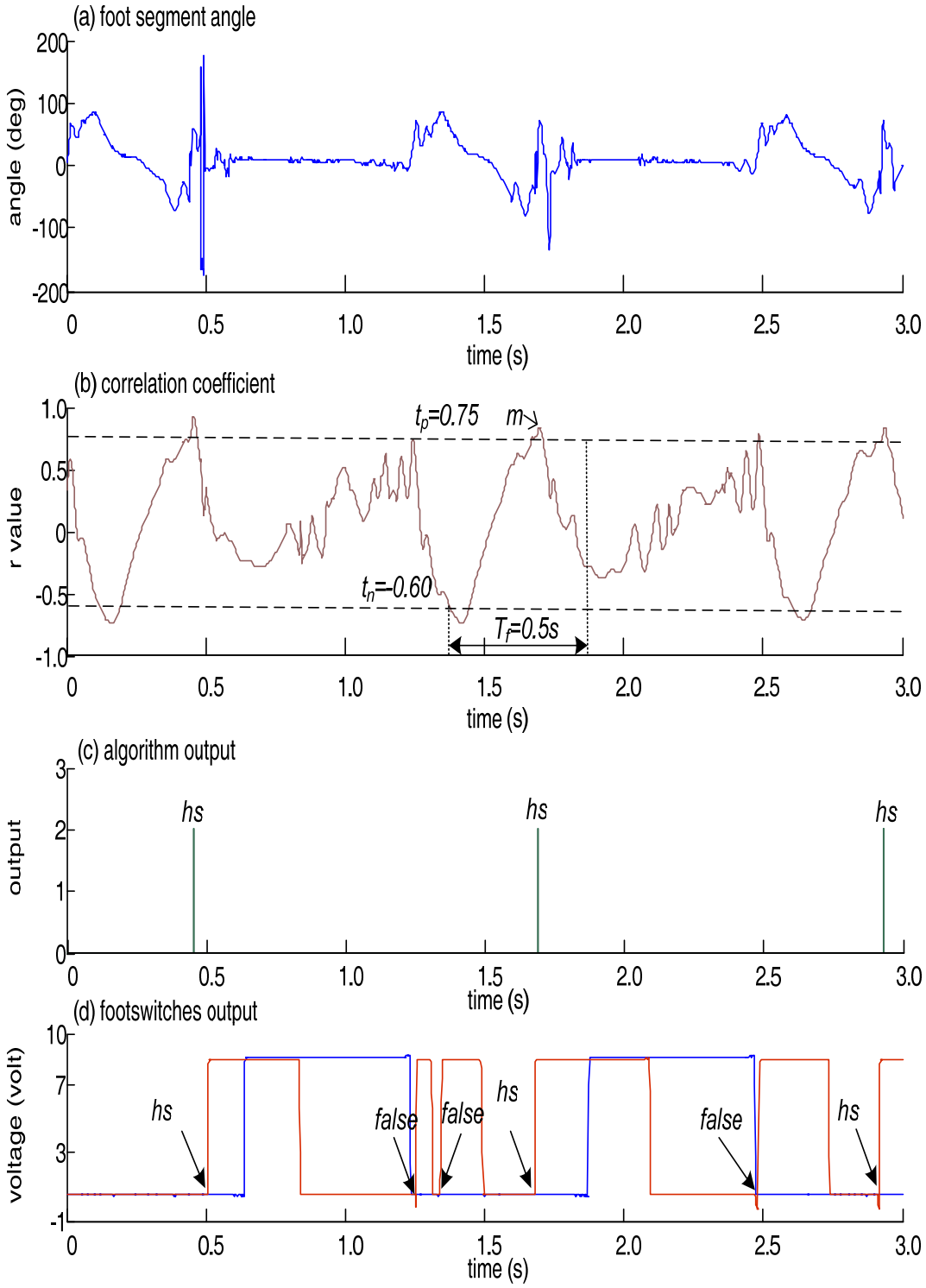

Figure 8-6 Heel strike events in Subject 4 (right foot). (a) foot segment angle (b) correlation coefficient between foot segment angle and a sample window (t_p = positive threshold, t_n = negative threshold, T_f= time frame and m=first maximum point) (c) algorithm output (0=no event, 2=event detected and hs=heel strike) and (d) heel (red line) and toe switch (blue line) output.

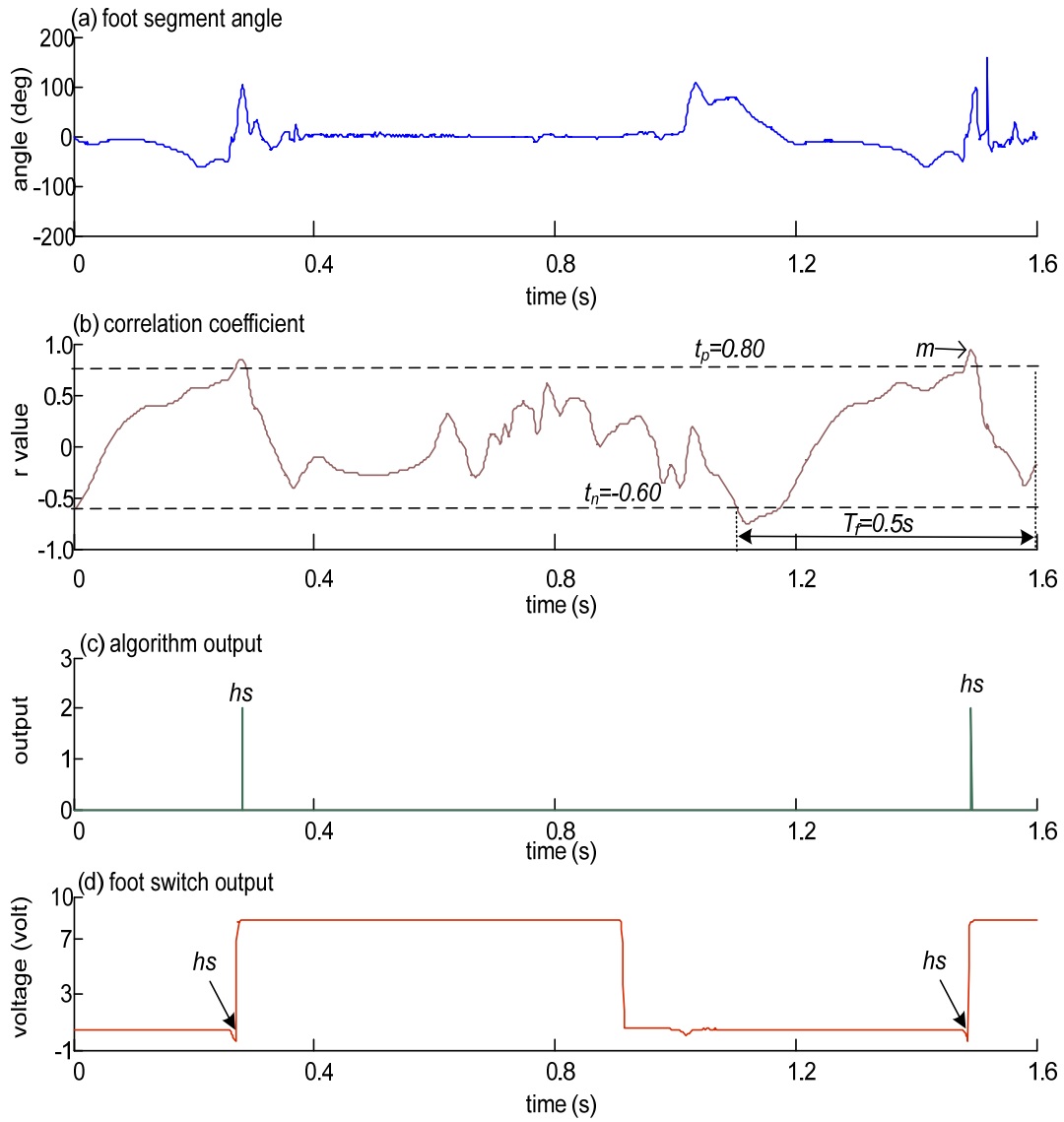

Figure 8-7 Heel strike events in Subject 5 (right foot). (a) foot segment angle (b) correlation coefficient between foot segment angle and a sample window (t_p = positive threshold, t_n = negative threshold, T_f= time frame and m=first maximum point) (c) algorithm output (0=no event, 2=event detected and hs=heel strike) and (d) heel switch output.

8.4.2 Time Difference of the Heel Strike Events Detection for Healthy Subjects

Table 8-2 presents the mean, standard deviation, mode, median and range of the time difference for the heel strike events detected during walking between the algorithm and the footswitch. The time difference has a range between -53ms and 35ms. The largest time difference observed was in Subject 4 (-53ms).

Table 8-3 presents the mean, standard deviation, mode, median and range of the stride time. The stride time has a range between 0.99s to 1.53s. Figure 8-8 to Figure 8-12 show the distribution of the time difference calculated in the healthy subjects.

Table 8-2 The mean, standard deviation, mode, median and range of the time difference in ms for heel strike events detected using the algorithm compared to the footswitch in five healthy subjects.

Subject	Number of events detected	Mean ± SD of time difference in ms	Mode (number of events)	Median	Range
1	47	2.53 ± 4.17	4 (13)	4	-20 to 6
2	43	-11.51 ± 14.53	8 (4)	-7	-51 to 8
3	24	-5.13 ± 6.87	2 (4)	-1	-20 to 2
4	27	-1.85 ± 20.16	-26 (3)	3	-53 to 35
5	20	-3.30 ± 13.12	-10 (2)	0	-31 to 15

Table 8-3 The mean, standard deviation, mode, median and range of the stride time in seconds calculated from the heel rise to the next heel rise in a gait cycle.

Subject	Mean ± SD of stride time in s (number of strides)	Mode	Median	Range
1	1.15 ± 0.09 (43)	1.11	1.14	1.00 to 1.39
2	1.34 ± 0.06 (28)	1.30	1.34	1.24 to 1.43
3	1.09 ± 0.12 (13)	1.07	1.07	0.99 to 1.47
4	1.26 ± 0.07 (19)	1.19	1.26	1.18 to 1.49
5	1.29 ± 0.11 (14)	-	1.28	1.13 to 1.53

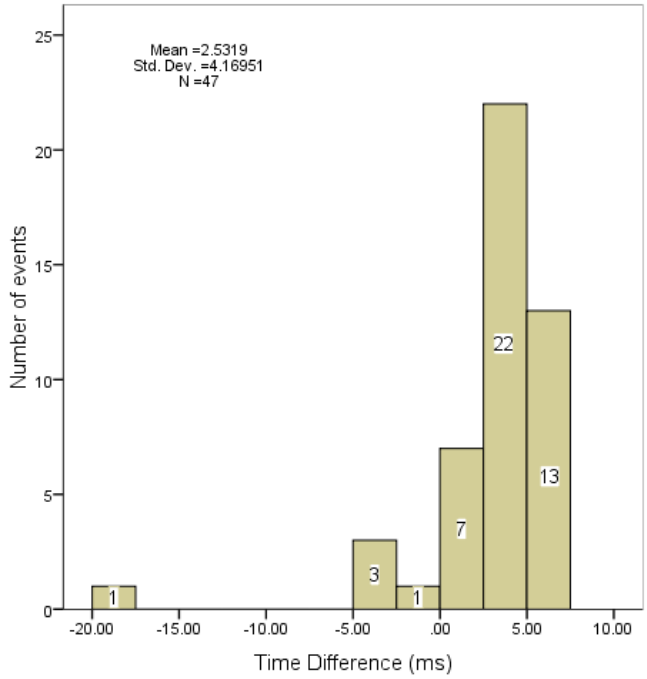

Figure 8-8 Time difference of the heel strike events detection between the algorithm and footswitch in Subject 1.

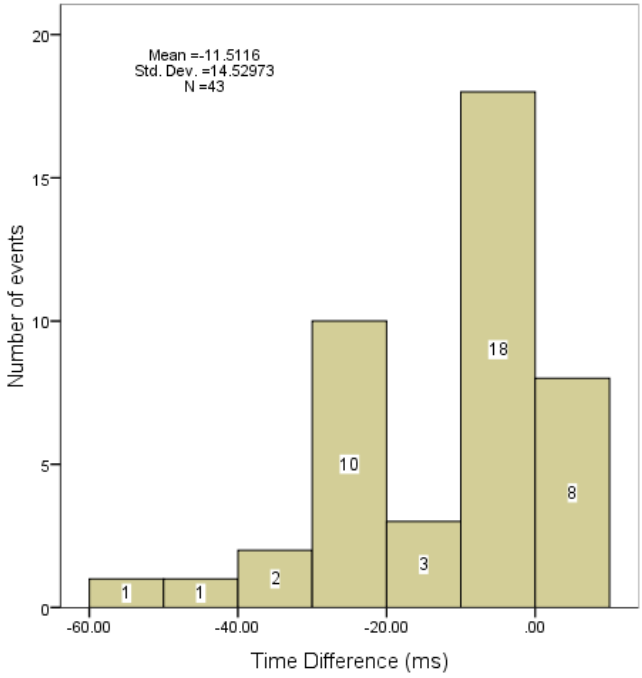

Figure 8-9 Time difference of the heel strike events detection between the algorithm and footswitch in Subject 2.

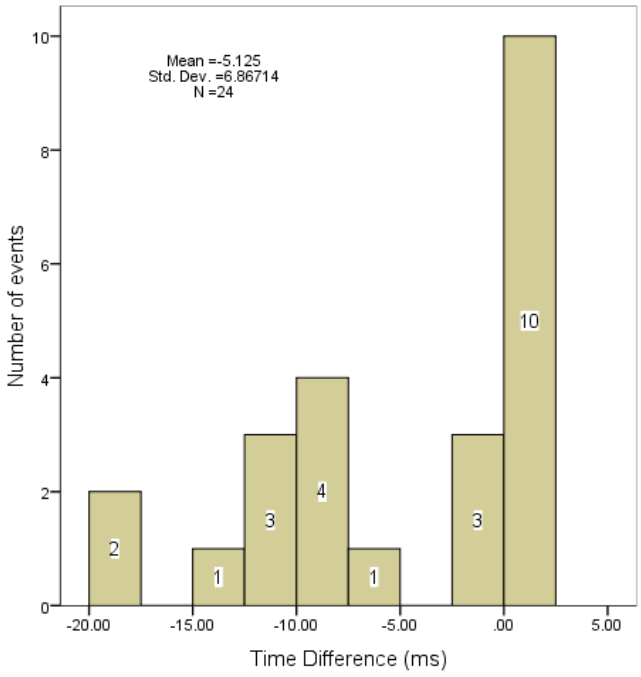

Figure 8-10 Time difference of the heel strike events detection between the algorithm and footswitch in Subject 3.

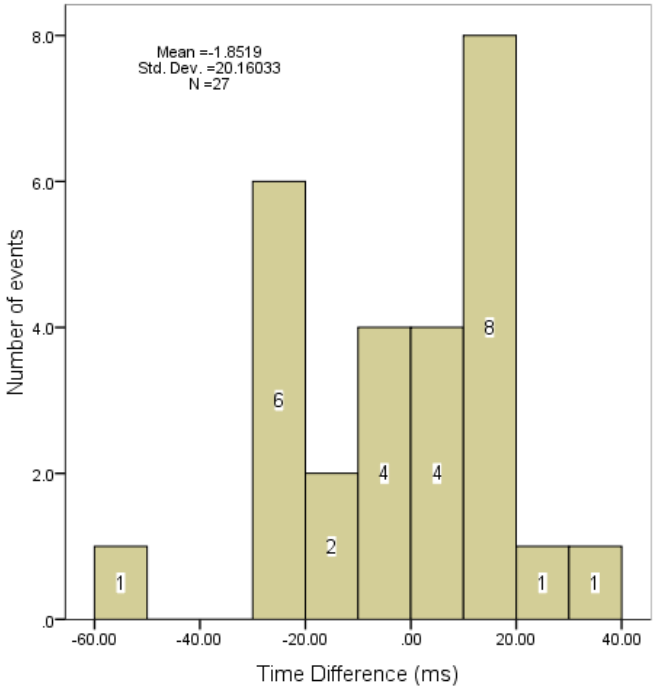

Figure 8-11 Time difference of the heel strike events detection between the algorithm and footswitch in Subject 4.

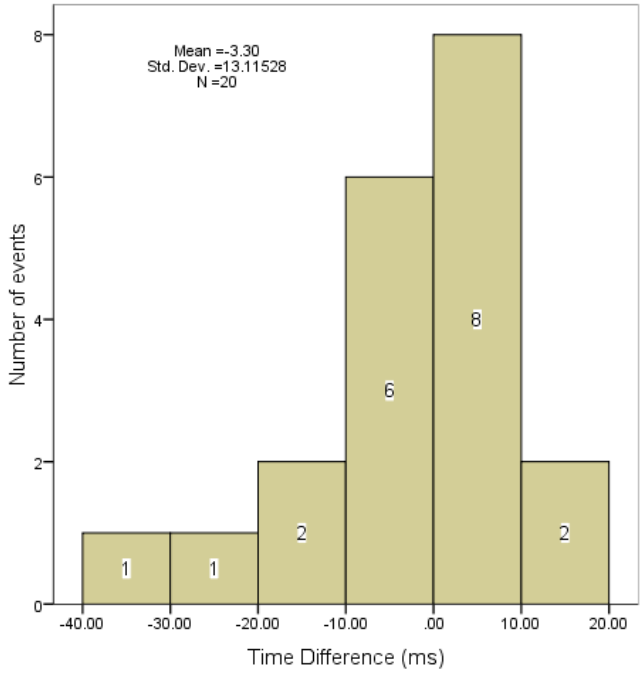

Figure 8-12 Time difference of the heel strike events detection between the algorithm and footswitch in Subject 5.

8.5 Discussion

The same type of footswitch and circuit used in the study has been evaluated by (Findlow et al. (2004)). They compared the footswitch with the gold standard system, the force plate, and reported a mean time difference of -7±19ms. As can be seen in the results for examples Figure 8-4 and Figure 8-6, the footswitch that is expected to be a gold standard reference as an alternative to the force plate for the detection of heel strike has detected false events. These false events occurred during swing. The same problem has been reported elsewhere (Aminian et al. (1999), Mansfield and Lyons (2003)), which is due to the foot shuffling or small forces exerted by the sole on the footswitch during swing. In different literature, false heel strike detection occurred immediately after heel off that could result from a slow heel off (Aminian et al. (1999)). In the study presented in this thesis, false detection only occurred in Subject 2 (left foot) and Subject 4 (right foot). This could be due to the footswitch position, the type of footwear and how tight the shoe was during the trials. In these circumstances, the detection algorithm (Chapter 7, p133) has an advantage over the footswitch as the sensor unit used in the algorithm is not affected by the pressure between the shoe and insole, the type of footwear and could be used barefoot.

From the off-line evaluation, the algorithm (Chapter 7, p133) has detected 161 true heel strike events when compared to the footswitch with no missing events for five healthy subjects during walking. This showed that the algorithm is reliable and better than a footswitch for the detection of heel strike events in healthy subjects during walking. However, more evaluations such as walking on rough terrain, walking with obstacle, walking on slopes, walking upstairs and downstairs could be done in the future to confirm the reliability of the algorithm in different walking environments.

Mansfields and Lyons (2003) reported that the delay (time difference) in the heel strike event detection using the accelerometer signal compared to footswitch was consistent with different speed of walking (normal or constant speed and faster than normal or slower than normal) for all the four unimpaired subjects. However, for these subjects, the time delay was different when walking in hemiplegic gait mode (asymmetrical gait). The time delay was also different between the subjects. Willemsen et al. (1990a) reported that the chances of missing heel strike detection and an early heel strike detection were largest for slow walking and fast walking respectively. They also reported that the speed of walking was not a good indicator for applicability of the method used but the walking pattern and the foot movements are the good indicator for a specific subject.

In the study, all five healthy subjects walked with their normal walking speed. The stride time for these subjects has a range between 0.99s and 1.53s. Based on the result presented in Table 8-2, the shortest to longest times for the standard deviation of the stride time are 0.06s (Subject 2), 0.07s (Subject 4), 0.09s (Subject 1), 0.11s (Subject 5) and 0.12s (Subject 3). The shortest to longest times for the standard deviation of the time difference in the detection of heel strike events are 4.17ms (Subject 1), 6.87ms (Subject 3), 13.12ms (Subject 5), 14.53ms (Subject 2) and 20.16ms (Subject 4). These data show that there was no clear relationship observed between the stride time and the time difference in the detection of heel strike event. However, in the future, the trials should be carried out with various speeds of walking such as slow, intermediate (normal) and fast to determine the effect of walking speed on the detection accuracy and reliability. Beauchet et al. (2009) have reported that a decrease in walking speed is accompanied by an increase in the stride time variability and the relationship is not linear but quadratic.

From 161 true heel strike events detected, 46.58% were detected earlier by the algorithm compared to the footswitch while 49.07% were detected later and 4.35% were detected at the same time (0ms time difference). These events were detected within 53ms. The time difference distribution has a range from -20 to 6ms, -51 to 8ms, -20 to 2ms, -53 to 35ms and -31 to 15ms for Subjects 1,2,3,4 and 5 respectively (Figure 8-8 to Figure 8-12). The largest time differences in percentage of the gait cycle are 1.74%, 3.81%, 1.83%, 4.21% and 2.40% for Subjects 1, 2, 3, 4 and 5 respectively which demonstrates the effectiveness of the system. In the results, the algorithm (Chapter 7, p133) and the footswitch agreed within 40ms (98% of total events detected). From the literature (Hart et al., 2006), the typical frequency used for stimulation of peroneal nerve or tibialis anterior muscles is 40Hz (pulses per second), therefore if stimulation is used, the events are detected less than 2 stimulation pulses before or after the footswitch detection. This level of response is very good and would be acceptable in the clinical and home environments. In addition, even the longest result (-53ms) is only 3 pulses away.

The median of the time difference are -7ms, -1ms, 0ms, 3ms and 4ms for Subject 2, Subject 3, Subject 5, Subject 4 and Subject 1, respectively (see Table 8-2). The largest standard deviation of the time difference for the detection of heel strike event compared with footswitch was observed in Subject 4 (20.16ms). This value is smaller than the standard deviation for normal subjects reported in other studies (Han et al. (2009), Jasiewicz et al. (2006), Willemsen et al. (1990a), and Mansfield and Lyons (2003)).

The algorithm (Chapter 7, p133) applied the threshold method to the correlation coefficient signal calculated between the kinematic signal (foot segment angle) and a selected sample window. The correlation coefficient obtained is more consistent even when there is a change in the amplitude of the kinematic signal and this makes the events detection process more simple and robust. The algorithm used one sample window selected from a subject and applied to all other four subjects. This simplicity of the algorithm makes it suitable for clinical application.

Table 8-4 lists the average time difference reported by other studies in the detection of heel strike with accelerometers and gyroscopes when compared to detection with a footswitch. From the reported results, the mean time difference in the heel strike or

initial contact detection in healthy subjects ranged between 10 and 147 ± 91ms. In this study, the absolute mean time difference has a ranged between 1.85 and 11.51 ms and standard deviation between 4.17 and 20.16 ms for five healthy subjects. Han et al. (2009) and Jasiewicz et al. (2006) have reported the time difference and standard deviation of initial heel contact for healthy subjects walking at normal speed while (Willemsen et al. (1990a) and Mansfield and Lyons (2003)) have presented results at different speeds. The mean time difference and standard deviation obtained from the study presented in this thesis are smaller and therefore better. Only the mean time difference where foot acceleration was used for the detection reported by (Jasiewicz et al. (2006)) is slightly smaller when compared to the largest mean time difference in this study (11.51ms) with a difference of 0.51ms. The variation of the mean time difference reported in the literature could be due to the different type of footswitch or pressure sensor (reference sensor) and measurement methods used as well as the type of footwear and the footswitch positioned during the trials.

Other researchers have reported the mean time difference of initial contact events detection for patients such as Parkinson Disease (PD) (Han et al. (2009)), Spinal Cord Injury (SCI) (Jasiewicz et al. (2006)) and stroke (Kotiadis et al. (2004)). As reported, the mean time difference in the heel strike or initial contact detection in these patient groups ranged between 15 and 53 ± 20 ms as compared to footswitch.

Han et al. (2009) have reported in their study that there were no missing events while there were three missed heel strikes in healthy subject and one missed heel strike in hemiplegic subjects (Willemsen et al (1990a)). There was no false detection when walking on a flat surface, carpet or rough terrain (Kotiadis et al. (2004)). In a study using one accelerometer the reliability of heel contact detection was between 98.2% and 99.8% as compared to footswitch (Mansfield and Lyons (2003)).

Table 8- 4The time difference in the heel strike events detection compared with footswitch as reported by other researchers.

Researchers	**Participants and procedure**	**Sensor used**	**Average time difference in ms**
Han et al. (2009)	Seven healthy and seventeen Parkinson Disease (PD) patients. Walked on level ground with normal speed.	Two dual axis accelerometer	Healthy Initial Contact = 41 ± 33 PD Initial Contact = 46
Jasiewicz et al. (2006)	Nineteen normal and thirteen spinal cord injury (SCI). Footswitch failed in the trials with two SCI and seven normal subjects. Walked at normal self-selected speed.	A sensor pack consists of a rate gyroscope and two biaxial accelerometers	Normal Initial Contact: Foot acceleration = -11 ± 23 Foot sagittal angular velocity = -12 ± 22 Shank sagittal angular velocity = -14 ± 23 SCI (non affected side) Initial Contact: Foot acceleration = -24 ± 15 Foot sagittal angular velocity = -20 ± 20 Shank sagittal angular velocity = -15 ± 17 SCI (affected side) Initial Contact: Foot acceleration = -22 ± 16 Foot sagittal angular velocity = -17 ± 18 Shank sagittal angular velocity = -53 ± 11

Kotiadis et al. (2004)	A stroke subject. Walking on a flat surface, carpet and rough terrain.	Inertial measurement unit (IMU) consists of three accelerometers and three gyroscopes attached to the shank	Heel Strike = 50
Aminian et al. (2002)	Nine young and eleven elderly adults. Walking on a treadmill and over ground.	Gyroscopes attached to shank and thigh using a rubber band.	Heel Strike = 10
Willemsen et al. (1990a)	Four unimpaired and four hemiplegic adults (only three of the hemiplegics data were analysed). Walk in three speeds, slow, comfortable and fast.	Four accelerometers attached to the shank on a bracket	Heel Contact for unimpaired = -30 ± 60
Mansfield and Lyons (2003)	Four unimpaired adults. Walking on a carpeted corridor with different speed, normal, faster than normal and slower than normal.	One accelerometer placed on the trunk	Heel Contact = 147 ± 91

8.6 Conclusions

A total of 161 true heel strike events have been detected in five healthy subjects using the algorithm (Chapter 7, p133) with no missing events when compared to the footswitch. The footswitch has a mean time difference of -7±19ms compared with the force plate as reported by Findlow et al. (2004). From 161 true heel strike events detected, 46.58% were detected earlier by the algorithm compared to the footswitch while 49.07% were detected later and 4.35% were detected at the same time (0ms time difference). The time difference for all five healthy subjects has a range between -53ms and 35ms. The largest absolute time difference (53ms) is within the acceptable timing limits for heel strike detection set by Kotiadis et al. (2010). The absolute mean time difference has a range between 1.85 and 11.51ms while standard deviation has a range between 4.17ms and 20.16ms. If method was applied to stimulate the peroneal nerve or tibialis anterior muscle using a typical frequency of 40Hz (pulses per second), even the longest result (-53ms) is only 3 pulses away from a true heel strike. This level of response is very good and would be acceptable in the clinical and home environments.

The processes involved in the detection algorithm are simple and robust; also it does not need any data training. Only one sample window selected from a healthy subject is needed to detect the heel strike for all other subjects (five in total). This evaluation will help to determine the suitability of the algorithm in the clinical and everyday use with FES system. A further evaluation will be carried out in the next chapter to detect tibial vertical event in healthy subject using the same algorithm.

Chapter 9

Evaluation of Tibial Vertical Event Detection in Healthy Subjects

9.1 Introduction

This chapter describes a method of estimating when the tibia is vertical (tibial vertical event) in healthy subjects using the same algorithm to detect heel strike as reported in the previous chapter. The footswitch has been used as a reference sensor to evaluate the reliability and the accuracy of the algorithm. Ideally, the events detected would have been compared with the kinematic data obtained from the Vicon™ system. However, the kinematic data from the Vicon™ system and the sensor unit are not comparable as different filtering techniques, mathematical models and sampling frequencies have been used. Moreover, the raw data is not accessible. Alternatively, to evaluate the algorithm, the estimated tibial vertical timing is compared with 13% of the gait cycle before initial foot contact or heel strike using a footswitch as a reference. In another study (Perry (1992)), the tibial vertical event occurs at 13% of gait cycle before initial contact in healthy subjects. Further, Kaufman and Sutherland (2006) have reported that the tibial vertical event occurs at 15% of the gait cycle before initial contact in healthy subjects. Sousa et al. (2007a, 2007b) have detected the tibial vertical event in healthy subjects using images from cameras while Park et al. (2007) have used a tilt sensor attached to the shank in patients and healthy subjects. However, none of these studies have reported on the accuracy of the detection. In this study, the tibial vertical event

should be detected within or close to the reported values of 13% (Perry (1992)) and 15% (Kaufman and Sutherland (2006)).

To detect the tibial vertical event in the same five healthy subjects, only one sample window is needed as in the previous chapter. Also, the sample window is selected from the foot segment angle of Subject 5 that is from the same subject as the sample window used to detect heel strike. Again, the foot segment angle has been chosen as a sample window since the foot segment angle requires less data points (smaller window) compared to a sample window selected from the shank segment angle.

9.2 Procedures

9.2.1 Subjects, Set-up and Protocol

The data of five healthy subjects obtained from the experiments described in section 6.2.1, 6.2.2 (i & ii) and 6.2.3 has been used in the analysis for the detection of the tibia vertical events. The analysis was done off-line using the algorithm described in Chapter 7. Data from a footswitch was used as a reference in the analysis to evaluate the algorithm for the detection of tibial vertical event in healthy subjects.

9.3 Data Analysis

9.3.1 Tibial Vertical Event Detection

For every subject, the segment angle shown in Figure 6-2 (Chapter 6, p101) obtained from the sensor units and the data from the footswitches of both lower limbs were analysed off-line. Only the foot segment angle was used to detect the tibial vertical event using the algorithm described in (Chapter 7, p133) which follows the heel strike event detection in healthy subjects. All of the subjects had heel strike as initial contact. Therefore, only the footswitch placed under the heel was used in the analysis. A sample window (WT1) selected from a foot segment angle data from one of the subject (Subject 5) was used in the correlation coefficient calculation for all the other subjects (five in total) to detect the tibial vertical events. Figure 9-1 shows the foot segment angle of a healthy subject (Subject 5) for a single gait cycle where the sample window

(WT1) has been selected. The sample window consists of 350 points (0.35ms). The signal begins just before the toe off event, ends at the tibial vertical as shown in Figure 9-2. This window was selected based on the 13% of gait cycle before heel strike with footswitch as reference. It was found that the selected sample window worked very well with other subject data. While no further sample windows were investigated from the other four healthy subjects, it is anticipated that very good results would also be obtained. The window size could be reduced to less than 350 points but there will be a size at which the algorithm starts to fail to detect events reliably. The chosen size incorporated data producing a representative pattern for robust event detection. For two of the subjects (Subject 1 and Subject 3), only the right lower limb data was analysed. The same program routines used in the detection of heel strike event in healthy subjects has been used to detect the tibial vertical event. All the program routines are included in Appendix G.

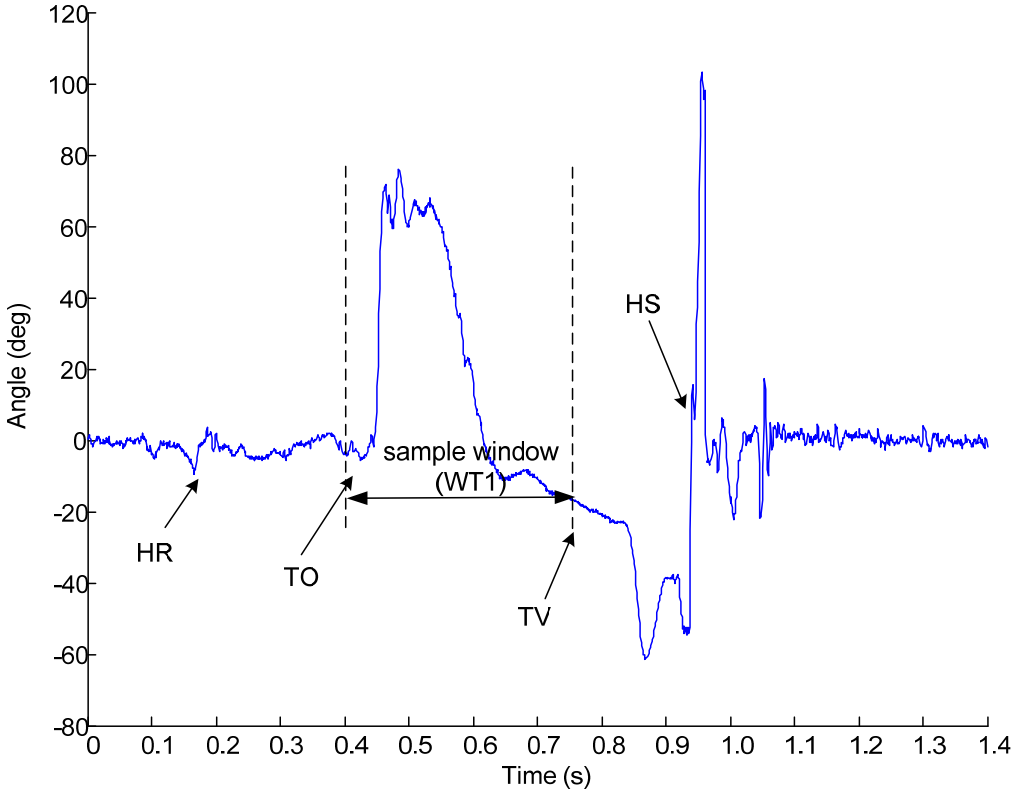

Figure 9-1 A single gait cycle of the foot segment angle during walking in Subject 5 showing the major gait events based on percentage of gait cycle and footswitches.

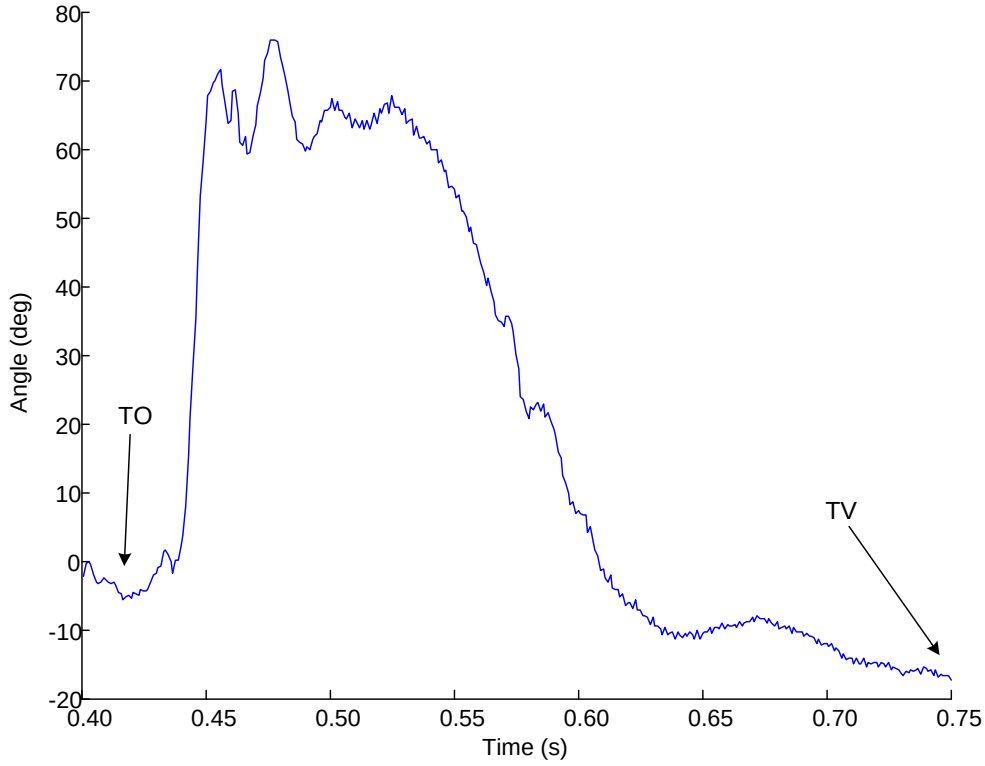

Figure 9-2 A sample window (WT1) selected from foot segment angle of Subject 5 for detection of tibial vertical event in healthy subjects.

The negative and positive threshold values and time frame which satisfied all the trials for that respective subject have been determined. Table 9-1 lists the threshold values and time frame used in the algorithm for the detection of the tibial vertical event for every subject. The threshold values and time frame were set for an individual subject based on the correlation coefficient signal obtained. For every subject, two horizontal lines which represent the thresholds were drawn on the correlation coefficient signal beginning with 0.3 for positive threshold and -0.3 for negative threshold (refer to Figure 9-3 for a correlation coefficient signal). The line was moved by 0.5 towards 1 for positive threshold and -1 for negative threshold. The last value before the line started to go beyond the positive or negative peak of the correlation coefficient signal in all trials for the respective subject, was set as the threshold. From the correlation coefficient signal, the tibial vertical event is detected using the Rules I as described in (Chapter 7, p137). The time frame, T_f was set for individual subject which start at the signal crossing the negative threshold (down slope) before the event and end slightly after the event has been detected and after crossing the positive threshold (down slope).

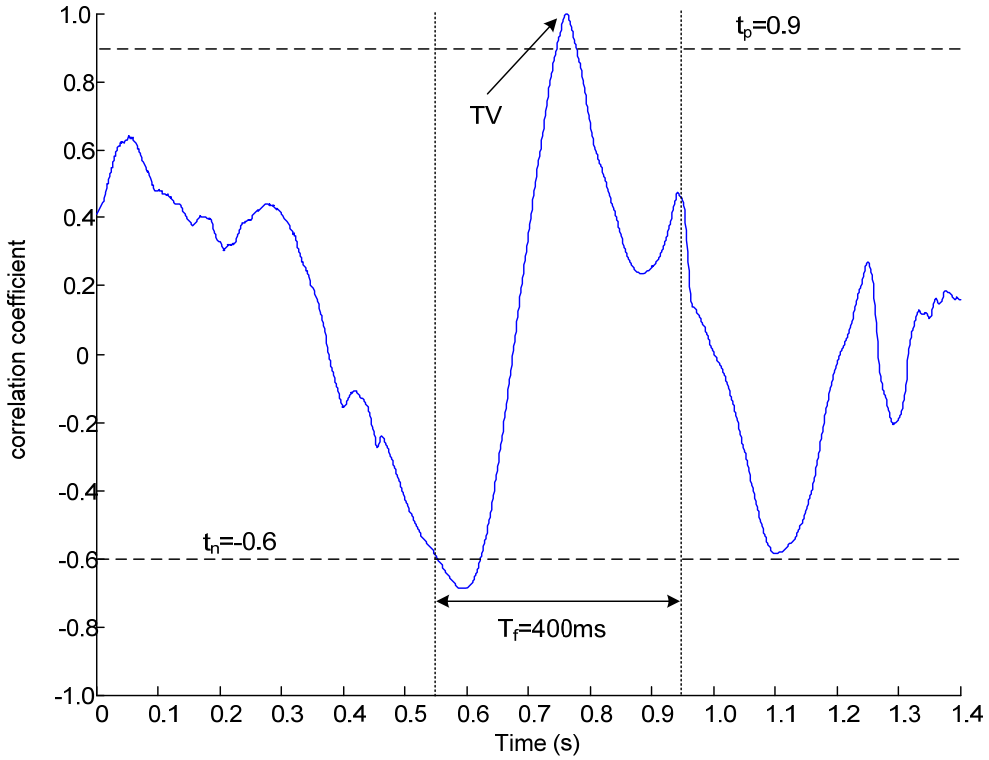

Figure 9-3 Correlation coefficient signal for tibial vertical (TV) event detection in Subject 5. The signal shows one TV event detected in a single gait cycle. (t_n=negative threshold, t_p=positive threshold and T_f=time frame)

Table 9-1 The thresholds for the correlation coefficient signal and time frame for tibial vertical event detection.

Subject	*Positive threshold, t_p*	*Negative threshold, t_n*	*Time frame, T_f in ms*
Subject 1	0.60	-0.50	400
Subject 2	0.60	-0.60	400
Subject 3	0.70	-0.50	400
Subject 4	0.80	-0.60	400
Subject 5	0.90	-0.60	400

9.3.2 Time of Tibial Vertical Event Detected in Percentage of Gait Cycle

The time at which the tibia is vertical, TE, is the time between when the tibia is vertical (TV) and the initial contact (IC) that is normally the heel strike (HS) (the one

that occurs after the TV event) as illustrated in Figure 9-4. A gait cycle time is the time between two consecutive heel strikes or initial contact and represents 100% of the gait cycle. Hence, the TE in percentage of gait cycle before initial contact can be calculated as,

$$\text{TE \% of GC before initial contact} = \frac{\text{TE (in ms)}}{\text{GC Time (in ms)}} \times 100\% \quad (9\text{-}1)$$

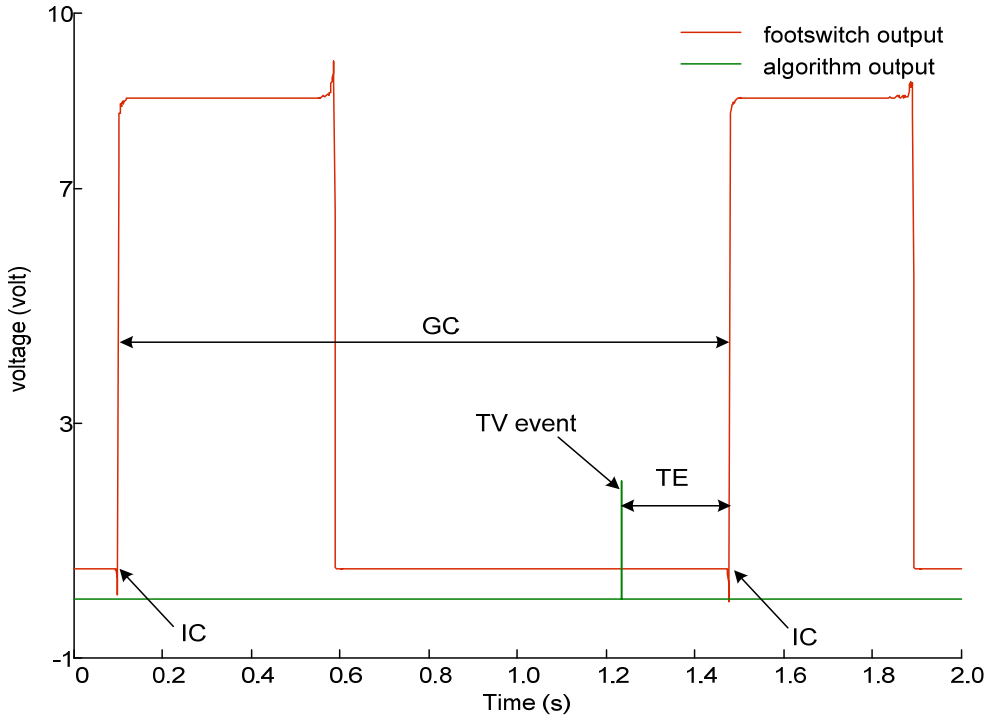

Figure 9-4 Time of tibial vertical event in percentage of gait cycle (GC=gait cycle, TE=time of tibial vertical event, TV=tibia vertical and IC=initial contact).

9.4 Results and Discussion

9.4.1 Tibial Vertical Event Detection

A total of 115 tibial vertical events have been detected in five healthy subjects as compared to the footswitch with no missing events. Figure 9-5 shows an example of the result for the detection of tibial vertical event in Subject 1. In Figure 9-5(c)-(d), all four tibial vertical events are consistently detected before the heel strike in swing phase. In Figure 9-5(b), the four red arrows show the correlation coefficient signal crossing the

negative threshold, however no tibial vertical event has been detected within 400ms as the signal does not cross the positive threshold and therefore the algorithm starts to search for the next negative peak with the signal crossing the negative threshold. The rest of the plots for Subject 1, 2, 3, 4 and 5 are appended in Appendix K.

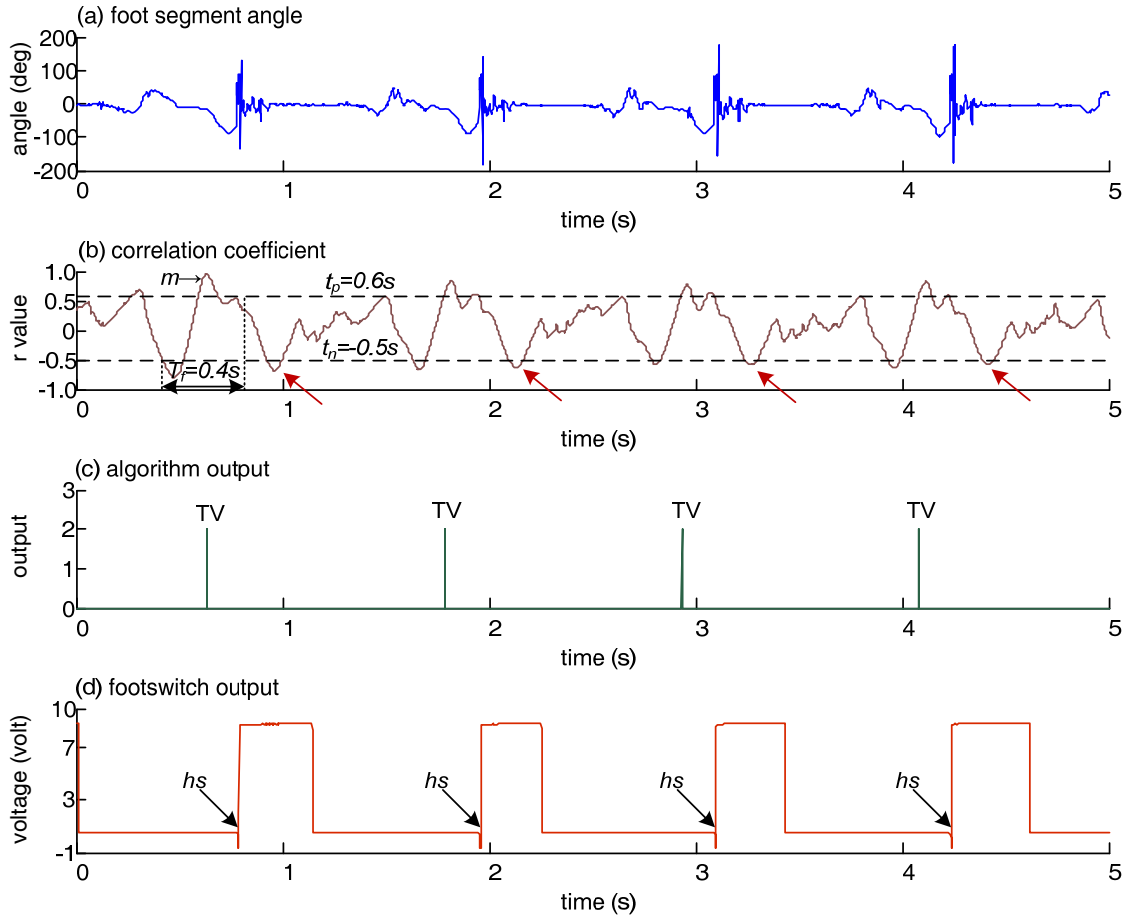

Figure 9-5 Tibial vertical events detection in Subject 1 (right foot). (a) foot segment angle (b) correlation coefficient between foot segment and sample window (WT1) (t_p=positive threshold, t_n=negative threshold, T_f=time frame and m=first maximum point) (c) algorithm output (0=no event, 2=event detected and TV=tibial vertical) and (d) heel switch output.

9.4.2 Time of Tibial Vertical Event as Percentage of Gait Cycle

Table 9-2 shows the mean and standard deviation of the time of tibial vertical events detected in five healthy subjects as compared to footswitch as well as the mean and standard deviation of the time difference between the time tibial vertical event and 13% of gait cycle before initial contact (the target). The mean of the time of tibial vertical

event has a range between 11.78% and 14.99%. The standard deviation of the time of tibial vertical event has a range between 0.81% and 2.61%. The absolute mean of the time difference between the time tibial vertical event and 13% of gait cycle before initial contact has a range between 0.01% and 1.99%. Table 9-3 presents the mode, median and range of the time of tibial vertical event detected in percentage of gait cycle before heel strike. Figure 9-6 to Figure 9-10 show the distribution of the time of tibial vertical event detected in percentage of gait cycle before heel strike in the healthy subjects. The data has a range from 4.23% to 20.66%.

Table 9-2 The mean and standard deviation of the time of tibial vertical event detected before heel strike.

Subject	*Number of events detected*	*Mean ± SD of TE% of GC before heel strike*	*Mean ± SD (TE % of GC before heel strike compared to 13% of GC before initial contact)*
Subject 1	34	14.01 ± 1.99	1.01 ± 1.99
Subject 2	29	14.59 ± 2.61	1.59 ± 2.61
Subject 3	23	12.99 ± 2.00	-0.01 ± 2.00
Subject 4	17	11.78 ± 0.81	-1.22 ± 0.81
Subject 5	12	14.99 ± 1.88	1.99 ± 1.88

Table 9-3 The mode, median and range of the time of tibial vertical event detected in % of gait cycle before initial contact.

Subject	*Mode*	*Median*	*Range*
Subject 1	-	14.33	4.23 to 16.01
Subject 2	-	14.97	5.71 to 20.66
Subject 3	11.57	13.34	9.23 to 17.45
Subject 4	11.88	11.77	10.30 to 13.53
Subject 5	-	15.06	11.41 to 17.70

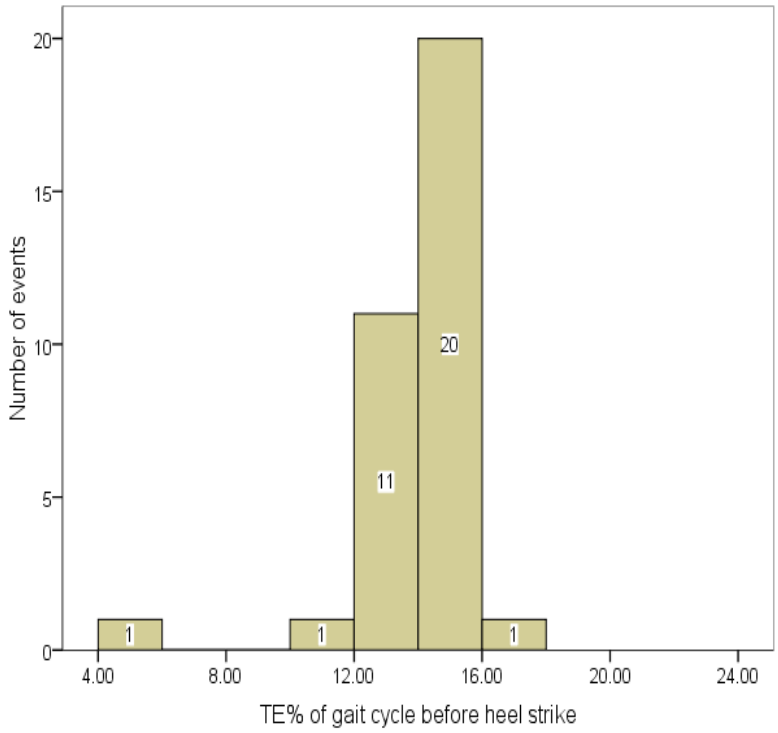

Figure 9-6 Distribution of the time of tibial vertical event detected in percentage of gait cycle before heel strike in Subject 1. (N=34, median=14.33% and range from 4.23% to 16.01%)

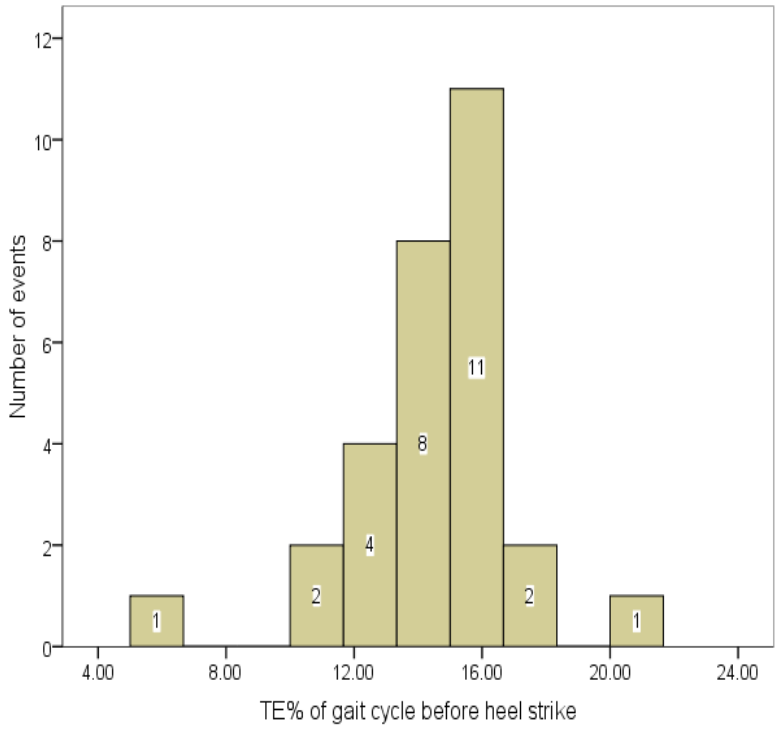

Figure 9-7 Distribution of the time of tibial vertical event detected in percentage of gait cycle before heel strike in Subject 2. (N=29, median=14.97% and range from 5.71% to 20.66%)

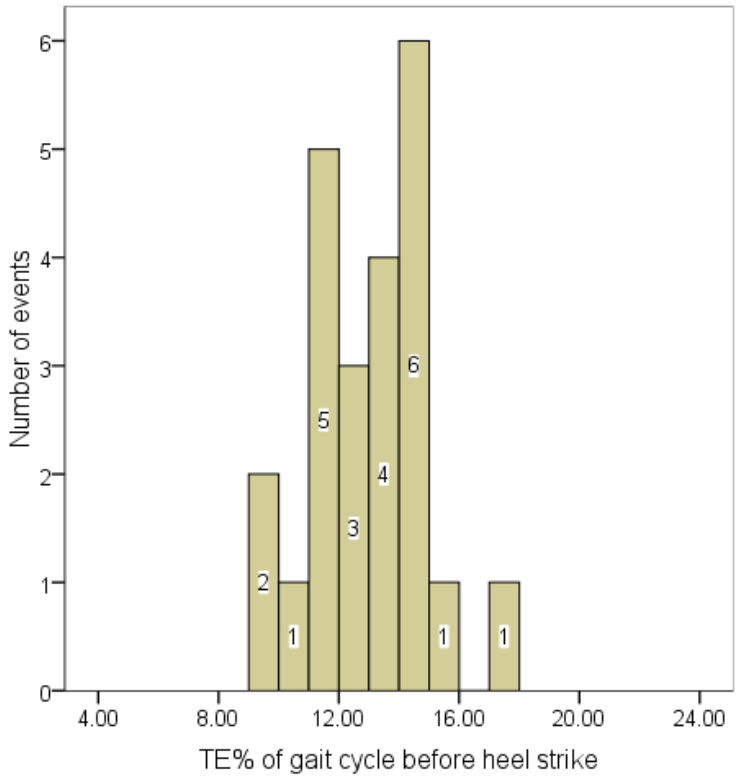

Figure 9-8 Distribution of the time of tibial vertical event detected in percentage of gait cycle before heel strike in Subject 3. (N=23, median=13.34% and range from 9.23% to 17.45%)

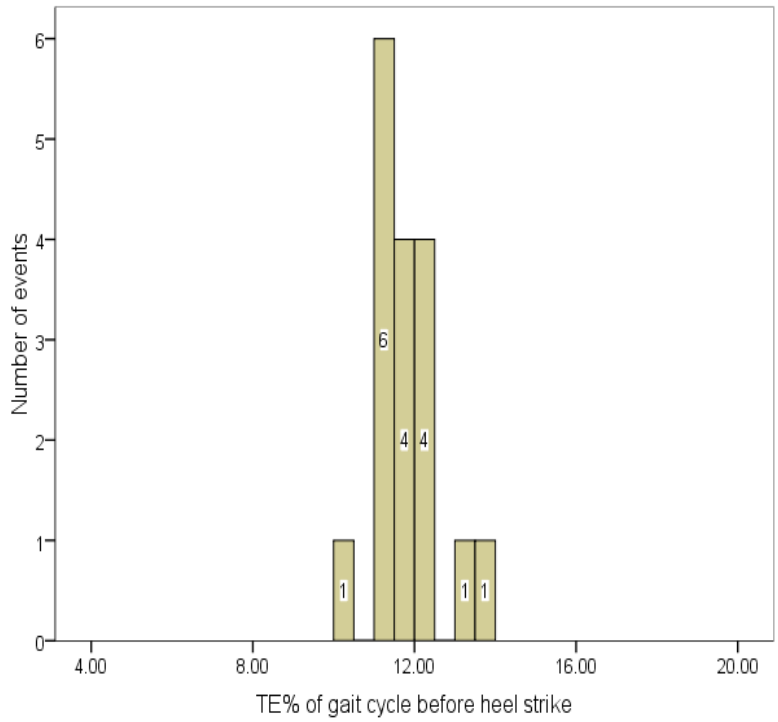

Figure 9-9 Distribution of the time of tibial vertical event detected in percentage of gait cycle before heel strike in Subject 4. (N=17, median=11.77% and range from 10.30% to 13.53%)

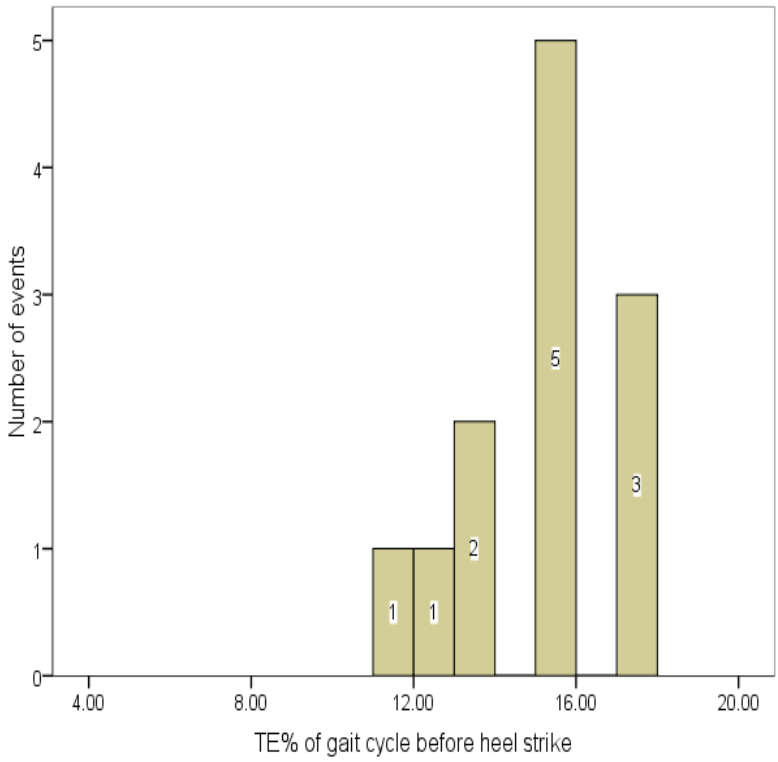

Figure 9-10 Distribution of the time of tibial vertical event detected in percentage of gait cycle before heel strike in Subject 5. (N=12, median=15.06% and range from 11.41% to 17.70%)

In the literature, the tibial vertical (TV) event occurs at 13% (Perry (1992)) and 15% (Kaufman and Sutherland (2006)) of a gait cycle before initial contact in healthy subjects. In the study, an event (which should correspond to when the tibia is vertical) is detected based on the TV event defined by (Perry (1992)) using a footswitch as a reference sensor. From Table 9-3, the median of the time of TV event detected has a range between 11.77% and 15.06% of gait cycle before heel strike. This range is close to the time of the event occurrence described by Perry (1992), and Kaufman and Sutherland (2006). Other studies that have detected this event were reported by Sousa et al. (2007a, 2007b) and Park et al. (2007). These studies, however did not report any evidence on the accuracy of the detection.

A search of the literature revealed no studies of the variability of the point at which the tibia becomes vertical in either people with normal neurology or those with a neurological condition. In a study of the gait variability of old adults, one hundred people aged 75 and older were divided into the three categories of nonfrail, prefrail and frail (Montero-Odasso et al. (2011)). Data were collected for gait velocity, stride time,

cadence, stride length, double support time and step width. The variability of these data are shown in Figure M-1 to Figure M-5 (see Appendix M), where the standard deviation of the data has been divided by the mean and expressed as a percentage. The values lie between 6% and 24% with a median value of 11%. However of interest is the double support time events as these data indicate the variability of an event within a gait cycle. They range between 11% and 15%. It is not rigorous to make a direct comparison of the variability of the double support time of the old adults with the TV events. However, nearly all of the TV events of the five subjects (Figure 9-6 to Figure 9-10) are in the range from 10% to 18% of the gait cycle before heel strike. This discussion indicates that the TV events have a similar variability to the data of (Montero-Odasso et al. (2011)).

9.5 Conclusions

A total of 115 tibial vertical events have been detected in five healthy subjects as compared to footswitch with no missing events. Only one sample window (WT1) selected from a foot segment angle data from one of the subjects (Subject 5) has been used to detect tibial vertical event in all five subjects. The standard deviation for the time of tibial vertical event ranged between 0.81% and 2.61% of gait cycle. The absolute mean of the time difference has a range between 0.01% and 1.99% of gait cycle.

The median of the time of the TV event detected in the healthy subjects has a range between 11.77% and 15.06% of gait cycle before heel strike. This range is close to the time of the TV event occurrence described by Perry (1992), and Kaufman and Sutherland (2006). Nearly all of the TV events detected in the five subjects are in the range from 10% to 18% of the gait cycle before heel strike. This range is also close to the occurrence of the TV event described by Perry (1992), and Kaufman and Sutherland (2006).

Chapter 10 Detection of Tibial Vertical Event in Neurological Patients

10.1 Introduction

This chapter describes a method of estimating when the tibia is vertical (tibial vertical event) in neurological patients using the same algorithm to detect tibial vertical event in healthy subjects as reported in the previous chapter. Ideally, the event detected would have been compared with kinematic data obtained from the Vicon^{TM} system. However, as described in the introduction section of previous chapter as a result of the underlying differences between the two systems, it is not possible to perform a direct comparison. Furthermore, there is no access to the raw data. Therefore, a direct comparison of the data from the patients is also not possible. Perry (1992) has described the tibial vertical event to be 13% of the gait cycle before initial contact in healthy subjects. As reported in the previous chapter, nearly all of the tibia vertical events of the five subjects are in the range from 10% to 18% of the gait cycle before heel strike with a small standard deviation of 2.61% of gait cycle. Based on this result, the use of 13% of the gait cycle before the initial contact to detect tibial vertical event would be reasonable in patients, even though the data in patients is anticipated to be more variable. The acceptable time to start stimulation would be 5% earlier from the detected event as defined in section 1.2 (Chapter 1, p3).

Although the same algorithm will be used to detect the tibial vertical event in patients, there is a slight different in the rule as the correlation coefficient signal used in the algorithm is slightly different in patients. A second time frame has been added to prevent any false detection. The same sample window used in the detection of heel strike in healthy subjects will be used to estimate the tibial vertical event in patients.

Park et al. (2007) have detected the tibial vertical event in patients and healthy subjects using a tilt sensor attached to the shank. However, they have not reported on the accuracy of the detection. To the best knowledge of the author, there is no other study which has focused on the detection of tibial vertical events for stimulation of the gluteals or hamstrings muscles prior to heel strike in neurological patients.

10.2 Procedures

10.2.1 Subjects

Seven patients with various neurological problems were recruited in the trials as shown in Table 10-1. They were using the Odstock Two-channel FES device (O2CHS) at the time of the trials. Four of the participants had multiple sclerosis, two have had a stroke and one person has spinal cord injury C4/5 incomplete tetraplegia. All participants were medically stable, able to walk with and without a stimulator and single-side affected. The study was granted ethical approval by the Wiltshire Research Ethics Committee (REF reference number: 08/H0104/77) and the participants gave informed consent.

Table 10-1 Information of the participants in the study, (F=female, M=male, MS=multiple sclerosis, SCI=Spinal cord injury, TA=tibialis anterior and CPN=Common peroneal nerves).

Patient	Age	Gender	Condition	Muscles/Nerves Stimulated	Gait problems (Affected Side)
P1	63	F	MS	Gluteal and TA/CPN	Drop foot during swing and excessive hip flexion/adduction at heel strike (Left)

P2	68	M	Stroke	Gluteal and TA/CPN	Drop foot during swing and excessive hip flexion/adduction at heel strike (Left)
P3	66	M	SCI C4/5	Gluteal and Pop. Fossa	Knee hyperextension and excessive hip flexion/adduction at heel strike (Right)
P4	66	F	MS	Hamstrings and TA/CPN	Knee hyperextension at terminal stance and drop foot during swing (Left)
P5	76	M	Stroke	Hamstrings and TA/CPN	Drop foot and insufficient knee flexion during swing (Left)
P6	65	M	MS	Gluteals and TA/CPN	Drop foot during swing and excessive hip flexion/adduction at heel strike (Right)
P7	45	F	MS	Gluteals and TA/CPN	Drop foot during swing and excessive hip flexion/adduction at heel strike (Right)

10.2.2 Set Up and Protocol

A sensor unit algorithm (Chapter 4, p57) was attached to the thigh, shank and foot of both lower limbs for the kinematic measurement (segment angle and acceleration) as shown in Figure 10-1. Two footswitches were placed under the heel and the first metatarsal head of the foot for both lower limbs; these were used as reference sensors. The outputs from the sensors were connected to two data acquisition systems (DAQPad-6015 and DAQ6036E from National Instrument Ltd). All signals were sampled at 1 kHz and acquired using the LabVIEW™ 8.0. The data was then analysed off-line using Microsoft Office Excel© and Matlab® R2006b. Every participant was asked to walk with stimulation on and with stimulation off at normal walking speed for about 4 metres for each trial in the Salisbury Gait Laboratory (SGL). All the participants walked using a cane/stick as walking aid. A clinician was asked to walk behind the participant to ensure the participant safety during the trials. The average of

stride time for P1, P2, P3, P5, P6 and P7 is 2.56s, 1.39s, 1.76s, 2.12, 1.73 and 1.88 respectively.

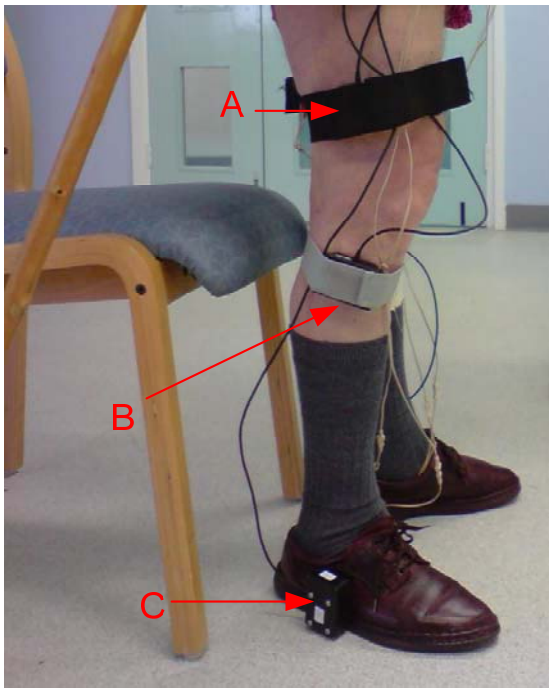

Figure 10-1 Sensor units attachment to both lower limbs. Right lateral view. (A:thigh segment, B:shank segment and C:foot segment).

10.3 Data Analysis

10.3.1 Kinematic Measurement

In the study, the foot segment angle of the affected side has been used in the detection of the tibial vertical events using the algorithm described in (Chapter 7, p138). There were two types of initial contact observed in the patients, either the heel or foot flat contact (heel and toe contact the ground about the same time). In Patient 1, there are four last steps and one first step with toe as initial contact. In Patient 6, there are two last steps with toe as initial contact. Information from the footswitch that first contacted the ground is used for the calculation of the time of the tibial vertical event in percentage of gait cycle as described in section 9.3.2. For patient (P4), their walking was very poor at the time of trials and no footswitch information was obtained; therefore the data was excluded from the analysis. The affected foot does not lift at all and the foot was dragged all the time during the trials.

10.3.2 Tibial Vertical Event Detection

In the detection of the tibial vertical event, the correlation coefficient signal was calculated between the sample window (W1) and the foot segment angle of the affected side of the patients (P1, P2, P5, P6 and P7). For patient (P3), the sample window (W2) was used to calculate the correlation coefficient. The negative (t_n) and positive (t_p) thresholds values have been chosen for every patient. Table 10-2 and Table 10-3 list the thresholds values and both time frames (T_f and T_{f1}) for every patient for the detection of tibial vertical events during walking with stimulation on and with stimulation off respectively using Rules II (Chapter 7, p141). For three patients, the same parameters are used with stimulation on and with stimulation off. The other patients have small changes in some of their parameters. The threshold values and time frame were set for an individual patient based on the correlation coefficient signal obtained. For every patient, two horizontal lines which represent the thresholds were drawn on the correlation coefficient signal beginning with 0.3 for positive threshold and -0.3 for negative threshold (refer to Figure 7-10 (Chapter 7, p141) for a correlation coefficient signal). The line was moved by 0.5 towards 1 for positive threshold and -1 for negative threshold. The last value before the line started to go beyond the positive or negative peak of the correlation coefficient signal in all trials for the respective subject, was set as the threshold. From the correlation coefficient signal, the tibial vertical event is detected using the Rules II. The time frame, T_f was set from negative threshold to between the first maximum crossing the positive threshold and the additional minimum crossing the negative threshold but closed to the first maximum crossing the positive threshold that satisfied with all the trials of the individual patient. As sometimes there is an additional maximum and minimum in the correlation coefficient signal, another time frame is needed. Time frame 1, T_{f1} has been used to cancel the additional minimum and maximum in the algorithm that occur during the stance phase of a gait. T_{f1} is from the first maximum crossing the positive threshold (the event) to right before the minimum crossing the negative threshold (in swing phase).

Table 10-2 The thresholds and time frames for the detection of the tibial vertical events (with stimulation on).

Participant	t_p	t_n	T_f *in ms*	T_{fl} *in ms*
P1	0.35	-0.50	550	1500
P2	0.50	-0.55	550	1000
P3	0.80	-0.50	800	1000
P5	0.45	-0.40	550	1500
P6	0.55	-0.60	550	1400
P7	0.40	-0.50	550	1000

Table 10-3 The thresholds and time frames for the detection of the tibial vertical events (with stimulation off).

Participant	t_p	t_n	T_f *in ms*	T_{fl} *in ms*
P 1	0.50	-0.50	550	2300
P 2	0.50	-0.55	550	1000
P3	0.80	-0.50	800	1000
P 5	0.50	-0.50	550	1800
P 6	0.55	-0.40	550	1500
P 7	0.40	-0.50	550	1000

10.4 Results and Discussion

10.4.1 Kinematic Measurement and Tibial Vertical Events Detection

Figure 10-2 and Figure 10-3 show examples of tibial vertical events detection in patient (P1) when walking with stimulation off and with stimulation on. From observation, the type of initial contact with the ground and amplitude of the foot segment angle are different when walking with stimulation on and stimulation off. In Figure 10-2(d) and Figure 10-3(d), the type of initial contact of the foot has changed from foot flat to heel contact when walking with stimulation on. In Figure 10-2(a) and Figure 10-3(a), the amplitude of the positive peak of the foot segment angle during the swing becomes greater when walking with stimulation on.

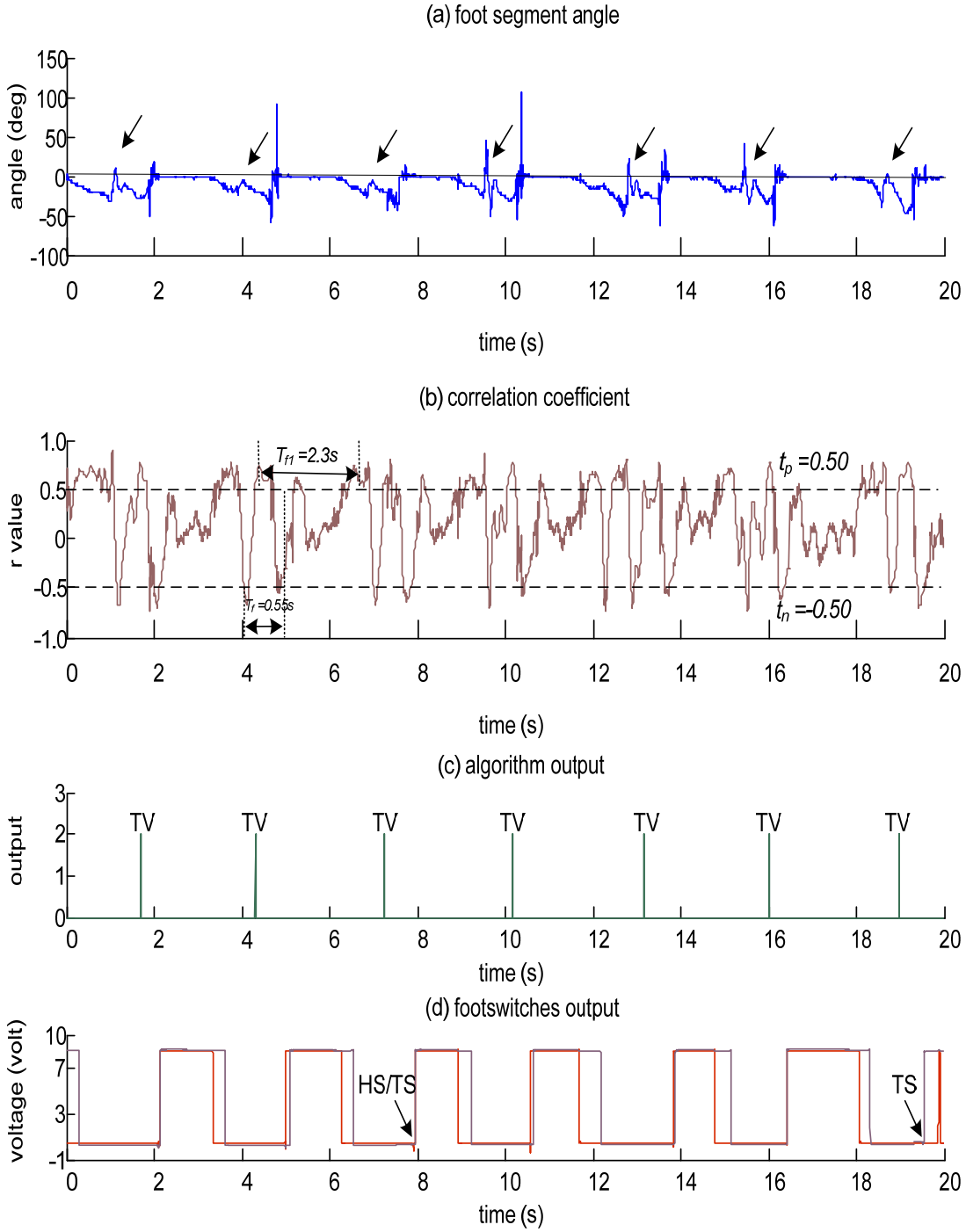

Figure 10-2 Tibial vertical event detection in patient (P1) when walking with stimulation off. Footswitches output: heel switch (red) and toe switch (purple), (TS=toe strike, HS=heel strike and TV=tibia vertical).

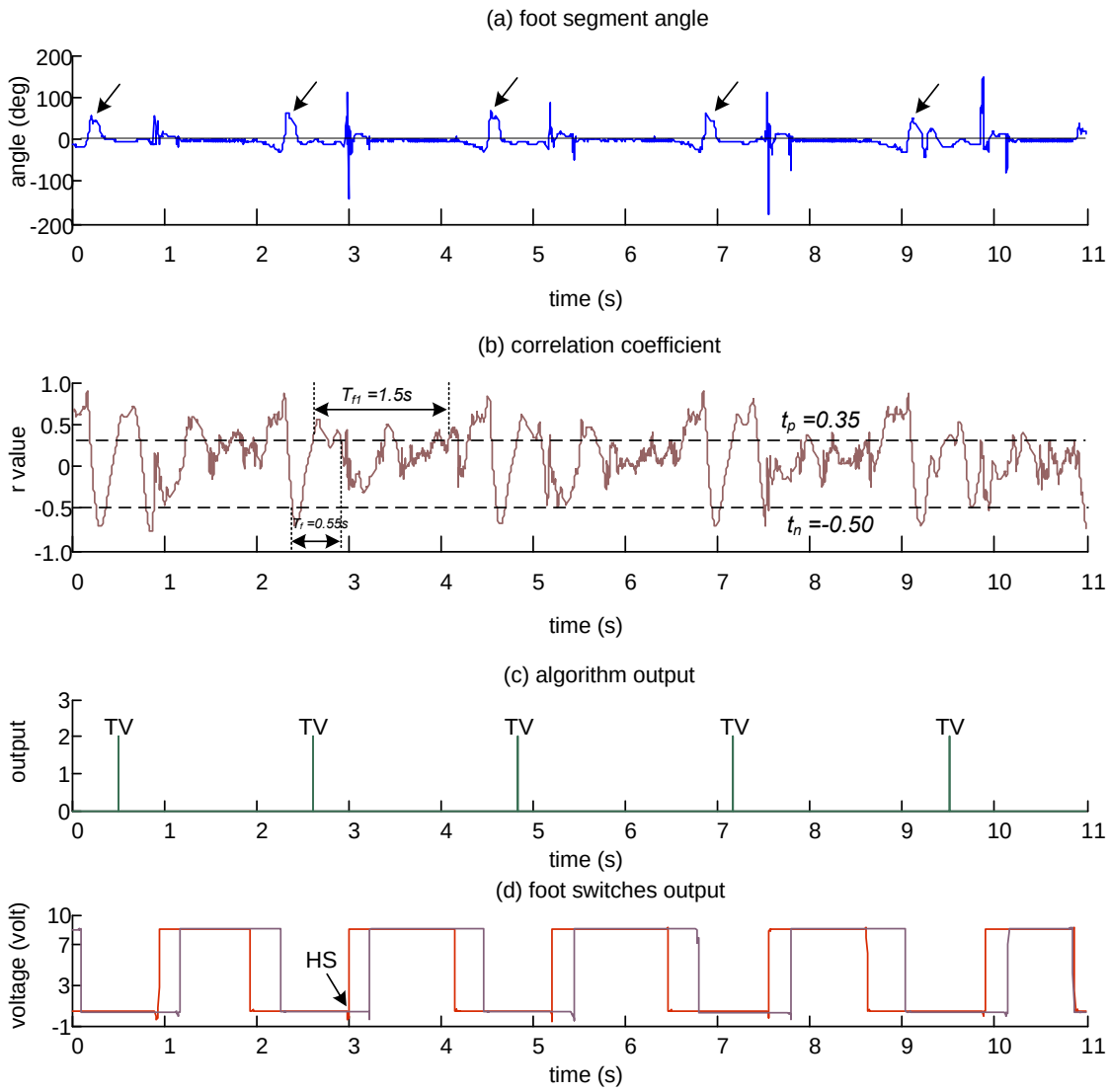

Figure 10-3 Tibial vertical event detection in patient (P1) when walking with stimulation on. Footswitches output: heel switch (red) and toe switch (purple), (HS=heel strike and TV=tibia vertical).

In patient (P1), the initial contact observed was heel contact when walking with stimulation on and foot flat when walking with stimulation off. The toe contact as initial contact was also observed in patient (P1) in four trials (last step) and a single trial (first step). Despite of all the differences, the correlation coefficient signal is consistent as the foot segment angle pattern is consistent. Therefore, the events can be detected reliably. In one trial of patient (P1), one stance is suspected to be missing between 8-12 s (Figure 10-4(d)) and according to the heel switch output of the contralateral leg (point b of Figure 10-4(e)), there should be one stance occuring at about 9-10s (point a of Figure 10-4(d)) as the contralateral leg is in swing phase.

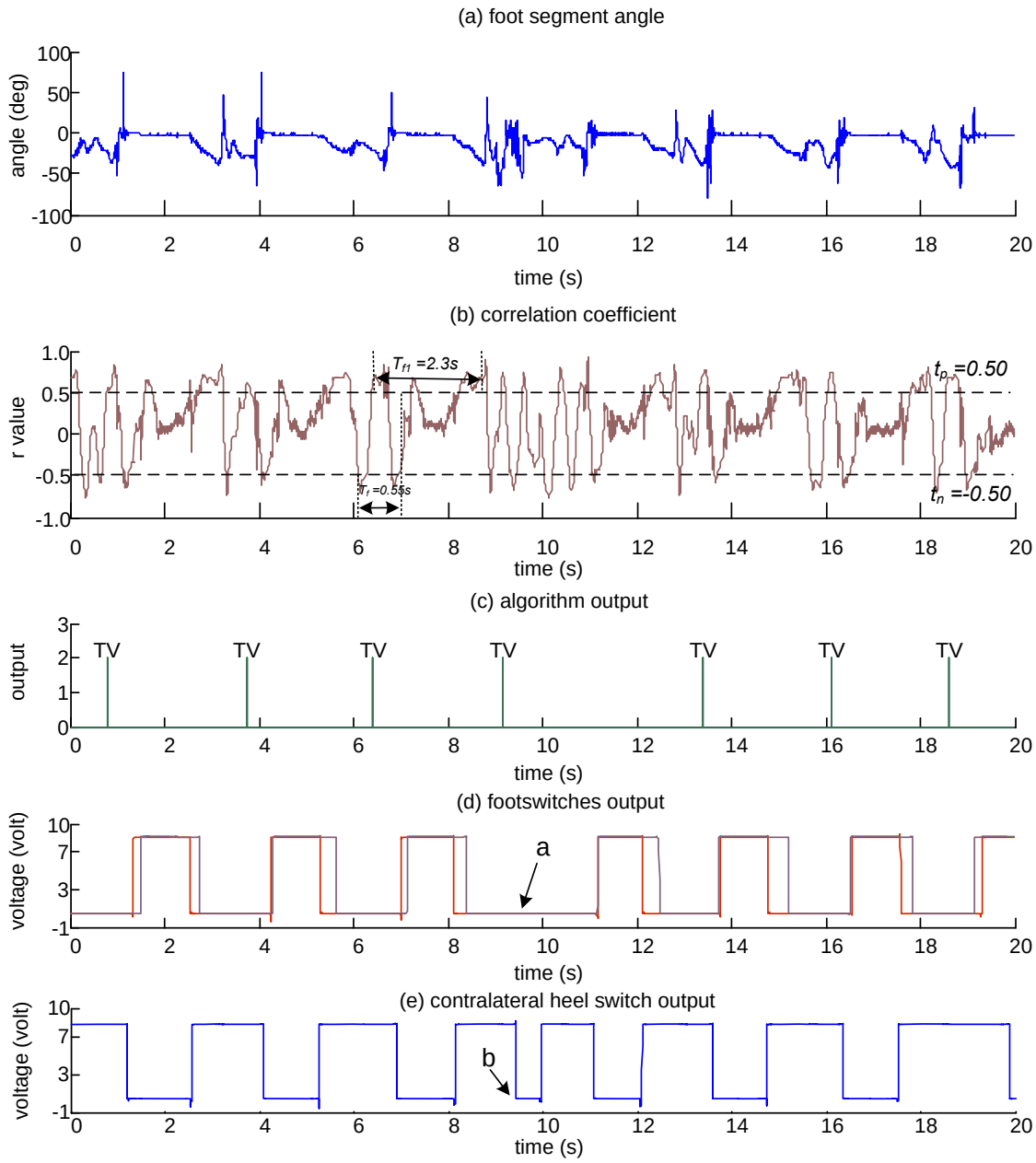

Figure 10-4 Tibial vertical event detection in patient (P1) when walking with stimulation off. Footswitches output: heel switch (red) and toe switch (purple), (HS=heel strike and TV=tibia vertical).

In patient (P2), the initial contact observed was foot flat and in seven out of ten trials the toe switch information was not obtained therefore only the heel switch information was presented. Figure 10-5 and Figure 10-6 show examples of tibial vertical event detection in patient (P2) when walking with stimulation on and stimulation off.

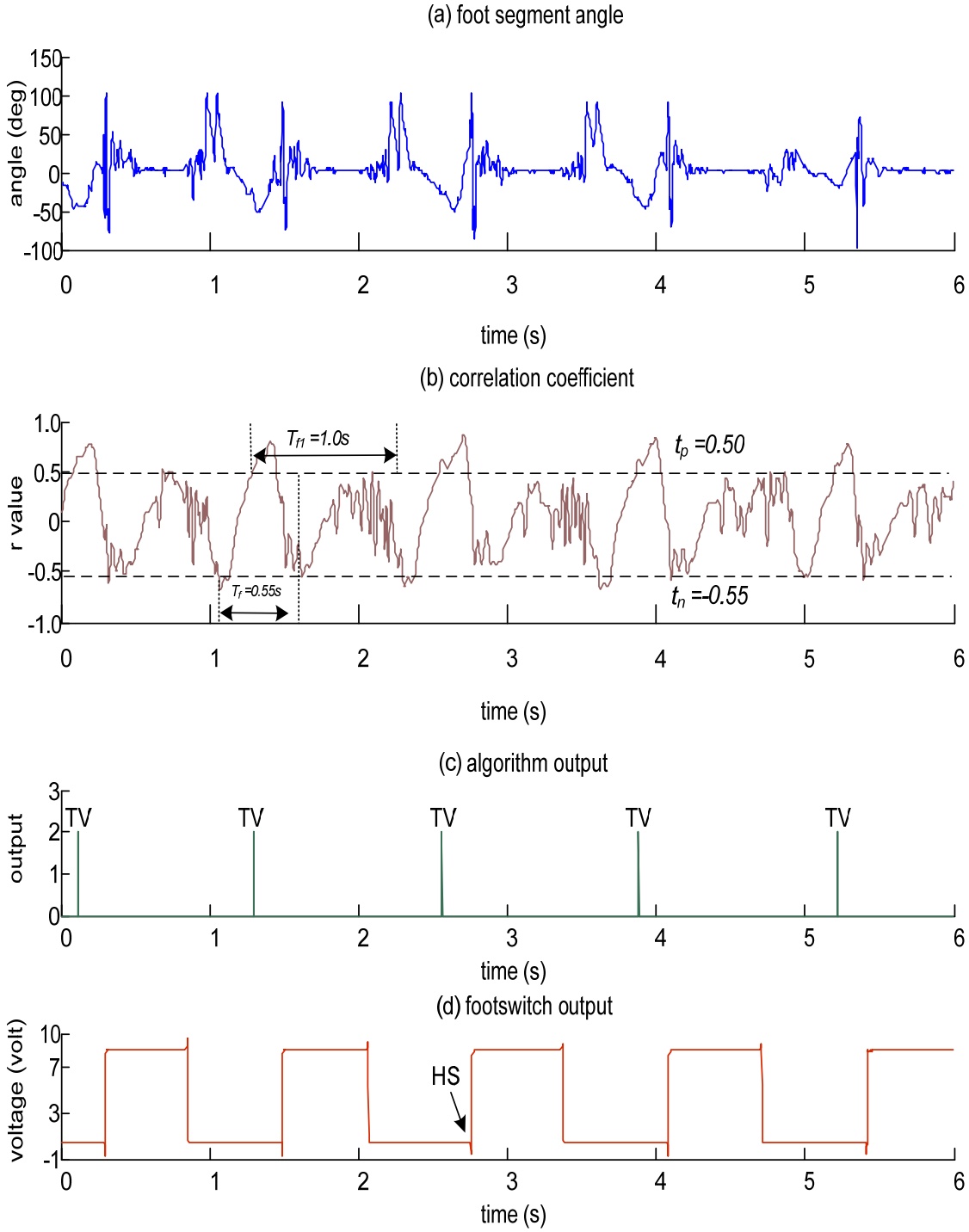

Figure 10-5 Tibial vertical event detection in patient (P2) when walking with stimulation on. Footswitch output: heel switch (red), (HS=heel strike and TV=tibia vertical).

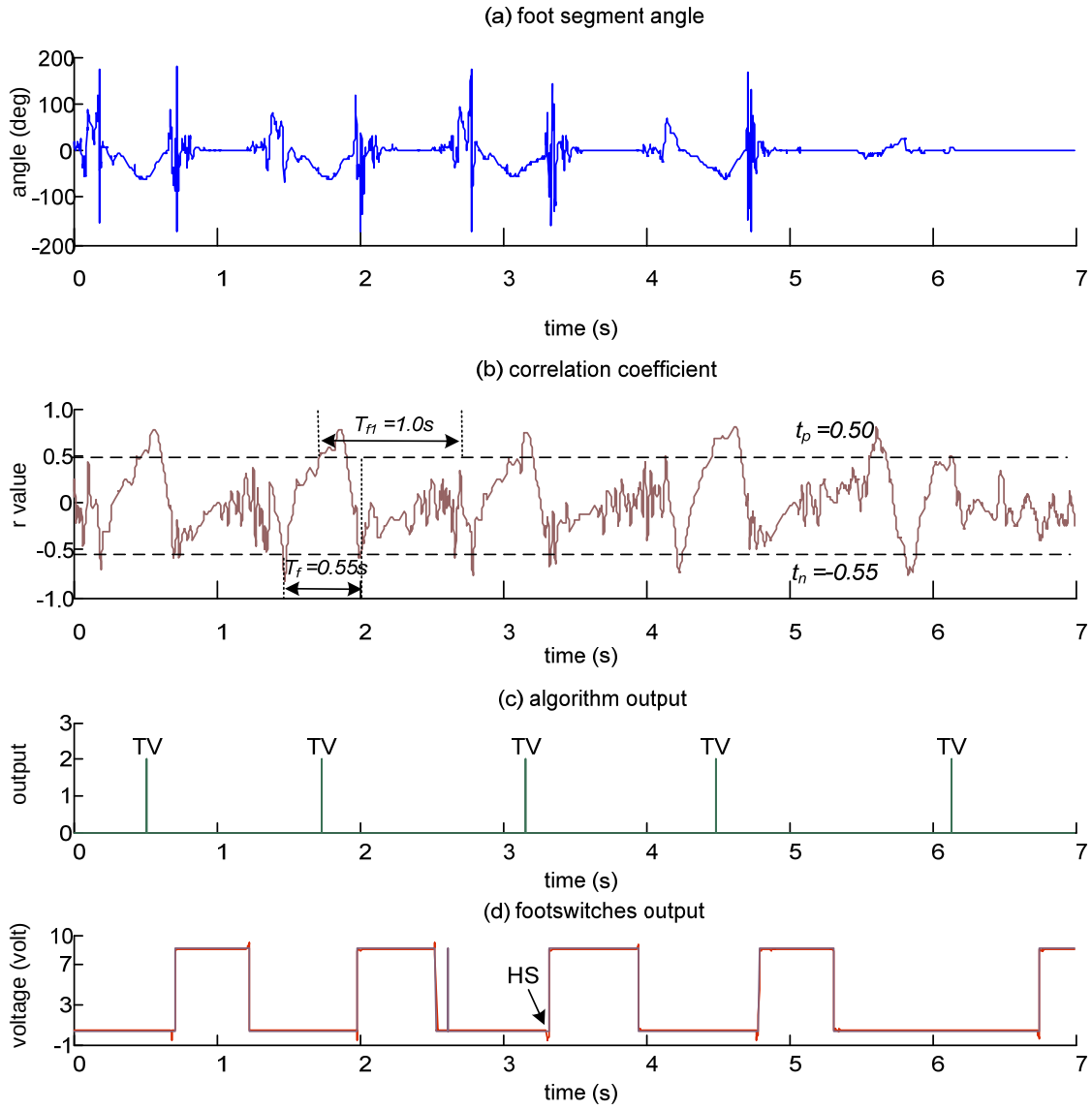

Figure 10-6 Tibial vertical event detection in patient (P2) when walking with stimulation off. Footswitches output: heel switch (red) and toe switch (purple), (HS=heel strike and TV=tibia vertical).

All fours trials (Figure L-13 to Figure L-15 and Figure 10-7) of patient (P3) when walking with stimulation on were excluded in the calculation of the mean and standard deviation of the time of tibial vertical event detection as presented in section 10.4.2. In these trials, the heel contact detected by the footswitch was suspected to occur at the wrong time when compared to the heel contact based on the foot segment angle. Figure 10-7 shows an example of tibial vertical event detection in patient (P3) when walking with stimulation on. In the figure, four vertical lines labelled with (i, ii, iii and iv) were drawn to indicate the heel contact (initial contact) based on the foot segment angle

pattern and in Figure 10-7 (d) the four small arrows show the heel contact detected by the footswitch. These could be that the footswitch detected the small force exerted between the sole and the shoe during swing as the foot everted and dorsiflexed when stimulated. These only happened when the patient walked with the stimulation switched on.

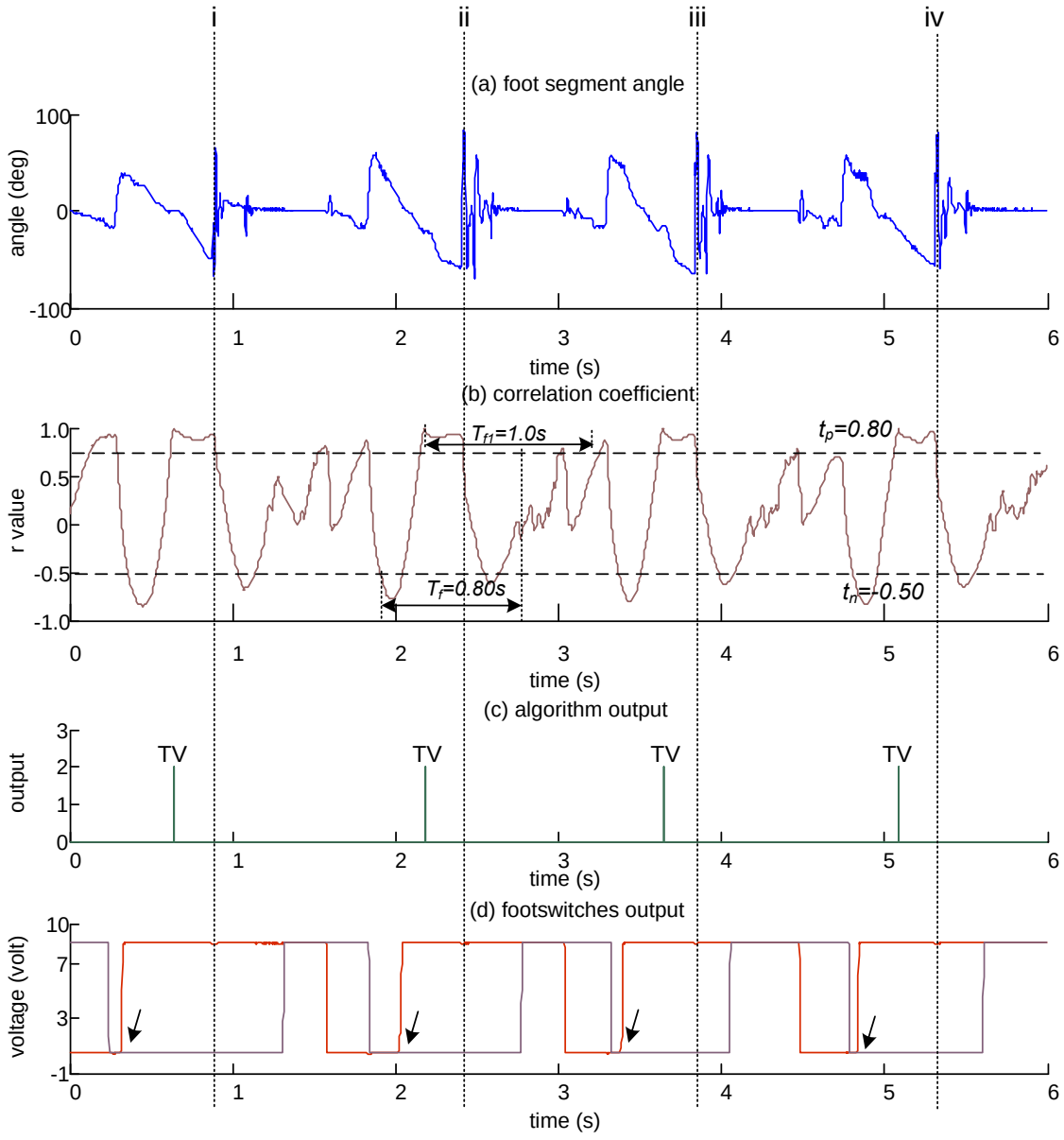

Figure 10-7 Tibial vertical event detection in patient (P3) when walking with stimulation on. Footswitches output: heel switch (red) and toe switch (purple), (TV=tibia vertical).

For patients (P3, P5, P6 and P7), the initial contact observed was heel contact. Only in two trials the last step of patient (P6), the initial contact observed was toe contact. The rest of the plots for patients (P1, P2, P3, P5, P6 and P7) are appended in Appendix L.

10.4.2 Time of Tibial Vertical Events Detected in Percentage of Gait Cycle

For all patients, there were no missing events as compared to the footswitch (heel switch) of the ipsilateral leg. Table 10-4 and Table 10-5 show the result of the tibial vertical events detected using sample window (W1) for patients (P1, P2, P5, P6 and P7) walking with stimulation off and with stimulation on, respectively. The column on the right hand side of these tables shows the differences between the values measured and the 13% target. These differences are in the range 7 to13% (walking with stimulation off) and 1 to 20% (walking with stimulation on). The differences for all others are smaller when walking with stimulation on except for one patient (P5). For patients (P1, P2, P6 and P7), the muscles that need to be stimulated are the gluteal for correction of excessive hip flexion/adduction at heel strike. If a typical 40 pulses per second stimulation is used, based on the result on Table 10-4, P2, P7 and P1 walking with stimulation off would have 1 pulse, 2 pulses and 5 pulses away respectively from the acceptable time to start gluteal muscles stimulation defined as 5% earlier than the detected event. It is anticipated that the deceleration of the hip and reduction of the limb advancement start slightly earlier. This effect could result in reduced step length and a slowing down of the walking activity. This subtle effect may not be obvious as the hip flexion contracture or spasticity in the patients will balance out the gluteal action. For P5 and P6, the standard deviation is small when walking with stimulation off and the values are within the defined range.

As can be seen in the table, patient (P5) has the largest mean time difference compared to 13% of GC before IC. This patient uses stimulation of the hamstrings muscles as the second channel to correct for the ‘insufficient knee flexion during swing’ as identified by the FES clinician at the set up of their stimulator in normal clinic. The time difference is more when walking with stimulation on; it could be that the stimulation has altered the gait pattern and therefore has changed the time of the event occurrence.

Table 10-6 shows the result of the tibial vertical events detected using sample window (W2) for patient (P3) walking with stimulation off. The mean time difference of the detected events is very close to the 13% with a small standard deviation. Therefore, the events detected in patient (P3) are within an acceptable range for stimulation of the gluteal muscles and no harm will cause to the patient during walking.

Table 10-4 The mean, standard deviation, median and range of tibial vertical events detection in percentage of gait cycle before initial contact when walking with stimulation off using sample window (W1).

Patient	*No. of events detected*	*Mean ± SD (TE % of GC before initial contact)*	*Median*	*Range*	*Mean ± SD (TE % of GC before heel strike compared to 13% of GC before initial contact)*
P1	23	22.54 ± 9.24	20.31	14.04 to 51.17	9.54 ± 9.24
P2	26	20.84 ± 6.81	20.09	2.47 to 39.90	7.84 ± 6.81
P5	30	25.76 ± 4.05	25.51	14.64 to 33.96	12.76 ± 4.05
P6	21	22.11 ± 4.43	21.31	17.58 to 36.53	9.91 ± 4.43
P7	17	20.49 ± 6.69	17.42	13.41 to 36.63	7.49 ± 6.69

Table 10-5 The mean, standard deviation, median and range of tibial vertical events detection in percentage of gait cycle before initial contact when walking with stimulation on using sample window (W1).

Patient	*No. of events detected*	*Mean ± SD (TE % of GC before initial contact)*	*Median*	*Range*	*Mean ± SD (TE % of GC before heel strike compared to 13% of GC before initial contact)*
P1	14	17.07 ± 3.94	17.47	4.43 to 21.10	4.07 ± 3.94
P2	24	17.11 ± 2.09	16.28	14.08 to 20.92	4.11 ± 2.09
P5	23	33.03 ± 9.36	30.96	21.27 to 59.83	20.03 ± 9.36
P6	15	16.25 ± 5.19	14.76	11.73 to 32.93	3.25 ± 5.19
P7	22	14.33 ± 3.04	13.37	10.75 to 22.83	1.33 ± 3.04

Table 10-6 The mean, standard deviation, median and range of tibial vertical events detection in percentage of gait cycle before initial contact when walking with stimulation off using sample window (W2).

Patient	*No. of events detected*	*Mean ± SD (TE % of GC before initial contact)*	*Median*	*Range*	*Mean ± SD (TE % of GC before heel strike compared to 13% of GC before initial contact)*
P3	16	14.10 ± 2.79	14.41	5.83 to 17.25	1.10 ± 2.79

Figure 10-8 to Figure 10-13 show the distribution of time of tibial vertical detection in percentage of gait cycle before initial contact for patients (P1, P2, P3, P5, P6 and P7) when walking with stimulation on and with stimulation off. In the figures, all the events have been detected before the initial contact of the footswitch. Time difference of tibial vertical event detection compared to 13% was small in patient (P3) and the time range is between 5-18%. The largest time for the detection of tibial vertical event was observed in patient (P5). The time was 59.83% of GC before IC.

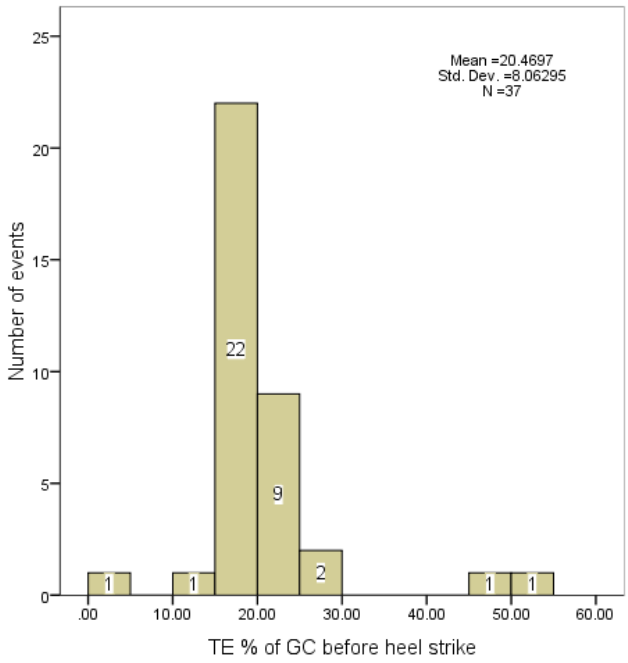

Figure 10-8 Distribution of time of tibial vertical event detected in percentage of gait cycle before initial contact in patient (P1) walking with stimulation on and stimulation off. (GC=gait cycle and TE= time of tibial vertical)

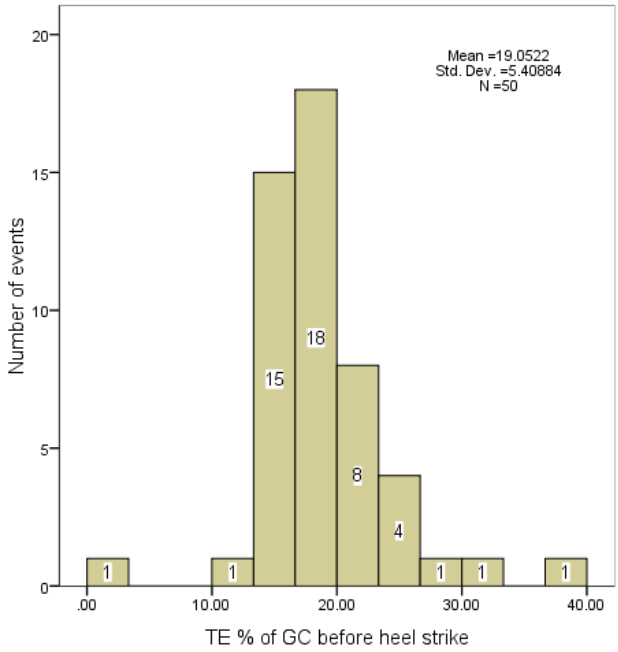

Figure 10-9 Distribution of time of tibial vertical event detected in percentage of gait cycle before initial contact in patient (P2) walking with stimulation on and stimulation off. (GC=gait cycle and TE= time of tibial vertical)

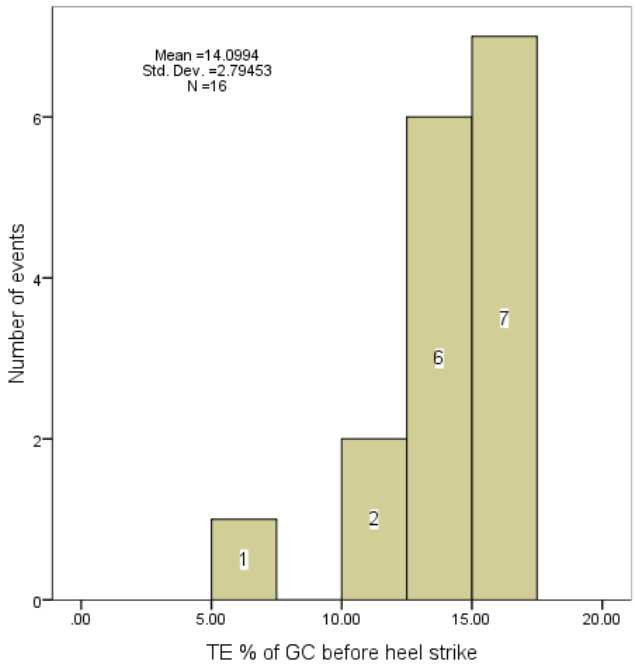

Figure 10-10 Distribution of time of tibial vertical event detected in percentage of gait cycle before initial contact in patient (P3) walking with stimulation off. (GC=gait cycle and TE= time of tibial vertical)

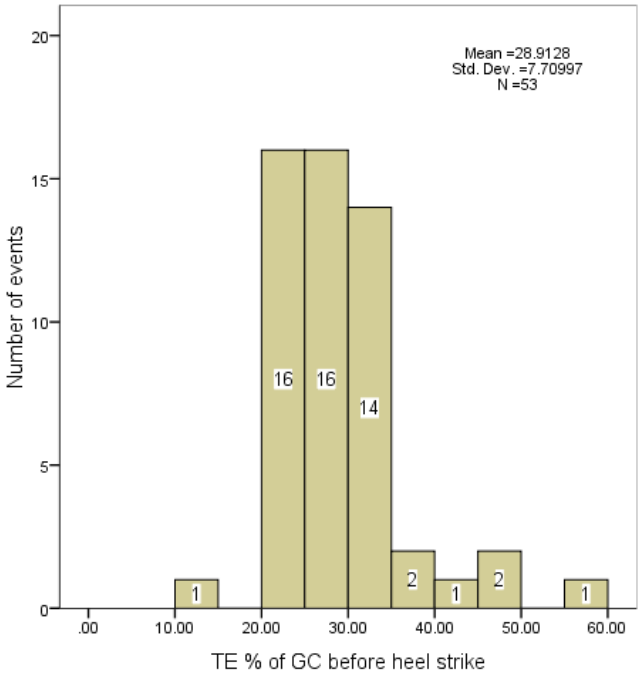

Figure 10-11 Distribution of time of tibial vertical event detected in percentage of gait cycle before initial contact in patient (P5) walking with stimulation on and stimulation off. (GC=gait cycle and TE= time of tibial vertical)

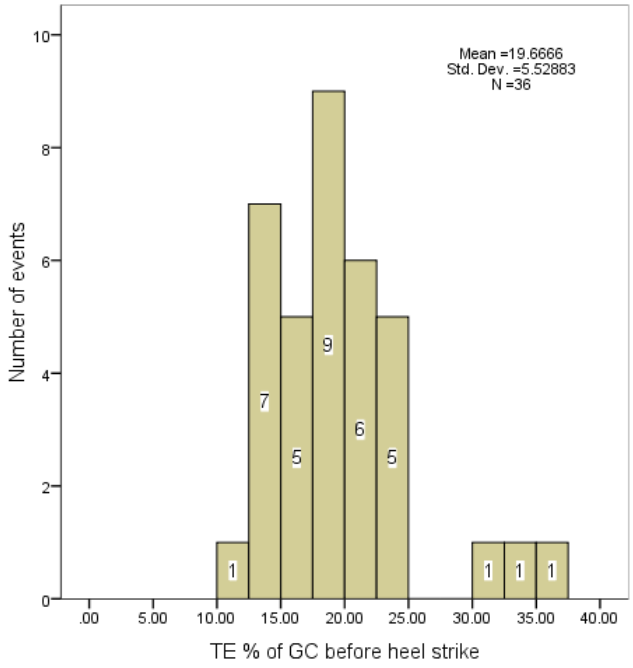

Figure 10-12 Distribution of time of tibial vertical event detected in percentage of gait cycle before initial contact in patient (P6) walking with stimulation on and stimulation off. (GC=gait cycle and TE= time of tibial vertical)

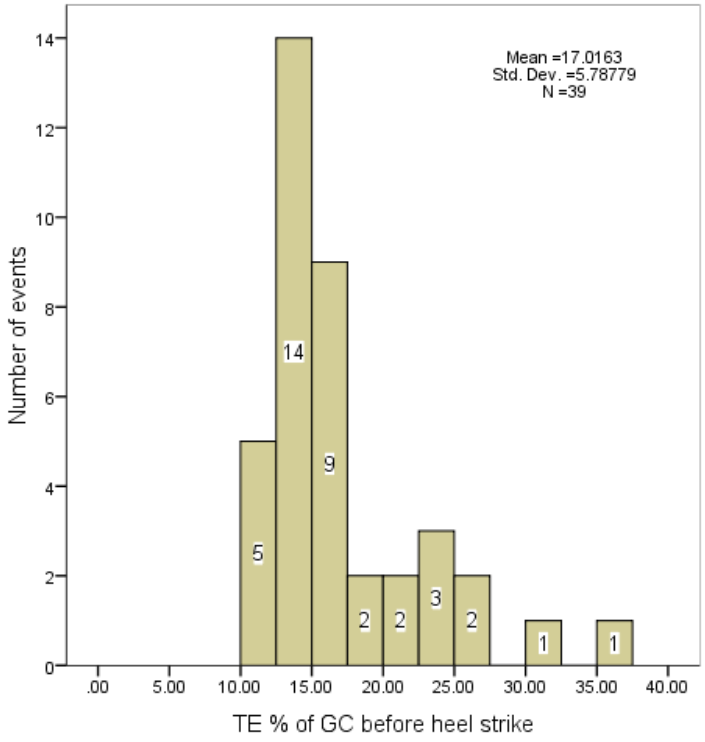

Figure 10-13 Distribution of time of tibial vertical event detected in percentage of gait cycle before initial contact in patient (P7) walking with stimulation on and stimulation off. (GC=gait cycle and TE= time of tibial vertical)

The data distribution of the time of tibial vertical (TV) event detected in percentage of gait cycle before initial contact for all the patients has a range between 2.47% to 51.17%. The range is wider compared to the data distribution obtained from the healthy subjects. Most of the data is in the range of 10% to 25% of gait cycle before heel strike except for patient 5. In the literature, the TV event in healthy subjects occurs at 13% (Perry (1992)) and 15% (Kaufman and Sutherland (2006)) of a gait cycle before initial contact. In the study, an event (which should correspond to when the tibia is vertical) is detected based on the 13% of gait cycle before initial contact defined by (Perry (1992)) using a footswitch as a reference sensor. For patients (P1, P2, P3, P6 and P7), the ranges of the median values of the time of TV event detected in percentage of gait cycle before heel strike are from 13.37% to 17.47% and 14.41% to 21.31% when walking with stimulation off and on, respectively. These ranges are close to the occurrence of TV event described by Perry (1992), and Kaufman and Sutherland (2006). For patient 5, the median values are 25.51% and 30.96% of gait cycle before heel strike when walking with stimulation off and on, respectively. The swing phase

(from toe off to heel strike) for patient 5 walking with stimulation on and off (Figure L-19 to Figure L-25) is longer compared to the stance phase of the same patient and the swing phase of other patients. The prolonged swing phase could be the reason for the deviation in the median values when compared to the occurrence of TV event described by Perry (1992), and Kaufman and Sutherland (2006). Most of the data for patient 5 is in the range of 20% to 40% of gait cycle before heel strike. The standard deviation of the time of TV event detected in the patients (9.36%) is larger than the standard deviation observed in the healthy subjects (2.61%).

10.5 Conclusions

A total of 231 tibial vertical events have been detected in six patients as compared to footswitch with no missing event. The mean time of tibial vertical events compared to 13% of GC before initial contact detected in P1, P2, P5, P6 and P7 using sample window (W1) is between 7-13% of GC (walking with stimulation off) and 1-20% of GC (walking with stimulation on). The standard deviation of time differences (compared to 13% of GC) for P1, P2, P6 and P7 when walking with stimulation on are smaller which is between 2.09% and 5.19% except for one patient (P5).

If a typical 40 pulses per second stimulation is used, when walking with stimulation off, P2, P7 and P1 would have 1 pulse, 2 pulses and 5 pulses away respectively from the acceptable time to start gluteal muscles stimulation defined as 5% earlier than the detected event. It could be that the deceleration of the hip and reduction of the limb advancement start slightly earlier. For P5 and P6, the standard deviation is small when walking with stimulation off and the values are within the defined stimulation range.

For P3, a sample window (W2) has been selected from the same patient data. The time difference of tibial vertical event detection compared to 13% was small in patient (P3) and the time range is between 5 and 18%. The events detected in patient (P3) are within an acceptable range for stimulation of the gluteal muscles and no harm will cause to the patient during walking.

Most of the data of the time of tibial vertical (TV) event detected is in the range of 10% to 25% except for patient 5 (20% to 40%). The range of 10% to 25% is close to the

occurrence of the TV event described by Perry (1992), and Kaufman and Sutherland (2006). For patient 5, the data range and median values of the time of TV event detected are deviated from the TV event described by Perry (1992), and Kaufman and Sutherland (2006). This could be due to the prolonged swing phase observed in this patient. The time of TV event detected in the patients (standard deviation of 9.36% of gait cycle) is more variable than the time observed in the healthy subjects (standard deviation of 2.61% of gait cycle).

Chapter 11
Final Conclusions and Future Work

11.1 Final Conclusions

A sensor system to detect tibial vertical events during gait has been developed with a future aim of triggering a stimulator for the contraction of the hamstrings or gluteals muscles and subsequent correction of knee hyperextension into early stance or excessive hip flexion/adduction at heel strike in neurological patients. Two algorithms namely the sensor unit algorithm and the detection algorithm have been combined to detect the specific events. The overall conclusions which can be drawn from the study are as follows.

The first sensor unit was developed using accelerometers with ±2g range. However, the preliminary experiments carried out have encountered saturation in the output signals during swing when the sensor unit was attached to the arm of the inverted pendulum. The accelerometers of the sensor unit were replaced with ones that have a higher acceleration range of ±6g. The first finding is that the ±2g acceleration range is not sufficient to be used for the measurement of linear acceleration of a rotating mechanical arm movement corresponding to a limb segment. Furthermore, the vertical acceleration measured during normal walking was found to be above 2.5g.

The estimated error in the sensor unit as an effect of non-linearity of the accelerometers is ±1degree. The output from the sensor unit shows more variability in the dynamic condition compared to static condition. When the sensor unit was attached to the arm of the test apparatus (inverted pendulum) and a comparison made between the segment angle measured from the sensor unit and the output from the potentiometer of the test apparatus, the error in the measurement of angle has a range between 3.62^0 and 5.44^0. These values can be lowered to 0.96^0 and 4.33^0 with a moving average of 0.3s.

The sensor unit used for the measurements is small in size, light-weight, inexpensive and has low power consumption. These characteristics are most suitable for clinical or everyday use with any ambulatory system including FES. An advantage of the sensor unit is that it is not affected by the pressure changes between the shoe and insole or the type of footwear used. The sensor unit can perform the measurement without the need for integration and therefore drift problems are totally avoided. As no complex calculation was involved and no further processing such as filtering or smoothing was required (the moving average was used for comparison test purposes only), the sensor unit can be implemented in a real time system.

The detection algorithm employed correlation coefficient calculations and a set of rules with thresholds. A sample window selected from kinematic data was used to obtain the correlation coefficient signal. The set of rules with a threshold was then applied to the signal to detect the desired event. The detection algorithm has an advantage of comparing a threshold with the correlation coefficient for the event detection as the correlation coefficient is within -1 to 1 only and not dependent on individual absolute values. The segment angle has a larger range of values and will vary between the subjects, making the threshold more difficult to set. Therefore the advantage of using the correlation coefficient calculation is that the clinical setting will be simple.

For all five healthy subjects walking with normal speed, the range of the correlation coefficient and standard deviation calculated between measurements from the sensor unit and Vicon^{TM} for thigh and foot segments angle for a single stride are between (r = 0.185 and r = 0.643) and (r = 0.363 and r = 0.898) and (10.29°and 19.19°) and (3.48°and 18.27°) respectively. For shank segment angle for a single stride, the correlation coefficient and standard deviation are between (r = 0.834 and r = 0.992) and

(2.83°and 13.72°) respectively. From all the segments measured using the sensor unit, only the shank segment angle has a similar pattern with the angle measured using the Vicon^{TM} for inter-subject and intra-subject. For thigh and foot angles, the measurements from the two systems have a different pattern. However, the thigh and foot segment angle measured using the sensor unit are similar and consistent between the subjects. Despite the large deviation between the two systems measurements, it is possible to use any of the segments angles measured using the senor unit to detect events as these angles have shown consistent patterns.

The sensor system can detect heel strike events in five healthy subjects with no missing events as compared to a footswitch. The largest absolute mean and standard deviation are 11.51ms (Subject 2) and 20.16ms (Subject 4). If the typical frequency used for stimulation of peroneal nerve or tibialis anterior muscles is 40Hz (pulses per second), the events are detected within two stimulation pulses. Moreover, even the largest time difference is 53ms (Subject 4) which is three pulses away and within the defined timing limit for heel strike detection 150ms (before or after the event).

The sensor system can also estimate an event that is 13% of the gait cycle before the heel strike that represents when the tibial is vertical in five healthy subjects and six neurological patients with no missing events. Although the study has defined that the earliest acceptable time to start the stimulation of hamstrings and gluteals muscles is 5% before the detected event (tibial vertical event), the effect of stimulating these muscles earlier than the 5% or within the 5% is still unknown and further work is needed to determine and confirm this effect. The standard deviation for the time of tibial vertical event ranged between 0.81% and 2.61%. The absolute mean of the time difference has a range between 0.01% and 1.99%. The median of the time of tibial vertical event detected in the healthy subjects has a range between 11.77% and 15.06% of gait cycle before heel strike. Nearly all of the tibia vertical events of the five subjects are in the range from 10% to 18% of the gait cycle before heel strike. The standard deviation of the time of tibial vertical event detected was small (2.61% of gait cycle).

For patients, if a typical 40 pulses per second stimulation is used, when walking with the stimulation off, patients P2, P7 and P1 would be one pulse, two pulses and five pulses away respectively from the acceptable time to start the gluteal muscles

stimulation defined as 5% earlier than the detected event. When walking with stimulation on, patients P6 and P5 would have less than one pulse and four pulses away respectively from the acceptable time to start gluteal muscles stimulation defined as 5% earlier than the detected event. Patients P3, P5 and P6 when walking with the stimulation off and for patients P1, P2 and P7 when walking with stimulation on, the events detected are within the acceptable time to start gluteal muscles stimulation. Even the worst case is five pulses away from the defined acceptable time to start the gluteal muscles stimulation and the established effect of this is not known. However, a possible effect could be that there is reduced step length and a slowing down of the walking activity due to the deceleration of the hip and reduction of the limb advancement that started slightly earlier.

Most of the data of the time of tibial vertical event detected for all the patients is in the range of 10% to 25% except for patient 5 (20% to 40%). For patient 5, the data range and median values of the time of tibial vertical event detected seem to be affected by the prolonged swing phase observed in the patient. The time of tibial vertical event detected in the patients is more variable than the time observed in the healthy subjects.

Furthermore, in total, only three sample windows have been used to detect heel strike and tibial vertical events in five healthy subjects and neurological patients. This result shows the simplicity and robustness of the sensor system in event detection and therefore, it could be used as a trigger to start the stimulation of hamstrings or gluteals muscles group with FES systems.

11.2 Future Work

Overall, the sensor system can be programmed in a microcontroller to trigger a stimulator for hamstrings or gluteals muscles stimulation during walking. The trials on the patients can be carried out to measure the improvement and the outcome of the stimulation.

The sensor unit algorithm can be further explored in different applications such as gait analysis, diagnosis of gait abnormalities, wheelchair stability and ambulatory

monitoring while the detection algorithm can be further explored in gait analysis studies.

11.2.1 Sensor Unit Measurement

The measurement of the sensor unit was limited to two dimensional (2D) measurements. If the sensor is to be used in any applications that involve with three dimensional (3D) measurements, the number of accelerometers in the sensor unit has to be increased.

The algorithm used for the sensor unit can be explored by having a different accelerometers arrangement for example 120° between the sensors axes. This configuration can reduce the number of accelerometers needed to perform the same measurements as the current sensor.

The sensor unit algorithm can be executed in a microcontroller for use in real time applications. The angle calculation steps for execution in microcontroller are shown in Figure 11-1. Any accelerometers with the same specifications can be employed in the sensor unit. Therefore a smaller sensor unit can be built by using smaller accelerometers. Also, for used with FES system, the sensor unit can be built in a smaller box or embedded into fabric or shoes to improve the cosmetic appearance.

The sensor unit could also be used in any vehicles for measurement of linear accelerations or incline but for this purpose, the bandwidth and sensitivity of the sensor will need to be selected appropriately.

The experimental work on assessment of the sensor unit measurement during walking can be improved by using a reference sensor that uses the same frequency sampling and method of calculation. A motion capture system that samples at a frequency of 1ksamples/sec is required.

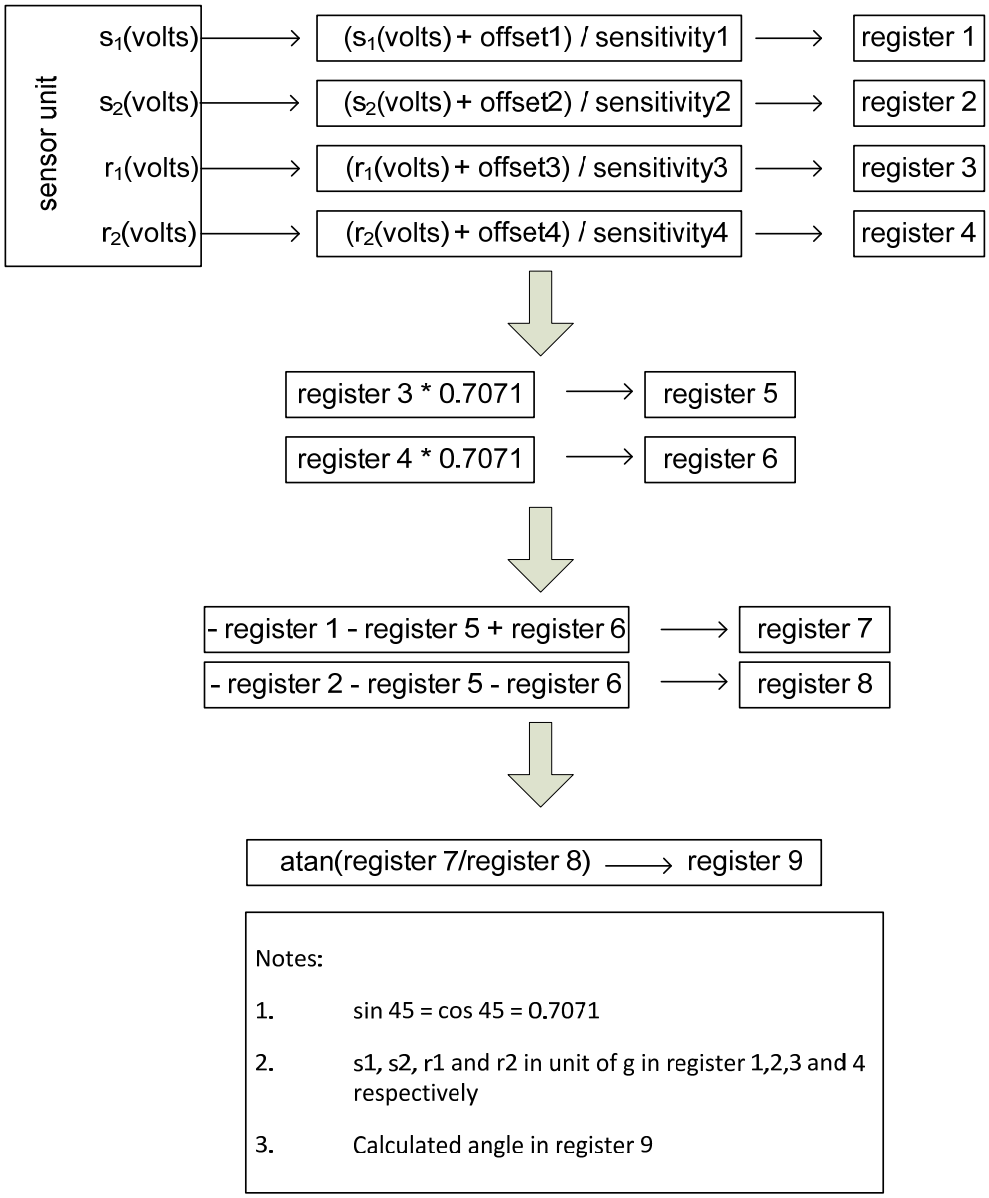

Figure 11-1 The angle calculation steps for execution in microcontroller.

11.2.2 Events Detection

The experimental work on the detection of events in healthy subjects and patients can be further explored before it is used for FES to confirm on the reliability and accuracy of the algorithm by having the participants walk:

- on different terrains for example walking on slopes
- at a longer distance and outside the laboratory

- upstairs and downstairs
- at different speeds and wearing different type of shoes

The detection algorithm can make use of other kinematic measurements made by the sensor unit such as linear accelerations and from different segment such as thigh or shank for the gait event detection. More gait events can be detected using the algorithm by selecting different sample windows for different events. It could be that by using a different sample window, a different pattern of the correlation coefficient signal will be produced. Therefore a different set of rules will be needed.

References

Aminian, K., Najafi, B., Büla, C., Leyvraz, P. F. and Robert, P. (2002) Spatio-temporal parameters of gait measured by an ambulatory system using miniature gyroscopes. *Journal of Biomechanics,* 35 (5)**,** 689-699.

Aminian, K., Rezakhanlou, K., De Andres, E., Fritsch, C., Leyvraz, P. and Robert, P. (1999) Temporal feature estimation during walking using miniature accelerometers: an analysis of gait improvement after hip arthroplasty. *Medical and Biological Engineering and Computing,* 37 (6)**,** 686-691.

Analog Devices Inc. (1995a) *ADXL311: Ultracompact ±2g Dual-Axis Accelerometer.* Available from: http://www.analog.com/en/sensors/inertial-sensors/ adxl311/ products/product.html [Accessed 20 January 2007]

Analog Devices Inc. (1995b) *ADXL320: Small and Thin, ±5 g Accelerometer.* Available from: http://www.analog.com/en/sensors/inertial-sensors/ adxl320/ products/ product.html [Accessed 26 April 2007]

Analog Devices Inc. (1995c) *ADXL203: Precision ±1.7g Dual-Axis iMEMS® Accelerometer.* Available from: http://www.analog.com/en/mems-sensors/inertial-sensors/adxl203/products/product.html [Accessed 26 February 2011]

Auvinet, B., Berrut, G., Touzard, C., Moutel, L., Collet, N., Chaleil, D. and Barrey, E. (2002) Reference data for normal subjects obtained with an accelerometric device. *Gait & Posture,* 16 (2)**,** 124-134.

Barnes, P. G., Gaik, K. H., Shaarani, N. H., Bani, N. A., Ab Aziz, N. F. and Kahoul, A. (2006) Biomechanical Motion Analysis. University of Southampton.

Beauchet, O., Annweiler, C., Lecordroch, Y., Allali, G., Dubost, V., Herrmann, F. and Kressig, R. (2009) Walking speed-related changes in stride time variability: effects of decreased speed. *Journal of NeuroEngineering and Rehabilitation,* 6 (1)**,** 32.

Bell, A. L., Brand, R. A. and Pedersen, D. R. (1989) Prediction of hip joint centre location from external landmarks. *Human Movement Science,* 8 (1)**,** 3-16.

Biometrics Ltd (2010) *Goniometer and Torsiometer.* Available from: http://www.biometricsltd.com/gonio.htm [Accessed 26 February 2011]

Bioness Inc. (2010) *Bioness® Live On.* Available from: http://www. bioness.com/ Home. php [Accessed 20 November 2010]

Boakes, J. L. and Rab, G. T. (2006) Muscle Avtivity During Walking. *In:* Rose, J.andGamble, J. G. (Eds.) *Human Walking.3rd ed* Philadelphia: Lippincott Williams & Wilkins.

Boonstra, M. C., van der Slikke, R. M. A., Keijsers, N. L. W., van Lummel, R. C., de Waal Malefijt, M. C. and Verdonschot, N. (2006) The accuracy of measuring the kinematics of rising from a chair with accelerometers and gyroscopes. *Journal of Biomechanics,* 39 (2)**,** 354-358.

Bouten, C. V. C., Koekkoek, K. T. M., Verduin, M., Kodde, R. and Janssen, J. D. (1997) A triaxial accelerometer and portable data processing unit for the assessment of daily physical activity. *IEEE Transactions on Biomedical Engineering,* 44 (3)**,** 136-147.

Brandes, M., Zijlstra, W., Heikens, S., van Lummel, R. and Rosenbaum, D. (2006) Accelerometry based assessment of gait parameters in children. *Gait & Posture,* 24 (4)**,** 482-486.

Burridge, J. (1997) Improvement of hemiplegic gait with single channel surface stimulation. *IEE***,** 3/1-3/3.

Burridge, J. H., Elessi, K., Pickering, R. M. and Taylor, P. N. (2007) Walking on an Uneven Surface: The Effect of Common Peroneal Stimulation on Gait Parameters and Relationship Between Perceived and Measured Benefits in a Sample of Participants With a Drop-Foot. *Neuromodulation,* 10 (1)**,** 59-67.

Burton, J. L. (1997) *Aids to undergraduate medicine 6th ed.* Edinburgh ; New York: Churchill Livingstone.

Carnstam, B., Larsson, L. E. and Prevec, T. S. (1977) Improvement of gait following functional electrical-stimulation .1. Investigations on changes in voluntary strength and proprioceptive reflexes. *Scandinavian Journal of Rehabilitation Medicine,* 9 (1)**,** 7-13.

Catalfamo, P., Ghoussayni, S. and Ewins, D. (2010) Gait Event Detection on Level Ground and Incline Walking Using a Rate Gyroscope. *Sensors,* 10 (6)**,** 5683-5702.

Churchill, Sarah and Peters, D.M. and Bevins, Joe (2007) *The Validity of Marker Reconstruction Modelling for Biomechanical Analysis in Sport.* In: 6th International Symposium on Computer Science in Sport, 3rd - 6th June, 2007, Calgary, Canada.

Dai, R., Stein, R. B., Andrews, B. J., James, K. B. and Wieler, M. (1996) Application of tilt sensors in functional electrical stimulation. *IEEE Transactions on Rehabilitation Engineering,,* 4 (2)**,** 63-72.

Davidson, S., Edwards, C. R. W., Bouchier, I. A. D., Haslett, C. and Chilvers, E. R. (1995) *Davidson's principles & practice of medicine. 17th ed.* Edinburgh ; New York: Churchill Livingstone.

Davis, I., Ounpuu, S., Tyburski, D. and Gage, J. (1991) A gait analysis data collection and reduction technique. *Human Movement Science,* 10 (5)**,** 575-587.

Dejnabadi, H., Jolles, B. M. and Aminian, K. (2005) A new approach to accurate measurement of uniaxial joint angles based on a combination of accelerometers

and gyroscopes. *IEEE Transactions on Biomedical Engineering,* 52 (8)**,** 1478-1484.

Dejnabadi, H., Jolles, B. M., Casanova, E., Fua, P. and Aminian, K. (2006) Estimation and visualization of sagittal kinematics of lower limbs orientation using body-fixed sensors. *IEEE Transactions on Biomedical Engineering,* 53 (7)**,** 1385-1393.

Dugdale, D.C., Hoch, D.B & Zieve, D. (2009) *Walking abnormalities- Overview.* Available from: http://www.umm.edu/ency/article/003199.htm [Accessed 30 August 2010]

Durham, S., Eve, L., Turner-Simmonds, C., Daniel, C., Stevens, C. and Ewins, D. J. (2004) An investigation of effect of functional electrical stimulation to assist the gait of children with cerebral palsy IN:9th Annual Conference of the International FES Society Bournemouth, UK.

Earth Day Colouring Book (1998) *Planet Earth, Love Your Mother.* Available from: http://parenting.leehansen.com/downloads/coloring/MISC/EarthPlanet.htm [Accessed 13 September 2010]

Favre, J., Jolles, B. M., Aissaoui, R. and Aminian, K. (2008) Ambulatory measurement of 3D knee joint angle. *Journal of Biomechanics,* 41 (5)**,** 1029-1035.

Findlow, A. H., Kenny, L. and Howard, D. (2004) Can alternatives to the forceplate be used for accurate detection of key gait events? IN:9th Annual Conference of the International FES Society Bournemouth, UK. 156-158.

Finetech Medical (2008) *STIMuSTEP® -Dropped Foot System.* Available from: http://www.finetech-medical.co.uk/Products/STIMuSTEPDroppedFootSystem/tabid/82/language/en-GB/Default.aspx [Accessed 20 November 2010]

Freescale Semiconductor (2006) *±1.5 g - 6 g Dual Axis Low-g Micromachined Accelerometer.* Available from: www.freescale.com/ files/sensors/doc/data_sheet/MMA6270QT.pdf [Accessed 26 April 2007]

Gaffney, M., O'Flyn, B., Mathewson, A., Buckle, J., Barton, J., Angove, P., Vcelak, J., Ó Conaire, C., Heal, G., Moran, K., O'Connor, N. E., Coyle, S., Kelly, P., Caulfield, B. and Conroy, L. (2009) Wearable Wireless Inertial Measurement for Sports Applications IN:33th International Conference and Exhibition IMAPS Gliwice - Pszczyna, Poland.

Ghoussayni, S. N., Catalfamo, P. C., Moser, D. and Ewins, D. J. (2004) Experience in the use of a single Gyroscope as a sensor for FES foot drop correction systems IN:9th Annual Conference of the International FES Society Bournemouth, UK.

Han, J., Jeon, H., Yi, W., Jeon, B. and Park, K. (2009) Adaptive windowing for gait phase discrimination in Parkinsonian gait using 3-axis acceleration signals. *Medical and Biological Engineering and Computing,* 47 (11)**,** 1155-1164.

Hansen, M., Haugland, M. K. and Sinkjaer, A. (2004) Evaluating robustness of gait event detection based on machine learning and natural sensors. *IEEE Transactions on Neural Systems and Rehabilitation Engineering,* 12 (1)**,** 81-88.

Hansen, M., Haugland, M., Sinkjaer, T. and Donaldson, N. (2002) Real Time Foot Drop Correction using Machine Learning and Natural Sensors. *Neuromodulation,* 5 (1)**,** 41-53.

Hart, D. J., Taylor, P. N., Chappell, P. H. and Wood, D. E. (2006) A microcontroller system for investigating the catch effect: Functional electrical stimulation of the common peroneal nerve. *Medical Engineering & Physics,* 28 (5)**,** 438-448.

Henriksen, M., Lund, H., Moe-Nilssen, R., Bliddal, H. and Danneskiod-Samsoe, B. (2004) Test-retest reliability of trunk accelerometric gait analysis. *Gait & Posture,* 19 (3)**,** 288-297.

Heyn, A., Mayagoitia, R. E., Nene, A. V. and Veltink, P. H. (1996) The kinematics of the swing phase obtained from accelerometer and gyroscope measurements In: IEEE (ed.) *Proceedings of the 18th Annual International Conference of the IEEE Engineering in Medicine and Biology Society* pp.463-464

Innovative Neurotronics (2006) *The WalkAide System for treatment of foot drop.* Available from: http://www.walkaide.com/en-US/Pages/default.aspx [Accessed 15 July 2008]

Jacobs, L.D., Wende, K.E., Brownscheidle, C.M., Apatoff, B., Coyle, P.K., Goodman, A., Gottesman, M.H., Granger, C.V., Greenberg, S.J., Herbert, J., Krupp, L., Lava, N.S., Mihai, C., Miller, A.E., Perel, A., Smith, C.R., Snyder, D.H., Sciarra, L.M., Baird, W.C., Justinger, T.A., Planter, M., Umhauer, M.A., Green, L.A., Krantz, S., Miller, C.E., Munschauer III, F.E., Patrick, K., Galey, T., Davidson, A.L., Hahn, T., Hovey, K.M., Bent, G.R., Mammano, R.L., Doxey, D.A., Galante, K., Periconi, P., Madonna, M., McCulloch, J., Shabus, D., Wheatley, J.A., Donohoe, K., Petrie, M., Pollock, M.L., Scheid, E., Schwid, S., Fraser C.Reilly, S., Brownscheidle, C.M., Jubelt, B., Delorenzo, T., Traugott, U., Wiesel-Levison, P. A profile of Multiple Sclerosis: The New York State Multiple Sclerosis Consortium. Multiple Sclerosis (1999) 5, 369-376

Jasiewicz, J. M., Allum, J. H. J., Middleton, J. W., Barriskill, A., Condie, P., Purcell, B. and Li, R. C. T. (2006) Gait event detection using linear accelerometers or angular velocity transducers in able-bodied and spinal-cord injured individuals. *Gait & Posture,* 24 (4)**,** 502-509.

Johson, C. D. (1997) Process Control Instrumentation Technology. Prentice Hall.

Kadaba, M. P., Ramakrishnan, H. K. and Wotten, M. E. (1990) Measurement of lower extremity kinematics during level walking. *Journal of Orthopaedic Research,* 8 (3)**,** 383-392.

Kaufman, K. R. and Sutherland, D. H. (2006) Kinematics of Normal Human Walking. *In:* Rose, J.andGamble, J. G. (Eds.) *Human Walking.3rd ed* Philadelphia: Lippincott Williams & Wilkins.

Kennaugh, K. (2007) The Functional Electrical Stimulation Single Channel Course. Salisbury District Hospital.

Kotiadis, D., Hermens, H. J. and Veltink, P. H. (2010) Inertial Gait Phase Detection for control of a drop foot stimulator: Inertial sensing for gait phase detection. *Medical Engineering & Physics,* 32 (4)**,** 287-297.

Kotiadis, D., Hermens, H. J., Veltink, P. H. and Slycke, P. (2004) Inertial Gait Phase Detection System: Design IN:9th Annual Conference of the International FES Society Bournemouth, UK.

Kottink, A. I., Oostendorp, L. J., Buurke, J. H., Nene, A. V., Hermens, H. J. and Ijzerman, M. J. (2004) The Orthotic Effect of Functional Electrical Stimulation on the Improvement of Walking in Stroke Patients with a Dropped Foot: A Systematic Review. *Artificial Organs,* 28 (6)**,** 577-586.

Lau, H. and Tong, K. (2008) The reliability of using accelerometer and gyroscope for gait event identification on persons with dropped foot. *Gait & Posture,* 27 (2)**,** 248-257.

Lauer, R. T., Smith, B. T. and Betz, R. R. (2005) Application of a neuro-fuzzy network for gait event detection using electromyography in the child with cerebral palsy. *IEEE Transactions on Biomedical Engineering,* 52 (9)**,** 1532-1540.

Liberson, W. T., Holmquest, H. J., Scott, D. and Dow, M. (1961) Functional electrotheraphy, stimulation of the peroneal nerve synchronized with the swing phase of hemiplegic subjects. *Arch Phys Med Rehabil,* 42**,** 101-105.

Lu, T.-W. and O'Connor, J. J. (1999) Bone position estimation from skin marker co-ordinates using global optimisation with joint constrains. *Journal of Biomechanics,* 32**,** 129-134.

Luinge, H. J. and Veltink, P. H. (2005) Measuring orientation of human body segments using miniature gyroscopes and accelerometers. *Medical & Biological Engineering & Computing,* 43 (2)**,** 273-282.

Mansfield, A. and Lyons, G. M. (2003) The use of accelerometry to detect heel contact events for use as a sensor in FES assisted walking. *Medical Engineering & Physics,* 25 (10)**,** 879-885.

Matsunaga, T., Misawa, A., Sato, M., Chida, S., Hatakeyama, K., Shimada, Y., Shirahata, T., Takeshima, M., Iwami, T. and Iizuka, K. (2007) FES assisted swing-through gait using accelerometer and neural network IN:12th Annual Conference of the International FES Society Philadelphia, PA USA.

Mayagoitia, R. E., Nene, A. V. and Veltink, P. H. (2002) Accelerometer and rate gyroscope measurement of kinematics: an inexpensive alternative to optical motion analysis systems. *Journal of Biomechanics,* 35 (4)**,** 537-542.

Mayagoitia, R. E., Nene, A. V. and Veltink, P. H. (2002) Accelerometer and rate gyroscope measurement of kinematics: an inexpensive alternative to optical motion analysis systems. *Journal of Biomechanics,* 35 (4)**,** 537-542.

McCormick, A, Fleming, D, Charlton, J. Morbidity statistics from general practice: fourth national study 1991-1992: a study carried out by the Royal College of General Practitioners, Office of Population Censuses and Surveys, and the Department of Health. London: HMSO; 1995.

Mickelborough, J., van der Linden, M. L., Tallis, R. C. and Ennos, A. R. (2004) Muscle activity during gait initiation in normal elderly people. *Gait & Posture,* 19 (1)**,** 50-57.

Miyaoka, S., Hirano, H., Ashida, I., Miyaoka, Y. and Yamada, Y. (2005) Analysis of head movements coupled with trunk drift in healthy subjects. *Medical & Biological Engineering & Computing,* 43 (3)**,** 395-402.

Moe-Nilssen, R. (1998) A new method for evaluating motor control in gait under real-life environmental conditions. Part 1: The instrument. *Clinical Biomechanics,* 13 (4-5)**,** 320-327.

Monaghan, C. C., van Riel, W. and Veltink, P. H. (2009) Control of triceps surae stimulation based on shank orientation using a uniaxial gyroscope during gait. *Medical & Biological Engineering & Computing,* 47 (11)**,** 1181-1188.

Monaghan, C. C., Veltink, P. H., Bultstra, G., Droog, E., Kotiadis, D. and van Riel, W. (2004) Control of Triceps Surae Stimulation based on shank orientation using a uniaxial gyroscope IN:9th Annual Conference of the International FES Society Bournemouth, UK.

Montero-Odasso, M., Muir, S. W., Hall, M., Doherty, T. J., Kloseck, M., Beauchet, O. and Speechley, M. (2011) Gait Variability Is Associated With Frailty in Community-dwelling Older Adults. *The Journals of Gerontology Series A: Biological Sciences and Medical Sciences,* 66A (5)**,** 568-576.

Mulder, A., Boom, H., Hermens, H. and Zilvold, G. (1990) Artificial-reflex stimulation for FES-induced standing with minimum quadriceps force. *Medical and Biological Engineering and Computing,* 28**,** 483-488.

Murata (2011) *ADXL203: Piezoelectric Vibrating Gyroscope (Gyrostart®).* Available from: http://www.murata.com/products/catalog/pdf/s42e.pdf [Accessed 26 February 2011]

National Institute for Health Research (1996) *Stroke Case Study.* Available from: http://www.hta.ac.uk/publicationspdfs/casestudies/strokecasestudy_lv.pdf [Accessed 25 February 2011]

Neurodan A/S (2008) *Neurodan.* Available from: http://neurodan.dk/actigait.asp [Accessed 15 July 2008]

Neurological Alliance. (2003) *Neuro Numbers.* Available from: http://www .neural. org.uk/store/assets/files/20/original/NeuroNumbers.pdf [Accessed 8 January 2010]

Newsom-Davis, J. (2010) *paralysis.* Available from: http://www.answers.com/topic/ paralysis [Accessed 1 February 2010]

Odstock Medical Limited (2008) *Odstock Medical.* Available from: http: //www. odstockmedical.com/ [Accessed 15 July 2008]

O'Halloran, T., Haugland, M., Lyons, G. M. and Sinkjaer, T. (2004) An investigation of the effect of modifying stimulation profile shape on the loading response phase of gait, during FES-corrected drop foot: Stimulation profile and loading response. *Neuromodulation,* 7 (2)**,** 113-125.

Pappas, I. P. I., Keller, T., Mangold, S., Popovic, M. R., Dietz, V. and Morari, M. (2004) A reliable gyroscope-based gait-phase detection sensor embedded in a shoe insole. *IEEE Sensors Journal,* 4 (2)**,** 268-274.

Pappas, I. P. I., Popovic, M. R., Keller, T., Dietz, V. and Morari, M. (2001) A reliable gait phase detection system. *IEEE Transactions on Neural Systems and Rehabilitation Engineering,* 9 (2)**,** 113-125.

Park, S., Son, J., Kang, S. and Kim, Y. (2007) A FES sensor system using a tilt sensor for improving gait. IN:International Conference on Advanced Nondestructive Evaluation II. Busan, Korea. pg 151-156

Patrick, E. C., Hpward, J. C., Michael, R. N. and Hambrecht, F. T. (1986) Sensors for Use with Functional Neuromuscular Stimulation. *Biomedical Engineering, IEEE Transactions on,* BME-33 (2)**,** 256-268.

Perry, J. (1992) Gait analysis normal and pathological function. Thorofare, N.J.: SLACK.

Persian Poet Gal (2006) *Diagram of the Human Nervous System.* Available from: http://upload.wikimedia.org/wikipedia/commons/b/ba/Nervous_system_diagram.png [Accessed 21 May 2010]

Robbins, S. M., Houghton, P. E., Woodbury, M. G. and Brown, J. L. (2006) The Therapeutic Effect of Functional and Transcutaneous Electric Stimulation on Improving Gait Speed in Stroke Patients: A Meta-Analysis. *Archives of Physical Medicine and Rehabilitation,* 87 (6)**,** 853-859.

Ru"zi"c, A. (1996) *Biocybernetic Laboratory.* Available from: http://www.ijs.si/~ruzic/e1/bio.html [Accessed 15 July 2008]

Sawcer, S., Goodfellow, P. N. and Compston, A. (1997) The genetic analysis of multiple sclerosis. *Trends in Genetics,* 13 (6)**,** 234-239.

Shimada, Y., Ando, S. and Chida, S. (2000) Functional electrical stimulation. *Artificial Life and Robotics,* 4 (4)**,** 212-219.

Shimada, Y., Ando, S., Matsunaga, T., Misawa, A., Aizawa, T., Shirahata, T. and Itoi, E. (2005) Clinical Application of Acceleration Sensor to Detect the Swing Phase of Stroke Gait in Functional Electrical Stimulation. *The Tohoku Journal of Experimental Medicine,* 207 (3)**,** 197-202.

Sigmedics, Inc. (2000) *Rehabilitation technology for the neurologically impaired.* Available from: http://www.sigmedics.com/index.htm [Accessed 15 July 2008]

Simcox, S., Parker, S., Davis, G. M., Smith, R. W. and Middleton, J. W. (2005) Performance of orientation sensors for use with a functional electrical stimulation mobility system. *Journal of Biomechanics,* 38 (5)**,** 1185-1190.

Skelly, M. M. and Chizeck, H. J. (2001) Real-time gait event detection for paraplegic FES walking. *IEEE Transactions on Rehabilitation Engineering, ,* 9 (1)**,** 59-68.

Smith, B. T., Coiro, D. J., Finson, R., Betz, R. R. and McCarthy, J. (2002) Evaluation of force-sensing resistors for gait event detection to trigger electrical stimulation to improve walking in the child with cerebral palsy. *IEEE Transactions on Neural Systems and Rehabilitation Engineering,* 10 (1)**,** 22-29.

Smith, L. N. (2006) Setting the agenda for neurological nursing: strategic directions. *International Journal of Nursing Studies,* 43 (8)**,** 1063-1072.

Sousa, D., Tavares, J., Correia, M., Mendes, E., Veloso, A., Silva, V. and João, F. (2007a) Registration Between Data from Visual Sensors and Force Platform in Gait Event Detection IN:3rd International Symposium on Measurement, Analysis, and Modeling of Human Functions 2007 (ISHF 2007) Lisbon, Portugal.

Sousa, D., Tavares, J., Correia, M., Mendes, E., Veloso, A., Silva, V. and João, F. (2007b) Selecting Biomechanical Variables for Detects Gait Events using Computational Vision IN:III International Congress on Computational Bioengineering Isla de Margarita, Venezuela.

STMicroelectronics (2007) *MEMS inertial sensor: 2-axis-+/-2g/+/-6g linear accelerometer.* Available from: http://www.st.com/stonline/books/ pdf/docs/10219.pdf [Accessed 26 April 2007]

Sunnerhagen, K. S., Svantesson, U., Lönn, L., Krotkiewski, M. and Grimby, G. (1999) Upper motor neuron lesions: Their effect on muscle performance and appearance in stroke patients with minor motor impairment. *Archives of Physical Medicine and Rehabilitation,* 80 (2)**,** 155-161.

Swain, I. D., Burridge, J. H., Johnson, C. A., Mann, G. E., Taylor, P. N. and Wright, P. A. (2000) The efficacy of Functional Electrical Stimulation in improving walking ability for people with Multiple Sclerosis IN:5th Annual International FES Society Conference Aalborg, Denmark.

Swain, I. D., Mann, G. E., Taylor, P. N., Wood, D. E. and Wright, P. A. (2003) Clinical use of FES to improve walking in people with Multiple Sclerosis IN:8th Annual International FES Society Conference Queensland, Australia.

Taylor, P. N. (2004a) The Odstock Two Channel Stimulator O2CHS II Clinician Instruction Manual. Salisbury: STOCK.

Taylor, P. N. (2004b) The Odstock Dropped Foot Stimulator ODFS III Clinician Manual Salisbury: STOCK.

Taylor, P. N. (2005) ODFS III V6.22., Salisbury Health Care NHS Trust.

Taylor, P. N. (2011) Potential Users of the Odstock Drop Foot Stimulator (ODFS). Salisbury.

Tong, K. Y. and Granat, M. H. (1999) A practical gait analysis system using gyroscopes. *Medical Engineering & Physics,* 21 (2)**,** 87-94.

University of Texas (2002) *Plug-in-Gait Marker Placement.* Available from: http://www3.uta.edu/faculty/ricard/Grad%20Biomech/Vicon%20Manuals/Plug-in-Gait%20Marker%20Placement%20&%20Force%20-%20Torque%20Directions.pdf [Accessed 10 June 2010]

Veltink, P. H., Franken, H. M., Verboon, A. W. and Boom, H. B. K. (1993) Detection of knee instability using accelerometers tfs and potential use in the control of FES-assisted paraplegic standing IN:Proceedings of the 15th Annual International Conference of the IEEE 1232-1233.

Vicon^{TM} (2010) *Plug In Gait Model Details.* Available from: http://www.irc-web.co.jp/vicon_web/news_bn/PIGManualver1.pdf [Accessed 10 June 2010]

Whittle, M. (2007) *Gait analysis : an introduction 4th ed.* Oxford: Butterworth-Heinemann.

Wilkinson, I. A. and Taylor, P. N. (2004) Retrospective study of patients using Funcional Electrical Stimulation for drop foot correction and increased hip stability. IN:9th Annual Conference of International FES Society. Bournemouth, UK. 305-307.

Willemsen, A. T. M., Bloemhof, F. and Boom, H. B. K. (1990a) Automatic stance-swing phase detection from accelerometer data for peroneal nerve-stimulation. *IEEE Transactions on Biomedical Engineering,* 37 (12)**,** 1201-1208.

Willemsen, A. T. M., Vanalste, J. A. and Boom, H. B. K. (1990b) Real-time gait assessment utilizing a new way of accelerometry. *Journal of Biomechanics,* 23 (8)**,** 859-863.

Williamson, R. and Andrews, B. J. (2000a) Sensor systems for lower limb functional electrical stimulation (FES) control. *Medical Engineering & Physics,* 22 (5)**,** 313-325.

Williamson, R. and Andrews, B. J. (2000b) Gait event detection for FES using accelerometers and supervised machine learning. *IEEE Transactions on Rehabilitation Engineering,,* 8 (3)**,** 312-319.

Williamson, R. and Andrews, B. J. (2001) Detecting absolute human knee angle and angular velocity using accelerometers and rate gyroscopes. *Medical & Biological Engineering & Computing,* 39 (3)**,** 294-302.

Winter, B. and Pattani, H. (2008) Spinal cord injury. *Anaesthesia & Intensive Care Medicine,* 9 (9)**,** 401-403.

Winter, D. A. and Yack, H. J. (1987) EMG profiles during normal human walking: stride-to-stride and inter-subject variability. *Electroencephalography and Clinical Neurophysiology,* 67 (5)**,** 402-411.

World Health Organization. (2010) *Neurological disorders affect millions globally: WHO report.* Available from: http://www.who.int/mediacentre /news /releases /2007/pr04/en/index.html [Accessed 4 January 2010]

Wright, P. A., Burridge, J. H., Ewins, D. J., Mann, G. E., McLellan, D. L., Swain, I. D., Taylor, P. N. and Wood, D. E. (1999) The Compustim 10B in stroke: control algorithms and patient selection criteria. IN:4th Annual Conference of International FES Society. Sendai, Japan.

Zijlstra, W. and Hof, A. L. (2003) Assessment of spatio-temporal gait parameters from trunk accelerations during human walking. *Gait & Posture,* 18 (2)**,** 1-10.

.

Appendix A

A.1 Earth horizontal plane.

The segment angle measured by the sensor unit (Chapter 4) is calculated with respect to the earth horizontal plane. Figure A-1 shows the examples of the earth horizontal plane at point A,B and C. These planes are orthoganal to the plane that originated from point O (center of the earth).

Figure A-1 The examples of the earth horizontal planes (red line) at point A, B and C. The earth image is adapted from (Earth Day Colouring Book (1998)).

Appendix B

Example 1, 2, 3, 4 and 5 show the equations to solve for θ. Example 1 uses four sensors output while example 2,3,4 and 5 use only three sensors output. No solution has been obtained when using only three sensors output, equation B-31, B-42, B-63 and B-74. When B-31 is substituted into equation B-15, this will give a division by zero. Also, there is another division by zero when B-42 is substituted into B-20. Therefore, no solution for any of the examples.

Example 1

Using four sensors output: s_1, s_2, r_1, r_2

$$s_1 = \ddot{x}\cos\theta - \ddot{y}\sin\theta - g\sin\theta \quad \text{(B-1)}$$

$$s_2 = -\ddot{x}\sin\theta - \ddot{y}\cos\theta - g\cos\theta \quad \text{(B-2)}$$

$$r_1 = \ddot{x}\cos\theta_2 - \ddot{y}\sin\theta_2 - g\sin\theta_2 \quad \text{(B-3)}$$

$$r_2 = -\ddot{x}\sin\theta_2 - \ddot{y}\cos\theta_2 - g\cos\theta_2 \quad \text{(B-4)}$$

Multiply (B-1) with cosθ

$$s_1\cos\theta = \ddot{x}\cos^2\theta - \ddot{y}\sin\theta\cos\theta - g\sin\theta\cos\theta \quad \text{(B-5)}$$

Multiply (B-2) with sinθ

$$s_2\sin\theta = -\ddot{x}\sin^2\theta - \ddot{y}\sin\theta\cos\theta - g\sin\theta\cos\theta \quad \text{(B-6)}$$

Subtracting (B-6) from (B-5),

$$s_1 \cos\theta - s_2 \sin\theta = \ddot{x} \tag{B-7}$$

Multiply (B-1) with sinθ

$$s_1 \sin\theta = \ddot{x}\sin\theta\cos\theta - \ddot{y}\sin^2\theta - g\sin^2\theta \tag{B-8}$$

Multiply (B-2) with cosθ

$$s_2 \cos\theta = -\ddot{x}\sin\theta\cos\theta - \ddot{y}\cos^2\theta - g\cos^2\theta \tag{B-9}$$

Adding (B-8) with (B-9),

$$s_1 \sin\theta + s_2 \cos\theta = -\ddot{y} - g \tag{B-10}$$

Expand (B-3) and multiply with sinθ,

$$r_1 \sin\theta = \ddot{x}\left(\sin\theta\cos\theta\cos\alpha - \sin^2\theta\sin\alpha\right) - \left(\ddot{y} + g\right)\left(\sin^2\theta\cos\alpha + \sin\theta\cos\theta\sin\alpha\right) \tag{B-11}$$

Expand (B-4) and multiply with cosθ,

$$r_2 \cos\theta = -\ddot{x}\left(\sin\theta\cos\theta\cos\alpha + \cos^2\theta\sin\alpha\right) - \left(\ddot{y} + g\right)\left(\cos^2\theta\cos\alpha - \sin\theta\cos\theta\sin\alpha\right) \tag{B-12}$$

Adding (B-11) and (B-12),

$$r_1 \sin\theta + r_2 \cos\theta = -\ddot{x}\sin\alpha - \left(\ddot{y} + g\right)\cos\alpha \tag{B-13}$$

Substitute (B-7) and (B-10) into (B-13),

$$r_1 \sin\theta + r_2 \cos\theta = -\left(s_1 \cos\theta - s_2 \sin\theta\right)\sin\alpha + \left(s_1 \sin\theta + s_2 \cos\theta\right)\cos\alpha \tag{B-14}$$

Solving for θ,

$$\theta = \tan^{-1}\left(\frac{-r_2 + s_2\cos\alpha - s_1\sin\alpha}{r_1 - s_1\cos\alpha - s_2\sin\alpha}\right) \tag{B-15}$$

Expand (B-3) and multiply with cosθ,

$$r_1 \cos\theta = \ddot{x}\left(\cos^2\theta\cos\alpha - \sin\theta\cos\theta\sin\alpha\right) - \left(\ddot{y} + g\right)\left(\sin\theta\cos\theta\cos\alpha + \cos^2\theta\sin\alpha\right) \tag{B-16}$$

Expand (B-4) and multiply with sinθ,

$$r_2 \sin\theta = -\ddot{x}\left(\sin^2\theta\cos\alpha + \sin\theta\cos\theta\sin\alpha\right) - \left(\ddot{y} + g\right)\left(\sin\theta\cos\theta\cos\alpha - \sin^2\theta\sin\alpha\right) \tag{B-17}$$

Subtract (B-17) from (B-16),

$$r_1 \cos\theta - r_2 \sin\theta = \ddot{x}\cos\alpha - (\ddot{y} + g)\sin\alpha \tag{B-18}$$

Substitute (B-7) and (B-10) into (B-18),

$$r_1 \cos\theta - r_2 \sin\theta = (s_1 \cos\theta - s_2 \sin\theta)\cos\alpha + (s_1 \sin\theta + s_2 \cos\theta)\sin\alpha \tag{B-19}$$

Solving for θ,

$$\theta = \tan^{-1}\left(\frac{-r_1 + s_1\cos\alpha + s_2\sin\alpha}{-r_2 + s_2\cos\alpha - s_1\sin\alpha}\right) \tag{B-20}$$

Example 2 :

Using three sensors output: s_1, s_2, r_1

$$s_1 = \ddot{x}\cos\theta - \ddot{y}\sin\theta - g\sin\theta \tag{B-21}$$

$$s_2 = -\ddot{x}\sin\theta - \ddot{y}\cos\theta - g\cos\theta \tag{B-22}$$

$$r_1 = \ddot{x}\cos\theta_2 - \ddot{y}\sin\theta_2 - g\sin\theta_2 \tag{B-23}$$

By multiplying Equation (B-21) with $\cos\theta$ and Equation (B-22) with $\sin\theta$, s_1 and s_2 can be written as,

$$s_1 \cos\theta = \ddot{x}\cos^2\theta - \ddot{y}\sin\theta\cos\theta - g\sin\theta\cos\theta \tag{B-24}$$

and

$$s_2 \sin\theta = -\ddot{x}\sin^2\theta - \ddot{y}\sin\theta\cos\theta - g\sin\theta\cos\theta \tag{B-25}$$

By subtracting Equation (B-25) from Equation (B-24), the $\ddot{x}$ is given by,

$$\ddot{x} = s_1\cos\theta - s_2\sin\theta \tag{B-26}$$

By multiplying Equation (B-21) with $\sin\theta$ and Equation (B-22) with $\cos\theta$, s_1 and s_2 can be written as,

$$s_1 \sin\theta = \ddot{x}\sin\theta\cos\theta - \ddot{y}\sin^2\theta - g\sin^2\theta \tag{B-27}$$

and

$$s_2 \cos\theta = -\ddot{x}\sin\theta\cos\theta - \ddot{y}\cos^2\theta - g\cos^2\theta \tag{B-28}$$

By adding Equation (B-27) and Equation (B-28), $\ddot{y}$ is given by,

$$\ddot{y} = -s_1 \sin\theta - s_2 \cos\theta - g \qquad \text{(B-29)}$$

Substituting (B-26) and (B-29) into (B-23),

$$r_1 = \left(s_1 \cos\theta - s \ \sin\theta\right)\cos\theta_2 - \left(-s_1 \sin\theta - s_2 \cos\theta - g\right)\sin\theta_2 - g\sin\theta_2$$

with $\theta_2 = \theta + \alpha$ (B-30)

Expand (B-30),

$$\boxed{r_1 = s_1 \cos\alpha + s_2 \sin\alpha} \qquad \text{(B-31)}$$

Example 3 :

Using three sensors output: s_1, s_2, r_2

$$s_1 = \ddot{x}\cos\theta - \ddot{y}\sin\theta - g\sin\theta \qquad \text{(B-32)}$$

$$s_2 = -\ddot{x}\sin\theta - \ddot{y}\cos\theta - g\cos\theta \qquad \text{(B-33)}$$

$$r_2 = -\ddot{x}\sin\theta_2 - \ddot{y}\cos\theta_2 - g\cos\theta_2 \qquad \text{(B-34)}$$

By mutiplying Equation (B-32) with $\cos\theta$ and Equation (B-33) with $\sin\theta$, s_1 and s_2 can be written as,

$$s_1 \cos\theta = \ddot{x}\cos^2\theta - \ddot{y}\sin\theta\cos\theta - g\sin\theta\cos\theta \qquad \text{(B-35)}$$

and

$$s_2 \sin\theta = -\ddot{x}\sin^2\theta - \ddot{y}\sin\theta\cos\theta - g\sin\theta\cos\theta \qquad \text{(B-36)}$$

By subtracting Equation (B-36) from Equation (B-35), the $\ddot{x}$ is given by,

$$\ddot{x} = s_1 \cos\theta - s_2 \sin\theta \qquad \text{(B-37)}$$

By multiplying Equation (B-32) with $\sin\theta$ and Equation (B-33) with $\cos\theta$, s_1 and s_2 can be written as,

$$s_1 \sin\theta = \ddot{x}\sin\theta\cos\theta - \ddot{y}\sin^2\theta - g\sin^2\theta \qquad \text{(B-38)}$$

and

$$s_2 \cos\theta = -\ddot{x}\sin\theta\cos\theta - \ddot{y}\cos^2\theta - g\cos^2\theta \quad \text{(B-39)}$$

By adding Equation (B-38) and Equation (B-39), $\ddot{y}$ is given by,

$$\ddot{y} = -s_1 \sin\theta - s_2 \cos\theta - g \quad \text{(B-40)}$$

Substituting (B-37) and (B-40) into (B-34),

$$r_2 = -(s_1 \cos\theta - s_2 \sin\theta)\sin\theta_2 - (-s_1 \sin\theta - s_2 \cos\theta - g)\cos\theta_2 - g\cos\theta_2$$

with $\theta_2 = \theta + \alpha$ (B-41)

Expand (B-41),

$$\boxed{r_2 = -s_1 \sin\alpha + s_2 \cos\alpha} \quad \text{(B-42)}$$

Example 4 :

Using three sensors output: s_2, r_1, r_2

$$s_2 = -\ddot{x}\sin\theta - \ddot{y}\cos\theta - g\cos\theta \quad \text{(B-43)}$$

$$r_1 = \ddot{x}\cos\theta_2 - \ddot{y}\sin\theta_2 - g\sin\theta_2 \quad \text{(B-44)}$$

$$r_2 = -\ddot{x}\sin\theta_2 - \ddot{y}\cos\theta_2 - g\cos\theta_2 \quad \text{(B-45)}$$

Now by multiplying Equation (B-44) with $\cos\theta_2$ and Equation (B-45) with $\sin\theta_2$, then multiplying Equation (B-44) with $\sin\theta_2$ and Equation (B-45) with $\cos\theta_2$, r_1 and r_2 can be written as,

$$r_1 \cos\theta_2 = \ddot{x}\cos^2\theta_2 - \ddot{y}\sin\theta_2\cos\theta_2 - g\sin\theta_2\cos\theta_2 \quad \text{(B-46)}$$

and

$$r_2 \sin\theta_2 = -\ddot{x}\sin^2\theta_2 - \ddot{y}\sin\theta_2\cos\theta_2 - g\sin\theta_2\cos\theta_2 \quad \text{(B-47)}$$

$$r_1 \sin\theta_2 = \ddot{x}\sin\theta_2\cos\theta_2 - \ddot{y}\sin^2\theta_2 - g\sin^2\theta_2 \quad \text{(B-48)}$$

and

$$r_2 \cos\theta_2 = -\ddot{x}\sin\theta_2\cos\theta_2 - \ddot{y}\cos^2\theta_2 - g\cos^2\theta_2 \quad \text{(B-49)}$$

By subtracting Equation (B-47) from Equation (B-46), the $\ddot{x}$ is given by,

$$\ddot{x} = r_1 \cos\theta_2 - r_2 \sin\theta_2 \qquad \text{(B-50)}$$

By adding Equation (B-48) and Equation (B-49), $\ddot{y}$ is given by,

$$\ddot{y} = -r_1 \sin\theta_2 - r_2 \cos\theta_2 - g \qquad \text{(B-61)}$$

Substituting (B-50) and (B-61) into (B-43),

$$s_2 = -(r_1 \cos\theta_2 - r_2 \sin\theta_2)\sin\theta - (-r_1 \sin\theta_2 - r_2 \cos\theta_2 - g)\cos\theta - g\cos\theta \qquad \text{(B-62)}$$

with $\theta_2 = \theta + \alpha$

Expand (B-62),

$$\boxed{s_2 = r_1 \sin\alpha + r_2 \cos\alpha} \qquad \text{(B-63)}$$

Example 5 :

Using three sensors output: s_1, r_1, r_2

$$s_1 = \ddot{x}\cos\theta - \ddot{y}\sin\theta - g\sin\theta \qquad \text{(B-64)}$$

$$r_1 = \ddot{x}\cos\theta_2 - \ddot{y}\sin\theta_2 - g\sin\theta_2 \qquad \text{(B-65)}$$

$$r_2 = -\ddot{x}\sin\theta_2 - \ddot{y}\cos\theta_2 - g\cos\theta_2 \qquad \text{(B-66)}$$

Now by multiplying Equation (B-65) with $\cos\theta_2$ and Equation (B-66) with $\sin\theta_2$, then multiplying Equation (B-65) with $\sin\theta_2$ and Equation (B-66) with $\cos\theta_2$, r_1 and r_2 can be written as,

$$r_1 \cos\theta_2 = \ddot{x}\cos^2\theta_2 - \ddot{y}\sin\theta_2\cos\theta_2 - g\sin\theta_2\cos\theta_2 \qquad \text{(B-67)}$$

and

$$r_2 \sin\theta_2 = -\ddot{x}\sin^2\theta_2 - \ddot{y}\sin\theta_2\cos\theta_2 - g\sin\theta_2\cos\theta_2 \qquad \text{(B-68)}$$

$$r_1 \sin\theta_2 = \ddot{x}\sin\theta_2\cos\theta_2 - \ddot{y}\sin^2\theta_2 - g\sin^2\theta_2 \qquad \text{(B-69)}$$

and

$$r_2 \cos\theta_2 = -\ddot{x}\sin\theta_2 \cos\theta_2 - \ddot{y}\cos^2\theta_2 - g\cos^2\theta_2 \quad \text{(B-70)}$$

By subtracting Equation (B-68) from Equation (B-67), the $\ddot{x}$ is given by,

$$\ddot{x} = r_1 \cos\theta_2 - r_2 \sin\theta_2 \quad \text{(B-71)}$$

By adding Equation (B-69) and Equation (B-70), $\ddot{y}$ is given by,

$$\ddot{y} = -r_1 \sin\theta_2 - r_2 \cos\theta_2 - g \quad \text{(B-72)}$$

Substituting (B-71) and (B-72) into (B-64),

$$s_1 = \left(r_1 \cos\theta_2 - r_2 \sin\theta_2\right)\cos\theta - \left(-r_1 \sin\theta_2 - r_2 \cos\theta_2 - g\right)\sin\theta - g\sin\theta \quad \text{(B-73)}$$

with $\theta_2 = \theta + \alpha$

Expand (B-73),

$$\boxed{s_1 = r_1 \cos\alpha - r_2 \sin\alpha} \quad \text{(B-74)}$$

Appendix C

Three single axis accelerometers are arranged with 120 degrees between the axes. Matrix A represents the derivatives of the three equations from the sensors output. The determinant of matrix A has been computed to check that the equations are linearly dependent

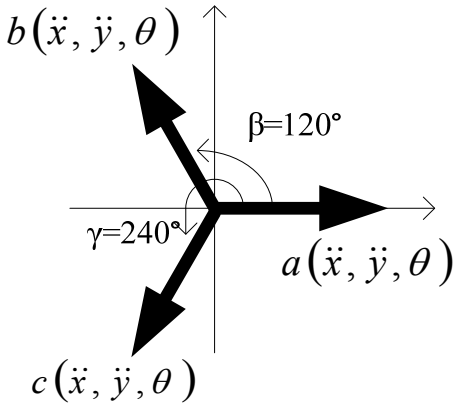

$$a = \ddot{x}\cos\theta + \ddot{y}\sin\theta + g\sin\theta \tag{C-1}$$

$$b = \ddot{x}\cos(\theta+\beta) + \ddot{y}\sin(\theta+\beta) + g\sin(\theta+\beta) \tag{C-2}$$

$$c = \ddot{x}\cos(\theta+\gamma) + \ddot{y}\sin(\theta+\gamma) + g\sin(\theta+\gamma) \tag{C-3}$$

Arrange in matrix 3x3,

$$A = \begin{vmatrix} \frac{\partial a}{\partial \ddot{x}} & \frac{\partial a}{\partial \ddot{y}} & \frac{\partial a}{\partial \theta} \\ \frac{\partial b}{\partial \ddot{x}} & \frac{\partial b}{\partial \ddot{y}} & \frac{\partial b}{\partial \theta} \\ \frac{\partial c}{\partial \ddot{x}} & \frac{\partial c}{\partial \ddot{y}} & \frac{\partial c}{\partial \theta} \end{vmatrix}$$

$$\det(A) = \frac{\partial a}{\partial \ddot{x}} \cdot \frac{\partial b}{\partial \ddot{y}} \cdot \frac{\partial c}{\partial \theta} + \frac{\partial a}{\partial \ddot{y}} \cdot \frac{\partial b}{\partial \theta} \cdot \frac{\partial c}{\partial \ddot{x}} + \frac{\partial a}{\partial \theta} \cdot \frac{\partial b}{\partial \ddot{x}} \cdot \frac{\partial c}{\partial \ddot{y}} - \frac{\partial a}{\partial \theta} \cdot \frac{\partial b}{\partial \ddot{y}} \cdot \frac{\partial c}{\partial \ddot{x}} - \frac{\partial a}{\partial \ddot{x}} \cdot \frac{\partial b}{\partial \theta} \cdot \frac{\partial c}{\partial \ddot{y}} - \frac{\partial a}{\partial \ddot{y}} \cdot \frac{\partial b}{\partial \ddot{x}} \cdot \frac{dc}{\partial \theta}$$

$$= \underbrace{\frac{\partial a}{\partial \ddot{x}}\left[\frac{\partial b}{\partial \ddot{y}} \cdot \frac{\partial c}{\partial \theta} - \frac{\partial b}{\partial \theta} \cdot \frac{\partial c}{\partial \ddot{y}}\right]}_{(C-4)} + \underbrace{\frac{\partial a}{\partial \ddot{y}}\left[\frac{\partial b}{\partial \theta} \cdot \frac{\partial c}{\partial \ddot{x}} - \frac{\partial b}{\partial \ddot{x}} \cdot \frac{dc}{\partial \theta}\right]}_{(C-5)} + \underbrace{\frac{\partial a}{\partial \theta}\left[\frac{\partial b}{\partial \ddot{x}} \cdot \frac{\partial c}{\partial \ddot{y}} - \frac{\partial b}{\partial \ddot{y}} \cdot \frac{\partial c}{\partial \ddot{x}}\right]}_{(C-6)}$$

Simplify (C-4),

$$\cos\theta\begin{bmatrix} -\ddot{x}\sin(\theta+\beta)\sin(\theta+\gamma) + (\ddot{y}+g)\sin(\theta+\beta)\cos(\theta+\gamma) \\ +\ddot{x}\sin(\theta+\beta)\sin(\theta+\gamma) - (\ddot{y}+g)\cos(\theta+\beta)\sin(\theta+\gamma) \end{bmatrix}$$

$$\Rightarrow -(\ddot{y}+g)\cos\theta\sin(\gamma-\beta) \qquad \text{(C-7)}$$

Simplify (C-5),

$$\sin\theta\begin{bmatrix} -\ddot{x}\sin(\theta+\beta)\cos(\theta+\gamma) + (\ddot{y}+g)\cos(\theta+\beta)\cos(\theta+\gamma) \\ +\ddot{x}\sin(\theta+\gamma)\cos(\theta+\beta) - (\ddot{y}+g)\cos(\theta+\beta)\cos(\theta+\gamma) \end{bmatrix}$$

$$\Rightarrow \ddot{x}\sin\theta\sin(\gamma-\beta) \qquad \text{(C-8)}$$

Simplify (C-6),

$$-\ddot{x}\sin\theta + (\ddot{y}+g)\cos\theta\left[\cos(\theta+\beta)\sin(\theta+\gamma) - \sin(\theta+\beta)\cos(\theta+\gamma)\right]$$

$$\Rightarrow -\ddot{x}\sin\theta\sin(\gamma-\beta) + (\ddot{y}+g)\cos\theta\sin(\gamma-\beta) \qquad \text{(C-9)}$$

Adding (C-7),(C-8) and (C-9),

$$-(\ddot{y}+g)\cos\theta\sin(\gamma-\beta) + \ddot{x}\sin\theta\sin(\gamma-\beta) + -\ddot{x}\sin\theta\sin(\gamma-\beta) + (\ddot{y}+g)\cos\theta\sin(\gamma-\beta)$$

$$= 0\,(\text{linearly dependent})$$

Appendix D

Figure D-1 Figure D-12 show the results of the dynamic acceleration from the sensor unit outputs.

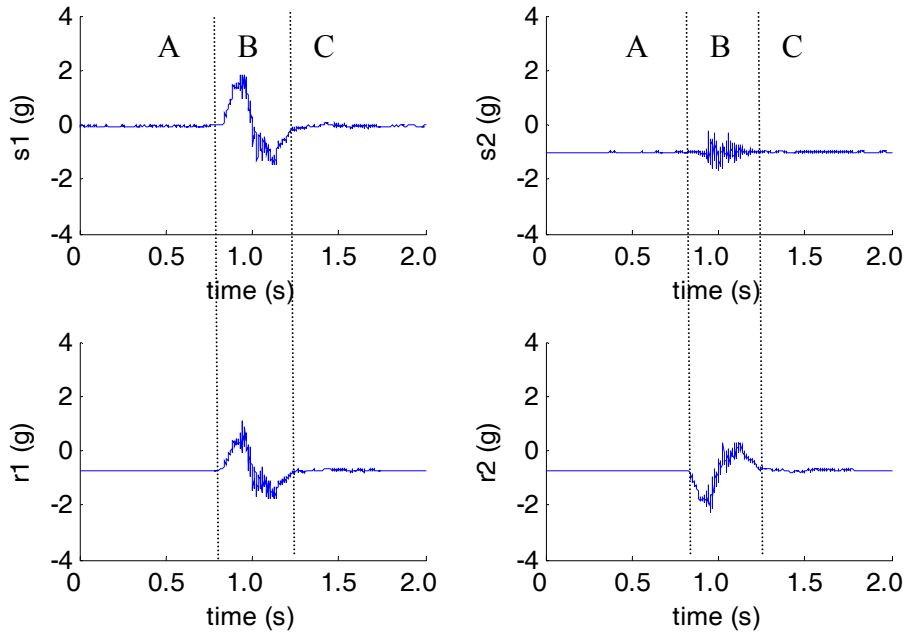

Figure D-1 The sensor unit outputs (s_1, s_2, r_1 and r_2) in unit of g at θ equals to 0 degree with movement to the left (-x). The means and standard deviations over the time in section B are -0.01g (±0.95), -1.00g (±0.18), -0.69g (±0.68) and -0.74g (±0.67) for s_1, s_2, r_1 and r_2 respectively.

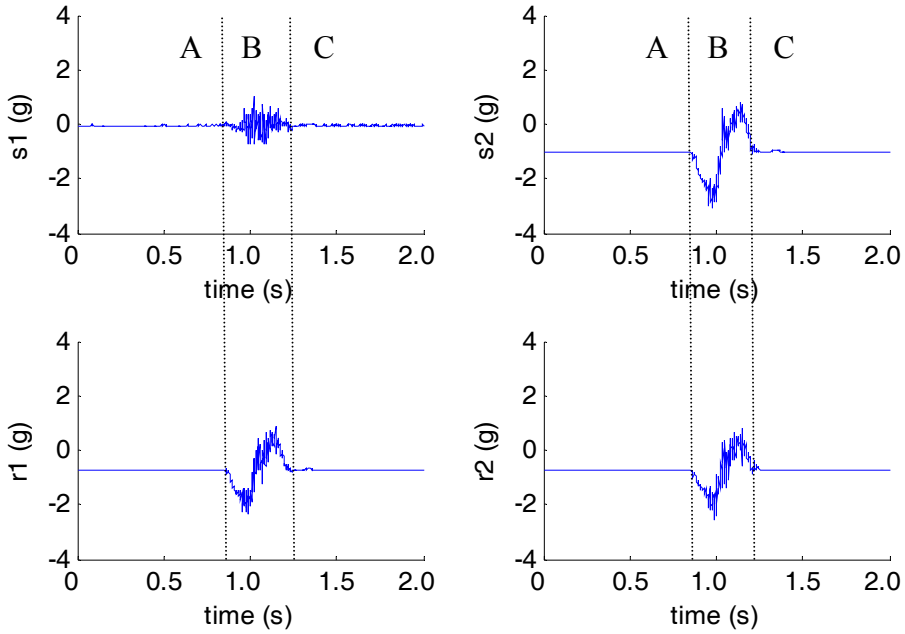

Figure D-2 The sensor unit outputs (s_1, s_2, r_1 and r_2) in unit of g at θ equals to 0 degree with movement to up (+y). The means and standard deviations over the time in section B are -0.04g (±0.24), -1.01g (±1.07), -0.72g (±0.79) and -0.74g (±0.78) for s_1, s_2, r_1 and r_2 respectively.

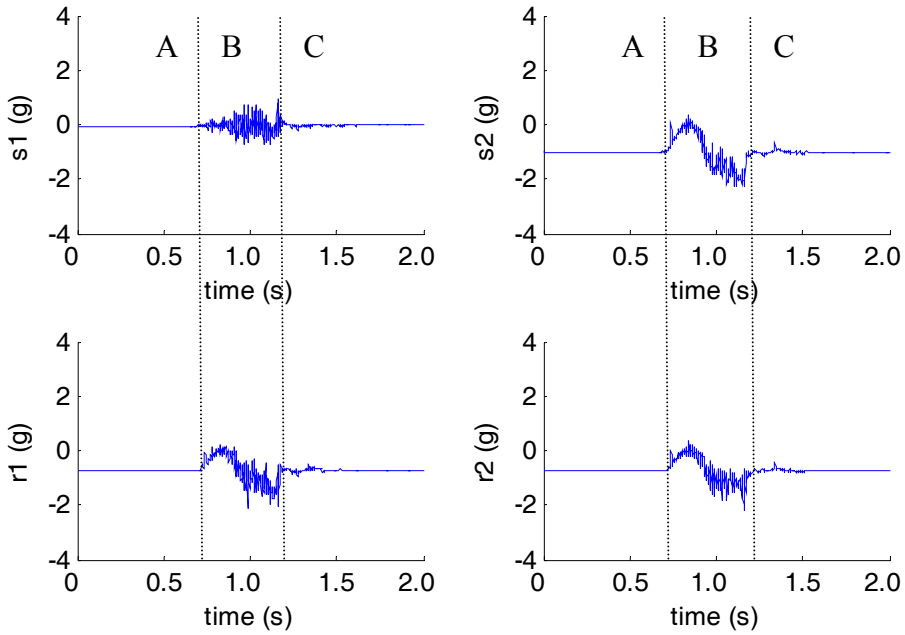

Figure D-3 The sensor unit outputs (s_1, s_2, r_1 and r_2) in unit of g at θ equals to 0 degree with movement to down (-y). The means and standard deviations over the time in section B are -0.04g (±0.24), -0.99g (±0.65), -0.71g (±0.49) and -0.71g (±0.49) for s_1, s_2, r_1 and r_2 respectively.

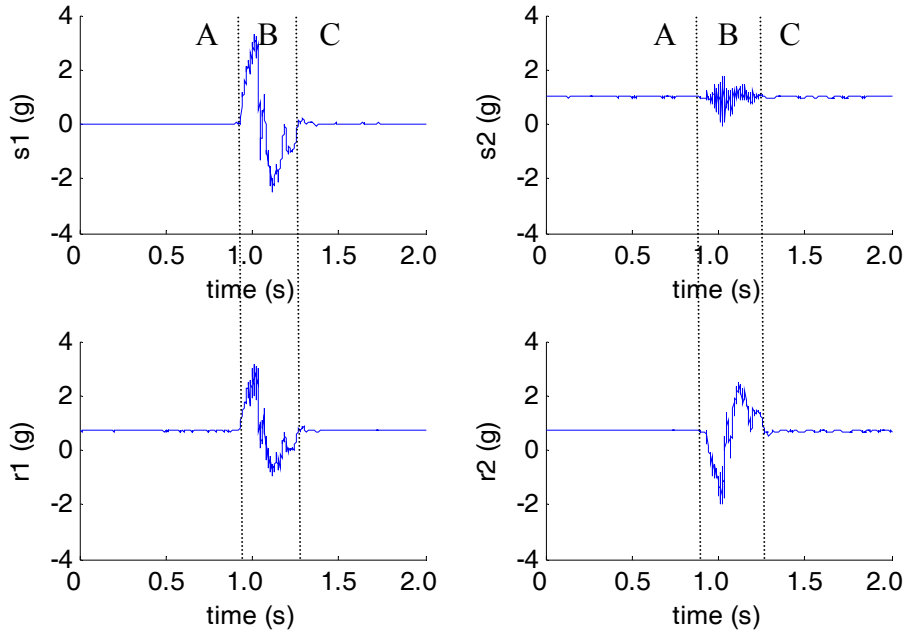

Figure D-4 The sensor unit outputs (s_1, s_2, r_1 and r_2) in unit of g at θ equals to 180 degrees with movement to the right (+x). The means and standard deviations over the time in section B are 0.02g (±1.37), 0.98g (±0.22), 0.71g (±0.94) and 0.70g (±0.98) for s_1, s_2, r_1 and r_2 respectively.

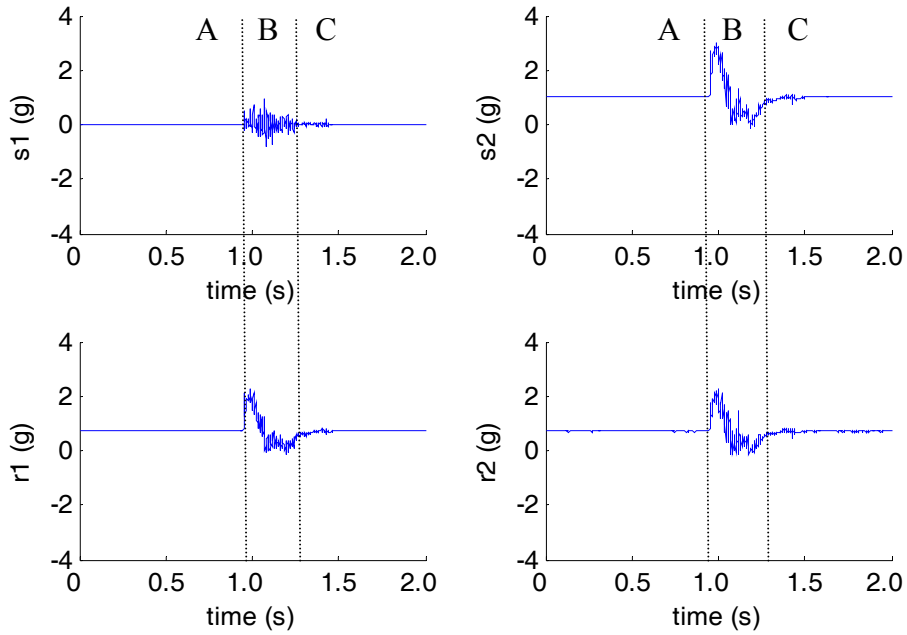

Figure D-5 The sensor unit outputs (s_1, s_2, r_1 and r_2) in unit of g at θ equals to 180 degrees with movement to up (+y). The means and standard deviations over the time in section B are 0.02g (±0.16), 1.00g (±0.63), 0.71g (±0.46) and 0.71g (±0.46) for s_1, s_2, r_1 and r_2 respectively.

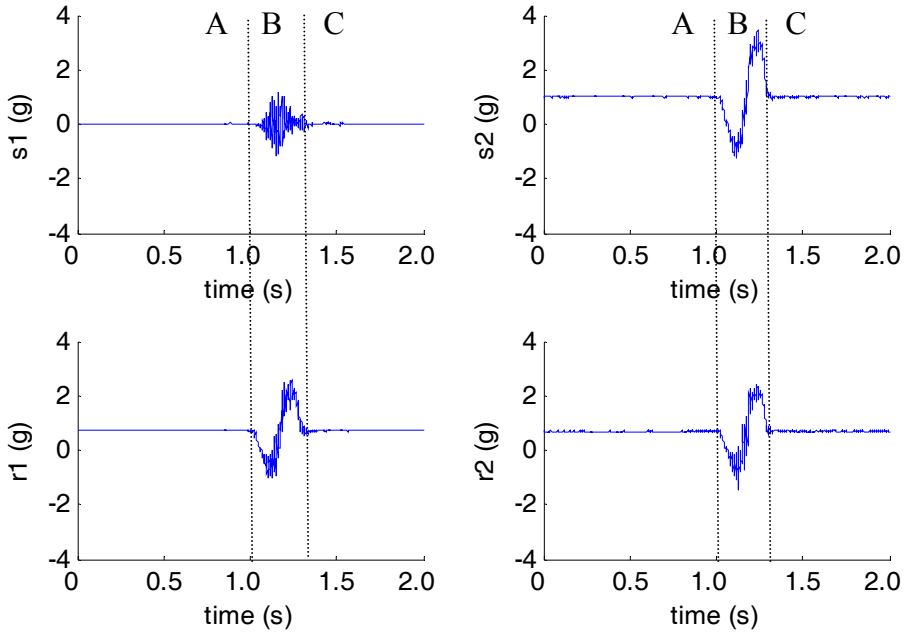

Figure D-6 The sensor unit outputs (s_1, s_2, r_1 and r_2) in unit of g at θ equals to 180 degrees with movement to down (-y). The means and standard deviations over the time in section B are 0.02g (±0.32), 0.99g (±1.33), 0.71g (±0.99) and 0.69g (±0.96) for s_1, s_2, r_1 and r_2 respectively.

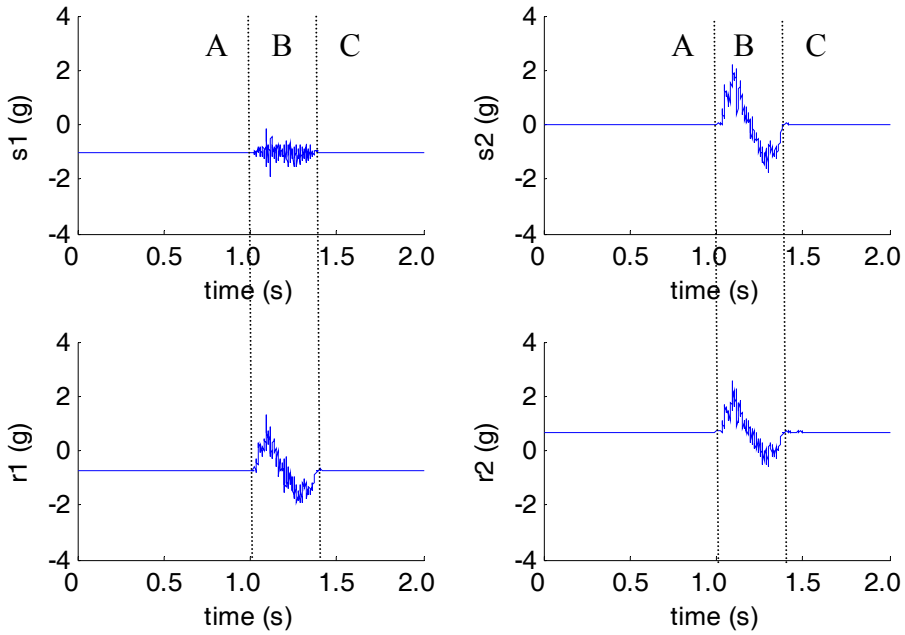

Figure D-7 The sensor unit outputs (s_1, s_2, r_1 and r_2) in unit of g at θ equals to 90 degrees with movement to the right (+x). The means and standard deviations over the time in section B are -1.02g (±0.18), 0.01g (±0.94), -0.72g (±0.67) and 0.70g (±0.68) for s_1, s_2, r_1 and r_2 respectively.

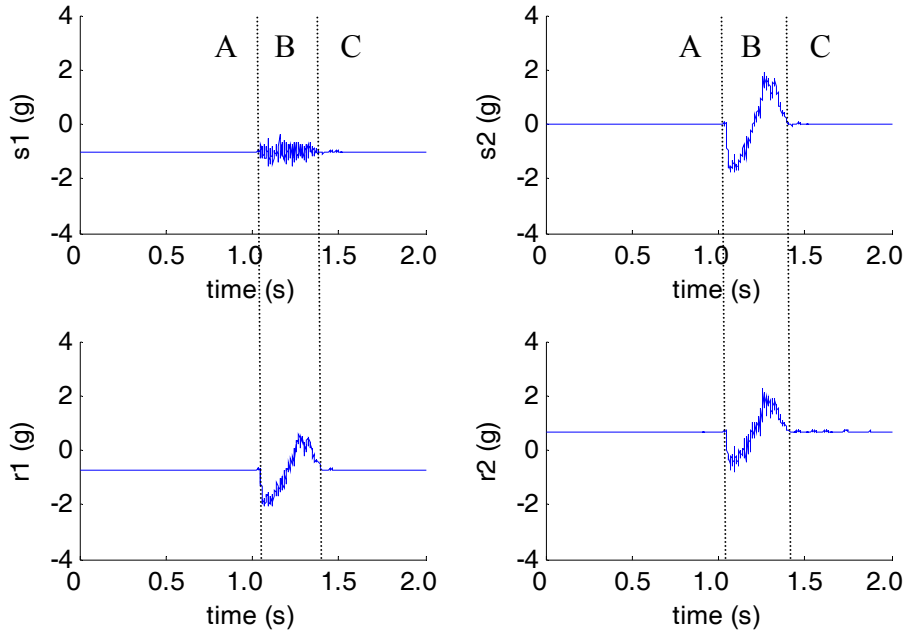

Figure D-8 The sensor unit outputs (s_1, s_2, r_1 and r_2) in unit of g at θ equals to 90 degrees with movement to the left (-x). The means and standard deviations over the time in section B are -1.02g (±0.17), 0.01g (±1.05), -0.72g (±0.75) and 0.69g (±0.75) for s_1, s_2, r_1 and r_2 respectively.

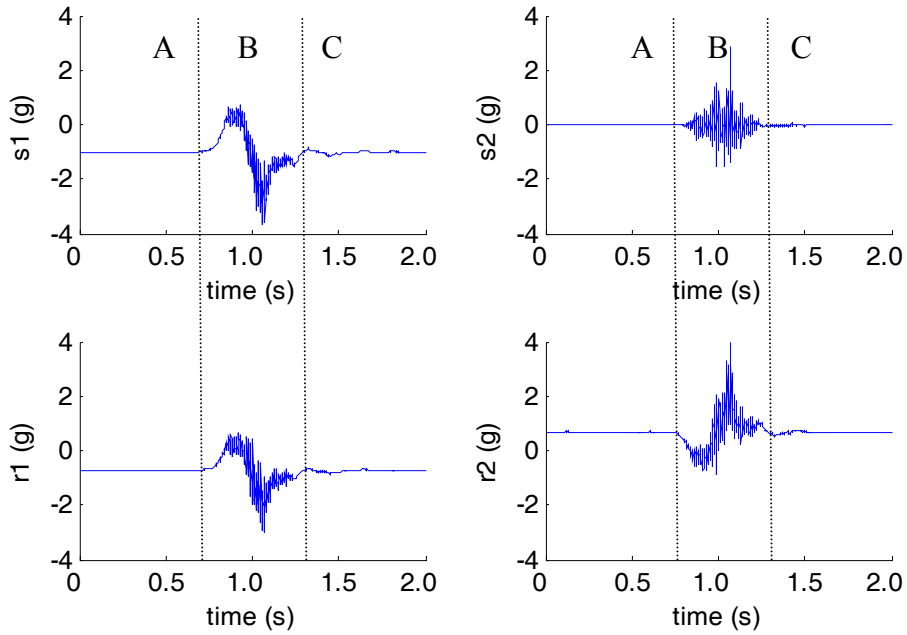

Figure D-9 The sensor unit outputs (s_1, s_2, r_1 and r_2) in unit of g at θ equals to 90 degrees with movement to down (-y). The means and standard deviations over the time in section B are -1.02g (±0.90), -0.01g (±0.39), -0.73g (±0.73) and 0.67g (±0.70) for s_1, s_2, r_1 and r_2 respectively.

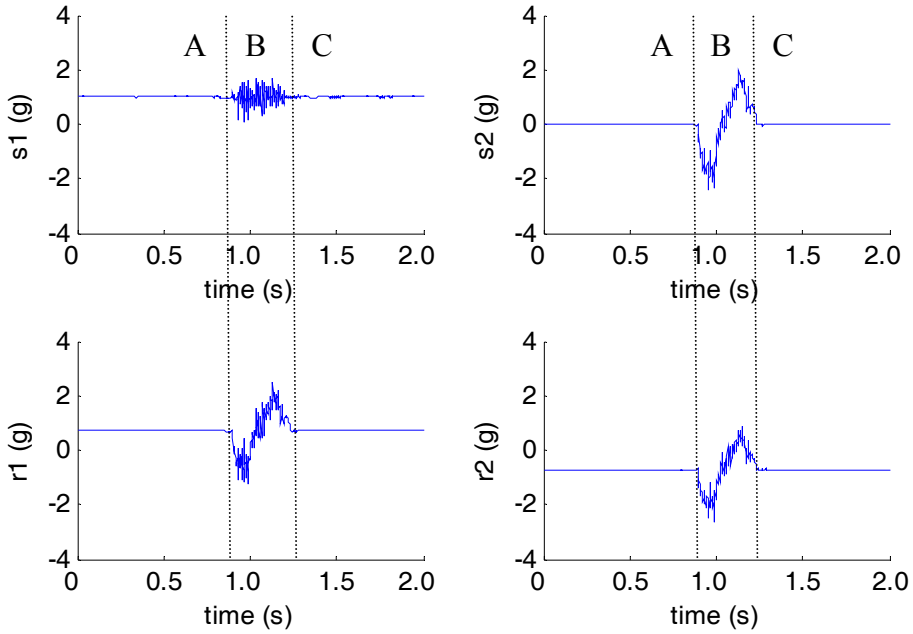

Figure D-10 The sensor unit outputs (s_1, s_2, r_1 and r_2) in unit of g at θ equals to 270 degrees with movement to the right (+x). The means and standard deviations over the time in section B are 1.00g (±0.25), -0.05g (±1.18), 0.70g (±0.88) and -0.73g (±0.85) for s_1, s_2, r_1 and r_2 respectively.

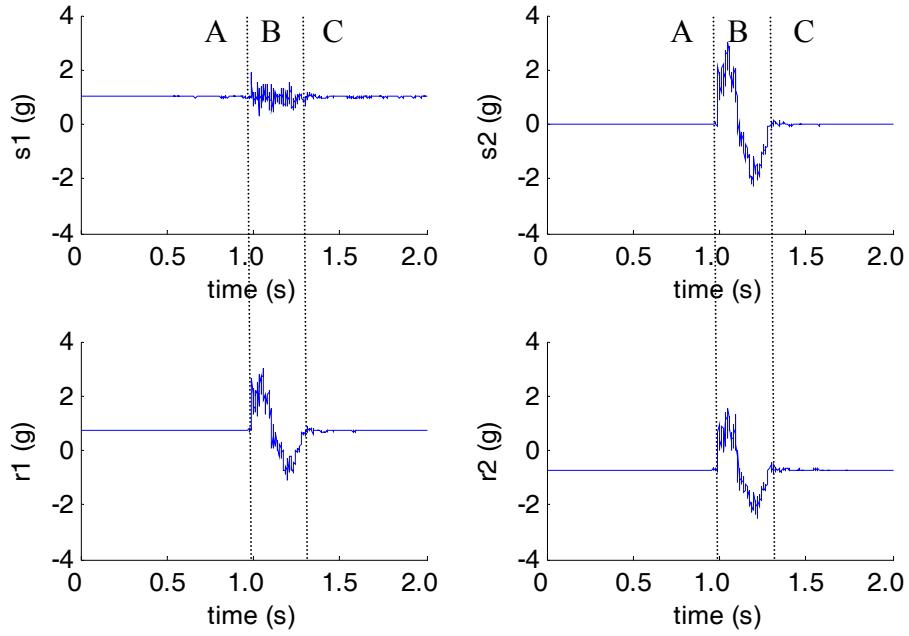

Figure D-11 The sensor unit outputs (s_1, s_2, r_1 and r_2) in unit of g at θ equals to 270 degrees with movement to the left (-x). The means and standard deviations over the time in section B are 0.99g (±0.20), -0.02g (±1.48), 0.70g (±1.06) and -0.72g (±1.07) for s_1, s_2, r_1 and r_2 respectively.

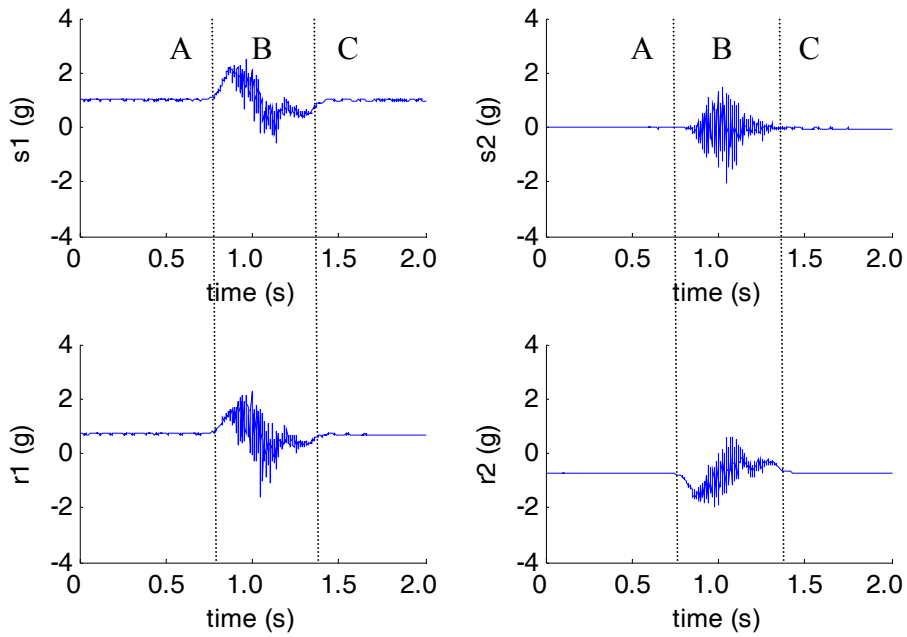

Figure D-12 The sensor unit outputs (s_1, s_2, r_1 and r_2) in unit of g at θ equals to 270 degrees with movement to up (+y). The means and standard deviations over the time in section B are 0.99g (±0.61), -0.03g (±0.37), 0.70g (±0.51) and -0.73g (±0.48) for s_1, s_2, r_1 and r_2 respectively.

Appendix E

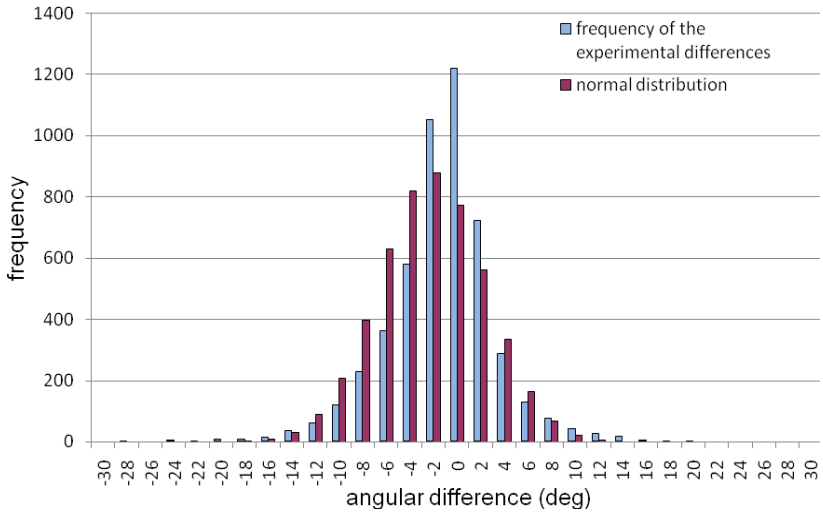

Figure E-1 The angular difference distribution for the angle measurement (180° to 0°) between sensor unit at 230mm from rotation point and potentiometer.

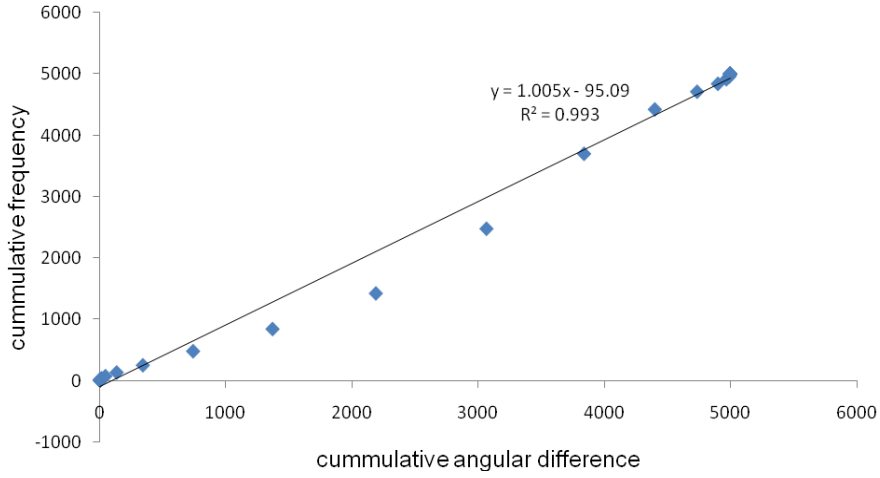

Figure E-2 The cumulative angular difference d for the angle measurement (180° to 0°) between sensor unit at 230mm from rotation point and potentiometer.

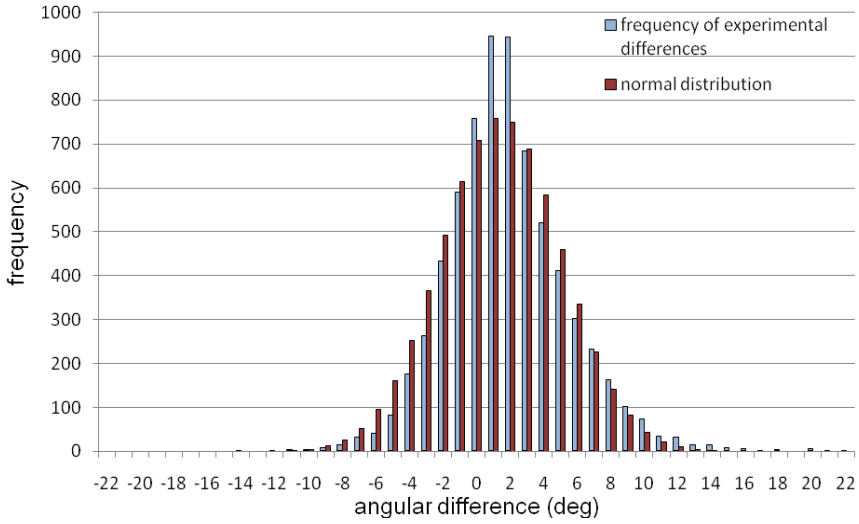

Figure E-3 The angular difference distribution for the angle measurement (0° to 180°) between sensor unit at 230mm from rotation point and potentiometer.

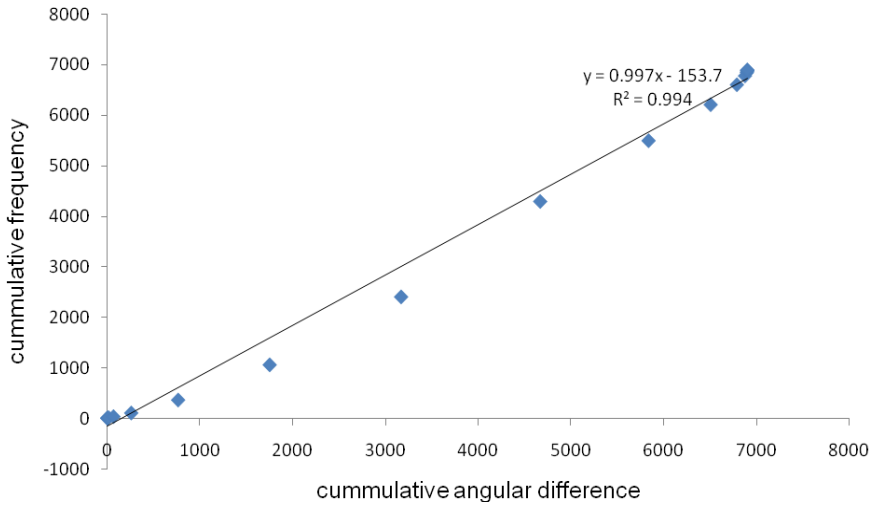

Figure E-4 The cumulative angular difference for the angle measurement (0° to 180°) between sensor unit at 230mm from rotation point and potentiometer.

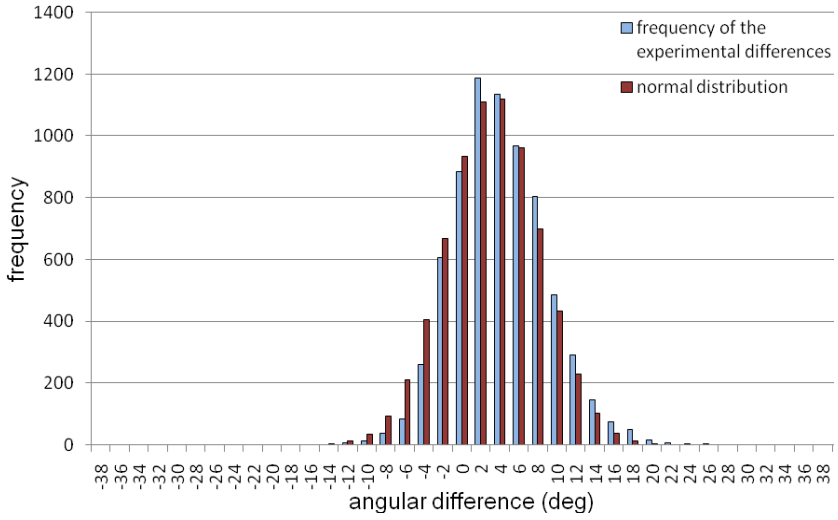

Figure E-5 The angular difference distribution for the angle measurement (180° to 360°) between sensor unit at 230mm from rotation point and potentiometer.

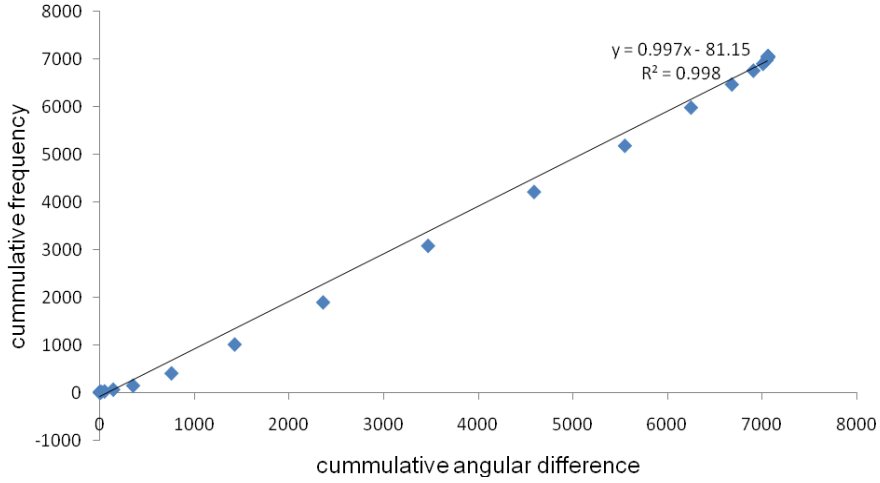

Figure E-6 The cumulative angular difference for the angle measurement (180° to 360°) between sensor unit at 230mm from rotation point and potentiometer.

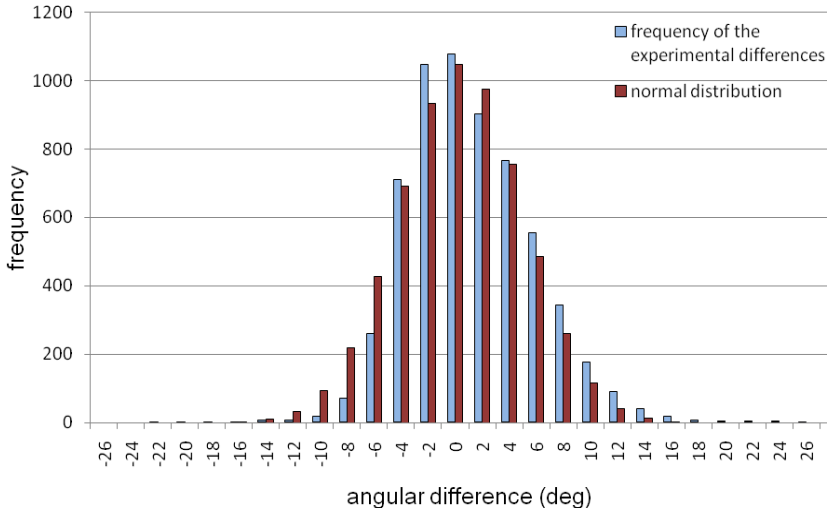

Figure E-7 The angular difference distribution for the angle measurement (360° to 180°) between sensor unit at 230mm from rotation point and potentiometer.

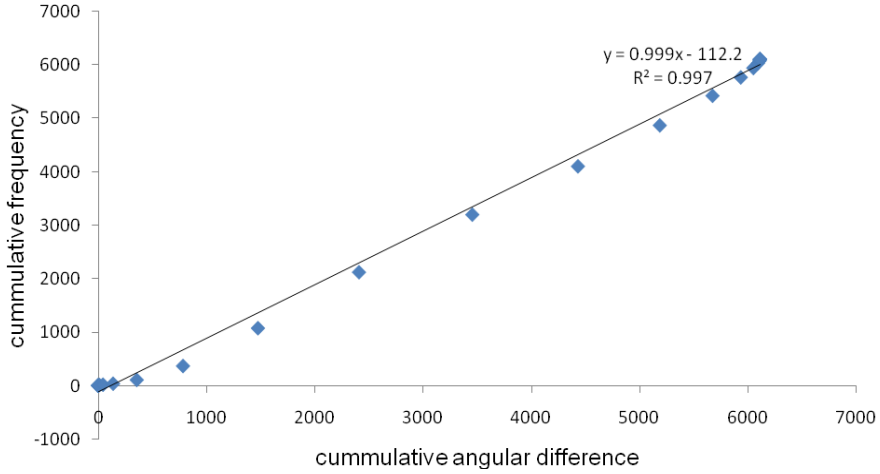

Figure E-8 The cumulative angular difference for the angle measurement (360° to 180°) between sensor unit at 230mm from rotation point and potentiometer.

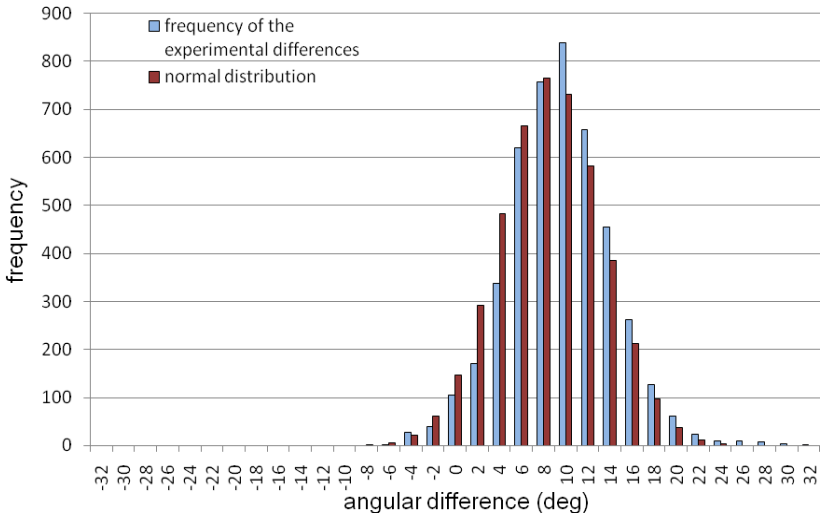

Figure E-9 The angular difference distribution for the angle measurement (180° to 360°) between sensor unit at 70mm from rotation point and potentiometer.

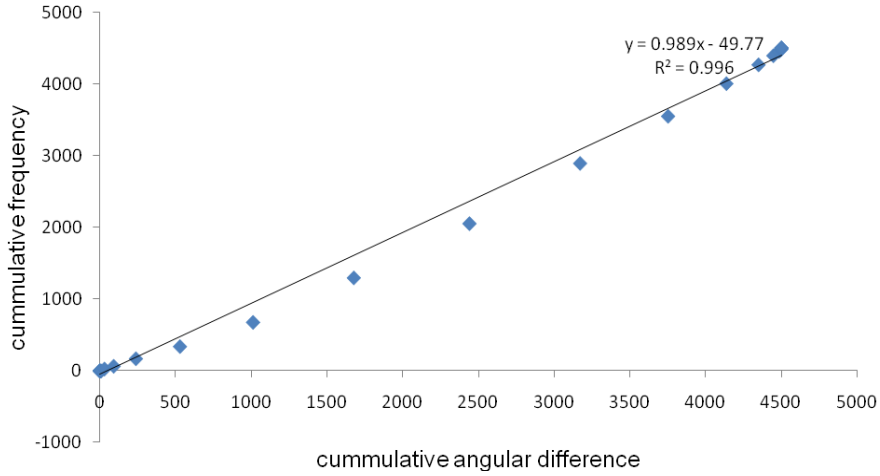

Figure E-10 The cumulative angular difference for the angle measurement (180° to 360°) between sensor unit at 70mm from rotation point and potentiometer.

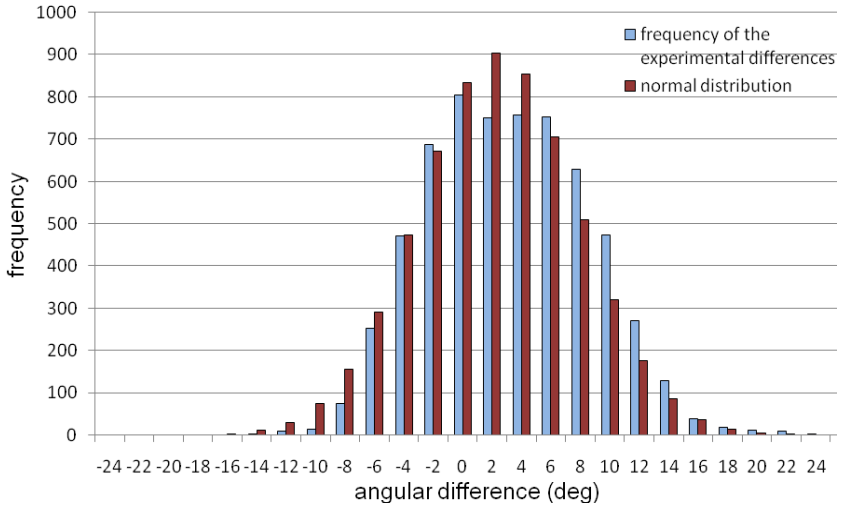

Figure E-11 The angular difference distribution for the angle measurement (360° to 180°) between sensor unit at 70mm from rotation point and potentiometer.

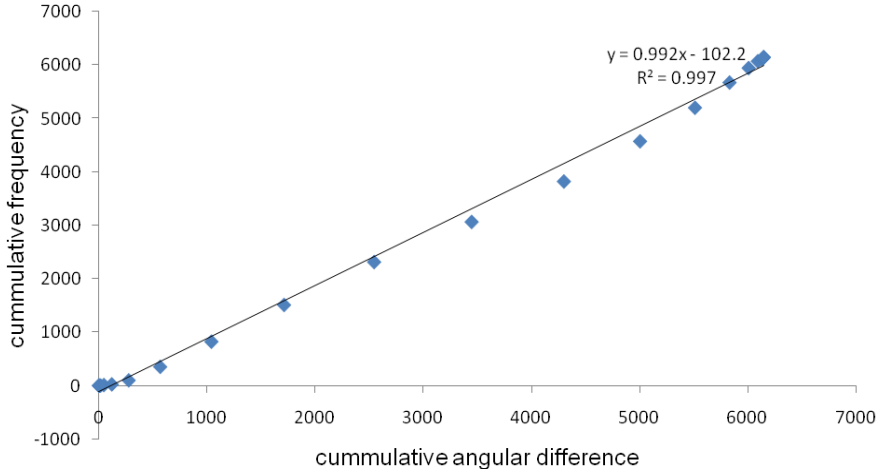

Figure E-12 The cumulative angular difference for the angle measurement (360° to 180°) between sensor unit at 70mm from rotation point and potentiometer.

Appendix F

Table F-1 The retroreflective markers attachment for pelvis, thigh, shank and foot (University of Texas (2002)).

Pelvis		
LASI	Left ASIS	Placed directly over the left anterior superior iliac spine
RASI	Right ASIS	Placed directly over the right anterior superior iliac spine
LPSI	Left ASIS	Placed directly over the left posterior superior iliac spine
RPSI	Right ASIS	Placed directly over the right posterior superior iliac spine
SACR	Sacral wand marker	Placed on the skin mid-way between the posterior superior iliac spines (PSIS). An alternative to LPSI and RPSI.
Leg Markers		
LKNE	Left knee	Placed on the lateral epicondyle of the left knee
RKNE	Right knee	Placed on the lateral epicondyle of the right knee
LTHI	Left thigh	Place the marker over the lower lateral 1/3 surface of the thigh just below the swing of the hand, although the height is not critical.
RTHI	Right thigh	Place the marker over the lower lateral 1/3 surface of the thigh just below the swing of

		the hand, although the height is not critical.
LANK	Left ankle	Placed on the lateral malleolus along an imaginary line that passes through the transmalleolar axis.
RANK	Right ankle	Placed on the lateral malleolus along an imaginary line that passes through the transmalleolar axis.
LTIB	Left tibial wand marker	Similar to the thigh markers, these are placed over the lower 1/3 of the shank to determine the alignment of the ankle flexion axis
RTIB	Right tibial wand marker	Similar to the thigh markers, these are placed over the lower 1/3 of the shank to determine the alignment of the ankle flexion axis
LMMA	Left medial malleolus	Placed on the medial malleolus to measure the shank offset
RMMA	Right medial malleolus	Placed on the medial malleolus to measure the shank offset

Foot Markers

LTOE	Left toe	Placed over the second metatarsal head, on the mid-foot side of the equinus break between fore-foot and mid-foot
RTOE	Right toe	Placed over the second metatarsal head, on the mid-foot side of the equinus break between fore-foot and mid-foot
LHEE	Left heel	Placed on the calcaneous at the same height above the plantar surface of the foot as the toe marker
RHEE	Right heel	Placed on the calcaneous at the same height above the plantar surface of the foot as the toe marker

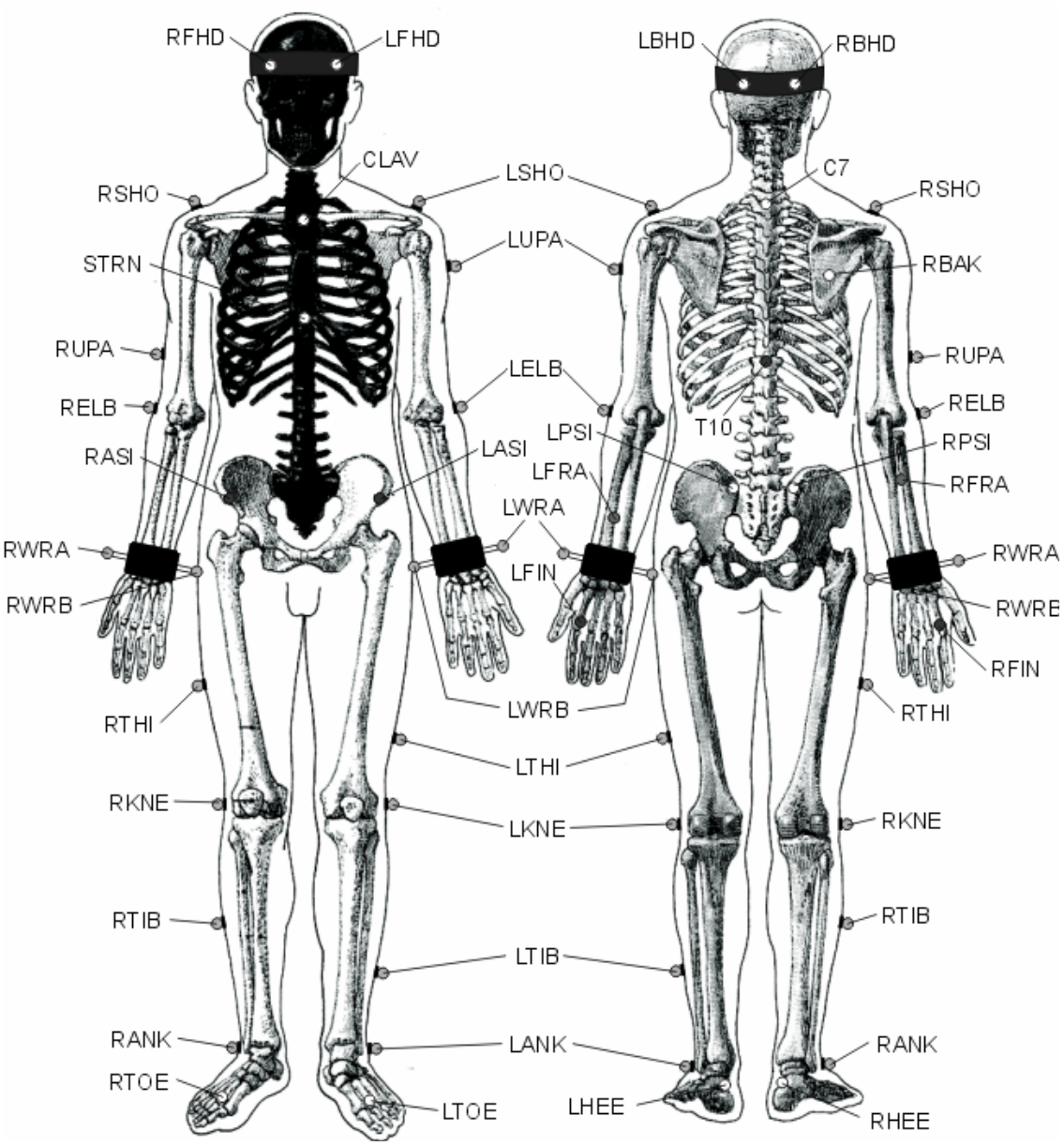

Figure F-1 The markers attachment positions (left figure: anterior view and right figure: posterior view) (University of Texas (2002)).

Appendix G

Program 1

```
% To calculate for the correlation coefficient between the data and the sample window
clc;
clear all;
load sample.txt;
load signal.txt;
w_result=fopen('corr_coeff.txt','wt');
[sample1]=textread('sample.txt','%f');      % read from sample window file
[sample2]=textread('signal.txt','%f');       % read from data file
count=0;
for start=1:1:12651
   A=sample1(1:350);
   B=sample2(start:start+349);
   R=corrcoef(A,B);                    % calculate the correlation coefficient
   fprintf(w_result,'%f\n',R(1,2));       % write the correlation coefficient value to a file
end
fclose(w_result);
```

Program 2

```
% To detect heel strike and tibia vertical event in healthy subjects
clc;
clear all;
load corr_coeff.txt;
w_result=fopen('event.txt','wt');
[sample1]=textread('corr_coeff.txt','%f');   % read correlation coefficient signal

state1=0;        % initialize states, state 1 for signal below negative threshold
state2=0;        % state 2 for signal in the middle after passing negative threshold
state3=0;        % state 3 for signal above positive threshold
state4=0;        % state 4 for signal in the middle after passing positive threshold
count=0;         % counter for the time frame
max=0.5;         % the value must less than the positive threshold

for start=1:1:20651
A=sample1(start);

   if(A<=-0.55) % negative threshold
      if(state3==1&&state4==1)
         count=0;
         state1=1;
         state3=0;
         state4=0;
         fprintf(w_result,' %f\n',0);            % no event detected

      else
         count=count+1; %continue count
         state1=1; %case 1
         state3=0;
         state4=0;
         fprintf(w_result,'%f\n',0);         % no event detected
      end
   end
```

```
if(A>-0.55&&A<0.65)      %middle
  if(state1==1&&count<550)       %continue counting if after negative threshold
      state2=1;        % start from state 1
      count=count+1;         %continue counting
      fprintf(w_result,'%f\n',0);         % no event detected
  else
      count=0;
      state4=1;
      state3=0;
      state2=0;
      state1=0;
      fprintf(w_result,'%f\n',0);         % no event detected
   end
end

if(A>=0.65) %positive threshold
   if(state1==1&&state2==1&&count<550)
      state3=1;
        if(A>max)
          max=A;
          count=count+1;
          fprintf(w_result,'%f\n',0);          % no event detected
        else
          fprintf(w_result,'%f\n',2);          % event detected
          state2=0;
          state1=0;
        end
   else
      count=0;
      state2=0;
      state1=0;
      fprintf(w_result,'%f\n',0);          %no event detected
   end
end
```

```
end
fclose(w_result);
```

Program 3

```
% To detect tibial vertical events in neurological patients
clc;
clear all;
load corr_coeff.txt;
w_result=fopen('event.txt','wt');
[sample1]=textread('corr_coeff.txt','%f');

state1=0;       % initialize states, state 1 for signal below negative threshold
state2=0;       % state 2 for signal in the middle after passing negative threshold
state3=0;       % state 3 for signal above positive threshold
state4=0;       % state 4 for signal in the middle after passing positive threshold
count=0;        % counter for time frame
count1=1000;            % counter for time frame 1
max=0.4;        % the value must less than the positive threshold

for start=1:1:7651
A=sample1(start);
   if(A<=-0.55) % negative threshold
      if(state3==1&&state4==1)
         count1=count1+1;
         count=0;
         state1=1;
         state3=0;
         state4=0;
         fprintf(w_result,' %f\n',0);            %no event detected
```

```
    else
        count1=count1+1;
        count=count+1;
        state1=1;
        state3=0;
        state4=0;
        fprintf(w_result,' %f\n',0);       %no event detected
    end
end

if(A>-0.55&&A<0.5)         %middle
  if(state1==1&&count<550)        %continue counting if after negative threshold
        count1=count1+1;
        state2=1;
        count=count+1;
        max=0.4;         % the value must less than the positive threshold value
        fprintf(w_result,'%f\n',0);          %no event detected
  else
        count1=count1+1;
        count=0;
        state4=1;
        state3=0;
        state2=0;
        state1=0;
        max=0.4;   % the value must less than the positive threshold value
        fprintf(w_result,'%f\n',0);         %no event detected
    end
 end
```

```
    if(A>=0.5)  % positive threshold
       if(state2==1&&count<550)
          state3=1;
          state1=0;
            if(A>max)
              max=A;
              count=count+1;    % increment time frame counter
              count1=count1+1;           % increment time frame 1 counter
              fprintf(w_result,'%f\n',0);     %no event detected
            else
               if(count1>1000)  % check time frame 1
              count=0;
              count1=0;
              fprintf(w_result,'%f\n',2);    % event detected
              state2=0;
              state4=1;
               else
              count=count+1;    % increment time frame counter
              count1=count1+1;           % increment time frame 1 counter
              fprintf(w_result,'%f\n',0);     % no event detected
               end
            end
       else
          count=0;
          count1=count1+1;     % increment time frame 1 counter
          state2=0;
          state1=0;
          fprintf(w_result,'%f\n',0);           % no event detected
       end
    end
end
fclose(w_result);
```

Appendix H

Figure H-1 and Figure H-2 show a typical foot segment angle pattern from Patient 3 walking with stimulation on and with stimulation off respectively. As can be seen in the figures, the segment angles pattern for both walking are similar with the typical foot segment angle of the healthy subject (Figure 7-2). Only the positive peak of the angle occurred after the foot has lifted from the ground is smaller in amplitude for P3 compared to the healthy subject.

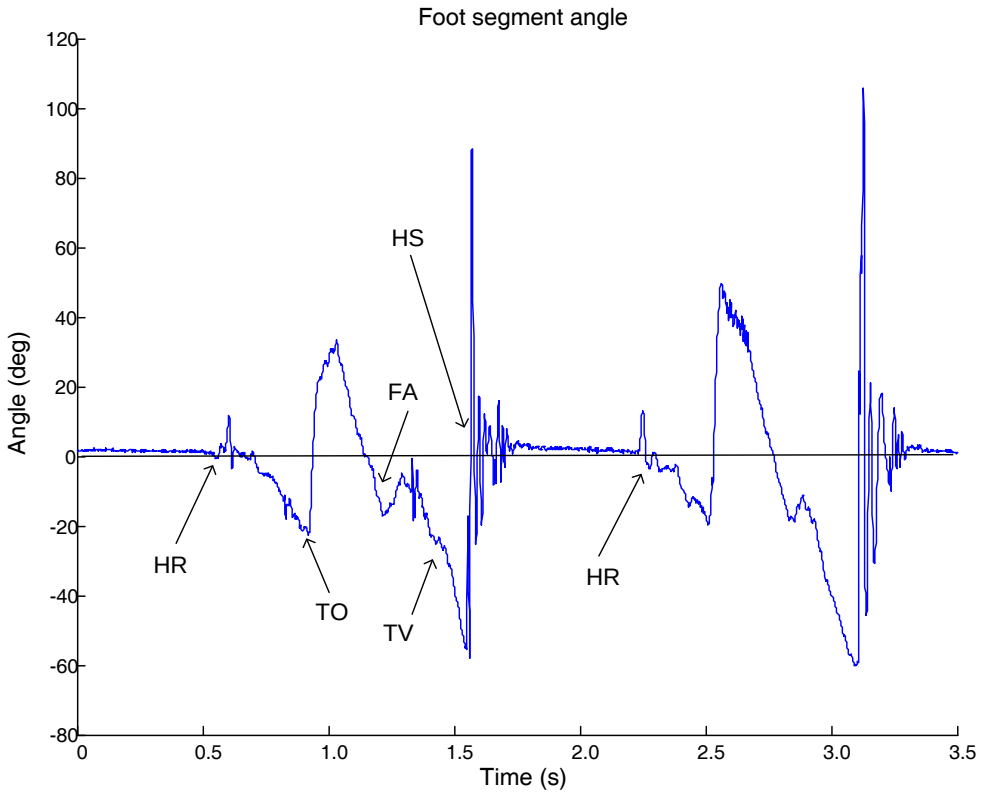

Figure H-1 A typical foot segment angle of the affected side of Patient 3 walking with stimulation on (gluteal and popliteal fossa muscles).

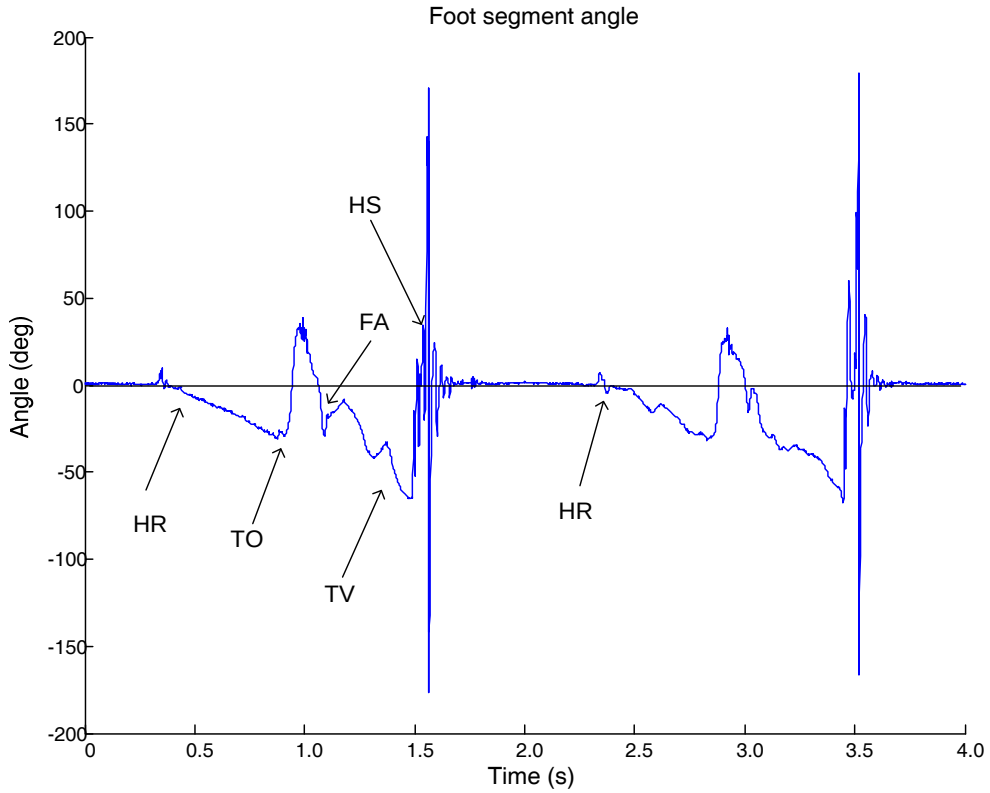

Figure H-2 A typical foot segment angle of the affected side of Patient 3 walking with stimulation off.

Figure H-3 and Figure H-4 show a typical foot segment angle of a patient (P4) walking with stimulation on and with stimulation off respectively. The angle pattern is different from the other patients and healthy subjects. The data from Patient 4 was not further analysed as no reference data was obtained. The walking was very poor at the time of trials, the patient drags the affected foot during walking without lifting the foot during the swing phase of the gait. Also, it is difficult to identify the events in the gait of P4 due to the poor walking, therefore only heel rise (HR) and heel strike (HS) events have been labelled in the figures.

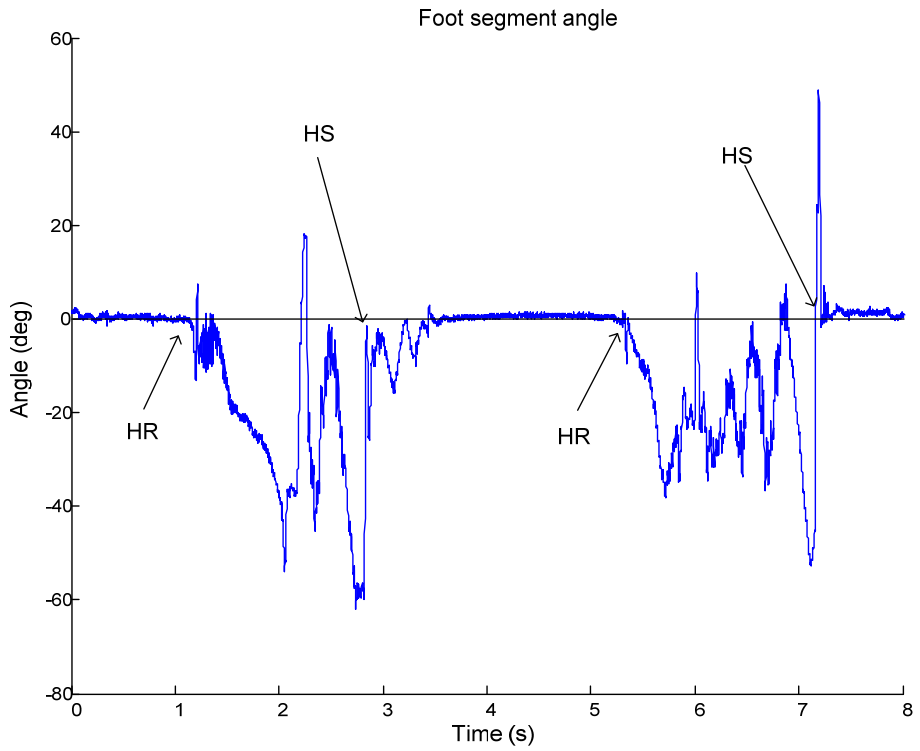

Figure H-3 A typical foot segment angle of the affected side of Patient 4 walking with stimulation on (hamstrings and tibialis anterior muscles).

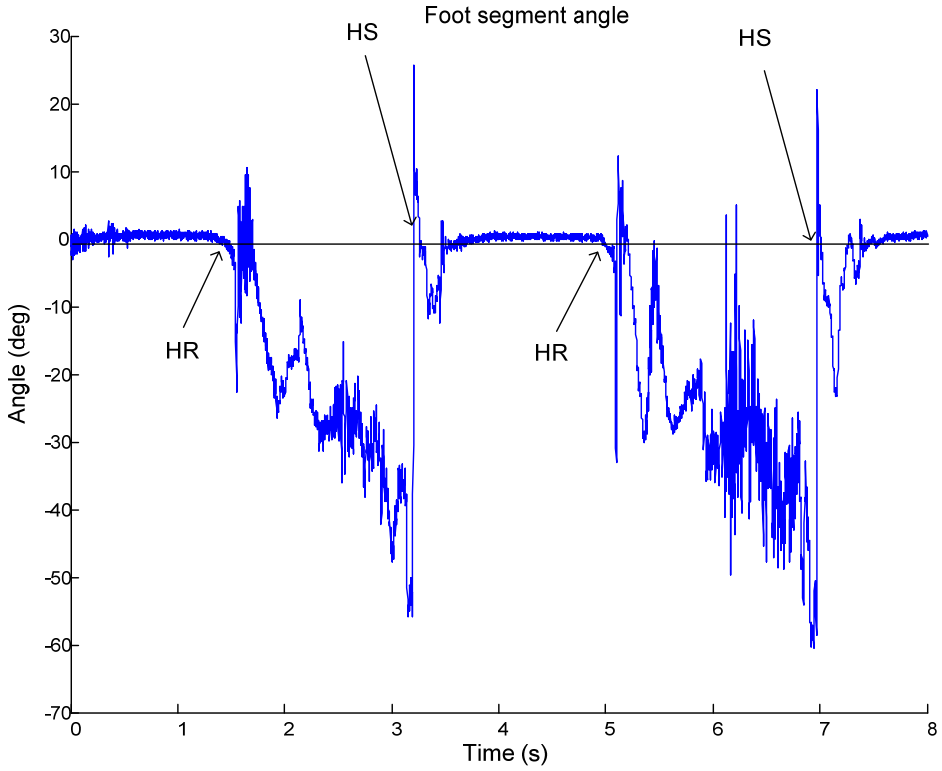

Figure H-4 A typical foot segment angle of the affected side of Patient 4 walking with stimulation off.

Appendix I

Figure I-1 and Figure I-2 show the output from a footswitch and a force sensor (FSG15N1A by Honeywell) in a static test when loaded with the same forces. The footswitch output changed from a low to high voltage (Figure I-1) between five and six newtons. The output changed from a high to low voltage (Figure I-2).between six and five newtons. For comparison purposes, the force sensor output voltage is shown where the applied force increments linearly in one newton increments ($0.5VN^{-1}$).

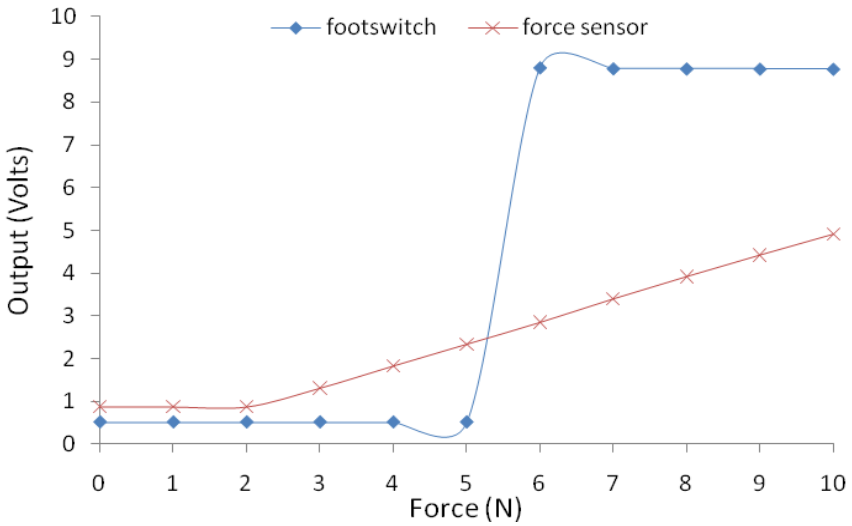

Figure I-1 Increasing load during a static test.

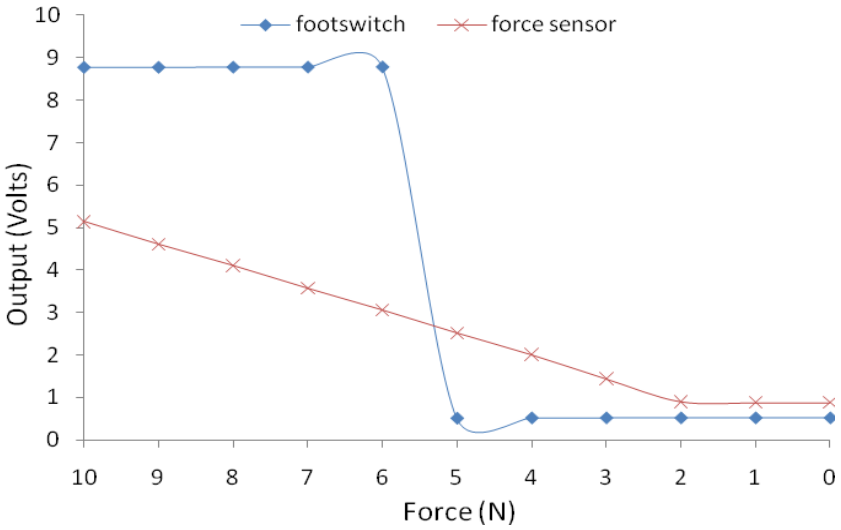

Figure I-2 Decreasing load during a static test.

Slow or fast unloading give no effect on the footswitch output as when normal loading or unloading. Only fast loading gives the feather edge effect on the output of the footswitch.

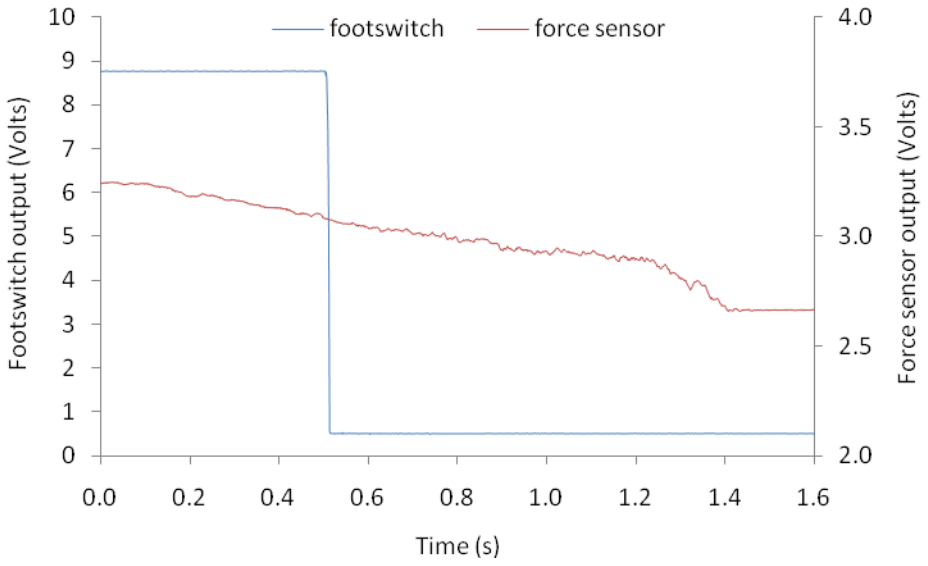

Figure I-3 Slow unloading.

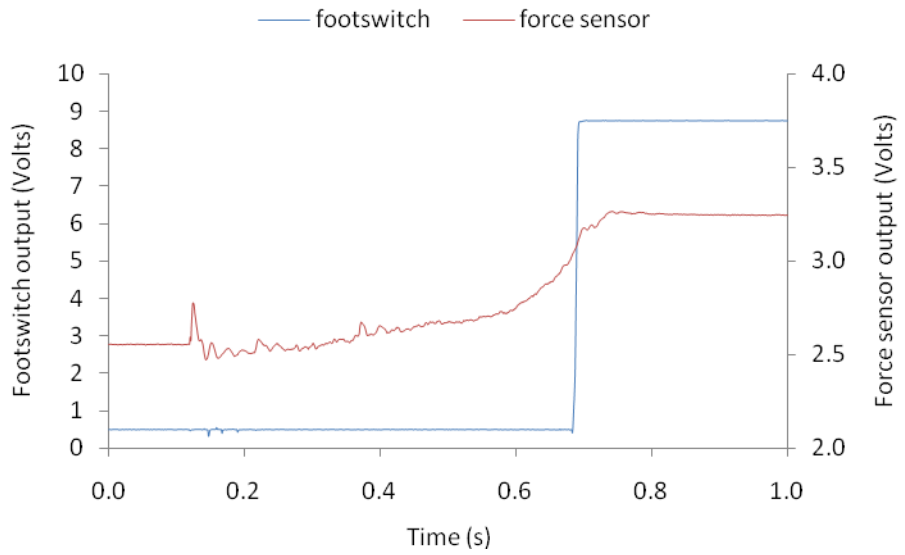

Figure I-4 Slow loading.

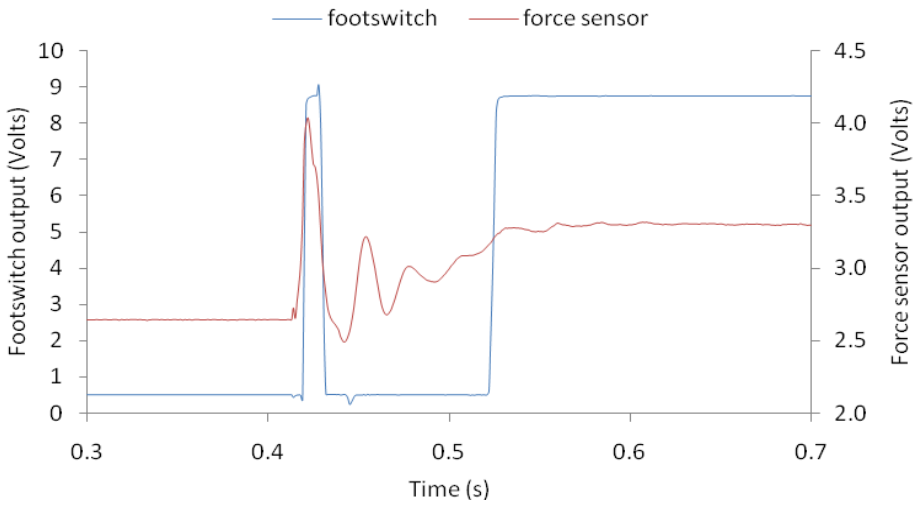

Figure I-5 Fast loading showing a feathered edge.

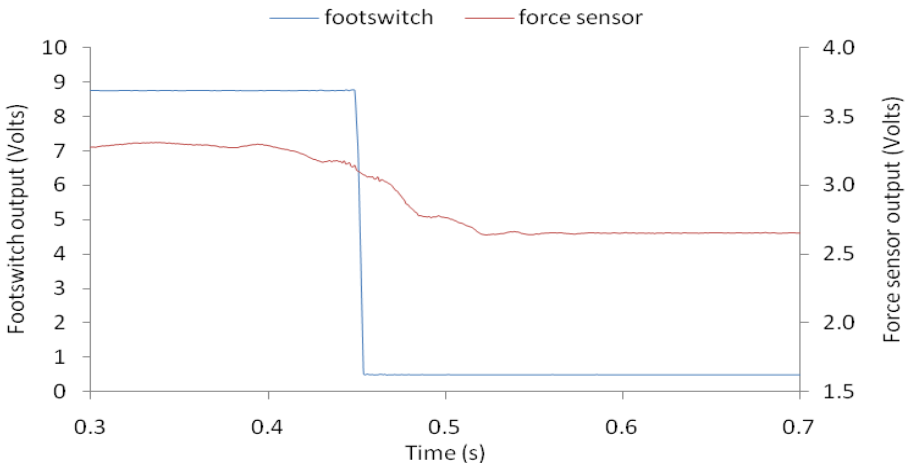

Figure I-6 Fast unloading.

Appendix J

Results for the heel strike events detection in healthy subjects.

Figure J-1 to Figure J-10: Heel strike events in Subject 1 (right foot). (a) foot segment angle (b) correlation coefficient between foot segment angle and a sample window (t_p = positive threshold, t_n = negative threshold, T_f = time frame and m=first maximum point) (c) algorithm output (0=no event, 2=event detected and hs=heel strike) and (d) heel switch output.

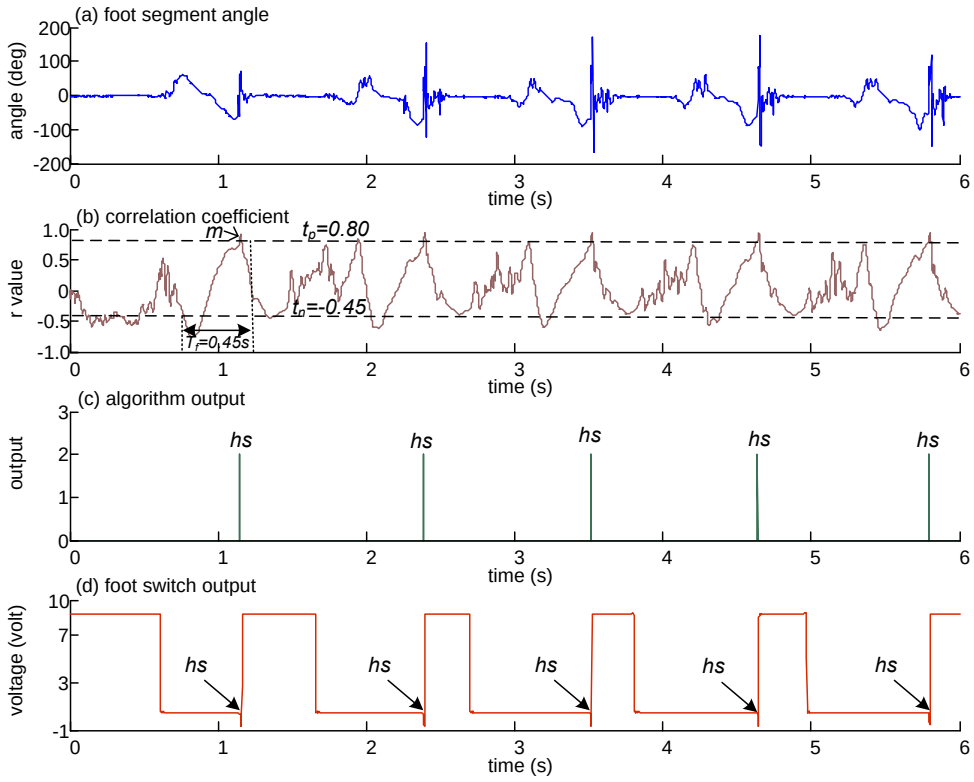

Figure J-1 Heel strike events in Subject 1 (right foot), n=5.

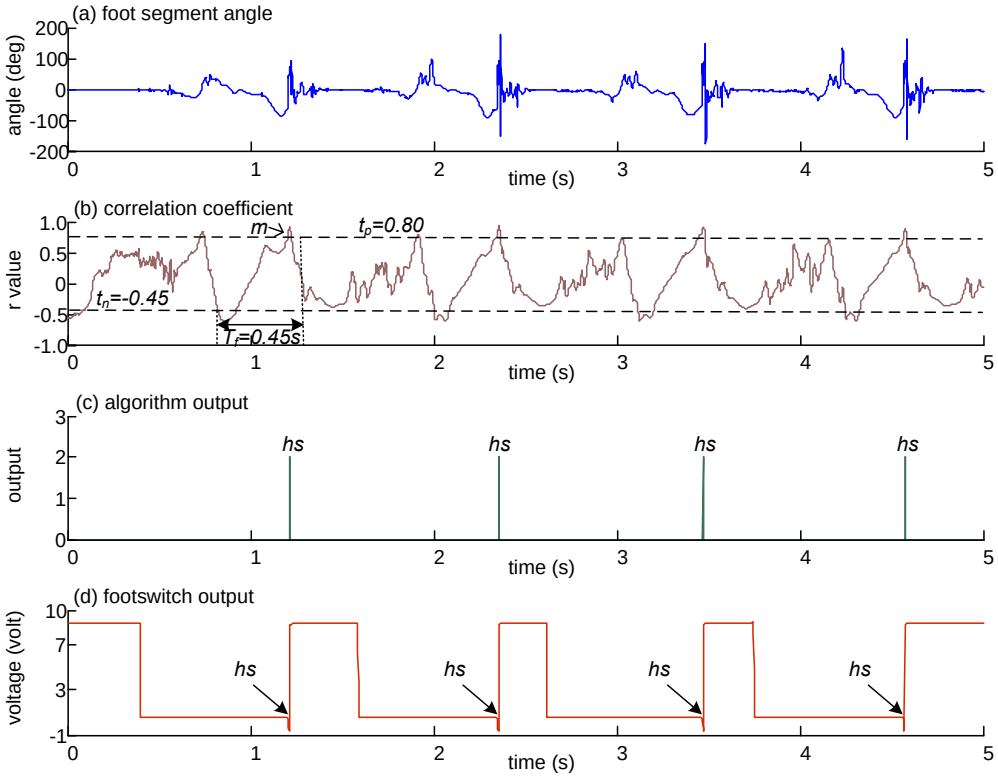

Figure J-2 Heel strike events in Subject 1 (right foot), n=4.

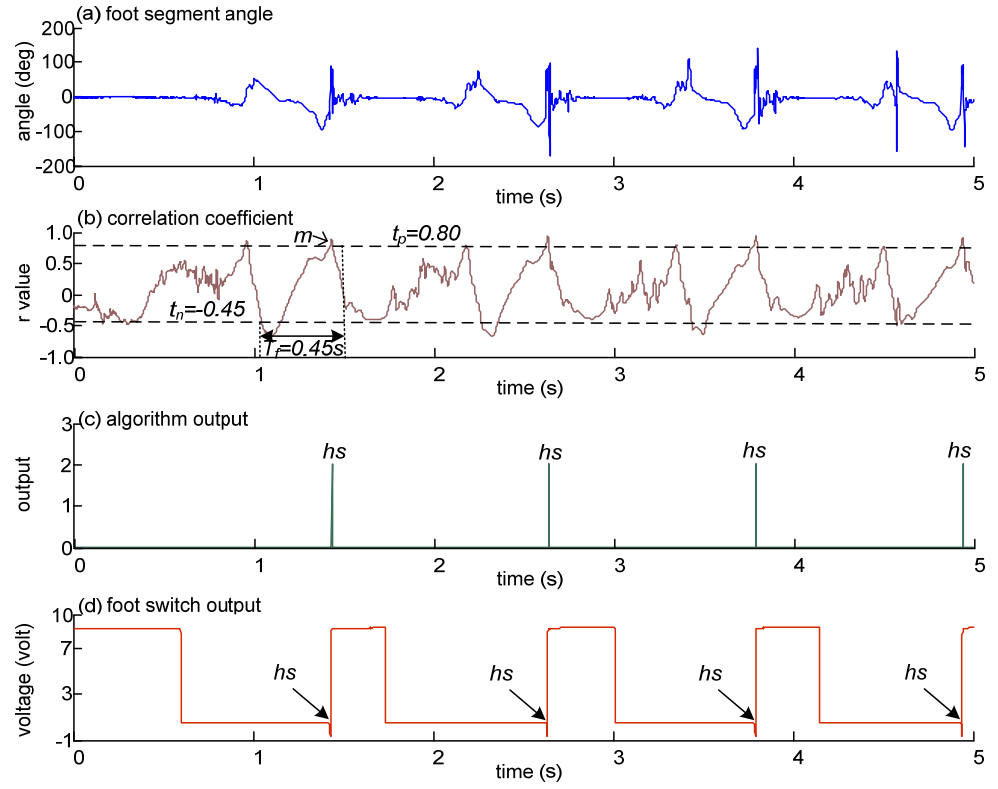

Figure J-3 Heel strike events in Subject 1 (right foot), n=4.

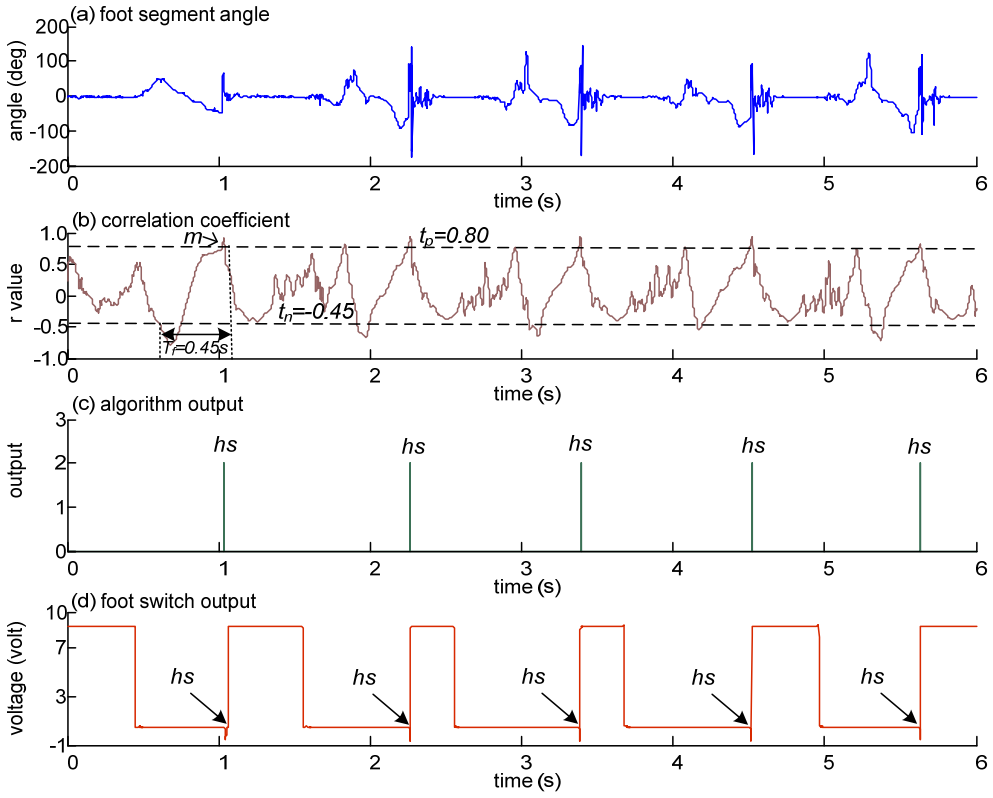

Figure J-4 Heel strike events in Subject 1 (right foot), n=5.

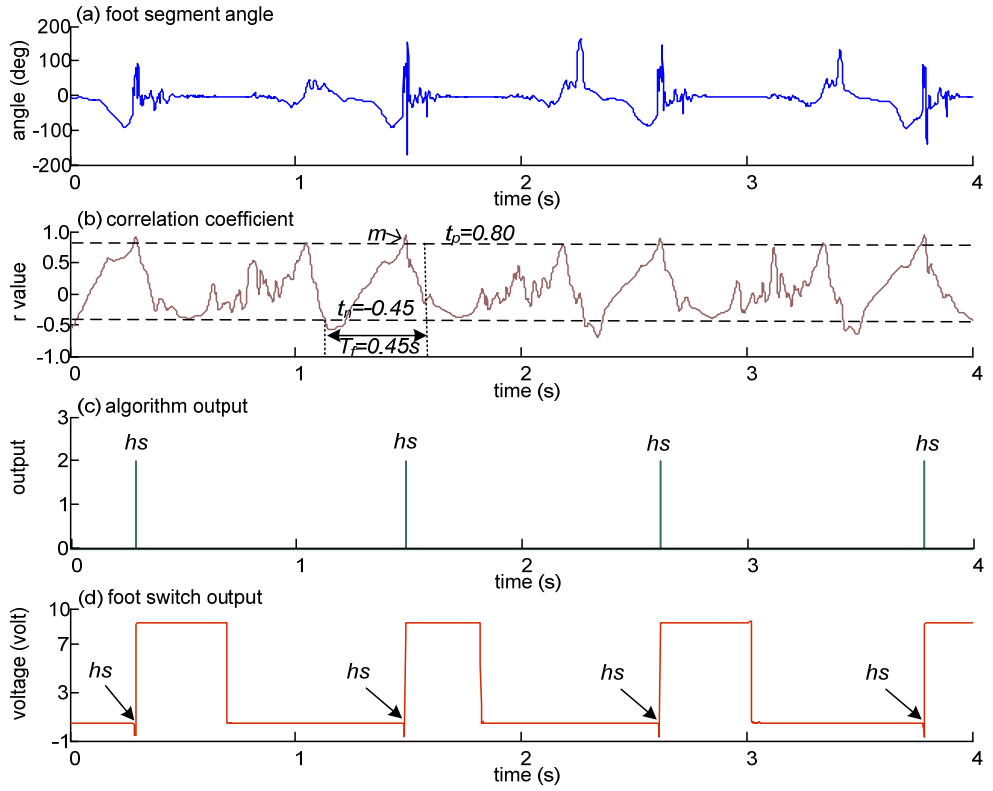

Figure J-5 Heel strike events in Subject 1 (right foot), n=4.

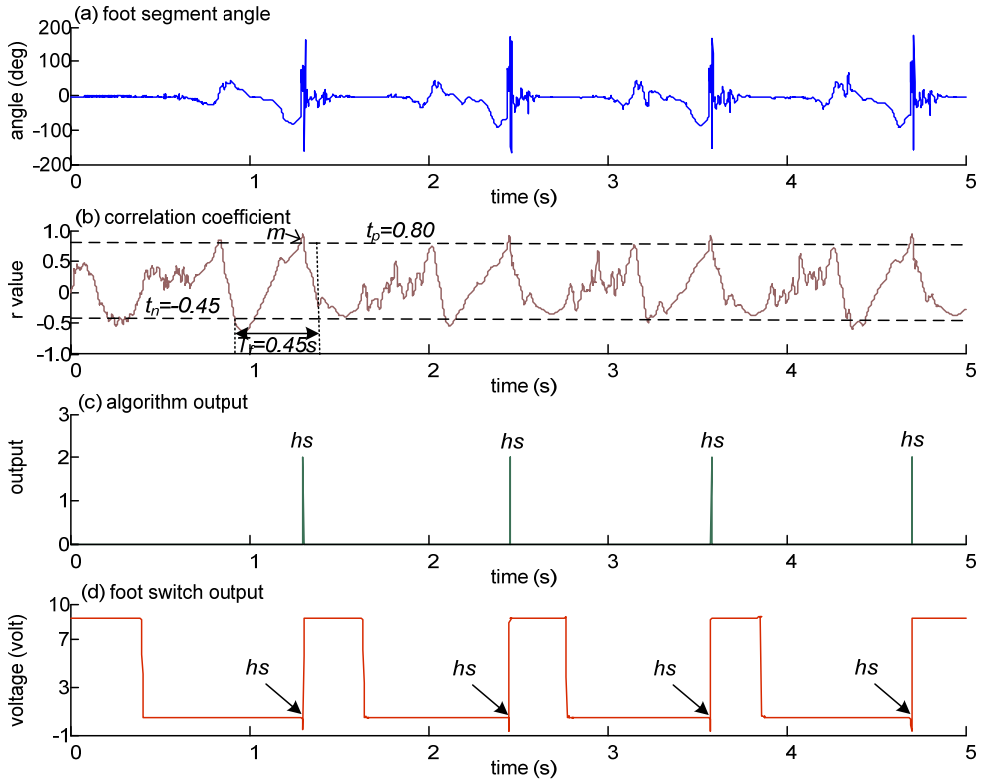

Figure J-6 Heel strike events in Subject 1 (right foot), n=4.

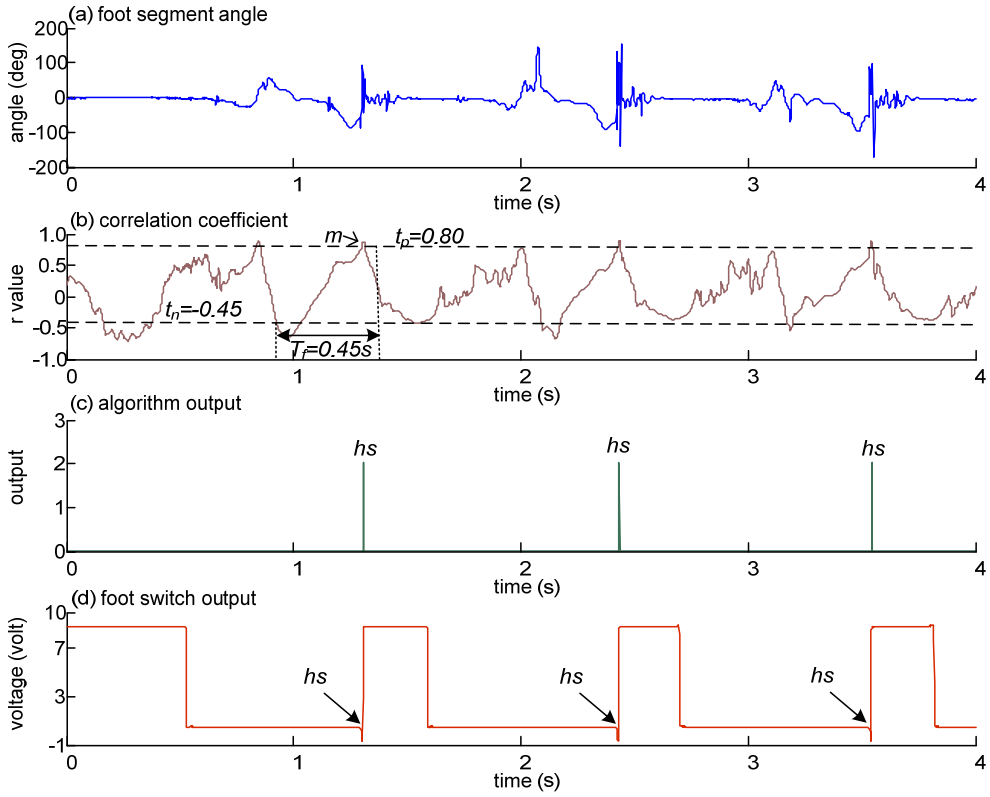

Figure J-7 Heel strike events in Subject 1 (right foot), n=3.

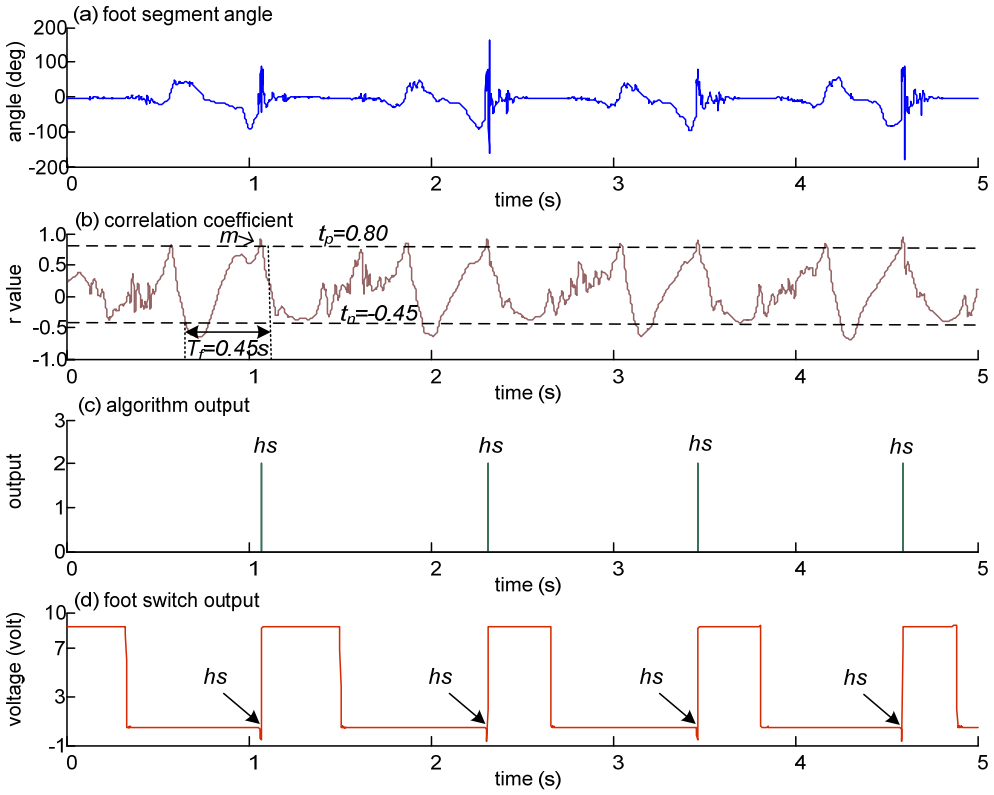

Figure J-8 Heel strike events in Subject 1 (right foot), n=4.

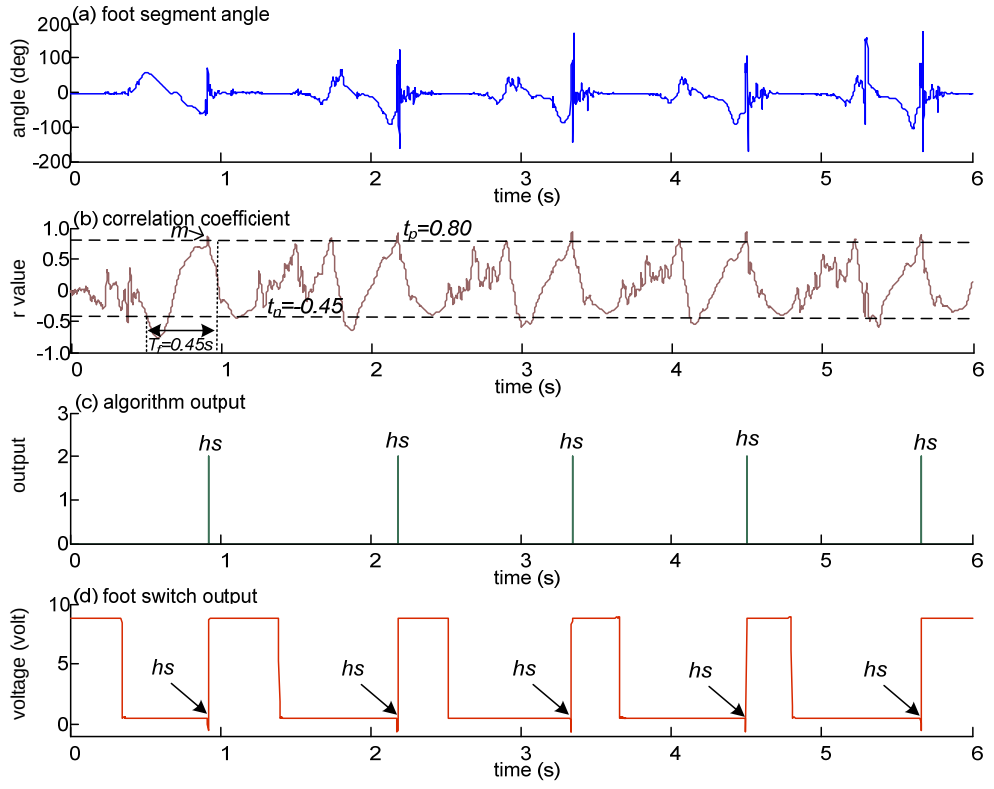

Figure J-9 Heel strike events in Subject 1 (right foot), n=5.

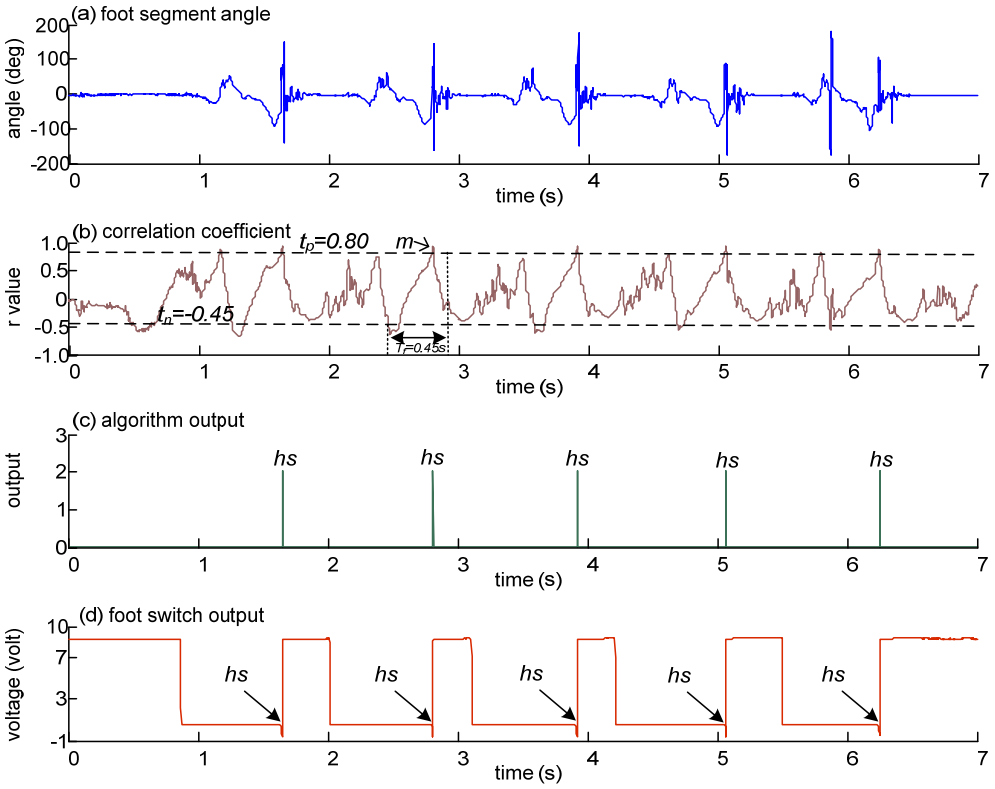

Figure J-10 Heel strike events in Subject 1 (right foot), n=5.

Figure J-11 to Figure J-19: Heel strike events in Subject 2 (right foot). (a) foot segment angle (b) correlation coefficient between foot segment angle and a sample window (t_p = positive threshold, t_n = negative threshold, T_f= time frame and m=first maximum point) (c) algorithm output (0=no event, 2=event detected and hs=heel strike) and (d) heel switch output.

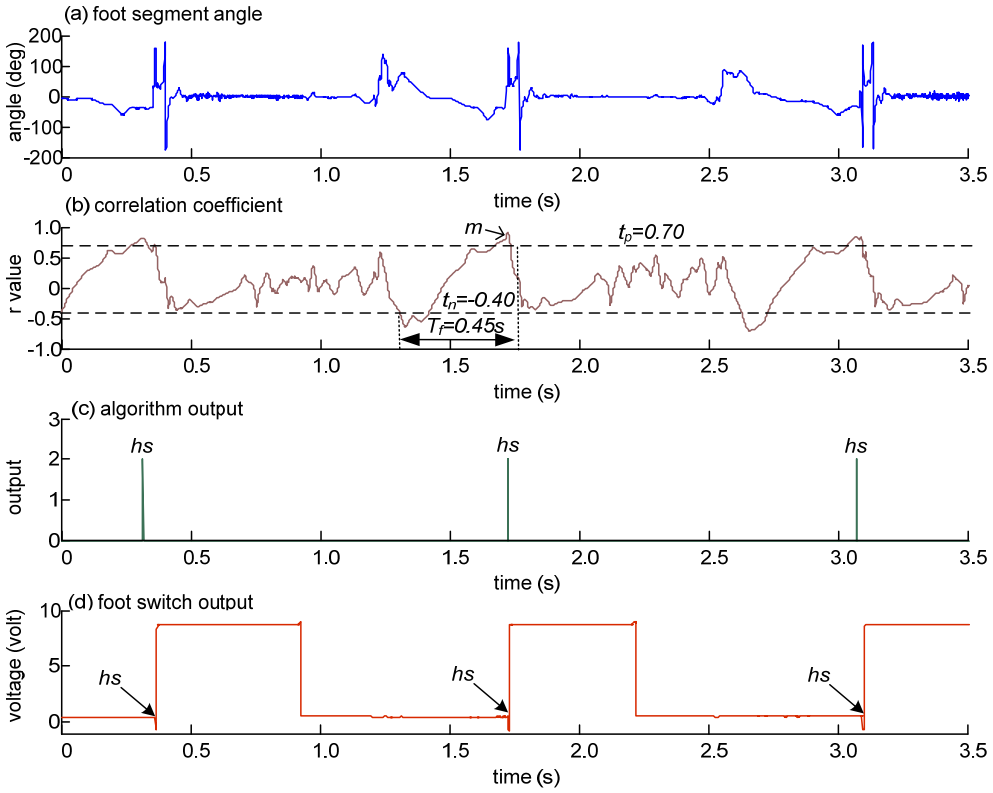

Figure J-11 Heel strike events in Subject 2 (right foot), n=3.

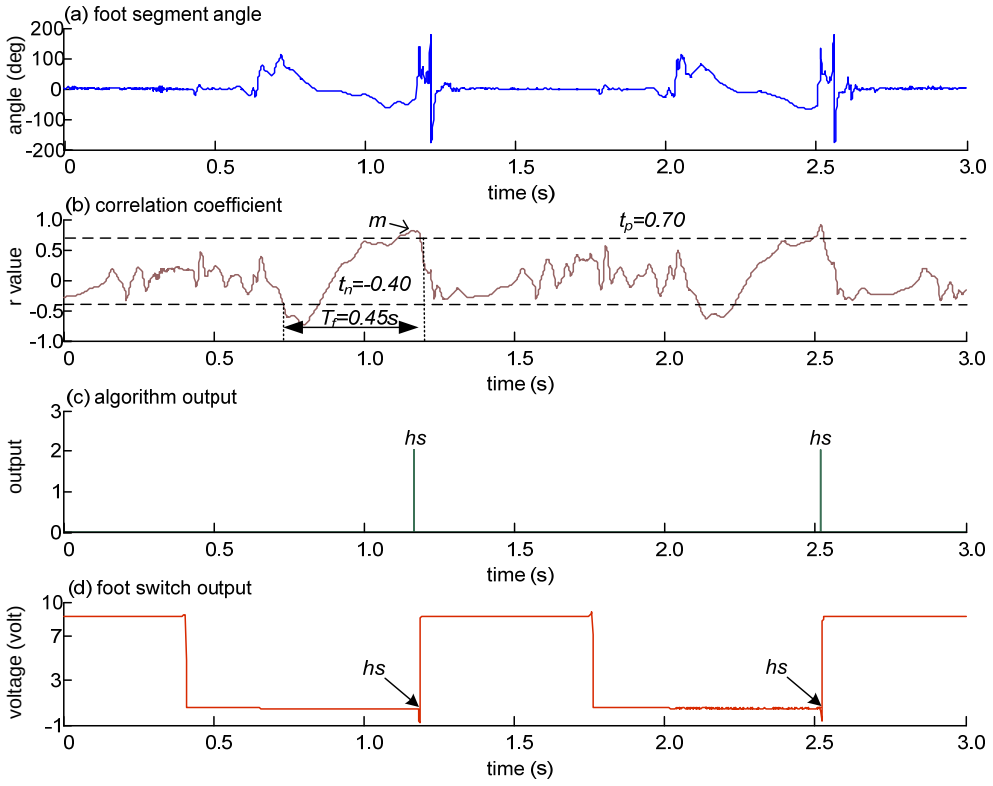

Figure J-12 Heel strike events in Subject 2 (right foot), n=2.

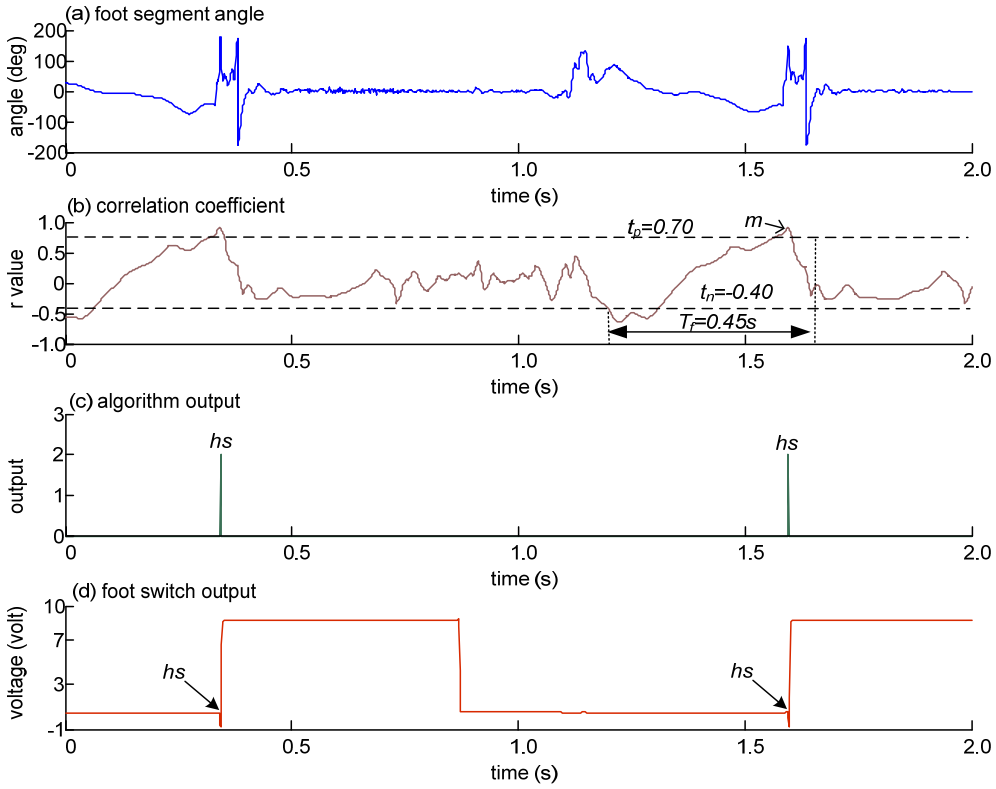

Figure J-13 Heel strike events in Subject 2 (right foot), n=2.

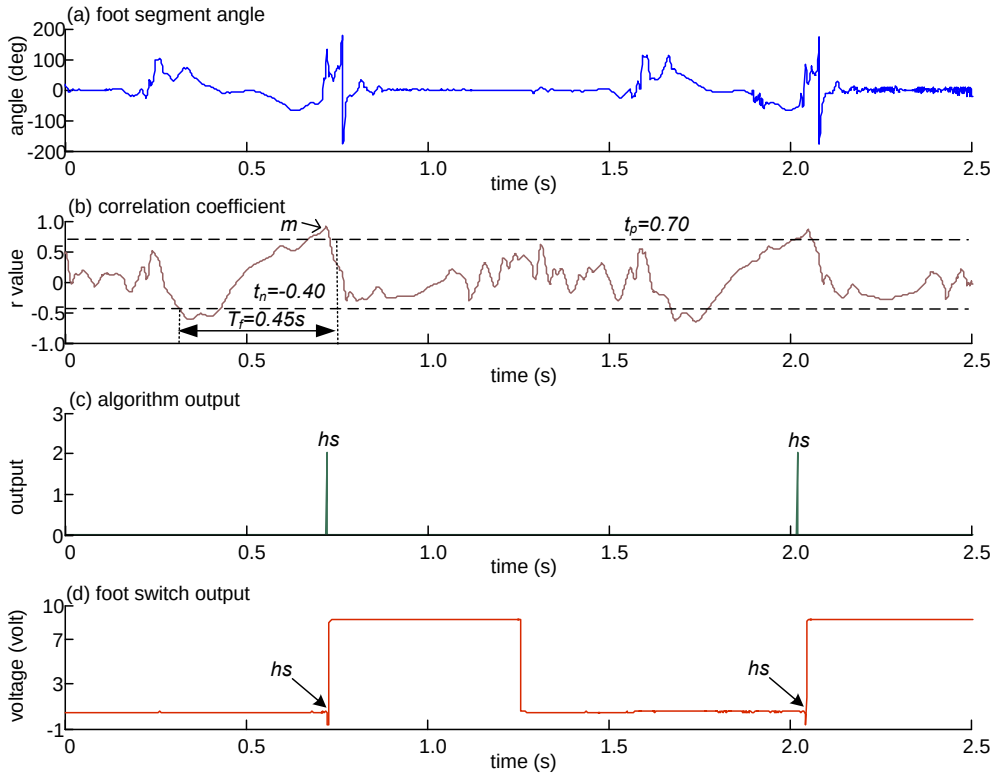

Figure J-14 Heel strike events in Subject 2 (right foot), n=2.

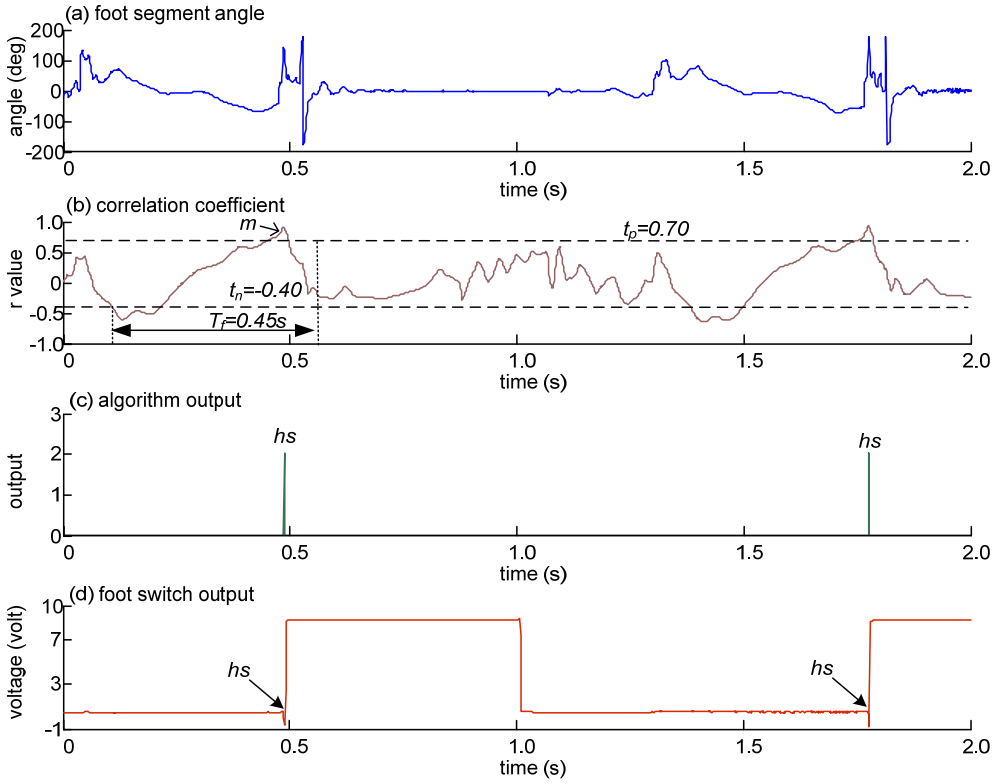

Figure J-15 Heel strike events in Subject 2 (right foot), n=2.

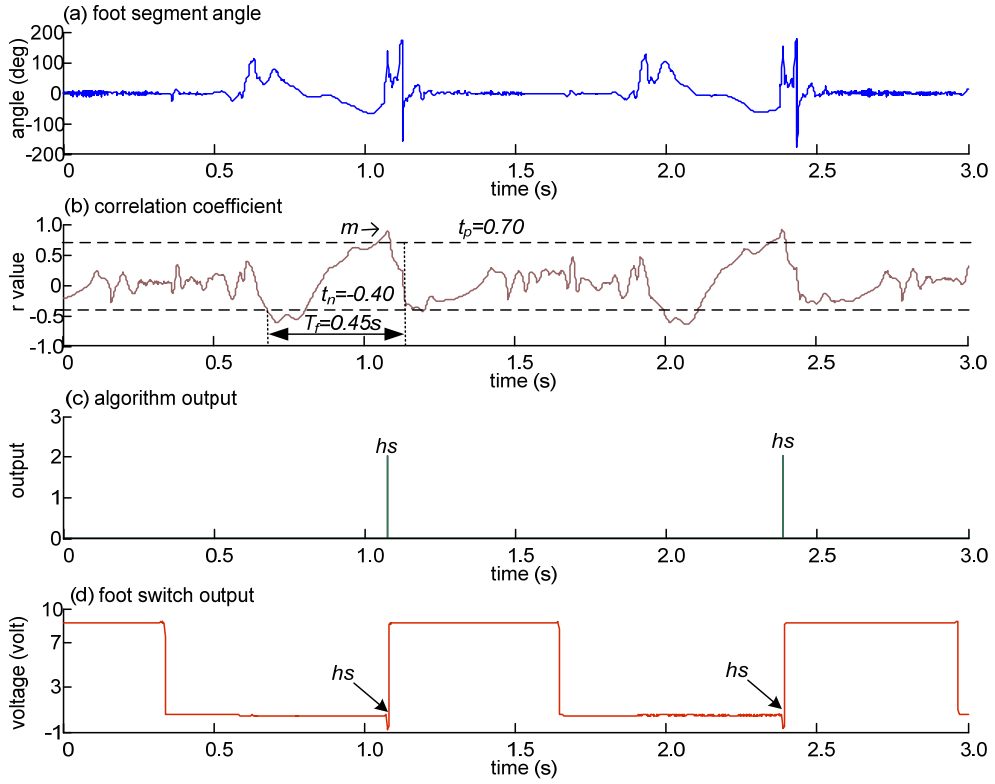

Figure J-16 Heel strike events in Subject 2 (right foot), n=2.

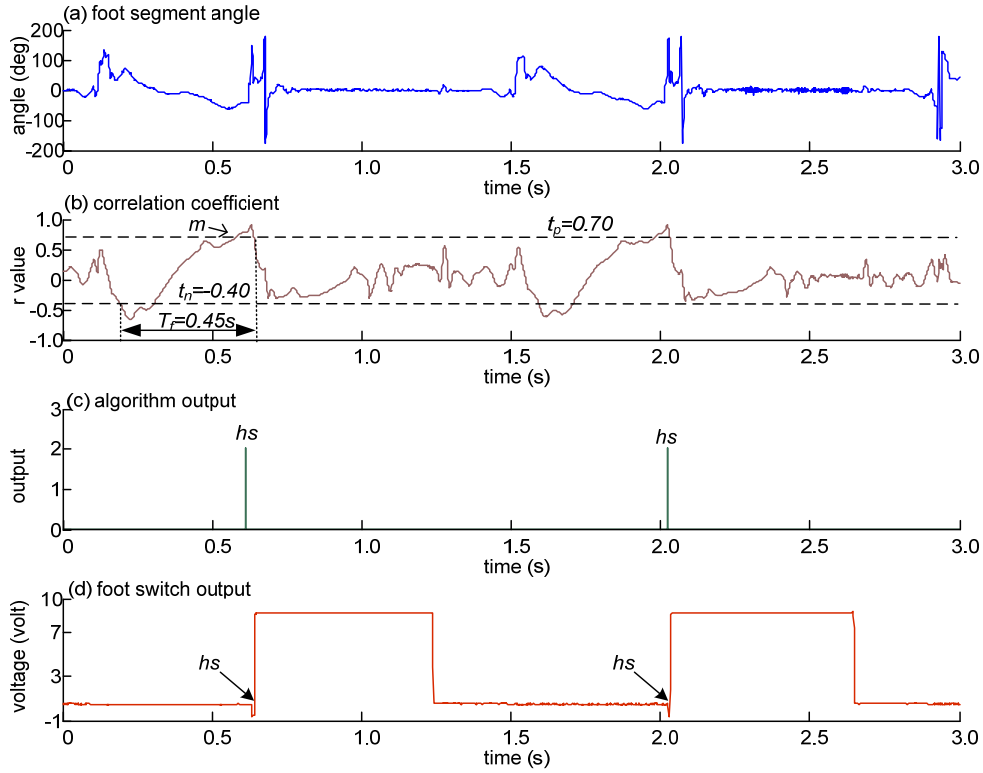

Figure J-17 Heel strike events in Subject 2 (right foot), n=2.

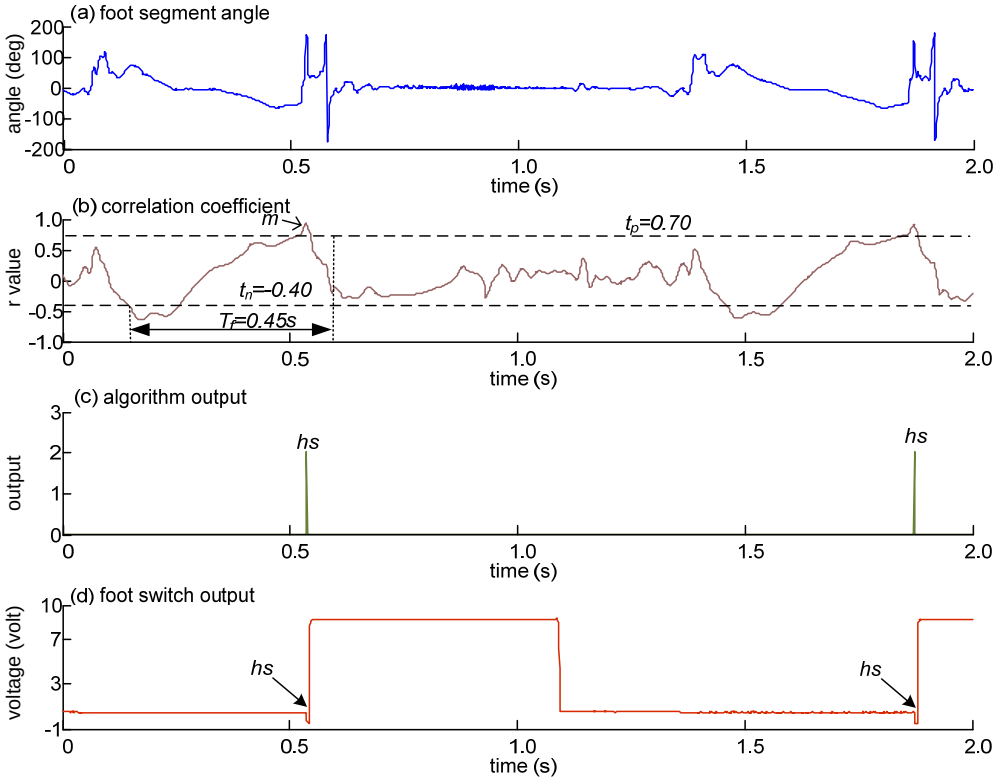

Figure J-18 Heel strike events in Subject 2 (right foot), n=2.

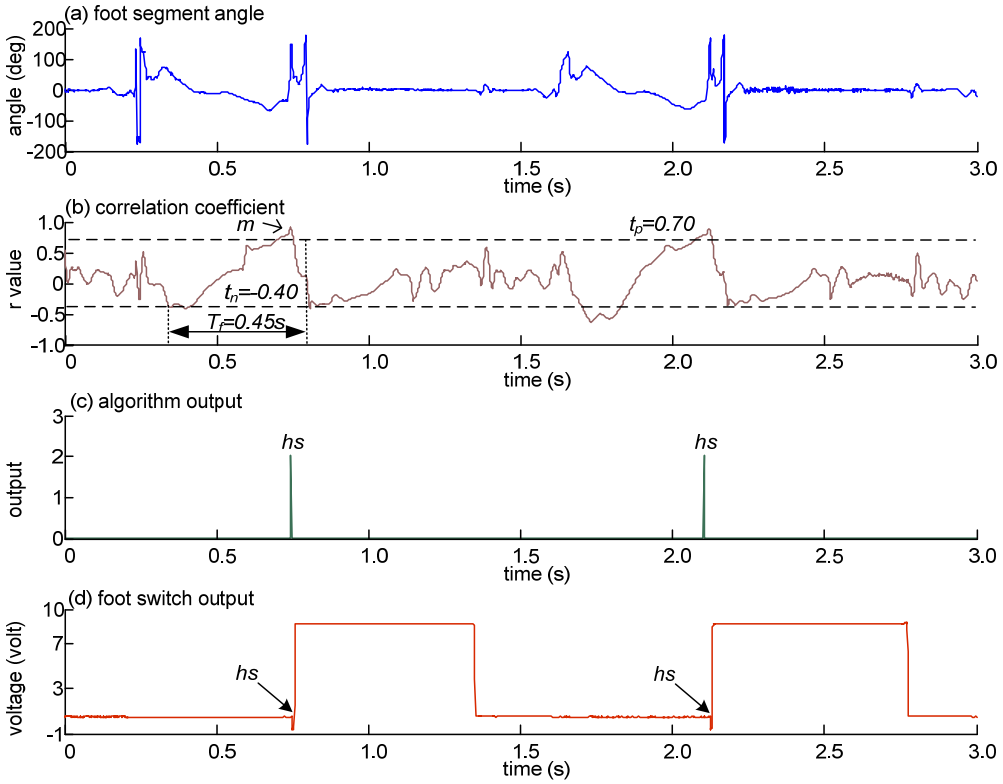

Figure J-19 Heel strike events in Subject 2 (right foot), n=2.

Figure J-20 to Figure J-27: Heel strike events in Subject 2 (left foot). (a) foot segment angle (b) correlation coefficient between foot segment angle and a sample window (t_p = positive threshold, t_n = negative threshold, T_f = time frame and m=first maximum point) (c) algorithm output (0=no event, 2=event detected and hs=heel strike) and (d) heel switch output.

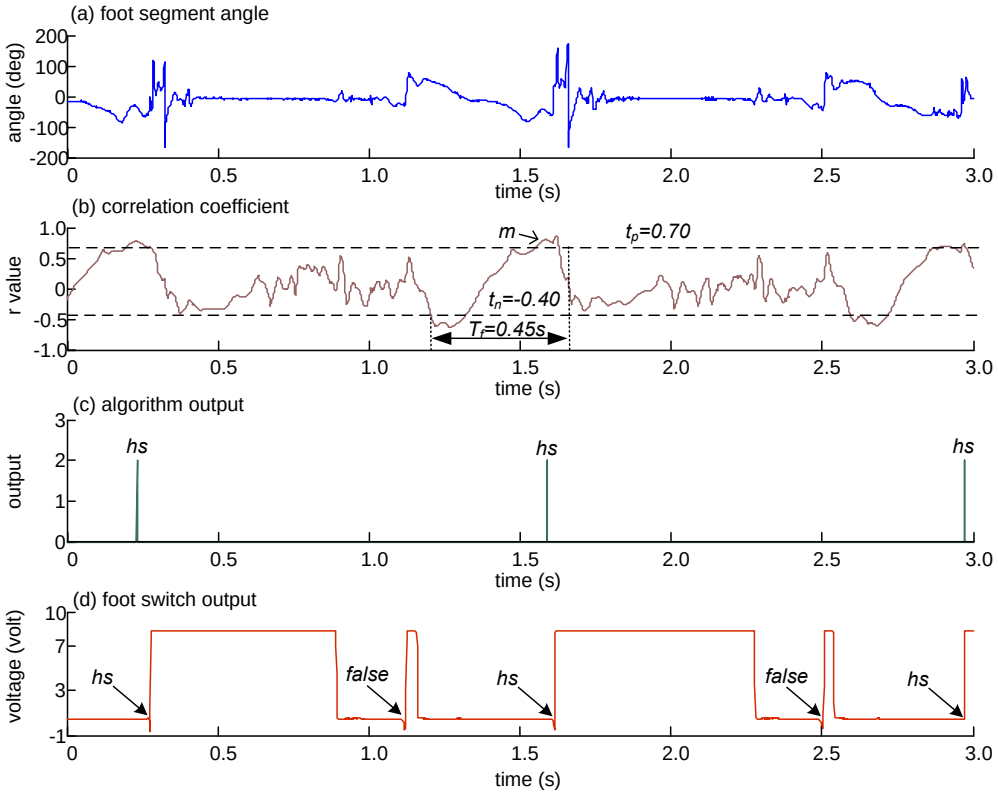

Figure J-20 Heel strike events in Subject 2 (left foot), n=3.

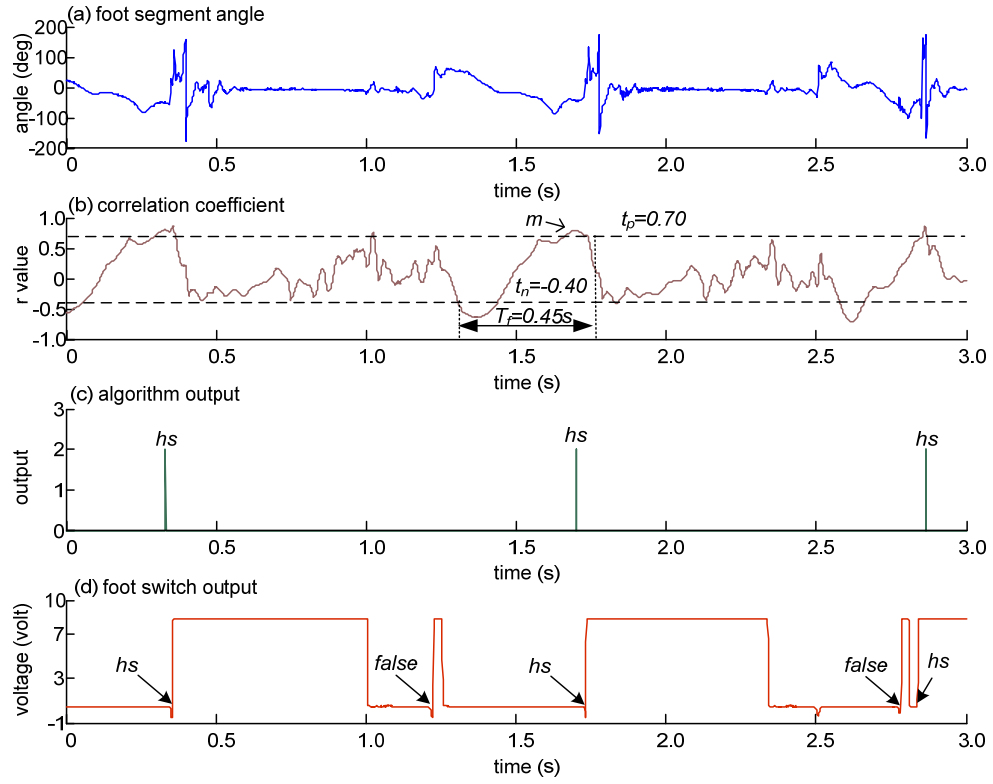

Figure J-21 Heel strike events in Subject 2 (left foot), n=3.

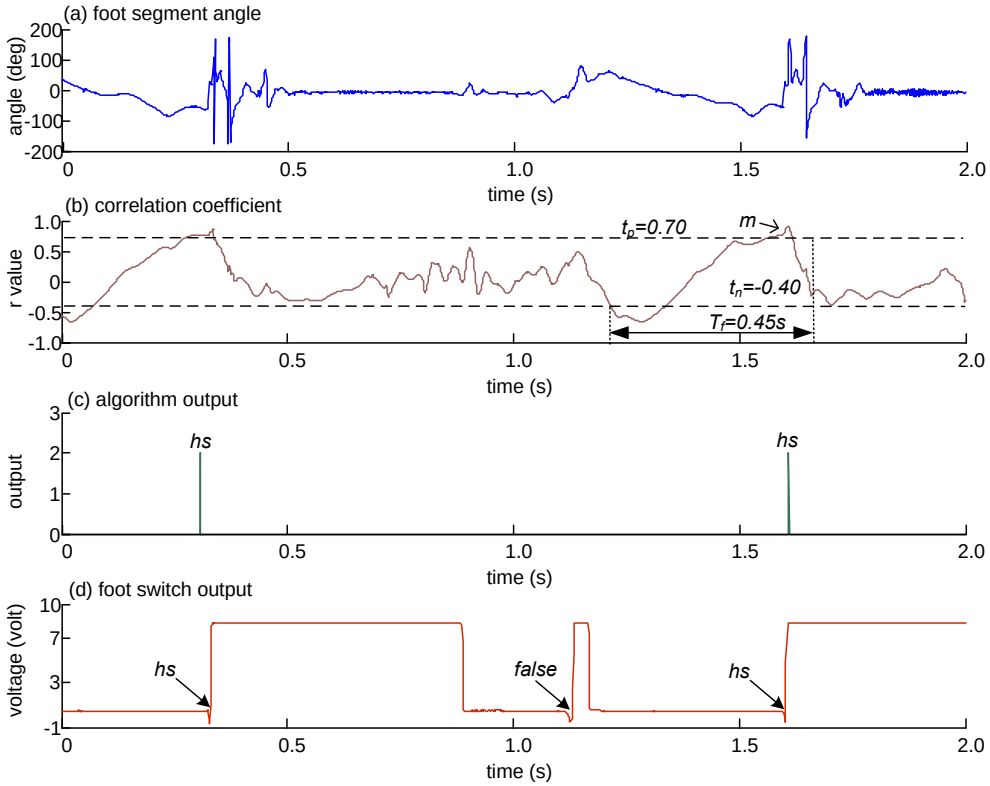

Figure J-22 Heel strike events in Subject 2 (left foot), n=2.

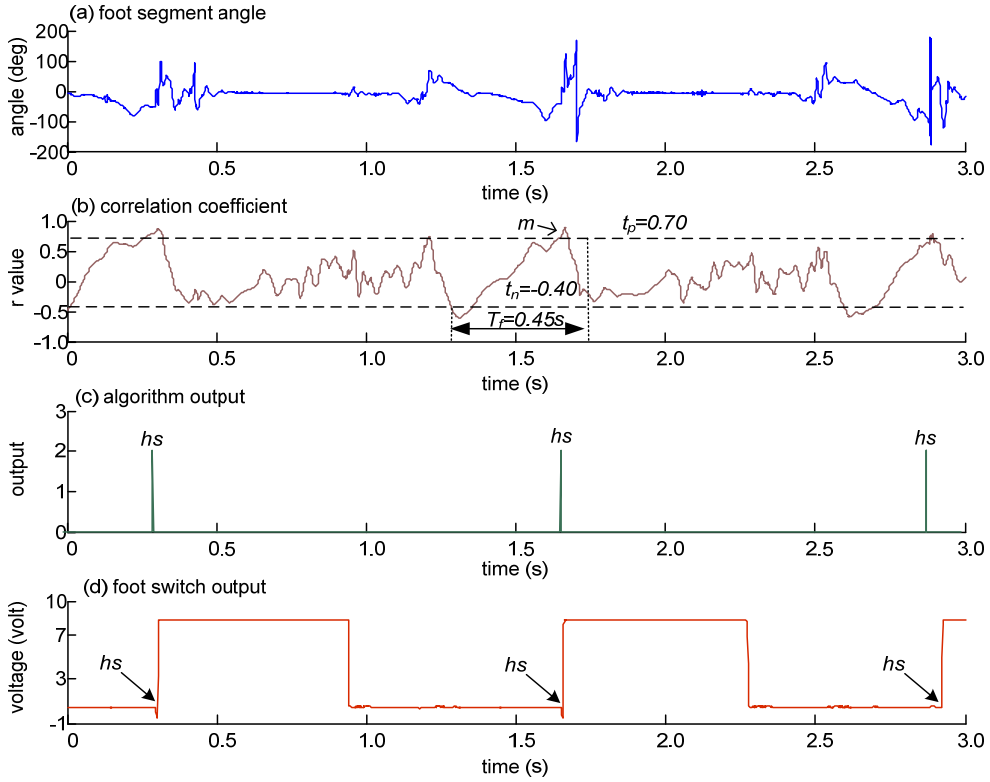

Figure J-23 Heel strike events in Subject 2 (left foot), n=3.

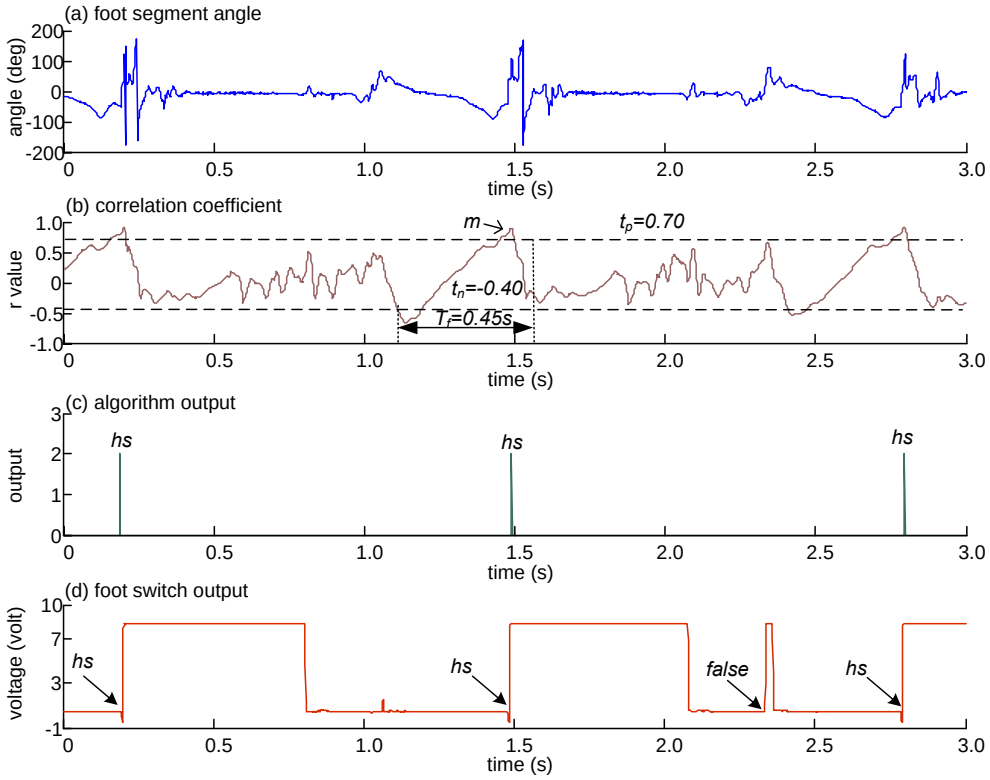

Figure J-24 Heel strike events in Subject 2 (left foot), n=3.

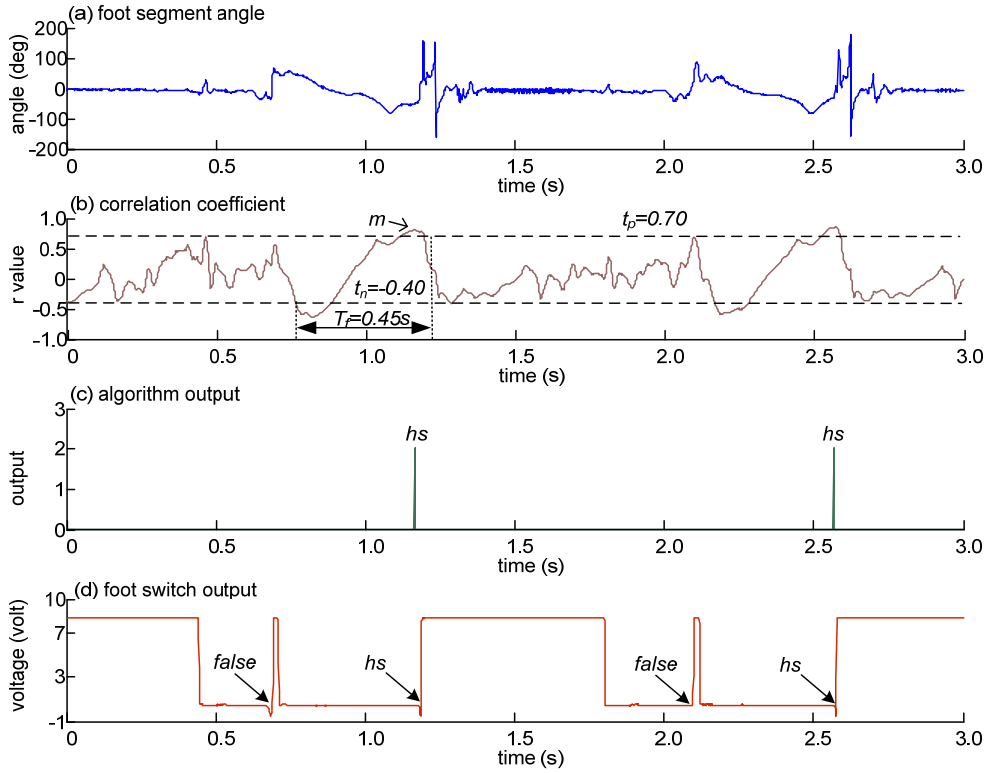

Figure J-25 Heel strike events in Subject 2 (left foot), n=2.

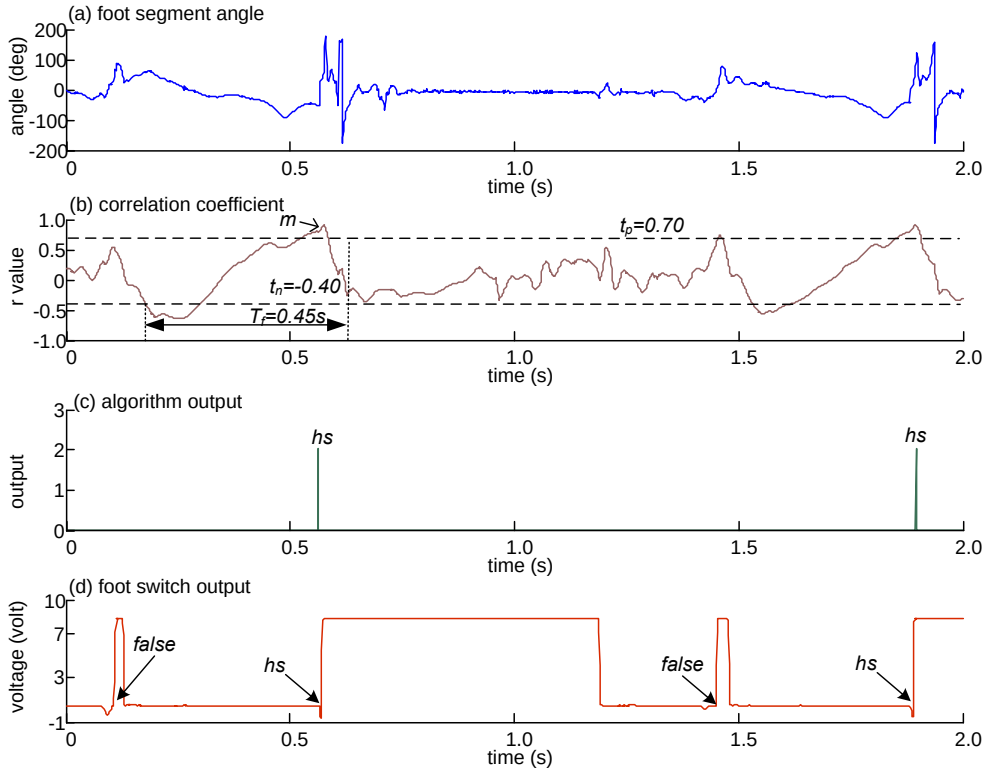

Figure J-26 Heel strike events in Subject 2 (left foot), n=2.

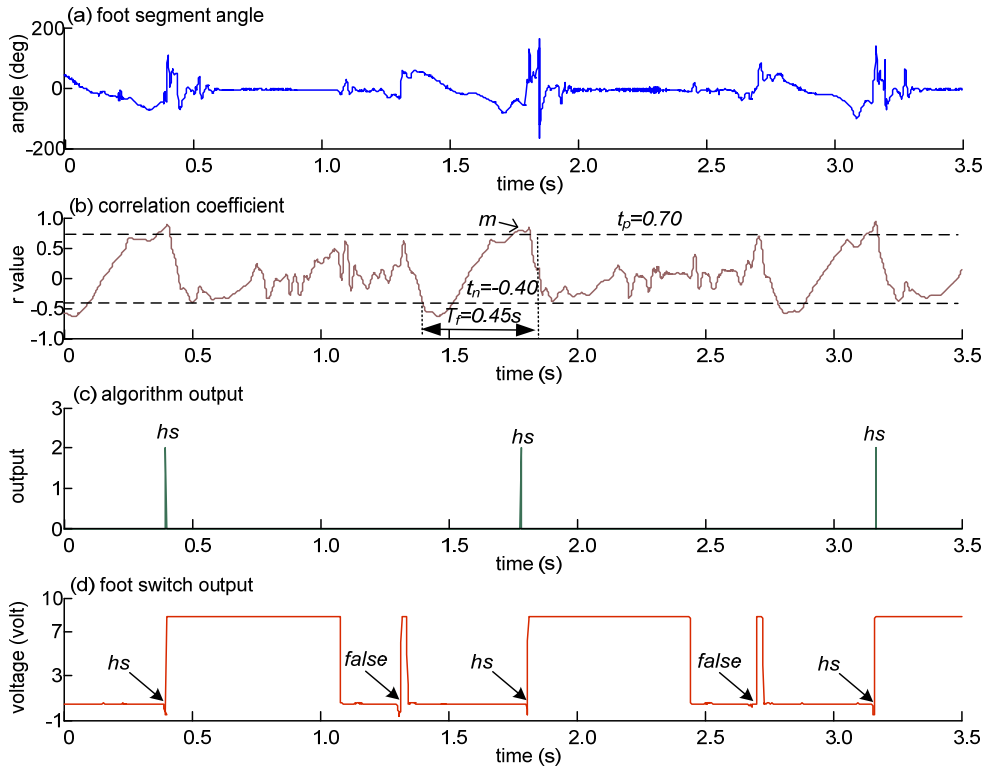

Figure J-27 Heel strike events in Subject 2 (left foot), n=3.

Figure J-28 to Figure J-38: Heel strike events in Subject 3 (right foot). (a) foot segment angle (b) correlation coefficient between foot segment angle and a sample window (t_p = positive threshold, t_n = negative threshold, T_f = time frame and m=first maximum point) (c) algorithm output (0=no event, 2=event detected and hs=heel strike) and (d) heel switch output.

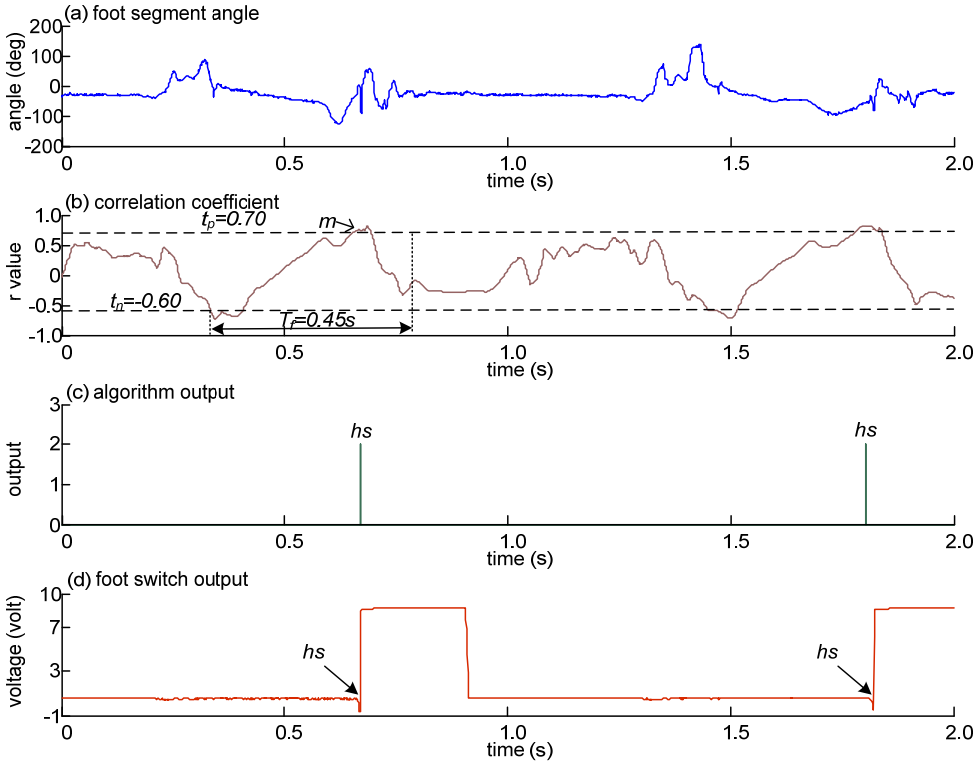

Figure J-28 Heel strike events in Subject 3 (right foot), n=2.

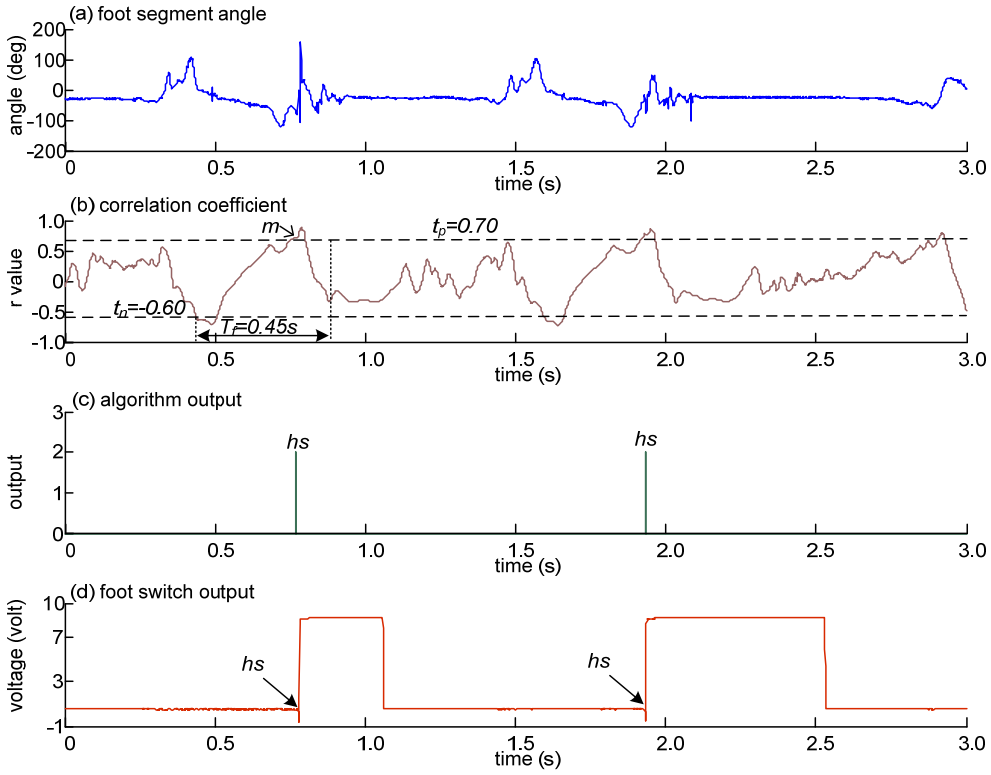

Figure J-29 Heel strike events in Subject 3 (right foot), n=2.

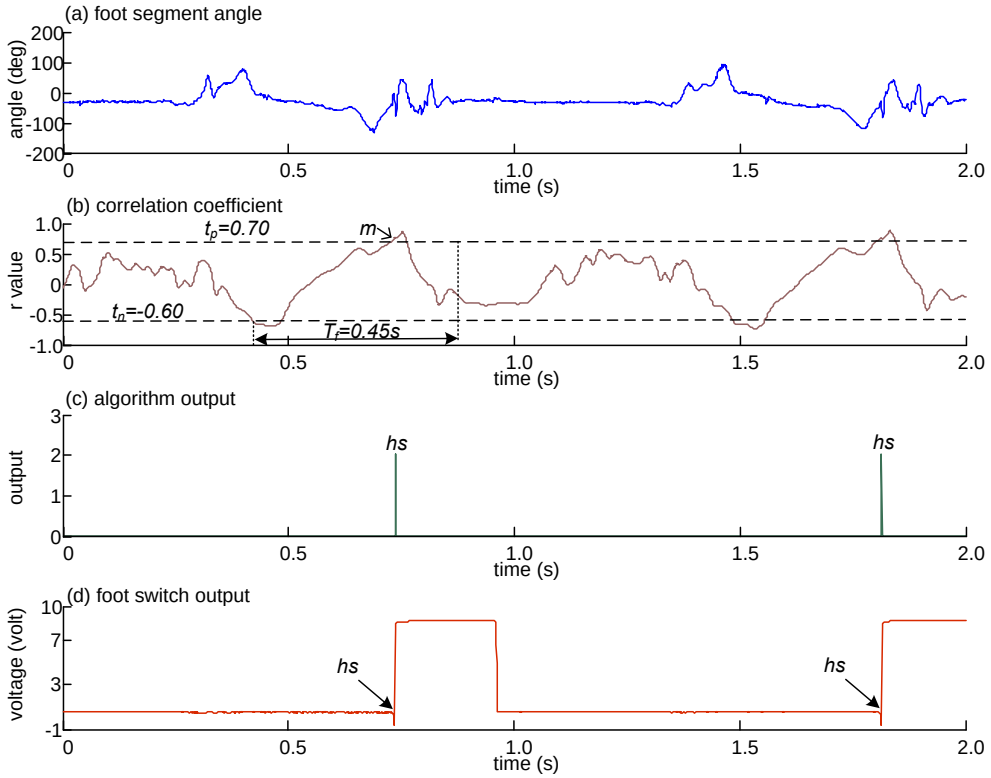

Figure J-30 Heel strike events in Subject 3 (right foot), n=2.

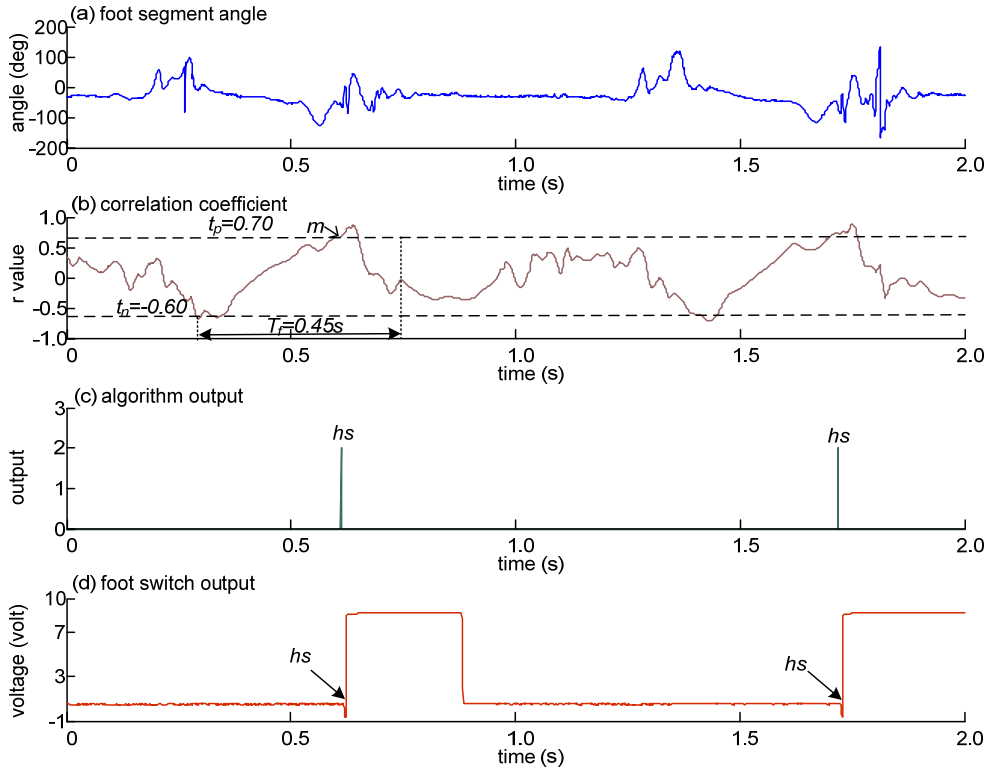

Figure J-31 Heel strike events in Subject 3 (right foot), n=2.

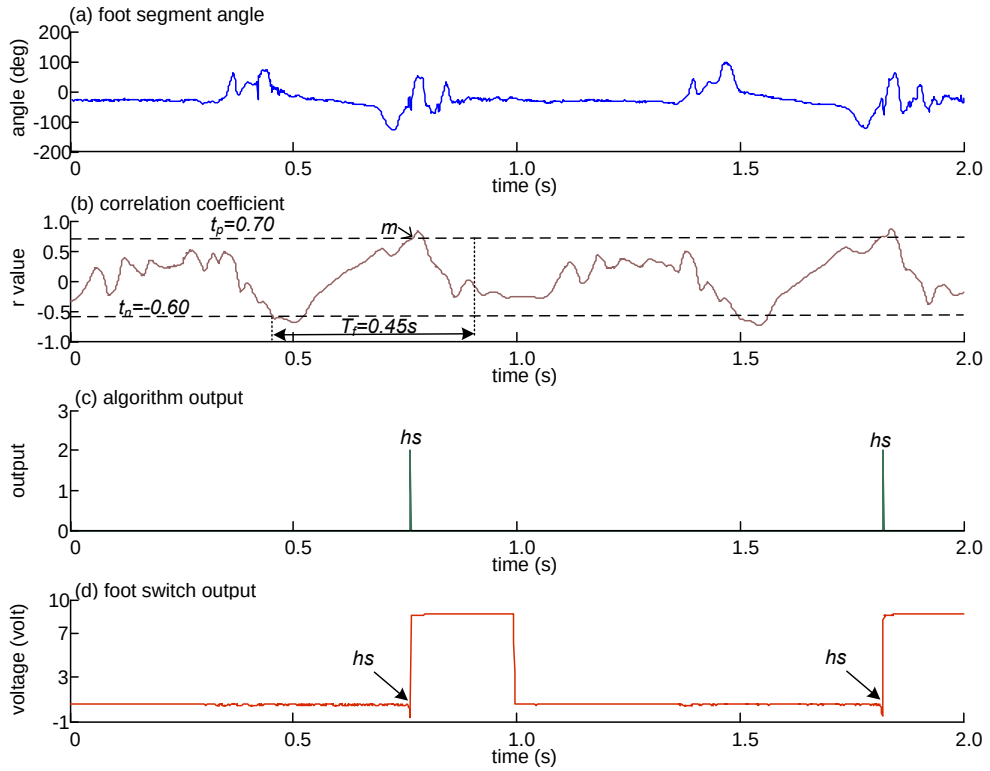

Figure J-32 Heel strike events in Subject 3 (right foot), n=2.

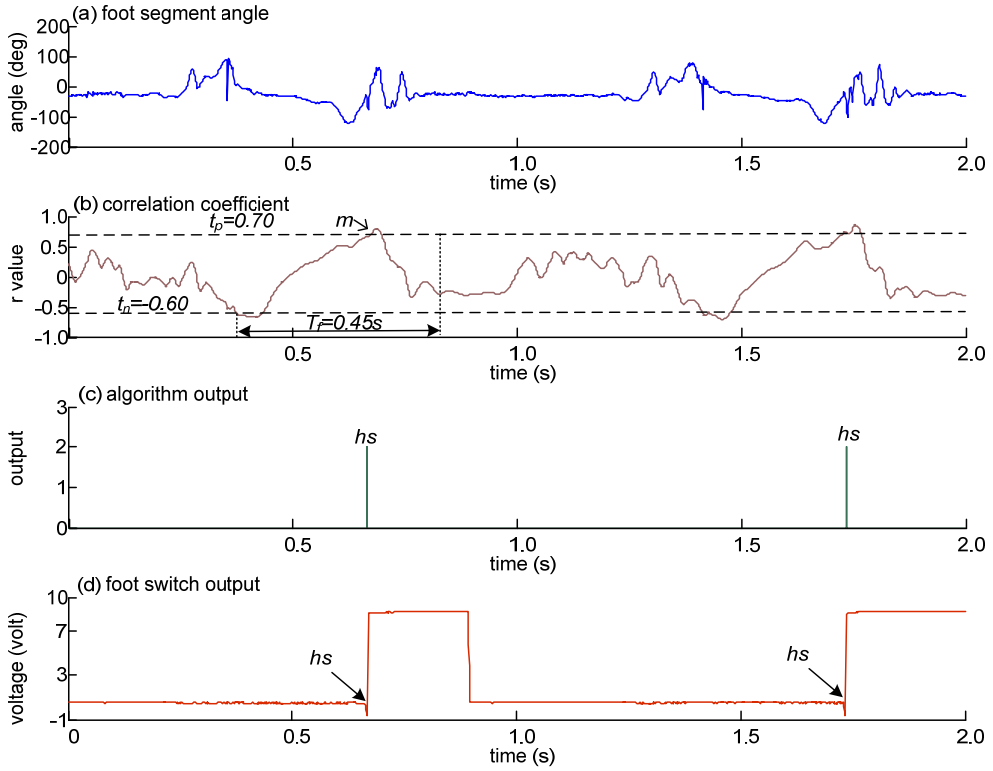

Figure J-33 Heel strike events in Subject 3 (right foot), n=2.

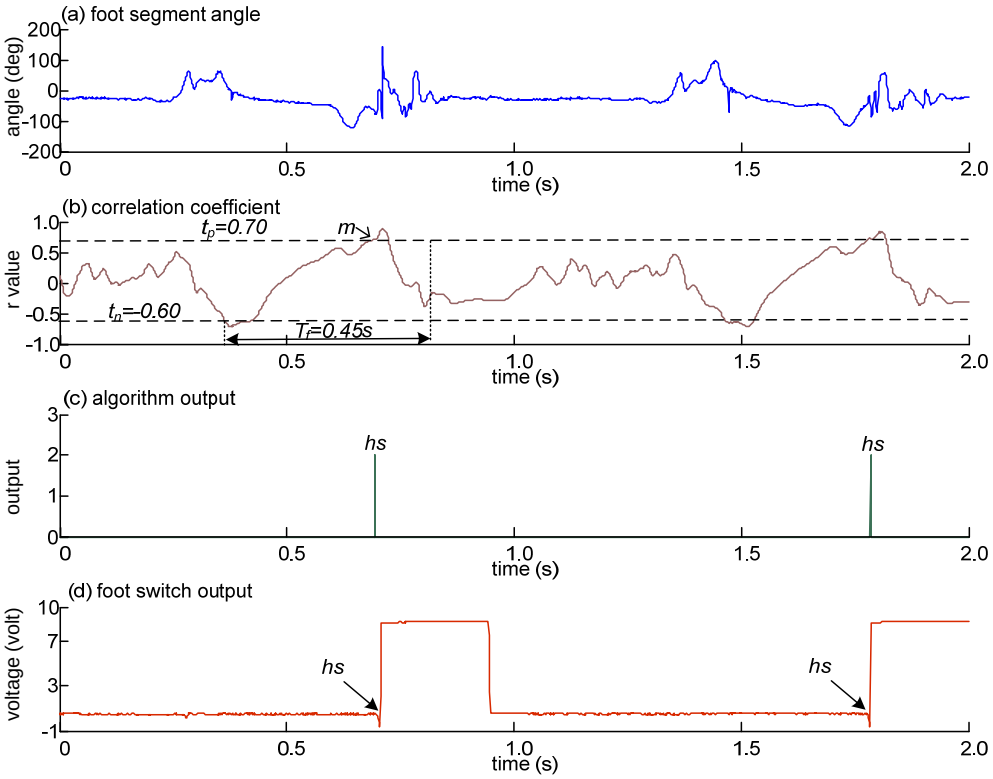

Figure J-34 Heel strike events in Subject 3 (right foot), n=2.

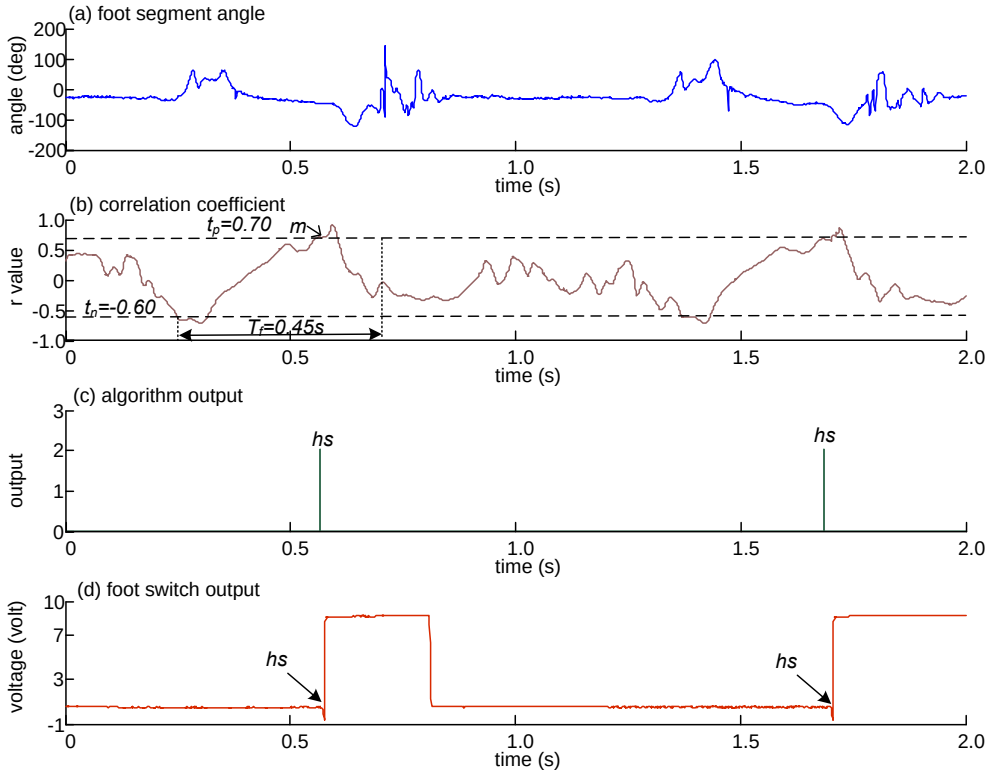

Figure J-35 Heel strike events in Subject 3 (right foot), n=2.

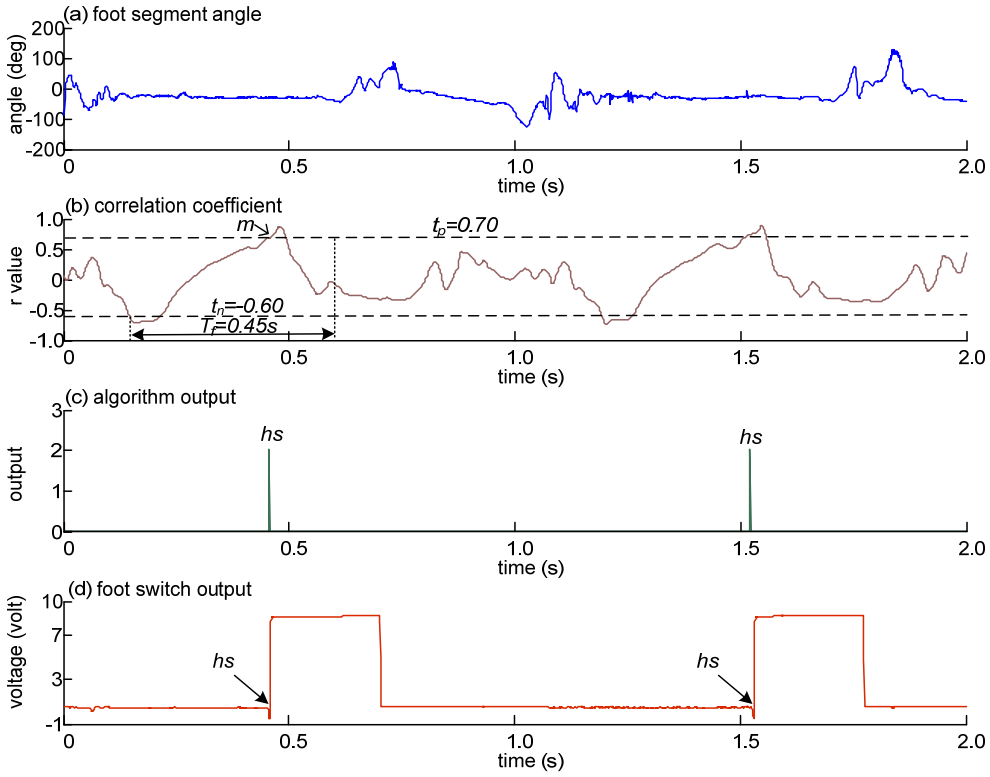

Figure J-36 Heel strike events in Subject 3 (right foot), n=2.

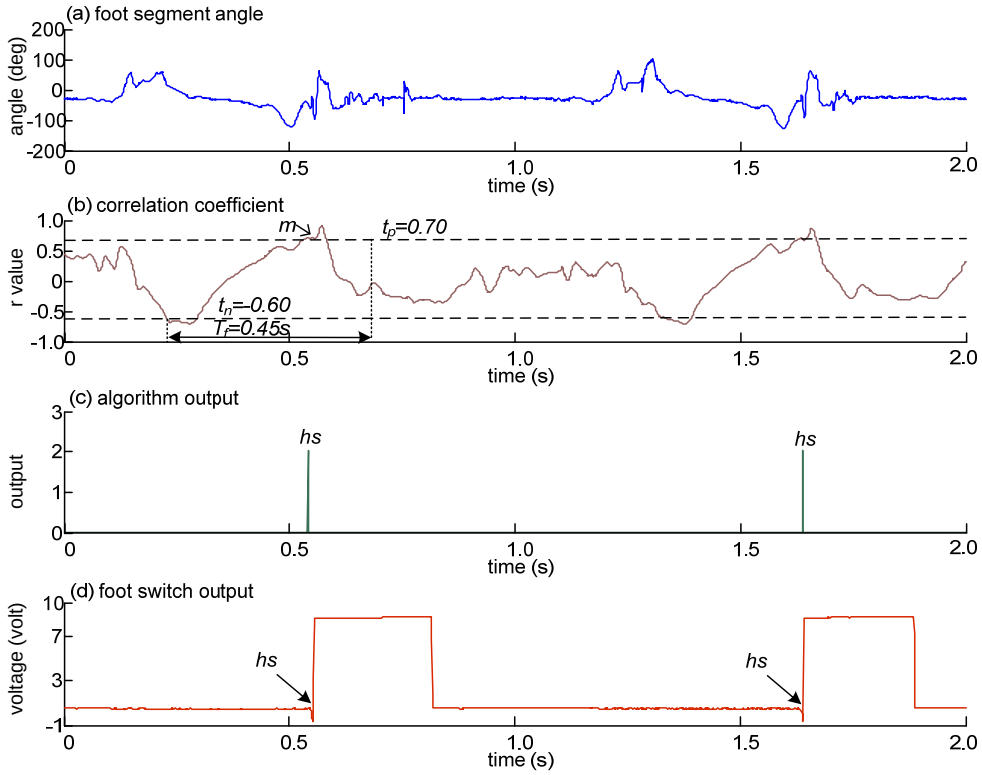

Figure J-37 Heel strike events in Subject 3 (right foot), n=2.

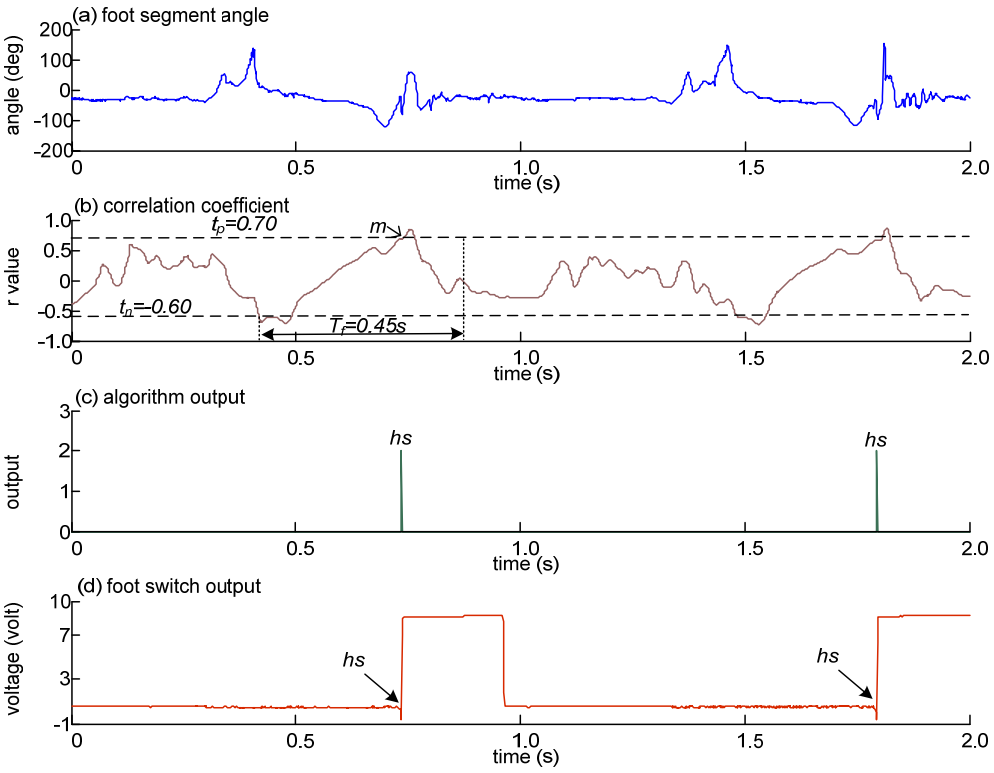

Figure J-38 Heel strike events in Subject 3 (right foot), n=2.

Figure J-39 to Figure J-42: Heel strike events in Subject 4 (right foot). (a) foot segment angle (b) correlation coefficient between foot segment angle and a sample window (t_p = positive threshold, t_n = negative threshold, T_f = time frame and m=first maximum point) (c) algorithm output (0=no event, 2=event detected and hs=heel strike) and (d) heel switch output.

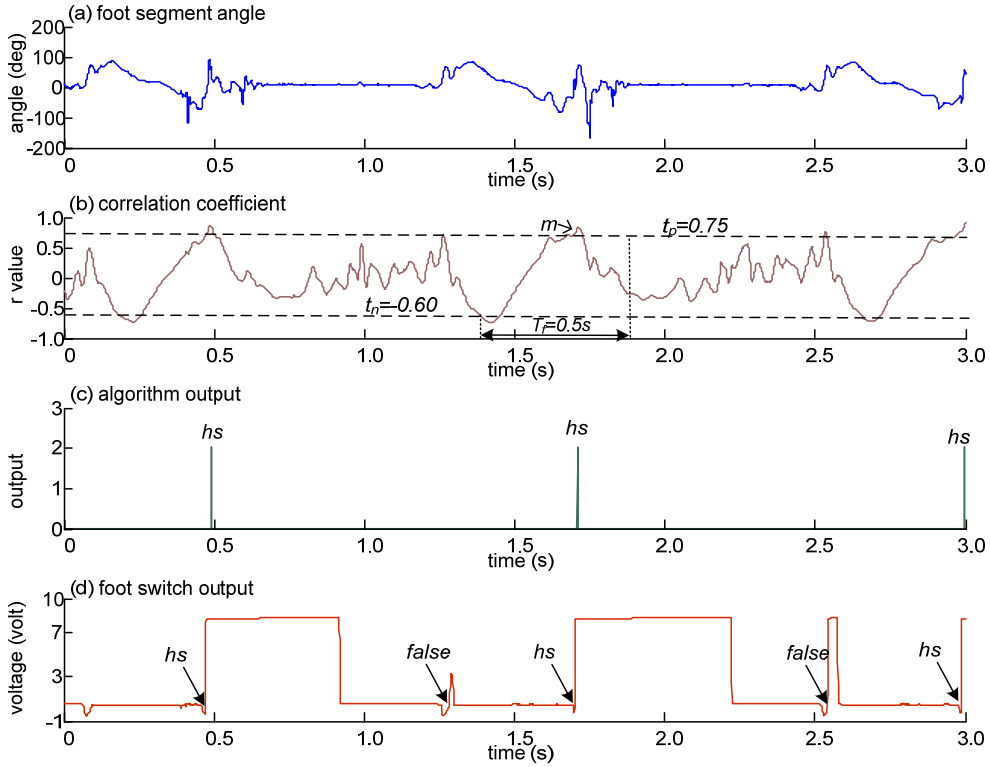

Figure J-39 Heel strike events in Subject 4 (right foot), n=3.

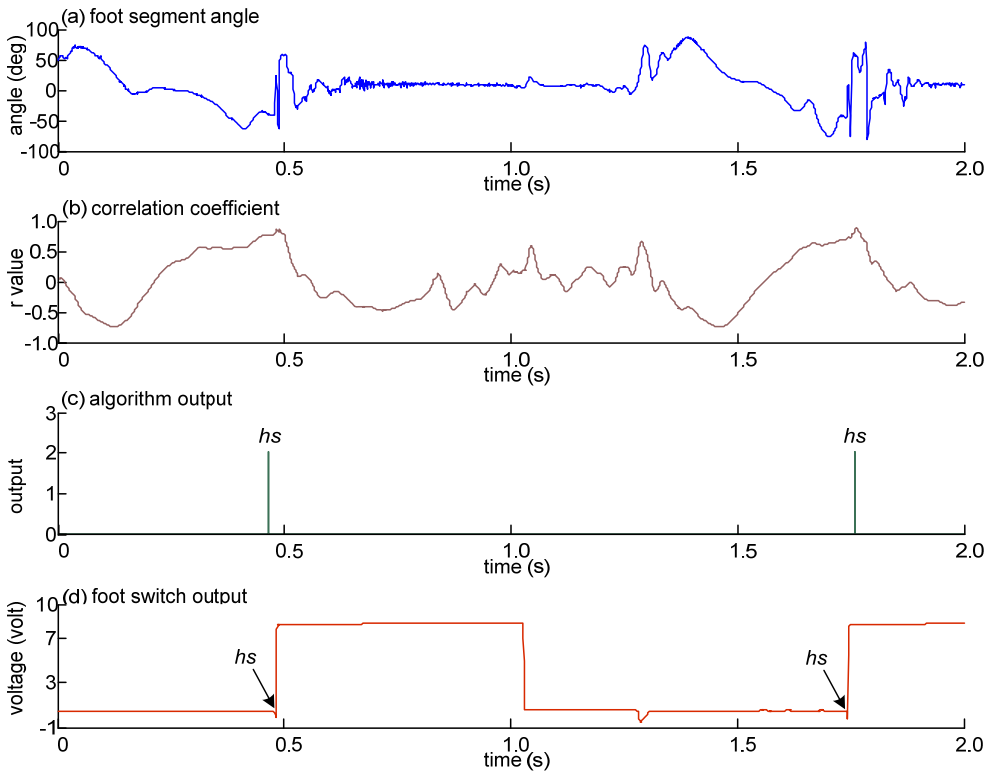

Figure J-40 Heel strike events in Subject 4 (right foot), n=2.

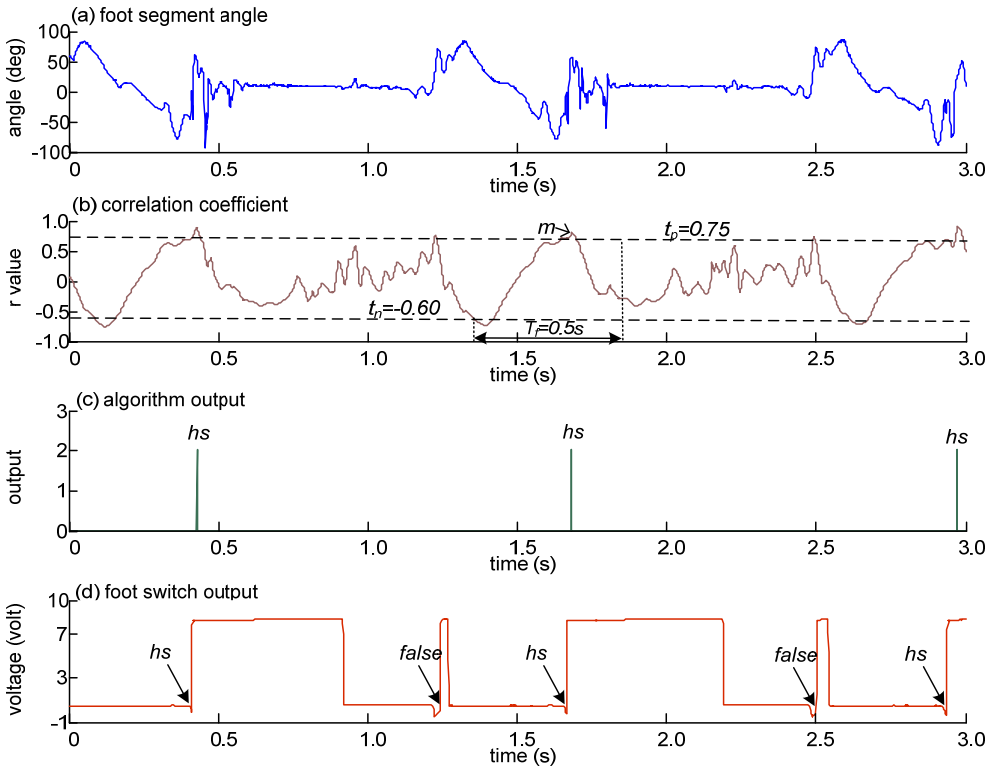

Figure J-41 Heel strike events in Subject 4 (right foot), n=3.

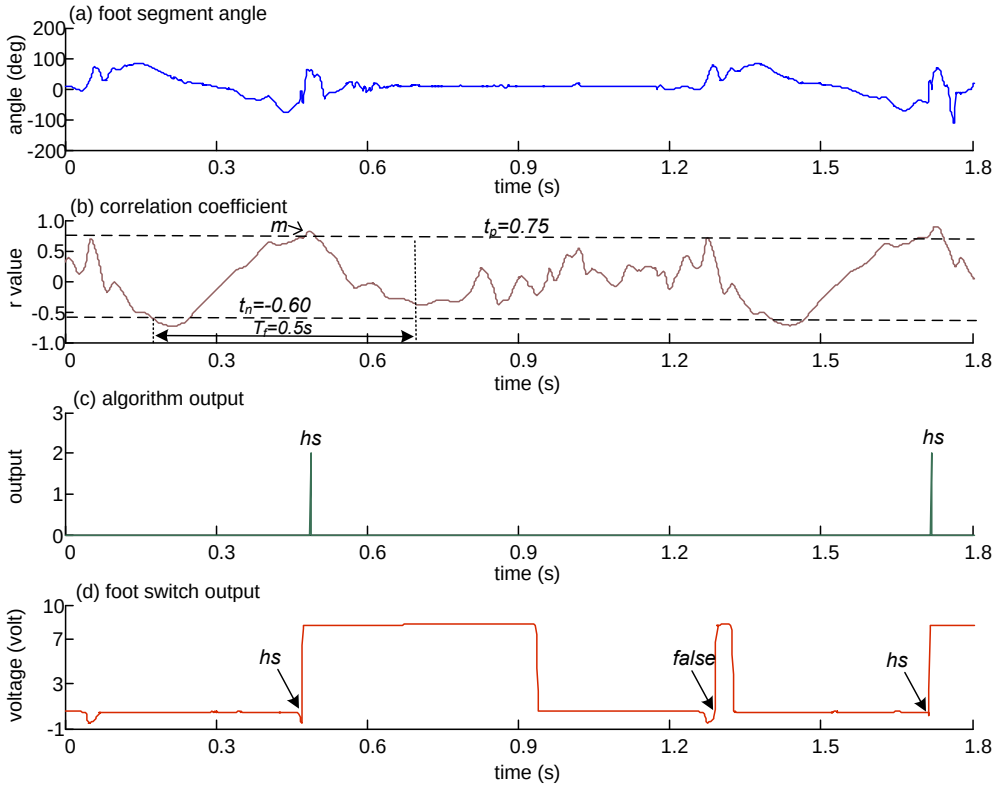

Figure J-42 Heel strike events in Subject 4 (right foot), n=2.

Figure J-43 to Figure J-47: Heel strike events in Subject 4 (left foot). (a) foot segment angle (b) correlation coefficient between foot segment angle and a sample window (t_p = positive threshold, t_n = negative threshold, T_f= time frame and m=first maximum point) (c) algorithm output (0=no event, 2=event detected and hs=heel strike) and (d) heel switch output.

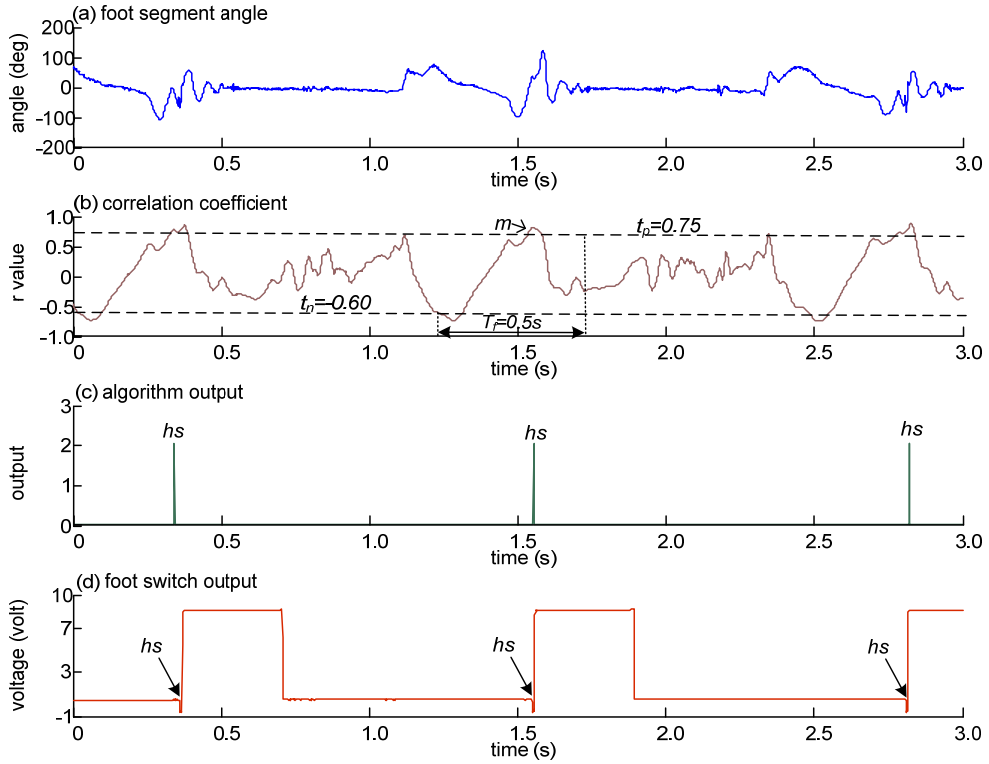

Figure J-43 Heel strike events in Subject 4 (left foot), n=3.

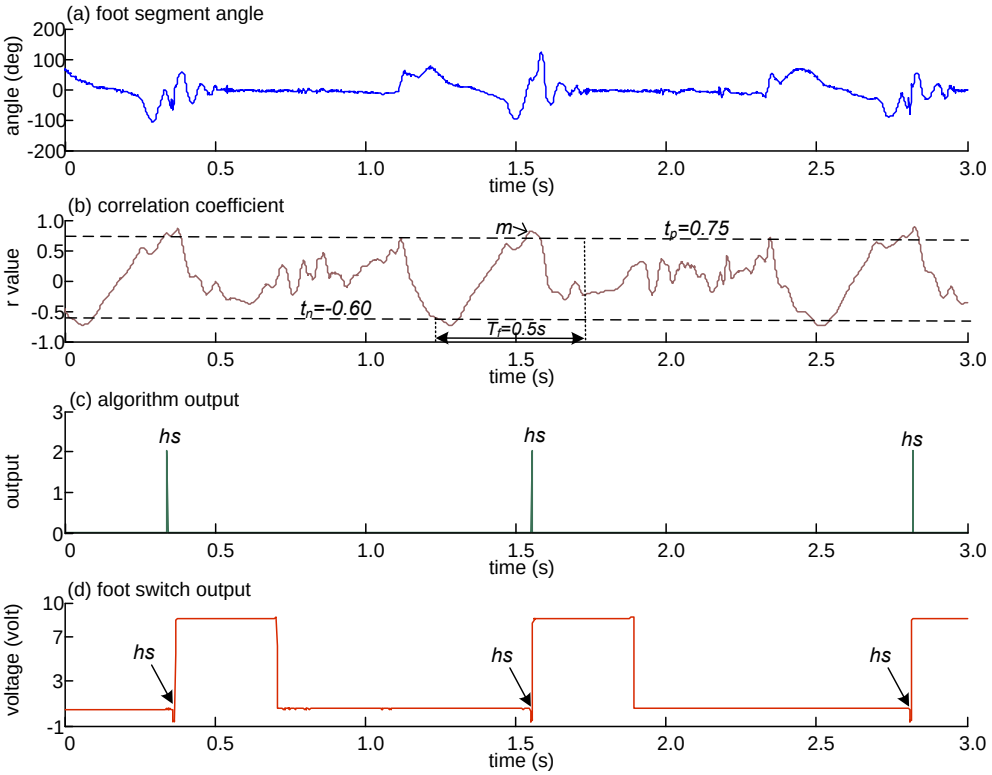

Figure J-44 Heel strike events in Subject 4 (left foot), n=3.

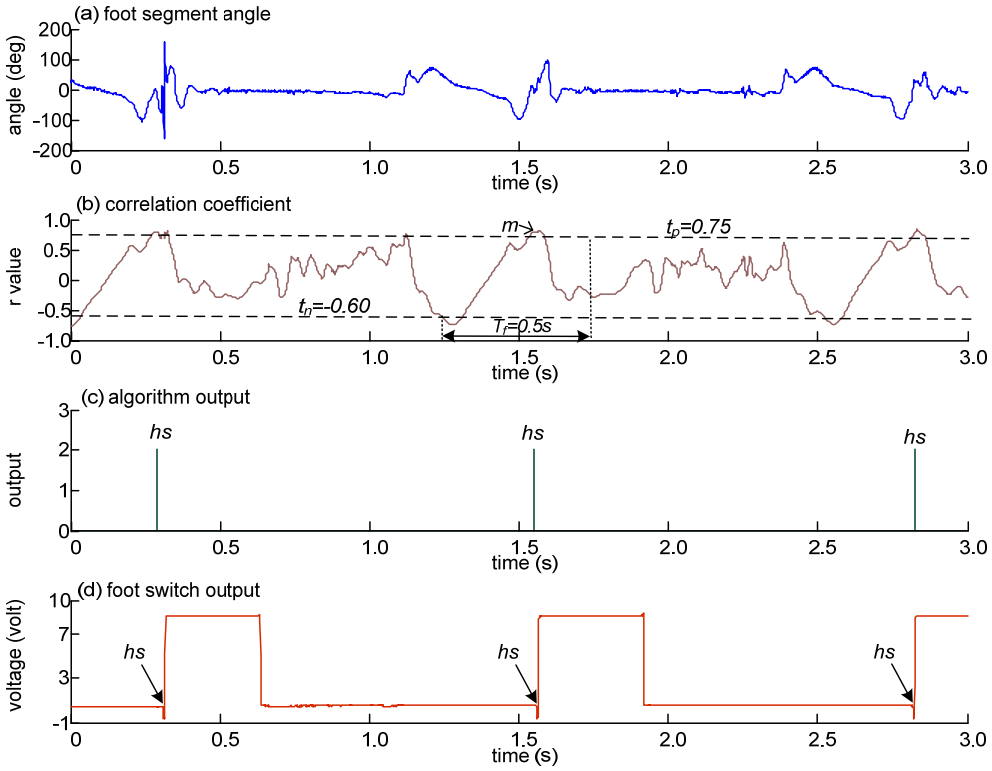

Figure J-45 Heel strike events in Subject 4 (left foot), n=3.

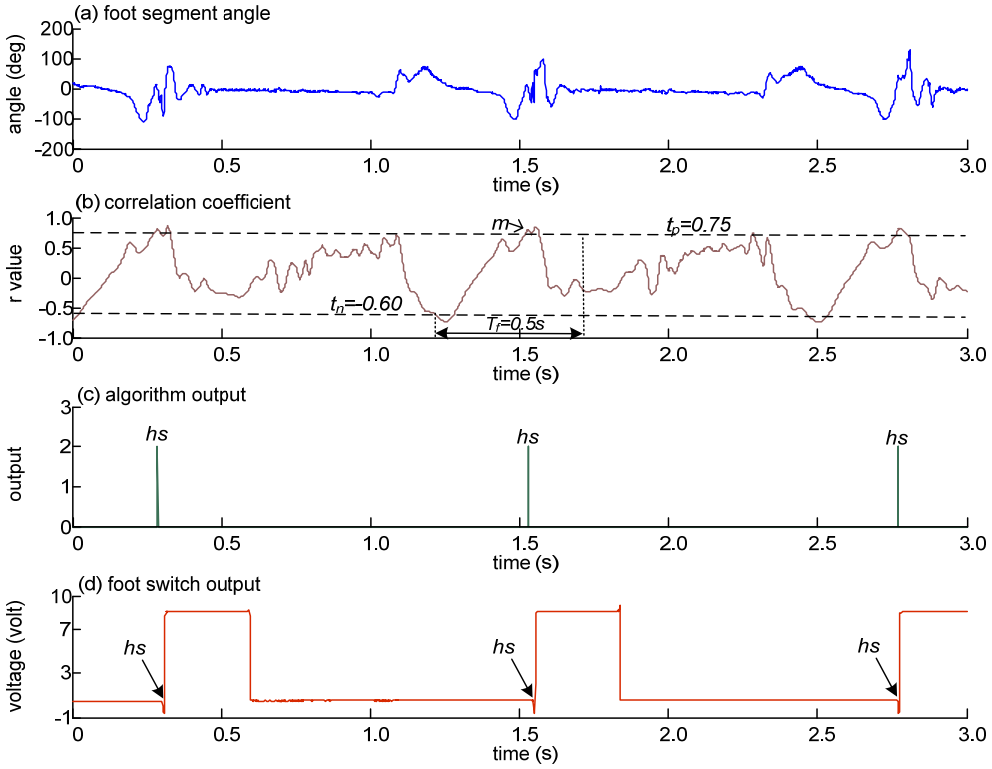

Figure J-46 Heel strike events in Subject 4 (left foot), n=3.

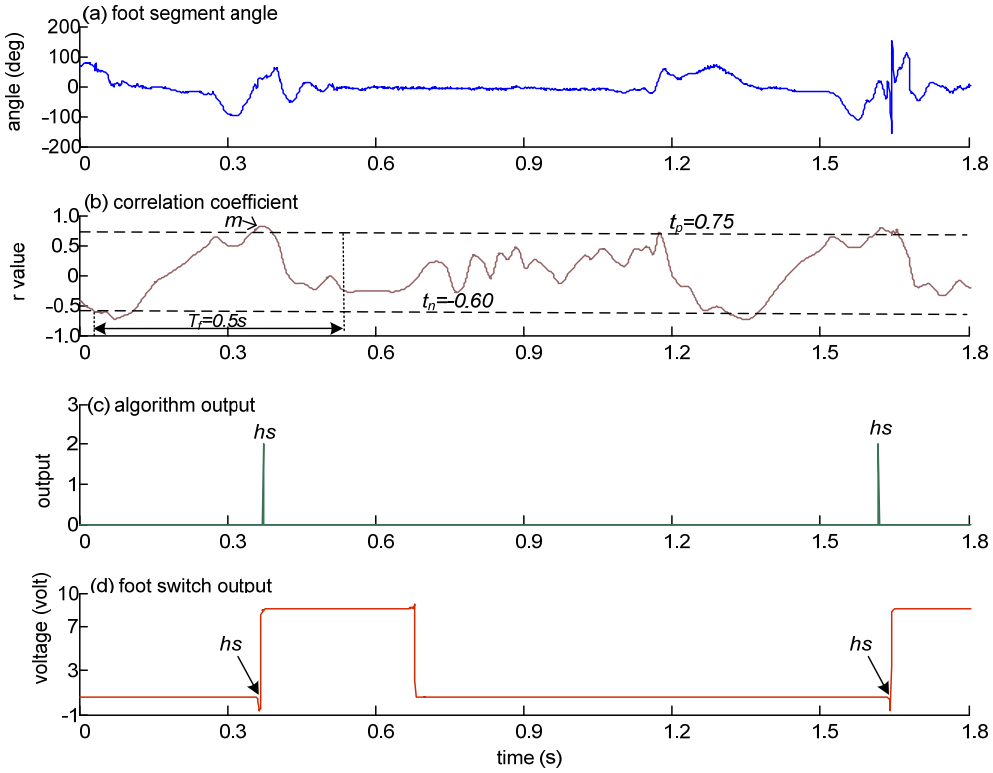

Figure J-47 Heel strike events in Subject 4 (left foot), n=2.

Figure J-48 to Figure J-52: Heel strike events in Subject 5 (right foot). (a) foot segment angle (b) correlation coefficient between foot segment angle and a sample window (t_p = positive threshold, t_n = negative threshold, T_f = time frame and m=first maximum point) (c) algorithm output (0=no event, 2=event detected and hs=heel strike) and (d) heel switch output.

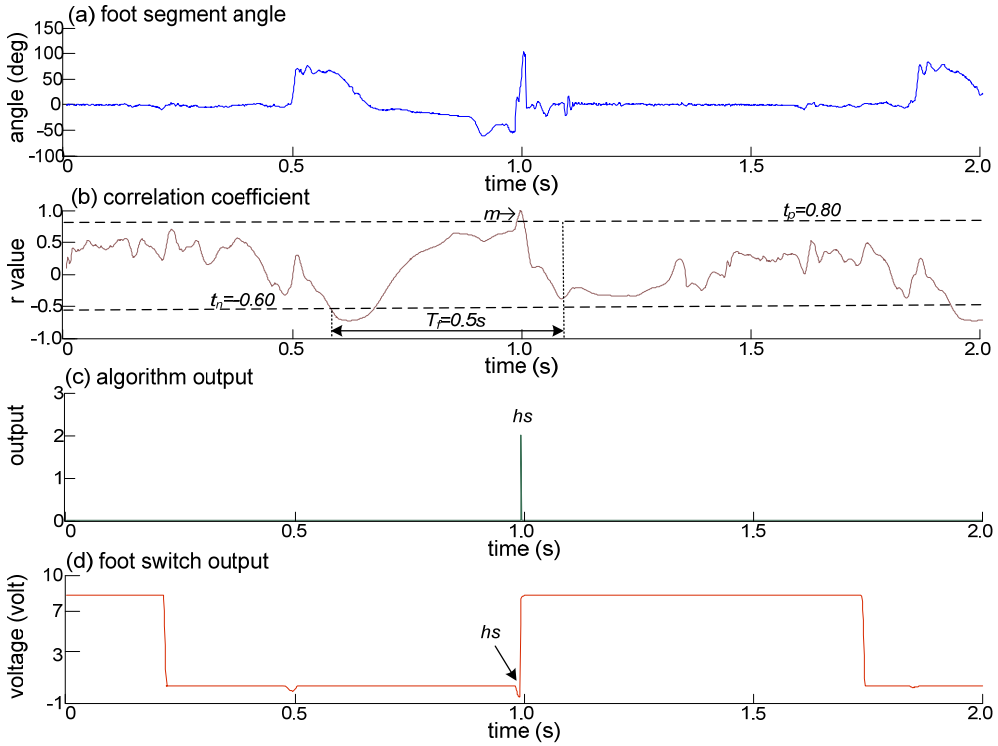

Figure J-48 Heel strike events in Subject 5 (right foot), n=1.

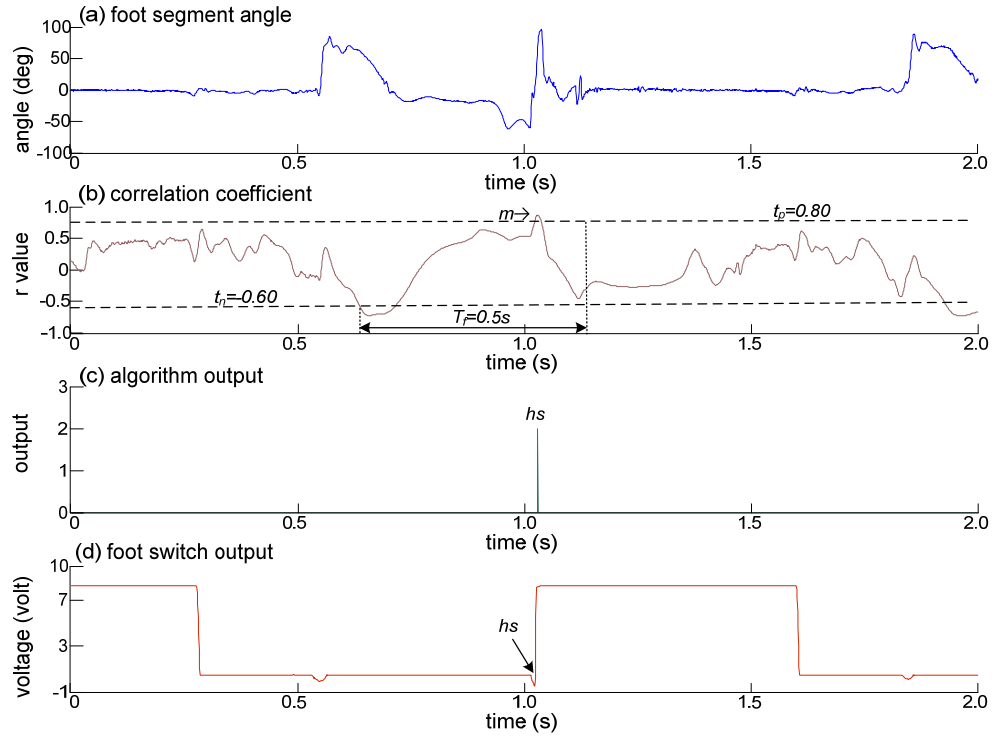

Figure J-49 Heel strike events in Subject 5 (right foot), n=1.

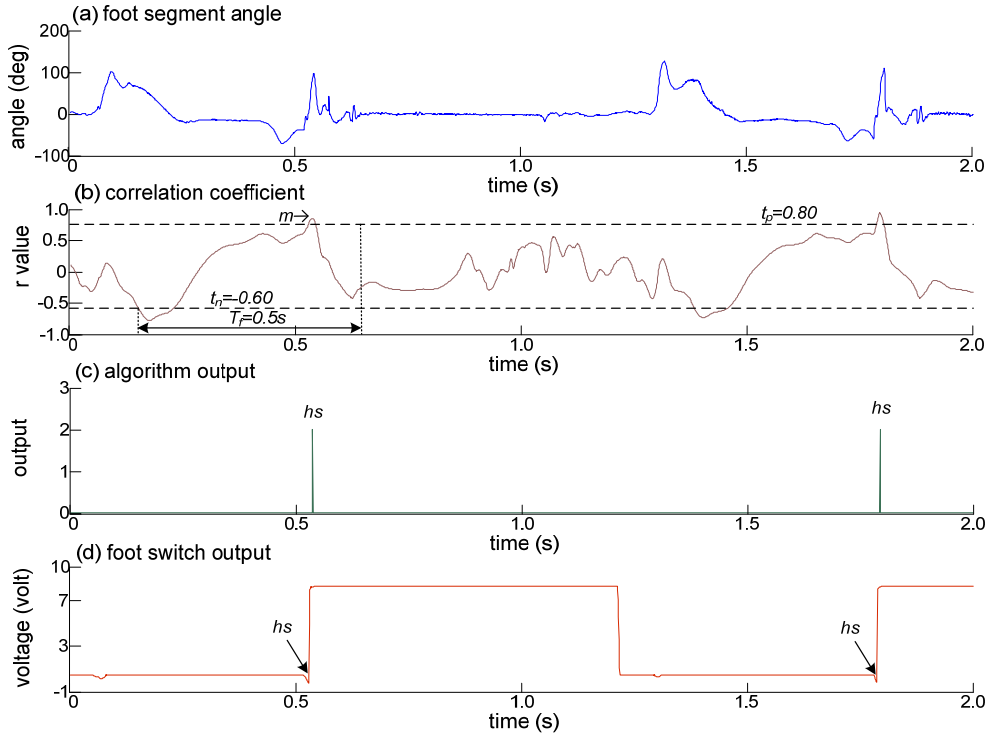

Figure J-50 Heel strike events in Subject 5 (right foot), n=2.

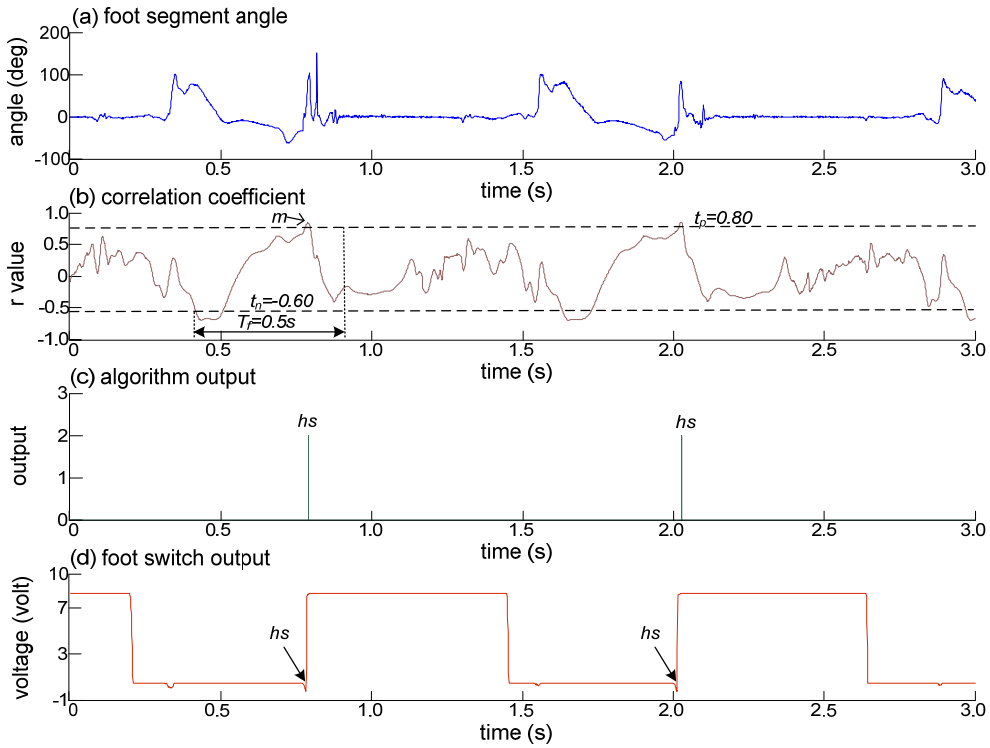

Figure J-51 Heel strike events in Subject 5 (right foot), n=2.

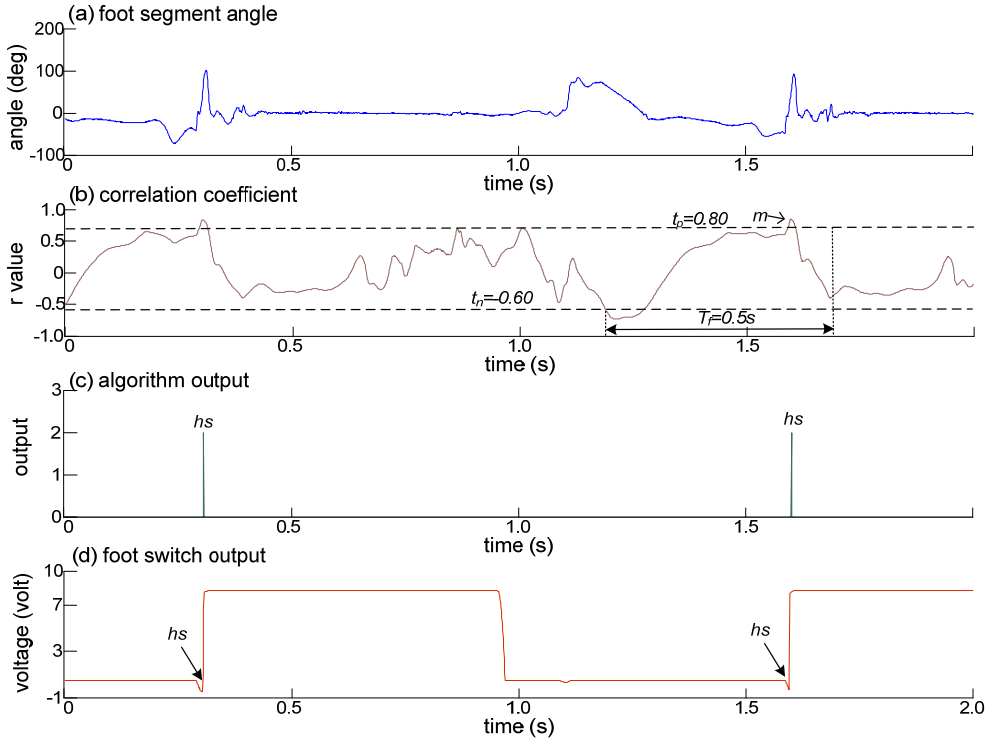

Figure J-52 Heel strike events in Subject 5 (right foot), n=2.

Figure J-53 to Figure J-58: Heel strike events in Subject 5 (left foot). (a) foot segment angle (b) correlation coefficient between foot segment angle and a sample window (t_p = positive threshold, t_n = negative threshold, T_f = time frame and m=first maximum point) (c) algorithm output (0=no event, 2=event detected and hs=heel strike) and (d) heel switch output.

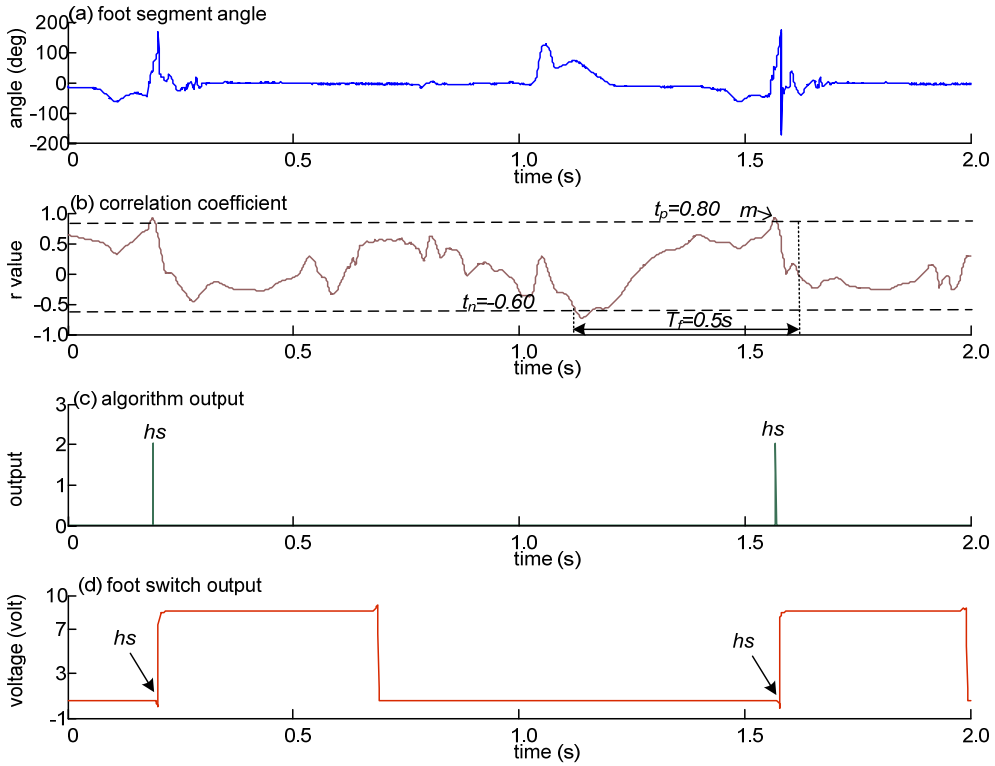

Figure J-53 Heel strike events in Subject 5 (left foot), n=2.

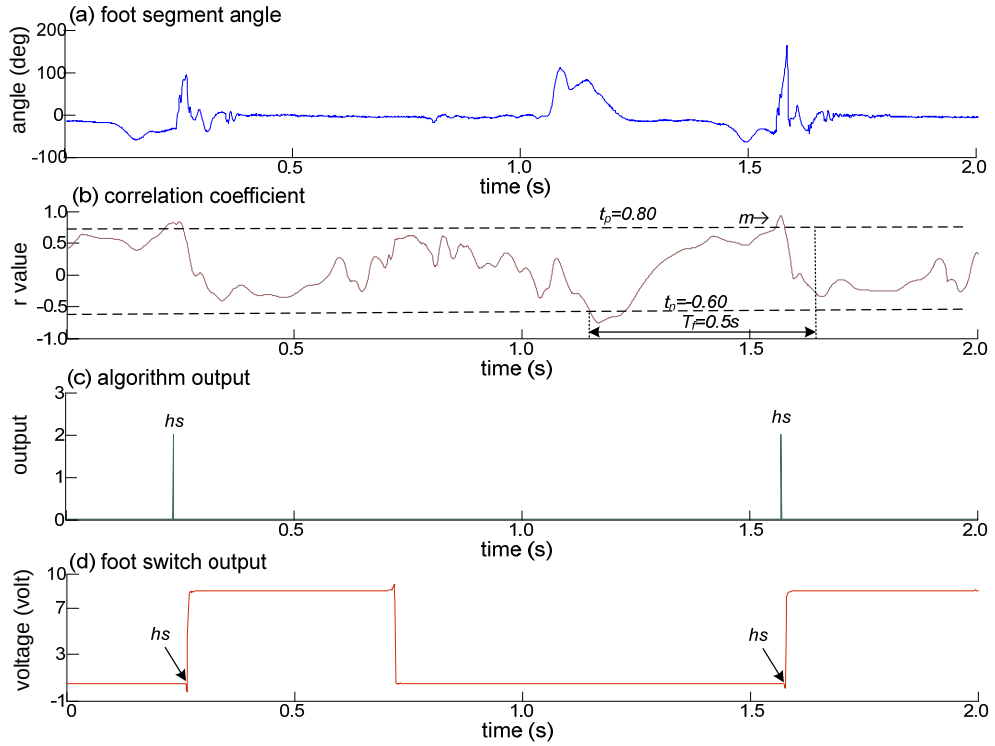

Figure J-54 Heel strike events in Subject 5 (left foot), n=2.

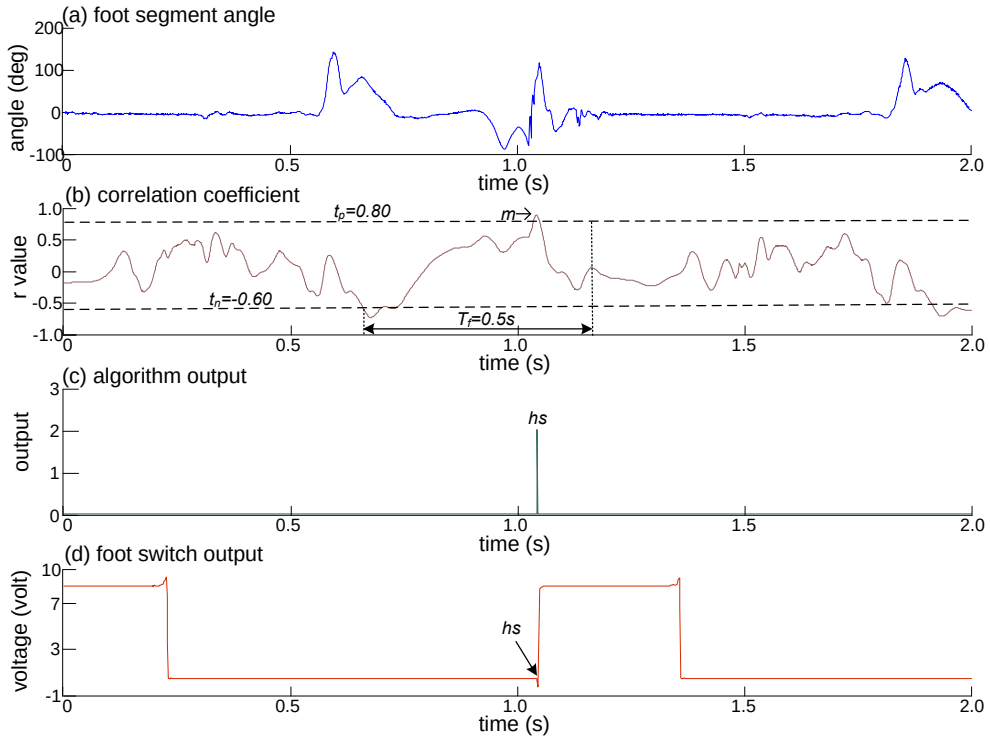

Figure J-55 Heel strike events in Subject 5 (left foot), n=1.

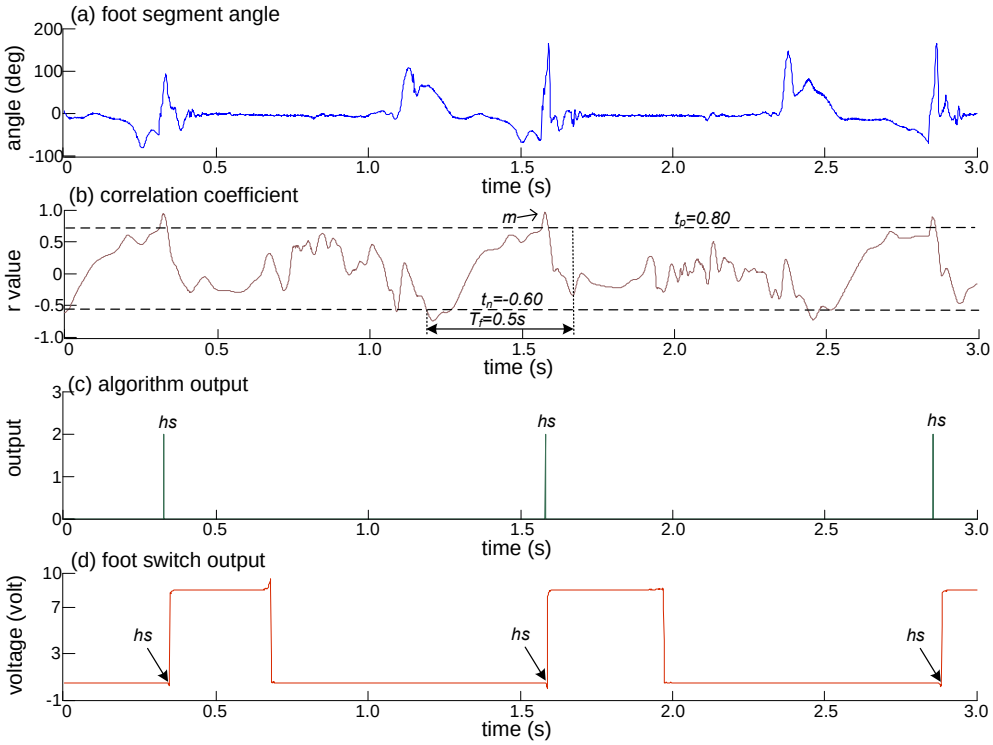

Figure J-56 Heel strike events in Subject 5 (left foot), n=3.

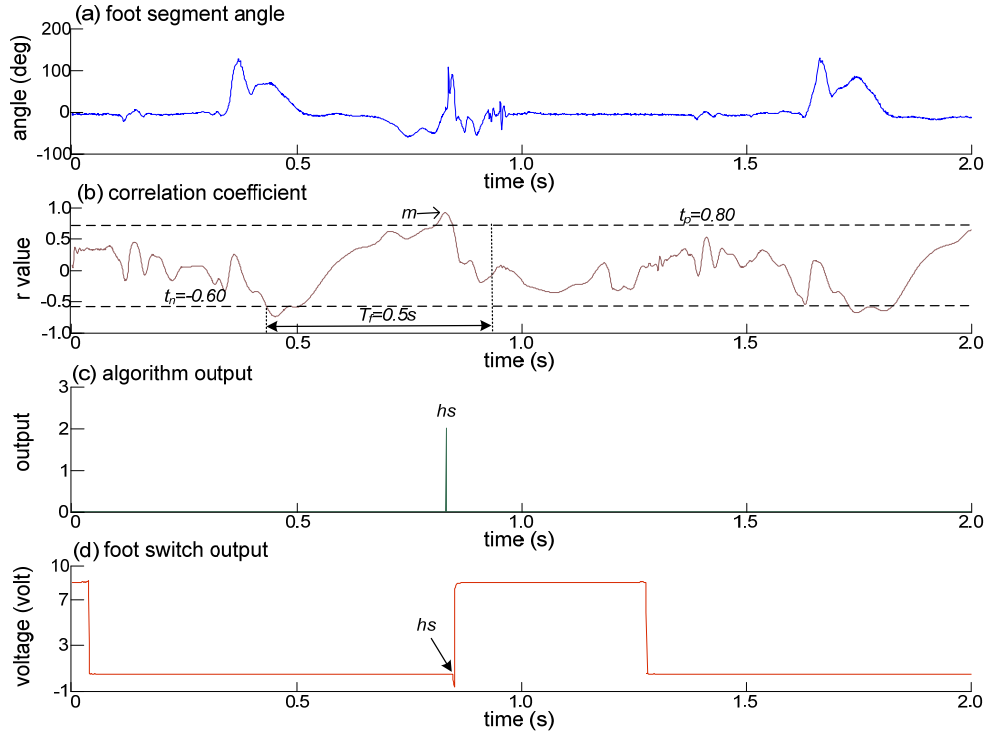

Figure J-57 Heel strike events in Subject 5 (left foot), n=1.

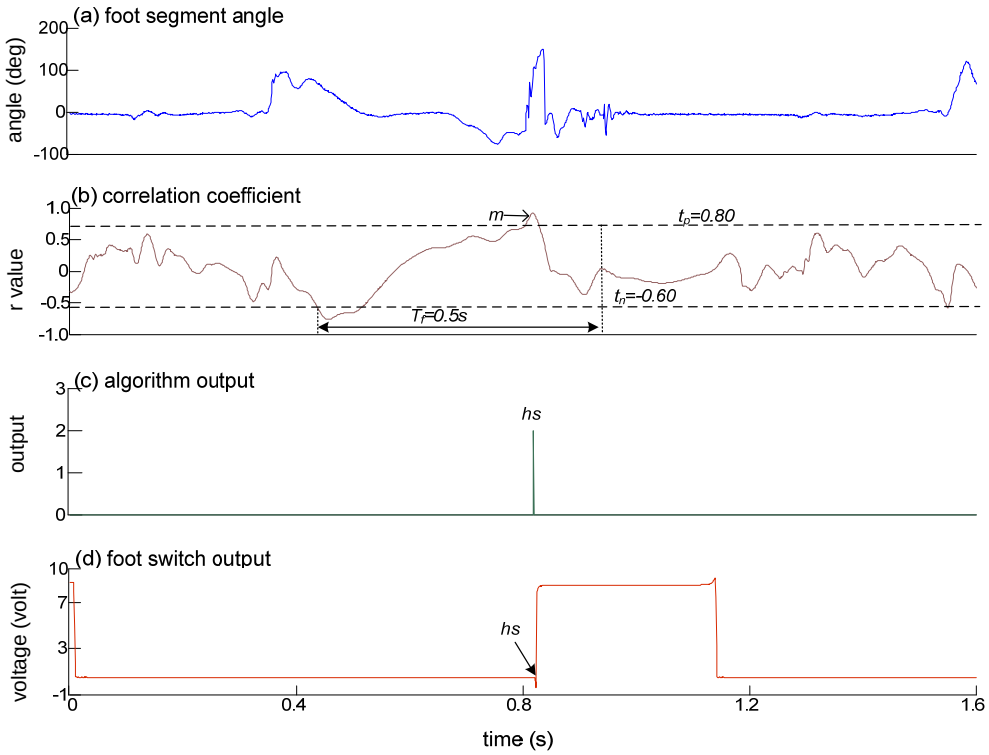

Figure J-58 Heel strike events in Subject 5 (left foot), n=1.

Appendix K

Results for the tibial vertical events detection in healthy subjects.

Figure K-1 to Figure K-10: Tibial vertical events in Subject 1 (right foot). (a) foot segment angle (b) correlation coefficient between foot segment angle and a sample window (t_p = positive threshold, t_n = negative threshold, T_f = time frame and m=first maximum point) (c) algorithm output (0=no event, 2=event detected and hs=heel strike) and (d) heel switch output.

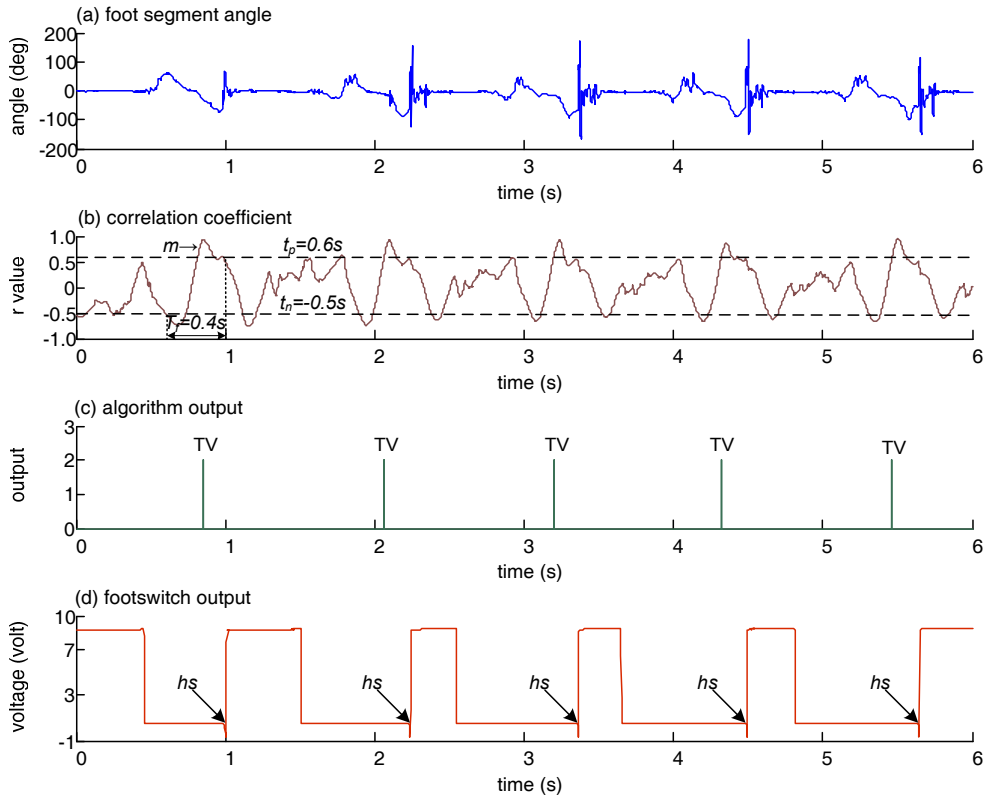

Figure K-1 Tibial vertical events in Subject 1 (right foot), n=5.

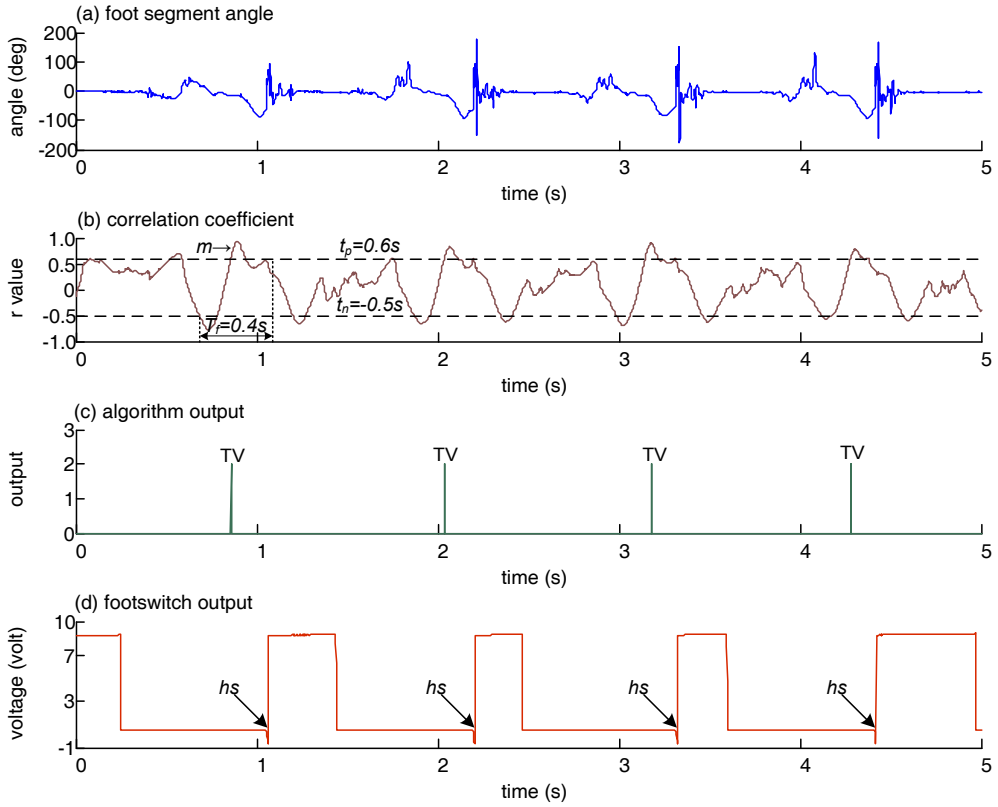

Figure K-2 Tibial vertical events in Subject 1 (right foot), n=4.

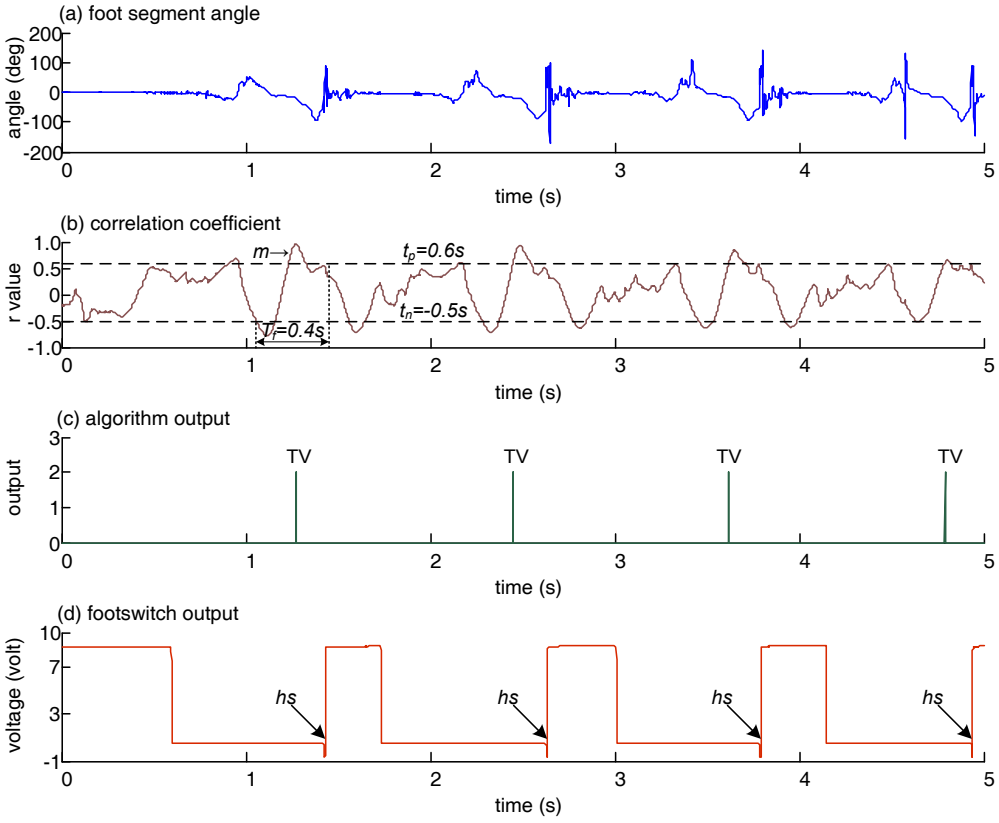

Figure K-3 Tibial vertical events in Subject 1 (right foot), n=4.

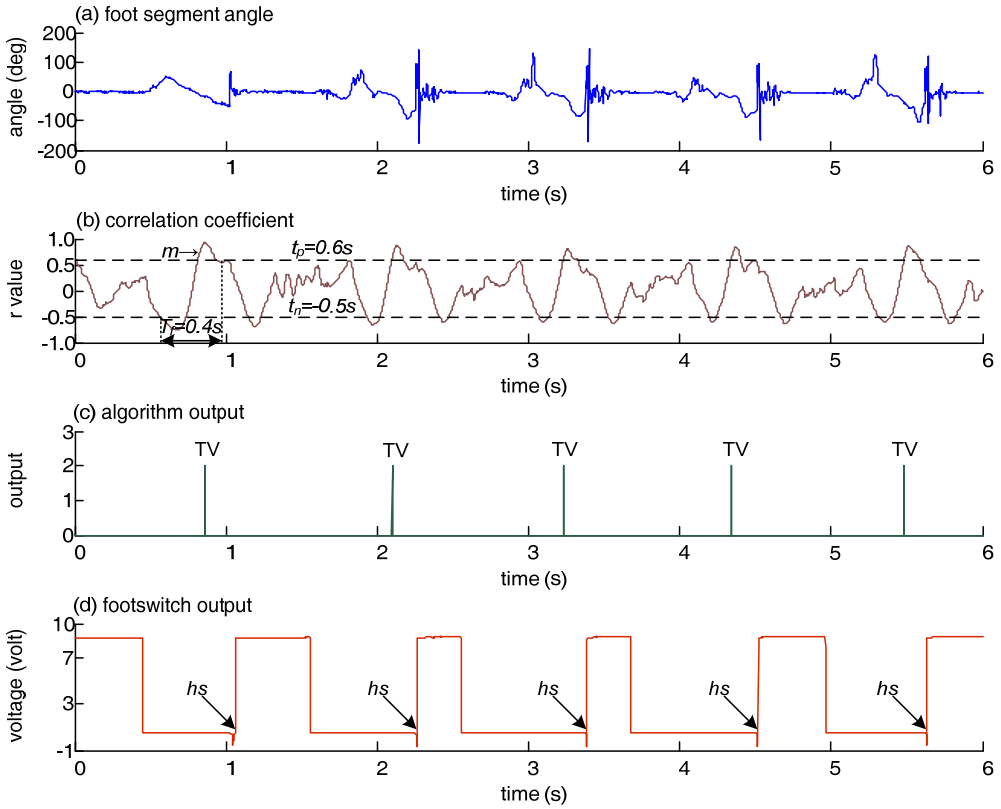

Figure K-4 Tibial vertical events in Subject 1 (right foot), n=5.

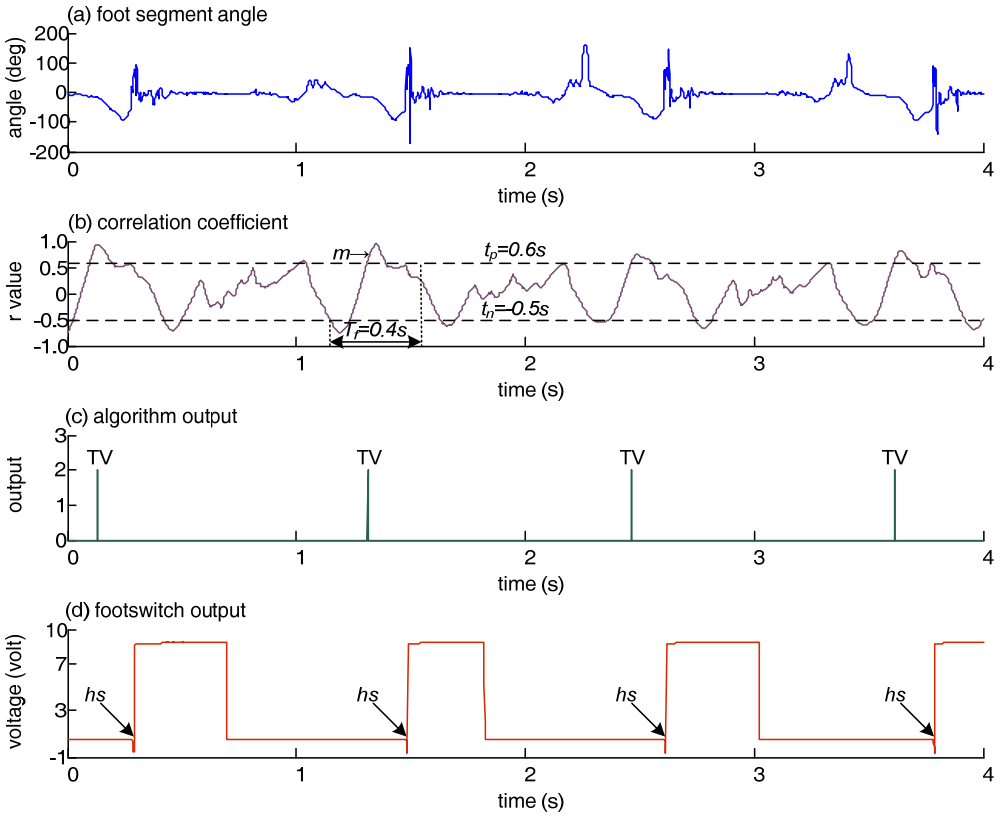

Figure K-5 Tibial vertical events in Subject 1 (right foot), n=4.

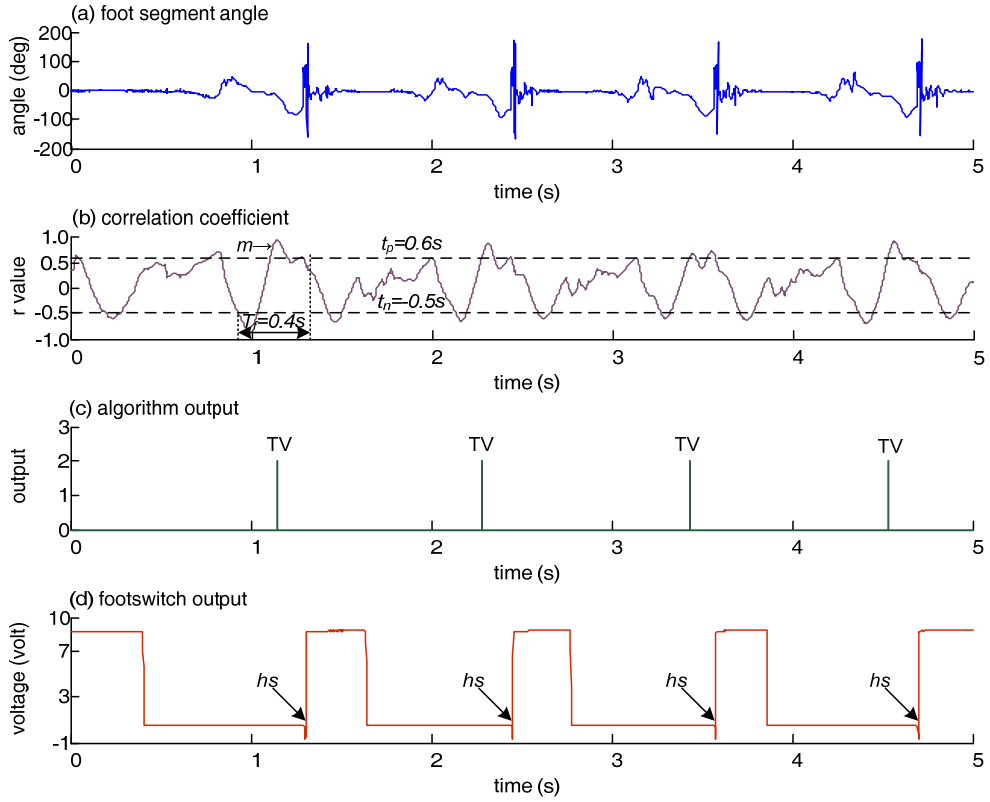

Figure K-6 Tibial vertical events in Subject 1 (right foot), n=4.

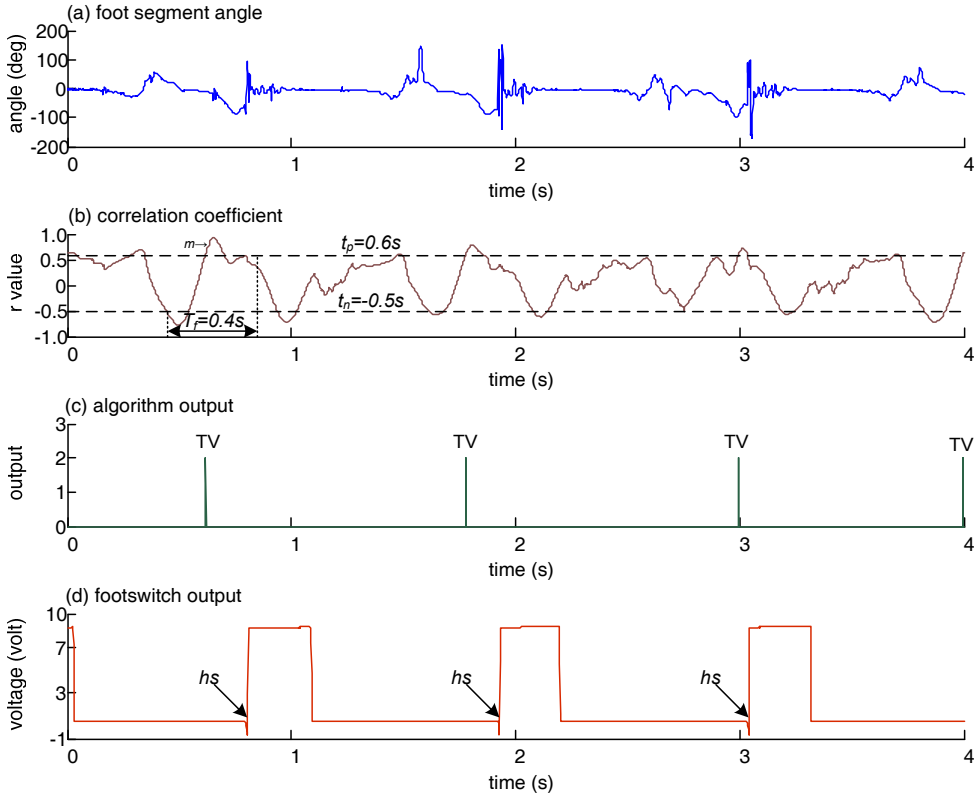

Figure K-7 Tibial vertical events in Subject 1 (right foot), n=4.

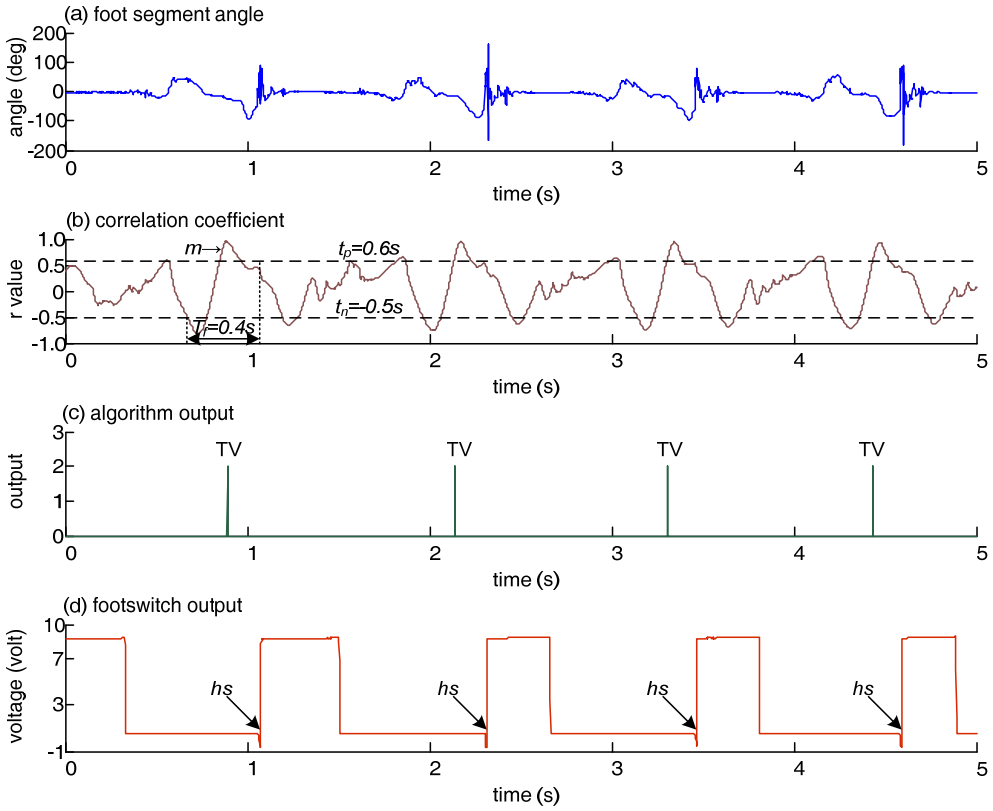

Figure K-8 Tibial vertical events in Subject 1 (right foot), n=4.

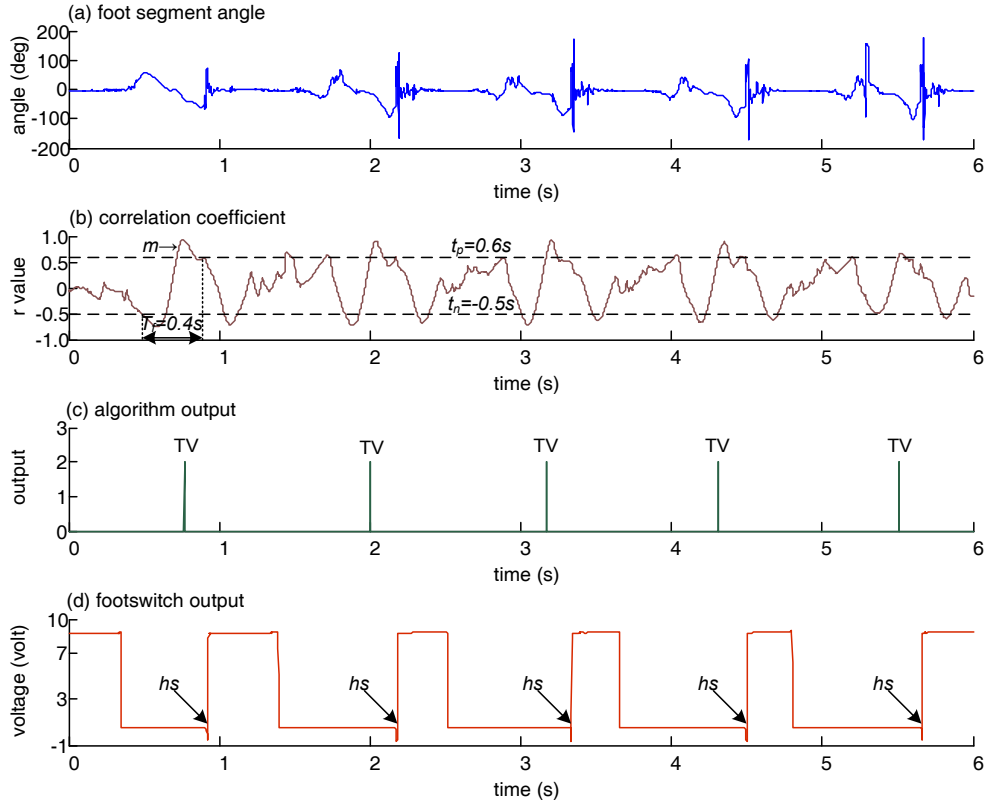

Figure K-9 Tibial vertical events in Subject 1 (right foot), n=5.

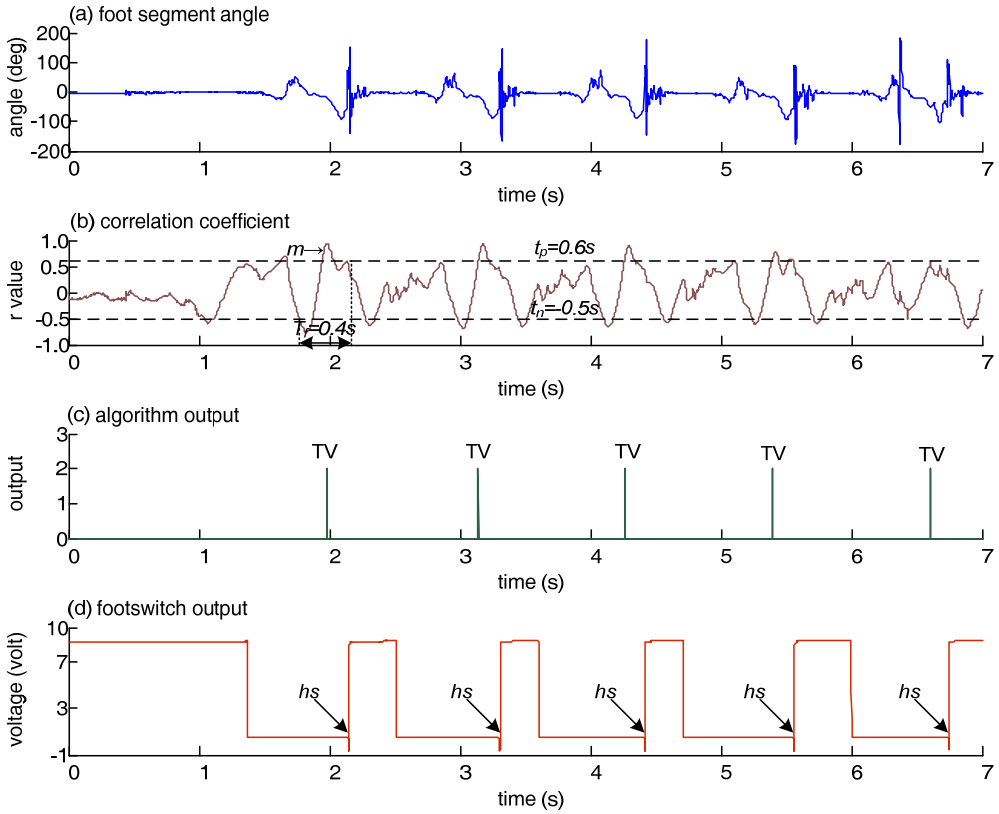

Figure K-10 Tibial vertical events in Subject 1 (right foot), n=5.

Figure K-11 to Figure K-19: Tibial vertical events in Subject 2 (right foot). (a) foot segment angle (b) correlation coefficient between foot segment angle and a sample window (t_p = positive threshold, t_n = negative threshold, T_f = time frame and m=first maximum point) (c) algorithm output (0=no event, 2=event detected and hs=heel strike) and (d) heel switch output.

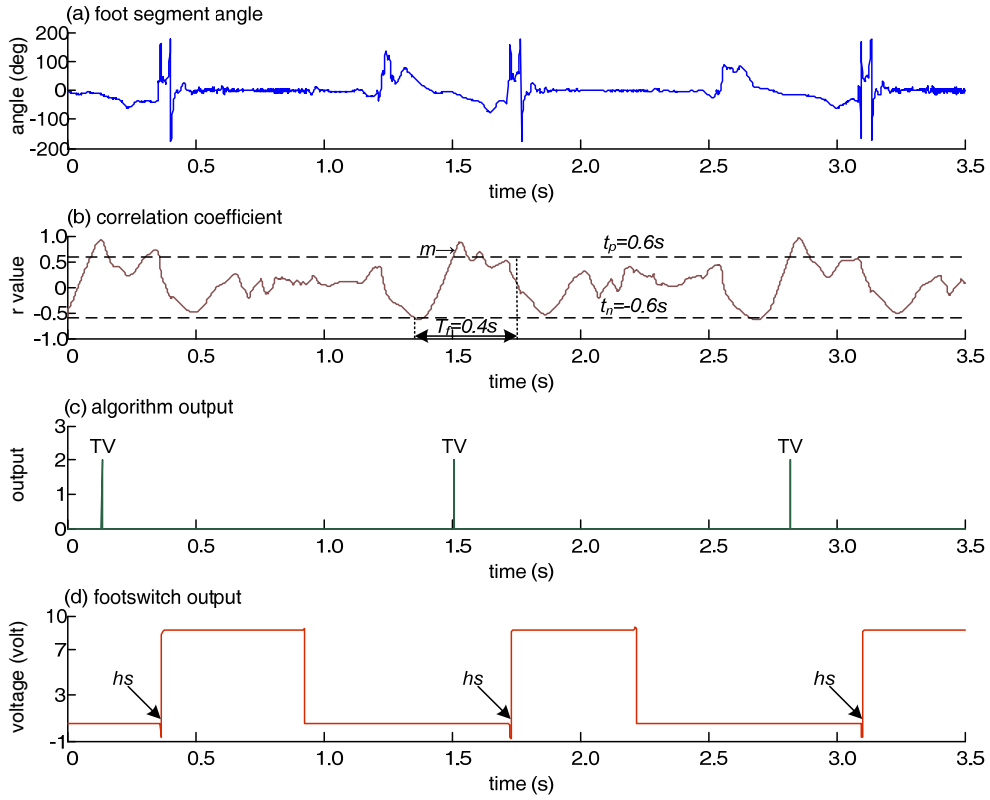

Figure K-11 Tibial vertical events in Subject 2 (right foot), n=3.

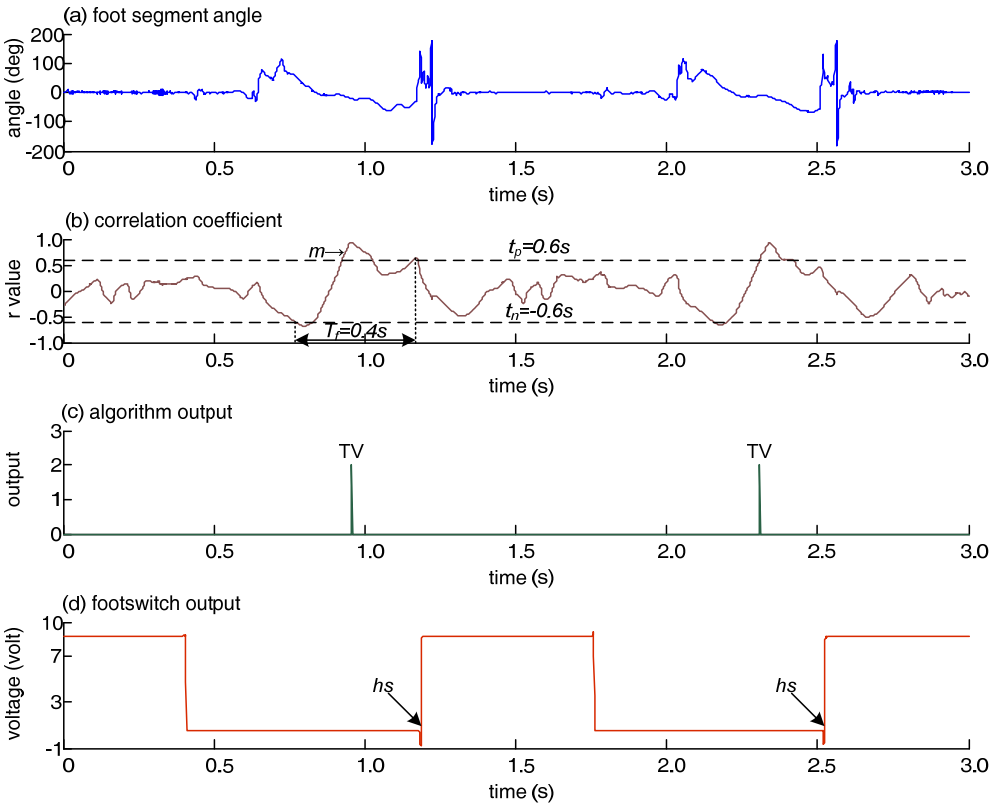

Figure K-12 Tibial vertical events in Subject 2 (right foot), n=2.

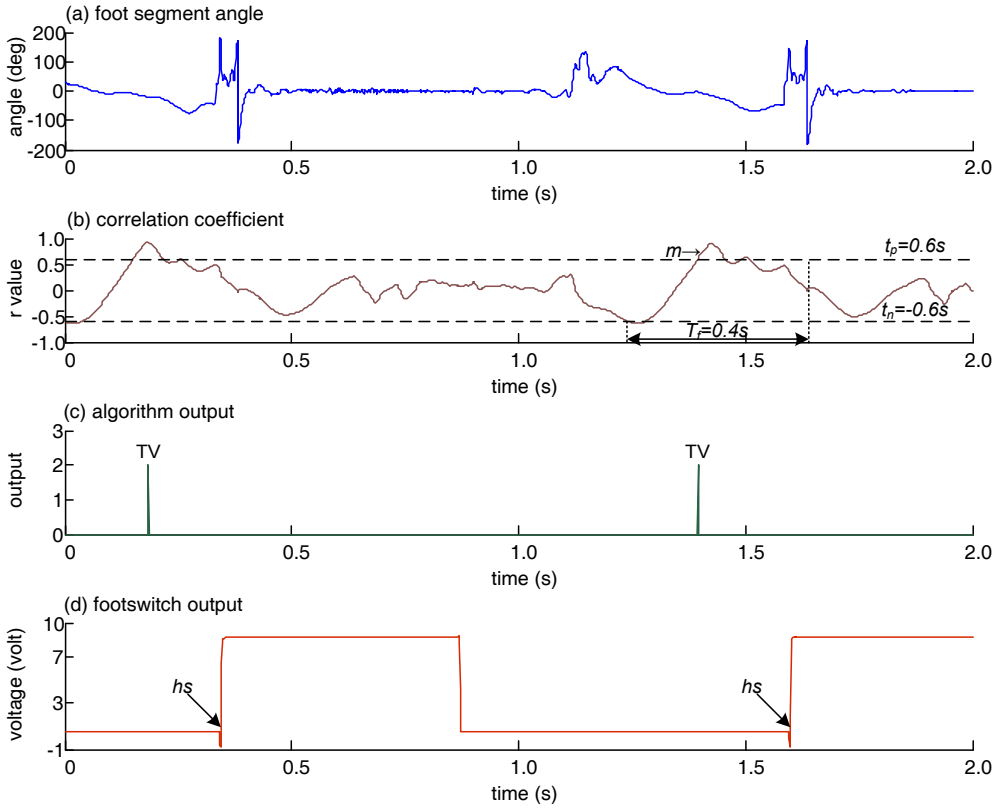

Figure K-13 Tibial vertical events in Subject 2 (right foot), n=2.

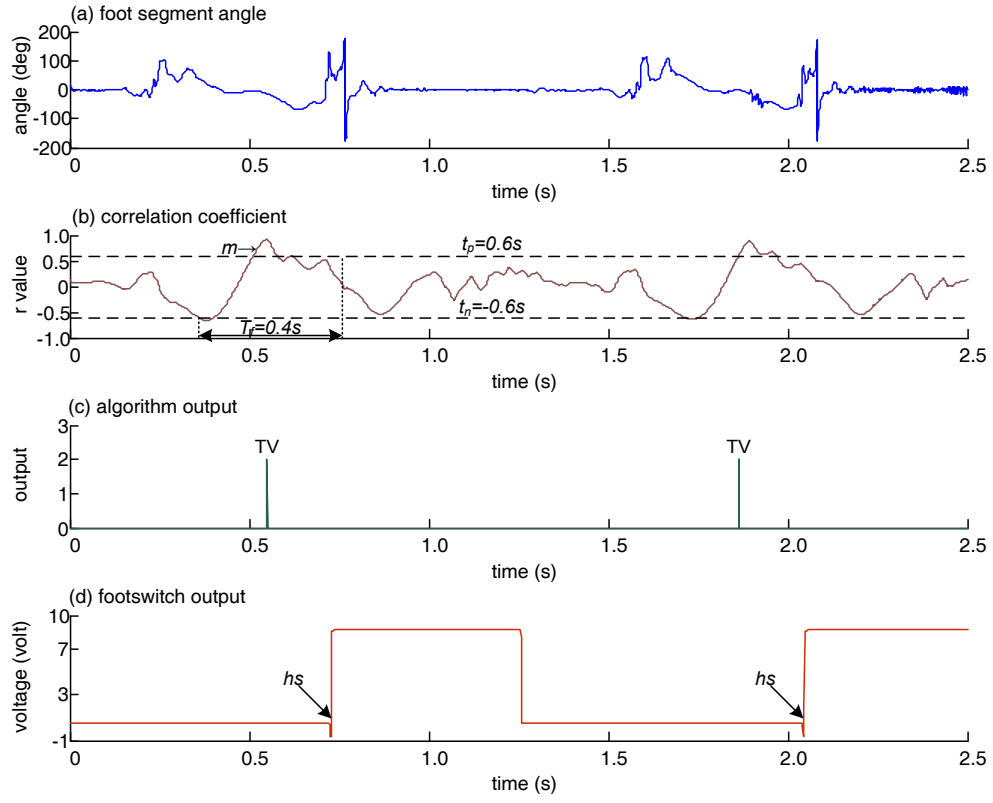

Figure K-14 Tibial vertical events in Subject 2 (right foot), n=2.

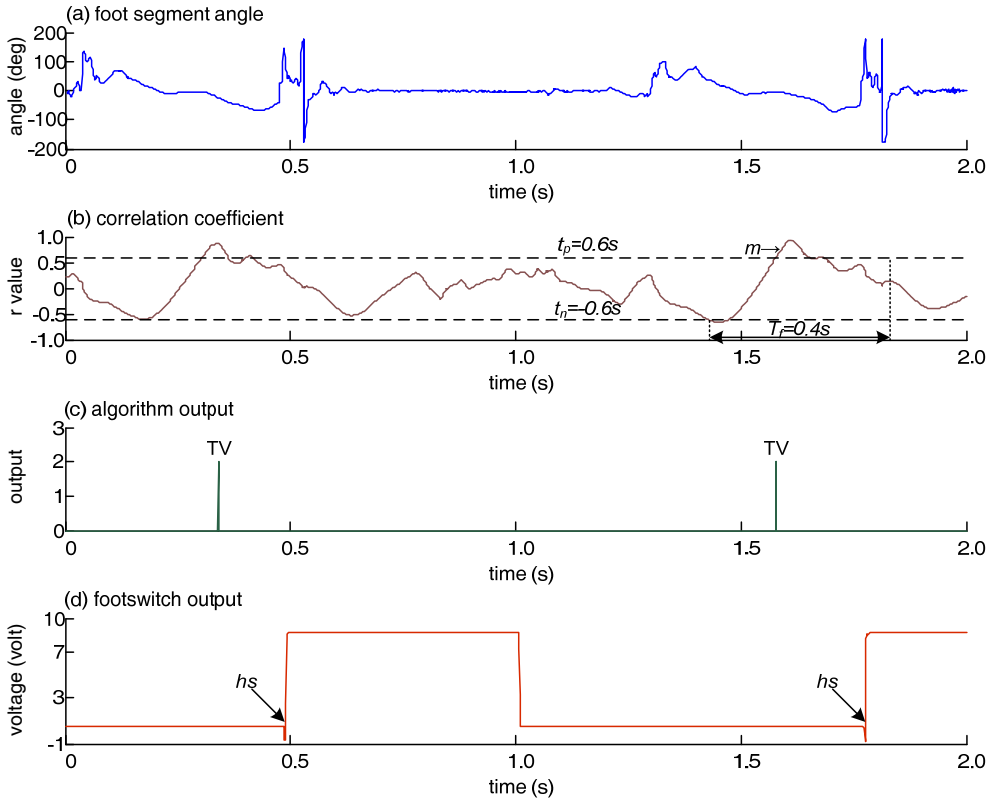

Figure K-15 Tibial vertical events in Subject 2 (right foot), n=2.

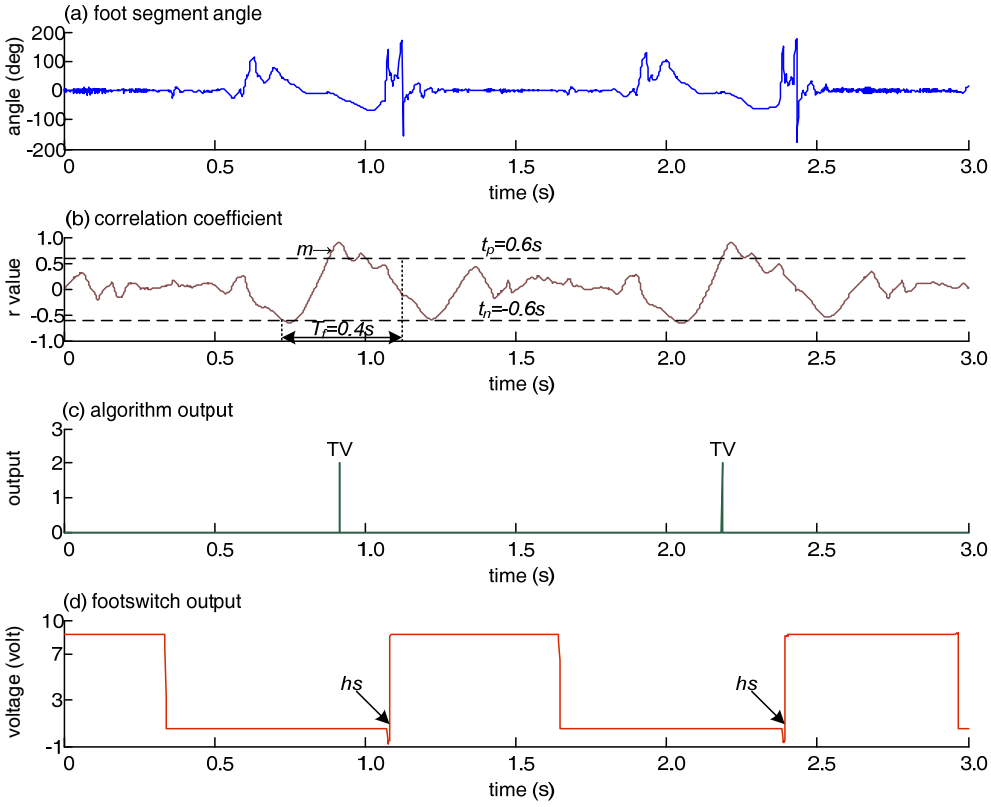

Figure K-16 Tibial vertical events in Subject 2 (right foot), n=2.

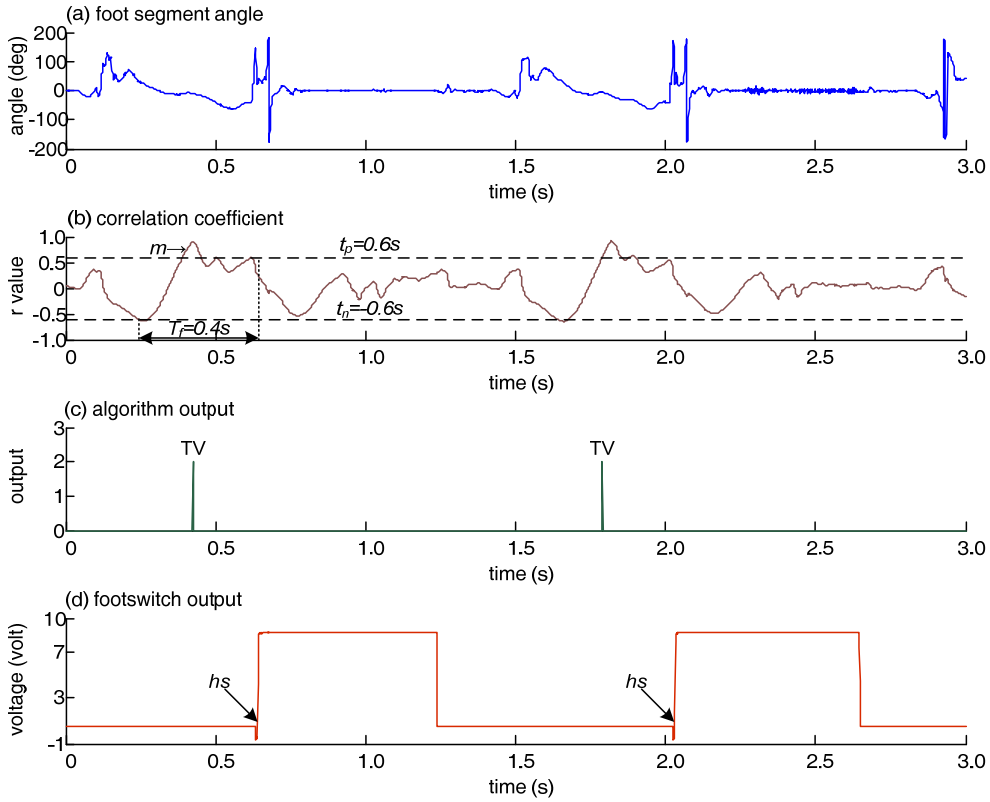

Figure K-17 Tibial vertical events in Subject 2 (right foot), n=2.

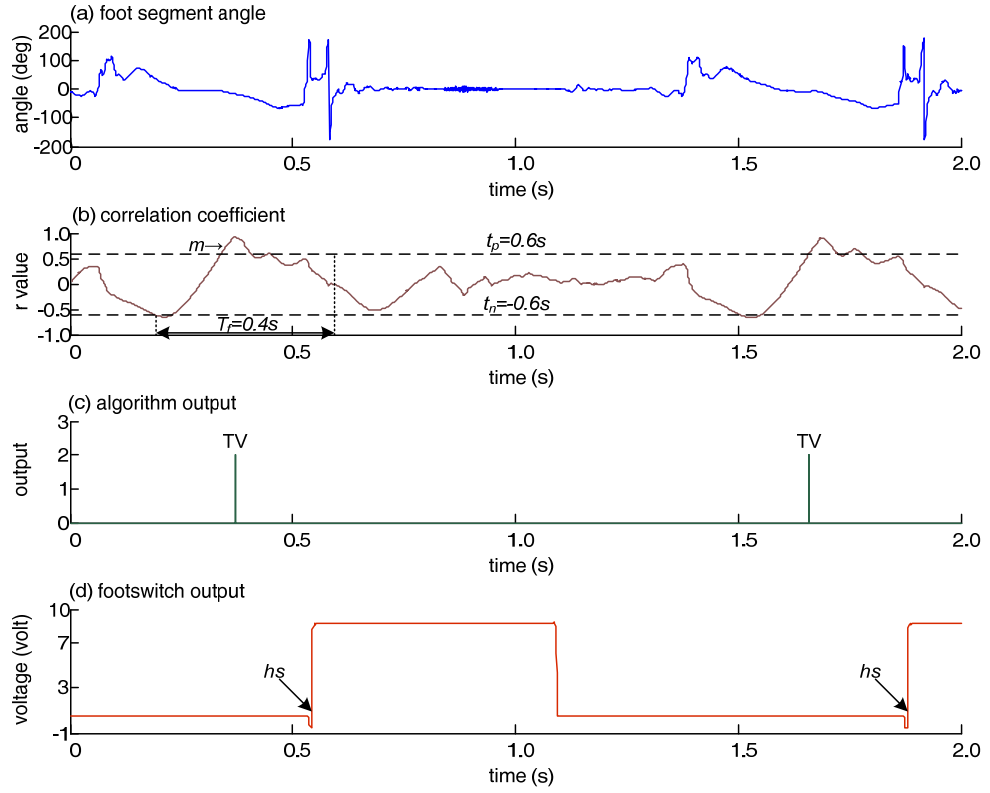

Figure K-18 Tibial vertical events in Subject 2 (right foot), n=2.

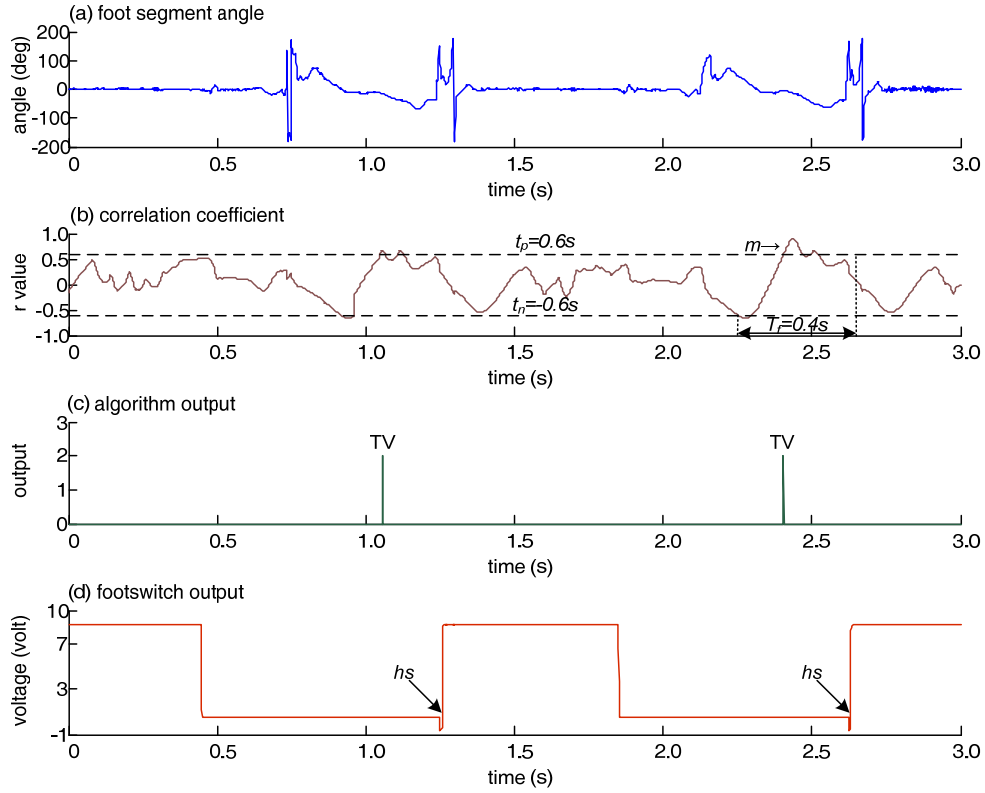

Figure K-19 Tibial vertical events in Subject 2 (right foot), n=2.

Figure K-20to Figure K-28: Tibial vertical events in Subject 2 (left foot). (a) foot segment angle (b) correlation coefficient between foot segment angle and a sample window (t_p = positive threshold, t_n = negative threshold, T_f = time frame and m=first maximum point) (c) algorithm output (0=no event, 2=event detected and hs=heel strike) and (d) heel switch output.

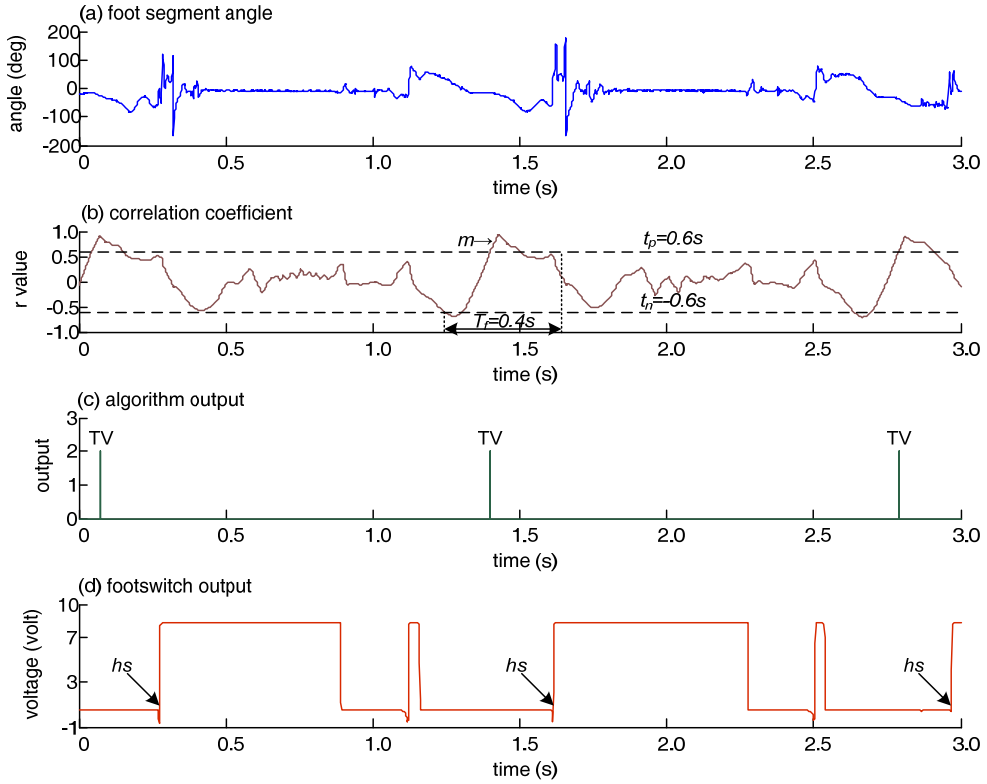

Figure K-20 Tibial vertical events in Subject 2 (left foot), n=3.

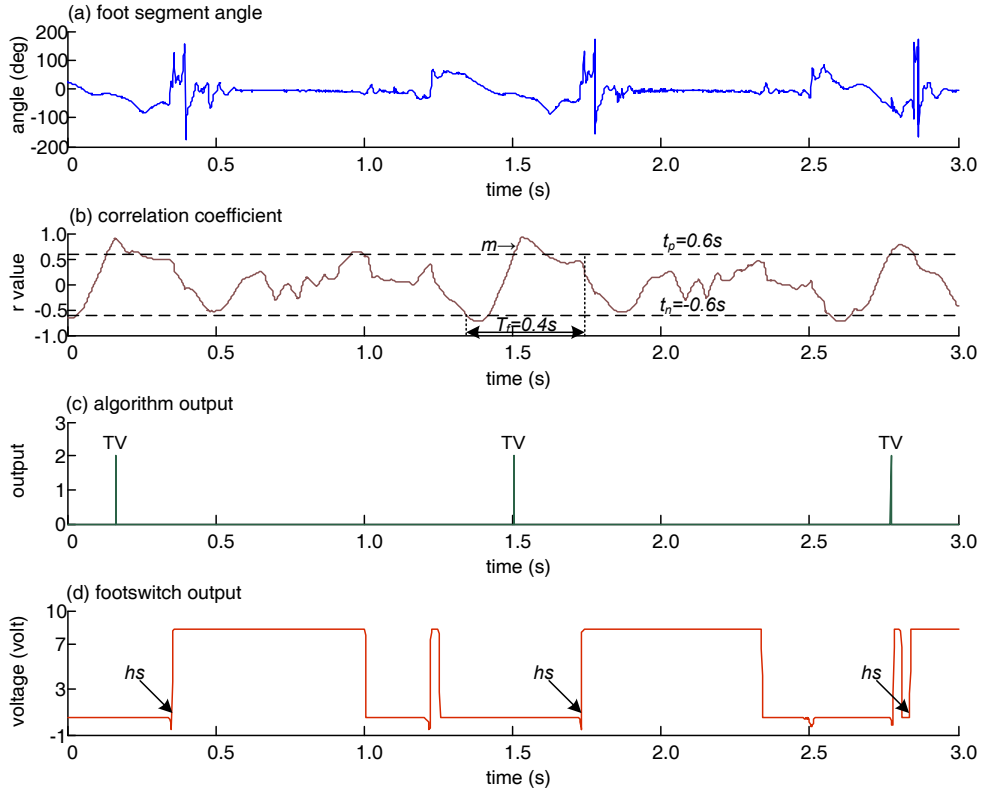

Figure K-21 Tibial vertical events in Subject 2 (left foot), n=3.

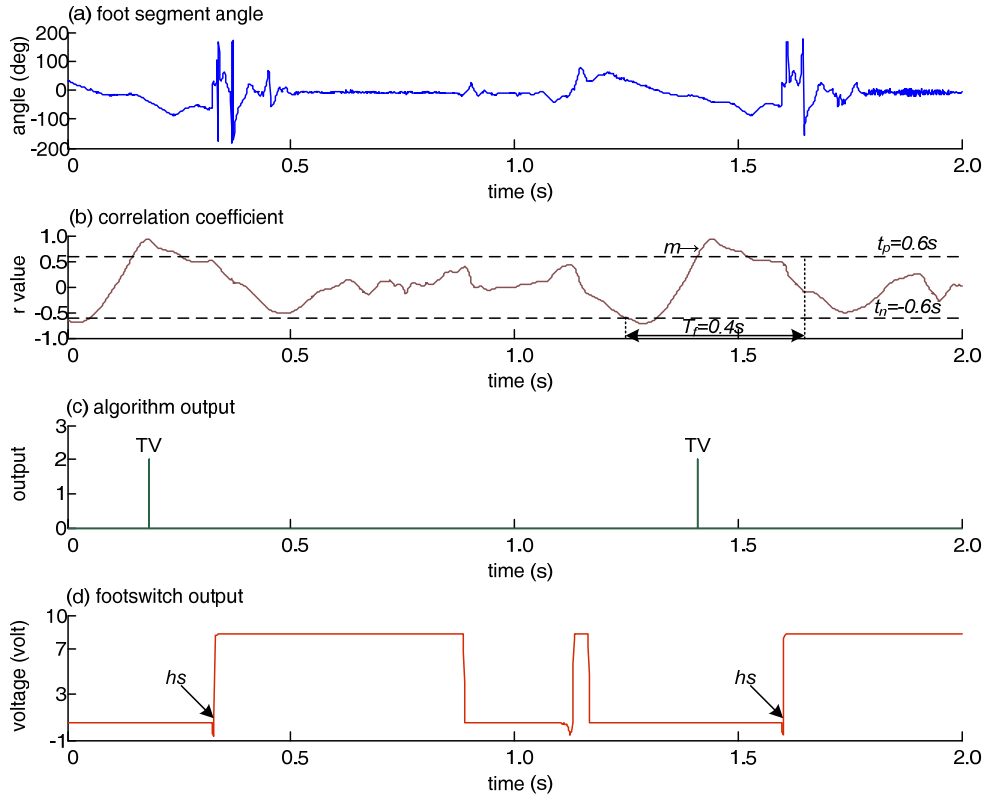

Figure K-22 Tibial vertical events in Subject 2 (left foot), n=2.

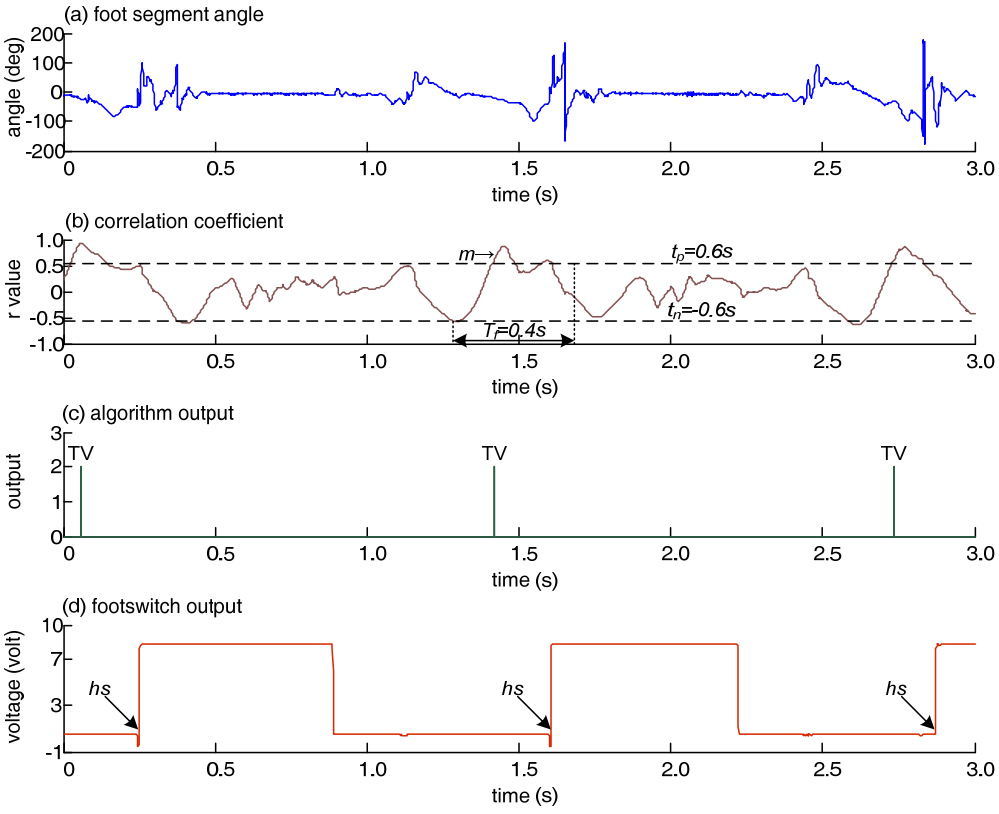

Figure K-23 Tibial vertical events in Subject 2 (left foot), n=3.

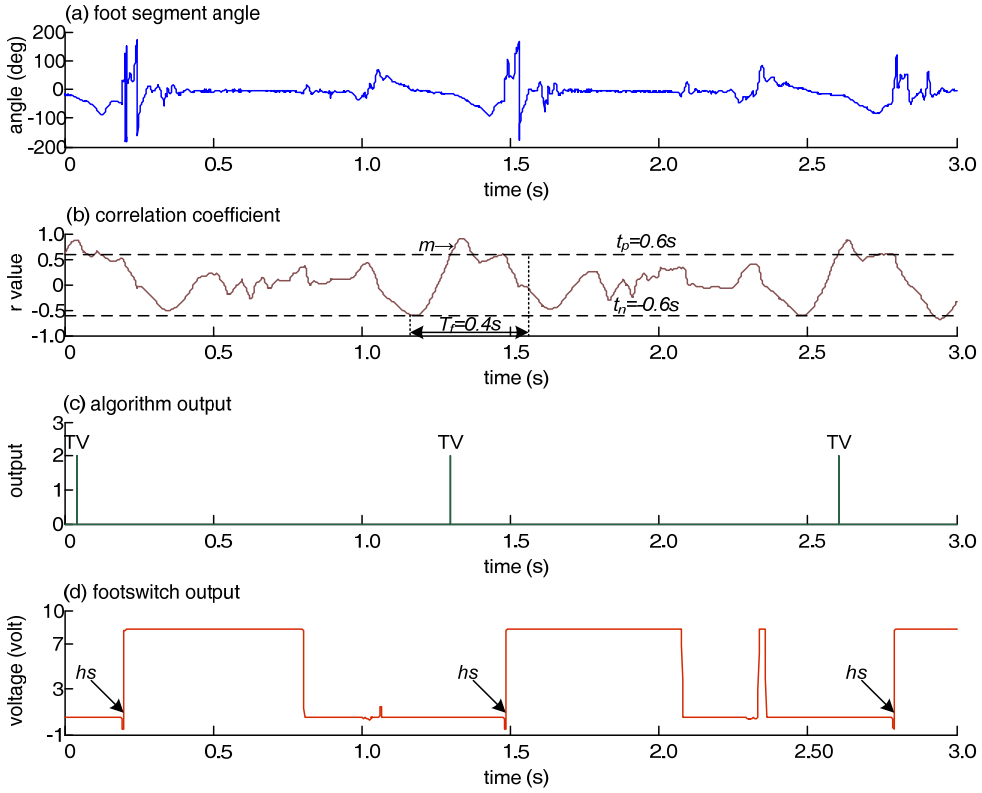

Figure K-24 Tibial vertical events in Subject 2 (left foot), n=3.

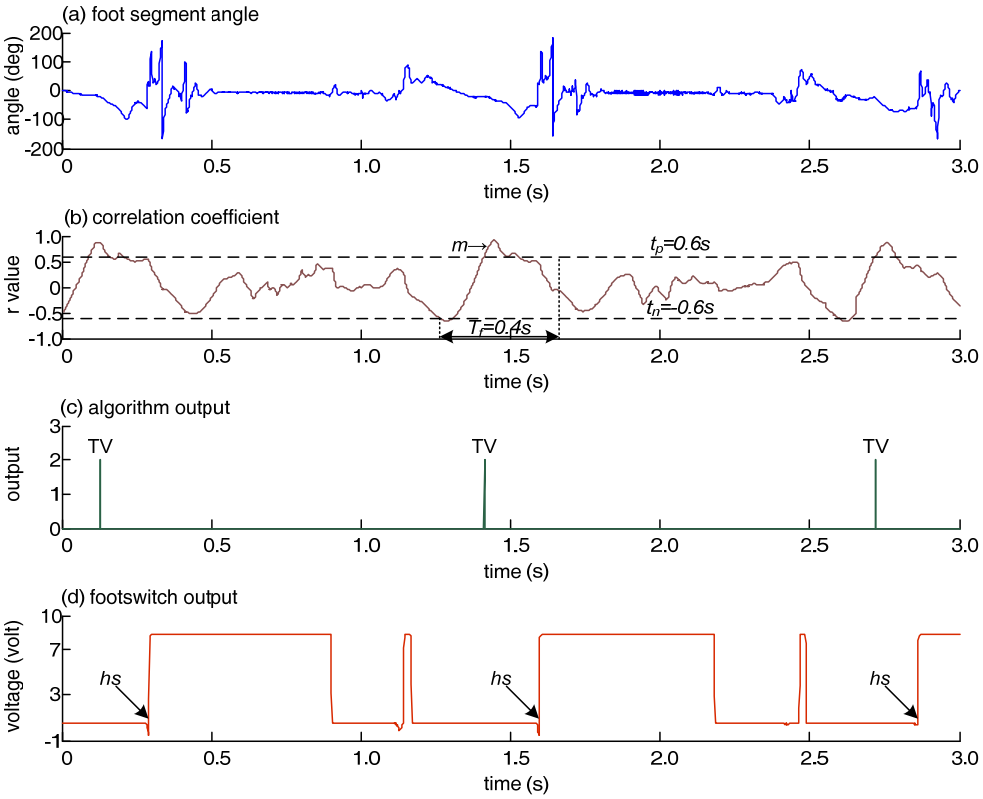

Figure K-25 Tibial vertical events in Subject 2 (left foot), n=3.

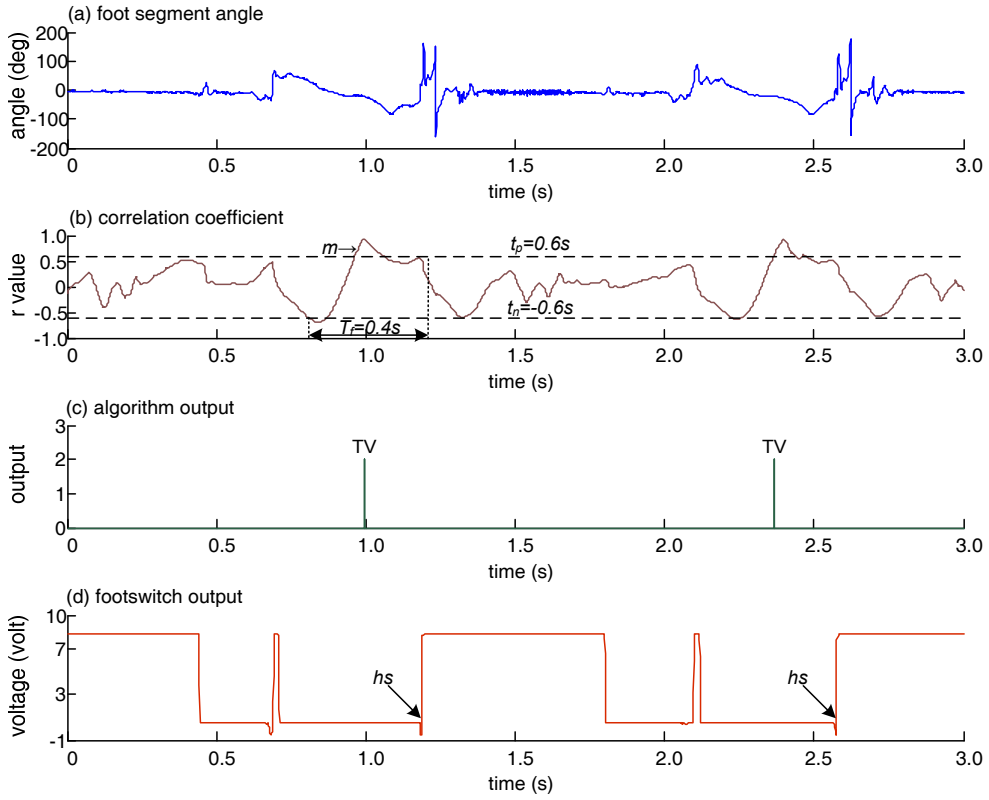

Figure K-26 Tibial vertical events in Subject 2 (left foot), n=3.

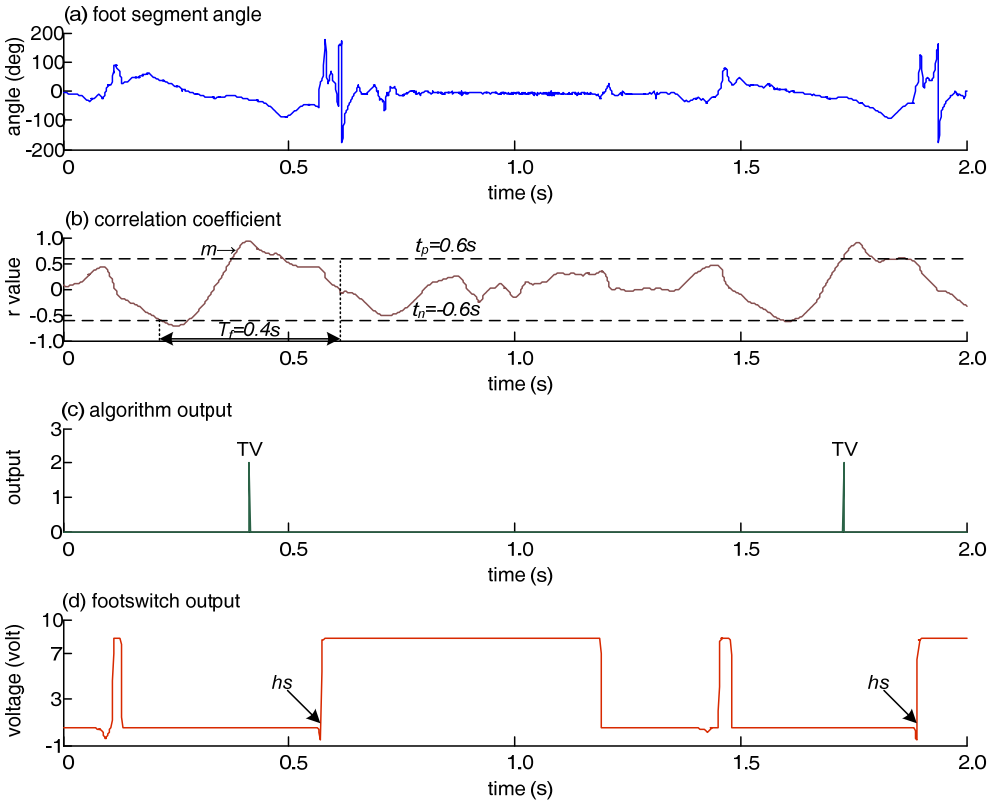

Figure K-27 Tibial vertical events in Subject 2 (left foot), n=2.

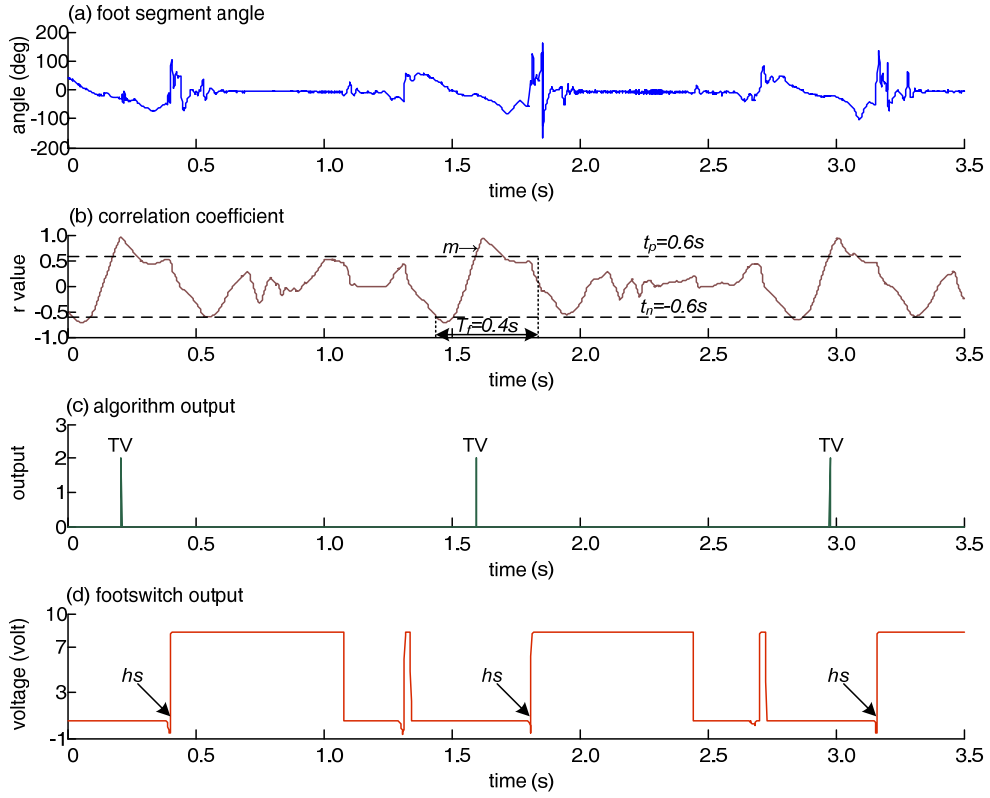

Figure K-28 Tibial vertical events in Subject 2 (left foot), n=3.

Figure K-29 to Figure K-40: Tibial vertical events in Subject 3 (right foot). (a) foot segment angle (b) correlation coefficient between foot segment angle and a sample window (t_p = positive threshold, t_n = negative threshold, T_f= time frame and m=first maximum point) (c) algorithm output (0=no event, 2=event detected and hs=heel strike) and (d) heel switch output.

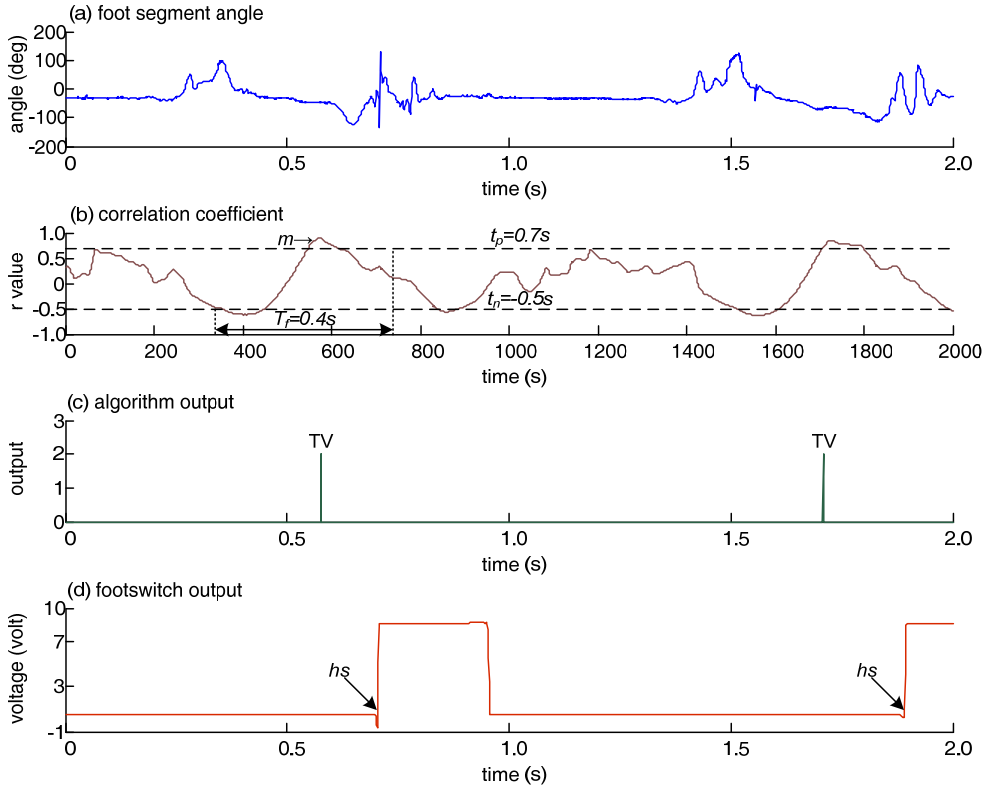

Figure K-29 Tibial vertical events in Subject 3 (right foot), n=2.

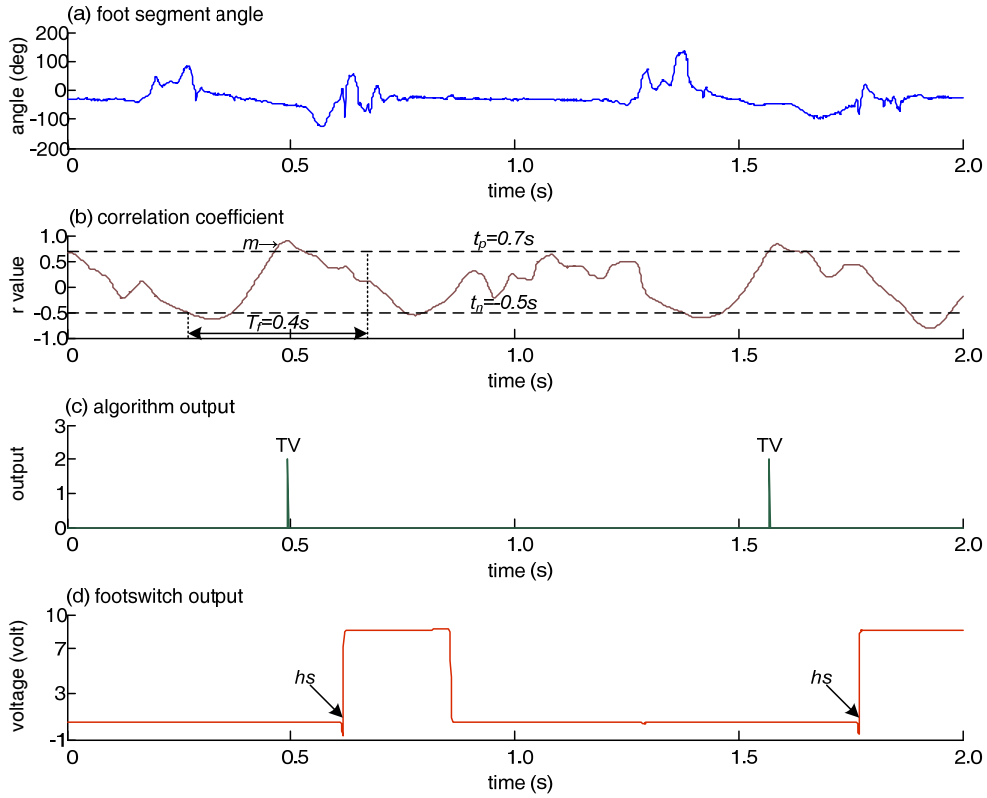

Figure K-30 Tibial vertical events in Subject 3 (right foot), n=2.

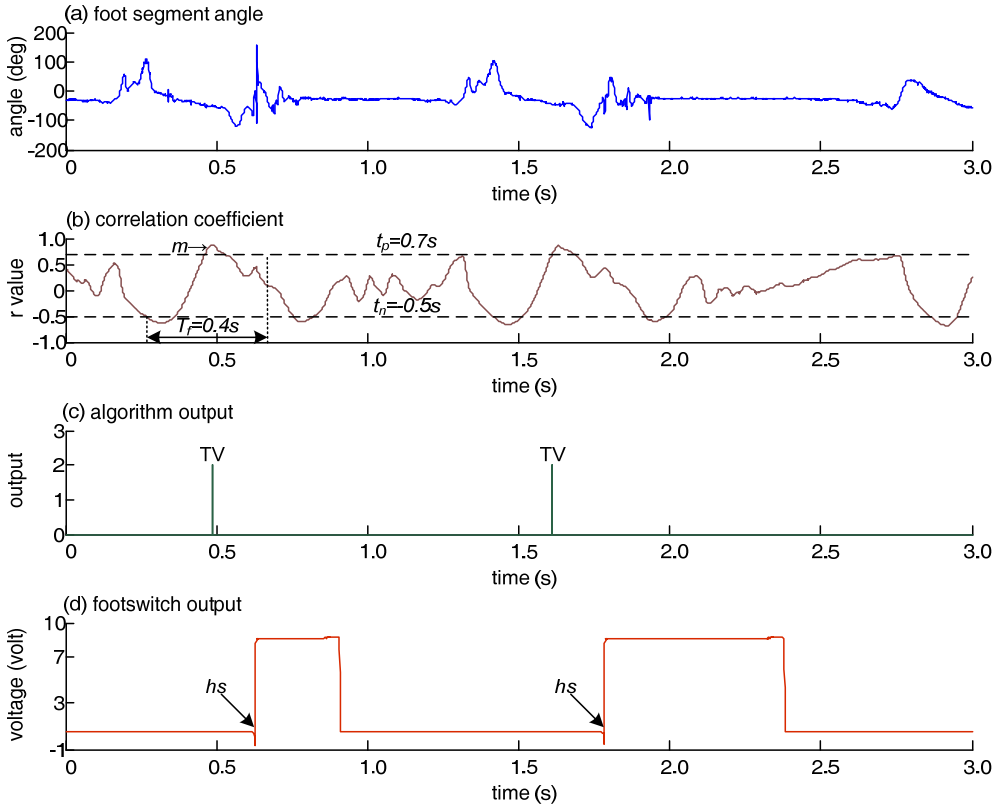

Figure K-31 Tibial vertical events in Subject 3 (right foot), n=2.

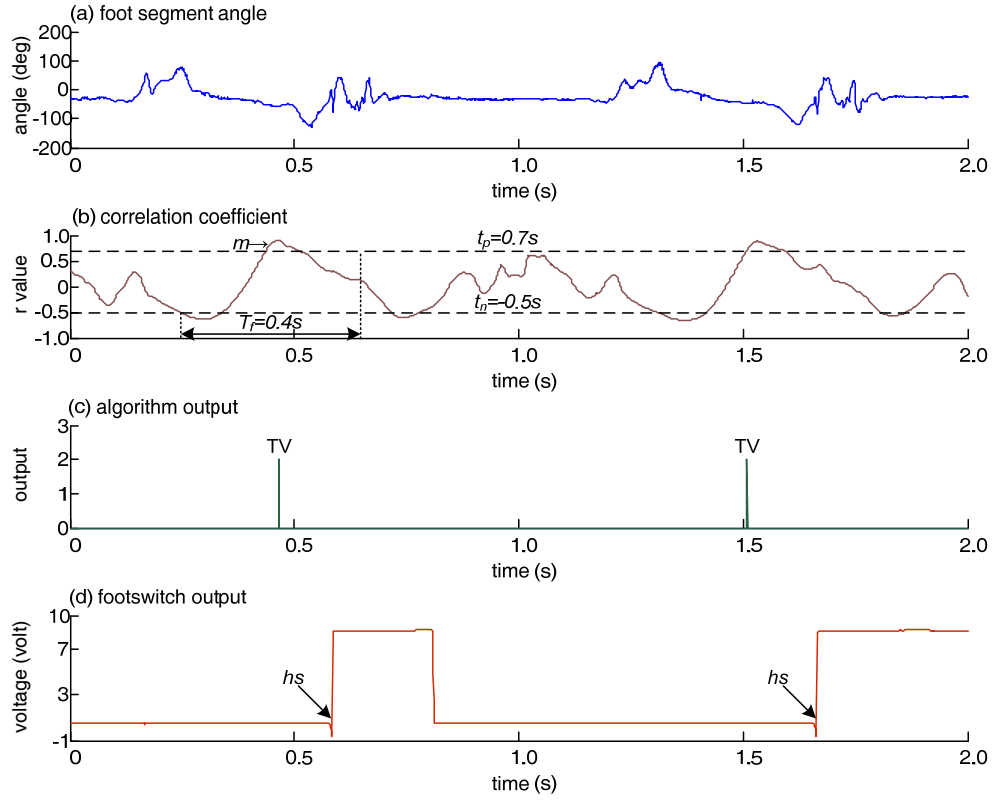

Figure K-32 Tibial vertical events in Subject 3 (right foot), n=2.

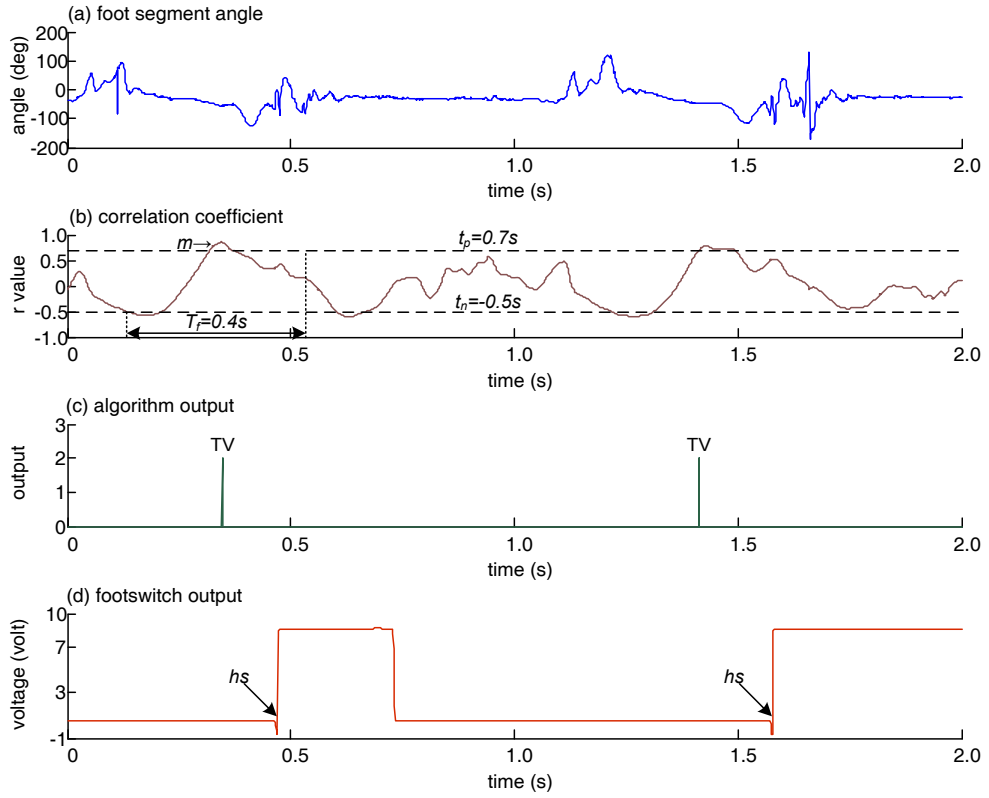

Figure K-33 Tibial vertical events in Subject 3 (right foot), n=2.

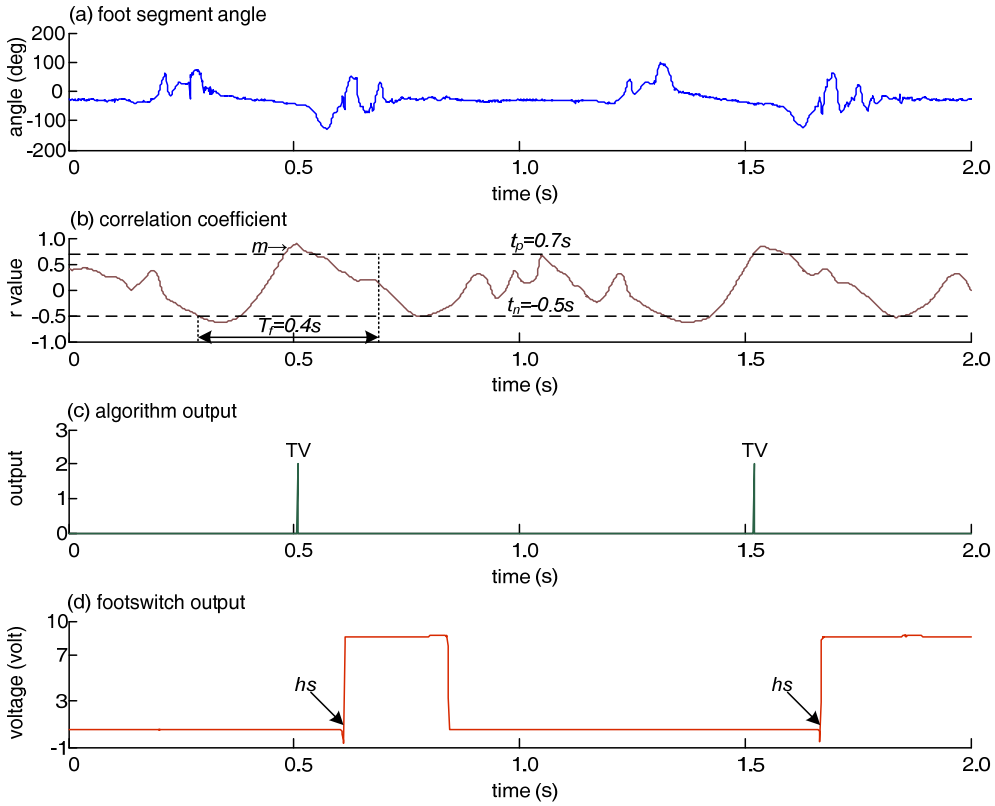

Figure K-34 Tibial vertical events in Subject 3 (right foot), n=2.

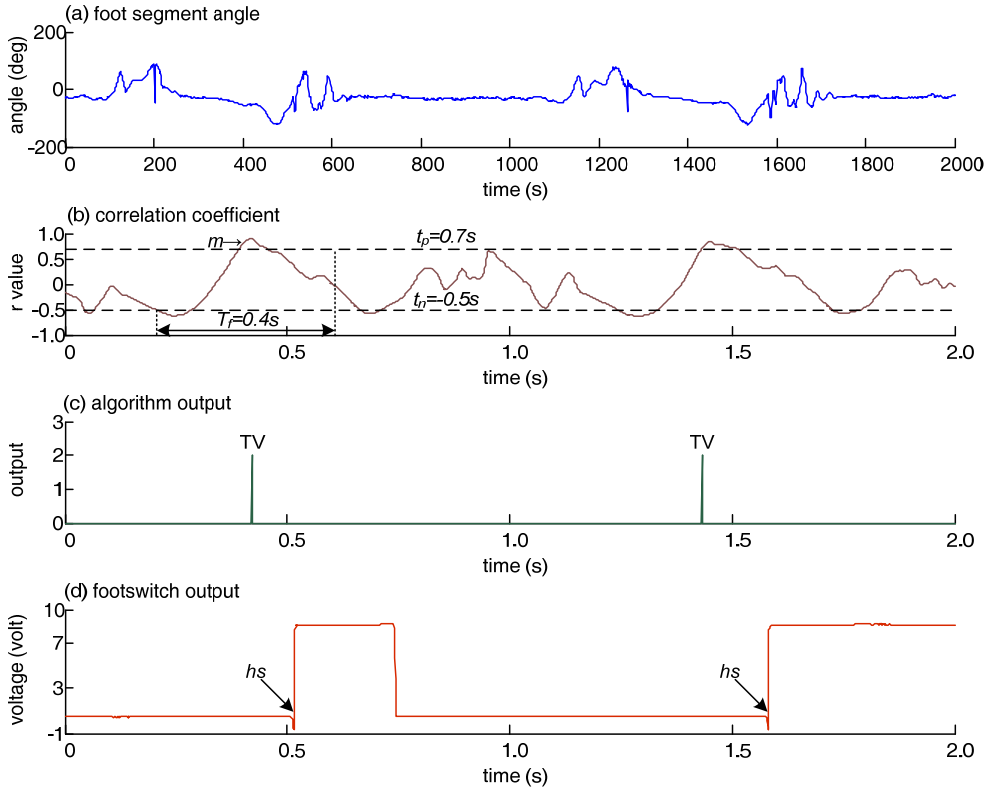

Figure K-35 Tibial vertical events in Subject 3 (right foot), n=2.

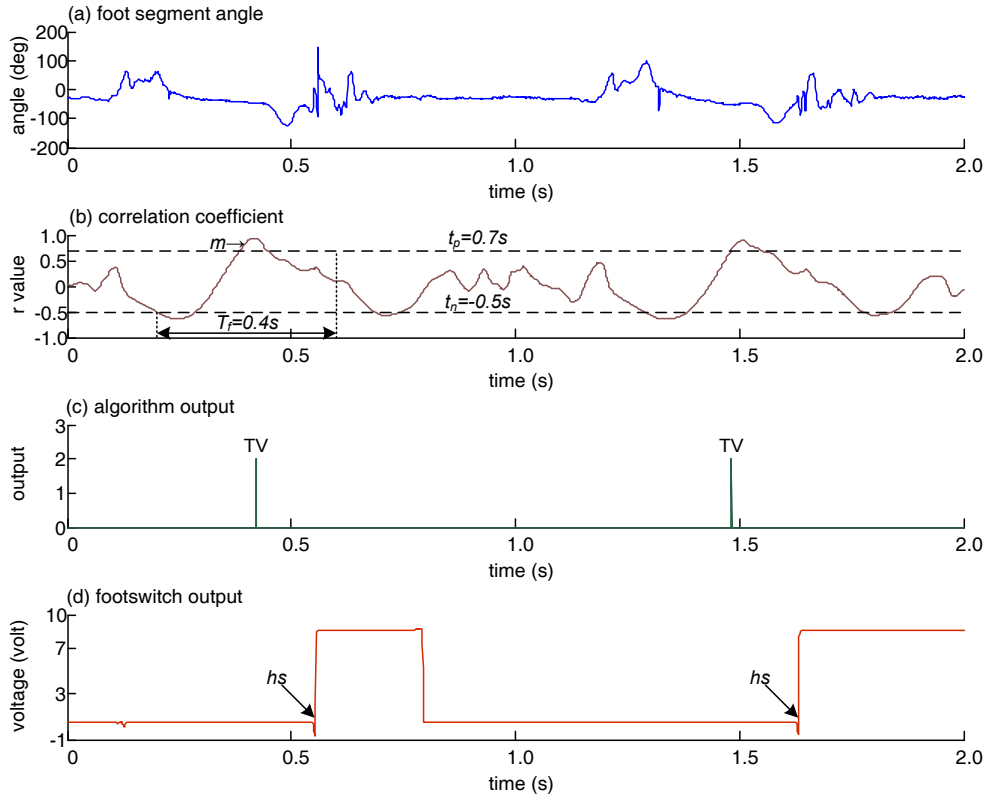

Figure K-36 Tibial vertical events in Subject 3 (right foot), n=2.

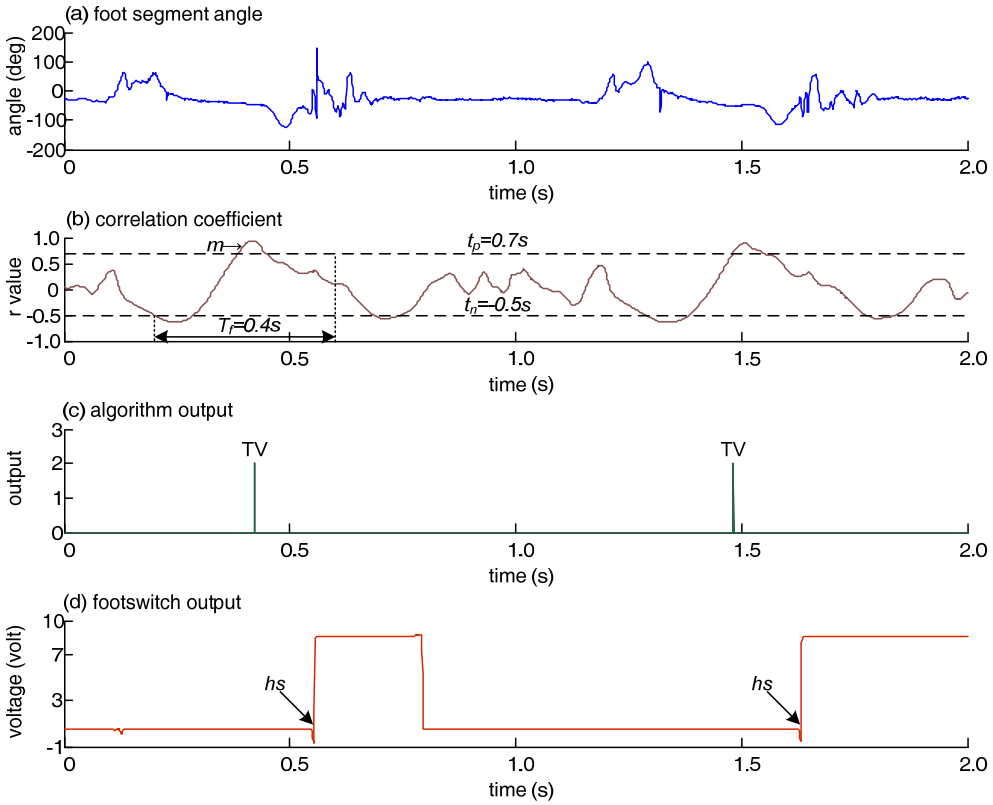

Figure K-37 Tibial vertical events in Subject 3 (right foot), n=2.

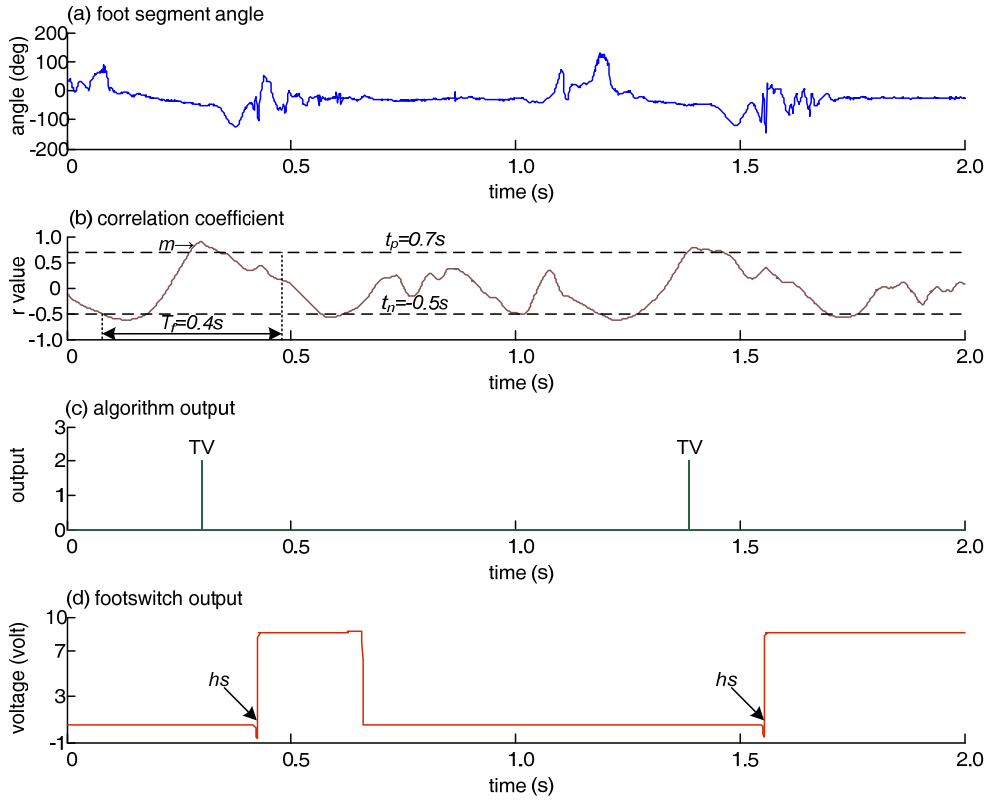

Figure K-38 Tibial vertical events in Subject 3 (right foot), n=2.

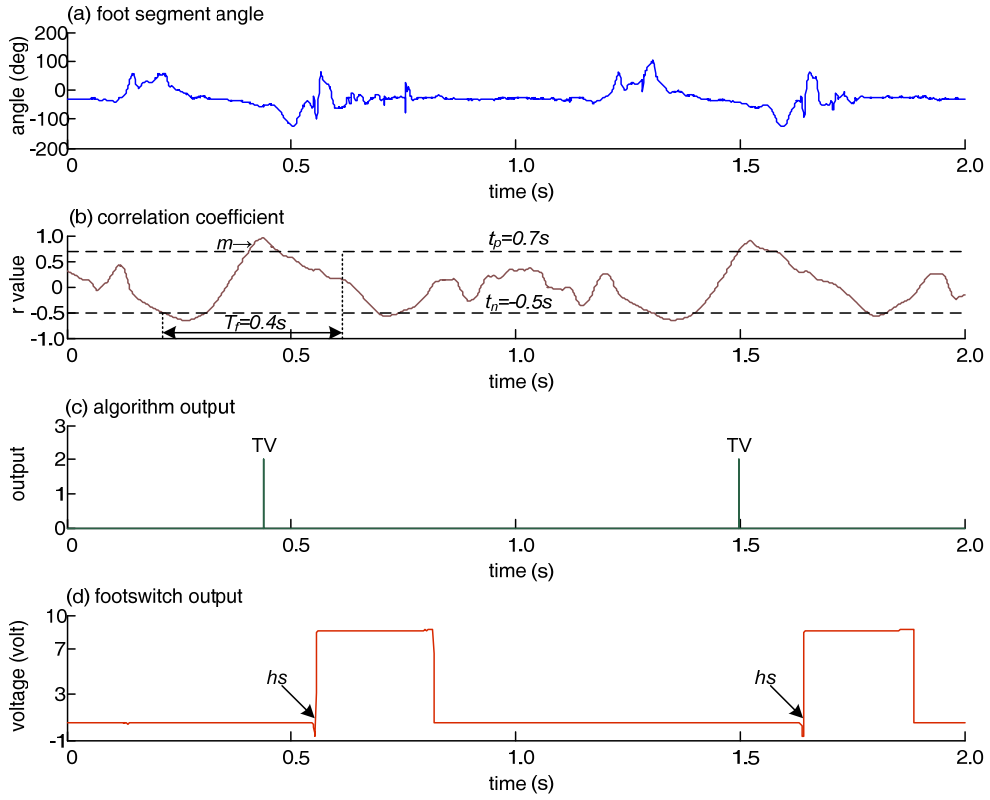

Figure K-39 Tibial vertical events in Subject 3 (right foot), n=2.

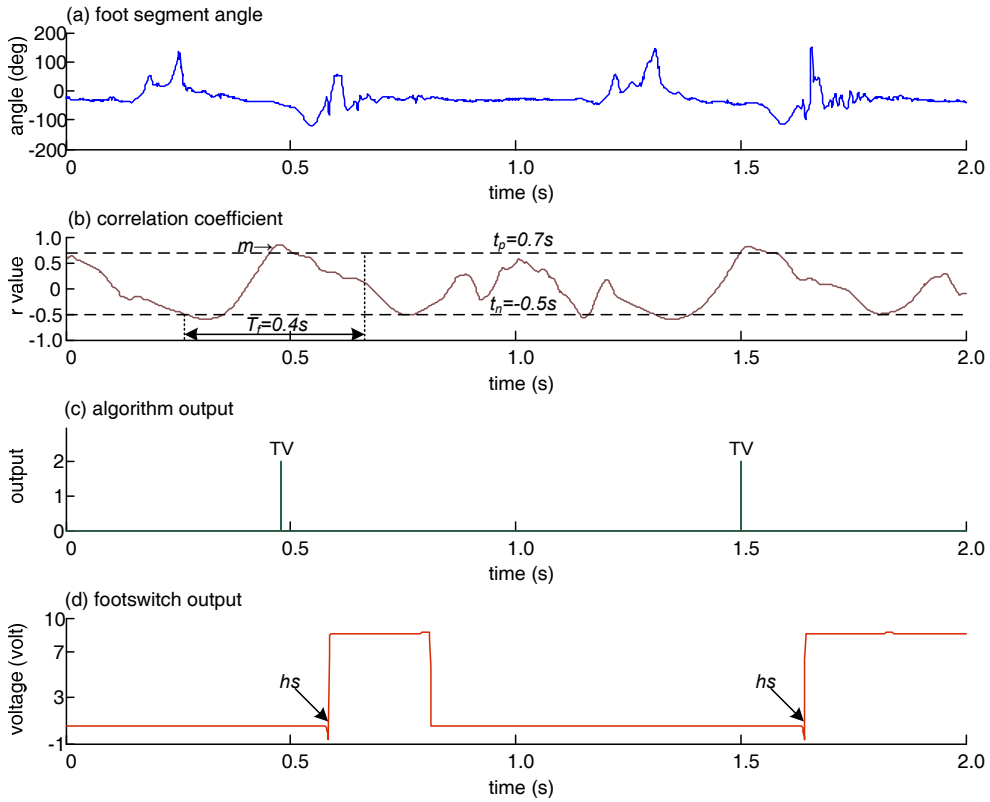

Figure K-40 Tibial vertical events in Subject 3 (right foot), n=2.

Figure K-41 to Figure K-45: Tibial vertical events in Subject 4 (right foot). (a) foot segment angle (b) correlation coefficient between foot segment angle and a sample window (t_p = positive threshold, t_n = negative threshold, T_f = time frame and m=first maximum point) (c) algorithm output (0=no event, 2=event detected and hs=heel strike) and (d) heel switch output.

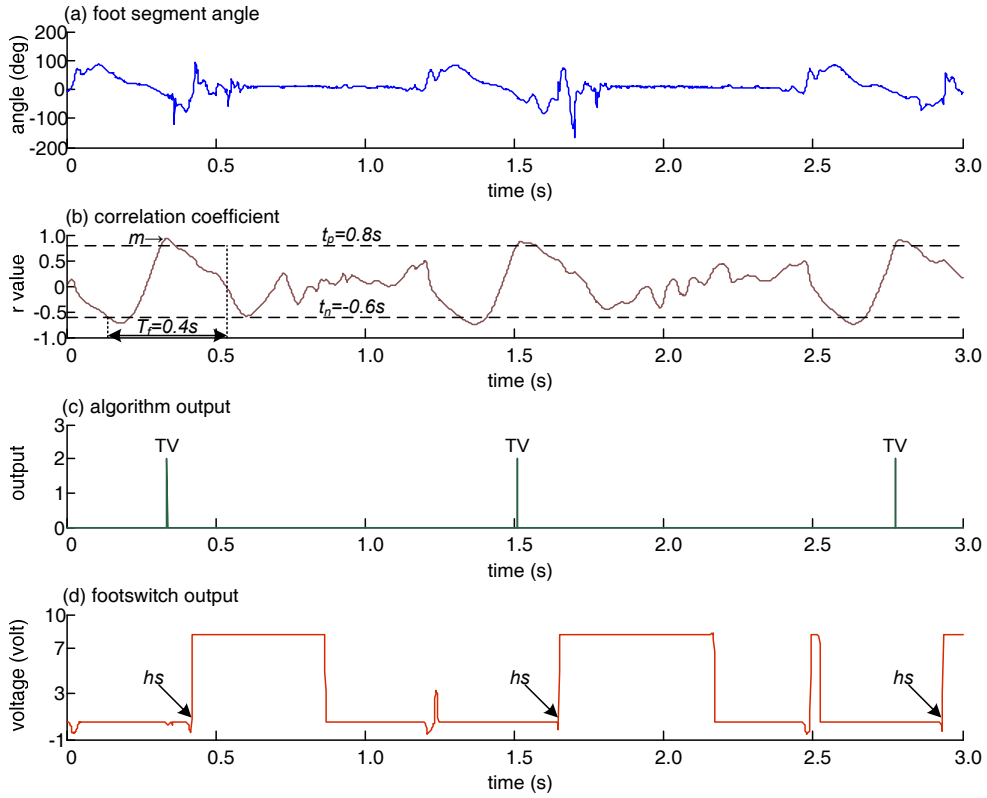

Figure K-41 Tibial vertical events in Subject 4 (right foot), n=3.

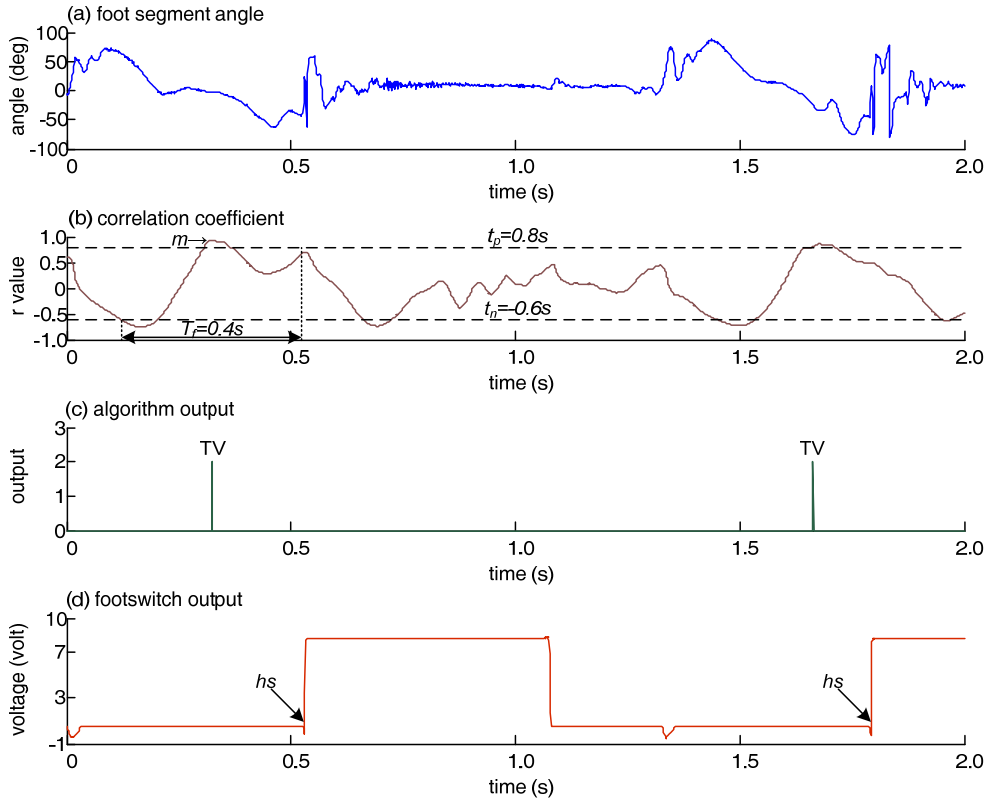

Figure K-42 Tibial vertical events in Subject 4 (right foot), n=2.

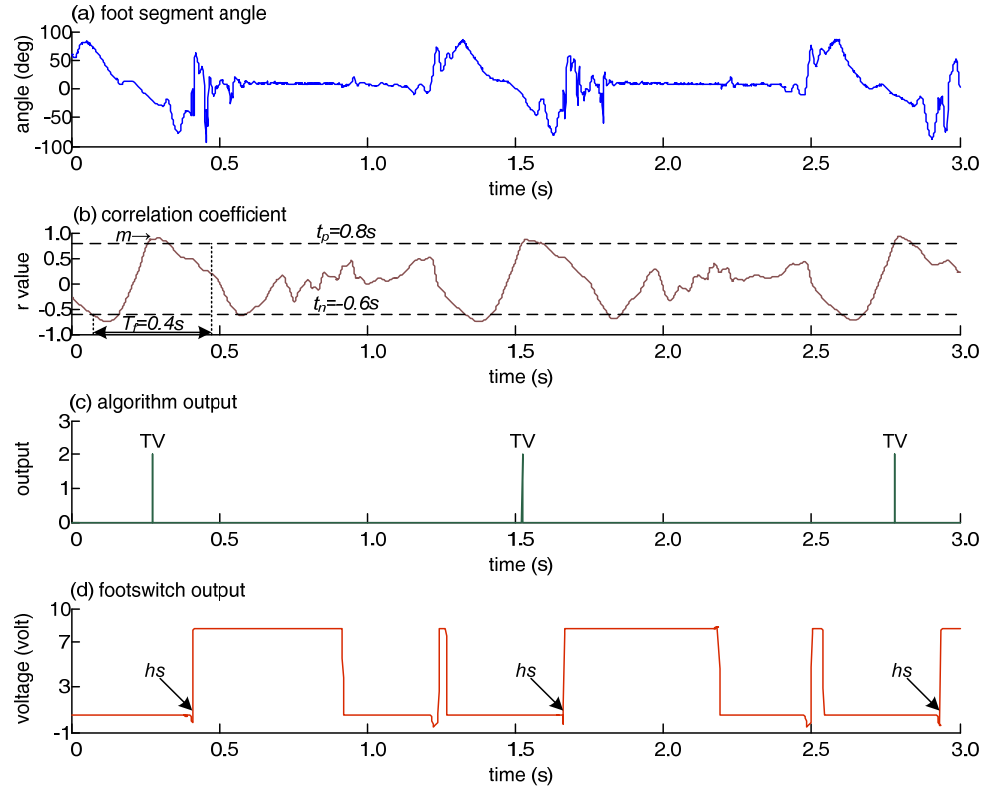

Figure K-43 Tibial vertical events in Subject 4 (right foot), n=3.

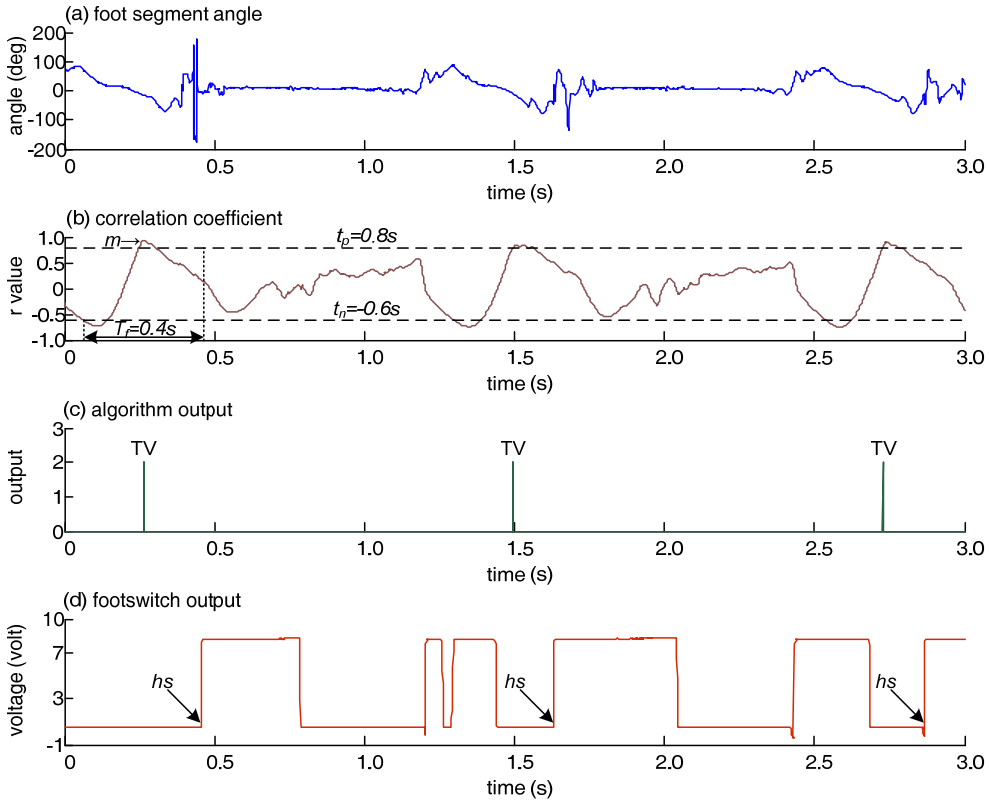

Figure K-44 Tibial vertical events in Subject 4 (right foot), n=3.

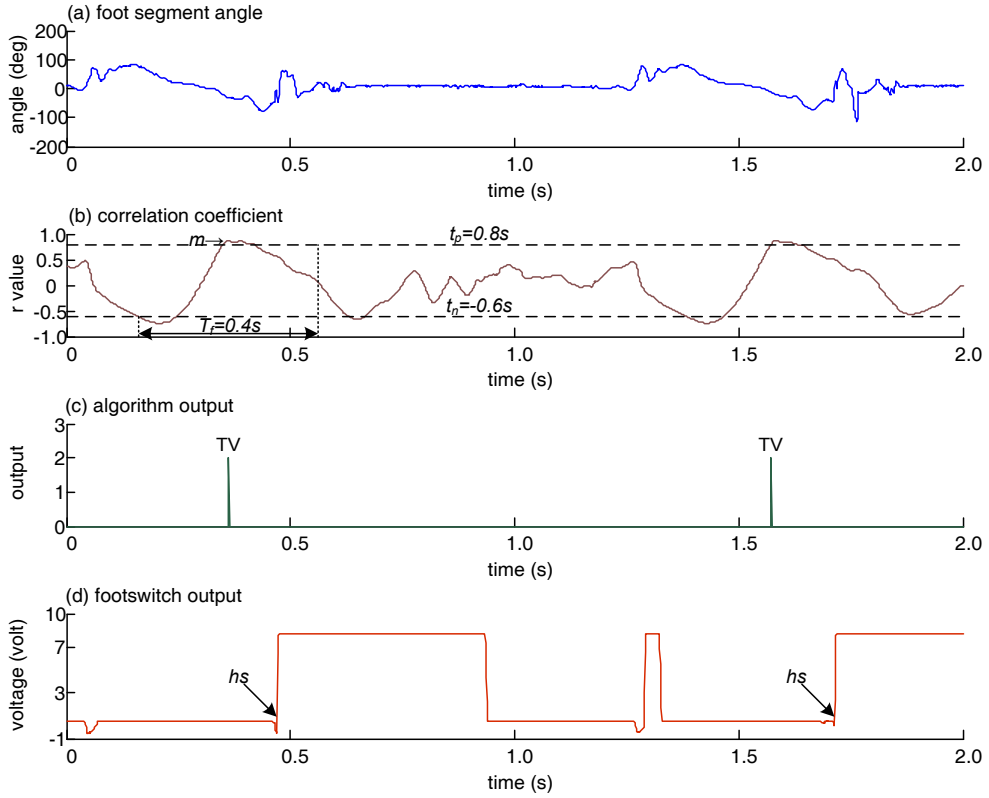

Figure K-45 Tibial vertical events in Subject 4 (right foot), n=2.

Figure K-46 to Figure K-50: Tibial vertical events in Subject 4 (left foot). (a) foot segment angle (b) correlation coefficient between foot segment angle and a sample window (t_p = positive threshold, t_n = negative threshold, T_f = time frame and m=first maximum point) (c) algorithm output (0=no event, 2=event detected and hs=heel strike) and (d) heel switch output.

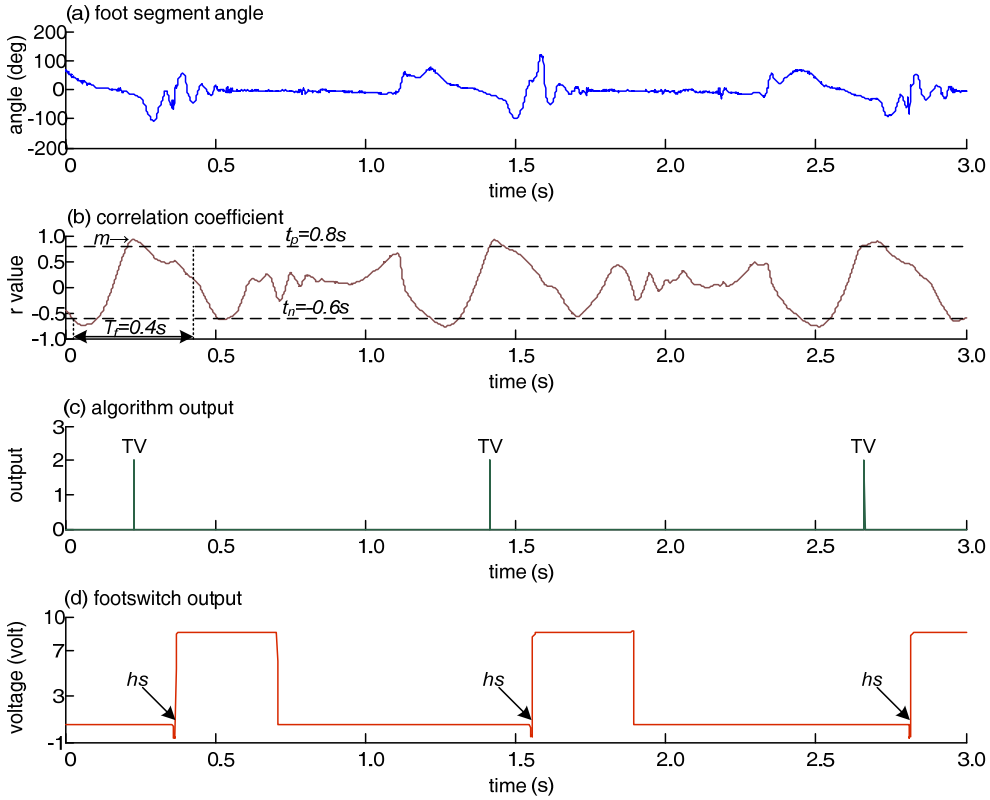

Figure K-46 Tibial vertical events in Subject 4 (left foot), n=3.

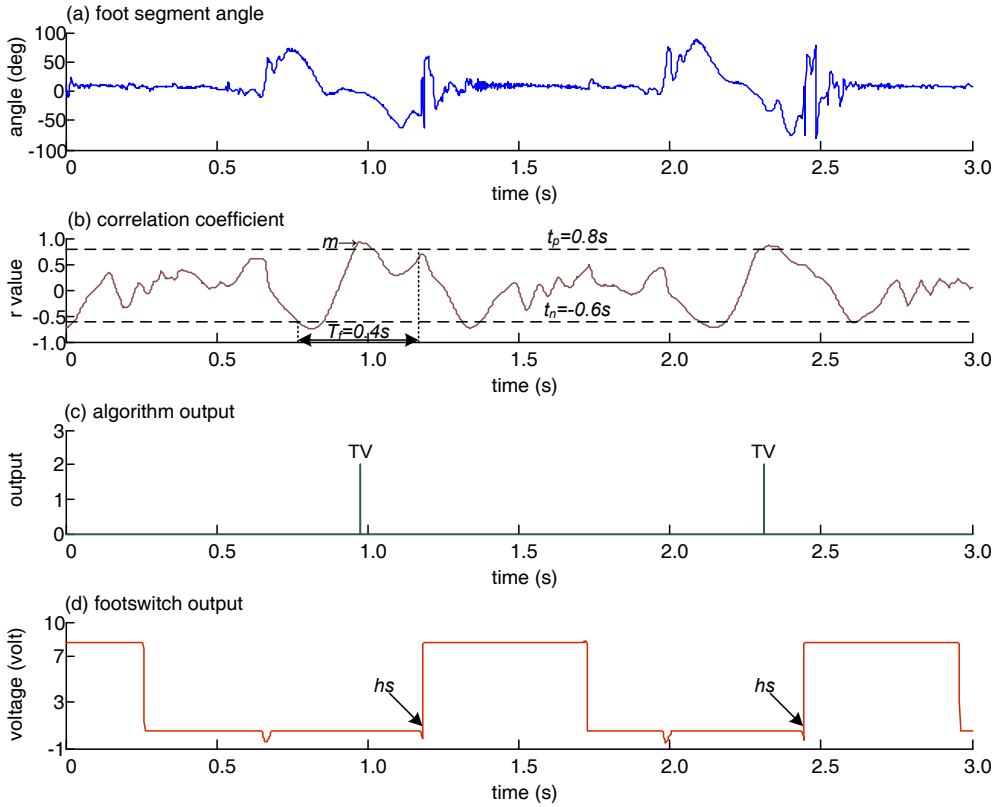

Figure K-47 Tibial vertical events in Subject 4 (left foot), n=2.

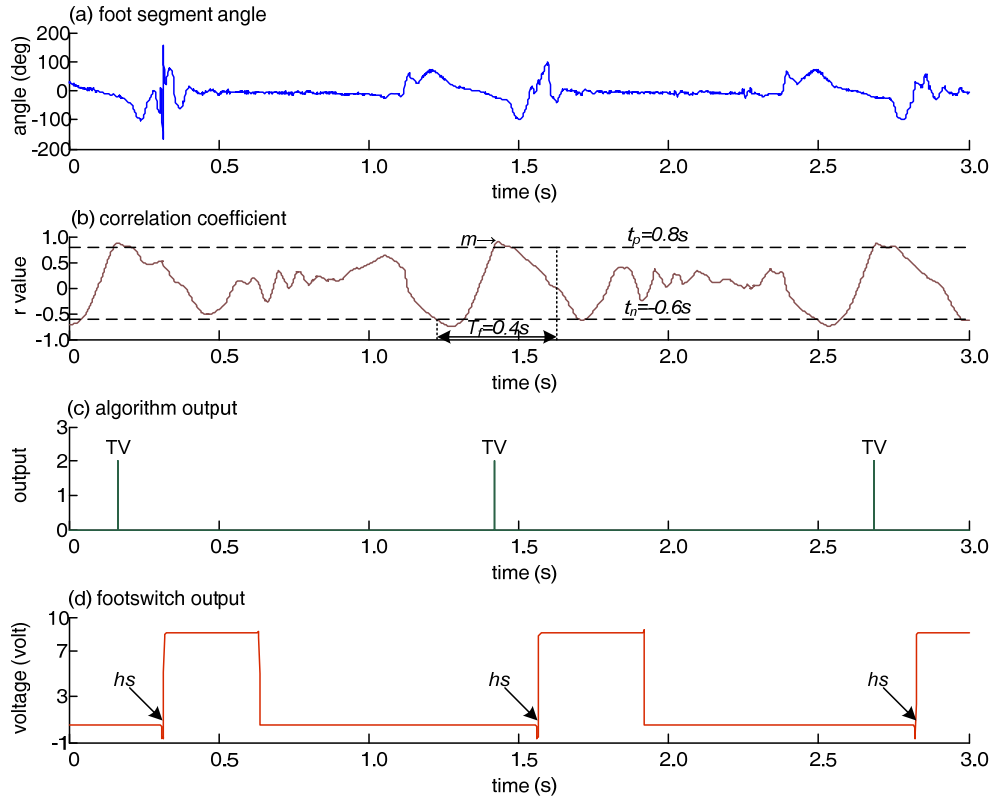

Figure K-48 Tibial vertical events in Subject 4 (left foot), n=3.

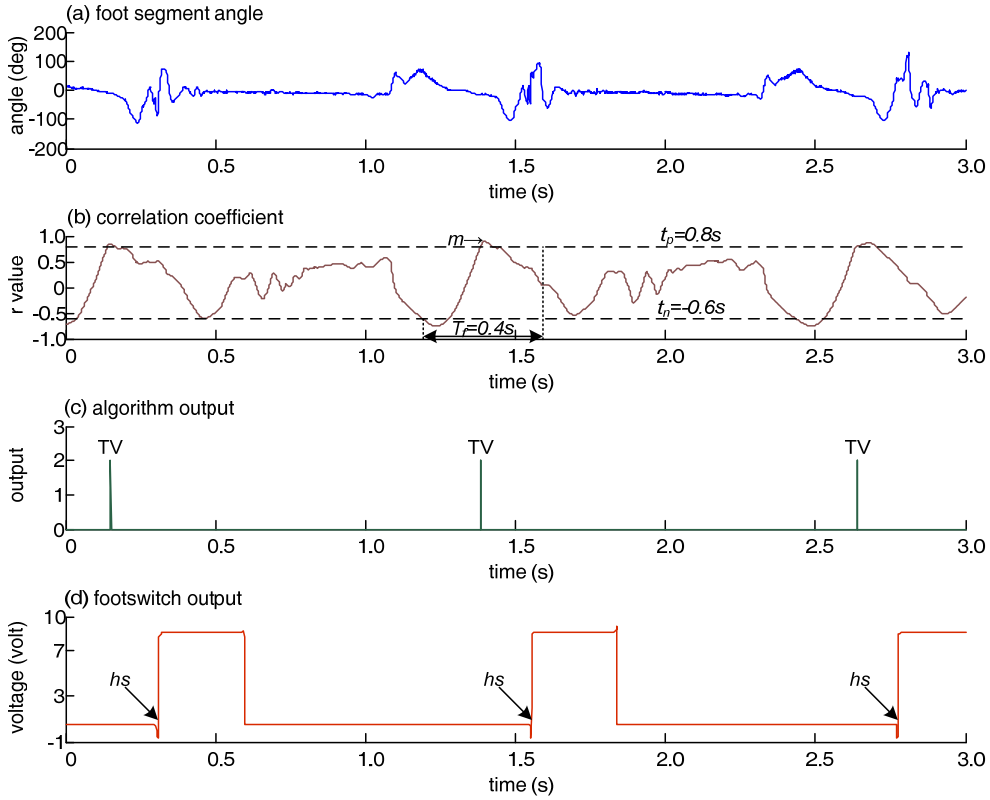

Figure K-49 Tibial vertical events in Subject 4 (left foot), n=3.

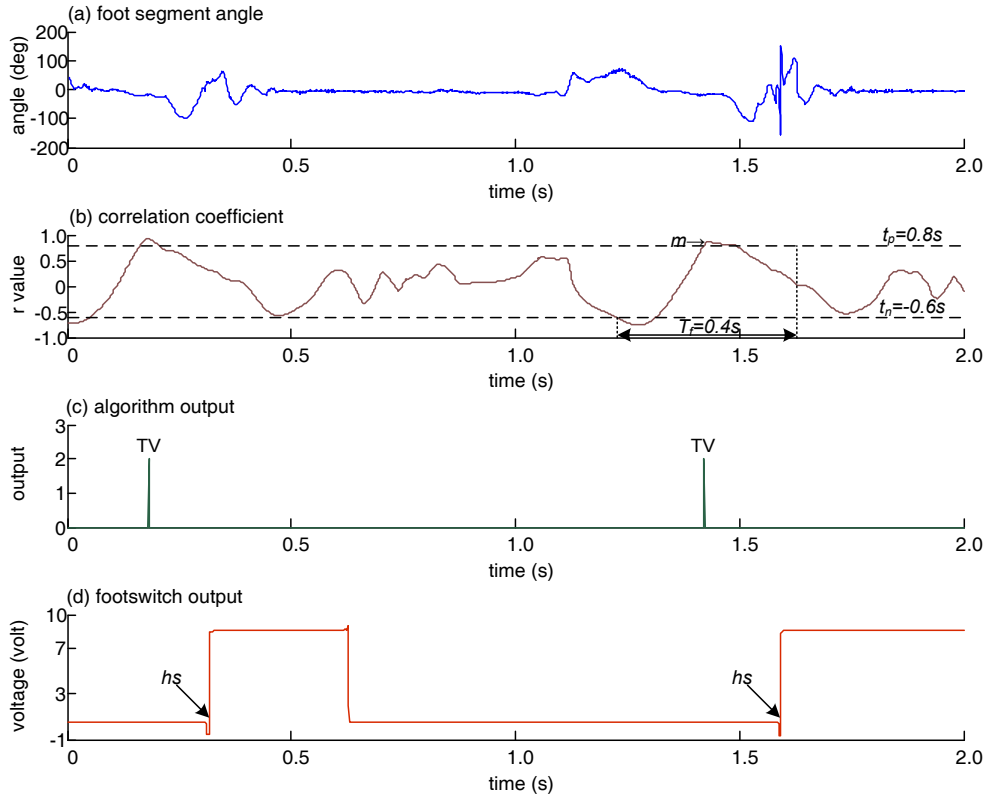

Figure K-50 Tibial vertical events in Subject 4 (left foot), n=2.

Figure K-51 to Figure K-56: Tibial vertical events in Subject 5 (right foot). (a) foot segment angle (b) correlation coefficient between foot segment angle and a sample window (t_p = positive threshold, t_n = negative threshold, T_f = time frame and m=first maximum point) (c) algorithm output (0=no event, 2=event detected and hs=heel strike) and (d) heel switch output.

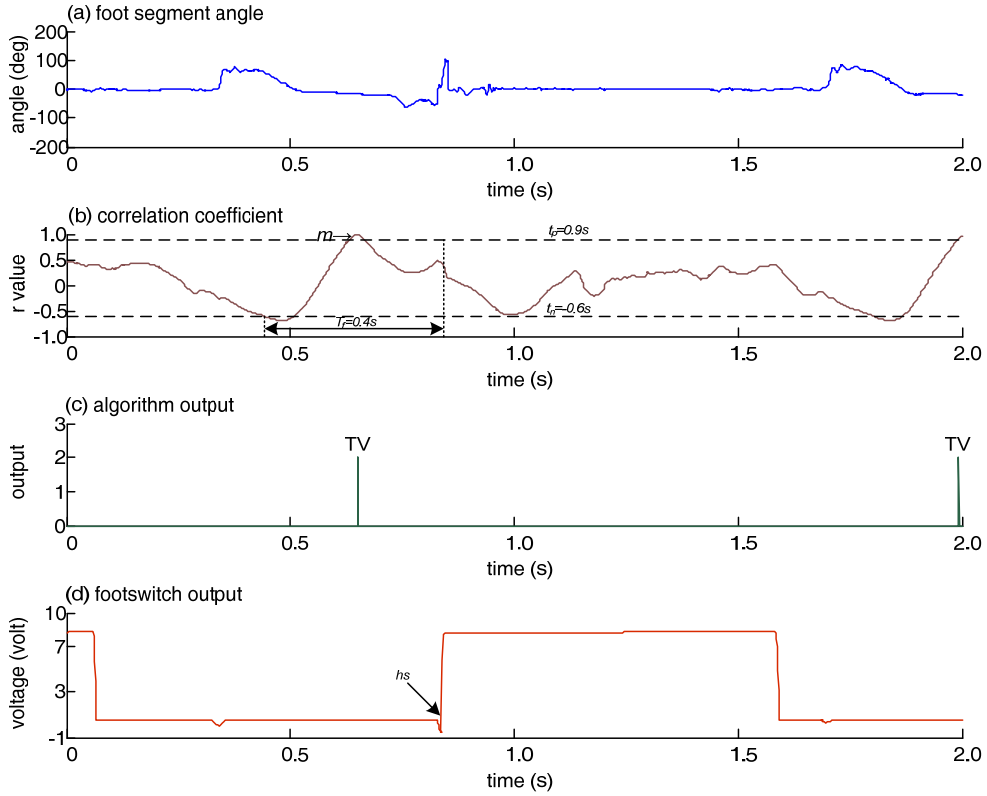

Figure K-51 Tibial vertical events in Subject 5 (right foot), n=2.

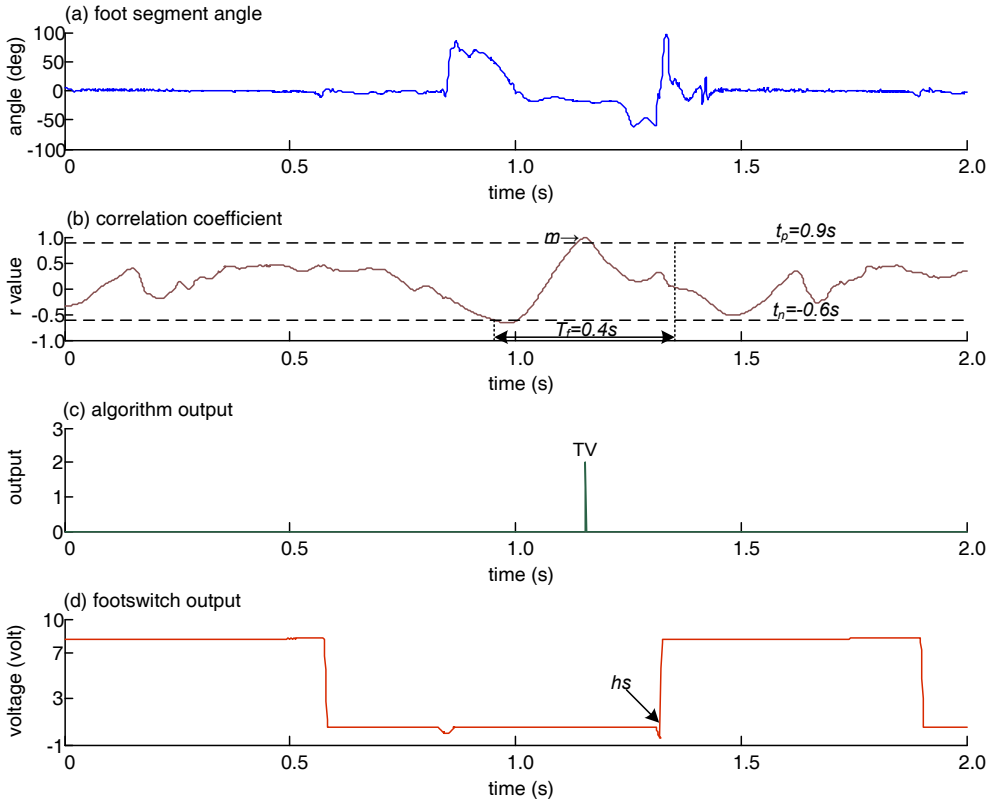

Figure K-52 Tibial vertical events in Subject 5 (right foot), n=1.

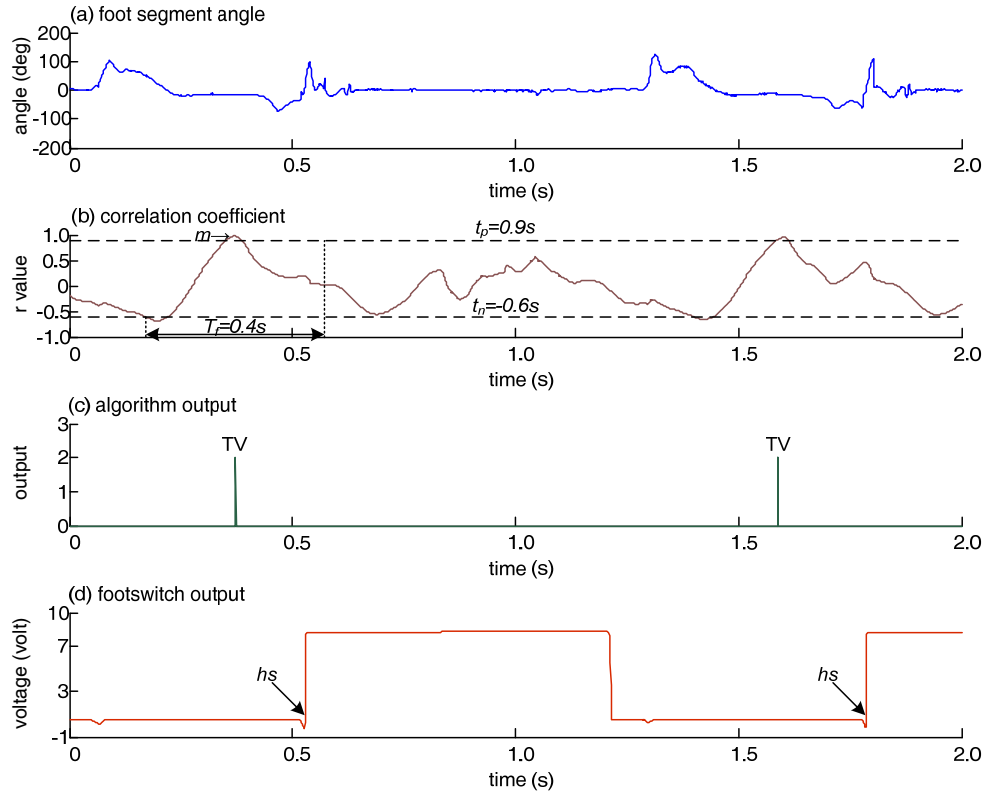

Figure K-53 Tibial vertical events in Subject 5 (right foot), n=2.

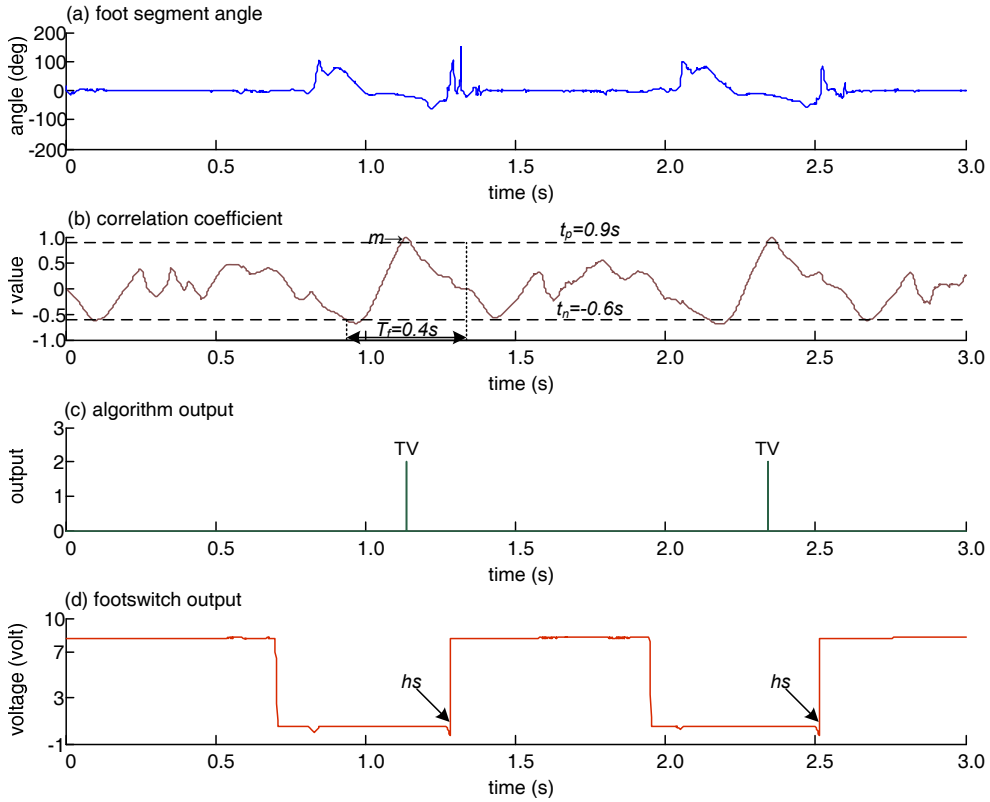

Figure K-54 Tibial vertical events in Subject 5 (right foot), n=2.

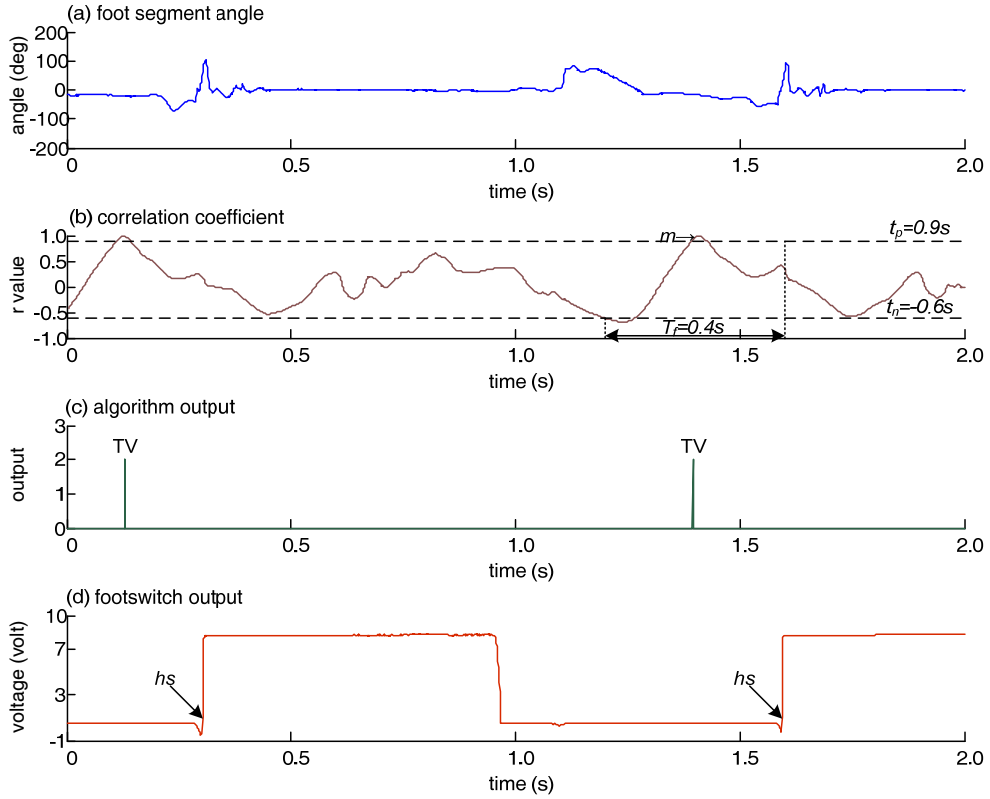

Figure K-55 Tibial vertical events in Subject 5 (right foot), n=2.

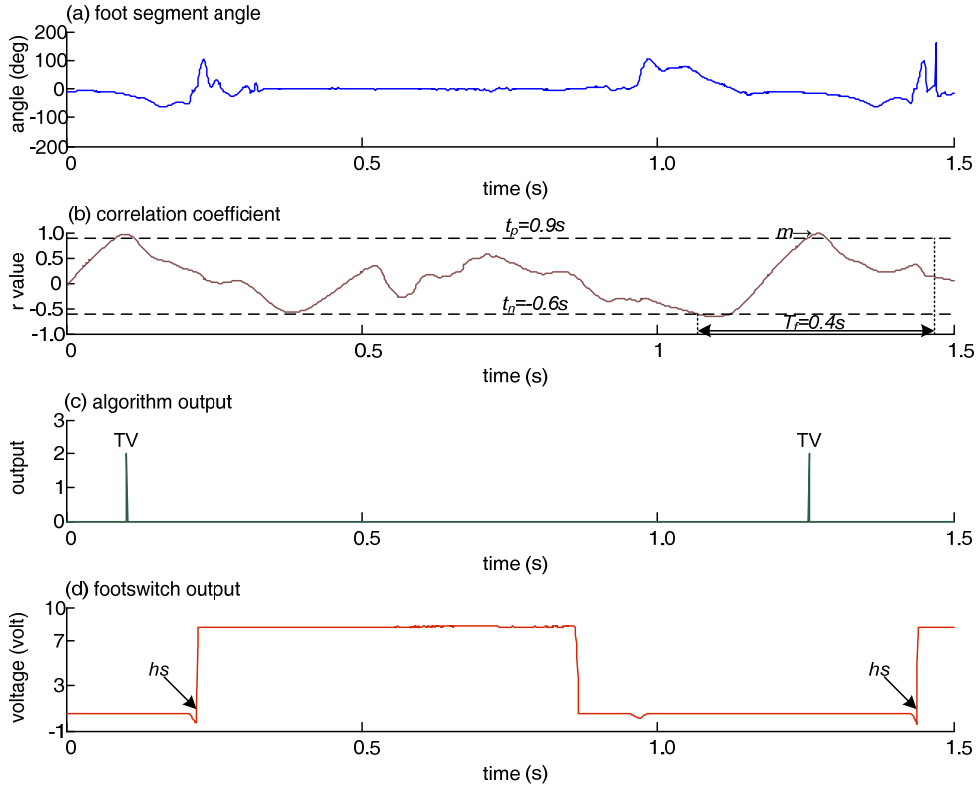

Figure K-56 Tibial vertical events in Subject 5 (right foot), n=2.

Figure K-57 to Figure K-62: Tibial vertical events in Subject 5 (left foot). (a) foot segment angle (b) correlation coefficient between foot segment angle and a sample window (t_p = positive threshold, t_n = negative threshold, T_f = time frame and m=first maximum point) (c) algorithm output (0=no event, 2=event detected and hs=heel strike) and (d) heel switch output.

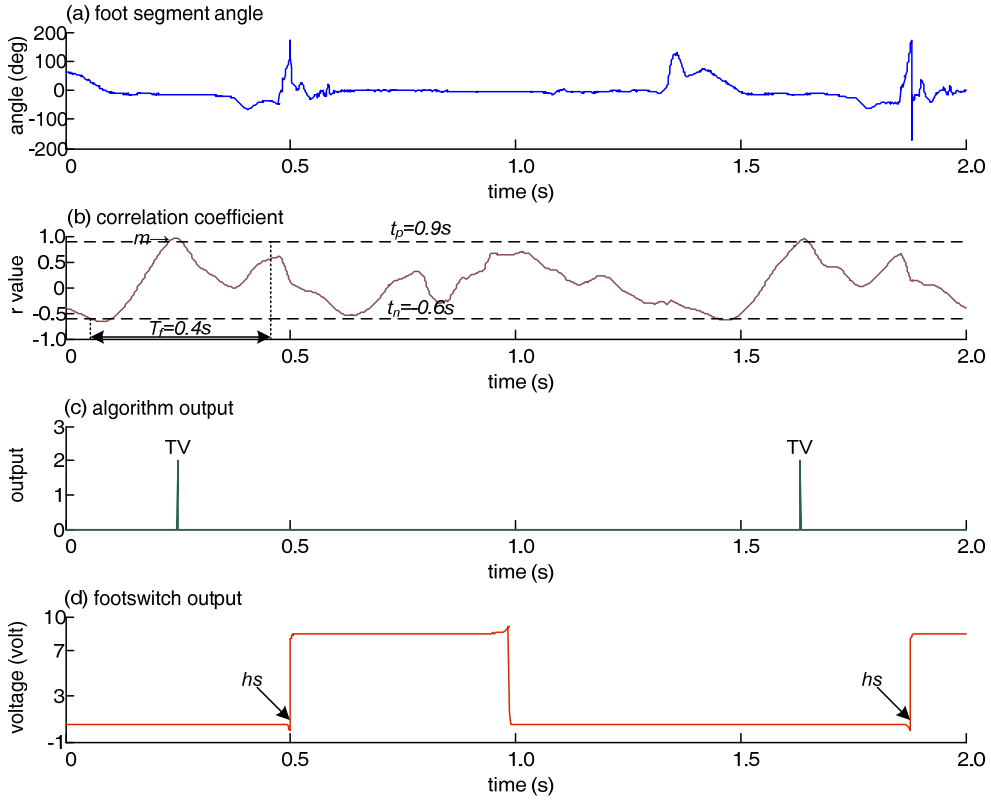

Figure K-57 Tibial vertical events in Subject 5 (left foot), n=2.

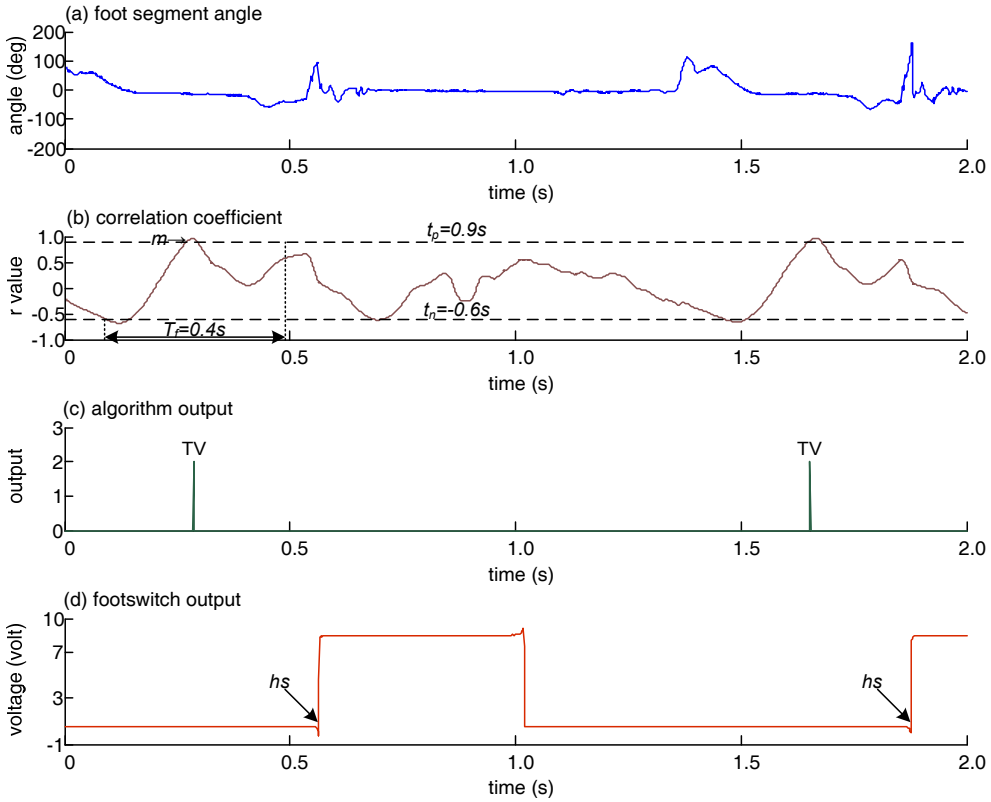

Figure K-58 Tibial vertical events in Subject 5 (left foot), n=2.

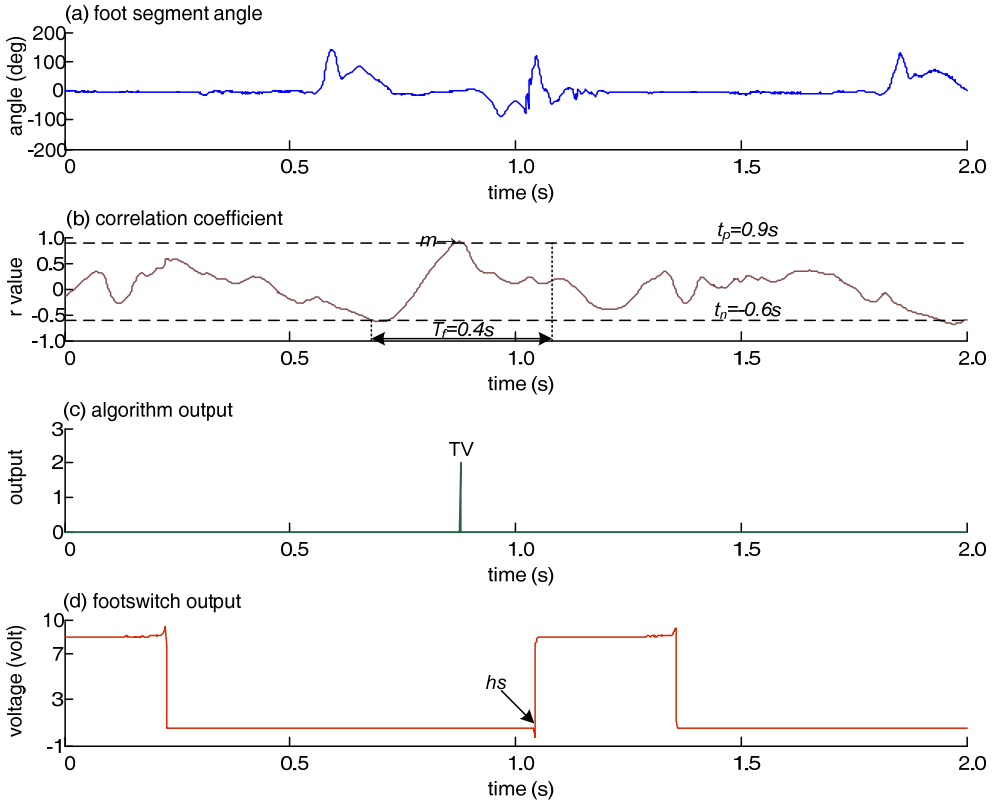

Figure K-59 Tibial vertical events in Subject 5 (left foot), n=1.

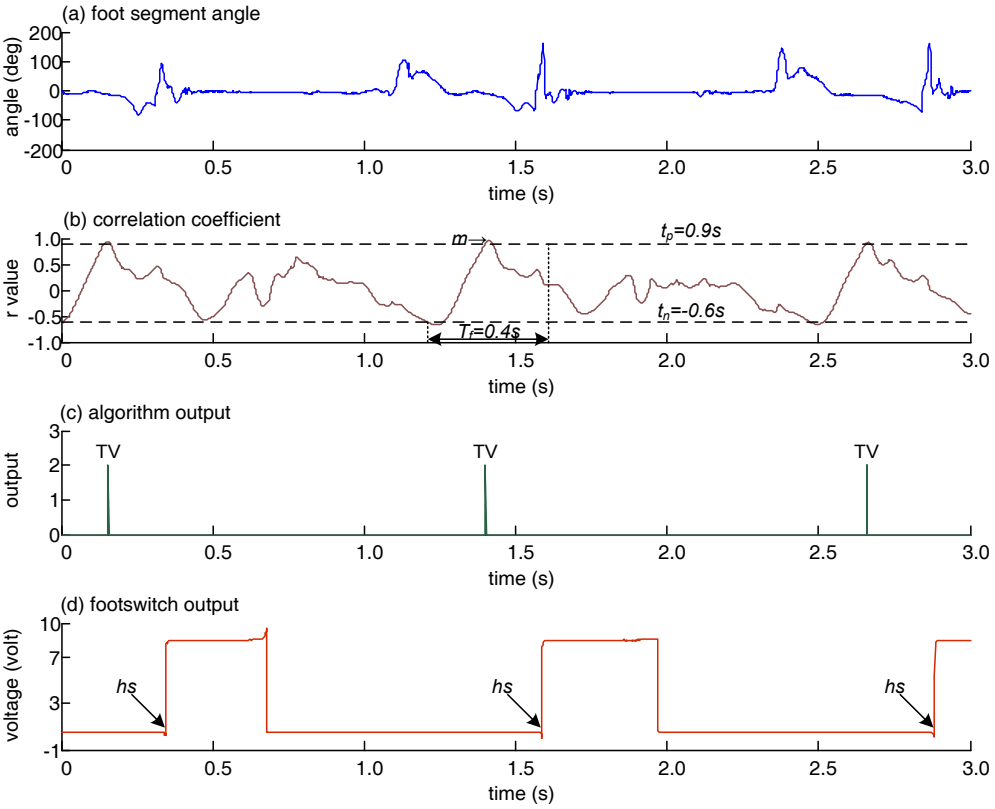

Figure K-60 Tibial vertical events in Subject 5 (left foot), n=3.

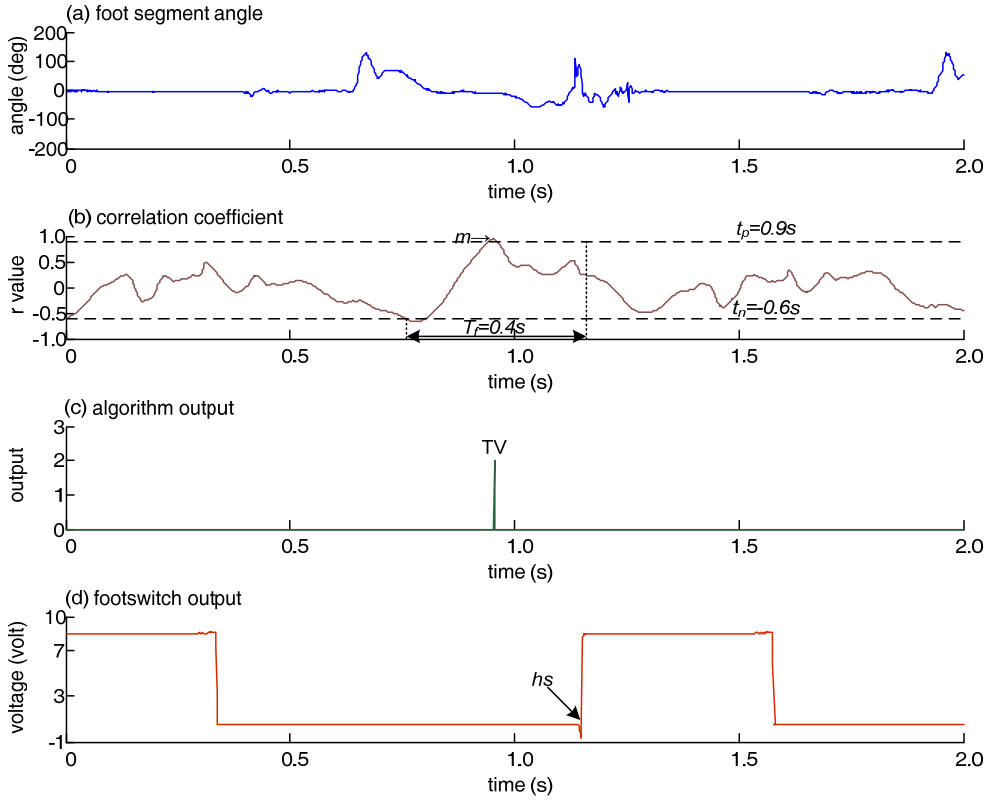

Figure K-61 Tibial vertical events in Subject 5 (left foot), n=1.

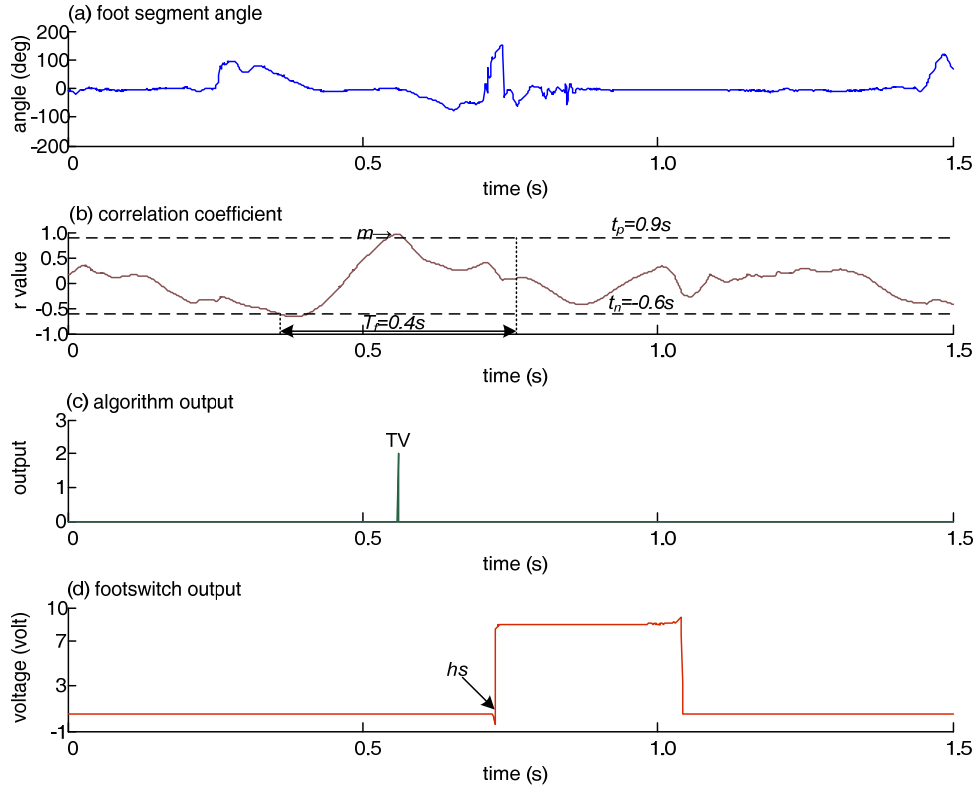

Figure K-62 Tibial vertical events in Subject 5 (left foot), n=1.

Appendix L

Results for the tibial vertical events detection in neurological patients.

Figure L-1 and Figure L-2: Tibial vertical event detection in patient (P1) when walking with stimulation on. Footswitches output: heel switch (red) and toe switch (purple). (TS=toe strike, HS=heel strike and TV=tibia vertical).

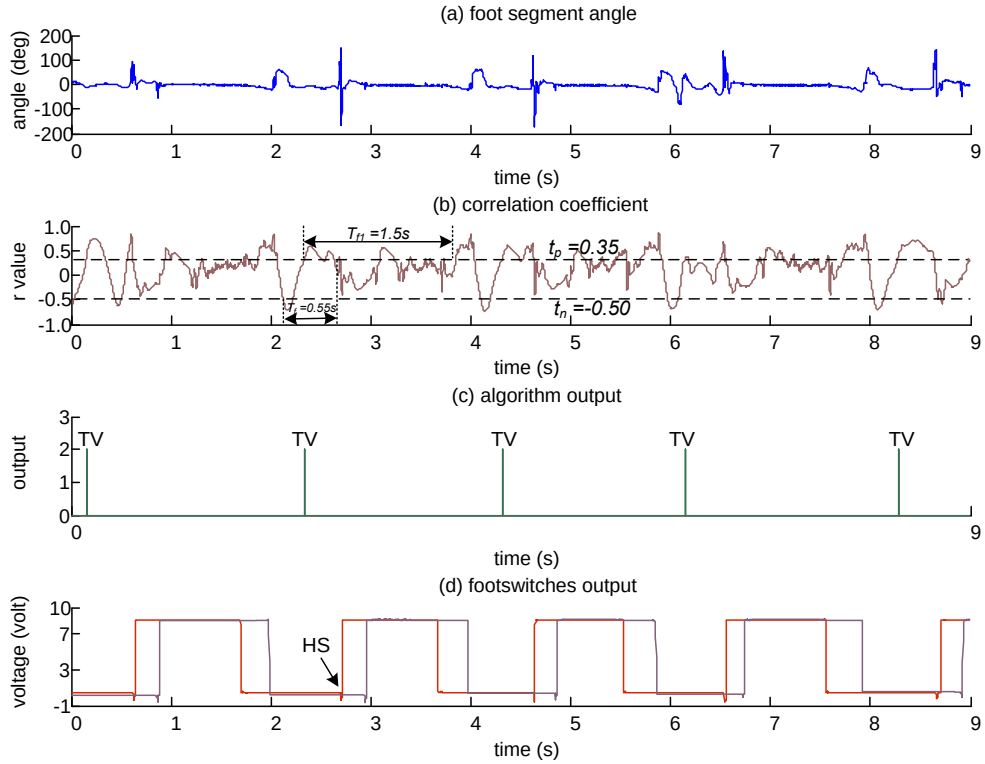

Figure L-1 Tibial vertical event detection in patient (P1) when walking with stimulation on, n=5.

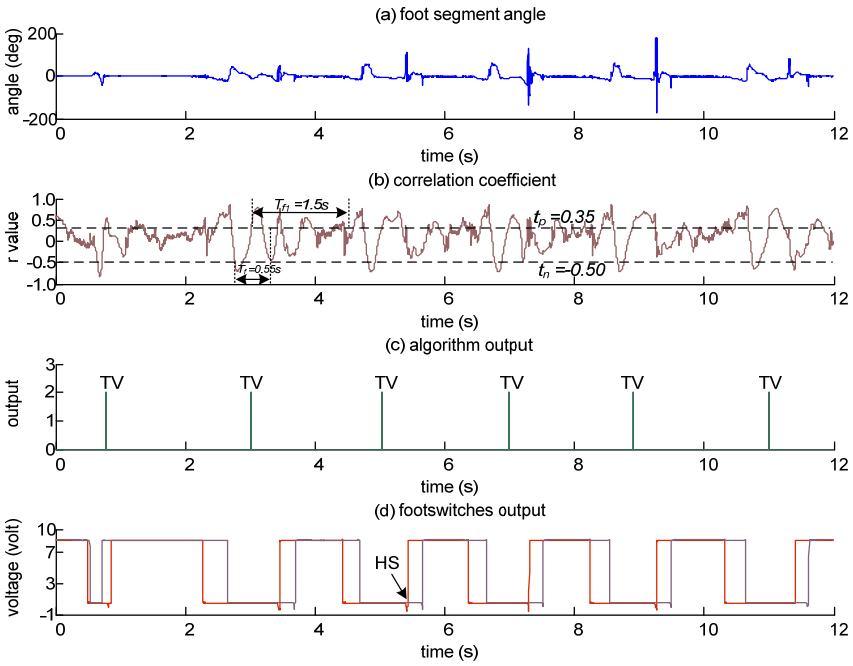

Figure L-2 Tibial vertical event detection in patient (P1) when walking with stimulation on, n=6.

Figure L-3 and Figure L-4: Tibial vertical event detection in patient (P1) when walking with stimulation off. Footswitches output: heel switch (red) and toe switch (purple). (TS=toe strike, HS=heel strike and TV=tibia vertical).

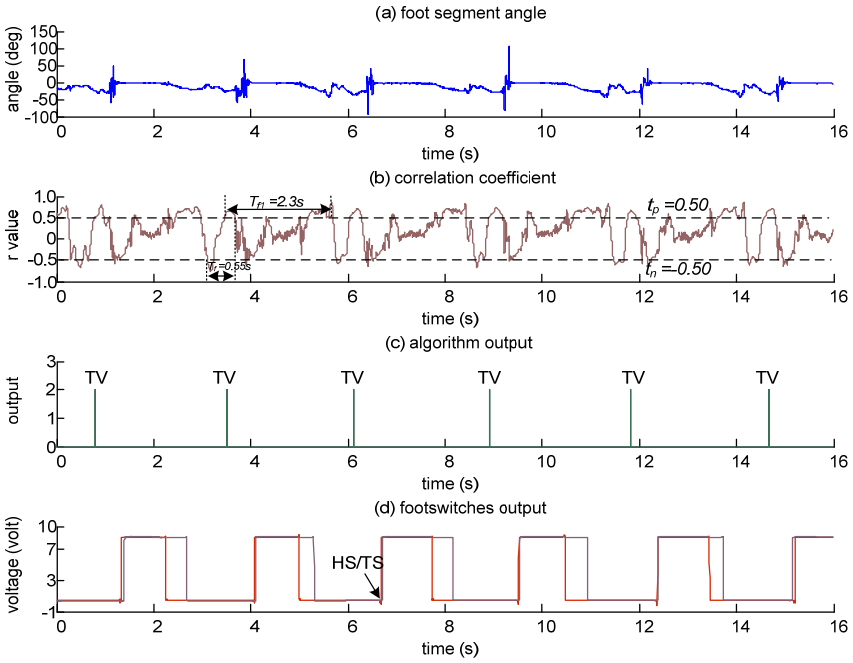

Figure L-3 Tibial vertical event detection in patient (P1) when walking with stimulation off, n=6.

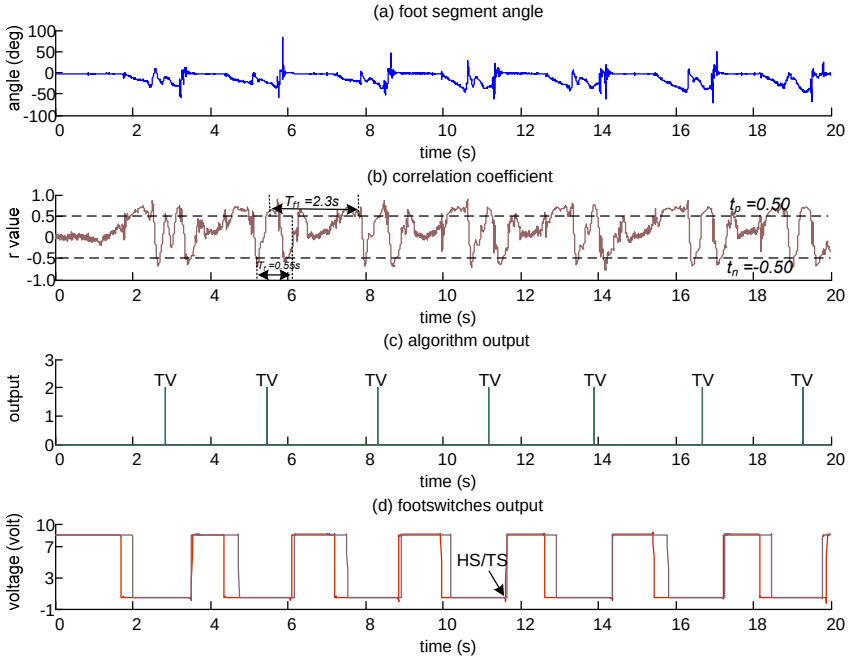

Figure L-4 Tibial vertical event detection in patient (P1) when walking with stimulation off, n=7.

Figure L-5 to Figure L-8: Tibial vertical event detection in patient (P2) when walking with stimulation off. Footswitches output: heel switch (red) and toe switch (purple). (HS=heel strike and TV=tibia vertical).

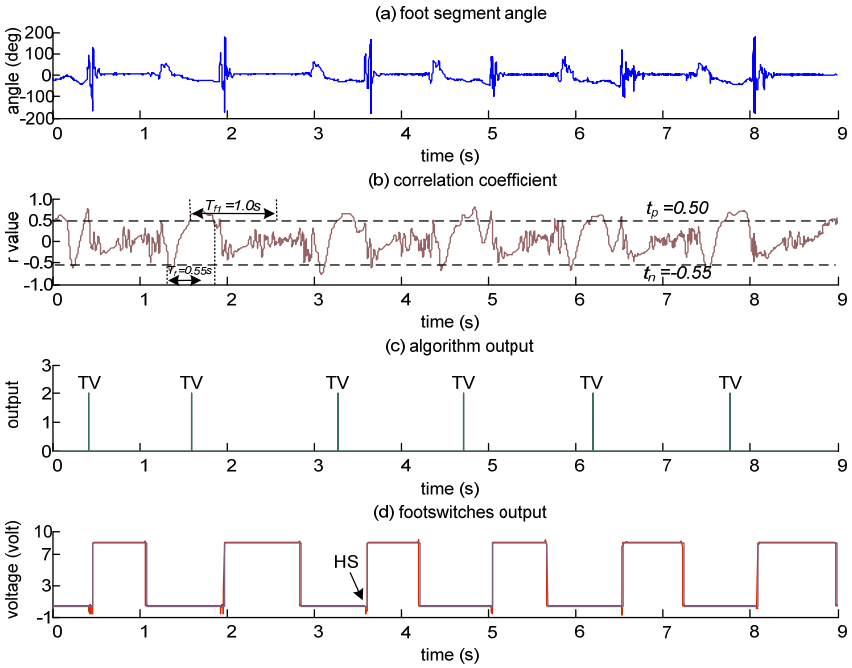

Figure L-5 Tibial vertical event detection in patient (P2) when walking with stimulation off, n=6.

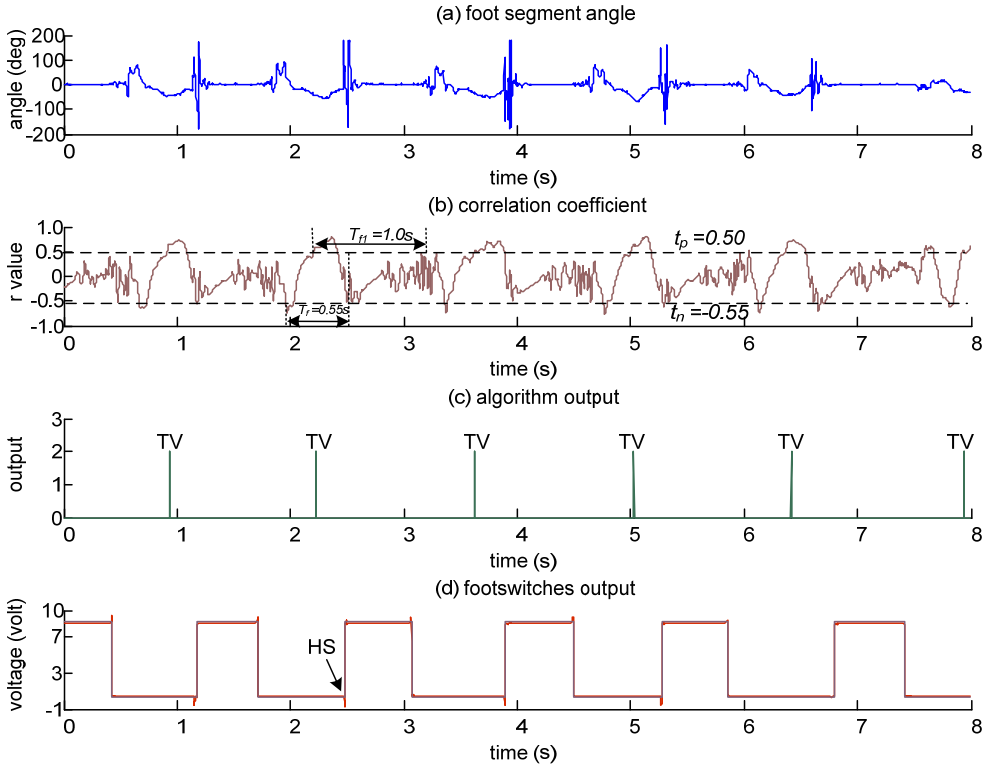

Figure L-6 Tibial vertical event detection in patient (P2) when walking with stimulation off, n=6.

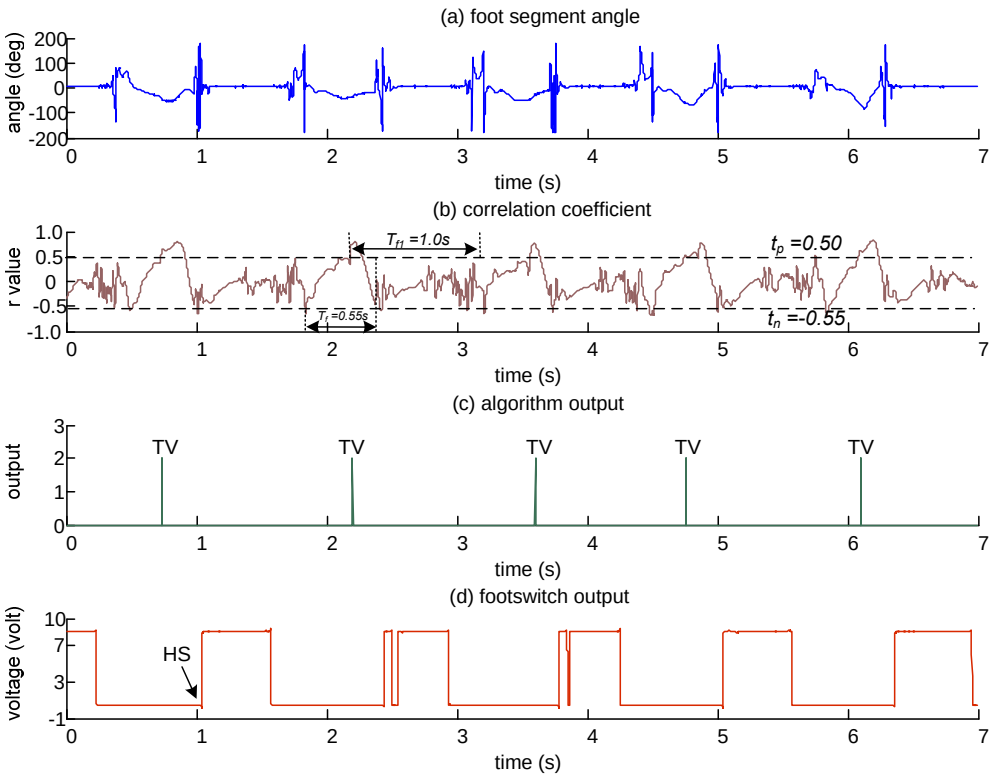

Figure L-7 Tibial vertical event detection in patient (P2) when walking with stimulation off, n=5.

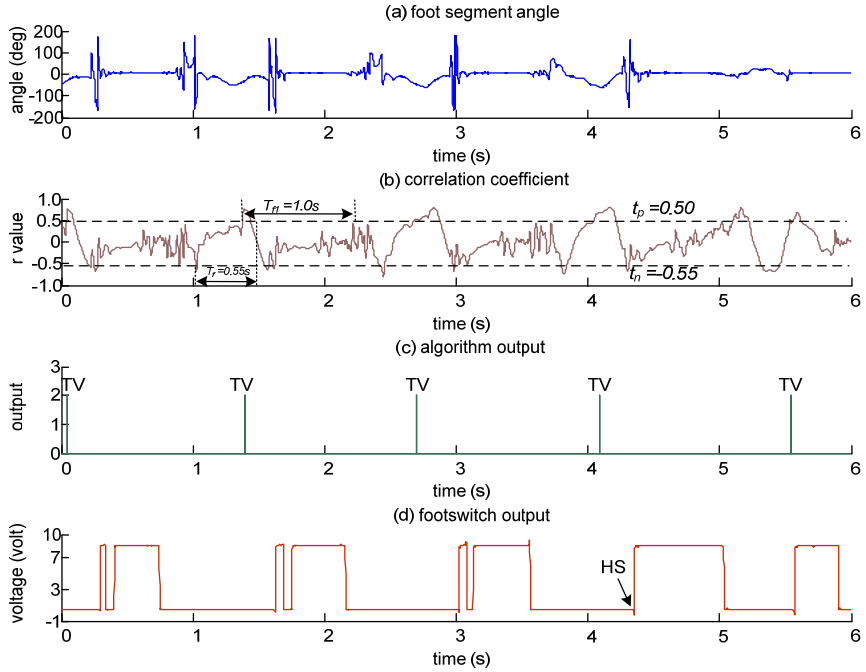

Figure L-8 Tibial vertical event detection in patient (P2) when walking with stimulation off, n=5.

Figure L-9 to Figure L-12: Tibial vertical event detection in patient (P2) when walking with stimulation on. Footswitches output: heel switch (red) and toe switch (purple). (HS=heel strike and TV=tibia vertical).

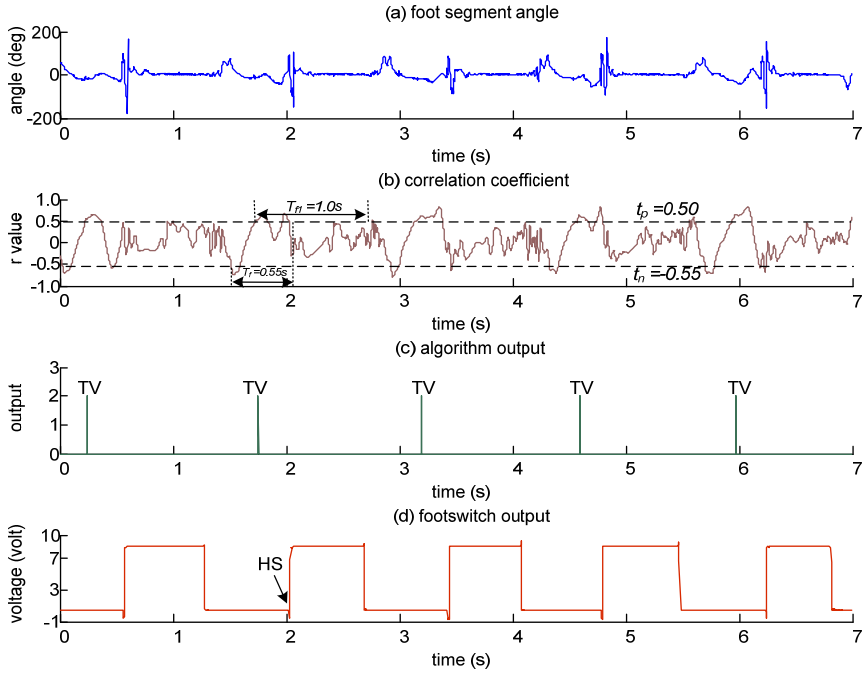

Figure L-9 Tibial vertical event detection in patient (P2) when walking with stimulation on, n=5.

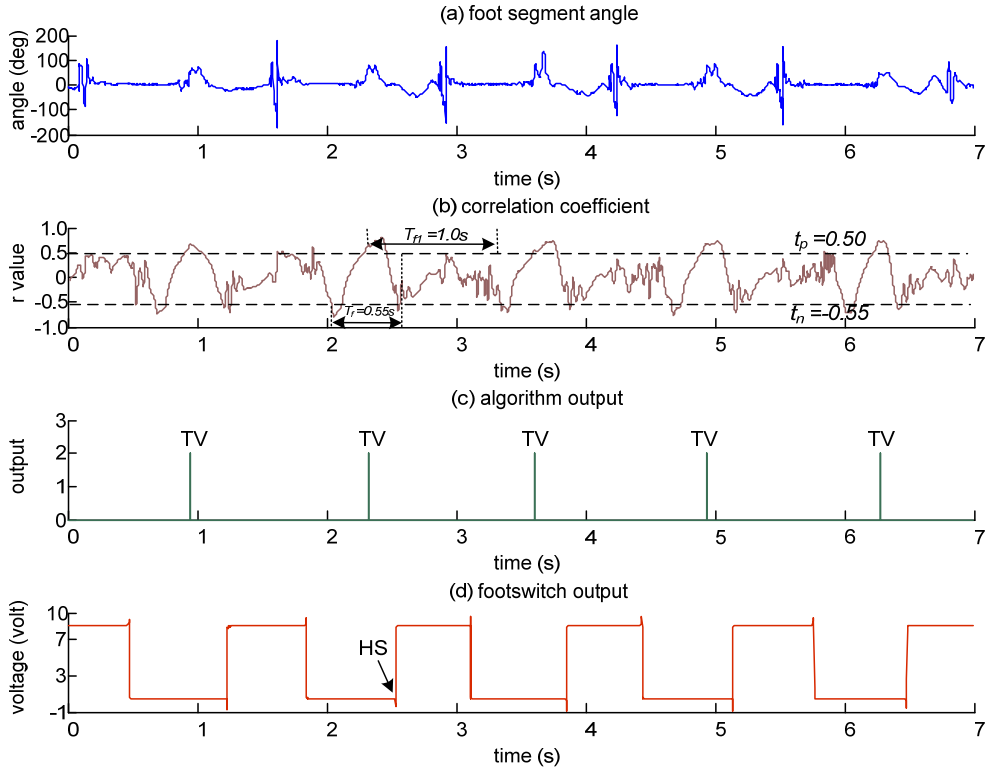

Figure L-10 Tibial vertical event detection in patient (P2) when walking with stimulation on, n=5.

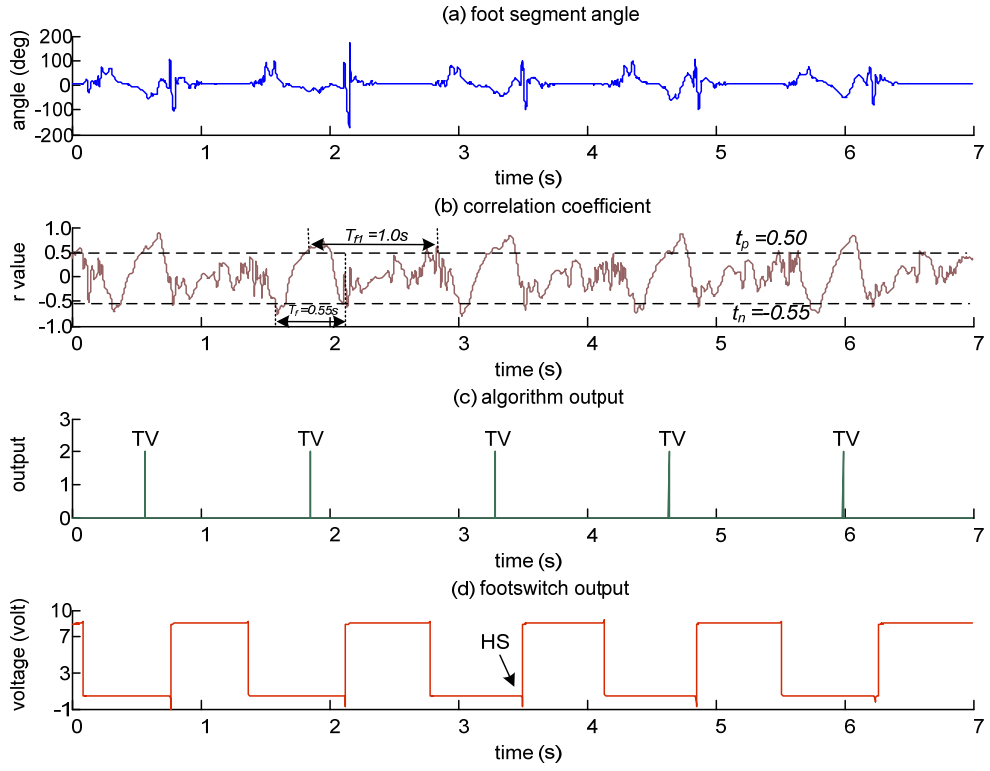

Figure L-11 Tibial vertical event detection in patient (P2) when walking with stimulation on, n=5.

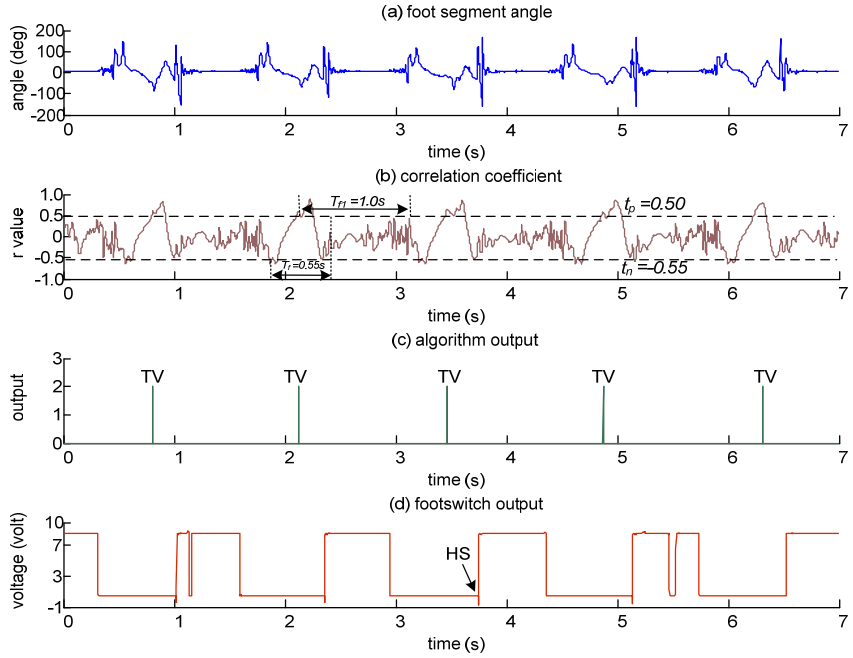

Figure L-12 Tibial vertical event detection in patient (P2) when walking with stimulation on, n=5.

Figure L-13 to Figure L-15: Tibial vertical event detection in patient (P3) when walking with stimulation on. Footswitches output: heel switch (red) and toe switch (purple). (TV=tibia vertical).

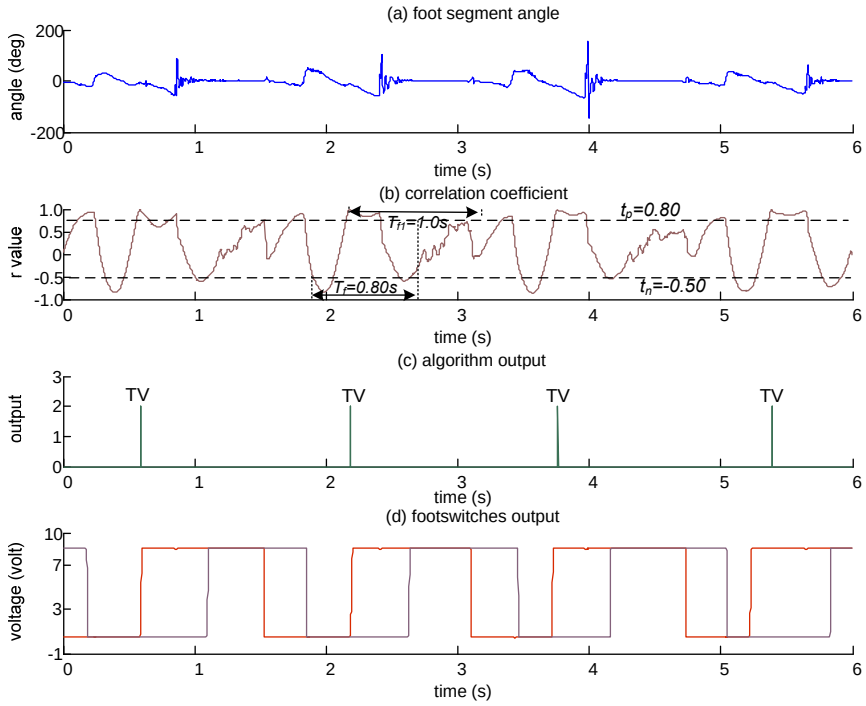

Figure L-13 Tibial vertical event detection in patient (P3) when walking with stimulation on, n=4.

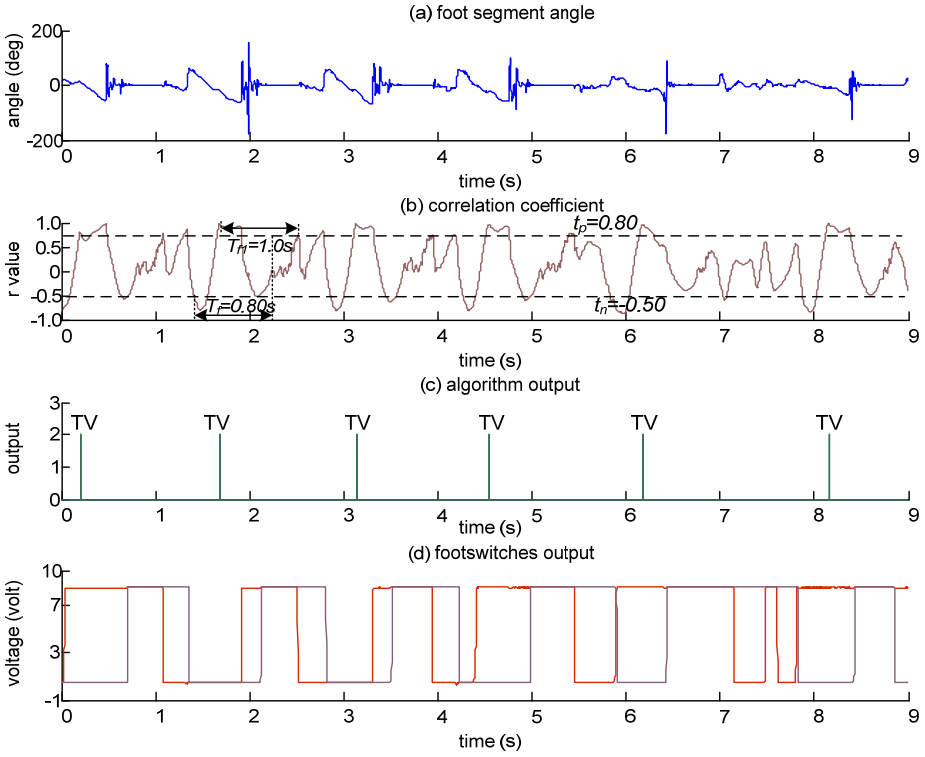

Figure L-14 Tibial vertical event detection in patient (P3) when walking with stimulation on, n=6.

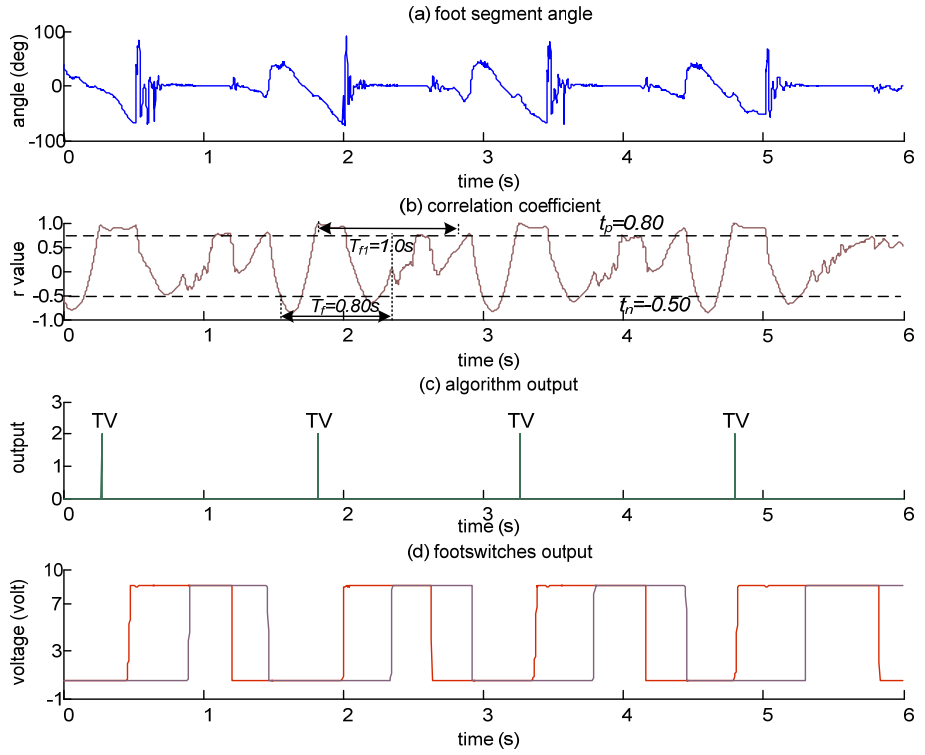

Figure L-15 Tibial vertical event detection in patient (P3) when walking with stimulation on, n=4.

Figure L-16 to Figure L-18: Tibial vertical event detection in patient (P3) when walking with stimulation off. Footswitches output: heel switch (red) and toe switch (purple). (TV=tibia vertical).

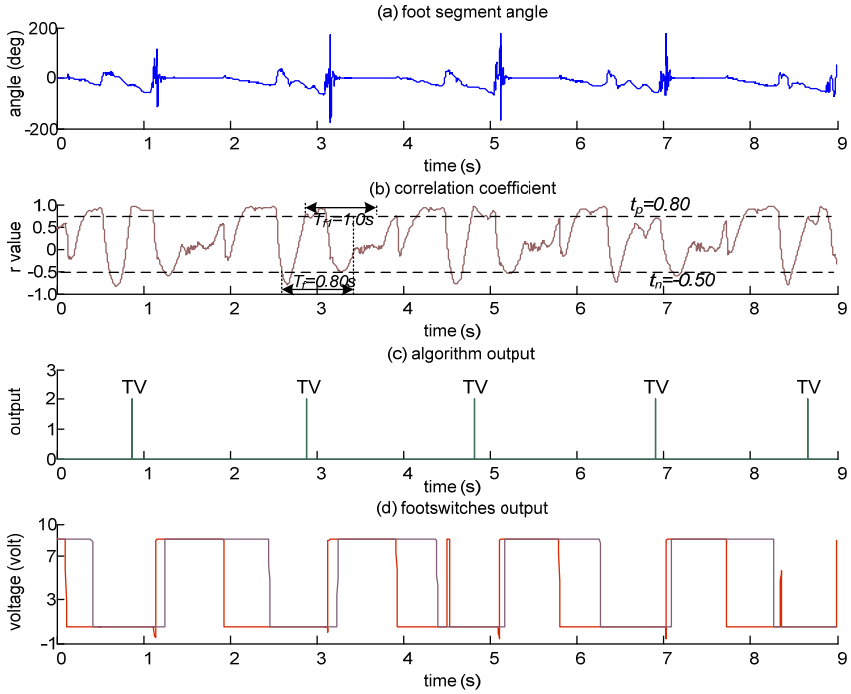

Figure L-16 Tibial vertical event detection in patient (P3) when walking with stimulation off, n=5.

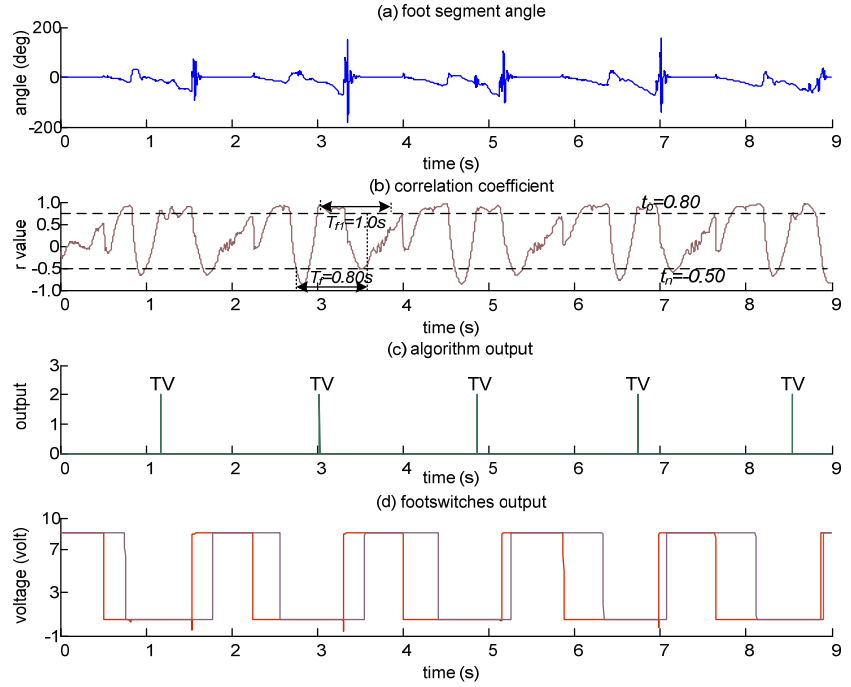

Figure L-17 Tibial vertical event detection in patient (P3) when walking with stimulation off, n=5.

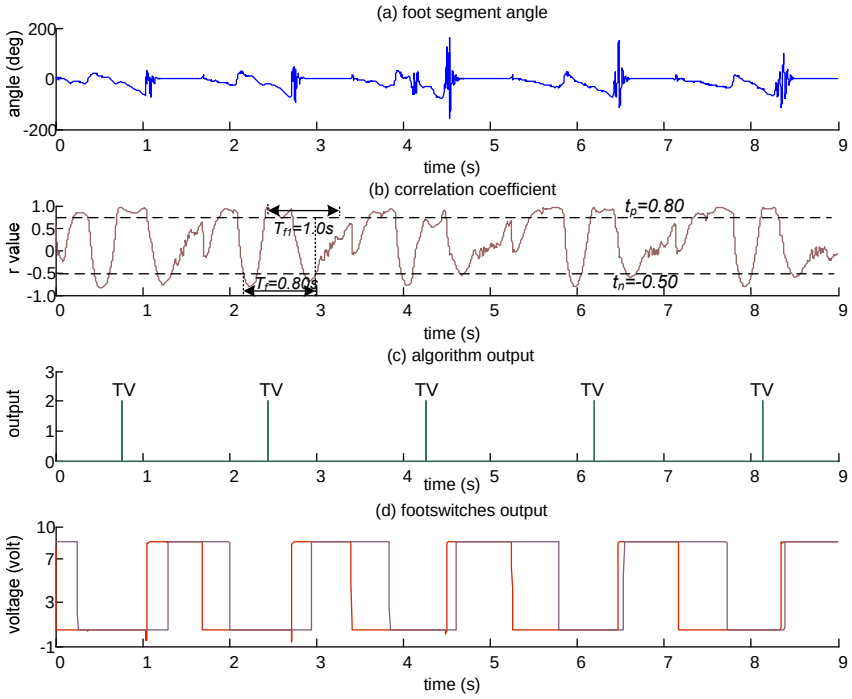

Figure L-18 Tibial vertical event detection in patient (P3) when walking with stimulation off, n=5.

Figure L-19 to Figure L-22: Tibial vertical event detection in patient (P5) when walking with stimulation off. Footswitches output: heel switch (red) and toe switch (purple). (TV=tibia vertical).

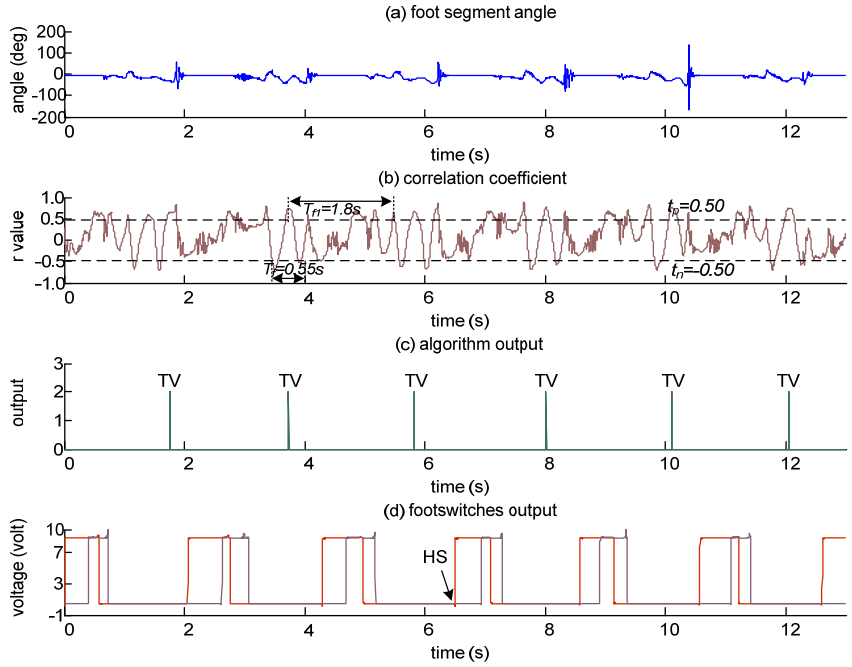

Figure L-19 Tibial vertical event detection in patient (P5) when walking with stimulation off, n=6.

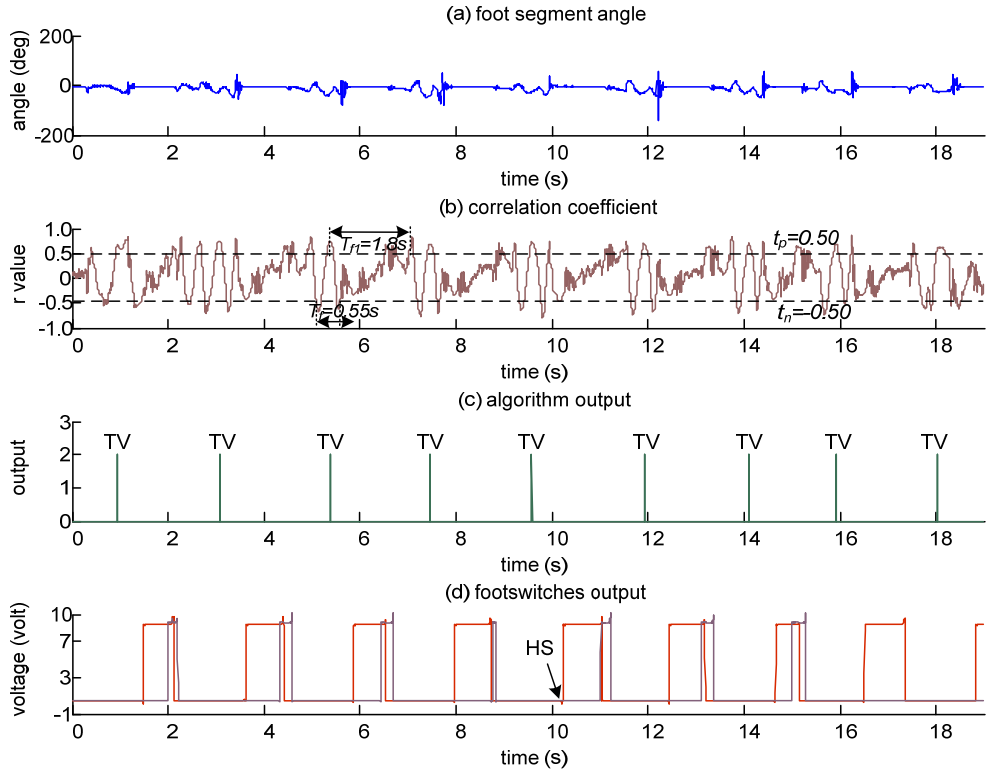

Figure L-20 Tibial vertical event detection in patient (P5) when walking with stimulation off, n=9.

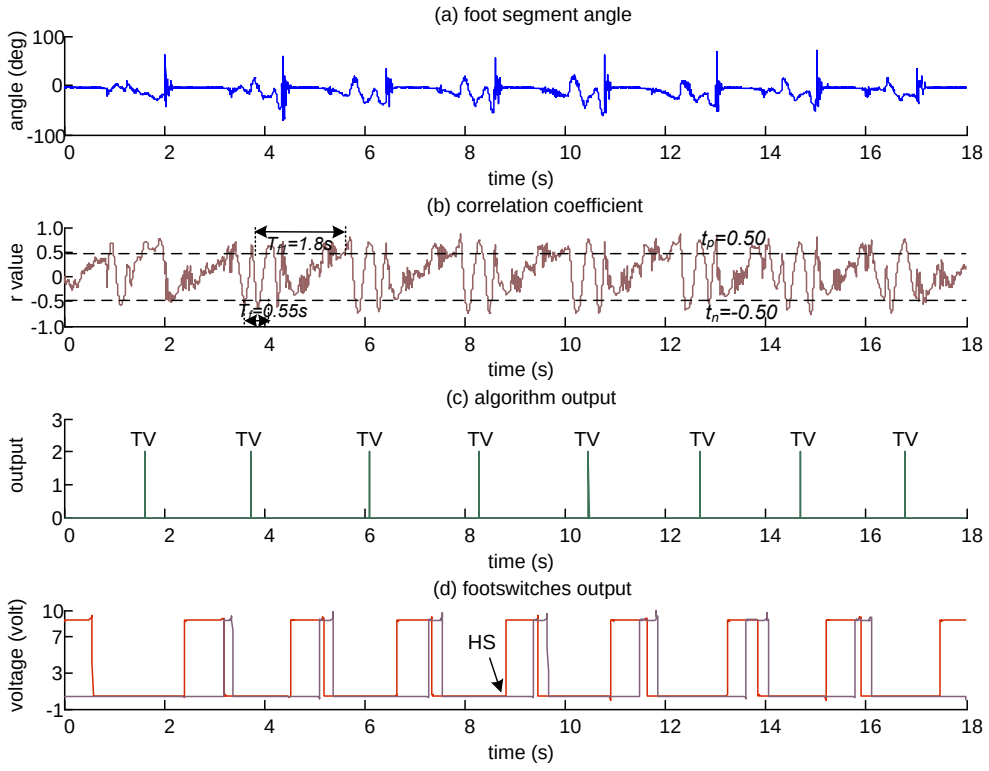

Figure L-21 Tibial vertical event detection in patient (P5) when walking with stimulation off, n=8.

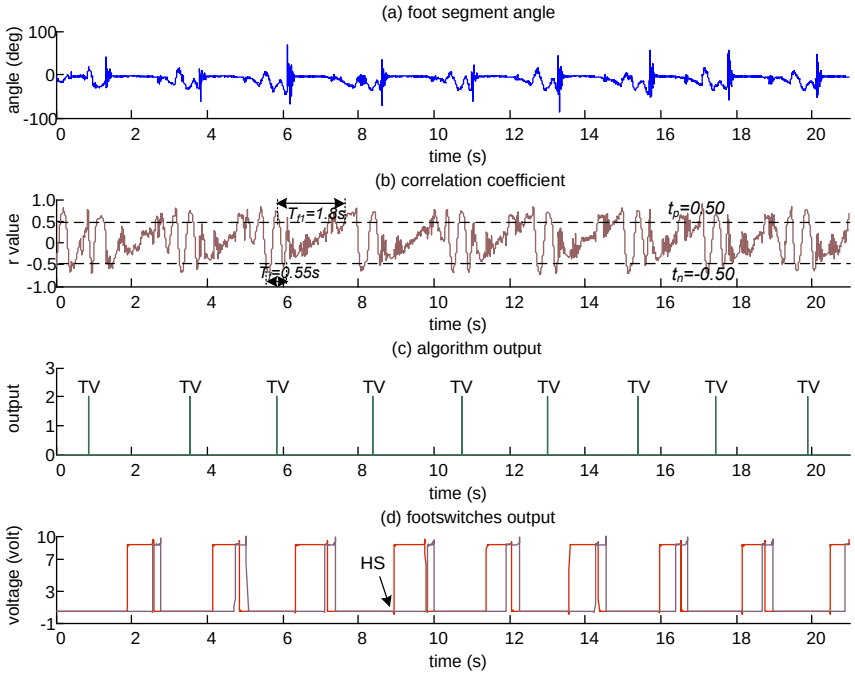

Figure L-22 Tibial vertical event detection in patient (P5) when walking with stimulation off, n=9.

Figure L-23 to Figure L-25: Tibial vertical event detection in patient (P5) when walking with stimulation on. Footswitches output: heel switch (red) and toe switch (purple). (TV=tibia vertical).

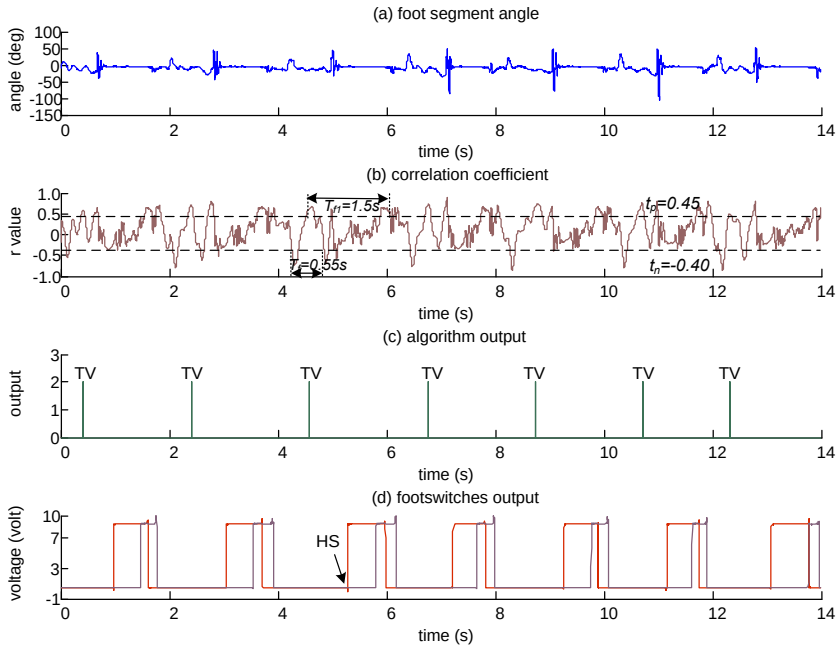

Figure L-23 Tibial vertical event detection in patient (P5) when walking with stimulation on, n=7.

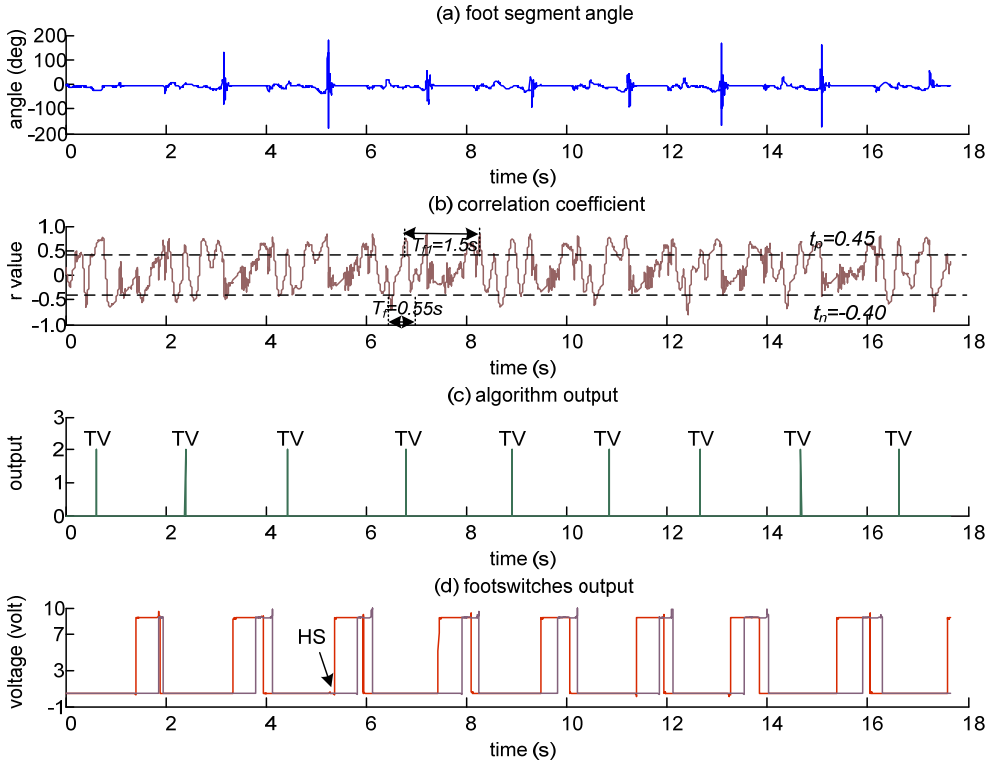

Figure L-24 Tibial vertical event detection in patient (P5) when walking with stimulation on, n=9.

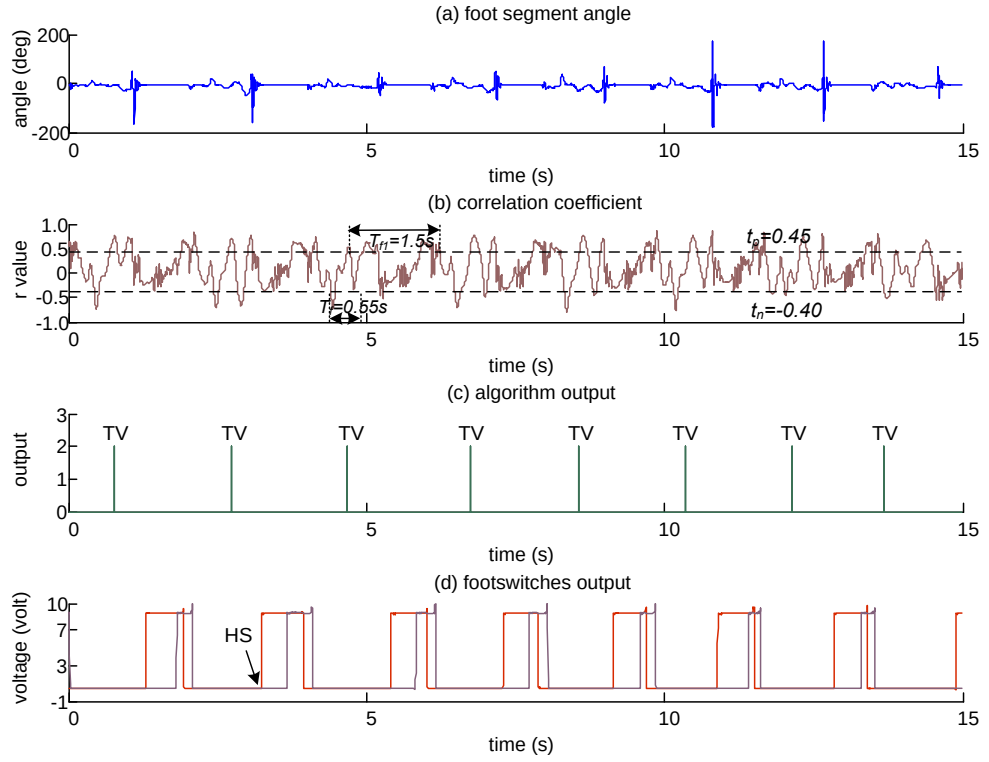

Figure L-25 Tibial vertical event detection in patient (P5) when walking with stimulation on, n=8.

Figure L-26 to Figure L-28: Tibial vertical event detection in patient (P6) when walking with stimulation off. Footswitches output: heel switch (red) and toe switch (purple). (TV=tibia vertical).

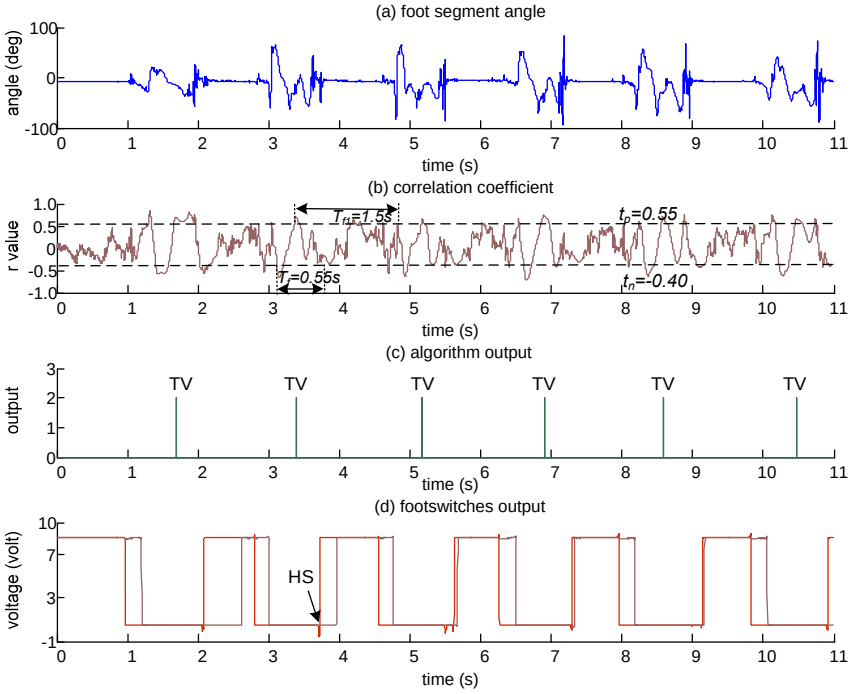

Figure L-26 Tibial vertical event detection in patient (P6) when walking with stimulation off, n=6.

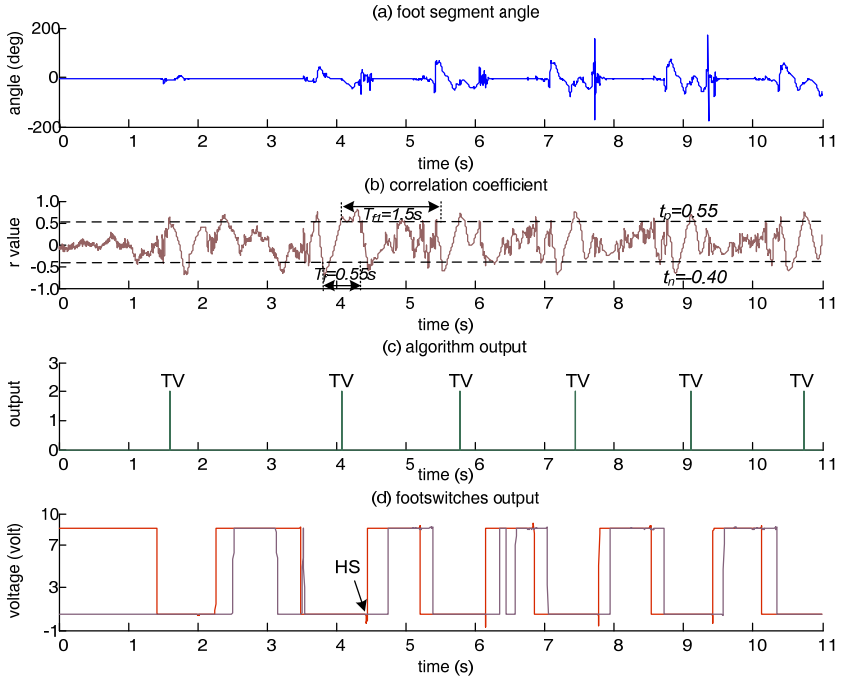

Figure L-27 Tibial vertical event detection in patient (P6) when walking with stimulation off, n=6.

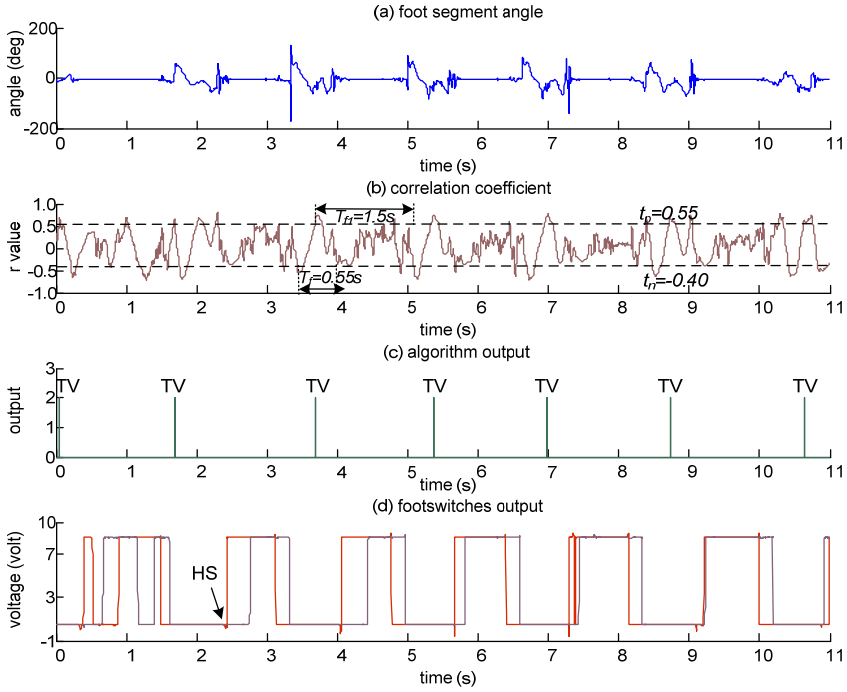

Figure L-28 Tibial vertical event detection in patient (P6) when walking with stimulation off, n=7.

Figure L-29 to Figure L-32: Tibia vertical event detection in patient (P6) when walking with stimulation on. Footswitches output: heel switch (red) and toe switch (purple). (TV=tibia vertical).

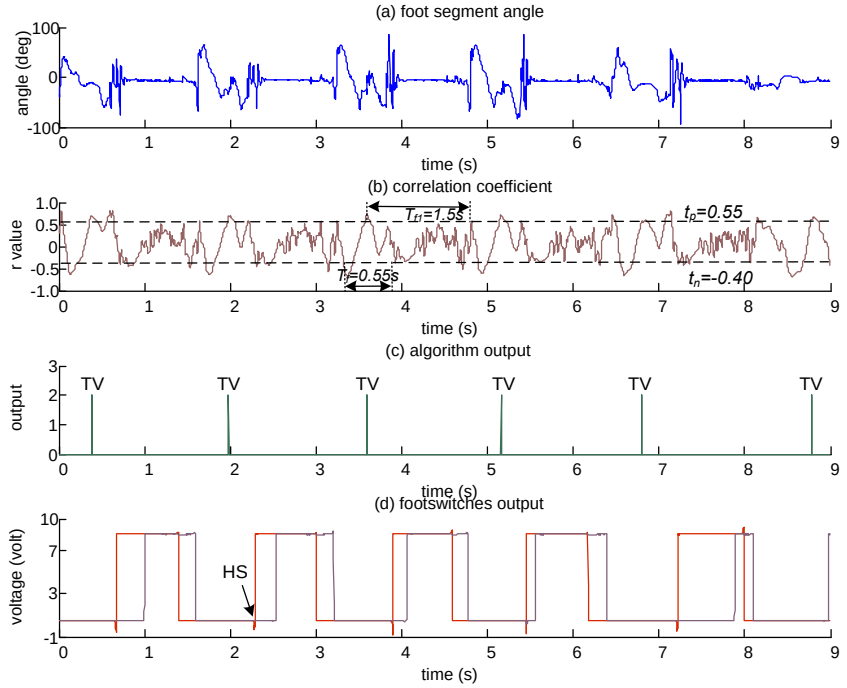

Figure L-29 Tibial vertical event detection in patient (P6) when walking with stimulation on, n=6.

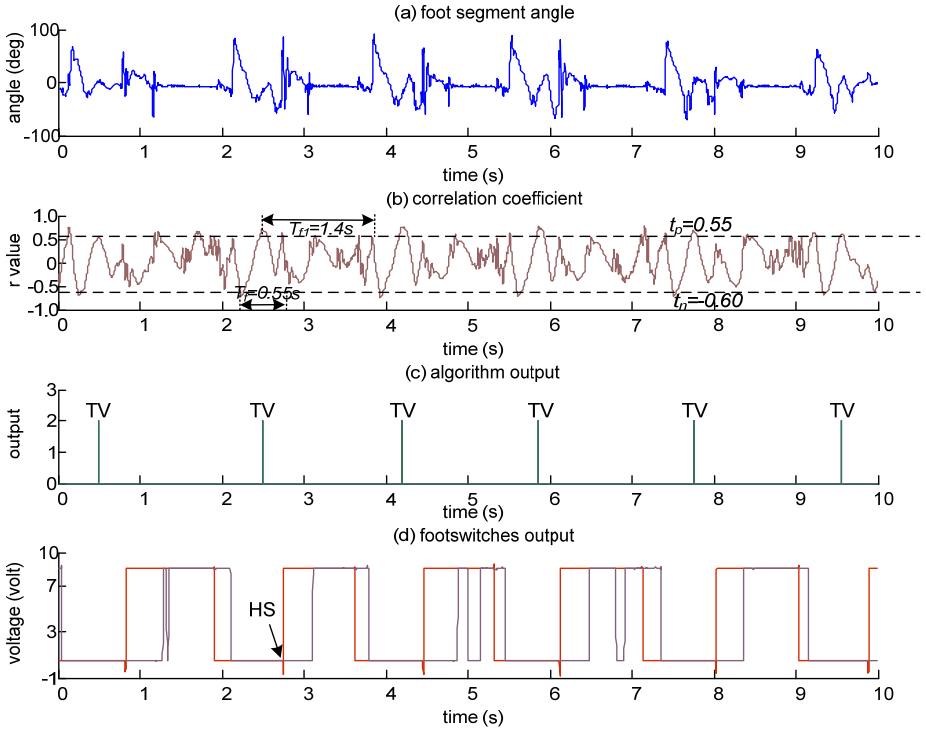

Figure L-30 Tibial vertical event detection in patient (P6) when walking with stimulation on, n=6.

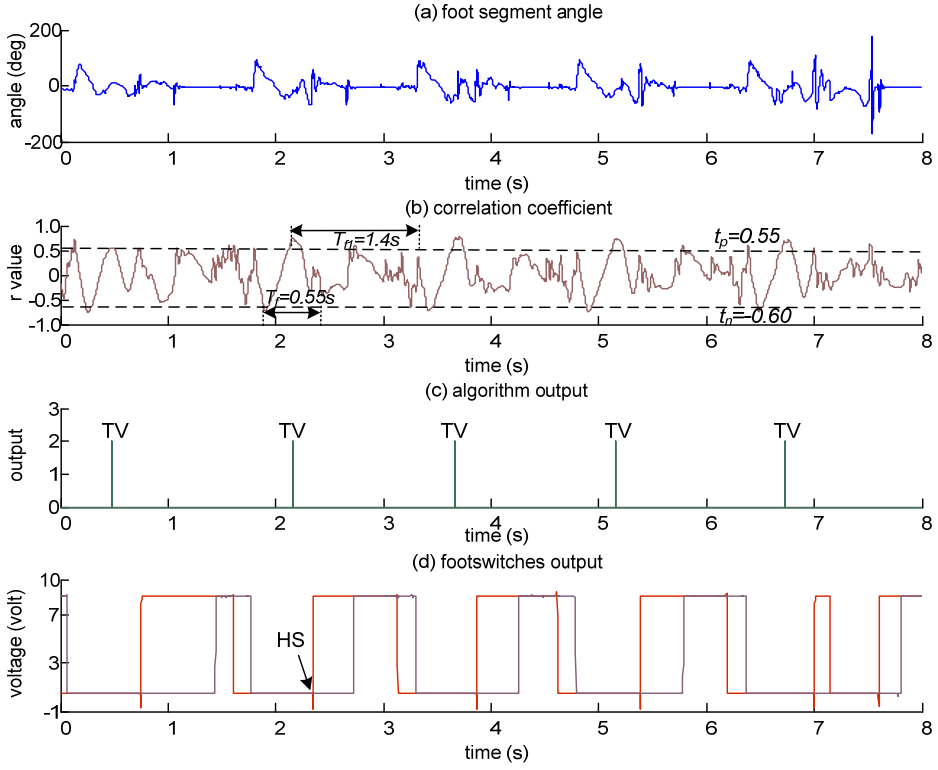

Figure L-31 Tibial vertical event detection in patient (P6) when walking with stimulation on, n=5.

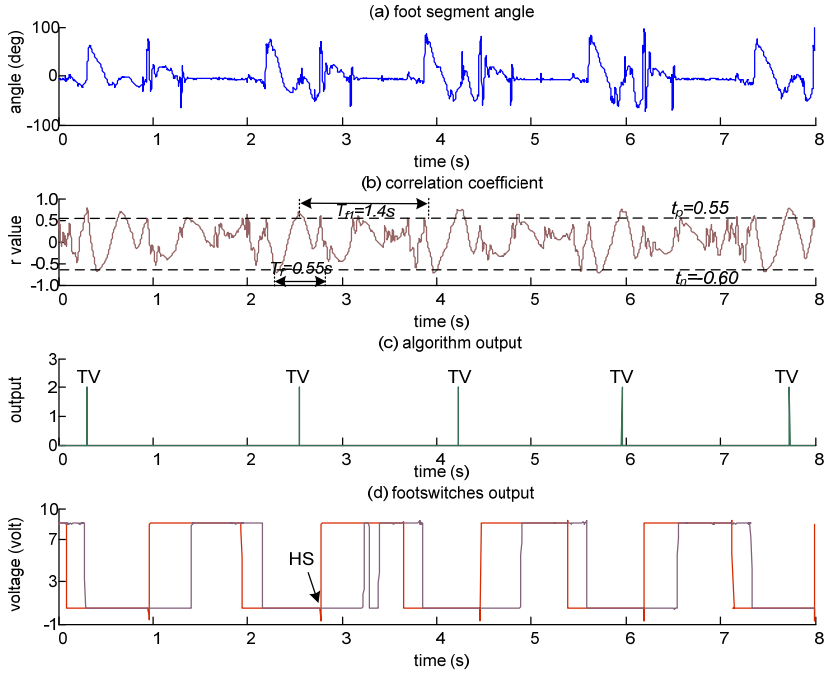

Figure L-32 Tibial vertical event detection in patient (P6) when walking with stimulation on, n=5.

Figure L-32 to Figure L-35: Tibial vertical event detection in patient (P7) when walking with stimulation off. Footswitches output: heel switch (red) and toe switch (purple). (TV=tibia vertical).

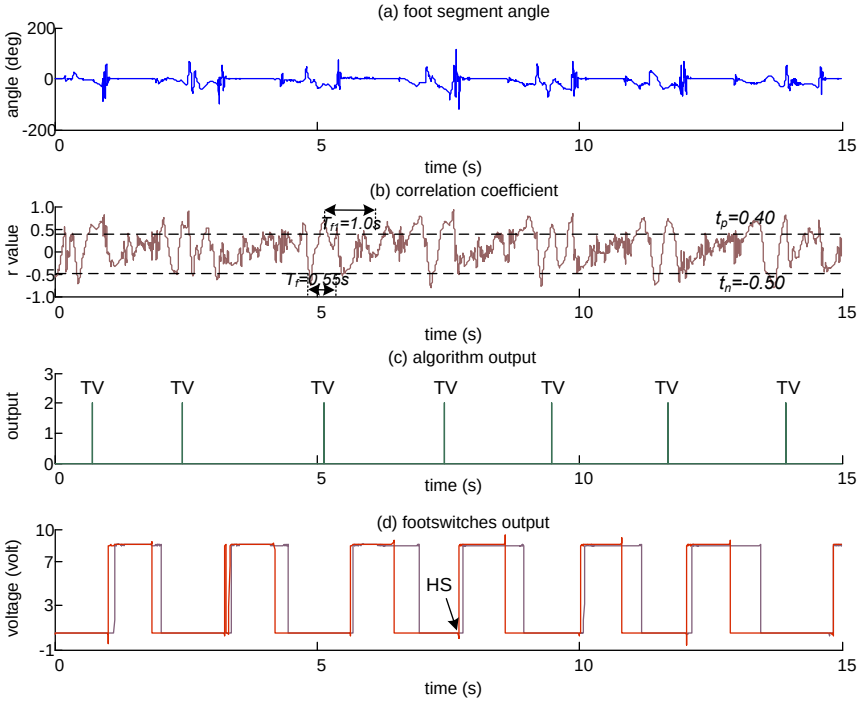

Figure L-33 Tibial vertical event detection in patient (P7) when walking with stimulation off, n=7.

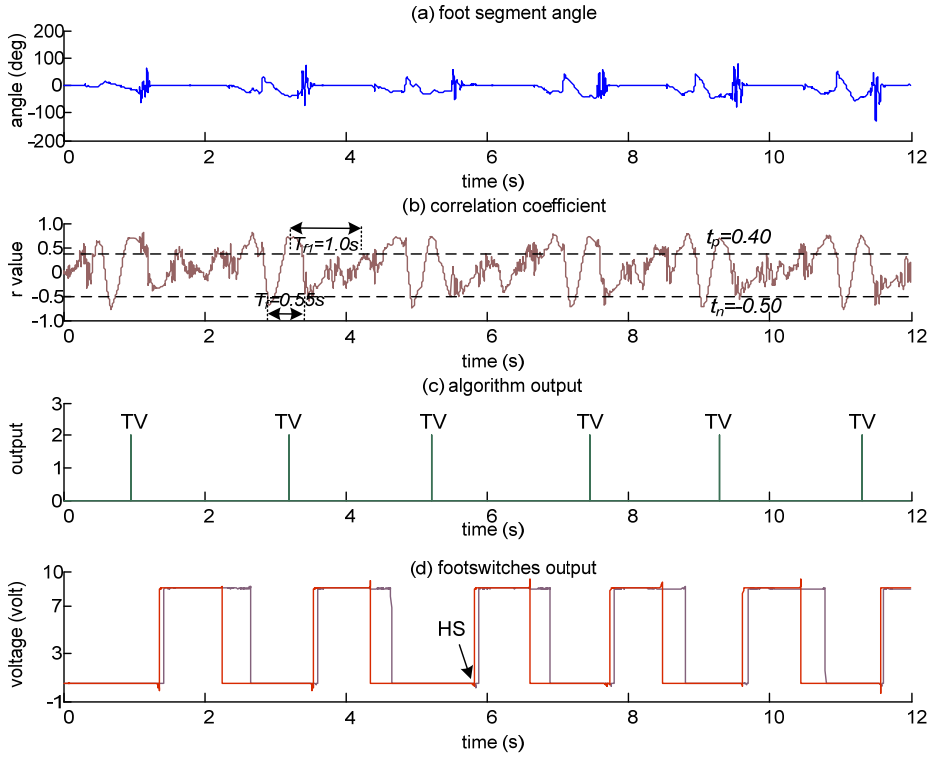

Figure L-34 Tibial vertical event detection in patient (P7) when walking with stimulation off, n=6.

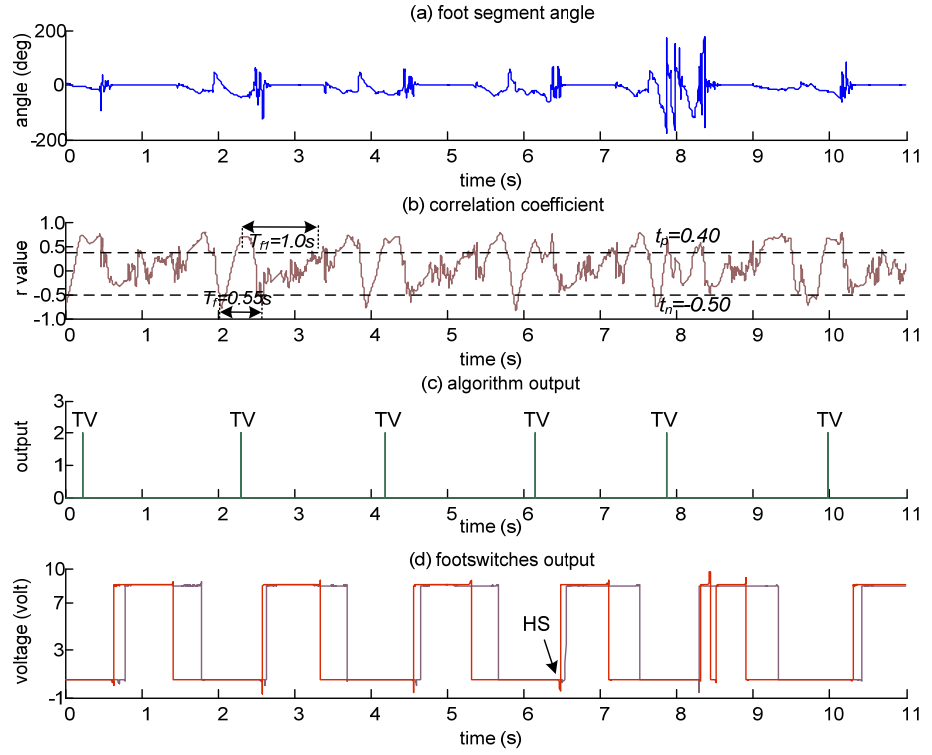

Figure L-35 Tibial vertical event detection in patient (P7) when walking with stimulation off, n=6.

Figure L-36 to Figure L-39: Tibial vertical event detection in patient (P7) when walking with stimulation on. Footswitches output: heel switch (red) and toe switch (purple). (TV=tibia vertical).

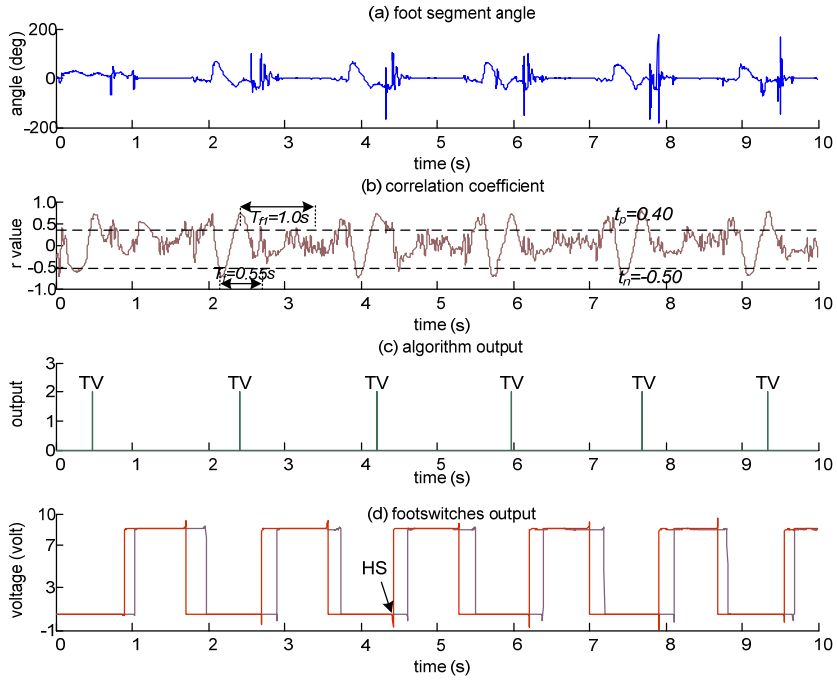

Figure L-36 Tibial vertical event detection in patient (P7) when walking with stimulation on, n=6.

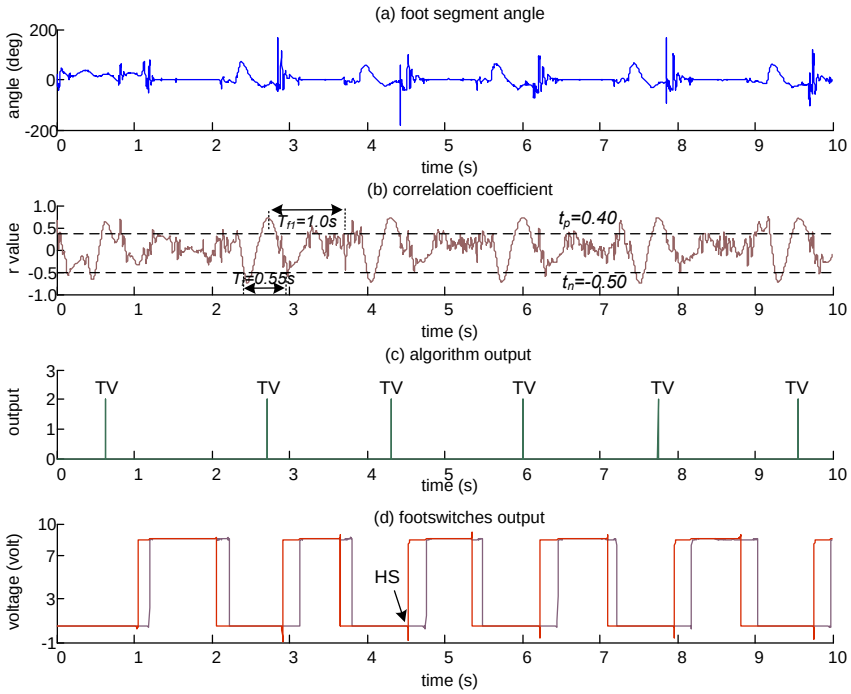

Figure L-37 Tibial vertical event detection in patient (P7) when walking with stimulation on, n=6.

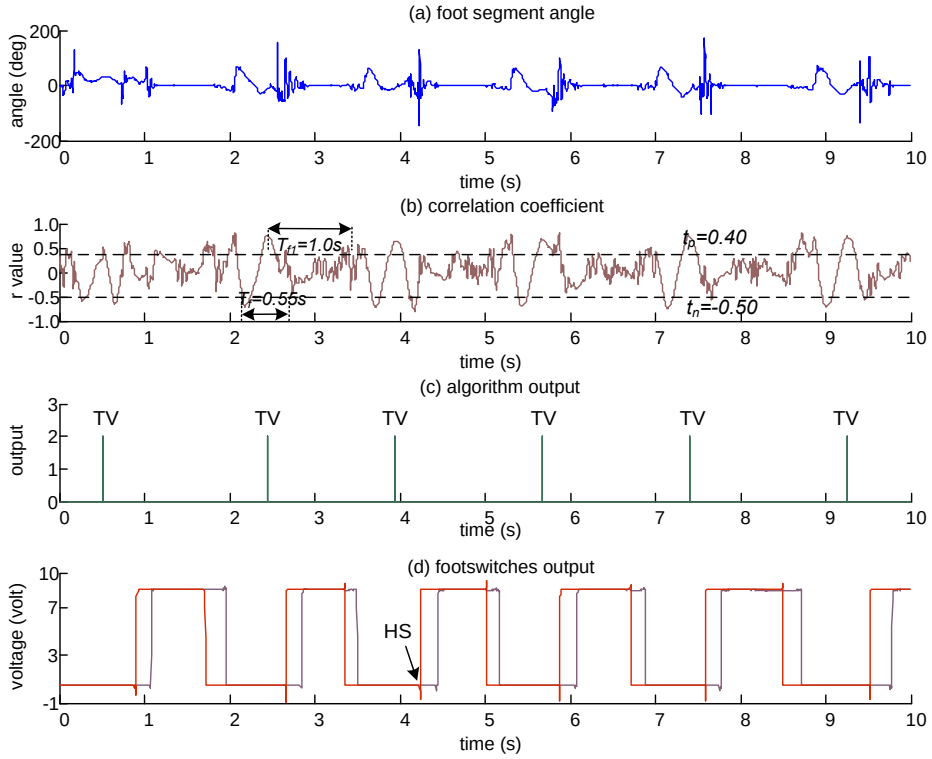

Figure L-38 Tibial vertical event detection in patient (P7) when walking with stimulation on, n=6.

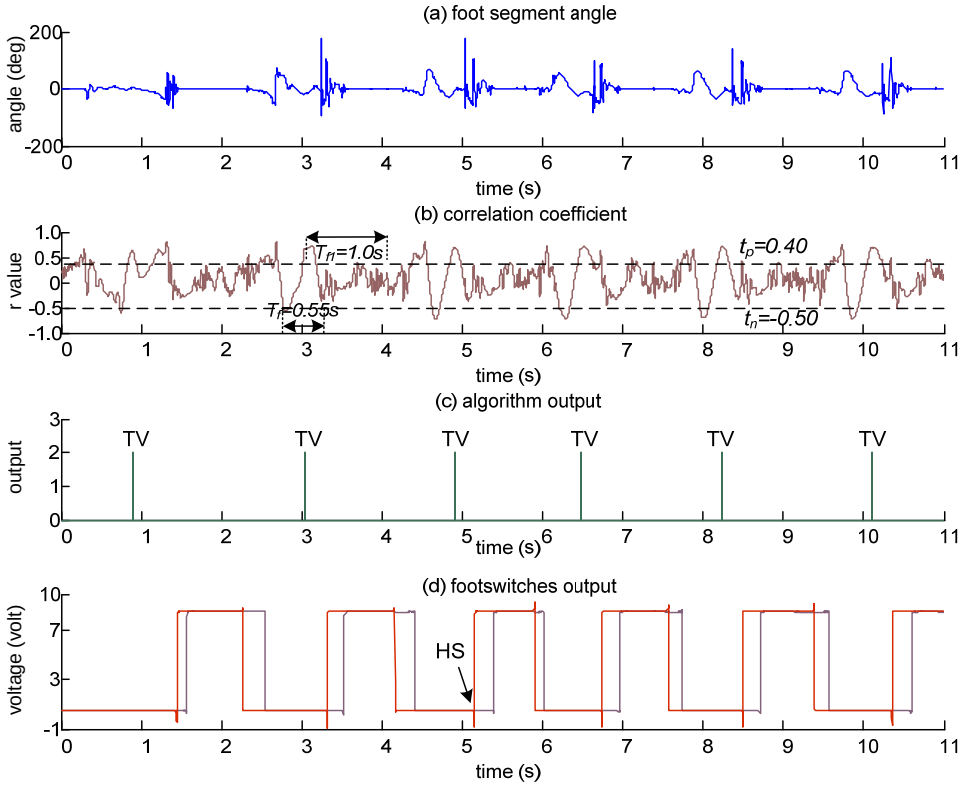

Figure L-39 Tibial vertical event detection in patient (P7) when walking with stimulation on, n=6

Appendix M

Figure M-1 to Figure M-5 show the mean and standard deviation of gait velocity, stride time, cadence, double support time and step width for nonfrail, prefrail and frail subjects.

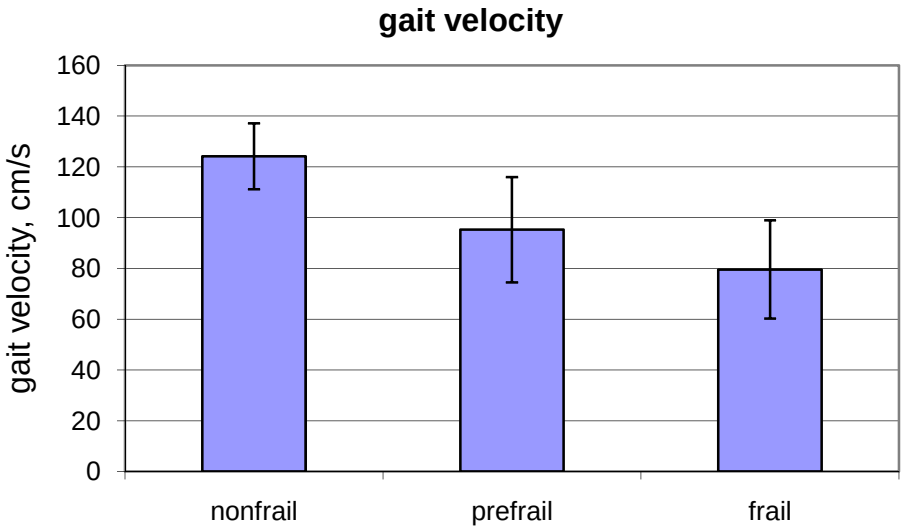

Figure M-1 The mean and standard deviation of gait velocity (cm/s) of nonfrail, prefrail and frail subjects.

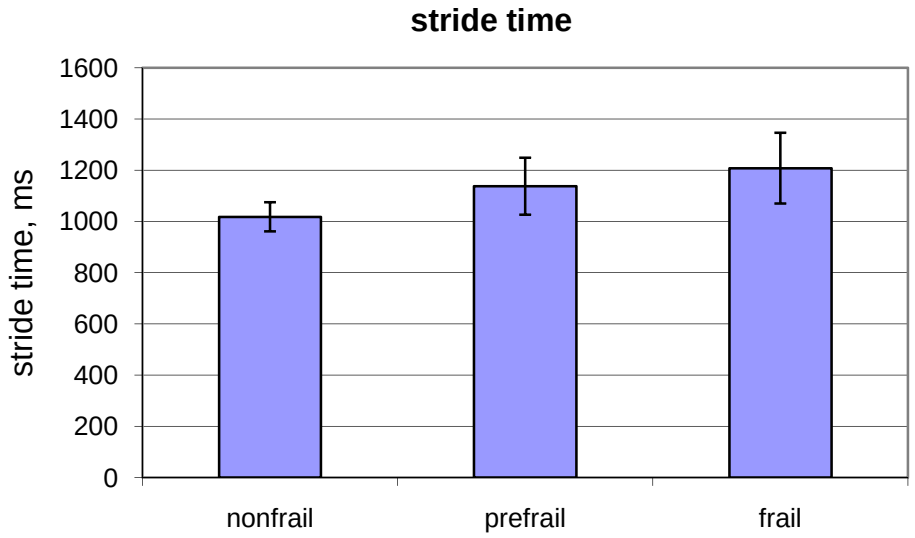

Figure M-2 The mean and standard deviation of stride time (ms) of nonfrail, prefrail and frail subjects.

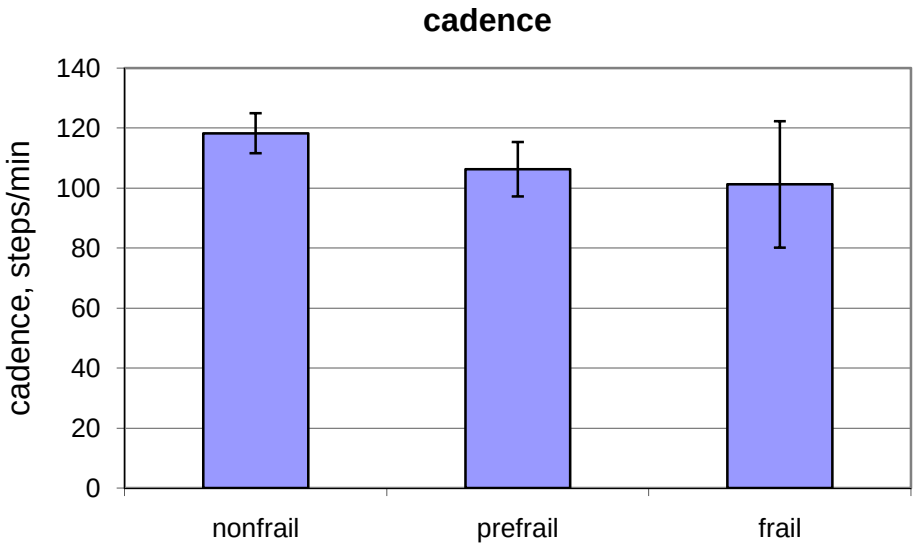

Figure M-3 The mean and standard deviation of cadence (steps/min) of nonfrail, prefrail and frail subjects.

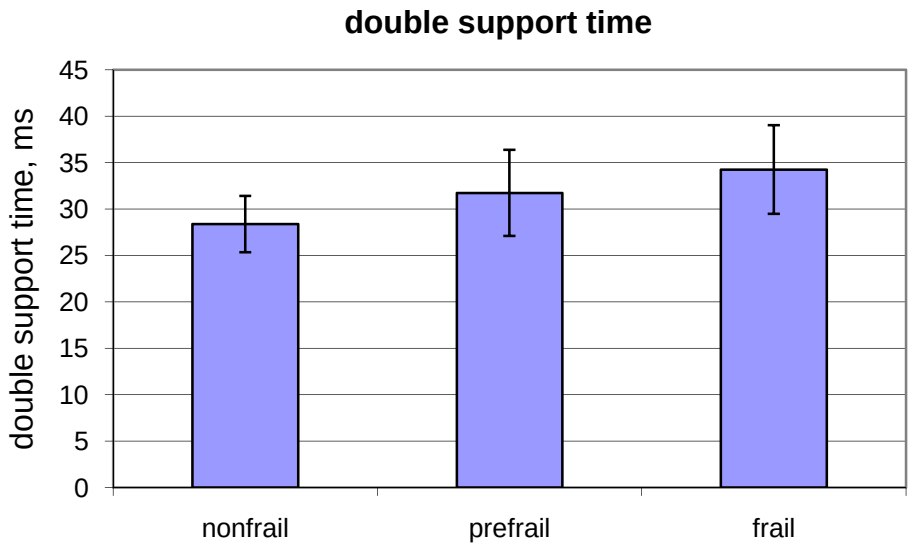

Figure M-4 The mean and standard deviation of double support time (ms) of nonfrail, prefrail and frail subjects.

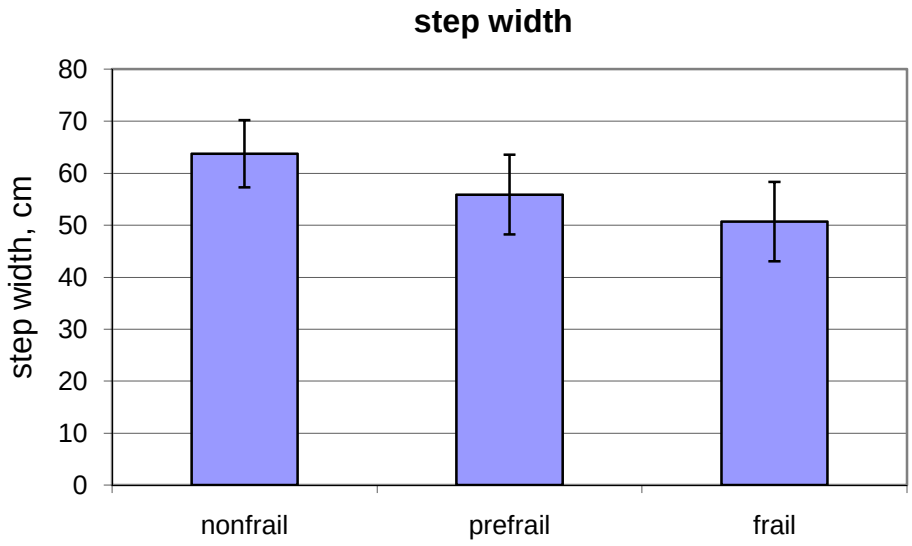

Figure M-5 The mean and standard deviation of step width (cm) of nonfrail, prefrail and frail subjects.